

**ROLE OF A LATE CRETACEOUS
VOLCANIC ARC AND RELATED UNITS IN
TECTONIC ASSEMBLY OF THE TETHYAN
SUTURE ZONE, CENTRAL AND EASTERN
PONTIDES, NORTH TURKEY**

Samuel P. Rice

THESIS SUBMITTED FOR THE DEGREE OF
DOCTOR OF PHILOSOPHY
UNIVERSITY OF EDINBURGH
2005



Dedicated to my Grandparents Doug and Elsie Griffin.

Note to the reader

The stratigraphic scheme set out in this thesis represents work in progress at the time of authorship. It is the author's intention to publish a formal stratigraphy in a peer-reviewed publication as a result of this work. The reader is advised to see subsequent publications if making use of the stratigraphy outlined here.

Acknowledgements

I am very greatly indebted to Prof. Alastair Robertson for his help and support throughout the project. He contributed a very great deal of effort and time to help make this project successful. Alastair's company in the field was inspirational and I am particularly grateful to Alastair for painstakingly reading my work. I am very grateful also to Timur Ustaömer for his kind help and support with essential logistical aspects of the fieldwork and thank Özge Karşlıoğlu for her kind help in the field during 2001. I would like to also thank Louise Meston for her help and company in the field during 2002 and also Yildiz Aydar who helped me to communicate and deal with the Turkish authorities during 2003.

Prof. Izver Ongen, Prof. Kemal Taşlı and Prof. Nurdan İnan very generously gave their time to provide expert biostratigraphic determinations essential to this project. I am very grateful for their contributions.

I also thank, Necdet and Ahmet abi in Tosya, and Umçuf umca and Rafat tazer in Ağvanis for their generous hospitality and friendly company. I am very thankful to Kadir Bey at the Emniyet Genel Müdürlüğü in Erzincan who kindly gave his time so that the fieldwork could continue.

At Edinburgh Dodi James, Pete Hill and Godffrey Fitton patiently explained and advised me on aspects of geochemical laboratory work. I am also grateful to John Dixon, who co-supervised the project. Hugh Sinclair also provided valuable support and advice for which I am very grateful. Many other staff at the University have been very helpful over the last four years, including Justin MacNeil, Shane Voss, and Di Williams.

Thanks also to Ricky for obtaining computer software critical to the production of this thesis. And many thanks to Ruth for her help and support during the writing-up of the project.

Abstract

The İzmir-Ankara-Erzincan suture zone (IAEZ) in the Central and the Eastern Pontides, N Turkey comprises a stack of mainly Upper Cretaceous-Early Tertiary thrust sheets that record the development of: 1) a subduction-accretion complex; 2) a rifted continental margin volcanic arc and associated fore-arc basin, and 3) a backarc basin and its sedimentary fill. Alternative tectonic models are considered in this thesis in the light of structural, sedimentary, igneous geochemical and palaeontological evidence. A tectonostratigraphic revision of the Late Cretaceous-Early Tertiary Neotethyan units in the Central and Eastern Pontides, combined with new biostratigraphic ages is used to constrain the timing of events associated with the assembly of the suture zone. All of the Late Cretaceous Neotethyan units exhibit a pervasive north-vergent shear. The age of north vergent deformation is constrained by the oldest overlying sediments (Kadıkızı Formation and Sipikör Formation) as pre-Eocene. Large-scale southward thrusting followed, forming the present thrust stack. Whole-rock geochemical analyses of basic igneous rocks obtained by X-ray fluorescence indicate the presence of a volcanic arc within the suture zone. The geochemistry of the Neotethyan ophiolites (found to the north of the arc units in both areas) suggests they may represent emplaced backarc basin lithosphere. Screens of metamorphic rocks within the ophiolite in the Eastern Pontides, together with geochemical evidence for a partially enriched mantle source of arc volcanic rocks in the Central Pontides suggest that the arc-backarc system formed by rifting of the continental margin of Eurasia. Using petrographic evidence thick (<1500 m) sedimentary successions found within the suture zone are interpreted as arc apron, forearc, backarc and syn-collisional basins respectively.

From the distribution of tectonic facies within the suture zone it is inferred that Neotethys was subducted northwards beneath the Eurasian margin associated with oceanwards trench-retreat, development of a volcanic arc and a backarc basin during Late Cretaceous time (Santonian-Maastrichtian; ~85-65 Ma). During Maastrichtian time (71-65 Ma) the northward-subducting trench collided with the Tauride-Anatolide Platform, driving northward and southward emplacement of accretionary mélangé, volcanic arc and ophiolitic units. This incipient collision was accompanied by accumulation of nummulitic carbonates in a shelf-depth setting during Palaeocene-Early Eocene time (65-49 Ma) in the Eastern Pontides, and Mid Eocene time (48.6-37.2 Ma) in the Central Pontides. The suture tightened in the Mid-Eocene ("hard collision"), causing large-scale southward imbrication and northward backthrusting in some areas. By way of discussion the results are compared with modern tectonic settings and are relevant to the initiation of subduction, the transition from accretionary to collisional processes, suture zone development and, the conditions of ophiolite genesis.

Contents

1 Introduction	1
1.1 Context	1
1.2 Ophiolites and ophiolitic suture zones: development of concepts	3
1.3 Development of ophiolite genesis and emplacement models in the Eastern Mediterranean and Oman	7
1.3.1 Trench-margin collision model (Oman)	7
1.3.2 Ridge-collapse model	9
1.3.3 Strike-slip-related emplacement	9
1.3.4 Non-tectonically emplaced ophiolites	10
1.3.5 Ophiolite emplacement along active margins in the Eastern Mediterranean	10
1.4 Geological background	15
1.4.1 The Pontides	18
1.4.2 The Tauride-Anatolide Platform (Kirşehir Block and Munzur Platform)	20
1.4.3 The İzmir-Ankara-Erzincan Suture Zone	22
1.4.4 Cover Rocks	27
1.5 Alternative models for Upper Cretaceous ophiolites in the Pontides	28
1.6 Logistical aspects	35
1.7 Methods	36
1.8 Organisation of thesis/review of contents	40
1.8.1 Turkish language	41
2 Tectonostratigraphy of the Eastern Pontides	43
2.1 Revised stratigraphy	43
2.1.1 Campanian-Maastrichtian Ayıkayası Formation	43
2.1.2 Upper Cretaceous Refahiye Complex	45
2.1.3 Upper Cretaceous Karayaprak Mélange	47
2.1.4 Upper Cretaceous Karadağ Formation	49
2.1.5 Campanian-Lower Eocene Sütçinar Formation	50
2.1.6 Palaeocene-Lower Eocene Sipikör Formation	51
2.2 Miocene cover units	52

2.3 Conclusions: tectonostratigraphy of the Eastern Pontides	53
3 The İzmir-Ankara-Erzincan Suture Zone in the Eastern Pontides	55
3.1 Introduction	55
3.2 Trench-margin collision facies: Ayıkayası Formation	55
3.2.1 Structure	58
3.2.2 Sedimentary petrography	58
3.2.3 Discussion	58
3.2.4 Summary	59
3.3 Emplaced inferred marginal basin lithosphere: the Refahiye Complex	59
3.3.1 Structure	60
3.3.2 Peridotites	70
3.3.3 Cumulates	79
3.3.4 Gabbro	80
3.3.5 Sheeted diabase dykes	82
3.3.6 Isolated intrusions	85
3.3.6.1 Plagiogranite dykes	86
3.3.6.2 Isolated diabase dykes	86
3.3.6.3 Late-stage aplite dykes	87
3.3.7 Metamorphic rocks	88
3.3.8 Whole-rock geochemistry of diabase dykes	91
3.3.8.1 Method	91
3.3.8.2 Classification	92
3.3.8.3 Variation diagrams	94
3.3.8.4 Tectonic discrimination	97
3.3.8.5 Multi-element plots	106
3.3.8.6 Chromian spinel chemistry	108
3.3.9 Discussion: petrogenesis and tectonic setting	109
3.3.10 Summary	112
3.4 Late Mesozoic accretionary complex: Karayaprak Mélange	113
3.4.1 Structure	117
3.4.2 Sedimentary and igneous petrography of the Karayaprak Mélange	118
3.4.2.1 Radiolarite-lava-diabase association	118

3.4.2.2 Massive limestone-lava-volcaniclastic association	119
3.4.3 Petrology of metamorphic rocks within the Karayaprak Mélange	120
3.4.4 Whole-rock geochemistry of basic igneous rocks in the Karayaprak Mélange	120
3.4.5 Timing and tectonic setting of the Karayaprak Mélange	131
3.4.6 Summary	132
3.5 Emplaced oceanic volcanic arc: Karadağ Formation	132
3.5.1 Structure	136
3.5.2 Sedimentary facies of the Karadağ Formation	140
3.5.3 Igneous petrology of the Karadağ Formation	147
3.5.4 Metamorphism of the Karadağ Formation	148
3.5.5 Whole-rock igneous geochemistry of basic-intermediate lavas	149
3.5.6 Tectonic setting of the Karadağ Formation	158
3.5.7 Summary	160
3.6 Preserved forearc basin: Sütpınar Formation	160
3.6.1 Structure	164
3.6.2 Sedimentary facies	168
3.6.3 Sedimentary petrography	171
3.6.4 Environment of deposition and tectonic setting	175
3.6.5 Summary	177
3.7 Syn-collisional sedimentation: Sipikör Formation	177
3.7.1 Structure	178
3.7.2 Sedimentary facies	181
3.7.3 Petrography of the Sipikör Formation	183
3.7.4 Depositional setting	190
3.7.5 Summary	190
3.8 Summary of main results from the İzmir-Ankara-Erzincan Suture Zone in the Eastern Pontides	191
4 Tectonostratigraphy of the Central Pontides	195
4.1 Introduction	195
4.2 Revised stratigraphy	195
4.2.1 Upper Cretaceous Kalecik Group	197
4.2.2 Campanian Eskiköy Formation	199

4.2.3 Upper Cretaceous-Lower Eocene Kirazbaşı Mélange: emplaced accretionary complex	200
4.2.4 Campanian-Maastrichtian Kızılırmak Ophiolite	201
4.2.5 Campanian-Maastrichtian Ikiçam Formation: emplaced marginal basin sedimentary rocks	202
4.2.6 Campanian-Maastrichtian Yaylaçayı Formation: emplaced volcanic arc	203
4.2.7 Campanian-Maastrichtian Yapraklı Formation: arc-derived sedimentary rocks	205
4.2.8 Mid-Eocene (Lutetian) Kadıkızı Formation: post-collisional neritic limestones and deltaic clastic sedimentary rocks	206
4.3 Summary of tectonostratigraphy of the Central Pontides	206
5 The İzmir-Ankara-Erzincan Suture Zone in the Central Pontides	209
5.1 Introduction	
5.2 The Eskiköy Formation: Trench-margin collision facies	209
5.2.1 Structure of the Eskiköy Formation	209
5.2.2 Sedimentary facies of the Eskiköy Formation	214
5.2.3 Summary	218
5.3 Emplaced ophiolite slices: Kızılırmak Ophiolite	220
5.3.1 Structure of the Kızılırmak Ophiolite	221
5.3.2 Petrology of the Kızılırmak Ophiolite	231
5.3.3 Igneous Geochemistry of the Kızılırmak Ophiolite	233
5.3.3.1 Whole-rock geochemistry of basic igneous rocks	233
<i>chromian spinel chemistry</i>	242
5.3.4 Petrogenesis and tectonic setting of the Kızılırmak Ophiolite	242
5.3.5 Summary	244
5.4 Late Mesozoic accretionary complex: Kirazbaşı Mélange	245
5.4.1 Structure of the Kirazbaşı Mélange	247
5.4.2 Sedimentary facies and petrology of the Kirazbaşı Mélange	252
5.4.2.1 Radiolarite-basalt-serpentinite-clastic association	252
5.4.2.2 Massive limestone-lava-volcaniclastic association	254
5.4.3 Whole-rock geochemistry of basic igneous rocks in the Kirazbaşı Mélange	256
5.4.4 Age, petrogenesis and tectonic setting of the Kirazbaşı Mélange	265
5.4.5 Summary	266

5.5 Emplaced volcanic arc: Yaylaçayı Formation	267
5.5.1 Structure of the Yaylaçayı Formation	269
5.5.2 Sedimentary facies and igneous petrology of the Yaylaçayı Formation	278
5.5.3 Metamorphic petrology of the Yaylaçayı Formation	285
5.5.4 Whole-rock igneous geochemistry of basic-intermediate lavas	286
5.5.5 Discussion: age, petrogenesis and tectonic setting of the Yaylaçayı Formation	297
5.5.6 Summary	299
5.6 Volcanic arc cover: Yapraklı Formation	300
5.6.1 Structure of the Yapraklı Formation	300
5.6.2 Sedimentary facies	304
<i>Palaeocurrent data</i>	307
<i>Depositional setting</i>	308
5.6.3 Summary	310
5.7 Preserved back-arc basin sediments: Ikiçam Formation	310
5.7.1 Structure of the Ikiçam Formation	311
5.7.2 Sedimentary facies and igneous petrology of the Ikiçam Formation	318
5.7.3 Whole-rock igneous geochemistry of basic rocks within the Ikiçam Formation	321
5.7.4 Environment of deposition and tectonic setting of the Ikiçam Formation	332
5.7.5 Summary	332
5.8 Post-collisional sediments: Kadıkızı Formation	333
5.8.1 Structure of the Kadıkızı Formation	336
5.8.2 Age and sedimentary facies of the Kadıkızı Formation	341
5.8.3 Depositional setting	338
5.8.4 Summary	339
5.9 Summary of the suture zone in the Central Pontides	340
6 Discussion	343
6.1 introduction	343
6.1.1 Comparison of the İzmir-Ankara-Erzincan Suture Zone in the Eastern and Central Pontides	343
6.1.2 Structure of the İzmir-Ankara-Erzincan Suture Zone	355
6.1.3 Summary of comparisons	359
6.2 Tectonic evolution of the northern Neotethyan Ocean	359

6.2.1 Alternative models	359
6.2.2 Proposed new model	362
6.3 Modern and ancient examples of comparable tectonic processes	365
6.4 Wider implications	375
6.4.1 Role of the volcanic arc: Experimental work on preservation of volcanic arcs	375
6.4.2 Role of the volcanic arc during early collision: continental subduction, 'hard' and 'soft' collision.	376
6.4.3 Ophiolites and orogenesis: local v. global controls.	378
6.4.4 Future work	380
7 Conclusions	383

1 Introduction

1.1 Context

The Eastern Mediterranean region has received much attention from geologists due to a particularly challenging set of tectonostratigraphic problems and a complicated tectonic history associated with the closure history of the Palaeozoic-Mesozoic ocean, Tethys. This complicated history has led to the development of several suture zones in the region (Figures 1.1 and 1.2). These suture zones mark the traces of former oceanic basins and the boundaries of previously separated continental lithospheric plates (Şengör and Yılmaz 1981; Dercourt et al. 1986; 1991; Robertson and Dixon 1984; Okay and Tüysüz 1999). Models for the tectonic development of the region (and even of local areas within the region) have continuously developed over the last 50 years and it is now apparent that a former ocean (Tethys) that was located between Afro-Arabia and Eurasia, finally closed along the Upper Cretaceous Izmir-Ankara-Erzincan Suture Zone (Izmir-Ankara-Erzincan Suture Zone). The Tethyan ocean is commonly divided into an Upper Palaeozoic-Lower Mesozoic 'Paleotethys' and, an Upper Mesozoic 'Neotethys' (e.g. Robertson and Dixon 1984). Several Neotethyan sutures have been identified in the Eastern Mediterranean region and these are generally divided into southerly and northerly sutures representing at least two oceanic areas. Further explanation of these different Tethyan definitions is given later. The Izmir-Ankara-Erzincan Suture Zone represents the scar of the main Neotethys (Şengör and Yılmaz 1981; Dercourt et al. 1986; Robertson and Dixon 1984). This suture zone can be traced across northern Anatolia from Izmir, on the Aegean coast, to the Armenian border in the East, where it continues eastward into the Caspian region (Figures 1.1 and 1.2; Adamia et al. 1981; Şengör and Yılmaz 1981; Okay and Tüysüz 1999; Robertson 2004). However, most geological research has focused on south-Tethyan sutures (i.e. in the Taurides, southeast Turkey, Antalya and Cyprus) and there has been a paucity of data from the Upper Cretaceous Izmir-Ankara-Erzincan Suture Zone. Several studies have noted the existence of a volcanic arc-type unit within the Izmir-Ankara-Erzincan Suture Zone (Tüysüz 1990, 1995; Ustaömer and Robertson 1997; Koçyiğit 2003; Rojay 2001). In particular, uncertainty persists regarding the direction and timing of

subduction of Tethyan lithosphere during Late Cretaceous time, the origin and mechanism of emplacement of ophiolites in the Pontides (Figure 1.3), and the timing of the final closure of northern Neotethys. This study provides critical data from the Izmir-Ankara-Erzincan Suture Zone in the Eastern and Central Pontides in order to better understand the tectonic development of the Izmir-Ankara-Erzincan Suture Zone. The results of this study highlight the role of a volcanic arc related to northward subduction of northern Neotethyan oceanic lithosphere.

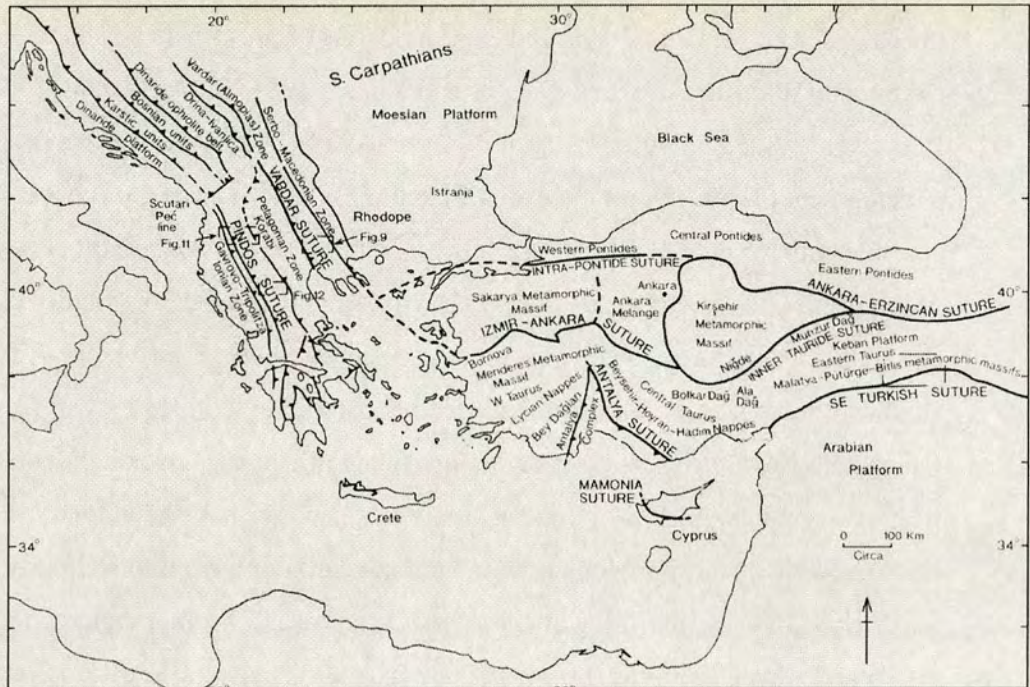


Figure 1.1. Outline map of the Eastern Mediterranean region showing the main suture zones (after Robertson 2002).

1.2 Ophiolites and ophiolitic suture zones: development of concepts

Suture zones represent the boundaries of former lithospheric plates. Their occurrence is associated in space and time with orogenesis (Dewey 1976). Suture zones are commonly associated with ophiolite complexes and typically contain ophiolitic mélange. In addition, it has long been recognised that ophiolites are a ubiquitous feature of major mountain belts globally (of both collisional and accretionary type; e.g. the Alpine-Himalayan Belt and the Andes respectively; e.g. Dalziel 1986). Early-on it was appreciated that the age of the vast majority of ophiolite complexes is very close to the age of their subsequent emplacement. Therefore, beyond providing information on the origin and nature of oceanic-type lithosphere (Parson and Murton 1992) ophiolites are central to concepts of how orogenesis operates in space and time.

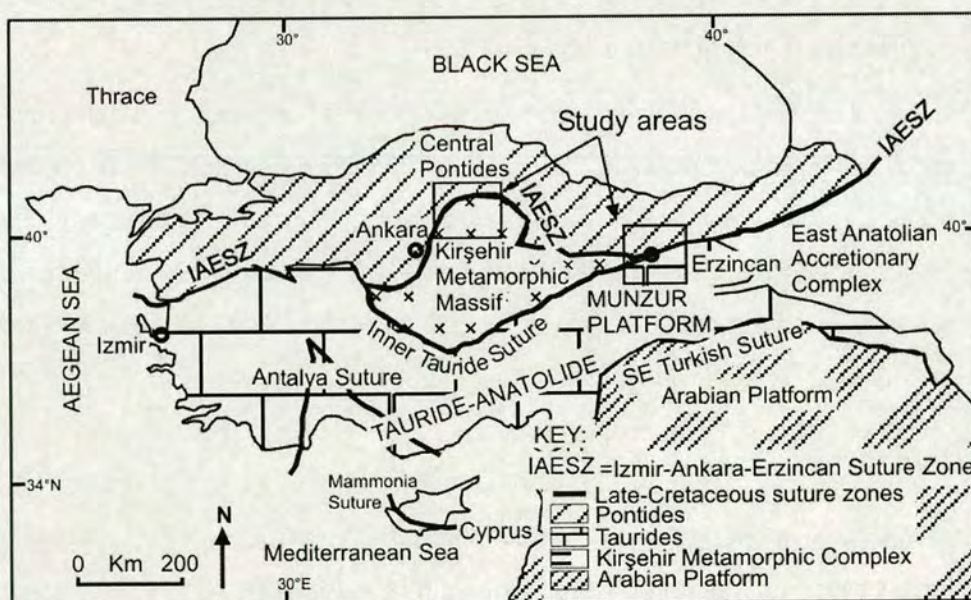


Figure 1.2. Tectonic map of Anatolia showing Upper Cretaceous-Early Tertiary suture zones. Izmir-Ankara-Erzincan Suture Zone = Izmir-Ankara-Erzincan Suture Zone. Boxes outline areas studied during this project.



Figure 1.3. Outline map of the Eastern Mediterranean region showing main ophiolite occurrences (after Robertson 2002).

The geological map of the world shows a greater density of ophiolites by area in the Mediterranean and Middle East than anywhere else in the world (except perhaps Indonesia or Alaska; Robertson 2004). Outcrops of the main ophiolites in the Eastern Mediterranean are shown in Figure 1.3. The Mediterranean region provides an excellent ‘natural laboratory’ in which interpretations of ophiolites and concepts regarding their emplacement and their role in orogenesis have been continuously tested and developed since the 1960’s.

One problem, however, is that in terms of their origin, the Eastern Mediterranean ophiolites may not be representative of all ophiolites, particularly those occurring in non-collisional mountain belts (e.g. the Andes). Another problem is that the Eastern Mediterranean ophiolites were generated and emplaced in great abundance within discrete brief intervals of geological time (Livermore and Smith 1984; Robertson and Dixon 1984). No directly equivalent process is known to be occurring today and there is no exact modern analogue for such extensive ophiolite development and emplacement (Pearce 2003; Robertson 2004). The formation and emplacement of ophiolites in mountain belts seems to occur in temporal pulses and

many workers have related the origin and emplacement of ophiolites to specific phases of drastic plate boundary reorganisation, or the generation of Large Igneous Provinces (e.g. Dalziel et al. 2000; Dilek 2003; Smith 2004; Robertson 2004). Therefore, ophiolites appear to present a challenge to uniformitarianism. Are ophiolites indicative of some drastic global tectonic event or can their emplacement be controlled by regional-scale tectonic processes (e.g. ridge subduction, arc-trench collision)?

Ophiolites were recognised well before the acceptance of the plate tectonic paradigm (e.g. Brogniart 1813; Suess 1909; Steinmann 1927; Bruhn 1954). It was suggested early-on that Alpine peridotites were formed by intrusion and extrusion of basic and ultrabasic magma within geosynclines (e.g. Harker 1909; Vogt 1921; see Young 2003). The sheeted dykes of the Troodos Massif (Cyprus) had been studied by Wilson (1959) before the hypothesis of seafloor spreading was proposed by Vine and Matthews in 1963. Mapping of the Troodos Massif by Gass (1968) and further studies by Moores and Vine (1971) led to the acceptance of ophiolites as fragments of oceanic crust formed at spreading centres. This view was retained when the Penrose Conference delegates in 1972 formally defined an ophiolite as a 'distinctive assemblage of mafic to ultramafic rocks'. In a complete Penrose-type ophiolite the rock types occur in the following sequence, starting from the bottom and working up:

1. Ultramafic complex.
2. Gabbroic complex.
3. Mafic sheeted dyke complex.
4. Mafic volcanic complex (Anonymous 1972).

more recently it was discovered that the Penrose-type definition does not apply well to the rifted-type ophiolites of e.g. the Eastern Alps and the Apennines (Robertson 2002).

During the 1970's basalts from a variety of tectonic settings including mid-oceanic spreading centres, seamounts and, volcanic arcs were geochemically analysed (e.g. Pearce and Cann 1973). Geochemical data from many ophiolites were shown not to match the composition of typical oceanic crust (Mid-Ocean Ridge Basalt; MORB; e.g. Pearce and Cann 1973; Shervais 1982; Pearce 1982). It was soon

recognised that the concept of ophiolites as analogues for typical oceanic lithosphere did not adequately explain these differences. The chemistry of ophiolitic lavas was shown to be, in many cases, more similar to that of volcanic arcs formed above subduction zones than to typical MORB (although it was also recognised that some ophiolites do have compositions similar to MORB; e.g. in the Western Mediterranean; Pearce et al. 1984). The geochemistry of ophiolites, very commonly, indicates that their formation was associated with subduction rather than the seafloor spreading stages of Wilson cycles. However, ophiolites are clearly neither structurally nor petrologically similar to well-developed volcanic arcs (Gass et al. 1975). In the search for modern analogues for the formation of suprasubduction zone (SSZ) ophiolites, extension-related magmatism in convergent tectonic settings such as backarc basins, forearc basins and, embryonic intraoceanic volcanic arcs became popular candidates. An embryonic arc setting was favoured (e.g. Pearce 1982; Clift and Dixon 1998; Robertson 2004) although modern analogues are apparently rare. One example could be the Trobriand arc/Woodlark Basin near Papua New Guinea (Davies 1984; Robertson et al. 2001). More recently, studies of ophiolites have shown that their composition, anatomy and origin are varied (MORB and Supra-Subduction Zone (SSZ) types are recognised; e.g. Pearce et al 1984) and a 'Tethyan'-type vs. 'Cordilleran'-type distinction has been made on the basis of oceanic settings and mode of emplacement (e.g. Robertson and Dixon 1984; Spaggari et al. 2003; Beccaluva et al. 2004). Western Mediterranean ophiolites are mostly similar, in terms of petrology and geochemistry, to oceanic lithosphere formed at mid-oceanic ridges (e.g. Subpelagonian ophiolites of the Albanide-Hellenide system; Beccaluva 1994). By contrast, the ophiolites of the Eastern Mediterranean are generally of SSZ-type (Robertson 2004).

In addition to the SSZ geochemical characteristics of most ophiolites the ubiquitous occurrence of ophiolites within orogenic belts and suture zones points to a close association between ophiolite genesis and convergent plate tectonics. The age of ophiolites is commonly close to the age of their emplacement (i.e. within ~15 M.y.; e.g. Dewey 1976). The formation of SSZ ophiolites is likely to be a response to the initiation of new subduction zones (Casey and Dewey 1984; Beccaluva et al. 2004). However, the initiation of subduction is a poorly understood process with no

well documented modern analogues. As is the case for ophiolite genesis, subduction zone initiation also appears to be non-uniformitarian and might have occurred at specific times of drastic global plate motion reorganisation (Casey and Dewey 1984; Dilek 2004). SSZ ophiolites could provide a tectono-magmatic record of the early stages of subduction and on the setting of its initiation (Flower and Dilek 2003).

1.3 Development of ophiolite genesis and emplacement models in the Eastern Mediterranean and Oman

Evidence from the Eastern Mediterranean and Oman has been used extensively to develop models for ophiolite genesis and emplacement. As mentioned above, the vast majority of data from the region have been obtained from south Tethyan suture zones. A brief outline of the development of these models in the Eastern Mediterranean provides a regional and historical context for this research which is concerned with the Izmir-Ankara-Erzincan Suture Zone in Turkey.

1.3.1 Trench-margin collision model (Oman)

The trench-margin collision model (Figure 1.4), which has been commonly applied to the Upper Cretaceous Semail Ophiolite of Oman (Glennie et al. 1973; Lippard et al. 1986), is the most popular model for the emplacement of Tethyan ophiolites. This model has since been successfully applied to many Eastern Mediterranean ophiolites, for example ophiolites which were emplaced southwards onto the Tauride platform (Lycian ophiolite: Collins and Robertson 1998; Çelik and Delaloye; Beyşehir ophiolite: Andrew and Robertson 2002; Pozantı-Karsanti ophiolite: Parlak et al. 2001; Kuthaya ophiolite, NW Turkey: Önen 2003; see Figure 1.3), ophiolites located along the Northern Arabian margin, through Iran, eastern Turkey and northern Syria (Ricou 1971; Glennie 2000) and ophiolites of the Balkans (Pindos and Vorinos Ophiolites: Capedri et al. 1980; Noiret et al. 1981). The Semail Ophiolite, Oman, developed above a north-dipping subduction zone during Late Cretaceous time as a result of SSZ extension and trench retreat ('rollback'). Several million years later the retreating trench reached the Arabian continental margin. The same lithospheric thrust zone that had been the subduction zone facilitated the emplacement of the new SSZ crust (i.e. the ophiolite) southwards over the Arabian

passive margin (Searle and Malpas 1980, 1982; Cox 1999; Robertson 2004). However, even with the possibility of temperature-induced buoyancy in the young ophiolitic slab it seems counter-intuitive that a vast slab of oceanic lithosphere could be obducted from an ocean basin, upwards, onto a continental margin against gravity. Analysis of syn-emplacment sedimentary rocks (Muti Formation) revealed that the margin and the abyssal plain subsided ahead of the advancing ophiolite nappe (Robertson 1987) due to the flexural bending of the lithosphere in response to slab-pull. Small granitic intrusions were inferred to have been derived by melting of passive margin sedimentary rocks that were partially subducted beneath the ophiolite (Cox 1999). Thus, the trench-margin collision model can be envisaged as the partial subduction of a continental margin rather than the forced upward-thrusting of oceanic lithosphere. In Oman, the thickness of subduction-resistant continental crust eventually 'choked' the subduction zone and the buoyancy of the partially consumed margin then uplifted the obducted ophiolite (Searle and Malpas 1980; Robertson 2004).

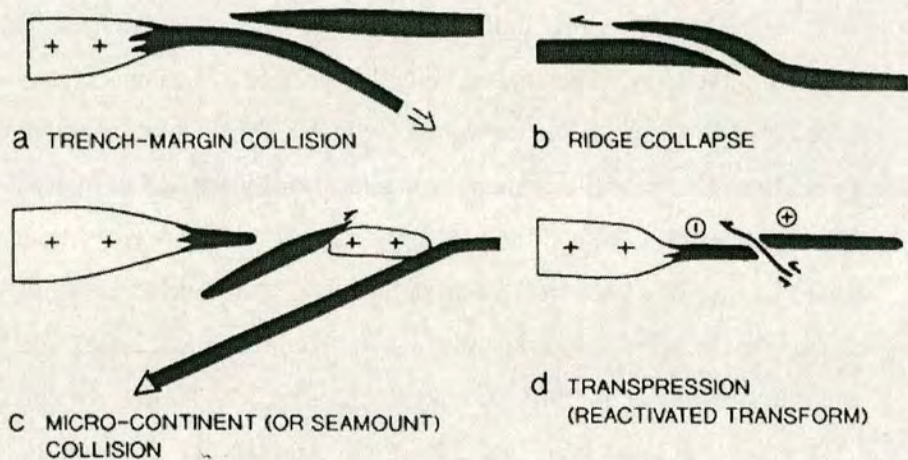


Figure 1.4. Some ophiolite emplacement models that have been applied in the Eastern Mediterranean (after Robertson 2004). a) Trench-passive margin collision (e.g. Oman); b) collapse of a spreading ridge; c) oceanward trench-jump following accretion of seamount or continental fragment; d) strike-slip (transpressional) emplacement (e.g. Antalya complex).

1.3.2 Ridge-collapse model

The high-temperatures necessary to generate the amphibolite facies rocks observed within the metamorphic soles of many ophiolites suggest that the basal thrust of the ophiolite developed near to the spreading ridge, where the crust was youngest and hottest (Hopson and Pallister 1980; Pallister and Hopson 1981; Nicolas and LePichon 1980). This led to the ridge-collapse model (Figure 1.4) in which a spreading ridge became the site of intraoceanic overthrusting. However, the geochemistry of metabasites within the metamorphic sole showed that they had a different petrogenetic origin (i.e. 'Within-Plate Basalt' and MORB) to the overriding SSZ ophiolite (Pearce 1981; Robertson 2004). This difference between the chemistry of the metamorphic sole and the overriding ophiolite would not be expected if the metamorphic sole rocks were accreted from the adjacent flank of a symmetrical spreading ridge (Harris 1992). Thus an asymmetrical ridge-collapse model is required in which only one side of the ridge subsided and retreated (Dixon and Robertson 1985). The SSZ ophiolite formed above the sinking flank of the ridge (composed of MORB lithosphere; the protolith of the accreted metamorphic sole rocks). The ophiolite was then obducted in essentially the same way as described above for Oman. However, there are no known modern analogues for this asymmetrical ridge-collapse process (Bloomer et al. 1995; Stern and Bloomer 1992; Robertson 2004).

1.3.3 Strike-slip-related emplacement

The Upper Cretaceous (Maastrichtian) Tekirova ophiolite in the southwest segment of the Antalya Complex (southwest Turkey) and related mélangé units are exposed within lozenge-shaped outcrops separated by high-angle strike-slip faults (Juteau 1979, 1980; Woodcock and Robertson 1985; see Figure 1.5 **Error! Reference source not found.**). The metamorphic sole of the ophiolite is only locally exposed (Çelik and Delaloye 2003) and the sediment stratigraphy of the adjacent carbonate platform, against which the Cretaceous Tekirova ophiolite is juxtaposed, does not exhibit evidence for subsidence during latest Cretaceous time when the ophiolite was being emplaced (Robertson 2004).

Few other examples of strike-slip settings have yet been recognised both regionally and globally.

1.3.4 Non-tectonically emplaced ophiolites

Ophiolites of the Inner Hellenide Ophiolite Belt (e.g. Guevgueli and related ophiolites; Figure 1.6) exhibit contact metamorphism against adjacent basement units that are correlative with Serbo-Macedonian continental crust. These ophiolites are interpreted to have formed within a narrow backarc basin formed within the rifted continental margin (i.e. an ensialic backarc basin). These ophiolites were deformed and uplifted without undergoing tectonic transport across the opposing lithospheric plate; they are preserved as parautochthonous tectonostratigraphic units. This type of ophiolite has been contrasted with the 'Oman' case by several workers (e.g. Robertson 2002; Spaggari et al. 2003; Dilek 2003; Beccaluva 2004).

1.3.5 Ophiolite emplacement along active margins in the Eastern Mediterranean

The term 'Cordilleran-type ophiolite' has been applied to ophiolites emplaced along Pacific-type active continental margins (e.g. Jurassic Californian ophiolites; Moores 1982). The term has also been used for ophiolites with MORB-type geochemical characteristics accreted to active margins from the down-going slab (e.g. Yakuno ophiolite, Japan; Osozawa et al. 2004), whereas the term 'Tethyan ophiolites' has been applied to ophiolites around the world that were emplaced over continental passive margins; exemplified by the Oman case (e.g. Spaggari et al. 2003; Beccaluva et al. 2004). However, these are genetic terms and should be used with caution because the causes and means of ophiolite genesis and emplacement in many individual cases are still poorly understood.

The 'Oman' model (Figure 1.4) has been commonly applied to ophiolites emplaced southwards over southerly passive margins of Tethyan oceanic basins (Robertson 2004). By contrast, within the Eastern Mediterranean region ophiolites

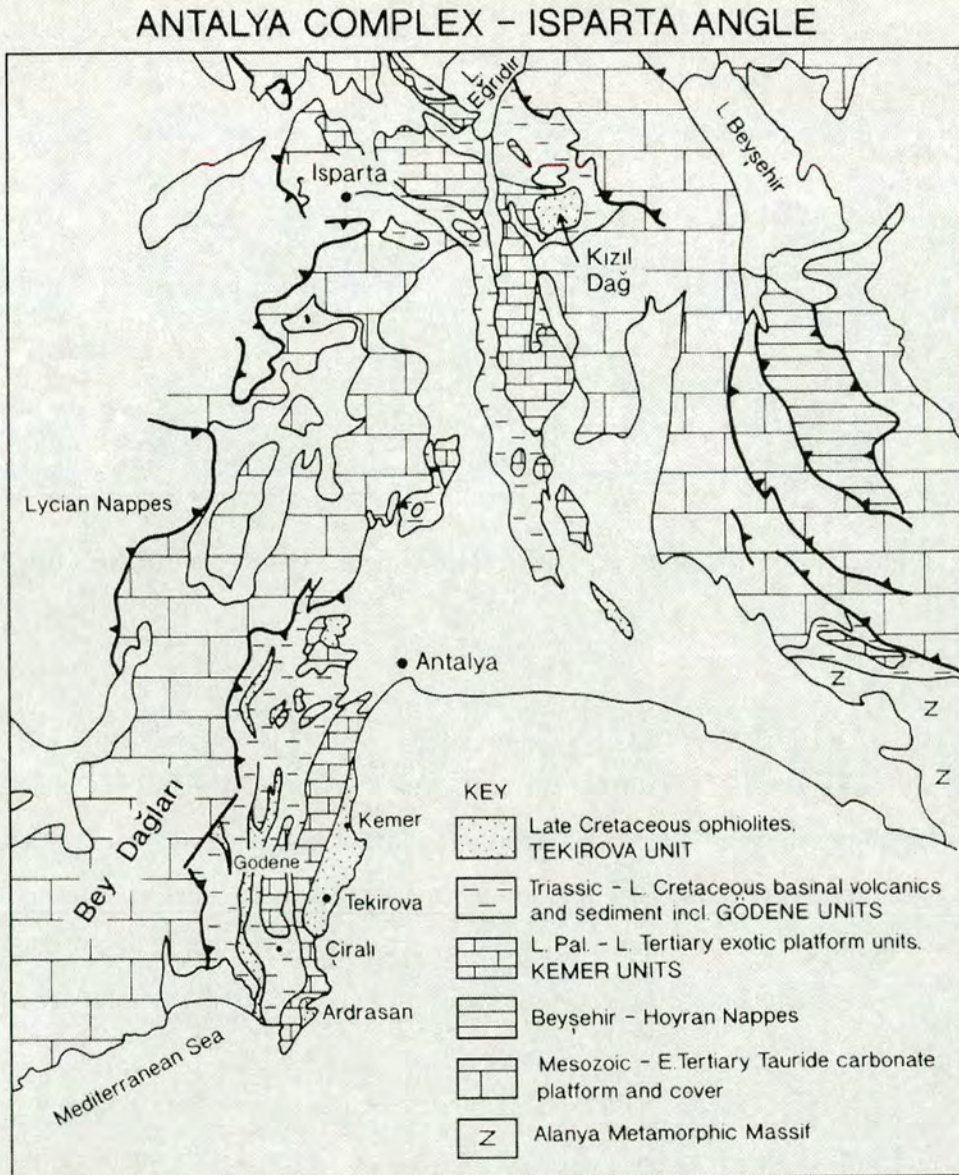


Figure 1.5. Map showing the geological setting of the Antalya Complex in southwest Turkey (after Robertson 2002).

were also emplaced onto the opposite northern margins of Tethyan oceanic basins (as 'Cordilleran'-type ophiolites). These northern margins generally record a long-term history of subduction-related and accretionary processes (Adamia et al. 1981; Robertson and Dixon 1984; Dercourt et al. 1986). Ophiolites were emplaced northward in the Pontides during Late Palaeozoic-Early Mesozoic time (e.g. Küre

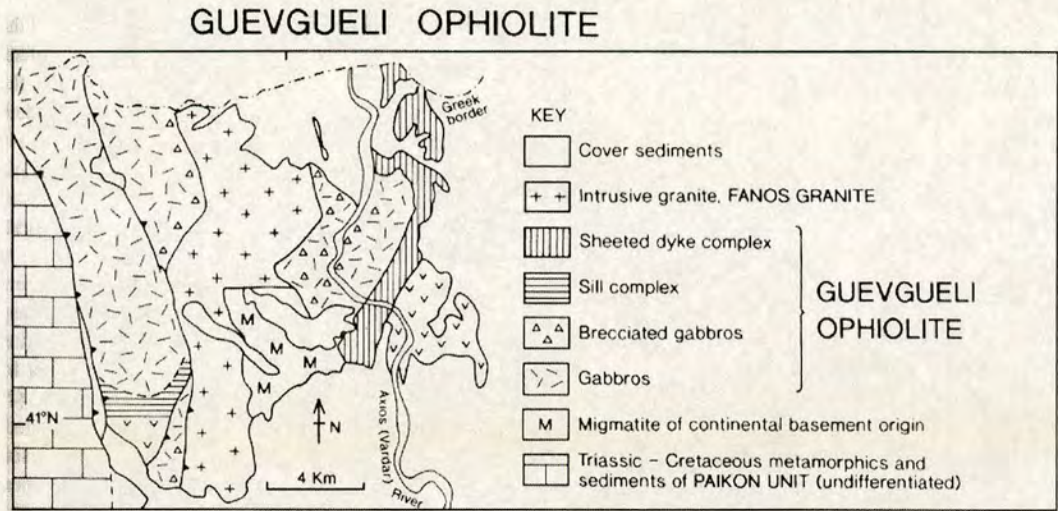


Figure 1.6. Sketch map of the Jurassic Guevgueli ophiolite in NE Greece (after Robertson 2002).

Bergougnan 1975; Şengör and Yılmaz 1981; Ustaömer and Robertson 1997; Okay and Şahintürk 1997; Yılmaz et al. 1997; and this study). The Upper Cretaceous ophiolites in the Pontides are important in this project because their characteristics are informative of past tectonic settings and processes and these are discussed below. Ophiolites were also emplaced onto the northerly active margin of a south Tethyan ocean basin and are exposed in southeastern Turkey. These examples are described briefly below.

Ophiolites in southeast Turkey were emplaced in latest Cretaceous time along the northern margin of a south Neotethyan ocean basin which is generally believed to have been subducted northwards (Hall 1976; Aktaş and Robertson 1984; Yılmaz 1993). Examples include the Guleman, Berit and Ispendere ophiolites (Figure 1.3). Their mode of emplacement remains poorly understood (Parlak et al. 2001; Robertson 2004). These ophiolites probably formed by SSZ spreading within southern Neotethys and were accreted to the Tauride active margin to the north. It is unclear what caused their obduction in an active margin setting. Due to the presence of arc-related plutonic rocks in the Taurides it is possible that two north-dipping subduction zones existed in southern Neotethys. The ophiolites are cut by arc-related

igneous rocks possibly related to northward subduction of the remaining south Neotethyan oceanic lithosphere (Robertson 1998).

Palaeotethyan (pe-Late Jurassic) ophiolites can also be considered to have been emplaced in an active margin setting (Robertson and Dixon 1984; Ustaömer and Robertson 1997; Okay and Şahintürk 1997). One model considers that ophiolite emplacement in the Pontides occurred in relation to northward subduction of Palaeotethys beneath the tectonically and magmatically active Laurasian margin during Late Palaeozoic-Early Mesozoic time (Adamia et al. 1977; Robertson and Dixon 1984; Dercourt et al. 1986, 1993), i.e. an active margin, or Cordilleran-type setting. In this model the Laurasian margin experienced terrane displacement, subduction-accretion, backarc basin formation and arc genesis comparable to the

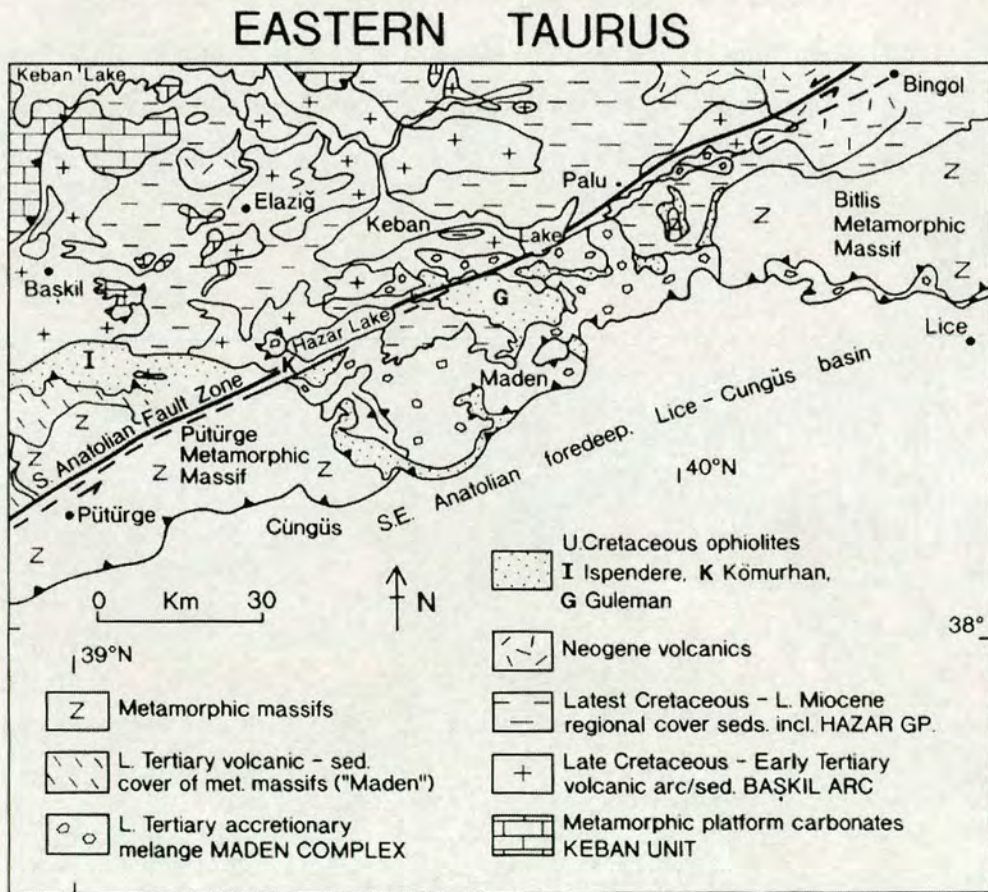


Figure 1.7. Sketch map showing the setting of Upper Cretaceous ophiolites in SE Turkey (after Robertson 2002).

southwest Pacific region (Ustaömer and Robertson 1997). The dismembered ophiolites (e.g. Küre Complex) were interpreted as forming in a backarc basin, which closed by Mid-Jurassic time. Other Upper Palaeozoic-Early Mesozoic igneous units, located slightly further south were interpreted as an emplaced volcanic arc (Çangaldağ unit) and accreted seamounts (Figures 1.8 and 1.10; Ustaömer 1993; Ustaömer and Robertson 1997, 1999). The model for their emplacement involved localised collisions of small continental fragments (e.g. Kargı Complex) with the subduction trench in the Early Triassic. In this model, with continued convergence the backarc basin began to close by north-directed thrusting which emplaced arc and backarc units onto the Laurasian margin as an accretionary prism related to southward subduction of the Küre marginal basin during the Late Jurassic (Ustaömer and Robertson 1997). The emplacement process was associated with a reversal of subduction polarity (*ibid.*). In this model closure of the Küre marginal basin by accretion of the arc and the continental fragment (Kargı Complex) to the Laurasian margin occurred during the Cimmerian orogenic event (Ustaömer and Robertson 1997).

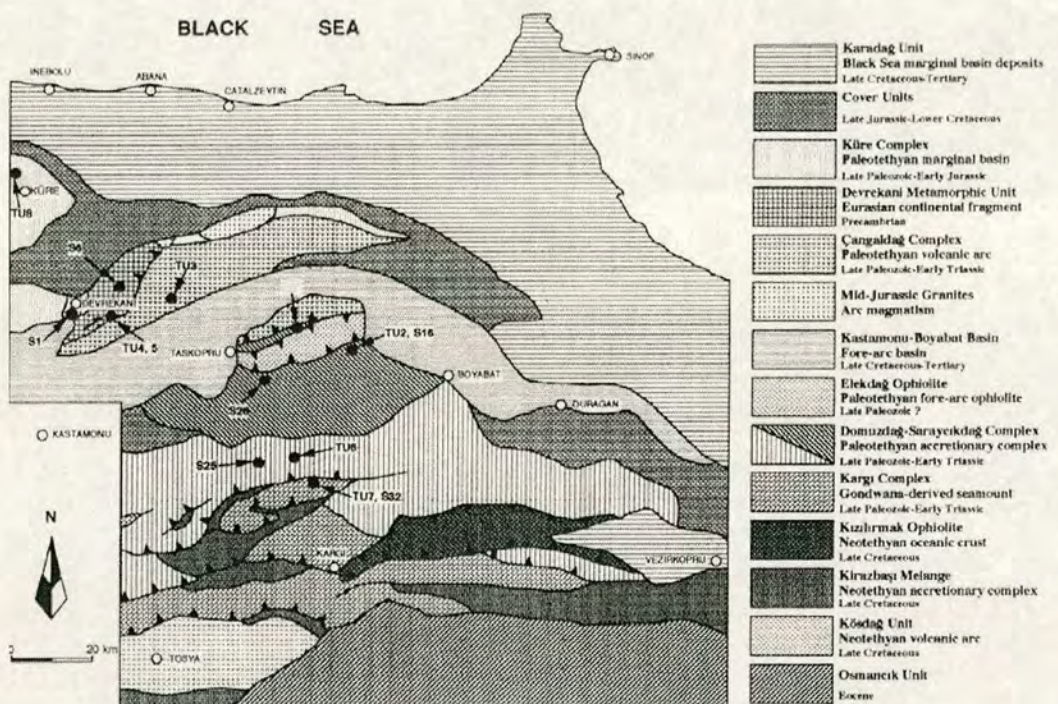


Figure 1.8. Simplified geological map of the northern Central Pontides, showing the main tectonic units (modified after Tüysüz 1990; Ustaömer and Robertson 1997).

By contrast, another model envisaged that the pre-Jurassic north Tethyan margin was a south-facing passive margin (Dewey et al. 1973; Şengör et al. 1980; 1984). In this model (Figure 1.9) Palaeotethys was subducted southward beneath the active southern (Gondwanan) Tethyan margin. An elongate microcontinent rifted away from the Gondwanan active margin and moved northwards with the trench, completely consuming Palaeotethys and eventually colliding with the northern passive margin in the Late Jurassic during the Cimmerian orogeny (Şengör et al. 1984). The root-zone of these ophiolites was a Palaeotethyan suture located in the Pontides north of the Izmir-Ankara-Erzincan Suture Zone and north of the Cimmerian continent. In this model the Cimmerian orogeny was a result of continent-continent collision and ophiolites were emplaced northward over a passive north Tethyan (Laurasian) margin in the same fashion as Oman.

In addition, the Upper Cretaceous ophiolites of the Pontides, and associated units, were emplaced onto the northern margin of Neotethys and are the main subject of this thesis, as outlined further below.

1.4 Geological background

It is first necessary to summarise what has been established from previous research in the Pontides.

The Pontides are a mountain range along the Black Sea coast of Turkey reaching altitudes of >3000 m in the east (Figures 1.1 and 1.2). During the Mesozoic the Pontides formed part of the Eurasian continental margin (Şengör and Yılmaz 1981; Robertson and Dixon 1984). The Upper Cretaceous Izmir-Ankara-Erzincan Suture Zone is located along the southern edge of the Pontides and separates Gondwana-derived (i.e. Tauride-Anatolide) blocks to the south from basement of Eurasian origin in the Pontides to the north (Figures 1.1 and 1.2; Bergougnan 1975; Şengör and Yılmaz 1981). The suture zone records the closure history of a northerly

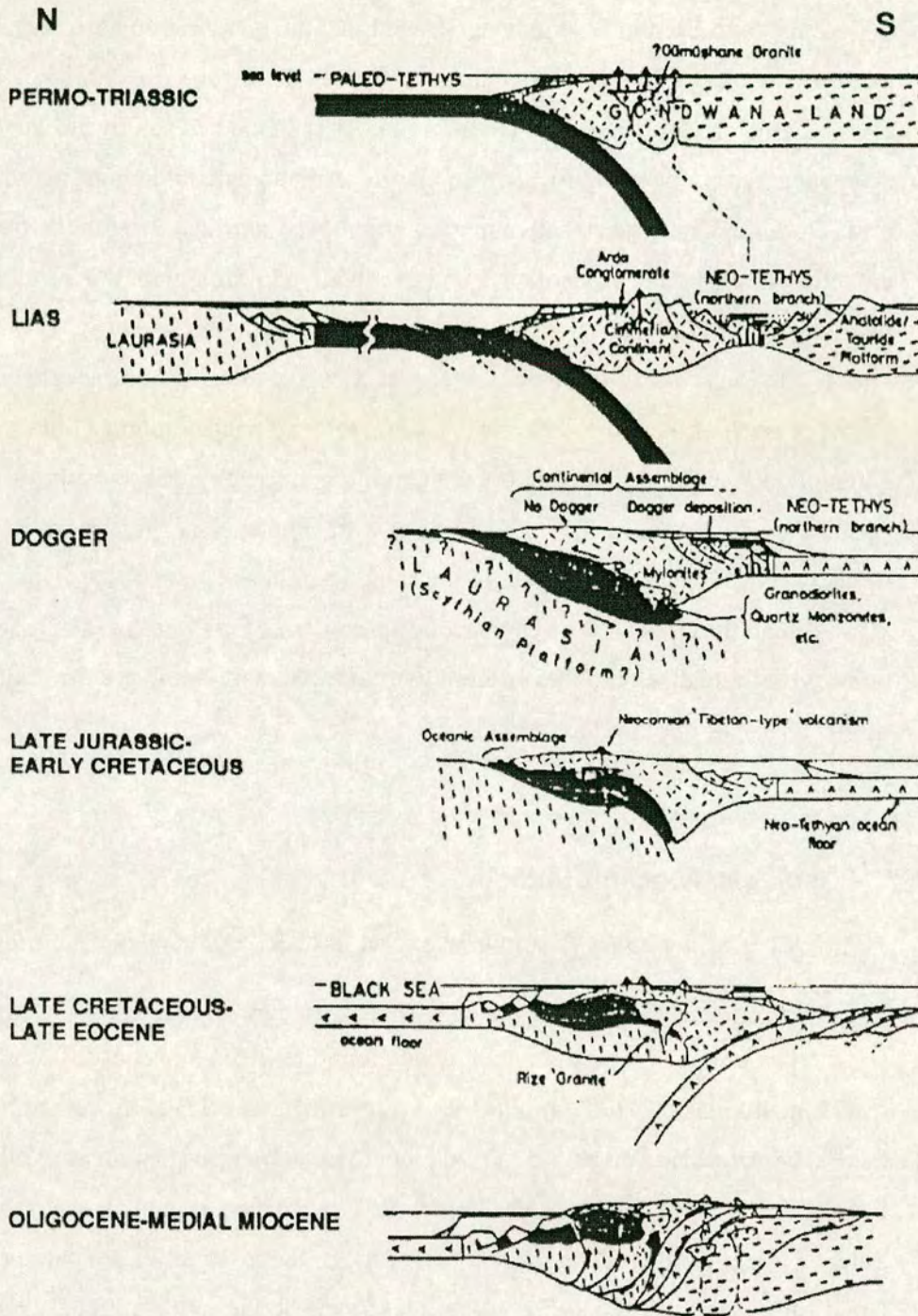


Figure 1.9. Model for the tectonic evolution of the north Tethyan margin after Şengör et al. (1980).

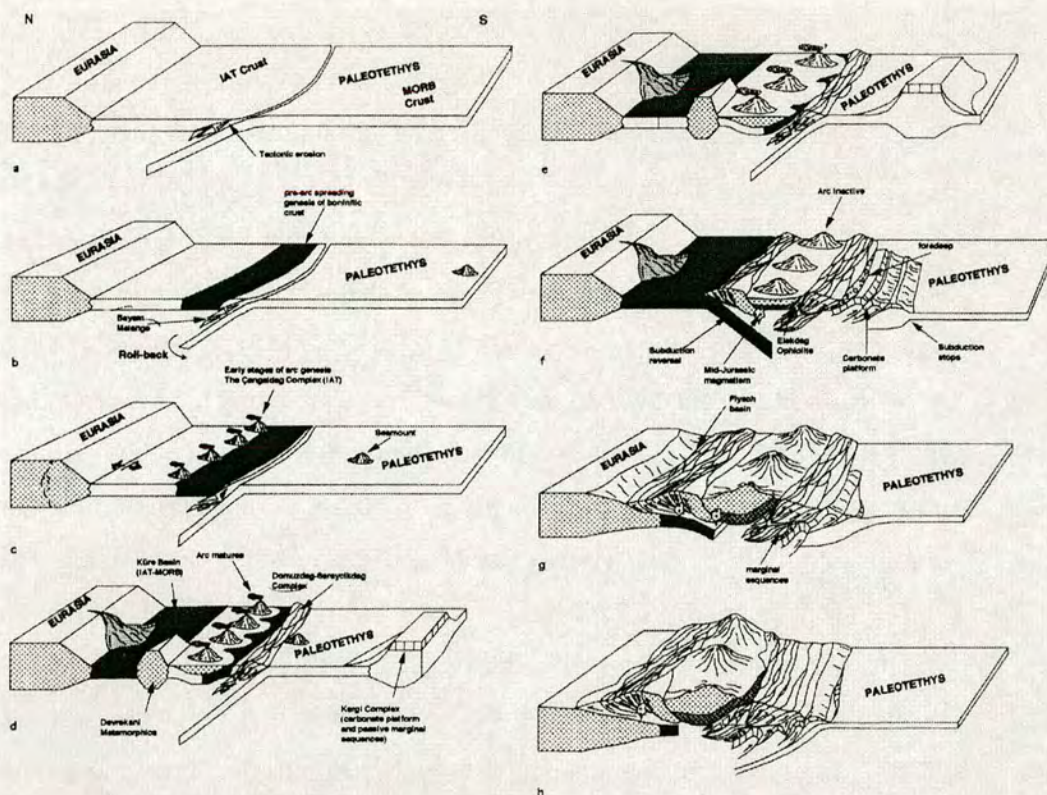


Figure 1.10. Sequential block-diagrams (a-h) showing the pre-Late Jurassic tectonic evolution of the Eurasian margin in the Central Pontides (after Ustaömer and Robertson 1997).

strand of the Tethys ocean (Northern Neotethys; Şengör and Yılmaz 1981; Robertson and Dixon 1984; Dercourt et al. 1986; Okay et al. 2001). This suture zone is well exposed as a dominantly south-vergent thrust belt, ~40 km wide, of mainly ophiolitic rocks and mélangé running across northern Anatolia (Yılmaz et al. 1997; Okay 1999). In the north of the suture zone, Upper Cretaceous units of the Izmir-Ankara-Erzincan Suture Zone are tectonically imbricated with Eurasian metamorphic basement rocks (i.e. Karakaya Complex and related units), whereas in the south these same units structurally overlie the southern margin of the Northern Neotethys, represented by the Tauride-Anatolide Platform (i.e. the Munzur Platform in the Eastern Pontides and the Kırşehir Massif in Central Anatolia; Figures, 1.1 and 1.2; Bergougnan 1975; Yılmaz 1985; Koçyiğit 1990; Tüysüz 1988, 1990).

1.4.1 The Pontides

The Pontides are traditionally divided into three major tectonic zones (Figure 1.11). The Sakarya zone (present study), the Istanbul-Zonguldak zone and, the Strandja zone (Şengor and Yilmaz 1981; Okay and Şahintürk 1997; Topuz et. al. 2004). The Sakarya zone borders the Izmir-Ankara-Erzincan Suture Zone along the southern part of the Pontides (Figure 1.11). Three types of metamorphic basement have been distinguished within the Sakarya zone (predating the Mesozoic units studied in this thesis): (1) High-T, low- to medium-P units of Carboniferous age intruded by granitoids, (2) low-T medium- to high-P Permo-Triassic rocks, and (3) non-metamorphic Carboniferous-Permian age sedimentary rocks (Topuz et. al. 2004). The Carboniferous high temperature low-medium pressure units comprise schists, gneisses, migmatites, amphibolites and marbles and crop out in both the Western and Eastern Pontides (Okay and Şahintürk 1997; Yilmaz et. al. 1997; Topuz et. al. 2004). Geochronological data from the granitoids that intrude these rocks yield a wide variety of ages and need to be considered with caution because of the lack of complete Sr homogenisation during granitoid genesis and the ubiquitous presence of inherited zircon domains (Topuz et. al. 2004). However, Late Carboniferous ages have been published for the high temperature low- to medium pressure metamorphic event (Topuz et. al. 2004). Low temperature-medium pressure and low temperature high pressure metamorphic rocks occur in several areas in the Western, Central and Eastern parts of the Sakarya zone (Topuz et al. 2004). These include the Karakaya Complex, which represents a tectonic *mélange* comprising slices of greenschists, phyllites, marbles (Nilüfer unit), LT-HP eclogites and blueschists, pelagic sedimentary rocks (e.g. Triassic radiolarites), Permian limestone blocks and mafic volcanics (Pickett and Robertson 1995, 2005; Yilmaz et. al. 1997; Okay and Şahintürk 1997). Blueschists and eclogites from this unit have yielded $^{40}\text{Ar}/^{39}\text{Ar}$ mica ages of 215-203 Ma (Okay and Monié 1997). This *mélange* is interpreted as a Triassic subduction-accretion complex related to northward subduction of Palaeotethys (e.g. Pickett and Robertson 1996) and is overlain transgressively by Liassic volcanic and sedimentary rocks (Rojay 1995; Robinson 1995; Yilmaz et al. 1997; Okay and Şahintürk 1997).

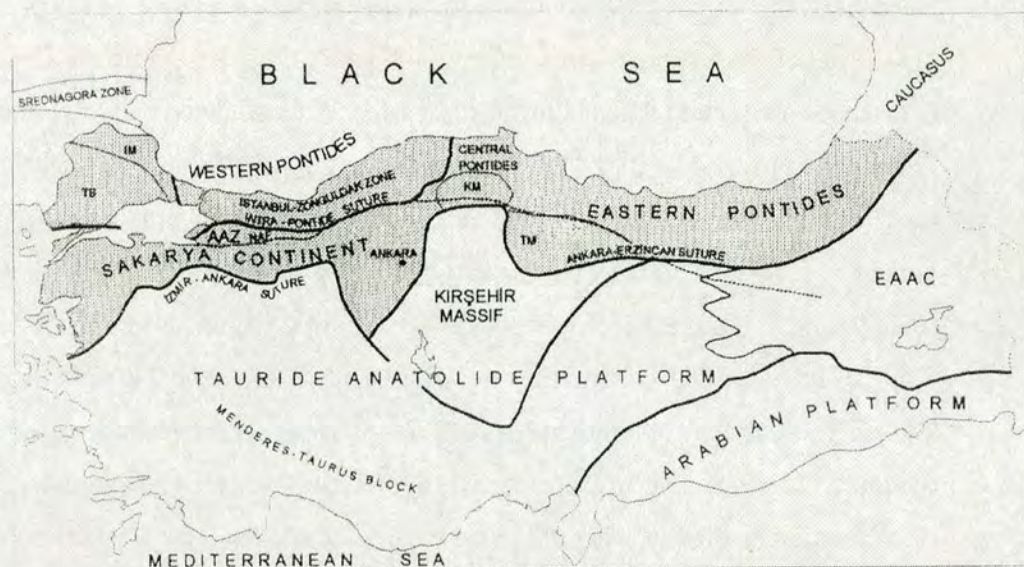


Figure 1.11. Outline map of Turkey showing main tectonic subdivisions of the Pontides (shaded grey) after Okay and Şahintürk (1997). IM = Istranca Massif, TB = Thrace Basin, AAZ = Armutlu-Almacık Zone, KM = Kargı Massif, NAF = North Anatolian Fault Zone, EEAC = eastern Anatolian accretionary complex.

The overlying Upper Jurassic-Lower Cretaceous succession begins with fluvial clastic sedimentary rocks and passes upwards into shallow marine platform carbonate rocks which record the development of an inferred south-facing passive margin in Early Jurassic-Early Cretaceous times (Şengör and Yılmaz 1981; Tüysüz 1990; Yılmaz et al. 1997; Ustaömer and Robertson 1997). In the Central Pontides the succession passes upwards into Upper Cretaceous deep-water volcanoclastic sedimentary rocks belonging to the Kastamonu-Boyabat Basin and the Karadağ Unit (Figure 1.8), which were deposited within extensional half-grabens (Ustaömer and Robertson 1997). No source for the volcanoclastic material is exposed in the Central Pontides and it is likely that the sedimentary rocks were derived from the Upper Cretaceous magmatic arc located to the southeast of Sinop in the Eastern Pontides (Figures 1.8 and 1.11; Ustaömer and Robertson 1997). The lack of Upper Cretaceous arc-related volcanic and plutonic rocks seen in the Central Pontides could indicate a ‘volcanic gap’ along the Eurasian active margin, possibly caused by oblique

subduction of the Neotethyan lithosphere beneath a geometrically irregular Eurasian margin (Ustaömer and Robertson 1997; see discussion chapter 6).

In contrast, the northern zone of the Eastern Pontides exhibits a thick Late Cretaceous arc related volcanoclastic succession and associated calc-alkaline granitic plutons (Şengör and Yılmaz 1981; Robinson et al. 1995; Yılmaz et al. 1997). The Eastern Pontide magmatic arc is generally interpreted as a continental margin volcanic arc formed above a northward subducting slab of Neotethyan lithosphere (Şengör and Yılmaz 1981; Robertson 2004). Granitic plutons from the Eastern Pontides have yielded radiometric ages of 89.3-65.5 Ma (Senonian) and associated volcanoclastic rocks are interbedded with fossiliferous sedimentary rocks of Santonian-Coniacian age (Yılmaz et al. 2003; Taner 1977). In an alternative interpretation Neotethys was subducted southwards beneath the Eastern Pontides (Bektaş 1999). Further south, near Erzincan (Figures 1.2 and 2.2), the metamorphic basement of the Pontides comprises the Pular Complex, interpreted as a Palaeotethyan accretionary complex associated with the continuous subduction of Tethys from Permian to Late Triassic (Topuz et al. 2004). The Pular Complex is transgressively overlain by Liassic conglomerates (Figure 1.12). The units discussed in this thesis belong to the southerly Sakarya Zone in the Central and Eastern Pontides.

1.4.2 The Tauride-Anatolide Platform (Kirşehir Block and Munzur Platform)

The Tauride-Anatolide Platform is located south of the Izmir-Ankara-Erzincan Suture Zone and represents the southern margin of Neotethys (Figure 1.2; Bergougnan 1975; Şengör and Yılmaz 1981; Okay 1999). In contrast to the Pontides the Tauride-Anatolide Platform shows a similar Palaeozoic stratigraphy to the Arabian Platform and Gondwana (Dercourt et al. 1986). The Tauride-Anatolide Platform forms a post-Palaeocene south-vergent thrust stack (Okay 1999). In the Eastern Pontides, immediately south of the suture zone in the area studied here, the Munzur Mountains (the northeasterly extension of the Tauride belt) expose a

continuous succession of algal, stromatolitic and rudistic neritic limestones of Late Triassic–Late Cretaceous age (Munzur Dağı Formation; Figure 1.13; Özgül and

Aşutka area

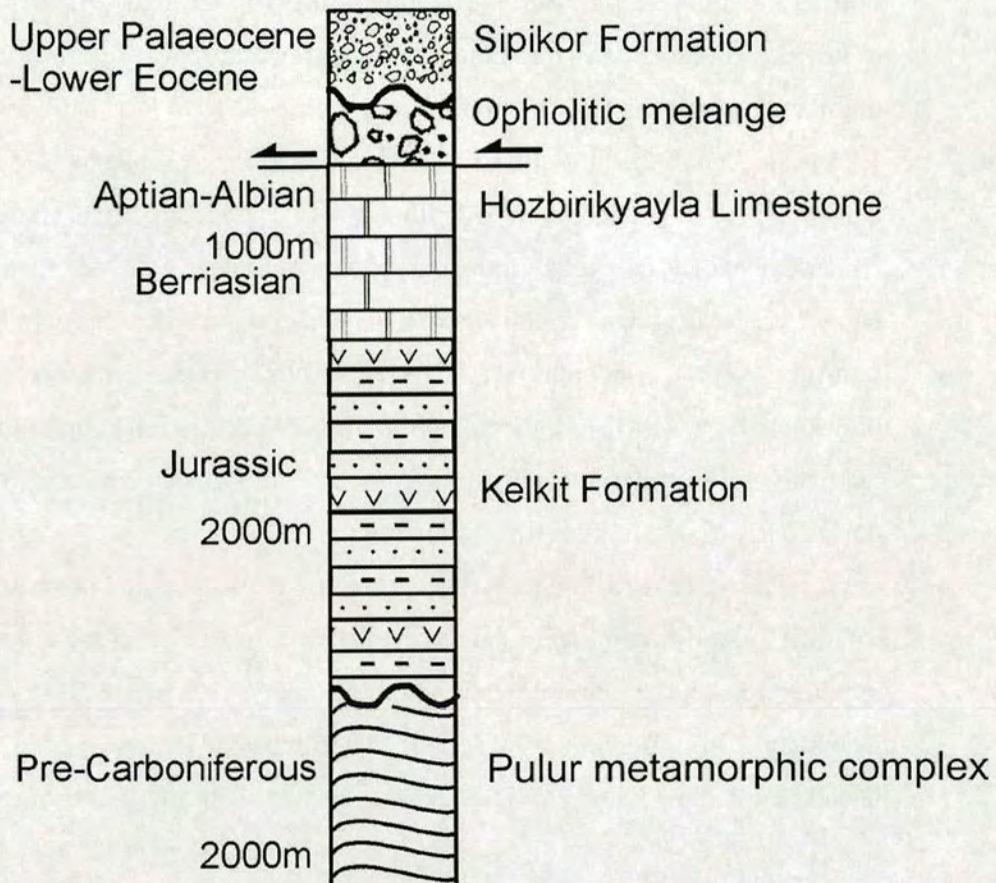


Figure 1.12. Tectonostratigraphy of the Pontides near Erzincan (after Okay and Şahintürk 1997).

Tuşucu 1984). The Upper Triassic–Upper Cretaceous succession of the Taurides and the Munzur Mountains is interpreted as a stable carbonate platform and is underlain by a schistose metamorphic basement (Yoncayolu Formation; Özgül and Turşucu 1984). The top of the succession exhibits a transition to deep-water facies of Turonian–Maastrichtian age and is tectonically overlain by ophiolites and ophiolitic mélangé emplaced from the north. The platform subsided ahead of the advancing

ophiolitic nappes during Late Campanian-Early Maastrichtian times (Kurtman 1961; Özgül and Turşucu 1984).

In Central Anatolia the south-Tethyan margin is represented by the Kirşehir/Niğde massifs (or Central Anatolian Crystalline Complex; Figures 1.2 and 1.11; Şengör and Yılmaz 1981). These massifs comprise high-temperature/medium- to low-pressure greenschist to granulite facies metamorphic rocks including gneiss, migmatite, mica schist and metaquartzite (Seymen 1981; Floyd et al. 1998; Okay 1999). The age of metamorphism is constrained as Late Cretaceous (75-80 Ma; Göncüoğlu 1986; Whitney and Hamilton 2004). The metamorphic rocks are cut by Upper Cretaceous calc-alkali monzogranites (Rb-Sr age 71 ± 1 Ma; Ataman 1972; Okay 1999). Maastrichtian-Palaeocene shallow-marine sedimentary rocks transgressively overlie both the metamorphic rocks and the dismembered ophiolite (Görür et al. 1984). Dismembered ophiolites (Central Anatolian ophiolite complex) were therefore emplaced southwards from the Izmir-Ankara-Erzincan Suture Zone during Maastrichtian time (Robertson 2002).

The Kirşehir/Niğde massifs may represent a continental promontory of the Tauride/Anatolide continent (Yalnız et al. 1996). In an alternative model the massifs are interpreted as a microcontinent within Neotethys (Yılmaz et al. 1997; Clark and Robertson 2002). A southerly Neotethyan ocean basin (Inner-Tauride Ocean) could have separated the Kirşehir/Niğde massifs from the Taurides (Andrew and Robertson 2002).

1.4.3 The Izmir-Ankara-Erzincan Suture Zone

The Izmir-Ankara-Erzincan Suture Zone, the subject of this thesis, forms a south-vergent imbricate thrust stack which separates Gondwana-derived blocks from Eurasian continental basement of the Pontides (Bergougnan 1975; Robertson and Dixon 1984; Tüysüz 1990; Koçyiğit 1991; Yılmaz et al. 1997). Upper Cretaceous units within the suture zone exhibit thrust faults, folds and pervasive shear fabrics that locally indicate a north-vergent deformational episode (Bergougnan 1975; Rojay 1995; Ustaömer and Robertson 1997). However, confusion persists as to the relative timing and cause of this north-vergent deformational event. In the Central Pontides

Upper Cretaceous rocks of the suture zone are thrust southward and eastward over Tertiary units (e.g. Çankırı Basin; Figure 1.14; Tüysüz 1995). Palaeozoic and Lower Mesozoic metamorphic rocks of the Pontides are in turn thrust southwards over the Upper Cretaceous Izmir-Ankara-Erzincan Suture Zone (Yılmaz et al. 1997). Thus, in general older rocks are exposed at structurally higher levels across the suture zone from south to north. In the Eastern Pontides the Upper Cretaceous Izmir-Ankara-Erzincan Suture Zone is thrust southward over the Tertiary sedimentary and volcanic fill of the Sivas Basin and, are also thrust directly over the Triassic-Cretaceous Munzur Dağı Formation of the Tauride Anatolide Platform (Bergougnan 1975; Özgül and Turşucu 1984).

Early studies did not attempt to distinguish individual units within the Izmir-Ankara-Erzincan Suture Zone (e.g. Bergougnan 1975). Yılmaz et al. (1997) described the suture zone as an ophiolite belt consisting of an ophiolitic association and a *mélange* association in thrust contact with the metamorphic basement rocks of the Pontides. The *mélange* was described as being composed mainly of blocks of red micritic limestones, black shales, ophiolitic fragments and metamorphic rocks, exposed as a series of north-dipping thrust slices (Yılmaz et al. 1997). In the Central Pontides outcrops of *mélange* exhibit a distinctive sedimentary succession above their unconformable southern contacts, while the northern contacts are south-vergent thrust faults (Ustaömer and Robertson 1997). The base of the *mélange* in the Central Pontides exhibits an internally ordered succession of pelagic limestone and shale containing pelagic *Globo truncana* microfossils that indicate a Campanian age (Yılmaz and Tüysüz 1984; Tüysüz et al. 1988; see chapter 5). In each thrust slice the pelagic and ophiolitic blocks increase in abundance towards the top (Yılmaz et al. 1997). The amount of pelagic and ophiolitic material and the thickness of the slices of *mélange* increase toward the south suggesting that *mélange* accretion began in a pelagic environment to the south and advanced northward toward the Eurasian continental margin (Yılmaz et al. 1997). Tüysüz et al.

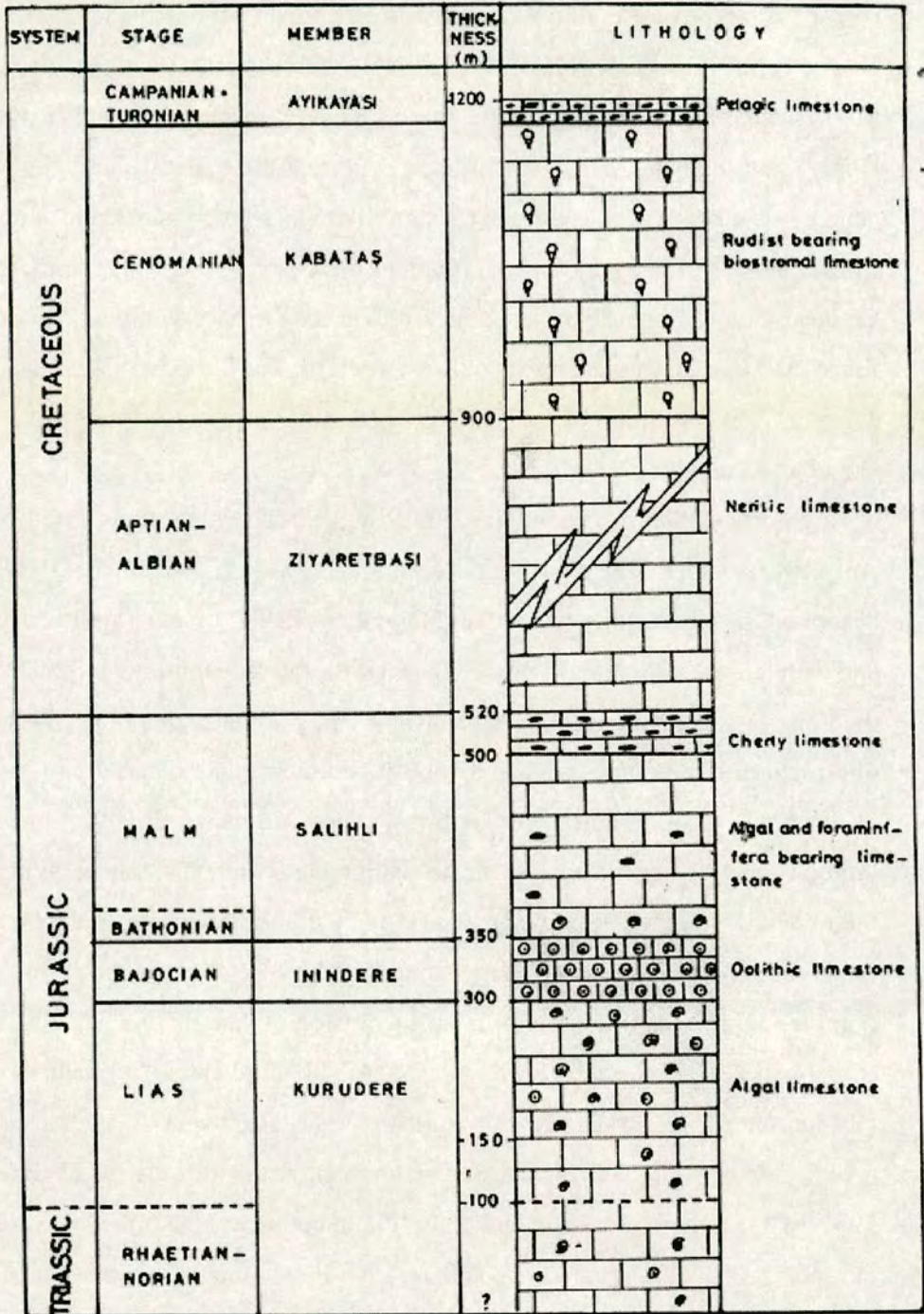


Figure 1.13. Tectonostratigraphy of the the Tauride platform (Munzur Mountains) in the Eastern Pontides after Özgül and Turşucu (1984).

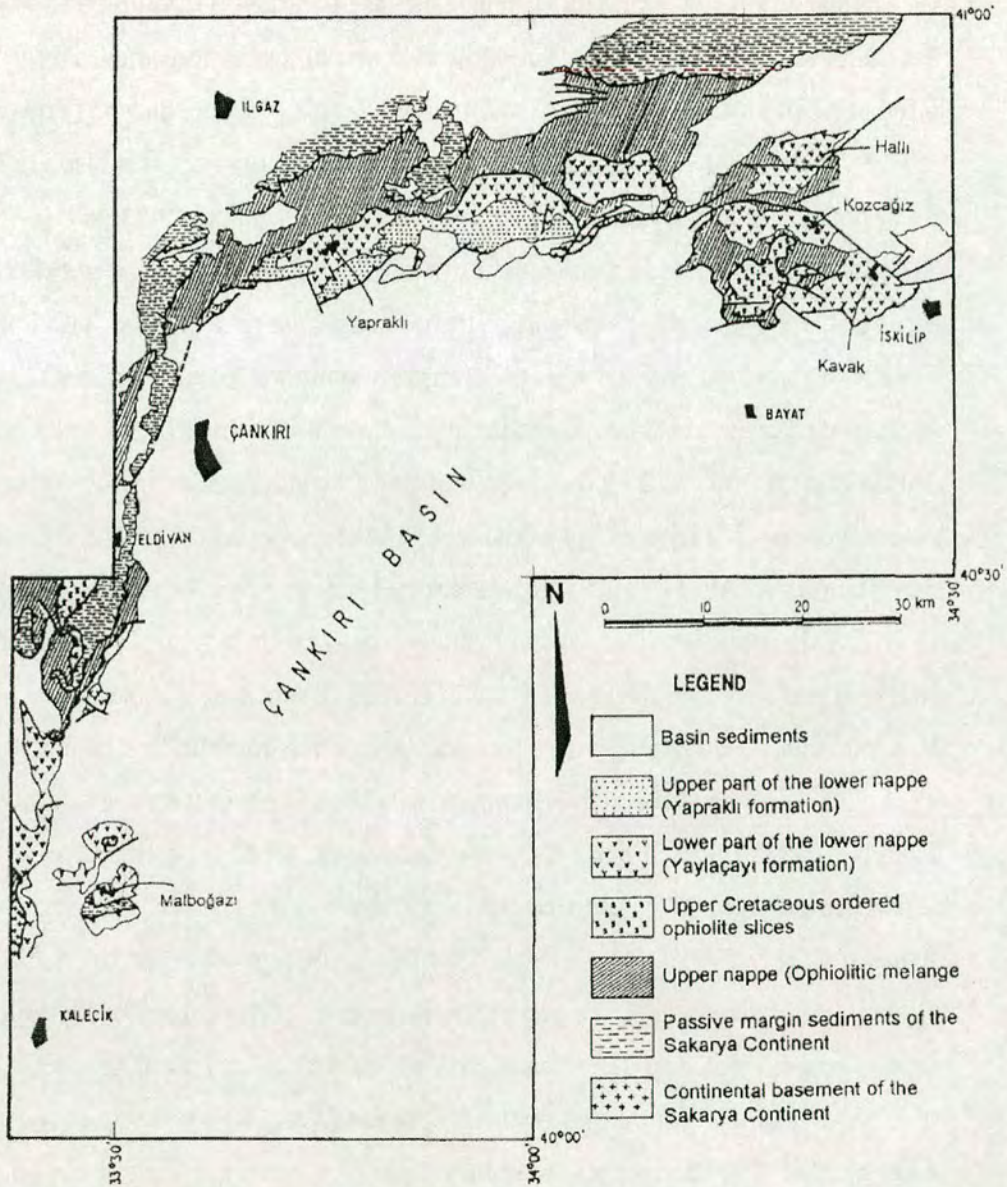


Figure 1.14. Geological map showing the internal structure of the İzmir-Ankara-Erzincan Suture Zone around the Çankırı Basin (after Tüysüz 1995).

(1995) postulated the existence of two separate mélangé belts that formed along two different subduction zones. This idea is supported by the interpretation of various units identified within the suture zone which are described below (i.e. oceanic volcanic arc (Tüysüz 1995), forearc basins (Koçyiğit 1988, 1991; Rojay 1995).

A volcanic unit (Yaylaçayı Formation) was identified within the suture zone in the Central Pontides (Yoldaş 1982) and was interpreted as an intraoceanic volcanic arc (Tüysüz et al. 1995). This was based on the observation of an ophiolitic basement to the volcanic succession, the absence of terrigenous material the intercalation of pelagic limestone and the geochemistry of the basalts (Tüysüz et al. 1995). Another volcanic unit identified in the Central Pontides was also interpreted as an oceanic volcanic arc and this is located further to the north (Köşdağ arc; Tüysüz 1990). Yet another volcanic arc was inferred on the basis of geochemical data for the Upper Cretaceous part of the Galatean Volcanic Province (isotopic age = 76 ± 2.4 Ma) located northwest of the suture zone in the Central Pontides (Koçyiğit et al. 2003). In contrast to the allochthonous arc units within the Izmir-Ankara-Erzincan Suture Zone, these rocks also crop-out north of the suture zone and are relatively autochthonous. No Upper Cretaceous volcanic arc is present upon the continental margin in the Central Pontides further north (Ustaömer and Robertson 1997).

A thick succession of distal turbidites of Late Cretaceous-Mid Eocene age was recognised within the suture zone in central Anatolia near Ankara (Haymana Basin; Ünalın 1976), lying unconformably above the ophiolitic *mélange* (Koçyiğit 1988). The Haymana Basin is interpreted as a forearc basin (Görür et al. 1984; Koçyiğit 1988, 1991). Thick sedimentary successions of Mid-Campanian to Maastrichtian age were identified within the suture zone further west near Tokat and Amasya (Rojay 1995). These successions lie unconformably upon the *mélange*, contain both volcaniclastic and terrigenous material and are therefore interpreted as forearc basins related to the volcanic arc, which was contemporaneously built upon the Pontide continental margin further to the northeast (Rojay 1995). However, as mentioned above, continental arc units are not exposed in the Central Pontides, which complicates the simple forearc basin model.

In the Eastern Pontides the northern part of the suture zone contains an extensive ophiolitic thrust sheet, composed dominantly of peridotite (serpentinised harzburgite; Bergougnan 1975; Yilmaz 1985). The ophiolite was named the Refahiye Complex by Yilmaz (1985). No age data are published for the ophiolite in the Eastern Pontides. Bergougnan described screens of metamorphic host rock within the intrusive diabase dyke complex of the Refahiye Complex near Erzincan. In the

Central Pontides smaller, discontinuous outcrops of ophiolite slices (~10 km long) are imbricated with other Upper Cretaceous units of the suture zone and older basement rocks of the Pontides (Yılmaz et al. 1997). A Campanian-Maastrichtian age for the ophiolite in the central Pontides is inferred from associated *Globo truncana*-bearing sedimentary rocks (Tüysüz 1990).

No volcanic arc units have previously been described from within the suture zone in the Eastern Pontides. The tectonic setting of the Eastern Pontide units has been determined for the first time during this study.

1.4.4 Cover rocks

In the Eastern Pontides a varied Palaeocene-Early Eocene sedimentary succession that includes Nummulitic and rudist limestones, sandstones and conglomerates unconformably overlies the Upper Cretaceous *mélange* and ophiolitic units of the Izmir-Ankara-Erzincan Suture Zone (Sipikör Formation; Bergougnan 1975; Yılmaz 1985; Koçyiğit 1990; Aktimur et al. 1995; Okay and Şahintürk 1997). Tüysüz (1990) suggested that closure of Neotethys is constrained to pre-Lutetian (48.6-40.4 Ma) by the observation of a sedimentary and volcanic succession of Lutetian age that unconformably overlies all of the units within the suture zone in the Central Pontides.

The Upper Cretaceous units of the Izmir-Ankara-Erzincan Suture Zone are unconformably overlain by sedimentary rocks of Tertiary basins; i.e. the Çankırı Basin (Figure 1.14) and Galatean Volcanic Province in the Central Pontides and, the Sivas Basin in the Eastern Pontides (Erol 1954; Görür et al. 1984). Development of these basins has been related to the late-stages of closure of Neotethys (Erol 1954; Görür et al. 1984; Çiner et al 2002).

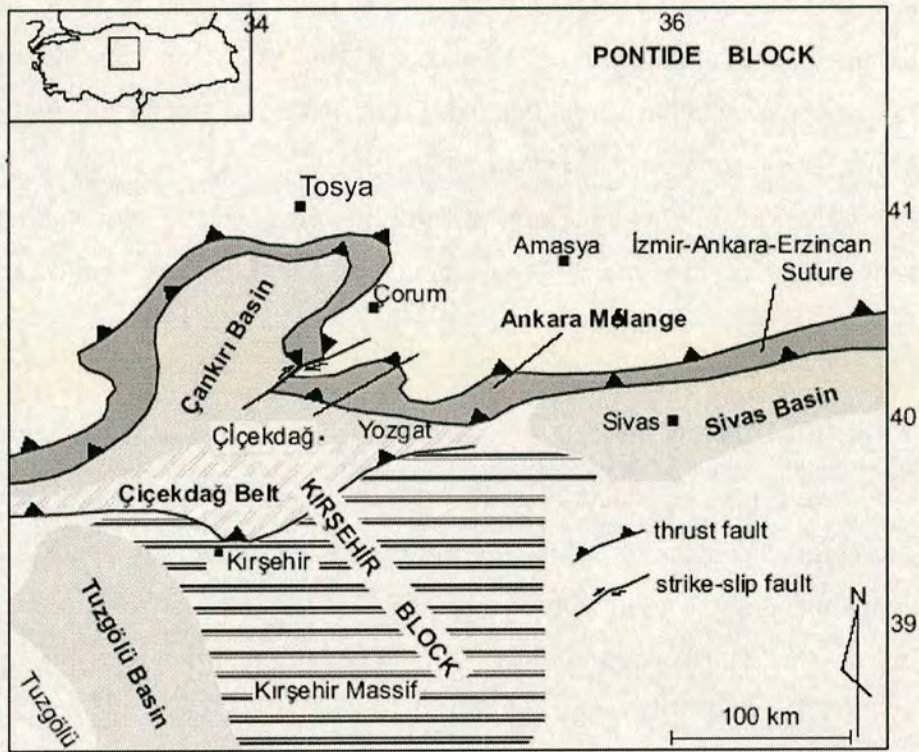


Figure 1.15. Map showing locations of the main Tertiary basins in Central Anatolia in relation to the Izmir-Ankara-Erzincan Suture Zone (modified after Tüysüz 1993).

1.5 Alternative models for Upper Cretaceous ophiolites in the Pontides

Several authors have recognised that ophiolites were emplaced in the Pontides during Late Cretaceous-Early Tertiary time and alternative tectonic scenarios have been proposed (Bergougnan 1975; Yılmaz 1985; Koçyiğit 1990; Tüysüz 1990; Okay and Şahintürk 1997; Yılmaz et al. 1997; Ustaömer and Robertson 1997). However, information on the age, structure and geochemistry of these units has remained sparse, necessitating the present study.

Early models for the tectonic development of the Eastern Pontides saw the ophiolites as slices of Neotethyan lithosphere that were scraped off from the subducting slab and accreted during Late Cretaceous-Palaeocene time (Bergougnan 1975; Yılmaz 1985). In these models Neotethys was consumed beneath the Eurasian margin by north-dipping subduction (Figure 1.16a). In addition, Bergougnan (1975)

recognised the importance of top-to-the-north thrusting of the ophiolite that occurred during Late Cretaceous time. This was explained by backthrusting of an associated accretionary complex during collision of the Taurides (Munzur Platform) with Eurasia (Pontides). This model would predict that the ophiolites were of mid-ocean ridge- (MOR) type.

North-dipping subduction beneath the Pontides is included in most models to account for thick calc-alkaline basaltic, andesitic and dacitic volcanic succession and associated large subduction-related granitic plutons of Late Cretaceous age that are located in the northern part of the Eastern Pontides (~100 km north of the Izmir-Ankara-Erzincan Suture Zone). However, as mentioned above in the Central Pontides (West of Sinop) there is no equivalent volcanic arc north of the suture zone. However, a volcanic arc unit of Late Cretaceous age was identified further south in the Central Pontides, within the suture zone (the Köşdağ arc; Tüysüz 1990). This unit was interpreted as an intraoceanic volcanic arc formed on an ophiolitic basement of Late Cretaceous (Campanian-Maastrichtian; 83.5-65.5 Ma) age. A model was proposed in which the Eurasian margin was an Atlantic-type passive margin until a magmatic arc developed during Turonian-Coniacian time (93.5-85.8 Ma) in response to northward subduction of Neotethys (Figure 1.16b; Şengör and Yilmaz 1981; Tüysüz 1990). Later, an intraoceanic magmatic arc developed further south, within Neotethys, during Campanian-Maastrichtian time (Tüysüz 1990, 1995). An accretionary complex grew and arc volcanism continued until the Late Maastrichtian when the intraoceanic arc, accretionary complex, and ophiolites were thrust-imbricated with the metamorphic basement of the Pontides (Tüysüz 1990, 1995). In this model, the northward emplacement of ophiolite and *mélange* occurred during Late Cretaceous-Early Palaeocene time due to backthrusting associated with growth of an accretionary prism (Tüysüz 1990, 1995). The deformed units are unconformably overlain by Mid Eocene (Lutetian; 48.6-40.4 Ma) limestones (Tüysüz 1990). In summary, this model involves two Late Cretaceous subduction zones; one formed adjacent to the Eurasian margin, and one further south within Neotethys above which a volcanic arc developed. The polarity of subduction beneath the intraoceanic arc was not included in the early model (Figure 1.16b). A later model suggested two contemporaneous north-dipping subduction zones. Emplacement

occurred during Late Cretaceous-Palaeocene time due to backthrusting (Tüysüz 1995).

In another model north-dipping subduction of Neotethys beneath the Eurasian margin was initiated during the Cenomanian-Campanian interval (93.5-83.5; Rojay 1995; Robinson 1995) and a thick forearc succession (identified in the Tokat and Haymana areas overlying the North Anatolian Ophiolitic Mélange) developed upon the accretionary complex adjacent to the continental margin (Koçyiğit 1991; Rojay 1995, 2001; Koçyiğit et al. 2003). In this model a single volcanic arc developed on the continental margin and there was only one north-dipping subduction zone (Figure 1.16a), ophiolitic mélangé was emplaced then southward over the southern Tethyan margin (Kırşehir Block) during collision in Eocene-Late Miocene times (55.8-5.33 Ma; Koçyiğit 1991; Rojay 1995, 2001; Koçyiğit et al. 2003). Northward emplacement was related to backthrusting which, in this model, occurred *later* than Lutetian time (40.4 Ma; Rojay 1995).

Okay and Şahintürk (1997) also recognised northwards emplacement of ophiolites had occurred in the Pontides and placed this deformational event in the Cenomanian (99.6-93.5 Ma). In Okay and Şahintürk's model Neotethys was subducted *southwards* at an intraoceanic subduction zone initiated during the Early Cretaceous (Figure 1.16c; Neocomian; 145.5-130 Ma). During this time the Pontides were part of an Atlantic-type passive margin (Şengör and Yılmaz 1981). Collision of the trench with that passive margin in Cenomanian time led to the northward emplacement of the ophiolites (Okay and Şahintürk 1997) in essentially the same way as the Semail ophiolite was emplaced in Oman (Figure 1.4). This was immediately followed by a reversal of subduction direction and the Pontides became magmatically active during the Late Cretaceous (Figure 1.16; Senonian; 89.3-65.5 Ma) as evidenced by isotopic ages of granitic plutons in the north of the Pontides (Okay and Şahintürk 1997). In this model the Late Cretaceous (Neotethyan) ophiolites in the Pontides are of 'Tethyan' type (1.3.1).

Bektaş (1999) proposed a model for the Eastern Pontides in which arc volcanism migrated southwards above a south-dipping subduction zone during the Late Cretaceous (Senonian; 89.3-65.5 Ma). In this model, the Pontides represent the

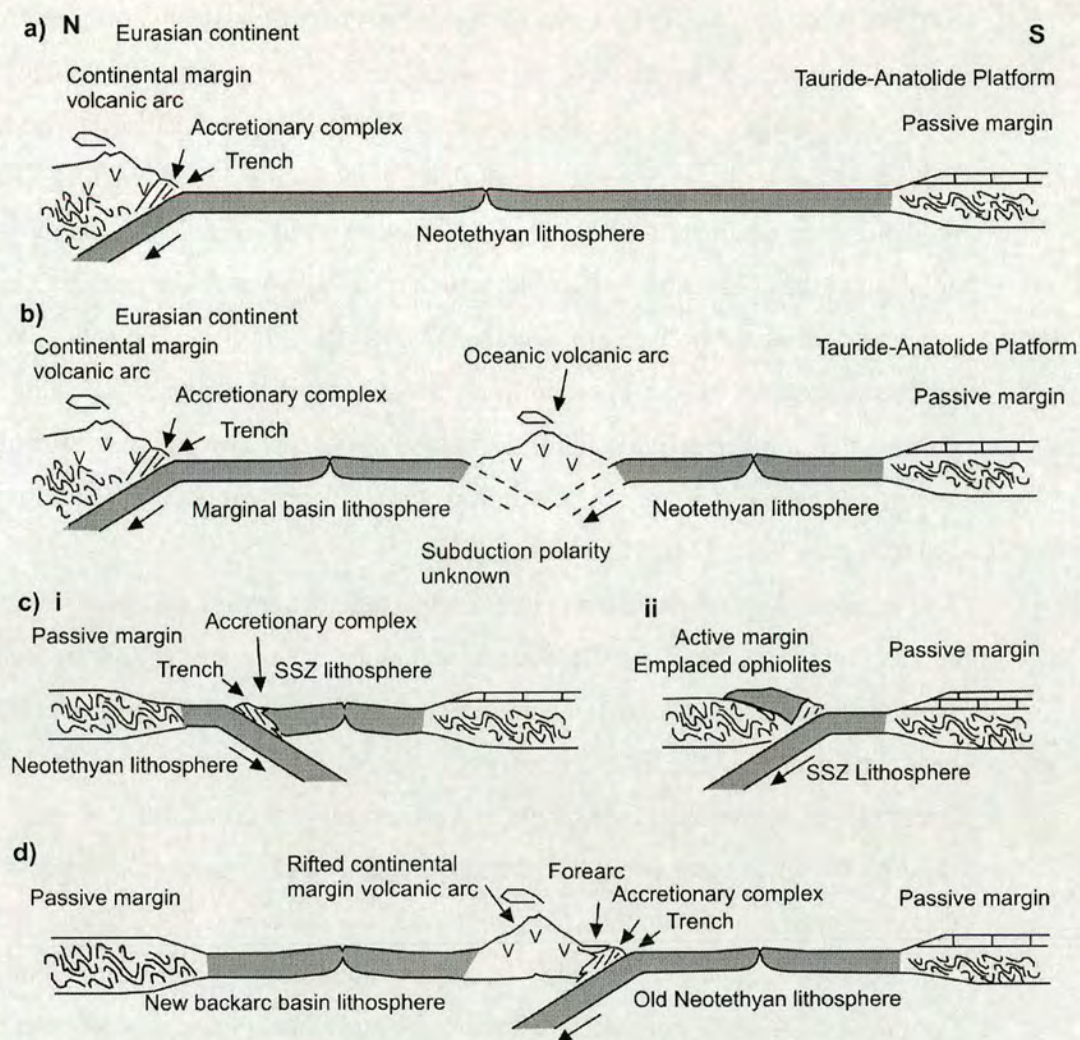


Figure 1.16. Previous tectonic models for the Late Cretaceous-Early Tertiary tectonic assembly of the suture zone in the Pontides; a) single northward-dipping subduction zone (Şengör and Yılmaz 1981); b) two northward-dipping subduction zones (polarity of oceanic arc not specified (Tüysüz 1990)); c) southward-dipping subduction zone, followed by reversal of subduction direction (Okay and Şahintürk 1997); d) single northward-dipping subduction zone with genesis and emplacement of a marginal basin (timing not specified (Ustaömer and Robertson 1997)). See text for discussion.

northern active margin of Gondwana which migrated northwards and the SSZ ophiolites of the Pontides were formed in the backarc region (Bektaş 1999).

Koçyiğit et al. (2003) suggested southward migration of the volcanic arc in the Central Pontides based on geochemical evidence that supports a backarc setting

for the Campanian Saraçköy Volcanic Suite (part of the Galatean Volcanic Province located northwest of the main suture zone in the Central Pontides and which yields a K-Ar isotopic age 76 ± 2.4 Ma; Koçyiğit et al. 2003). The chemical composition of these trachyandesites is consistent with slab rollback (Koçyiğit et al. 2003). This model favours northward subduction of Neotethys along a single subduction zone adjacent to the continental margin but which retreated southwards during Campanian time creating a backarc basin (Koçyiğit 1991; Rojay 1995; Koçyiğit et al. 2003). Collision occurred in post-Lutetian time (<40.4 Ma). This model explains the northwards emplacement of ophiolites in the Pontides in terms of backthrusting of an overgrown accretionary prism. The northward emplacement occurred during post Lutetian time (<40.4 Ma; Rojay 1995).

Ustaömer and Robertson (1997) suggested that northward intraoceanic subduction during the Early Cretaceous led to the development of an intraoceanic volcanic arc (Kösdağ arc) in the central Pontides (Figure 1.16d). The marginal basin between the arc and the Eurasian margin to the north (Pontides) was formed either from trapped Neotethyan lithosphere or newly created suprasubduction zone lithosphere which closed southward beneath the arc during regional compression in Campanian-Maastrichtian time (83.5-65.5 Ma; Ustaömer and Robertson 1997). This compression resulted in the northward emplacement of ophiolites in the Central Pontides prior to collision with the Anatolides and final closure of Neotethys during the Eocene (Şengör and Yılmaz 1981; Ustaömer and Robertson 1997). This model suggests that emplacement of ophiolites was an accretionary orogenic process because it pre-dates continental collision.

In summary, uncertainty persists regarding the direction and timing of subduction of Neotethyan lithosphere, the origin and mechanism of emplacement of ophiolites in the Pontides, and the timing of the final closure of northern Neotethys. The various models described above indicate a variety of different possible settings of ophiolite genesis and means of emplacement including; ophiolites formed at a Neotethyan mid-oceanic spreading centre and emplaced by off-scraping, accretion or backthrusting of an over-steepened accretionary wedge (Bergougnan 1975; Yılmaz 1985, 1997); ophiolites formed in a forearc, backarc or embryonic arc setting emplaced by trench-margin collision (Okay and Şahintürk 1997; Koçyiğit 1990,

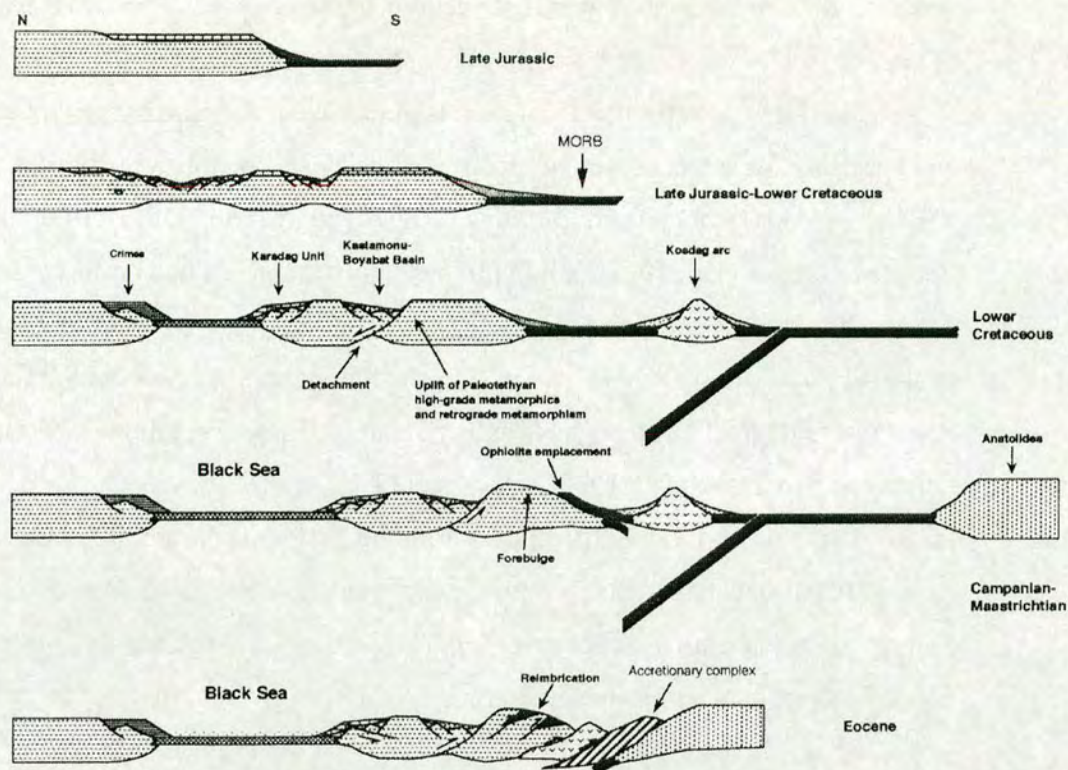


Figure 1.17. Sequential sections showing a model for post-Late Jurassic tectonic evolution of the Izmir-Ankara-Erzincan Suture Zone and emplacement of Upper Cretaceous ophiolites in the Pontides after Ustaömer and Robertson (1997). Note: ophiolite emplacement in this model was associated with southwards closure of the marginal basin during Campanian-Maastrichtian time, *before* the arrival of the Anatolides at the trench.

1991; Tüysüz 1990, 1995); ophiolites formed in forearc, backarc or embryonic arc settings emplaced during a subduction polarity reversal (Okay and Şahintürk 1997) or as parautochthonous 'cordilleran' ophiolites during a regional compression of the Eurasian active margin before collision occurred (Ustaömer and Robertson 1997). The models proposed include southward- (Bektaş 1999) or northward- (Rojay 1995) dipping subduction at a single trench and a continental margin volcanic arc; double subduction beneath a continental volcanic arc and an intraoceanic arc (Tüysüz 1990); subduction northwards beneath a single intraoceanic arc with no continental margin arc in the Central Pontides (Ustaömer and Robertson 1997); southwards intraoceanic

subduction followed by northwards subduction at the continental margin (Okay and Şahintürk 1997).

Published ages for the development of the accretionary mélangé (Karayaprak and Kirazbaşı Mélangé, commonly referred to as North Anatolian Ophiolitic Mélangé; NAOM) range from Carboniferous (Koçyiğit 1990; Yılmaz 1985) to Eocene (Aktimur et al. 1995). Timing of the emplacement-related north-vergent deformation in the Pontides ranges from Senonian (Okay and Şahintürk 1997) to post-Mid Eocene (Rojay 1995) in the published literature. Estimates of the timing of final closure of Neotethys ranges from Senonian (Okay and Şahintürk 1997) to Oligocene (Robinson et al. 1995; Koçyiğit et al. 1999).

This study provides critical data from the Eastern and Central Pontides in order to better understand the tectonic development of the Izmir-Ankara-Erzincan Suture Zone by testing the alternative models (section 6.3). The results of this study highlight the role of a volcanic arc during the early stages of collision.

Some of the key questions which this project therefore addresses are:

What was the tectonic setting of formation of the Neotethyan ophiolites in the Pontides?

What was the timing of the genesis and emplacement of ophiolitic and volcanic arc units?

How was ophiolite genesis and emplacement related to the volcanic arc?

What was the direction of subduction of Neotethys? How many subduction zones were involved?

When did northern Neotethys finally close?

Were ophiolites emplaced before or during collision and how were they emplaced (Cordilleran v. Tethyan type models)?

Was ophiolite emplacement in this case controlled by local or global factors?

1.6 Logistical aspects

Two areas of the Izmir-Ankara-Erzincan Suture Zone were studied in four fieldtrips during the course of this project. In the first fieldtrip, made during September 2001, the author met with the project supervisor (Prof. Alastair Robertson), Prof. Timur Ustaömer and field assistant Ozge Karşlıoğlu in Erzincan, northeastern Turkey. During this reconnaissance trip the stratigraphy and structure of the area were assessed and samples were collected for biostratigraphic and geochemical analysis. The weather was good and the trip was relatively problem-free. However, from the reconnaissance visit it did not at first appear that any volcanic arc unit was present within the Izmir-Ankara-Erzincan Suture Zone in the Eastern Pontides. Following presentation of the initial results to the school's postgraduate committee in April 2002 it was decided that a hypothesis-testing approach was needed. Therefore, the second fieldtrip, made in May 2002, was restricted to the Central Pontides area, where two volcanic arc units had been mapped previously (Tüysüz 1990, 1995). Our intention was to follow up the first-year's reconnaissance fieldtrip in the east by also re-visiting the Erzincan area in order to compare the two areas. The fieldwork in the Central Pontides did not go smoothly due to difficulties in obtaining satisfactory permission from national, military and local authorities to undertake research in the area. However, a substantial amount of data was collected from the Central Pontides in spring 2002 and a short visit was made to the Eastern Pontides in October of that year. Further data was needed, particularly from the Eastern Pontides and so a final trip was made in 2003 focusing on the Erzincan area.

1.6 Methods

This is a multidisciplinary study in which various types of data (e.g. structural, stratigraphic, geochemical, palaeontological, petrographic, sedimentological) are combined in order to establish the tectonic evolution of the areas using a 'tectonic facies' approach. A definition of tectonic facies is given by Robertson (1994) as:

"A tectonic facies constitutes the combined lithological and structural features that allow systematic recognition of past tectonic settings within an orogenic belt (e.g. an oceanic seamount)." (Robertson 1994).

Examples of tectonic facies are given in the following tables:

Tectonic facies	Characteristics	Examples
"Passive rifts"	Basin showing evidence of rifting, faulting and subsidence, followed by flexurally controlled uplift, then magmatism; typically rotated fault block geometry.	Rifting of Neotethys in Late Permian–Mid Triassic related to break-up of the northern margin of Gondwana prior to spreading from mid-Triassic onwards. Examples include Ionian and Pelagonian Zones, Greece; Antalya and Alanya units, southwestern Turkey. Development of early geanticlines, e.g. Helez, Levant and Hazro, southeastern Turkey suggest flexural uplift.
"Active rifts"	Basin showing evidence of thermally controlled uplift (mantle plume and/or more short-lived upwelling); typically marked by regional unconformity, then volcanism, followed by rift related faulting.	
Failed rifts (aulacogens)	Rift basins do not proceed to spreading stage, but fail and are infilled with shallowing upwards sedimentary successions; these zones of crustal weakness are easily deformed during later tectonic instability.	Budva Zone? of Serbia and Bosnia. Late Permian basins of Crete/Sicily; Ionian Zone in Greece and Albania.
Intra-platform basins	Pelagic and redeposited carbonates, floored by volcanics/sediments of stretched continental basement (where exposed). Long-ranging successions normally remain above the CCD and show gravity input from bordering carbonate platforms. May include condensed deposits on local volcanic highs.	Ionian Zone, western Greece and Albania; within the Pelagonian Zone in Argolis, Greece; Archangelos Unit of Rhodes; Kızılca Unit, southwestern Turkey; Çamova Unit, southwestern Turkey.

Table 1. Rift related tectonic facies, with examples from the Eastern Mediterranean Tethys (from Robertson 1994).

Tectonic facies	Characteristics	Examples
Spreading ridge	MOR-type ophiolites, basal metalliferous sediments, tensional faulting exposing plutonics, with ophicalcite in slow spreading, rifted ridges; overlying pelagic carbonates, then siliceous facies below CCD.	Western-type ophiolites, Albania; some Jurassic ophiolites in Croatia/Bosnia; Siptorrema, Othris, Greece; Migdhalitsa, Argolis, Greece; Karakaya, northwestern Turkey.
Abyssal plain	Laterally continuous blanket of deep-sea pelagic and hemipelagic sediments, deposited after subsidence below the CCD; siliceous in upwelling areas, may include inactive ridges, active ridges and/or within plate-type volcanics.	Upper thrust sheets of Pindos-Olonos nappes, western Greece; Various slices in accretionary complexes, both Palaeotethyan and Neotethyan.
Continental fragment	Fragments of continental crust, where preserved, overlain by siliciclastics and carbonate platform units, showing only limited subsidence; bordered by a small passive margin passing laterally into oceanic crust.	Palaeotethyan Kargı unit, Central Pontides, Turkey; Neotethyan Kemer units, Antalya Complex, southwestern Turkey; Olympos platform, central northern Greece; Parnassus platform, southern Greece.
Oceanic seamount or oceanic plateau	Thick piles of MORB/WPB-type basalts, locally overlain by rapidly subsiding carbonate platform units; pelagic carbonate/non-calcareous sediment capping; marginal talus, partly within flexural moat.	Palaeotethyan Karakaya complex, northwestern Turkey and central Turkey; Neotethyan Ankara Melange, Central Turkey; Avdella Melange, northwestern Greece; Besni unit, southwestern Turkey; Dhiarizos Gp, southwestern Cyprus.

Table 2. Spreading ridge tectonic facies, with examples from the Eastern Mediterranean Tethys (after Robertson 1994).

Tectonic facies	Characteristics	Examples
Supra-subduction zone ophiolite	Complete ophiolite, with harzburgitic depleted mantle, sheeted dykes and IAT-type/boninitic extrusives; locally includes acidic calcalkaline extrusives and volcanoclastics.	Eastern-type ophiolites, Albania; Pindos and Vourinos ophiolites, Greece; Troodos ophiolite, Cyprus; Hatay, Bâer-Bassit and Guleman ophiolites, south and southeastern Turkey.
Oceanic arc	Thick piles of basalts and basaltic andesites; subordinate more fractionated extrusives and volcanoclastics; tuffaceous, where shallow-water and/or subaerial.	Palaeotethyan Çangaldağ, Central Pontides, northern Turkey; Neotethyan units in central and southeastern Turkey (not well documented).
Subduction/accretion complex	Thick units of structurally repeated deep-sea sediments, often with slivers of scraped-off oceanic crust; successions ideally thicken and coarsen-upwards in individual thrust slices and show downward younging in age of accreted units; many structural complications; often melange units are present.	Palaeotethyan Karakaya Complex, western and central Turkey; Neotethyan Pindos-Olonos nappes, western Greece; Avdella Melange, northwestern Greece; Ermioni Complex, southeastern Greece; Cetmi and Ankara melanges, northwestern and central Turkey.
Fore-arc basin	Structurally overlies subduction/accretion units, comprises thick, variable sequences of moderately deep- to shallow-marine or sub-aerial deposits including carbonates, siliciclastics and/or volcanoclastics; often relatively structurally intact, with only low-grade metamorphism	Neotethyan Kastamonu-Bayobat basin, Central Pontides; Tüz-Gölü basin, central Turkey (in part); Bilecik Lst, and underlying clastics, northwestern Turkey.
Black-arc basin (intra-continental)	MORB- and/or IAT-type ophiolite overlain by terrigenous and/or volcanogenic sediment shed from both active arc and continental basement; locally siliceous and/or organic-rich sediments.	Palaeotethyan Küre Complex, Central Pontides; modern Black Sea basins.
Back-arc basin (intra-oceanic)	MOR- and/or IAT-type ophiolite, overlain by mainly volcanogenic sediments, including tuffs. Little or no coarse clastic sediment input; volcanoclastic turbidites and debris flows in areas proximal to active arcs.	Not specifically recognised, but may include some ophiolite-related units in Neotethys of southeastern Turkey.

Table 3. Convergent margin tectonic facies with examples from the Eastern Mediterranean Tethys (after Robertson 1994).

Tectonic setting	Characteristics	Examples
Intra-oceanic collision	Structurally complex assemblages of several ophiolitic and/or active margin related units (including oceanic arcs) often separated by serpentinitic melange; amalgamation by strike-slip and/or thrusting.	None specifically recognised in Eastern Mediterranean Tethys, but may be present, particularly in Palaeotethys in Pontides, also in Neotethys of southeastern Turkey
Remnant ocean basin	Ophiolite (where preserved) overlain by deep-sea sediments, then much younger gravity-deposited sediments, commonly with provenance including emplaced ophiolites and collision zones already sutured along strike; little or no associated arc volcanism.	Neotethyan Pindos "Flysch", western Greece; Killan Units; southeastern Turkey; modern Eastern Mediterranean Sea and Ionian Sea.
Pre-collisional extensional basin	Extensional fault-controlled basins developed on active continental margins (locally including ophiolites), above subduction zones, with little or no active subduction related volcanism.	Neogene sedimentary cover of Troodos ophiolite, Cyprus; Lower Tertiary Hazar basin, southeastern Turkey; modern Hellenic "trench" southwestern of Crete.
Post-collisional extensional basin	Basin formation above normal (detachment) faults that relieve stresses accumulated during collision and crustal thickening; subaerial to marine, clastic dominated basins; depocentre ideally migrates away from footwall faults with time; provenance mainly from footwall side of basin.	Extensional unroofing of Aegean metamorphic units, including Menderes, Pelagonian, Rhodope, Serbo-Macedonian and Cycladic.
Foredeep with emplaced oceanic crust	Collapsed passive margins, overlain by deepening-upwards sedimentary successions, including hemipelagic and pelagic sediments and debris flows; overthrust by accretionary units and/or ophiolites.	Collapse of Pelagonian Zone associated with emplacement of Jurassic ophiolite in Greece, Albania and Serbia; similar collapse of Arabian margin, related to Late Cretaceous ophiolite emplacement in southeastern Turkey.
Foreland basin with emplaced continental crust	Collapsed passive margins, overlain by deepening-upwards sedimentary successions—mainly terrigenous turbidites and mudstones; debris flows locally at the top; overthrust by continental thrust sheets; includes piggy-back basins and other complications.	Closure of Neotethys in Greece within Pelagonian, Pindos-Olonos and Ionian Zones (e.g. Ionian "flysch", similar Kaş basin in southwestern Turkey and Lice/Çüngüş basin in southeastern Turkey; piggy-basins include southern Tavaş basin, western Turkey and Meso-Hellenic Trough, Greece.
Uplift-related tectonic settings	Varies from regional to local with unconformities, structural evidence of uplift and/or diapirism; associated sediments deposited in basins, either locally or far-removed.	Quaternary uplift of Troodos Massif, Cyprus; Regional uplift of Anatolian Plateau; uplift of Pindos Mountains etc.

Table 4. Collision-related tectonic facies, with examples from the Eastern Mediterranean Tethys (after Robertson 1994).

Tectonic facies	Characteristics	Examples
Transform rifts and passive margins	Passive margin bordered by subsiding basin, with outer ridge composed of sediments and/or continental basement slivers; structural evidence of shear, especially near continent-ocean boundary; reduced subsidence and volcanism relative to "normal" margins.	Late Palaeozoic-Early Mesozoic (non emplaced) rifted Levant; western margin of Mesozoic Bey Dağları carbonate platform, southwestern Turkey; more local margin offsets, including Scutari-Peç, Albania.
Oceanic transform faults	Ophiolites cut by major fault zones showing pervasive strike-slip, fragmentation of ophiolitic crust; local rotations; fault-controlled sedimentary basins with intercalations of extrusives and coarse talus; ophicalcite where submarine exposure of ultramafics.	South Troodos Transform Fault Zone, Cyprus and Tekirova Zone, southwestern Turkey (both supra-subduction zone ophiolites); no well documented examples within MOR-type ophiolite in E. Mediterranean region.
Oceanic crust in pull-apart basins	MORB-type ophiolite overlain by relatively proximal terrigenous sediments; possible evidence of strike-slip within ophiolites; bordering margins may show thermal metamorphism related to intrusion/spreading.	Neotethyan Gevgueli ophiolite, and related ophiolitic units, (e.g. Meglenitsa ophiolite), Vardar Zone, northeastern Greece.
Convergence-related (pre-collisional)	Sedimentary basins in forearc/backarc locations that were influenced by oblique subduction and/or strike-slip. Hard to recognise as tectonic facies.	Palaeotethyan marginal basins (e.g. Küre); Neotethyan forearc basins (e.g. Kastomonu-Baybat, Central Pontides and Hazar, south-eastern Turkey; modern eastern Hellenic active margin; Cyprus active margin between Cyprus and Arabia).
Strike-slip and rotation (pre-collisional)	Complex and variable settings marked by compression, strike-slip and/or tectonic rotations (about vertical axes); also transtensional pull-apart basins related to oblique collision	Southwestern segments of the Antalya Complex, southwestern Turkey; Palaeorotation of the Troodos microplate and related deformation of the Mamonita Complex and Kyrenia Range, Cyprus; and Tertiary Lice "pull-apart" basin, southeastern Turkey.
Strike-slip and rotation (post-collisional)	Regions of pervasive strike-slip and distributed shear, including zones of compression, transtension; localised volcanism and deep-level (granitic) intrusion; block rotations; localised melange genesis; strike-slip pull-apart basins.	Neotethyan evolution of Vardar Zone, Greece, Macedonia and Serbia; Tectonic escape of Anatolia westwards, with compression, localised uplift, block-rotation and pull-apart basin development.

Table 5. Strike-slip related tectonic settings, with examples from the Eastern Mediterranean Tethys (after Robertson 1994).

From field observations; various tectonostratigraphic units are identified within the Upper Cretaceous Izmir-Ankara-Erzincan Suture Zone and are interpreted in terms of their tectonic facies. In combination with their stratigraphic and structural field-relations this forms the basis for the construction of a model for the tectonic evolution of the region through time.

Interpretation of tectonic facies is supported by geochemical data. Whole-rock geochemical analyses were made following a method developed by Godfrey Fitton and Dodie James and incorporating procedures outlined by de Jongh (1973), Govindaraju (1994), Jochum et al. (1990), Norrish and Hutton (1969) and Reynolds (1963) (Appendix 2). Chromite grains were analysed by electron microprobe following the method of Reed (1975). Geochemical analyses of basaltic rocks are used to identify past tectonic environments using the well established 'tectonic discrimination diagrams' of e.g. Pearce (1973), Pearce and Cann (1982) and Dick and Bullen (1984).

1.8 Organisation of thesis/review of contents

Two areas, ~500 km apart from each other, were studied during this project. This was advantageous because it allowed a direct comparison of the Izmir-Ankara-Erzincan Suture Zone in these two areas, which exhibit several important differences in terms of regional geology. The Erzincan area in the east has higher mean elevation and topographic relief than does the area in the Central Pontides; subduction-related plutonic and volcanic rocks crop out north of the Izmir-Ankara-Erzincan Suture Zone in the Eastern Pontides but not in the Central Pontides; the Izmir-Ankara-Erzincan Suture Zone in the east separates the Pontides from the Taurides whereas in the Central Pontides it separates the Pontides from the Kirşehir/Niğde massif.

Data from the Eastern Pontides is presented first and then the data from the Central Pontides is presented for comparison. Thus, the thesis contains two main data-bearing chapters (Chapters 3 and 5), which are each preceded by a review of the tectonostratigraphy. Chapters 3 and 5 also contain simple geographical maps of each area with a key to the Turkish grid references used throughout the thesis.

Where field-based data is presented either 6- or 10-figure grid references, obtained by GPS, preceded by a reference to the relevant Turkish 1:100 000 map sheet are quoted in parentheses (e.g. gr: F32, 4020069730).

The data are discussed and compared together in chapter 6, with reference to the regional and global tectonic context. The conclusions are summarised in chapter 7.

1.8.1 Turkish language

The thesis contains many references to Turkish place names or Turkish stratigraphic units. The Turkish language contains letters not found in the English alphabet. To help the reader, their pronunciation is given below:

Letter	Pronunciation
ıİ	‘uh’ as in put
üÜ	‘oo’ as in shoe
öÖ	not common in English; ‘ur’ as in the french fleur.
ğĞ	silent but emphasises the preceeding vowel
şŞ	‘sh’ as in ash
çÇ	‘ch’ as in chair

Turkish place names are often composed of simple words

Some useful geographical Turkish words are listed below:

Dağ	mountain
Çayır	stream
Nehiri	River
Tepe	hill
Köy	village
Yayla	highland pasture
Deniz	sea
Beyaz	white
Kara	black

2 Tectonostratigraphy of the Eastern Pontides

2.1 Revised stratigraphy

This revised stratigraphy applies to the Upper Mesozoic-Early Tertiary rocks of the suture zone and incorporates, with acknowledgements, previously published data. Previous stratigraphic nomenclature is retained as far as possible. The introduction of new stratigraphic names is avoided except where this is essential to conform to the requirements of the international stratigraphic guide (Murphy and Salvador 1994). Where there is disagreement between, and uncertainty regarding, different published stratigraphic schemes the merits of each division have been considered in the light of the field evidence collected during this project. For each of the proposed stratigraphic units a biostratigraphic age is assigned based on existing data combined with the new micropalaeontological data obtained during this project. The revised tectonostratigraphy for the Eastern Pontides is shown in Figure 2.1.

2.1.1 Campanian-Maastrichtian Ayıkayası Formation

Synonymy: Ayıkayası Formation (Özgül and Turşucu 1984).

Name: It is not known where the Ayıkayası Formation (Figure 2.1) initially takes its name from.

Lithology: Buff-grey-coloured thin-bedded pelagic limestones are interbedded with oolitic and bioclastic calcarenites with some mafic lithiclastic material. These rocks are interspersed with coarse, poorly sorted, graded, conglomerates containing angular to rounded clasts of neritic limestone, red mudstone and chert. The conglomerate beds have scoured, erosive bases.

Lower and upper boundaries: The unit lies with a sharp but conformable contact on neritic limestone (Kabataş Member) of the Munzur Dağı Formation

(Figure 3.1 and 3.3). Its upper stratigraphic boundary has been removed by south-vergent thrust faulting.

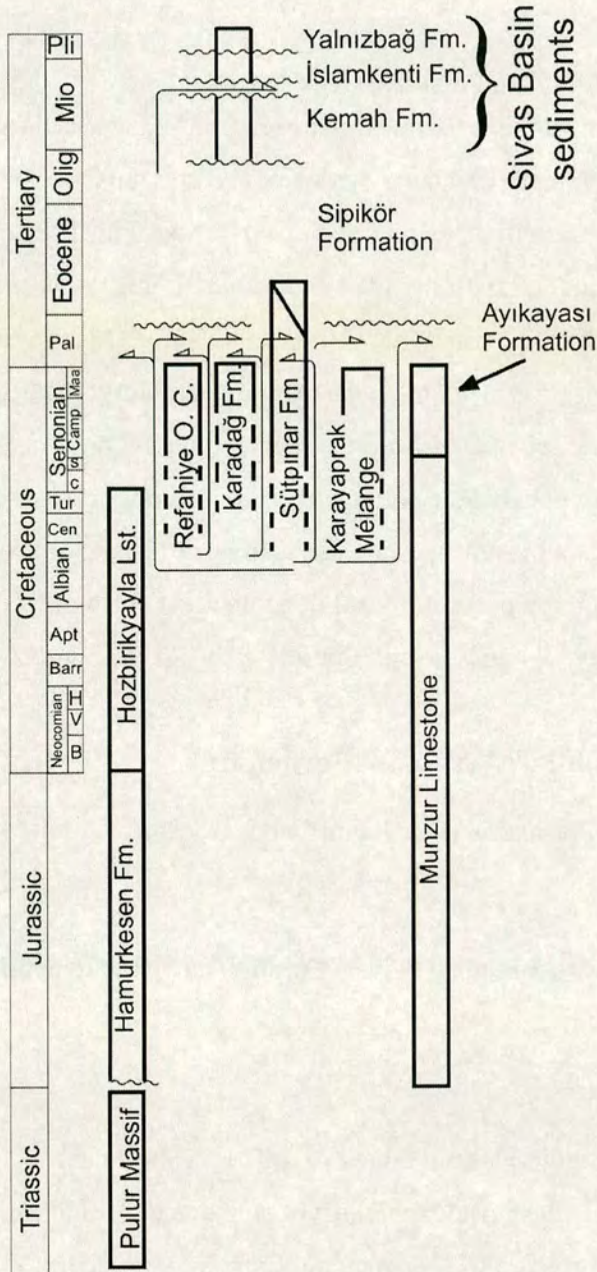


Figure 3.1. Revised tectonostratigraphy of the Eastern Pontides with units arranged in order of outcrop from north to south.

Thickness and lateral extent: The Ayıkayası Formation reaches a maximum exposed thickness of 25m in the Munzur Mountains area between Muratboynu and

Yeşilyazı (Figure 2.2). Its outcrop is limited, being only preserved as remnants of the thin uppermost part of the Munzur Dağı Formation that has escaped erosion. In addition, the thick limestone succession of the Munzur Dağı Formation itself gives rise to a fairly inaccessible terrain. The only accessible outcrop in the area is ~10 km south of Muratboynu (Figure 2.2).

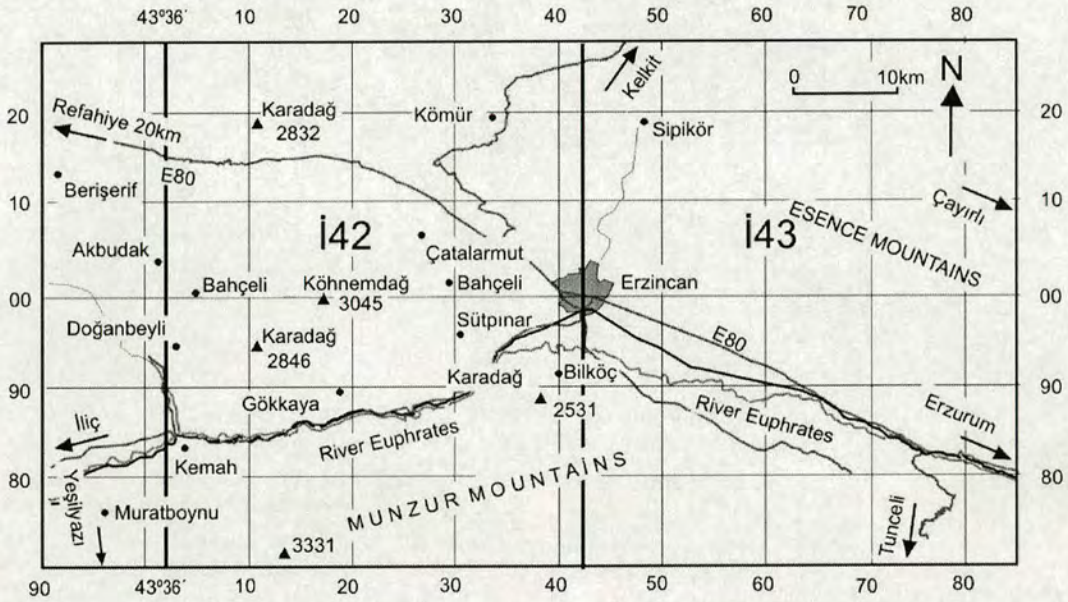


Figure 3.2. Map of the Erzincan area to show locations referred to in the text. I42 and I43 are Turkish map numbers.

2.1.2 Upper Cretaceous Refahiye Complex

Synonymy. Zone intermédiaire des péridotites d'Erzincan, Bergougnan (1975); Refahiye Karmaşığı/Erzincan Nappe, Yilmaz (1985); Karakaya Kompleksi (in part), Koçyiğit (1990); Karadağ Kompleksi (in part), Koçyiğit (1990); İç Toros Kompleksi (in part), Koçyiğit (1990); Refahiye Ophiolitic Complex (in part), Aktimur et al. (1995); Ofiyolitli Melanj (in part), Okay and Şahintürk (1997); Uluymaç Ophiolite, Ozer et al. (2004).

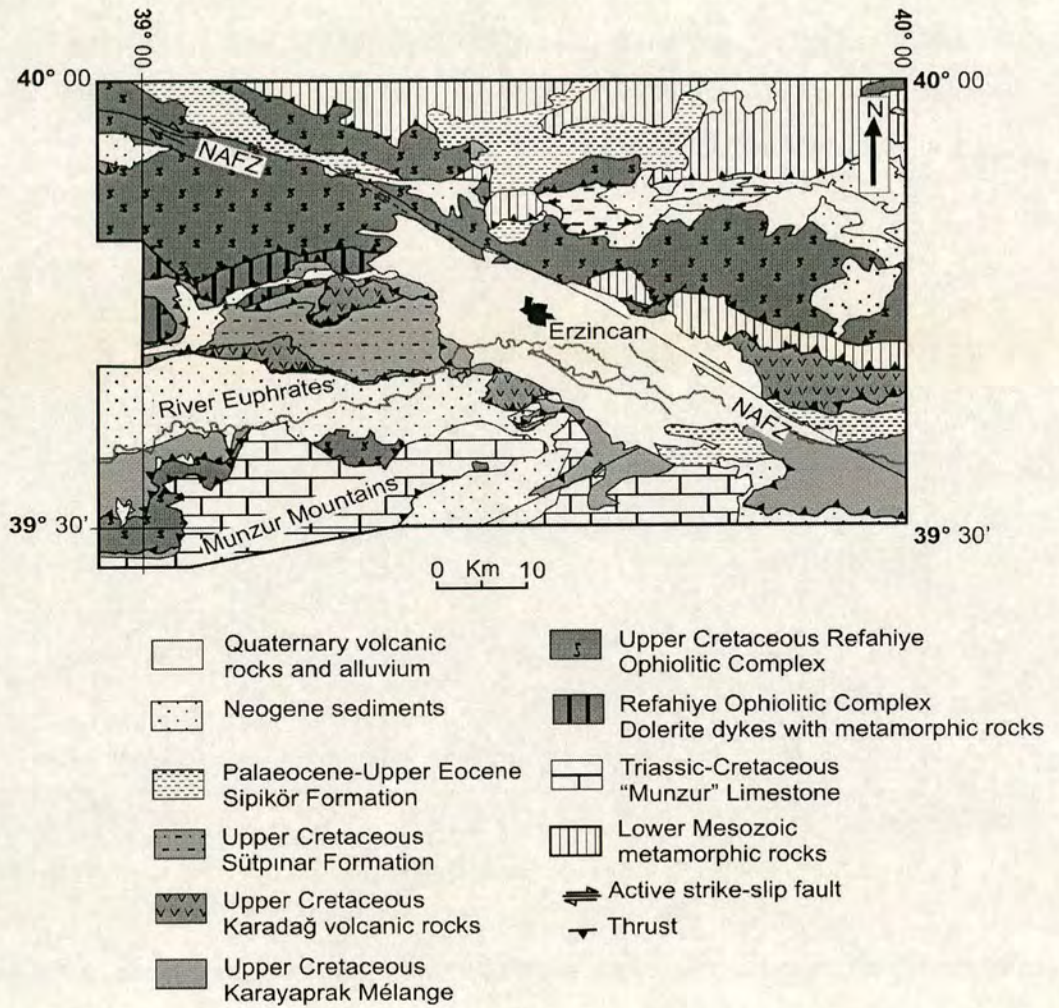


Figure 3.3. Simplified geological map of the Erzincan area to show outcrop of the Upper Cretaceous-Lower Tertiary units of the IAES suture zone; modified from Aktimur et al. (1995).

Name. The unit is named after the town of Refahiye which lies within a large outcrop area of the unit, about 70km west of Erzincan. The unit is well exposed along the international highway (E80) half way between Refahiye and Erzincan.

Lithology. The unit is composed of >75% by volume, serpentinised harzburgite, ~20% diabase and minor amounts of gabbro, and isolated trondhjemite

(plagiogranite) dykes. Tectonic slices, about 2000m thick, of a sheeted dyke complex crop out west of Çatalarmut and south of Akbudak (Figure 2.2). In the same area, the Refahiye Complex also contains a variety of metamorphic rocks which make up <5%, occurring as screens of various thickness between diabase dykes. Lithologies include epidote-actinolite schist, metabasite, metaserpentinite and massive marble. These metamorphic rocks probably belong to the Upper Palaeozoic-Early Mesozoic Karakaya Complex (see section 3.3.7).

Lower and upper boundaries. The base of the Refahiye Complex is a north-dipping thrust everywhere where it is observed. The boundaries are commonly thick, serpentinitised shear zones displaying S-vergent shear fabrics and fluid alteration of the surrounding rocks. At its upper boundary the unit is unconformably overlain by the Eocene Sipikör Formation or younger Tertiary cover rocks (sections 2.1.6 and 2.2; Figure 2.1).

Thickness and lateral extent. The estimated thickness of the Refahiye Complex is about 8km. The unit is very well exposed to the north and north-west of the Erzincan pull-apart basin and crops out in an ~8km-wide belt extending eastwards towards Çayırılı and westwards beyond Refahiye.

2.1.3 Upper Cretaceous Karayaprak Mélange

Synonymy. Mélange Ophiolitique Karayaprak, Bergougnan (1975); Karayaprak Karmaşığı, Yılmaz (1985); Karayaprak Napı (in part) of the Anadolu Kompleksi, Koçyiğit (1990); Refahiye Ophiolitic Complex (in part), Gülandere Formation (in part), Senek Ophiolitic Complex (in part), Aktimur et al. (1995); Ophiolitic Mélanj, Okay and Şahintürk (1997).

Name. The Karayaprak Mélange apparently takes its name from a village in the Suşeri area 130 km west of Erzincan which is outside the study area. The name was first used by Bergougnan (1975).

Lithology. The Karayaprak Mélange is a variably tectonised mixture of blocks and slices individually up to about 1km long. These blocks are dominantly hard pale-grey massive crystalline pelagic limestones associated with basalt. Hydrothermally altered basaltic pillow lava is commonly associated with red radiolarian chert, pelagic limestone and mudstone. Serpentinite occurs as blocks and slices of altered peridotite, and also as highly deformed masses along shear zones. Lesser components of the mélange include diabase, volcanoclastic shale and sandstone, gabbro, recrystallised and deformed pink pelagic limestone, rare plagiogranite, amphibolite and greenschist metavolcanic rocks. Matrix-supported olistostromal (ie. sedimentary) mélange crops out near Kömür village (north of Erzincan) where metre-scale blocks are set in a poorly-sorted but dominantly muddy sedimentary matrix. However, at most outcrops a sedimentary matrix is absent and the blocks of various lithologies are tectonically mixed. For more detailed discussion of the nature of the Karayaprak Mélange see section 3.4.

Lower and upper boundaries. The lower contact of the Karayaprak Mélange is a thrust where ever it is observed. North-dipping thrust faults imbricate the Karayaprak Mélange with units of various ages in the region, including the pre-Liassic Karakaya Complex and Miocene and younger cover rocks (section 2.2). The Karayaprak Mélange is unconformably overlain by the Upper Cretaceous-Lower Eocene Sipikör Formation at Muratboynu village (Figure 2.1; sections 2.1.6 and 3.7).

Thickness and lateral extent. The Karayaprak Mélange occurs as discrete slices, up to a maximum of about 4km thick. It is imbricated with various older units and its outcrop is distributed over a wide area. The most accessible outcrops occur along the international highway (E80) SE of Erzincan. Large outcrop areas are found 35km west of Erzincan between the villages of Akbudak and Bahçeli (Figure 2.2), and also between the River Euphrates and the Munzur Mountains, SW of the town of

Kemah near Muratboynu village (Figure 2.2). Outcrops have also been mapped outside the study area, south of the Munzur Mountains between Ovacık and Kemaliye (Özgül and Turşucu 1984).

2.1.4 Upper Cretaceous Karadağ Formation

Synonymy. Refahiye Ophiolitic Complex (in part), Yılmaz (1985); Karadağ Volcanitleri, Koçyiğit (1990); Karadağ basalt member (Çerpaçindere Formation), Aktimur et al. (1995); Pazarcık Volcanics, Atalay (1999).

Name. The Formation is named after Karadağ ('Black Mountain'). There are at least three mountains within 30km of Erzincan with the name Karadağ (Figure 2.2). One such mountain near the village of Bilkoç 10km south of Erzincan (Figure 2.2) was mapped by Koçyiğit (1990) as 'Karadağ volkanitleri' (Eocene) and the unit originally took its name from there. However, the stratigraphy of Aktimur et al. (1995) retained the name Karadağ for the volcanic unit but placed it in the Palaeocene and mapped the Karadağ Mountain area near Binkoç village as Eocene, in agreement with Koçyiğit (1990). However, they mapped the rocks under a new name (the Senek Formation) and described them as a mélangé. Their name Karadağ Formation therefore refers to the Karadağ Mountain near the village of Doğanbeyli (30km west of Erzincan, Figure 2.2) which they mapped as Upper Cretaceous-Palaeocene basalt. The name Karadağ Formation is retained here since both localities are interpreted here as outcrops of the same stratigraphic unit.

Lithology. The unit comprises a thick succession (~3km) of hornblende- and plagioclase-phyric basic and andesitic lavas interbedded with coarse volcanoclastic conglomerates of andesitic composition. Chlorite-epidote-albite- and quartz-bearing volcanoclastic, tuffaceous and carbonaceous schists occur between metabasic and meta-andesitic flows, 2-3m thick. These are interpreted as metamorphosed volcanoclastic sandstones, shale and tuff, bearing mineralogical and textural evidence of a regional metamorphic event reaching upper greenschist facies (see Chapter 3 for details).

Lower and upper boundaries. The lower contact of the Karadağ Formation is everywhere a N-dipping thrust. Where the upper boundary has not been cut out by thrusting the unit is overlain unconformably by the Lower Eocene Sipikör Formation (eg. at Bılkoç), or younger sedimentary rocks (Figure 2.1; sections 2.1.6 and 3.7).

Thickness and lateral extent. The formation occurs in discontinuous wedge-shaped thrust slices up to 20km long which, individually, reach a maximum estimated post-deformational thickness of ~3km. A total outcrop area of 250 square km was mapped within the suture zone in the Erzincan area. The best outcrop is found at Köhnemdağ Mountain, 20km west of Erzincan. Other outcrops are found east of the Erzincan pull-apart north of the main road, and west of Erzincan south off the road at the village of Berişerif (Figure 2.2).

2.1.5 Campanian-Lower Eocene Sütöinar Formation

Synonymy. Gözerek Formation (in part), Arıkaya Limestone (in part), Özgöl and Turşucu (1984); Sütöinar Formation, Koçyiğit (1990); Çerpaçin member (of the Çerpaçindere Formation), Aktimur et al. (1995); Kapıkaya Limestone, Okay and Şahintürk (1997).

Name. It is unclear where the names Gözerek and Arıkaya (Özgöl and Turşucu 1984) were taken from. Very limited information has been published regarding the outcrop and characteristics of the Gözerek and Arıkaya Formations and it is not even clear if these are of the same lithology and age. For this reason the name Sütöinar Formation (Koçyiğit 1990) is used here. The formation takes its name from the village of Sütöinar, 10km west of Erzincan. The main outcrop of the unit is located on the western edge of the Erzincan pull-apart basin.

Lithology. The formation consists of a 1500m-thick succession of sedimentary rock which generally coarsens upwards. The lower ~800m is a succession of medium-bedded calcarenites and quartzo-feldspathic sandstones with laminated, muddy-shaly calcareous partings. In places, the succession is dominated

by thin-bedded, fine-grained, dark, volcanoclastic shale, thick-bedded, pale calcarenites with rare andesitic lava flows and volcanoclastic debris-flow conglomerates. The Formation passes upwards conformably into the Sipikör Formation.

Lower and upper boundaries. Both the lower and upper boundaries of this unit are commonly north-dipping thrusts. In the centre of the suture zone, near Gökkaya village and at Köhnemdağ Mountain (Figure 2.2) the top of the Sütpinar Formation exhibits a conformable transition to the Sipikör Formation, marked by the appearance of thick (up to 4m) lenses of coarse polymict conglomerates, and massive, texturally immature and compositionally varied sandstones.

Thickness and lateral extent. The present apparent thickness is estimated to be up to 8km based on mapping. The succession at Gökkaya measures 1500m thick. West of Erzincan the formation crops out in a 25 km-long belt that extends into the mountains between the Euphrates River and the North Anatolian Fault Zone. Access by road to this large area of outcrop is difficult. Very good exposure occurs in deep gorges that drain to the south, west and east from Köhnemdağ Mountain. By far the best access is by foot from the village of Gökkaya (Figure 2.2).

2.1.6 Palaeocene-Lower Eocene Sipikör Formation

Synonymy. Sipikör Formation, Bergougnan (1975); Köroğlu Formasyonu, Koçyiğit (1990); Gülandere Formation, Aktimur et al. (1990, 1995); Sipikör Formation, Okay and Şahintürk (1997); Gülandere Formation, Atalay (1999); Sipikör Formation, Topuz et. al. (2004).

Name. In the Erzincan area this unit originally took its name from the village of Sipikör, 20km north of Erzincan (Bergougnan 1975). The name continues to be used in this area (eg. Okay and Şahintürk 1997; Topuz et. al. 2004). However, in the Sivas Basin, further west, the unit takes its name from the Gülandere River between Refahiye and Kemah (eg. Aktimur et. al. 1990), the name Gülandere Formation was subsequently extended to the Erzincan area (Aktimur et al. 1995) and continues to be

used in the Sivas Basin area (eg. Ayaz 2003). In this study Bergougnan's original name for this unit, the Sipikör Formation (1975) is retained in the Erzincan area. The Sipikör Formation is correlative with the Gülandere Formation in the adjacent Tertiary Sivas basin further west.

Lithology. The formation exhibits a variety of lithologies. Polymict, well-rounded conglomerate lenses and weakly bedded, to massive, fine- to coarse-grained sandstones interdigitate with discontinuous lenses of very fine, dark grey, hard, massive foraminiferal limestone, up to ~50m thick. In places medium- to thick-bedded, pale-creamy coloured sandy, oncoidal and bioclastic Nummulitic packstones and wackestones with rudist fauna, algae and large sponges represent shallow-marine carbonate environments (see section 3.7 for details of fossil occurrences). These limestones are interbedded with anhydrite beds. The shallow-marine facies pass upwards into deltaic and fluvial facies sedimentary rocks.

Lower and upper boundaries. The Formation rests unconformably on the Karayaprak Mélange and the Refahiye Complex (Figure 2.1). However, the base of the Sipikör Formation is a conformable transition from the Sütpınar Formation in a well exposed section between Gökkaya village and Köhnemdağ Mountain. The beginning of the Sipikör Formation is marked by the appearance of thick (ie. 4m) lenses of polymict conglomerates interbedded with thick (~40 m) lenses of massive fine-grained nummulitic limestone. The unit is unconformably overlain by Miocene and younger sedimentary or volcanic cover rocks (eg. near Kemah). The upper contact at many localities is a north-dipping thrust fault.

Thickness and lateral extent. The Sipikör Formation is less deformed than the older units and its thickness is estimated to be at least 500m in the Köhnemdağ area where the most complete section crops out.

2.2 Miocene cover units

The Miocene and younger cover rock units in the area are not revised here as they were not studied in detail during this project. The nomenclature of Aktimur et

al. (1995) is adopted informally in this thesis for the Tertiary cover units of the Sivas basin (Kemah Formation, İslamkenti Formation and Yalnızbağ Formation). These units have been described in great detail particularly from the Sivas Basin by other workers (eg. Aktimur et al. 1990). These sedimentary rocks comprise a variety of clastic sedimentary rocks, carbonates and evaporites that unconformably overlie Lower Tertiary and older rocks. Miocene and younger cover rocks crop out extensively in the large Sivas Basin to the west of Erzincan and also to the north in the Pontides.

2.3 Conclusions: tectonostratigraphy of the Eastern Pontides

This chapter has outlined a workable stratigraphic scheme that identifies six major formations of Late Cretaceous-Early Tertiary age within the suture zone. These are the Ayıkayası Formation, Refahiye Complex, Karayaprak Mélange, Karadağ Formation, Sütüinar Formation and the Sipikör Formation. The Sütüinar Formation extends into the Lower Eocene. In addition, the Sipikör Formation of Palaeocene-Lower Eocene age is included here for two main reasons: 1) sedimentological analysis of the Sipikör Formation provides a means to investigate the tectonic processes occurring during the early stages of collision and assembly of the suture zone; 2) the Sipikör Formation is the oldest unit unconformably overlying some of the assembled Upper Cretaceous units of the suture zone and thus constrains the timing of tectonic events. The Ayıkayası Formation is considered here because of its relevance to the investigation of the tectonic processes during final closure of Northern Neotethys. In contrast, a detailed consideration of the stratigraphy of the Tertiary sedimentary basins (eg. Sivas Basin) is outside the objectives of this research.

The lithostratigraphic division presented here allows meaningful, detailed comprehensible descriptions of each of the units to be made in the following chapters of this thesis.

3 The Izmir-Ankara-Erzincan suture zone in the Eastern Pontides

3.1 Introduction

This chapter details the diagnostic characteristics of each of the Upper Cretaceous-Early Tertiary units exposed within the Izmir-Ankara-Erzincan suture zone in the Eastern Pontides. Igneous, sedimentary and geochemical data are presented from each unit and an interpretation of each unit is given. The interpretations of the individual units are summarised together at the end of the chapter.

3.2 Trench-margin collision facies: *Ayıkayası Formation*

A small outcrop of the Ayıkayası Formation was logged south of the River Euphrates in the Munzur Mountains (e.g. south of Muratboynu at gr: J41, 9857770181), where the Ayıkayası Formation conformably overlies the platform limestone of the Munzur Dağı Formation. The stratigraphic top of the formation was not observed, being cut by north-dipping thrust faults (the unit is structurally overlain by the Karayaprak Mélange). Pelagic foraminifera present in the Ayıkayası Formation include the Lower Cretaceous species *Vercorsella*, *Pyrgo* and *Quinqueloculina* (Taşlı and İnan pers. comm. 2004). The Lower Cretaceous foraminifera could be reworked. Özgül and Turşucu (1984) dated the unit Turonian-Campanian.

The Ayıkayası Formation begins with ~3 m thickness of pink pelagic limestone (Figures 3.1 and 3.2). This pelagic limestone is followed by amalgamated, thickly-bedded, massive (~2 m) calcirudites. The calcirudites are matrix-supported conglomerates with large (<50 cm), rounded to sub-angular boulders and pebbles of grey coarse biosparite and angular to sub-angular pebbles and granules of red chert and red pelagic limestone in an oolitic biomicrite or calcarenite matrix. Individual

beds tend to be dominated by either angular red pelagic clasts or rounded neritic limestone clasts. The amalgamated calcirudites have scoured, erosive bases and are

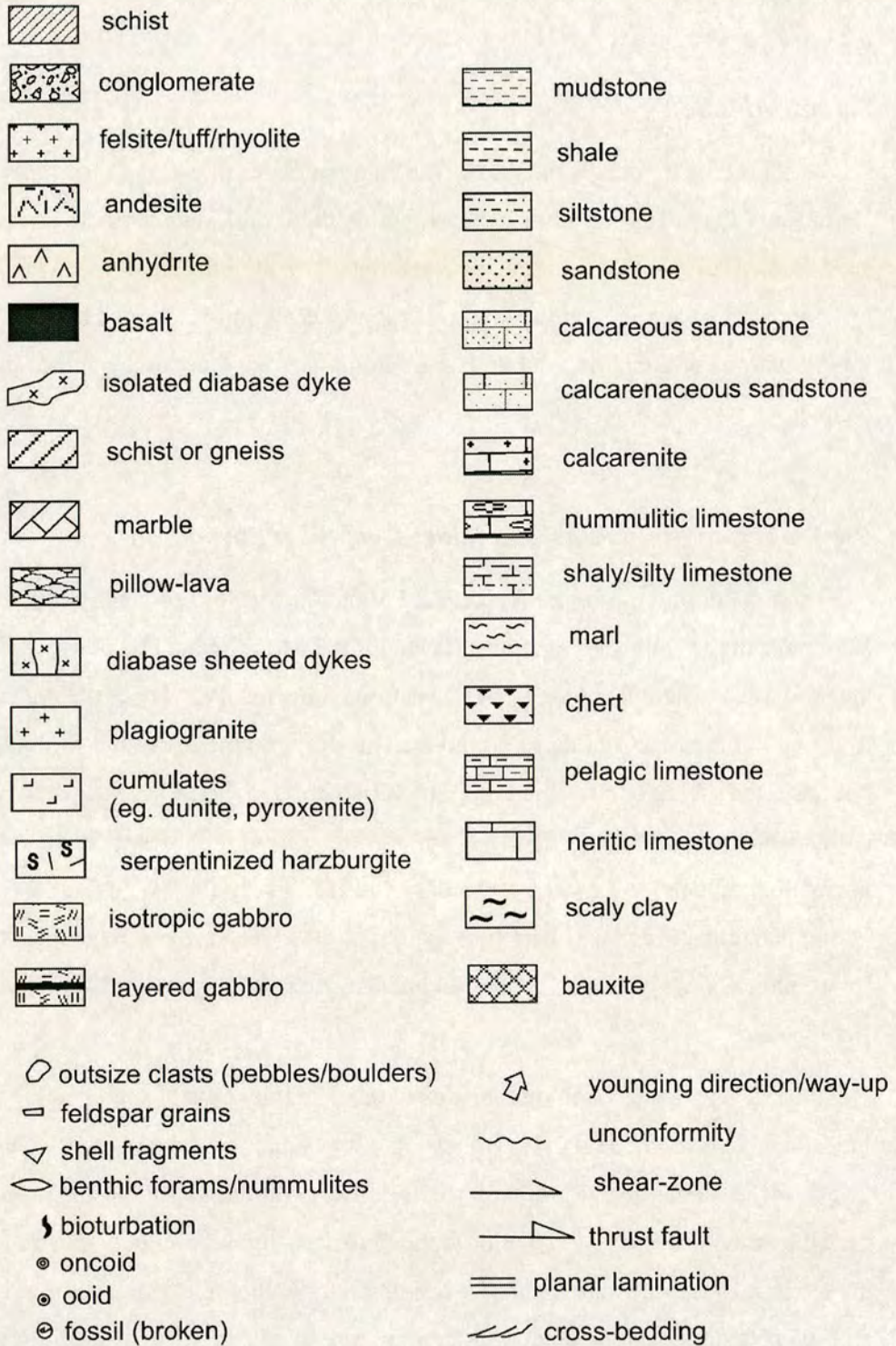


Figure 3.1. Key to logs, sections and maps.

Ayıkayası Formation

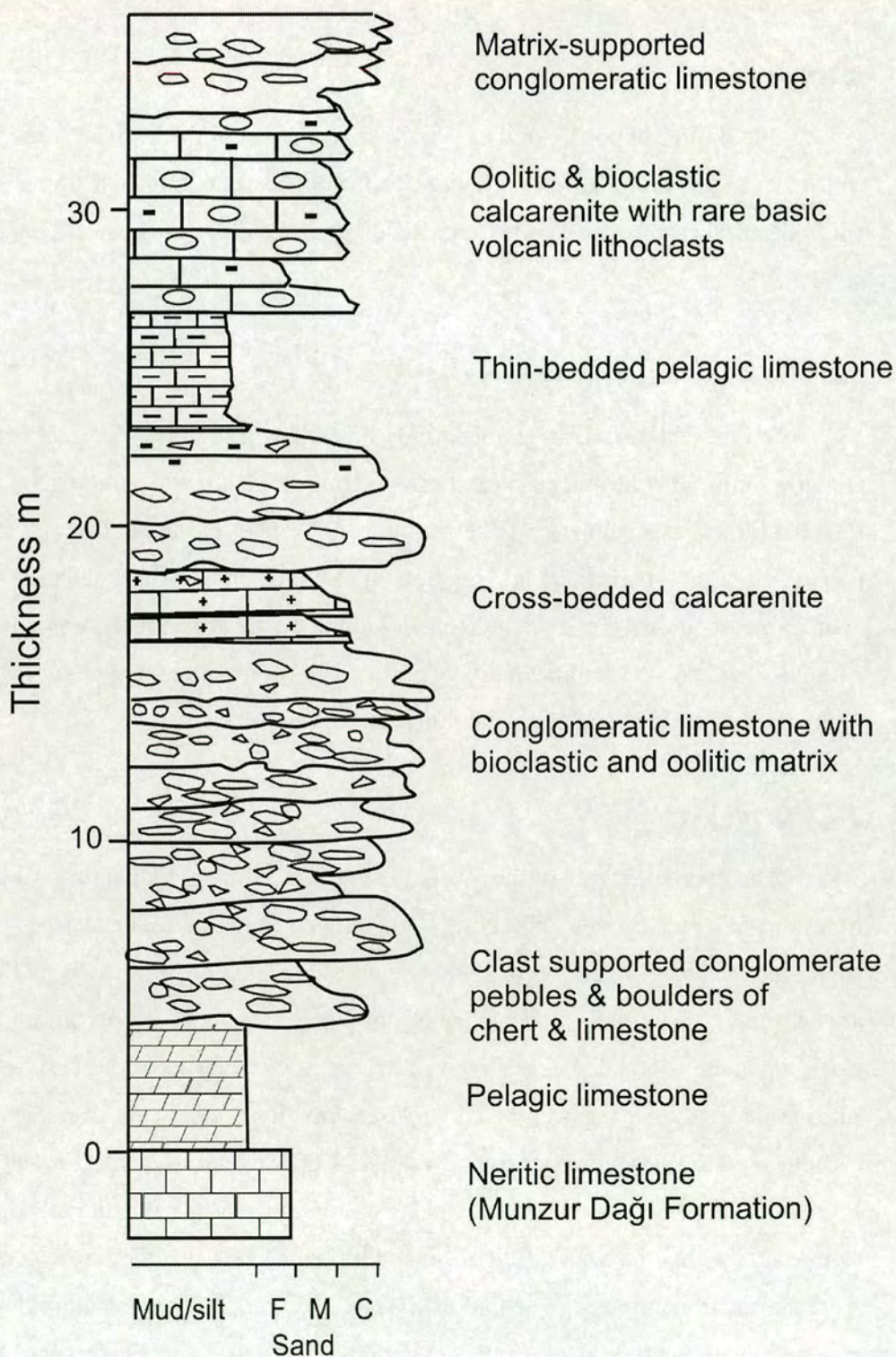


Figure 3.2. Sedimentary log of the Ayıkayası Formation.

interbedded with medium-bedded oolitic biosparite, cross-bedded calcarenites and, thinly-bedded pelagic limestones. Some conglomerate beds exhibit clast imbrication.

3.2.1 Structure

The limited exposure of the Ayıkayası Formation in the Erzincan area is not well-cleaved and no folds were observed. Some exposures exhibited a strong low-angle shear fabric or mylonitic texture. Bedding planes dip locally toward the south at $\sim 45^\circ$.

3.2.2 Sedimentary petrography

In thin section coarse-grained sandy limestone from the Ayıkayası Formation contains ooids, oncoids, bioclasts and calcite grains together with sub-angular to sub-rounded lithic clasts composed of serpentinite, chloritised basalt, diabase, chert and, plagiogranite in a sparite cement. Some sections contain abundant rounded or angular quartz grains. These include metamorphic quartz grains with strained extinction and polycrystalline quartzite grains with sutured grain boundaries. A mylonitic texture is observed in one thin section.

3.2.3 Discussion

The internal texture of the biosparite clasts is identical to that of the neritic limestone belonging to the underlying Munzur Dağı Formation. The matrix-supported, coarse-grained and massive texture of the conglomerates suggest that they are debrites, transported and deposited by 'proximal' sediment-gravity flows. The clasts are compositionally sorted to some degree, suggesting separate source regions. The neritic limestone clasts in the Ayıkayası Formation are derived from the carbonate platform represented by the Triassic-Upper Cretaceous Munzur Dağı Formation. The red pelagic chert and pelagic limestone clasts have no potential source area within the Munzur Platform and it seems likely that they were derived from the accretionary wedge behind the Neotethyan trench. The metamorphic quartz content may indicate exposure and denudation of the Palaeozoic basement of the Munzur Platform during the Late Cretaceous.

3.2.4 Summary

The Ayıkayası Formation is of Campanian-Maastrichtian age (83.5-65.5 Ma; Özgül and Turşucu 1984; 93.5-70.6 Ma; Gradstein et al. 2004).

The formation lies with conformable contact above the Munzur Dağı Formation (Özgül and Turşucu 1984).

The formation begins with pelagic limestones that pass stratigraphically upwards into redeposited coarse calcirudites, interpreted as debrites. The debrites were redeposited from the Munzur Platform to the south and the Neotethyan oceanic crust-derived nappes to the north (e.g. the Karayaprak Mélange and Refahiye Complex described below).

The formation records the foundering of the Munzur Platform and development of a foredeep during Campanian-Maastrichtian time (83.5-65.5 Ma) related to southward thrusting and emplacement of the Neotethyan ophiolitic nappes. The Ayıkayası Formation can be interpreted as a trench-margin collision facies. The Ayıkayası Formation and its tectonostratigraphic position are comparable to units of the same age found ~500 km southwest in the Taurides (Ozer et al. 2004).

3.3 Emplaced inferred marginal basin lithosphere: The Refahiye Complex

The outcrop of the Refahiye Complex is shown in Figure 3.3. The unit is well exposed in several deeply incised gorges that feed the Erzincan pull-apart basin from the north. In the Erzincan area the Refahiye Complex exhibits the lower- to mid-level components of an ophiolitic pseudo-stratigraphy (Figure 3.4): However, extrusive rocks and epiophiolitic sedimentary rocks are missing, and no metamorphic sole is present. No age data are yet available for this unit.

A peridotite thrust sheet, including largely serpentinitised harzburgite, is exposed in the central and northern sections of the complex (Figure 3.5). Mafic/ultramafic cumulates (websterite, dunite and layered gabbro) occur as isolated outcrops or fault-bounded blocks and undeformed shear-pods within the sheared serpentinite. North and west of Erzincan, near the villages of İşikpınar and Tandırılı (Figure 3.5) gabbro, diabase sheeted dykes, plagiogranite bodies and rare andesite

dykes are found within fault blocks separated by sheared serpentinite. Lithologies from different parts of the ophiolitic pseudo-stratigraphy (i.e. peridotite, cumulates and intrusives) are commonly tectonically mixed at outcrop-scale, occurring as trains of blocks, imbricated sigmoidal shear-pods or lozenges up to ~50 m long commonly within a matrix of sheared serpentinite (Figures 3.6 to 3.8). Sheeted dykes are best exposed within an internally deformed thrust sheet extending for >10 km west of Erzincan. The diabase dyke complex contains abundant screens of metamorphic rocks in the southwestern part of the complex (Figures 3.5 and 3.9). Thus, while the Refahiye Complex contains an ophiolitic rock assemblage the Complex does not strictly match the formal definition of an ophiolite (Anonymous 1972). The older metamorphic host is intruded by dense swarms of diabase dykes (<2 m thick), and thin isolated dykes containing aplite, trondjemite and pegmatitic gabbro (<1 m thick). Diabase and plagiogranite (trondhjemite) dykes are found as isolated intrusive bodies at all levels within the complex (Figure 3.4).

Although displaying evidence of intense polyphase deformation (section 3.3.1) the unit retains a degree of structural coherence and can be divided roughly into east-west trending lithological associations (Figure 3.5). The massive harzburgitic tectonites generally crop out furthest to the north; the central zone comprises a tectonic mixture of isolated diabase and plagiogranites (trondhjemite) dykes, layered cumulates and gabbro; the southern zone contains mainly diabase and metamorphic host rocks. Thus, the northern part of the ophiolitic complex comprises the lithologies of the lithospheric mantle, whereas the southernmost part exposes a upper-mid crustal section with metamorphic screens.

3.3.1 Structure

At outcrop-scale, the whole unit displays a pervasive north-vergent shear fabric (Figure 3.12). North and east of the Erzincan Basin the deeper parts of the unit are imbricated by north-dipping (top-to-the-south) thrusts on a large scale (tens of kilometres long thrust sheets) with metamorphic basement units of the Pontides (Figures 3.3 and 3.5). North-dipping thrust faults also separate kilometre-scale thrust slices within the ophiolitic complex (Figures 3.5 and 3.10). The Refahiye Complex

exhibits strike-slip shear-zones. The unit is bounded above and below by south-vergent shear zones.

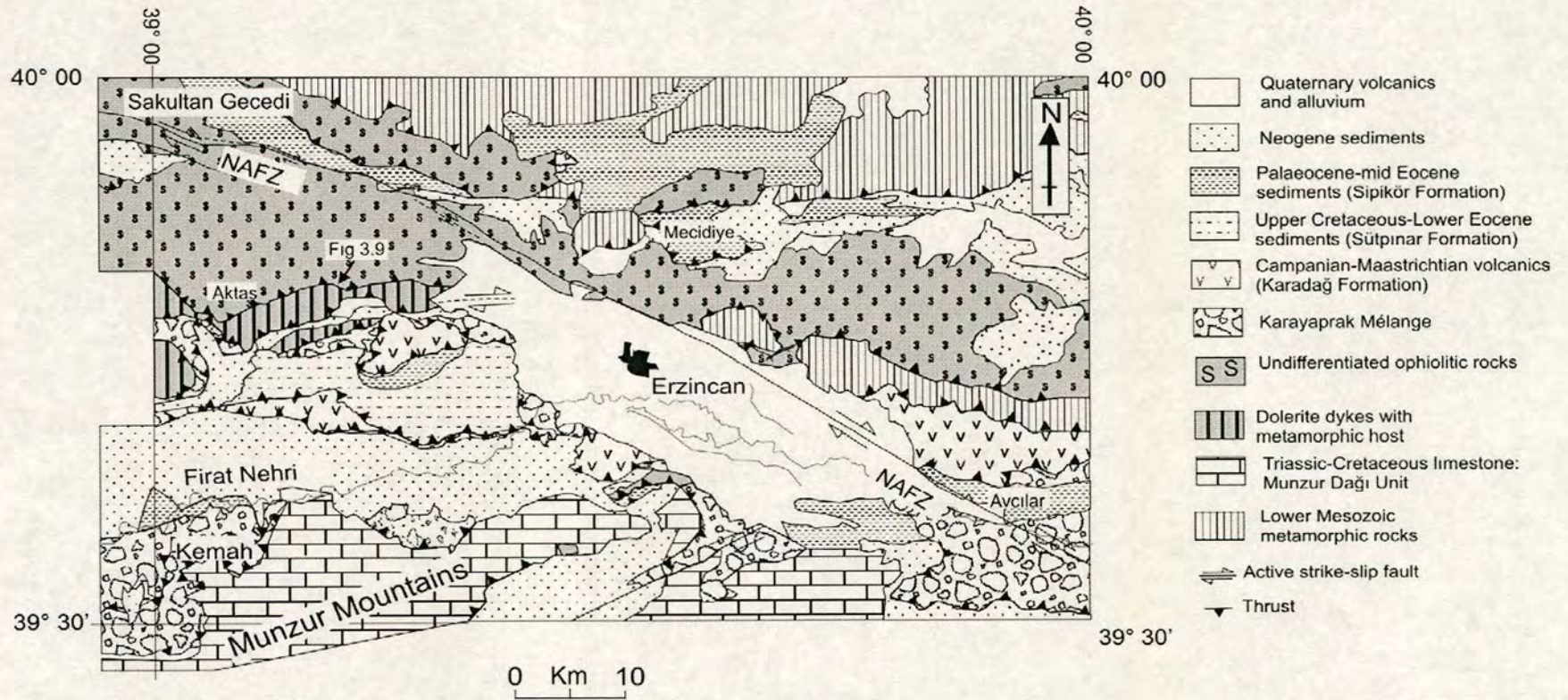


Figure 3.3. Simplified map of the Erzincan area to show outcrop of the Refahiye Complex.

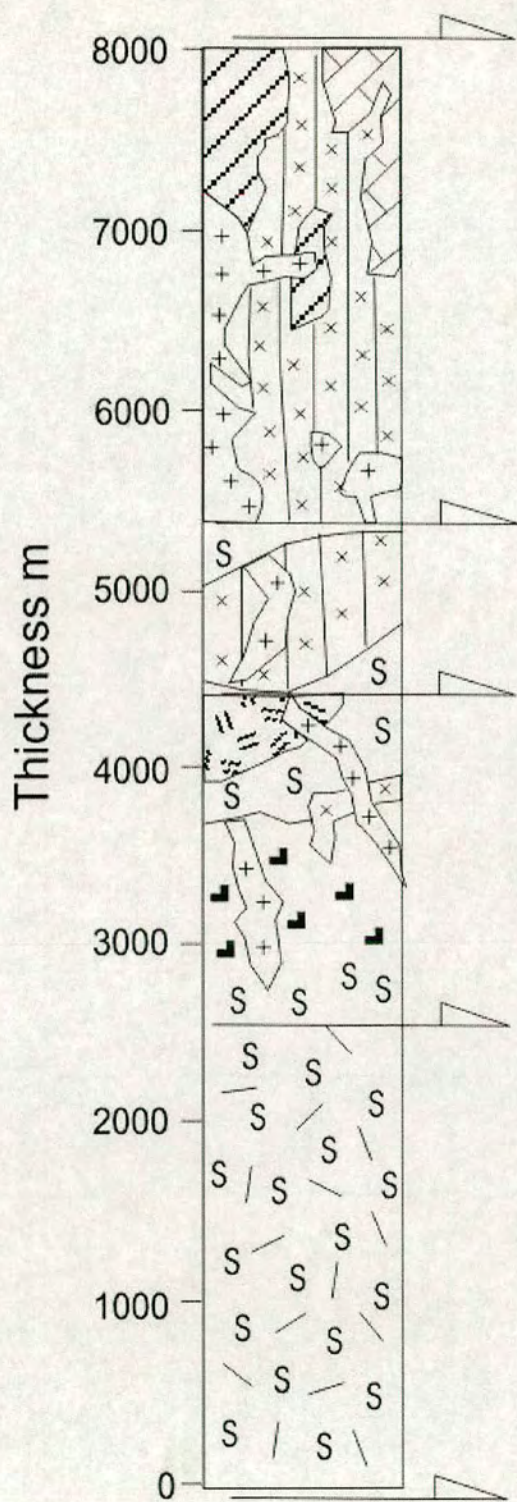


Figure 3.4. Composite log of the Refahiye Complex.

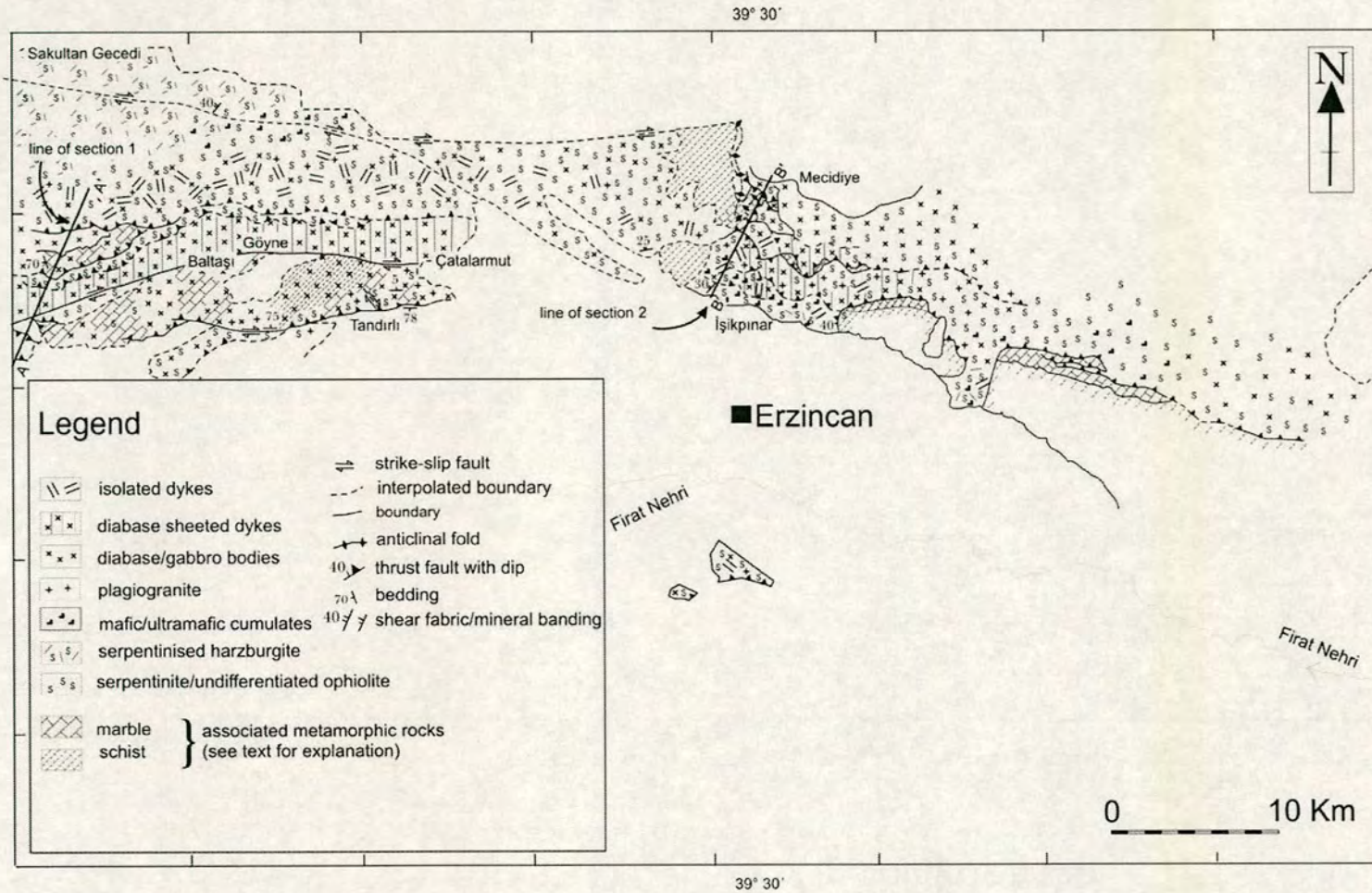


Figure 3.5. Geological map of the Refahiye Complex. Locations of sections 1 and 2 (shown in Figures 3.10 and 3.11) are given.

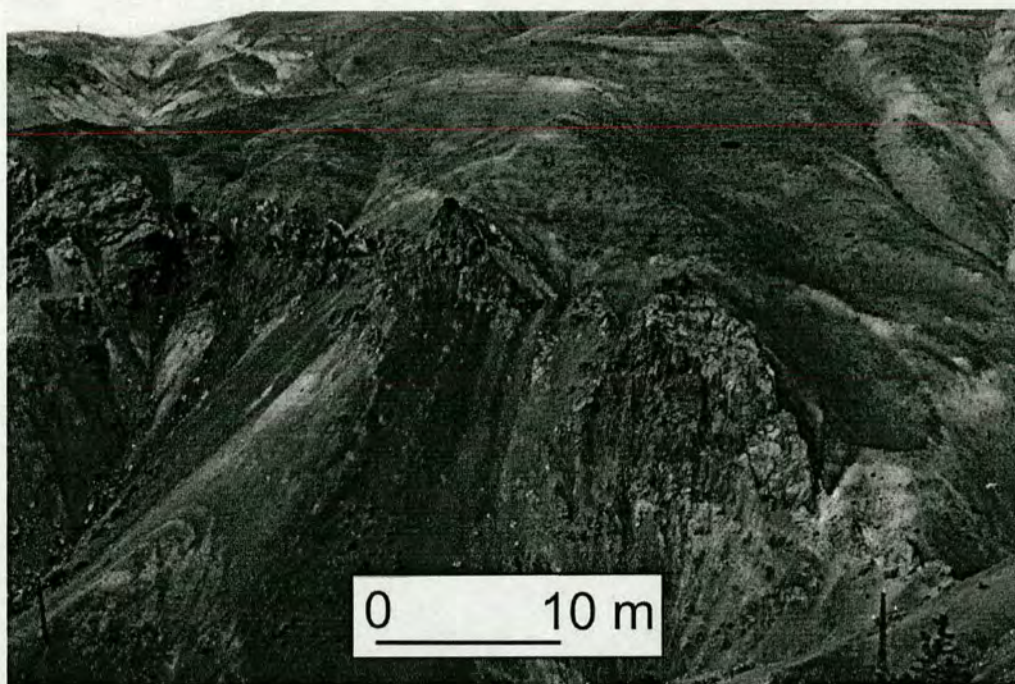


Figure 3.6. Train of blocks of marble and schist within sheared serpentinite (near Handere 5 km west of Işıkpınar (Figure 3.5).



Figure 3.7. Equant tectonically abraded blocks of serpentinitised harzburgite and diabase in sheared serpentinite (near Tandırılı; Figure 3.5).

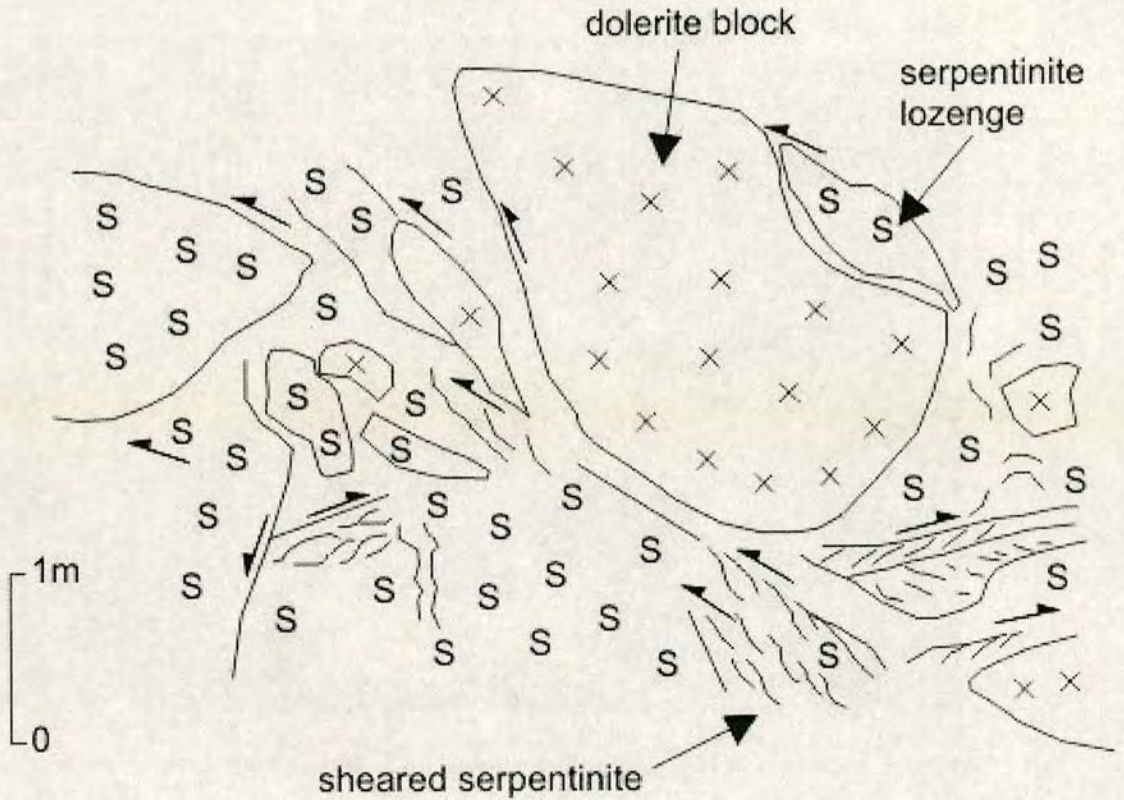


Figure 3.8. Field sketch of a typical exposure of the Refahiye Complex near İşikpınar.

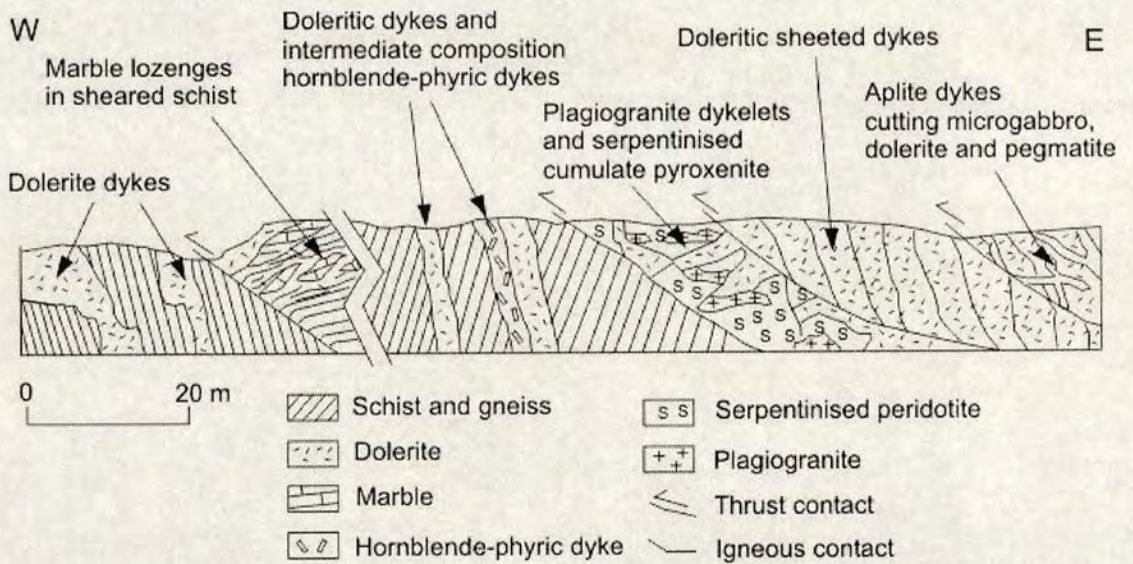


Figure 3.9. Field sketch near Göyne showing intrusive relationships and metamorphic screens in the Refahiye Complex. See Figure 3.3 for location.

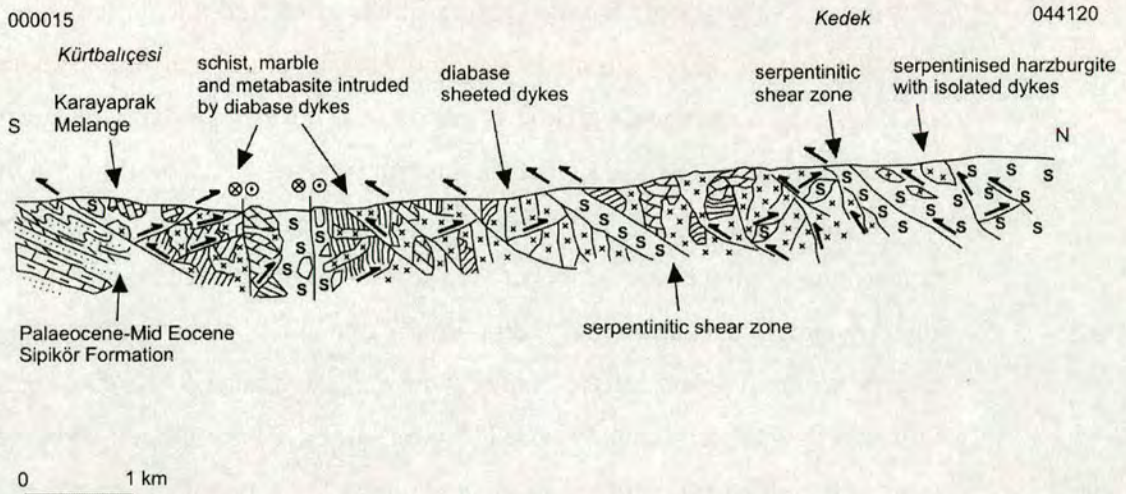


Figure 4.10. Section 1. See Figure 4.5 for location.

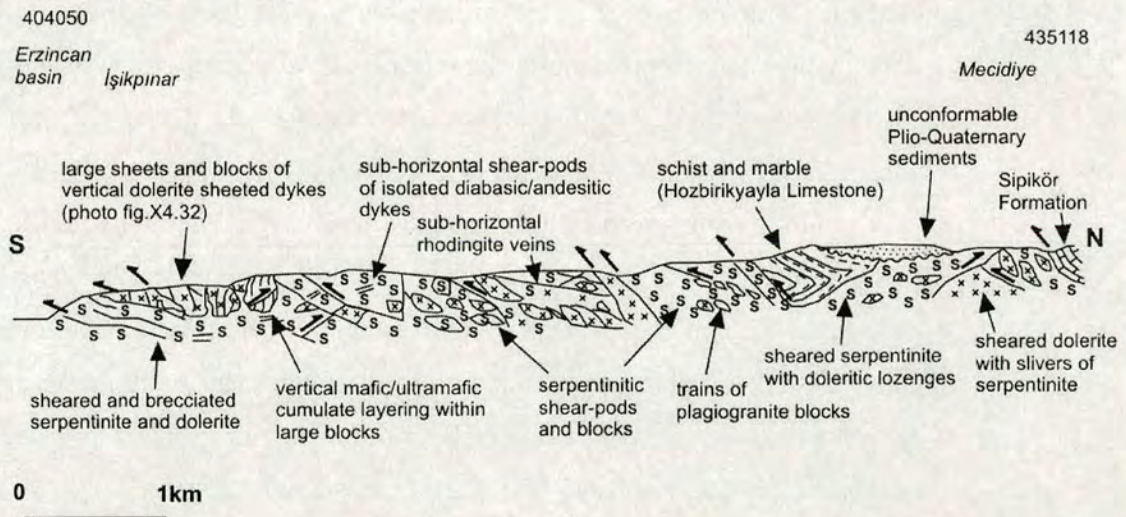


Figure 4.11. Section 2. See Figure 4.5 for location.

Harzburgites within the Refahiye Complex exhibit a foliation formed by the alignment of orthopyroxene crystals and aggregates of chromite. The foliation in harzburgite dips moderately to the north and northwest (Figure 3.13**Reference source not found**). The contact between harzburgite and gabbro (the 'petrological Moho') is exposed at Işıkpınar (Figure 3.5) dipping 80°S/105°. Mineral layers in gabbro are sub-vertical and dominantly strike NE-SW to E-W (060°-165°; Figure 3.13a). Chilled margins of sheeted dykes are steeply inclined to the north and

northwest and exhibit a range of strike orientations (Figures 3.13 and 3.14). Isolated dykes are generally steeply inclined and exhibit no preferred orientation.

The harzburgitic tectonite is commonly serpentinised and strongly sheared (Figure 3.12). Discrete shear zones exhibit c-s fabrics and slickensides that indicate a range of cross-cutting relations and kinematic directions. A pervasive top-to-the-north shear fabric is associated with discrete shear zones that exhibit a top-to-the-north c-s fabric, south-dipping thrust faults with top-to-the-north slickensides that form duplex structures and, reidal shears (north-dipping). A folded top-to-the-north mylonite was observed within diabase. Most commonly the pervasive shear fabric dips gently south although its orientation is varied (Figure 3.13c). Top-to-the-north shear fabric is seen to be folded and faulted by later structures. The top to the north structures are widespread and are commonly cut by top-to-the-south thrusts and shear zones. Top-to-the-north shear is preserved within north-dipping thrust horses of a top-to-the-south duplex structure exposed west of Erzincan near Çatalarmut (gr: İ42, 245066). Commonly blocks retaining a top-to-the-north shear fabric are set within a highly sheared tectonic matrix exhibiting a top-to-the-south fabric, e.g. near Tandırlı (Figures 3.5 and 3.7) and Göltepe (gr: İ43, 438869).

Top-to-the-south thrusts and shears dip northwards. Their measured orientations are shown in Figure 3.13c. Major north-dipping top-to-the-south thrusts are seen at the base and top of the Refahiye Complex where they juxtapose the Refahiye Complex against other units. Top-to-the-south shear zones are spaced ~1 m apart within the sheeted dyke complex 5 km north of Erzincan. The top-to-the-south shear fabric is pervasive and sub-horizontal near Işıkpınar (Figure 3.5). Asymmetrical south and east-vergent folds were seen to fold the top-to-the-north shear fabric in several places. These folds have recumbent to gently inclined axes and are disharmonic. Metamorphic segregation was observed in metabasic rocks adjacent to major top-to-the south shear zones.

Sub-vertical strike-slip faults exhibiting both dextral and sinistral slickensides and C-S fabrics cut all of the above structures. The orientation of strike-slip faults is shown in Figure 3.13c and b.

Top-to-the-east and top-to-the-west structures and shear fabrics are common in the Refahiye Complex. These tend to exhibit complex cross-cutting relationships.

Metamorphic host rocks within the Refahiye Complex (Figure 3.9) exhibit a sub-vertical cleavage striking NW-SE (Figure 3.16). The structure in the metamorphic rocks is coherent and cleavage is commonly sub-parallel to gneissose banding and bedding where these were observed. Stretching lineation and crenulations are sub-vertical. The NW-SE structural grain in the metamorphic rocks is roughly normal to the dominant structural grain in the ophiolitic rocks. Cleavage in the metamorphic rocks is cut by intrusive and tectonic contacts with the ophiolite, including top-to-the-north thrusts.

No relationship was directly observed between the foliation in harzburgite and the grain of the metamorphic host rocks. The NW-SE structural grain within the metamorphic host rocks, orientated roughly normal to the overall structural grain of the ophiolite, is cut by top-to-the-north thrusts and intrusive contacts. The grain of the metamorphic rocks, therefore, pre-dates ophiolite genesis and the top-to-the-north deformational event. The earliest deformational structure within the ophiolitic rocks of the Refahiye Complex is seen in harzburgitic tectonite and is an S-tectonite fabric (Hobbs et al. 1976) common in alpine-type peridotites. The foliation in the harzburgitic tectonite is interpreted as an inherited mantle flow fabric (Nicolas 1989). The top-to-the-north deformational event gave rise to a pervasive shear-fabric and associated top-to-the-north thrusts. Structures associated with this phase of deformation trend ENE-WSW (Figure 3.15) and are likely to have developed as a result of emplacement of the ophiolite northwards onto the Eurasian margin. The emplacement direction is interpreted to have been from the SSE towards the NNW. The next deformation produced south-directed thrusting, shearing and folding of previous structures. Structures exhibiting a top-to-the-south sense of motion trend NE-SW and NW-SE. Rocks adjacent to major top-to-the-south serpentinite shear zones are metamorphosed. This probably reflects the high activity of water (AH_2O) near the shear zone but also suggests that shearing was likely to have occurred at elevated pressure and/or temperatures, possibly at mid crustal depths (Best 2002). The top-to-the-east and top-to-the-west structures that were observed may be related to these phases of deformation and may indicate transpressional (oblique) deformation. All the previous structures are cut by sub-vertical strike-slip faults. NNW-SSE strike-slip faults are orientated at a low angle to the trend of the North

Anatolian Fault Zone. Some of the strike-slip and normal faults that cut the Refahiye Complex may be related to the North Anatolian Fault Zone (Chorowicz et al. 1999). Older strike-slip faults may also be present.



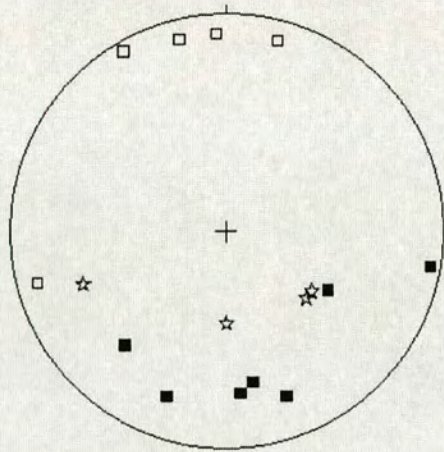
Figure 4.12. Pervasive north-vergent shear-fabric in serpentinised harzburgite. Photo taken near Handere, ~4 km east of Işıkpınar (Figure 3.3, 3.5).

3.3.2 Peridotites

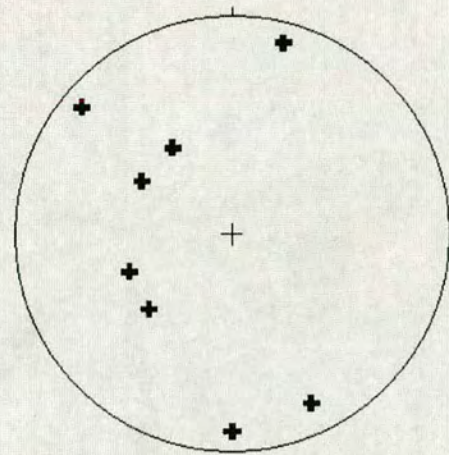
An extensive thrust sheet of deformed and serpentinised peridotite crops out north and west of Erzincan (Figure 3.5) and comprises ~ 75% of the Refahiye Complex. Serpentinised peridotite dominates the central and northern parts of the outcrop and is tectonically imbricated on a large scale with older basement units of the Pontides to the northeast of the Erzincan Basin (Figure 3.3). The peridotite is intruded by isolated plagiogranite (trondhjemite) and diabase dykes.

Hydrothermal (metasomatic) alteration of the ultrabasic rocks has largely replaced the original mineralogy with serpentine group minerals. The degree of serpentinisation is locally variable. In places patchy alteration was observed on the

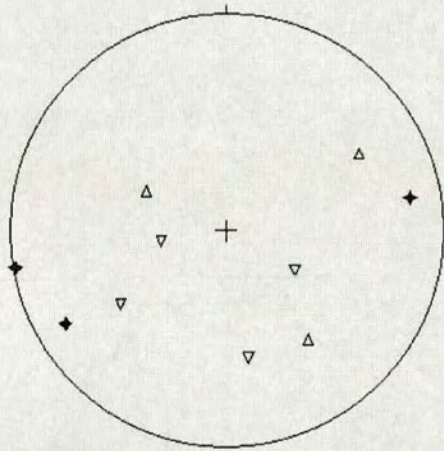
a) ophiolite genesis-related



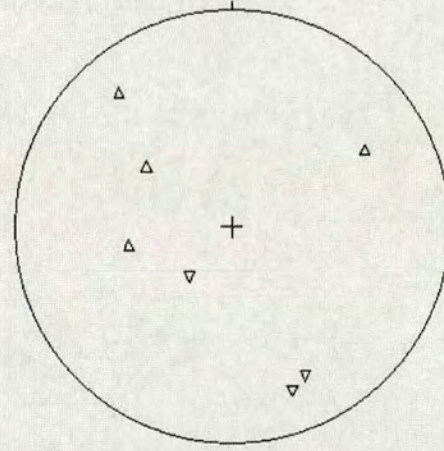
b) isolated dykes



c) shear fabrics



d) thrust faults



- ☆ poles to foliation in harzburgite
- poles to layers in gabbro
- poles to sheeted dyke chilled margins
- △ poles to top-to-the-north shear fabric
- ▽ poles to top-to-the-south shear fabric
- ◆ poles to strike-slip shear fabric

Figure 3.13. Equal-area plots (Lambert/Schmidt) showing structural data for the Refahiye Complex.

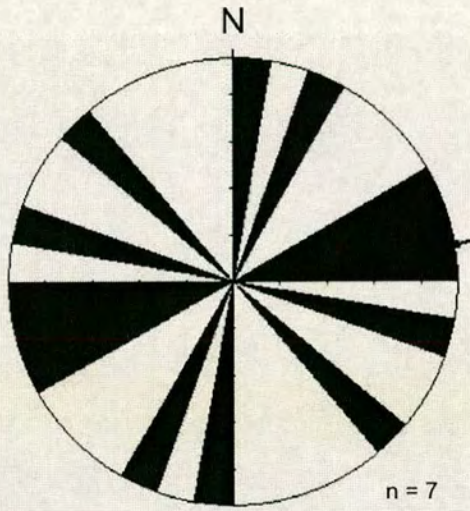
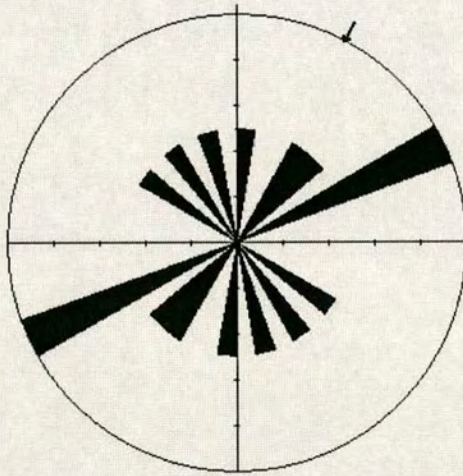


Figure 3.14. Rose diagram showing strike orientation of chilled margins in the sheeted dyke complex within the Refahiye Complex.

a) Thrust faults



b) Strike-slip shears

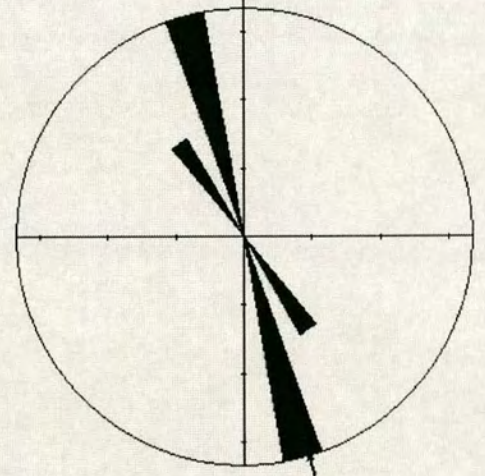


Figure 3.15. Rose diagrams showing strike orientation of fault planes within the Refahiye Complex.

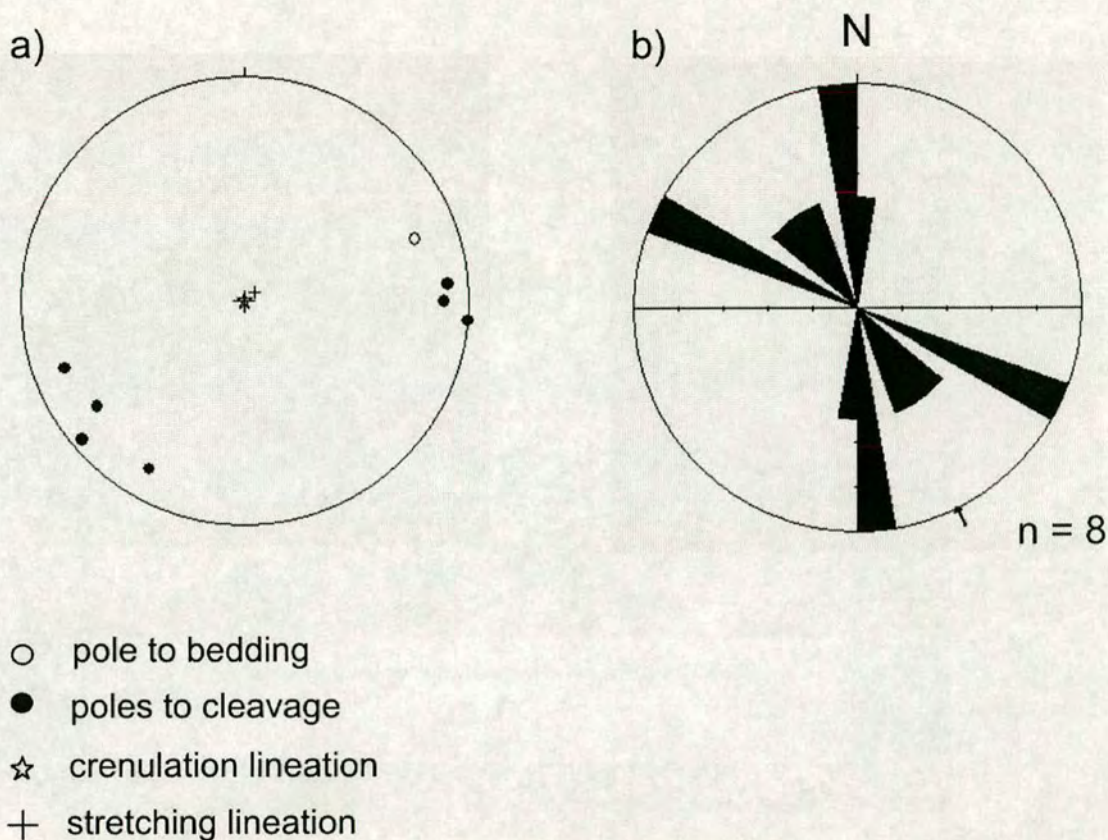


Figure 3.16. Structural data for the metamorphic host rocks within the Refahiye Complex. a) equal-area plot (Lambert/Schmidt); b) rose diagram showing strike orientations of cleavage planes.

scale of about 1 m. Where deformation is minimal the harzburgite is a hard, dark coloured rock with pale bluish weathered surfaces, a soapy feel and massive appearance. Relatively fresh surfaces exhibit a relict primary igneous texture of coarsely crystalline (~1.5 cm) dark brown bronzite and bastite pseudomorphs replacing orthopyroxene and black, brown or blue serpentine pseudomorphs after olivine. Primary igneous olivine or orthopyroxene crystals are rarely preserved intact. The only primary igneous mineral unaffected by the alteration are abundant small (~1 mm) black grains of accessory chrome spinel. The serpentine group minerals are not easily distinguished from each other without the use of X-ray techniques. In thin section the serpentine occurs as: 1) a mesh-textured pseudomorphic replacement of olivine (Figure 3.17); 2) platy pseudomorphs after

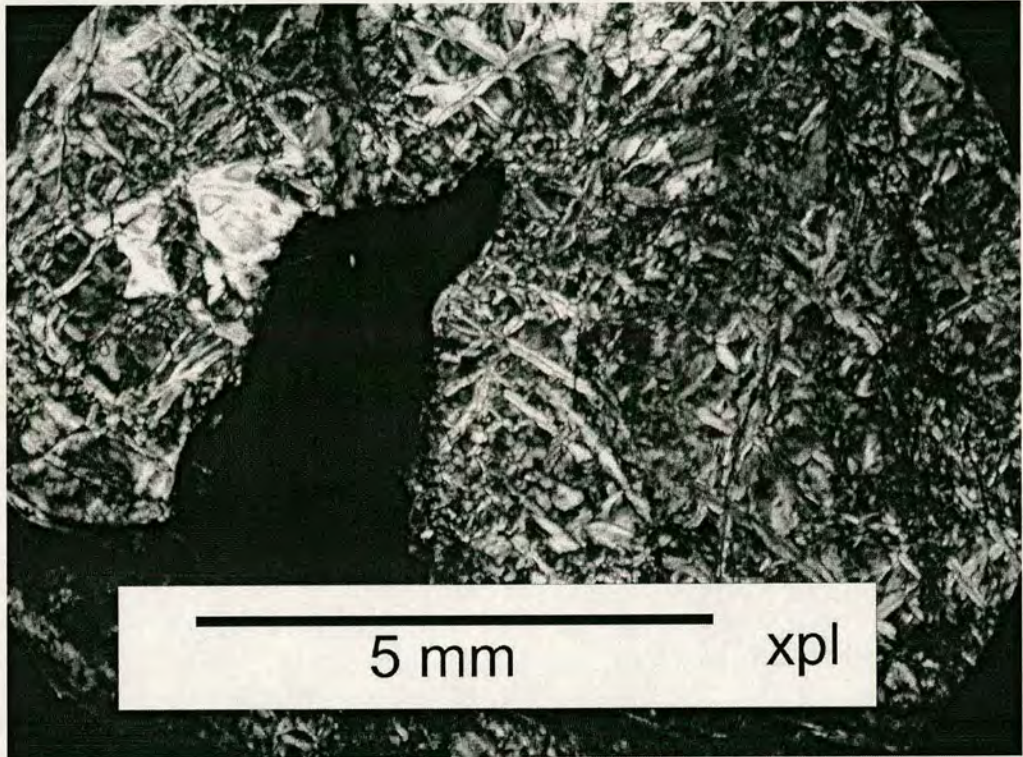


Figure 3.17. Photomicrograph of serpentined harzburgite from the Refahiye Complex showing mesh-textured pseudomorphic serpentine replacing olivine.

orthopyroxene (Figure 3.18) (bastite probably replacing enstatite/bronzite); and, 3) fibrous veins (Figure 3.19). Primary olivine and orthopyroxene are rarely preserved as complete crystals (up to 1.5 cm length); they commonly form remnant ‘blebs’, as seen in thin section (Figure 3.20).

Where present, the orthopyroxenes commonly display a lamellar structure with rows of flattened blebs of exsolved highly birefringent clinopyroxene, an occurrence known as pigeonite. Dark red chrome spinel crystals are ubiquitous and may be euhedral, partly resorbed or fragmentary (Figure 3.21). Secondary minerals other than serpentine are also present such as brucite, magnetite and hydromagnesite.

The harzburgite commonly exhibits a relict mineral foliation (S1) (Figure 3.22). S1 is a pervasive shear fabric, and the ophiolitic peridotite is, therefore, an S-tectonite. The S-tectonite fabric is commonly replaced by later deformational fabrics. An extensive (~30 km) outcrop of well preserved harzburgitic tectonite is

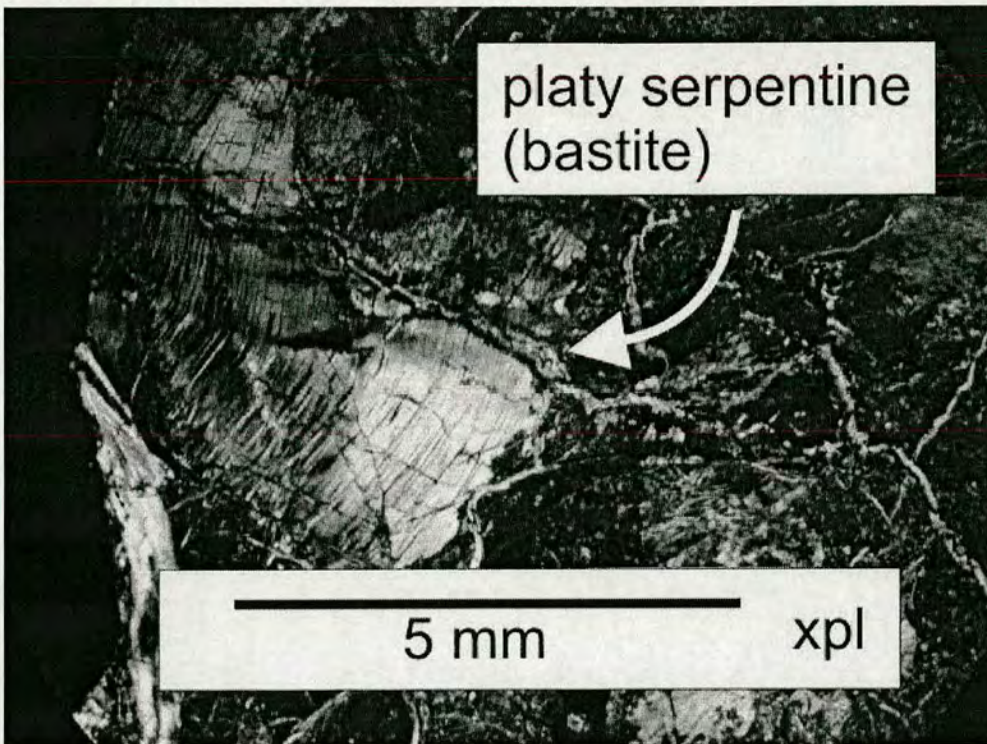


Figure 3.18. Photomicrograph of serpentinised harzburgite from the Refahiye Complex showing platy serpentine (bastite) replacing enstatite (orthopyroxene).

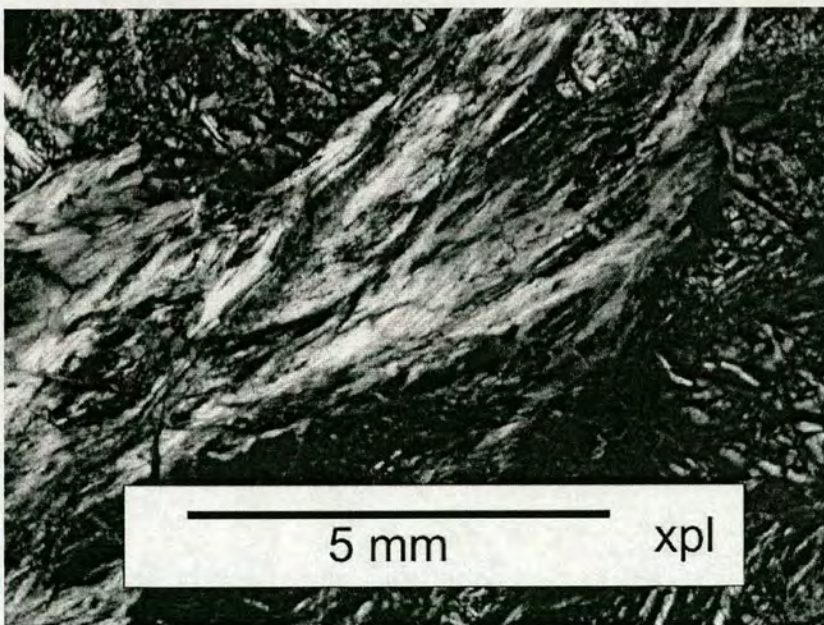


Figure 3.19. Photomicrograph of fibrous serpentine in serpentinised harzburgite from the Refahiye Complex.

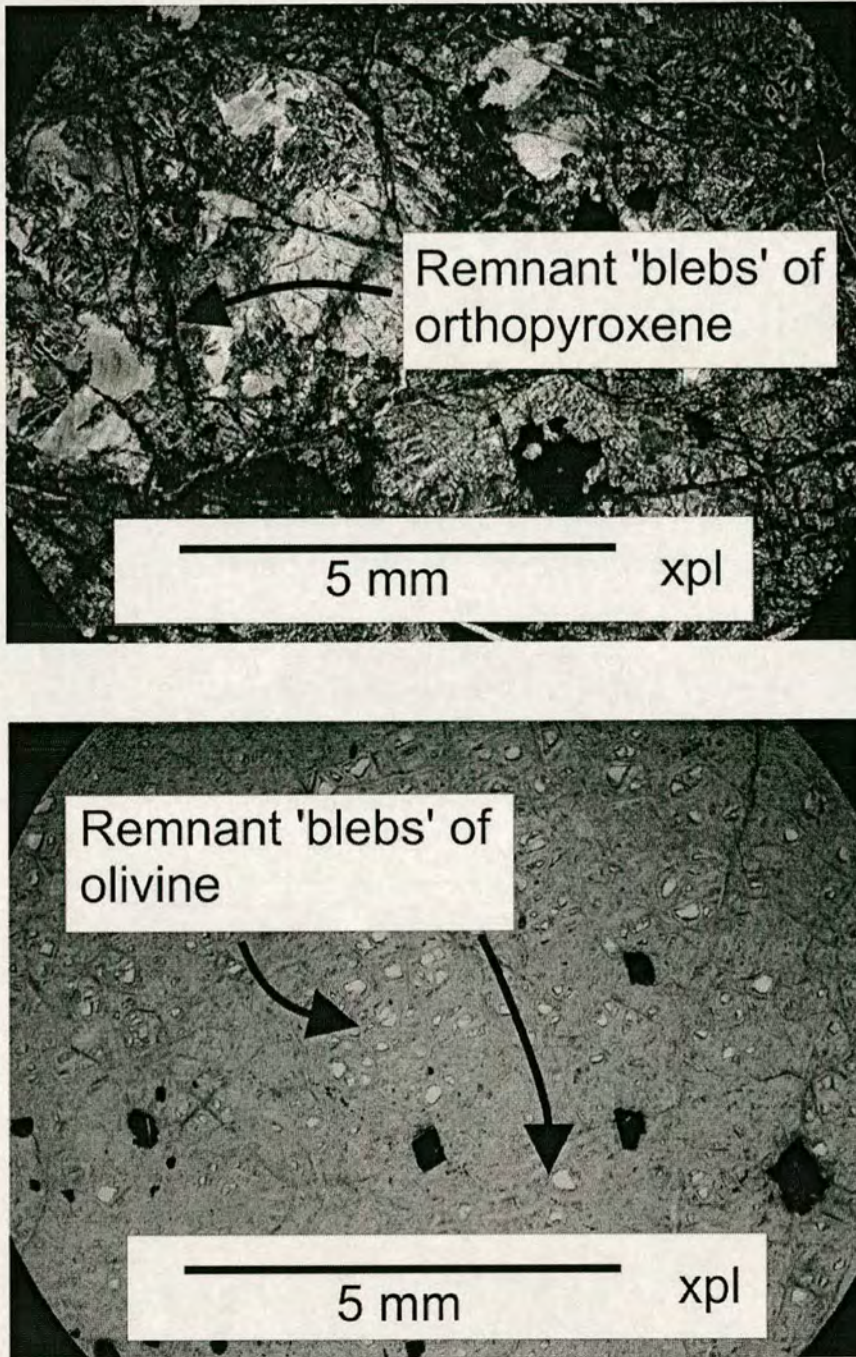


Figure 3.20. photomicrographs of serpentinitised hazburgite in the Refahiye Complex to show remnant blebs of primary orthopyroxene and olivine.

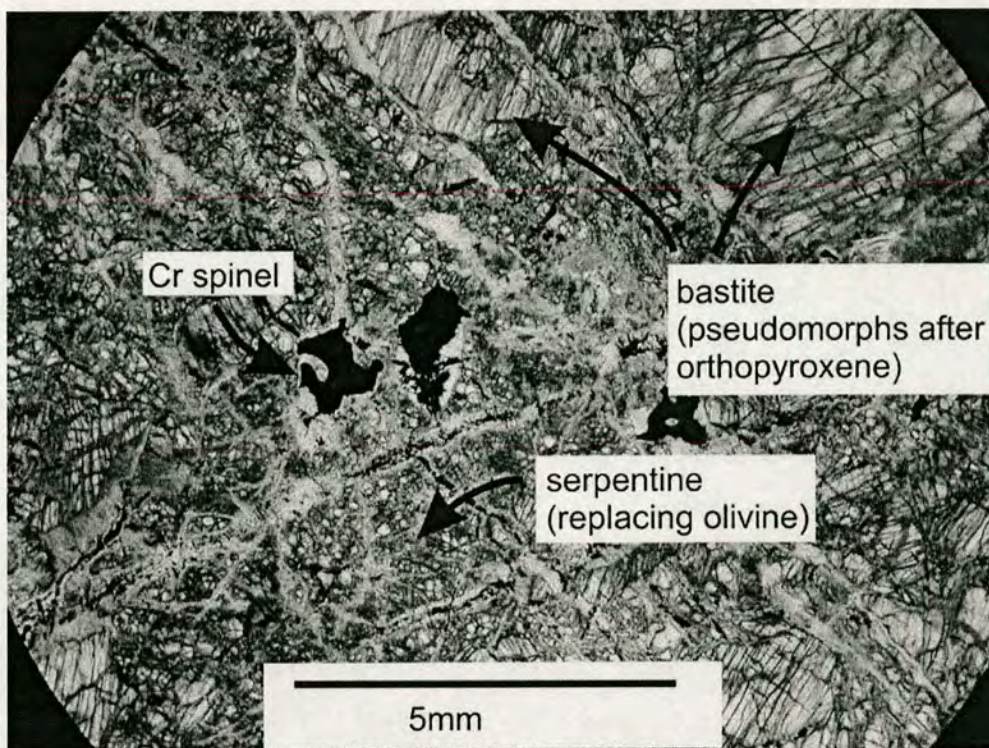


Figure 3.21. Photomicrograph of a typical serpentinised harzburgite of the Refahiye Complex with partially resorbed chrome spinel.



Figure 3.22. Photograph showing mineral foliation in harzburgitic tectonite along the E80 highway near Erzincan: preserved mantle flow-fabric.

exposed along the E80 highway 30 kilometres west of Erzincan (gr: İ42, 165152) where the mineral foliation was measured with the following trends: 35°N to 090°, 40°N to 040° and 40°N to 035°. 20 kilometres further southeast at Deryurt (gr: İ43, 370080), the flow fabric is locally variable but was measured at 75°N to 150°. However, in much of the ophiolitic complex the primary crystalline texture and mineral foliation has been destroyed by the development of later pervasive shear-fabrics (Figure 3.12). The more intensely serpentinised outcrops that commonly show more well-developed S2 and/or S3 shear fabrics are soft, fissile, and preferentially weathered. D2- and D3-deformed serpentinite is commonly present in discrete shear-zones (20 cm--~200 m). Where the unit is sheared, the primary texture of the peridotite is only preserved in undeformed shear-pods. S1, S2 and S3 fabrics are cut by brecciated and mineralised zones (10 m wide, up to ~1 km long) that contain anastomosing calcite, brucite, hydromagnesite, rhodinite dolomite and quartz veins.

The serpentinised harzburgitic tectonite represents the lowest part of the exposed ophiolitic pseudo-stratigraphy. The peridotite does not exhibit cumulate layering and is interpreted to represent residual lithospheric mantle from beneath the petrological Moho. The clinopyroxene-poor mineralogy of the harzburgite suggests the presence of a high depletion of the incompatible elements (e.g. calcium and aluminium). This depletion is consistent with the extraction of larger volumes of basaltic melt from the lithospheric mantle than is inferred to occur at normal mid-oceanic ridges, where clinopyroxene-rich lherzolites are representative of the lithospheric mantle (e.g. Bloomer et al. 1995; Dick and Bullen 1984; Nicholas and Le Pichon 1980; Boudier et al. 1988).

S-tectonite fabrics are commonly observed in ophiolitic peridotites and indicate ductile shearing at an oceanic spreading centre (e.g., Nicolas and Le Pichon 1980). The mineralogy, coarse igneous texture and S1 fabric indicate deformation and equilibration to mantle temperature and pressure conditions (Shipboard Scientific Party 2004 in: Keleman et al. 2004). Patchy replacement of the primary texture and mineralogy with hydrous phyllosilicates (serpentine) indicates that subsequent lower temperature hydrothermal activity followed. Preferential

serpentinisation within discrete, highly sheared zones (S2, S3) suggests that later, S2 deformation was synchronous with retrograde metamorphism and high fluid activity. Due to the abundance of phyllosilicates and hydroxides the serpentinite has low internal cohesion, low friction and low density and is capable of migrating along crustal weaknesses (Boudier et al. 1988), to form serpentinitic shear zones up to ~1 km wide, outside the outcrop area of the Refahiye Complex.

A later stage of hydrothermal mineralisation is recorded by veins, up to 10 cm thick that cut the deformational fabrics of the serpentinite. The presence of carbonate minerals (e.g., calcite, dolomite, hydromagnesite) in the ophiolitic peridotites indicates that late-stage carbonatization occurred at 200-300°C (Schandl and Wicks 1993). Late meteoric fluids more readily pervade the rock along sheared zones and react with the serpentine, forming clay minerals within the highly sheared zones (Boudier et al. 1988).

3.3.3 Cumulates

Cumulates are well exposed in the deeply incised gorges on the northern flanks of the Erzincan pull-apart basin (Figure 3.3, 3.5). The cumulates crop-out in the middle of the complex, generally occurring between the outcrops of gabbro and sheeted-dykes to the south, and the serpentinised harzburgite to the north. Basic-ultrabasic layering was observed in fault-bounded blocks and sigmoidal shear-pods within exposures of sheared serpentinite that also contain fragments of other ophiolitic lithologies (peridotite, gabbro, diabase dyke swarms, isolated diabase dykes and plagiogranite dykes). Sub-vertical dykes of microgabbro (~5 m) and hornblende-phyric andesite (<2 m) intrude the cumulates sub-parallel to the steeply oriented layering (observed at Işıkpınar (Figure 3.3)).

The layers (~1 cm-2 m thick) are coarse-grained (2-3 cm) monominerallic adcumulates of olivine (dunite) or pyroxene (pyroxenite), or polyminerallic orthocumulates of olivine, pyroxene, plagioclase and accessory oxides that form thin layers of dunite, harzburgite, lherzolite, and pyroxene-rich gabbro. Dunite is commonly red due to replacement of olivine by iddingsite. Serpentine also commonly replaces olivine and pyroxene. Orthocumulates were seen to contain needles of fresh black pyroxene, up to 3 cm long. Despite the intense thrust faulting

and shearing a degree of local structural consistency is shown by locally constant sub-vertical orientation of cumulate layers in different fault blocks (e.g. 80°S/076°).

The cumulates are interpreted as crystal concentrates that formed by fractional crystallisation of a basic magma body (Hall 1996). The volume of cumulates present (10%) implies that the body of basic magma remained at high temperature for a considerable period of time. Olivine, orthopyroxene and plagioclase were all liquidus phases. The melt continued to crystallize olivine, pyroxene and plagioclase and may have been repeatedly replenished. It is likely that the magma body formed by partial melting of the peridotites and was the source of diabase and plagiogranite within the Refahiye Complex.

3.3.4 Gabbro

Isotropic gabbro occurs as isolated outcrops and fault-bounded blocks in the central part of the complex north and west of Erzincan. Massive and coarse-grained (>5 mm) gabbro comprises <10% of the Refahiye Complex. In thin section interlocking crystals of clinopyroxene (<45%), plagioclase (<45%) and magnetite (10-25%) +/- pale green amphibole (<45%) are seen (Figure 3.23). Grains of plagioclase (labradorite) are mostly turbid. Pale green amphibole and bastite (serpentine) pseudomorphs commonly replace the pyroxene, and in some samples these have thick chlorite rims. Some samples contain anhedral, partially resorbed blebs of primary clinopyroxene adjacent to feldspar. Another petrographic feature is the presence of fibrous pale green hornblende pseudomorphs after clinopyroxene. Chlorite, iddingsite and serpentine pseudomorph rare olivine crystals.

The anhedral texture of primary clinopyroxene crystals could have formed during re-equilibration of the gabbro at lower temperature than its initial crystallisation. The replacement of primary igneous pyroxene by fibrous pale green amphibole resulted from a late-stage hydrothermal process known as 'uralitization' (Allaby and Allaby 1990), or alternatively from low-grade hydrous metamorphism. Fluid activity is further evidenced by the turbid feldspars, clay mineral rims and pseudomorphs of hydrous phyllosilicates (chlorite, iddingsite and serpentine).

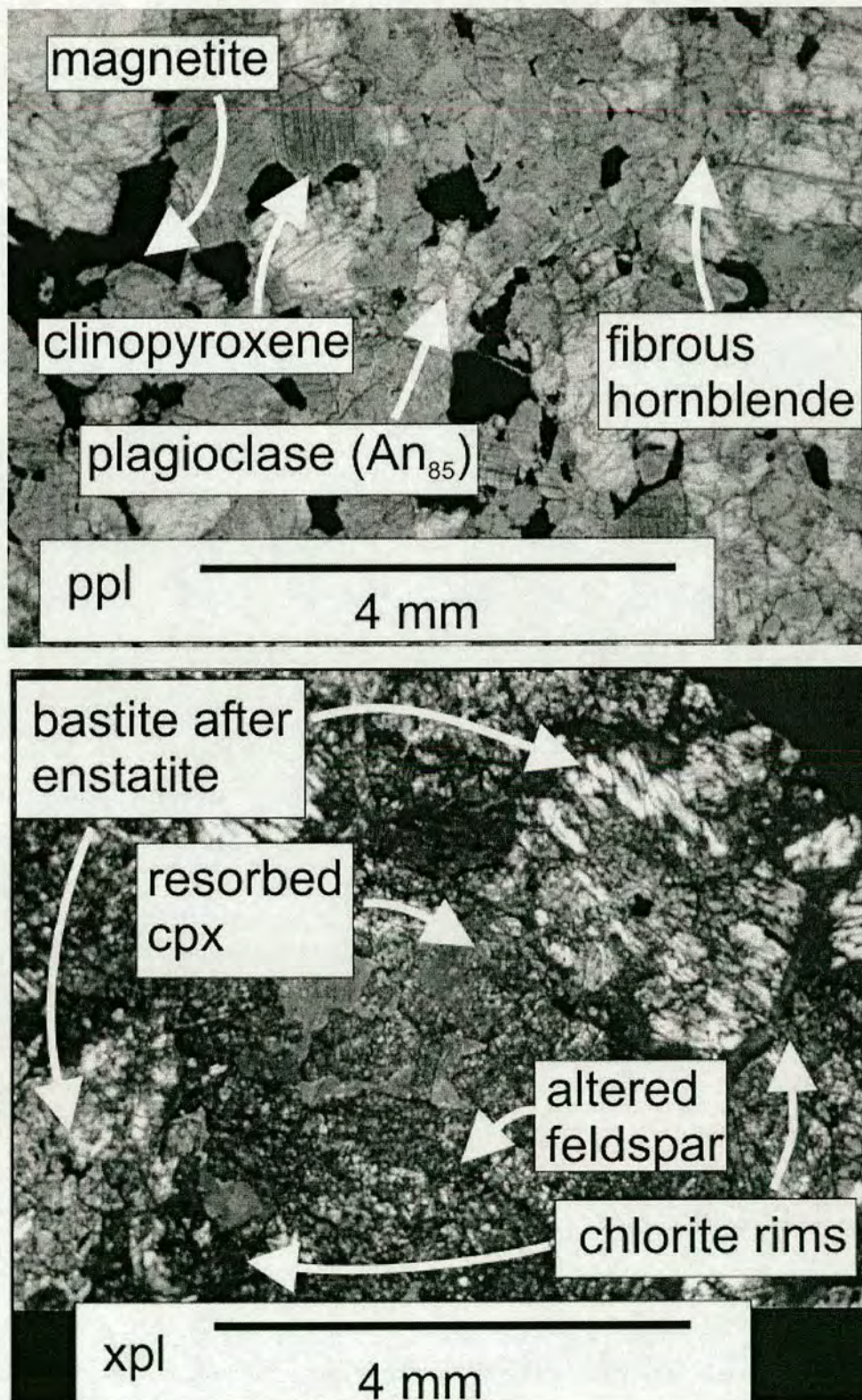


Figure 3.23. Photomicrographs of gabbro from the Refahiye Complex.

3.3.5 Sheeted diabase dykes

South of the T80 Highway an extensive outcrop (~5 km wide) of sheeted dyke complex extends west of Erzincan towards Aktaş village and beyond (Figure 2.2 and 3.3). The southern part of this complex exhibits metamorphic screens, whereas more northerly sections contain 100% dykes (Figure 3.5). In the southern part of the complex the dyke swarms exhibit chilled margins against metamorphic host rocks. Individual dykes are ~1.5 m thick. Dyke contacts commonly trend roughly E-W or NW-SE, although the trend is highly variable. The rock is medium grained (~1 mm), with visible crystals of white feldspar, green amphibole and, less commonly, grey pyroxene. Large blocks and shear-pods (up to ~75 m long) of multiple dyke swarms are found within a host of sheared serpentinite north of Erzincan (e.g. Işıkpınar, Figure 3.5) where rare thin screens of chert were seen between the dykes.

In thin section (Figure 3.25), the diabase is seen to contain ~50% actinolite replacing clinopyroxene, ~50% feldspar (primary labradorite An₆₀ and secondary albite). Some samples are slightly porphyritic, with small phenocrysts (<0.5 mm) of turbid albite. The feldspars are turbid or altered. Actinolite has been partly replaced by chlorite. An ubiquitous accessory opaque oxide phase (magnetite?), rare sphene and, secondary calcite crystals were also observed.

The aphyric doleritic texture of the sheeted dykes indicates coeval crystallization of both plagioclase and pyroxene together in roughly equal proportions. The magma did not fractionate at low temperature but rose rapidly from depth to the cool upper crust. The turbid texture of the feldspar, replacement of labradorite by albite (spilitization) and, of pyroxene by actinolite (uralitization), together with chlorite indicates greenschist facies, hydrous metamorphism, or late-stage hydrothermal alteration. Experimental data (Mottl 1983) and observations from the Sarmiento ophiolite, Chile (Elthon and Stern 1978) suggest that the observed metamorphic assemblage is likely to have formed by reaction with seawater at approximately 200-450°C and 500-600 bars. These observations are compatible with

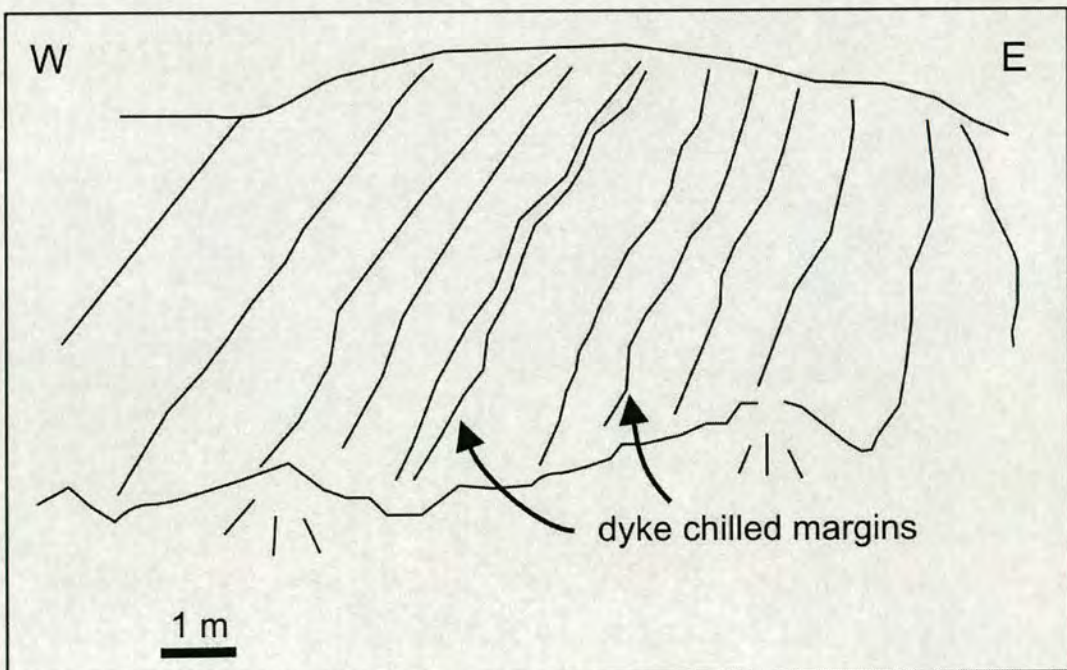
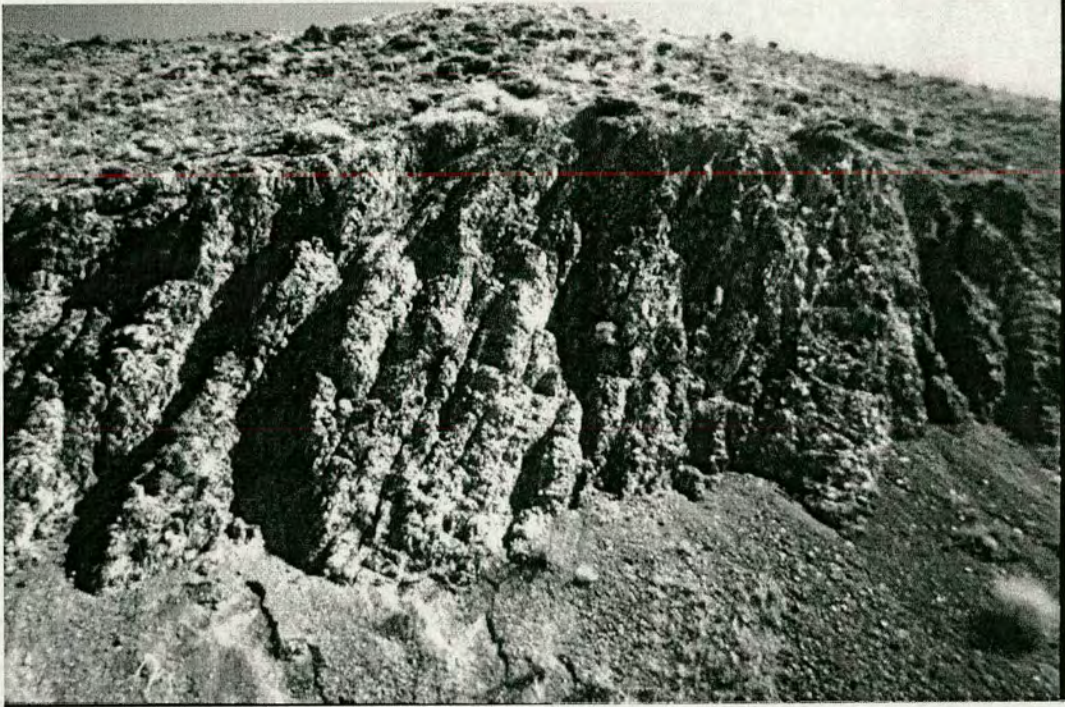


Figure 3.24. Photograph and sketch of sheeted dykes exposed north of Erzincan near Isikpinar.

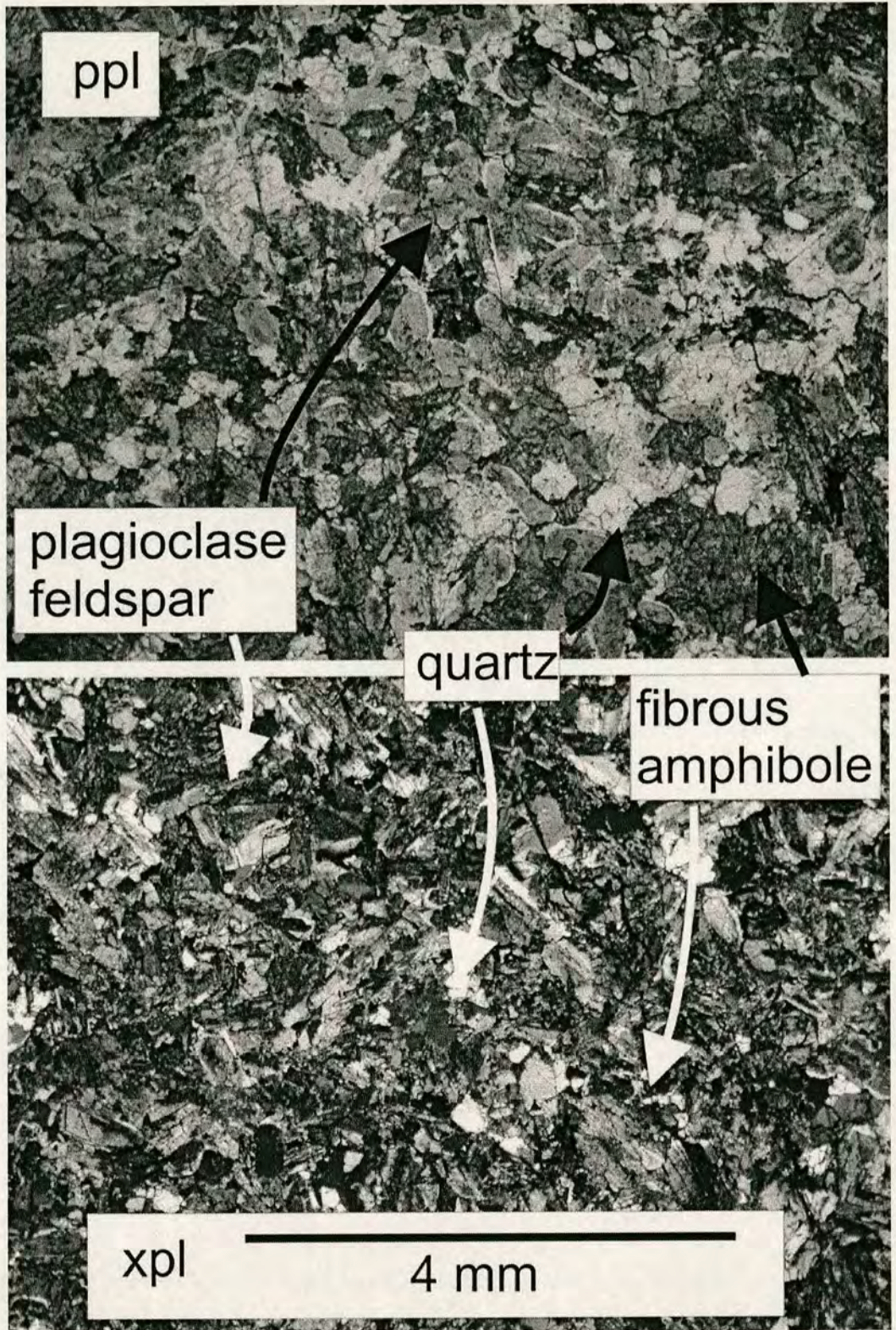


Figure 3.25. Photomicrograph of diabase from sheeted dyke complex.

sea-floor hydrothermal metasomatism of the mid- to shallow-level oceanic crust (Elthon and Stern 1978; Mottl 1983).

3.3.6 Isolated intrusions

The serpentinised harzburgitic tectonite, gabbro and the metamorphic host rocks are intruded by isolated plagiogranite (trondhjemite), diabase and rare aplite and andesite dykes (0.15 m-10 m). The isolated dykes commonly occur as trains of pulled-apart blocks which may be roughly equant, imbricated boudins, imbricated sigmoidal blocks, or lozenges in a matrix of fissile sheared serpentinite (Figure 3.26). The edges of some blocks exhibit a baked margin of metaserpentinite without a shear fabric. Isolated intrusions are found with chilled contacts against metamorphic basement, layered cumulates and sheeted diabase dykes. Some fault-bounded blocks contain fragmented swarms of dykes with evidence of multiple intrusion events; isolated intrusions commonly exhibit relatively undeformed but irregular igneous contacts. Igneous contacts were also observed between the various late-stage intrusions (aplite, diabase and plagiogranite).



Figure 3.26. Imbricated lozenges of isolated diabase and plagiogranite intrusions within a matrix of highly sheared serpentinite, south of Erzincan (gr: İ43, 435875).

3.3.6.1 Plagiogranite dykes

Plagiogranite (trondhjemite) dykes are small (<3 m) but fairly abundant within the Refahiye Complex (~5%). Plagiogranite bodies are commonly irregular and intrude peridotite, diabase and metamorphic hosts. These rocks are fine-grained with ~5% small (~1 mm) plagioclase phenocrysts in a groundmass of plagioclase and quartz.

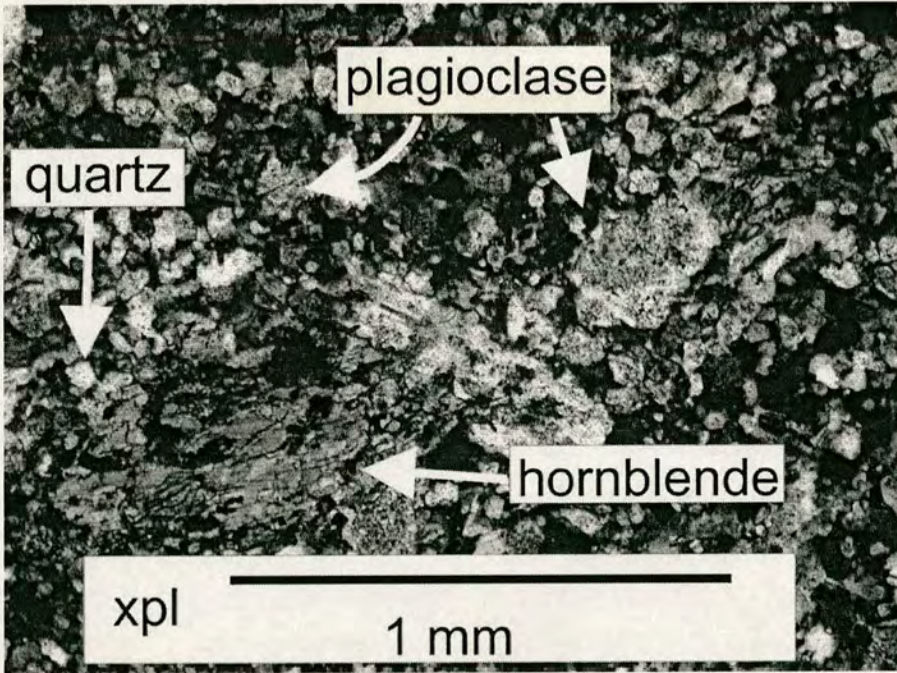


Figure 3.27. Photomicrograph of plagiogranite from an isolated intrusion within the Refahiye Complex.

3.3.6.2 Isolated diabase dykes

Diabase dykes are seen with chilled margins against plagiogranite, metamorphic and ultrabasic host rocks. These are fine- to medium-grained and contain ~50% plagioclase and up to 50% secondary actinolite, which, together with minor amounts of bastite, have completely replaced primary pyroxene (orthopyroxene (enstatite); Figure 3.28). Minor amounts of chlorite and epidote are also present. Plagioclase crystals are turbid.

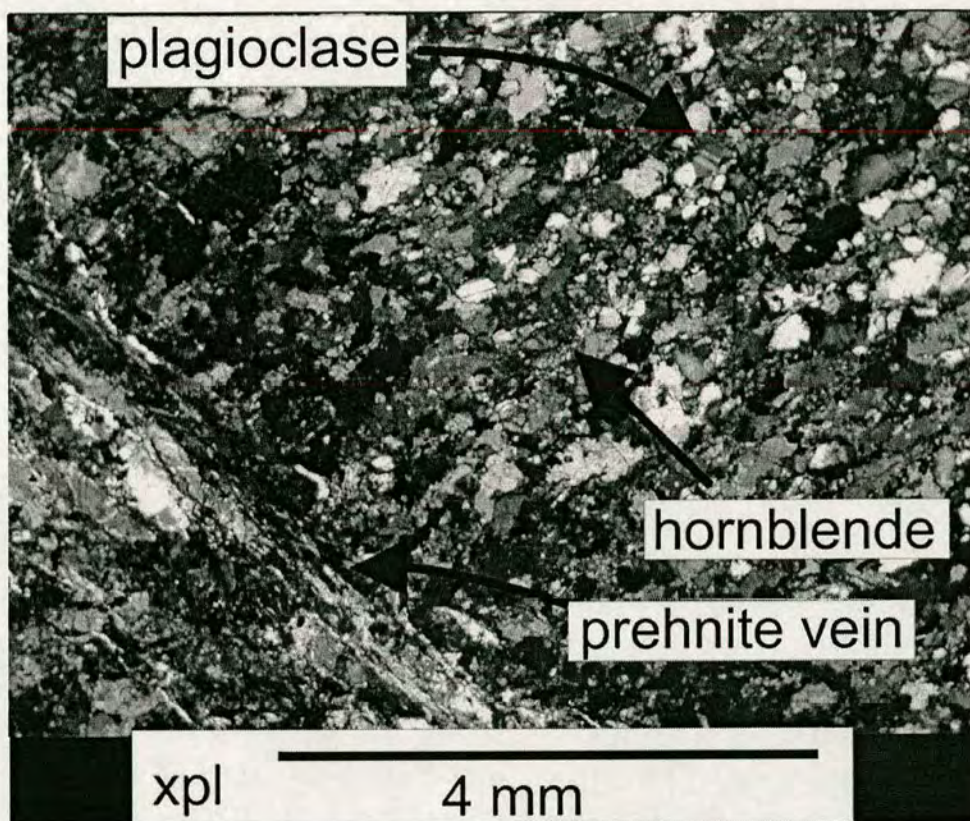


Figure 3.28. Photomicrograph of uralitic diabase from an isolated intrusion within the Refahiye Complex.

3.3.6.3 Late-stage aplite dykes

Aplite dykes (2 cm to 2 m across) with needles (~5 mm) of black amphibole, set in a fine-grained pale greenish-grey groundmass, occur as fragmented isolated bodies with the ultramafic and metamorphic host rocks described above. Chilled margins against trondhjemite and diabase dykes were again observed, suggesting late-stage emplacement of the aplite dykes.

More silica-rich rock compositions do not alter to hydrous phyllosilicates such as serpentine, which are more readily deformed (Best 2003). Thus, the silica-saturated, oversaturated and evolved isolated intrusions remained coherent throughout the combined hydrothermal/deformational event that is so clearly evident in the serpentinised ultrabasic host rock. Their occurrence as pulled-apart blocks indicates that they were intruded before the hydrothermal and deformational event.

Deformation of the serpentinite host-rock is likely to have been coeval with its alteration (serpentinisation; section 3.3.2). The lack of internal deformation and serpentinisation of the isolated intrusions should not be taken to suggest that the intrusive event post dates serpentinisation or deformation of the host rock.

Small isolated tholeiitic dykes intruding an ultrabasic host (harzburgitic tectonite and ultramafic cumulates) are rare in ophiolites but are however commonly observed in many of the Tauride ophiolites (e.g. Mersin, Beyşehir, Lycian, Tekirova, Antalya (Collins and Robertson 1998; Dilek et al. 1998; Andrew and Robertson 2001; Robertson 2002). These are all supra-subduction zone (SSZ)-island arc tholeiite (IAT) type and are interpreted as the products of incipient volcanic arc magmatism.

3.3.7 Metamorphic rocks

Southern sections of the Refahiye Complex include screens of schist, gneiss and marble. The main outcrops are found toward the southern side of the sheeted dyke complex, and are best exposed west of Erzincan on the road from Çatalarmut to Göyne and Baltaş (Figures 3.2 and 3.5). The relationship of these rocks to the rest of the ophiolite is complicated by neotectonic strike-slip faulting in this area. Individual outcrops of the metamorphic rocks range in extent from <1 m to >1 km.

The proportion of metamorphic rocks present within the sheeted-dyke complex varies locally. Metamorphic rocks are estimated to comprise ~15% of the total sheeted dyke complex. The igneous contacts between the dykes and the host lithologies are commonly highly irregular. Metamorphic fabrics (banding, schistosity) are cross-cut by the intrusions. The original structure is complicated by polyphase thrusting and strike-slip deformation.

A range of metamorphic lithologies are present within the ophiolite. They include quartzo-feldspathic and pelitic schists, grey crystalline massive and schistose marble, and highly deformed banded amphibole schists (Figures 3.29 and 3.30).

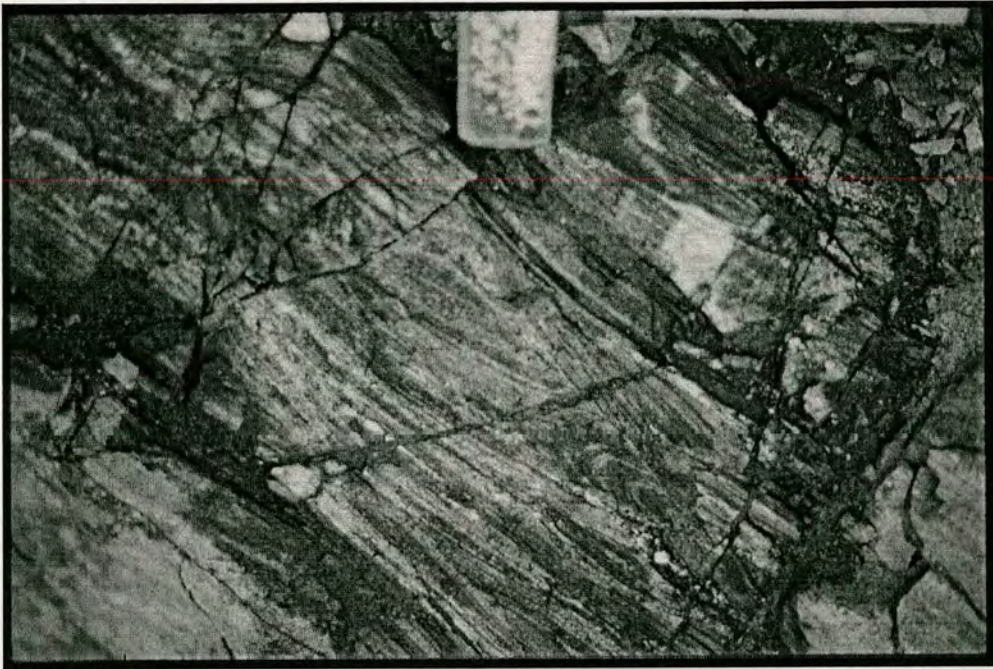


Figure 3.29. Thin screen of highly strained amphibolitic gneiss within the Refahiye Complex near Goyne (gr: İ42, 228067).



Figure 3.30. A thick (>100m) screen of massive crystalline marble within the Refahiye Complex (in contrast to the dark brown landscape in the background), typical of the surrounding outcrop of basic and ultrabasic lithologies. Near Aktas (gr: İ42, 070035).

These rocks occur as screens (~1 m to ~100 m wide) between dense swarms of diabase dykes.

An assemblage of quartz + feldspar + biotite + amphibole is present in the quartzofeldspathic schist. Abundant quartz and feldspar show irregular sutured grain boundaries and strained extinction patterns. Brown biotite and green-brown amphibole (<2 mm) exhibit a preferred orientation between small (~2 mm) lenses of 100% quartz (Figure 3.31). Amphibole-rich schists exhibit felsic-mafic mineral-layering and contain the assemblage: amphibole + plagioclase + clinopyroxene + epidote + chlorite ± muscovite ± quartz ± sphene ± biotite. Quartz and feldspar aggregates exhibit 'bearded' pressure-shadows with growths of mica, or form lenses and augen. These schists commonly show flaser textures. Marble occurs as thin beds between fissile pelitic schists and also as thick (~100m) screens of massive crystalline marble (Figure 3.30). Figure 3.30 shows a typical field occurrence of the marble which has been intruded by dense swarms of diabase dykes and heavily deformed by thrusts and strike-slip faults.

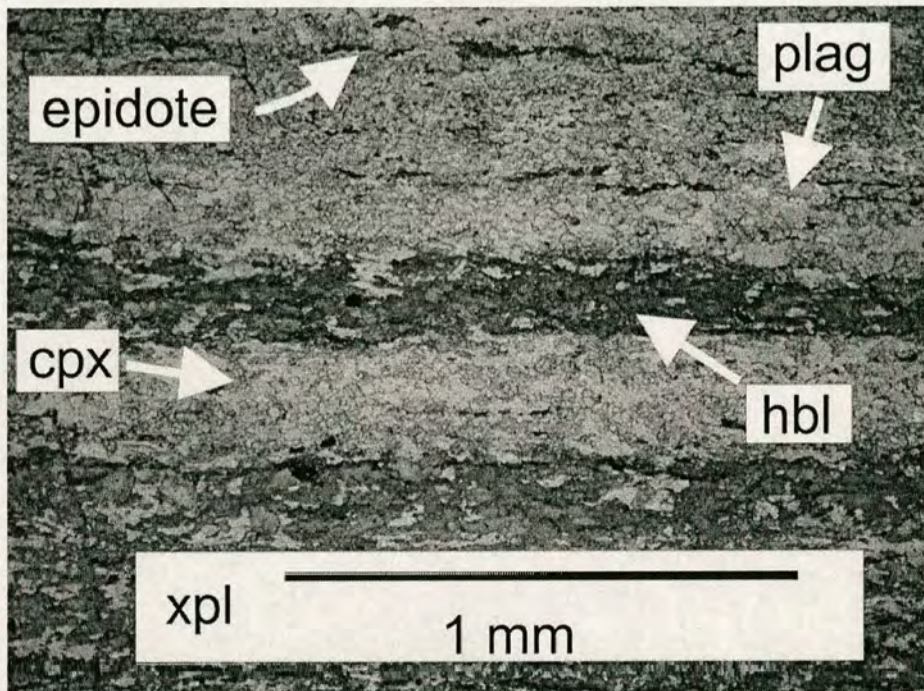


Figure 3.31. Photomicrograph of amphibolite schist from within the sheeted dyke complex of the Refahiye Complex; near Goyne (gr: İ42, 222065). plag = plagioclase, cpx = clinopyroxene, hbl = hornblende.

3.3.8 Whole-rock geochemistry of diabase dykes

Tectonic discrimination is a useful geochemical method for identifying the original tectonic setting of ancient basic volcanic rocks, especially where other geological observations are ambiguous. The principle behind the most successful methods of tectonic discrimination is the comparison of trace element concentrations in the unknown rock with their concentrations in present-day volcanic rocks of known tectonic settings (Pearce and Cann 1973).

Twenty five rock samples of basic intrusions that appeared to exhibit a low degree of alteration in hand specimen were collected from the Refahiye Complex and analyzed by X-Ray Fluorescence (XRF) to determine whole-rock major and trace element compositions. The data are used in this chapter to classify the rocks and make appropriate geochemical comparisons with rocks from modern tectonic settings.

3.3.8.1 Method

Basaltic samples were collected in the field, which appeared to be relatively unaffected by hydrothermal alteration or weathering. The samples were taken from isolated and sheeted diabase and basaltic dykes. They were then analysed for 10 major and 15 trace elements at the Edinburgh University School of GeoSciences using a Phillips PW2404 wavelength-dispersive, sequential X-ray fluorescence spectrometer. For details of the sample preparation, analytical method, accuracy and precision of the data see Appendix 2. Sixteen analyses gave a total major element wt.% outside the range 99-100.5% and were not useful in the interpretation because this could be due to either a hydrous magma source or post-crystallization hydration during metamorphism and/or alteration. The geochemistry and petrogenesis of the remaining nine analyses will be discussed in the following section.

The objective here is to investigate the processes that have led to the petrogenesis of the Refahiye Complex. This principally means understanding the conditions of melting, and requires a determination of the 'primary' magma composition. Thus, the affects of subsequent magmatic evolution, and alteration by

fluids during hydrothermal metasomatism ('sea-floor metamorphism') or weathering need to be identified and taken into account.

To obviate the effects of fractional crystallization only fine-grained aphyric samples were analysed. After analysis geochemical limits on the degree of evolution and alteration of the samples were applied. The widely accepted limit for silica (SiO_2 wt.%) in unaltered igneous rocks is <75% (Brown 1997; Pearce 1973; Best 2003). Basalts have SiO_2 <54 wt.% (Pearce and Cann 1973). None of the samples showed silica enrichment beyond this limit. Unaltered basic igneous rocks should have MgO+CaO values in the range 12-22wt.% (Pearce and Cann 1973). Thus, only whole-rock analyses with SiO_2 values below 54 wt.%, and MgO+CaO₂ within the range 12-22 wt.% were used here to investigate primary magma composition. The nine acceptable analyses are classified geochemically and compared with analyses from known tectonic settings by use of various 'discrimination' diagrams in the following section.

Judd (1886) and Harker (1909) postulated the existence of different petrogenetic provinces long before tectonic theory allowed later workers (e.g. Pearce and Cann 1973) to investigate the underlying processes that control petrological and geochemical variety in igneous rocks. What were once empirical distinctions are now more securely based on an appreciation of the controls of mantle source characteristics, degree and conditions of melting for different tectonic settings (Rolinson 1993; Brown 1997). There has been much geochemical research into igneous petrogenesis, the details of which are beyond the scope of this study; however, as a result, there now exists a variety of geochemical means for discriminating between different tectonic settings of eruption. The analyses are first assessed geochemically for their usefulness in tectonic discrimination diagrams. Then, several suitable discriminant plots are used to compare the analyses with data from known modern tectonic settings using well established diagrams.

3.3.8.2 Classification

The nine available whole-rock geochemical analyses of the basic igneous intrusions from the Refahiye Complex are presented in Appendix 3. Figure 3.32 is a

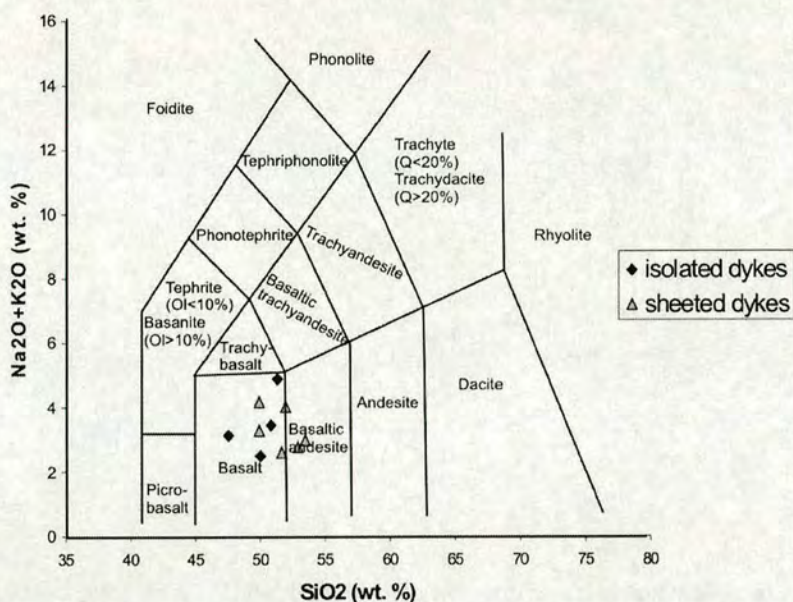


Figure 3.32. Relatively unaltered samples from the sheeted dyke complex of the Refahiye Complex plotted on the total alkali-silica (TAS) diagram (Le Maitre et al. 1989).

plot of total alkali elements versus silica (TAS; Le Maitre et al. 1989), showing the range of rock types and the degree of magmatic evolution of the nine basic igneous samples. The TAS diagram shows most of the samples to be of basaltic to slightly alkalic compositions.

Field and petrographic evidence from the Refahiye Complex as a whole attests to the variable degree to which alteration has affected the unit (sections 3.3.2 and 3.3.5). The basic igneous rocks are preserved as spilite, uralite, chlorite-rich basalt and relatively unaltered basalt. K_2O , Na_2O and SiO_2 are inferred to be potentially mobile during the P - T conditions of metamorphism and/or hydrothermal alteration indicated by the mineral assemblages observed (sections 3.3.5 and 3.3.6; Loughnan 1969). Thus, a more meaningful classification is provided by plotting components that are known to be immobile under greenschist facies hydrothermal and metamorphic conditions. A useful plot for classifying potentially altered basic rocks uses the relatively immobile trace elements Ti, Nb, Y and Zr (Winchester and

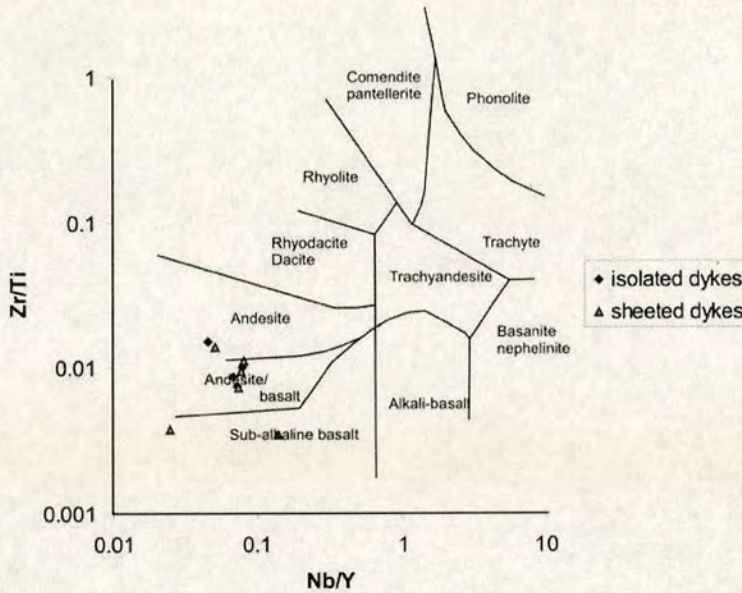


Figure 3.33. Classification of basic igneous intrusions from the Refahiye Complex using immobile trace elements (Zr/Ti versus Nb/Y). Diagram from Winchester and Floyd (1977).

Floyd 1977). On the basis of immobile trace elements the samples plot in the fields for sub-alkaline basalts, basalt/andesite and andesite with no distinction between isolated and sheeted dykes (Figure 3.33).

3.3.8.3 Variation diagrams

Figure 3.34 shows variation diagrams (Harker 1909) for Ni/Mg, Zr/Nb, Cr, MgO and Cr/Ni, all elements known to be immobile; they show good geochemical coherence among the samples. That such elements do not vary independently of each other suggests that concentrations of these elements in the samples were not affected by metamorphic, alteration or weathering processes and indicates that the samples are part of a co-magmatic suite, forming part of a series of rocks originating from a similar parental source and related by fractional crystallisation. The affect of alteration and weathering on the concentrations of other elements can be assessed by plotting the data for an element that is known to be immobile against the potentially.

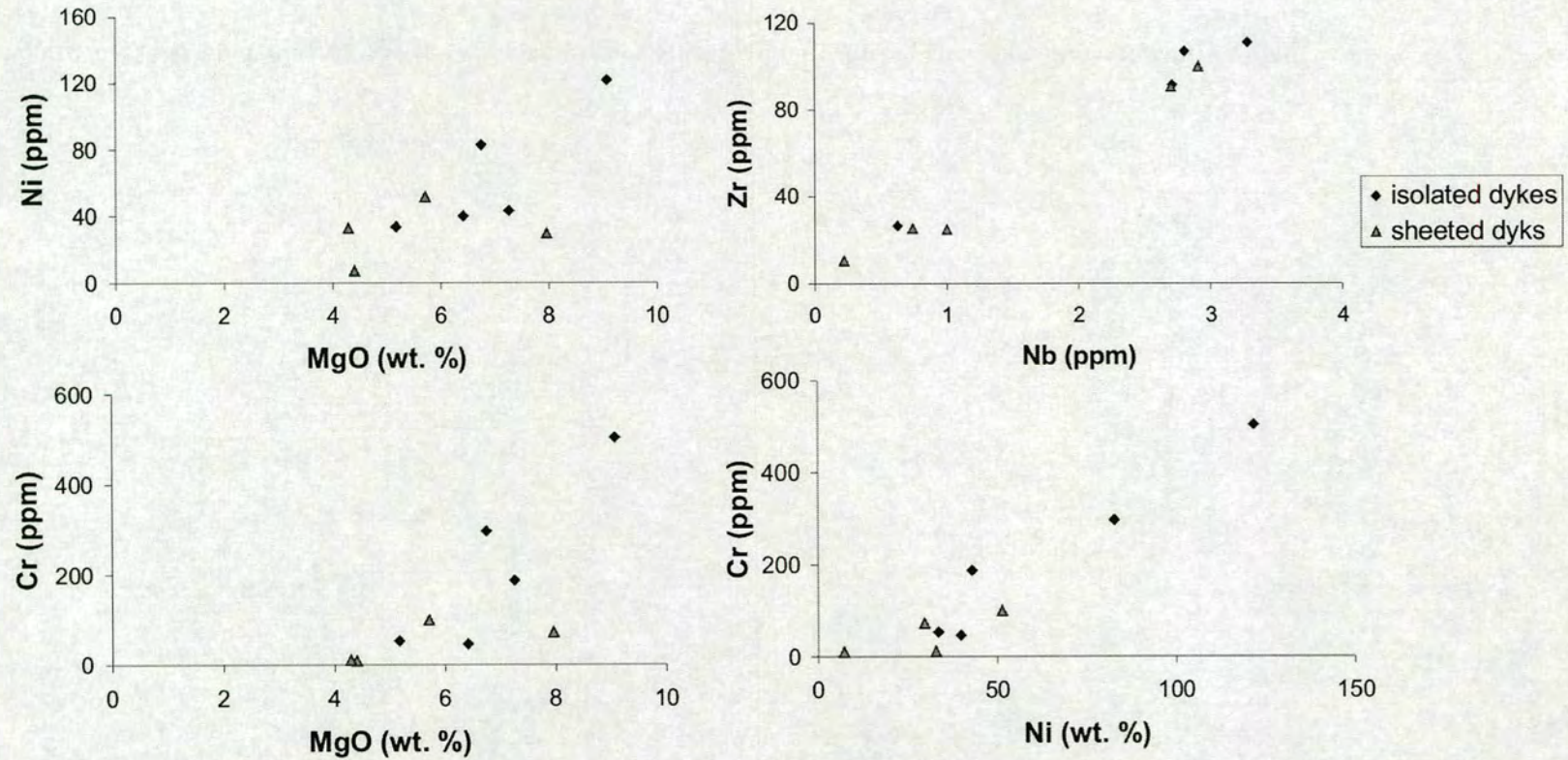


Figure 3.34. Variation diagrams between immobile trace elements for basic intrusions of the Refahiye Complex.

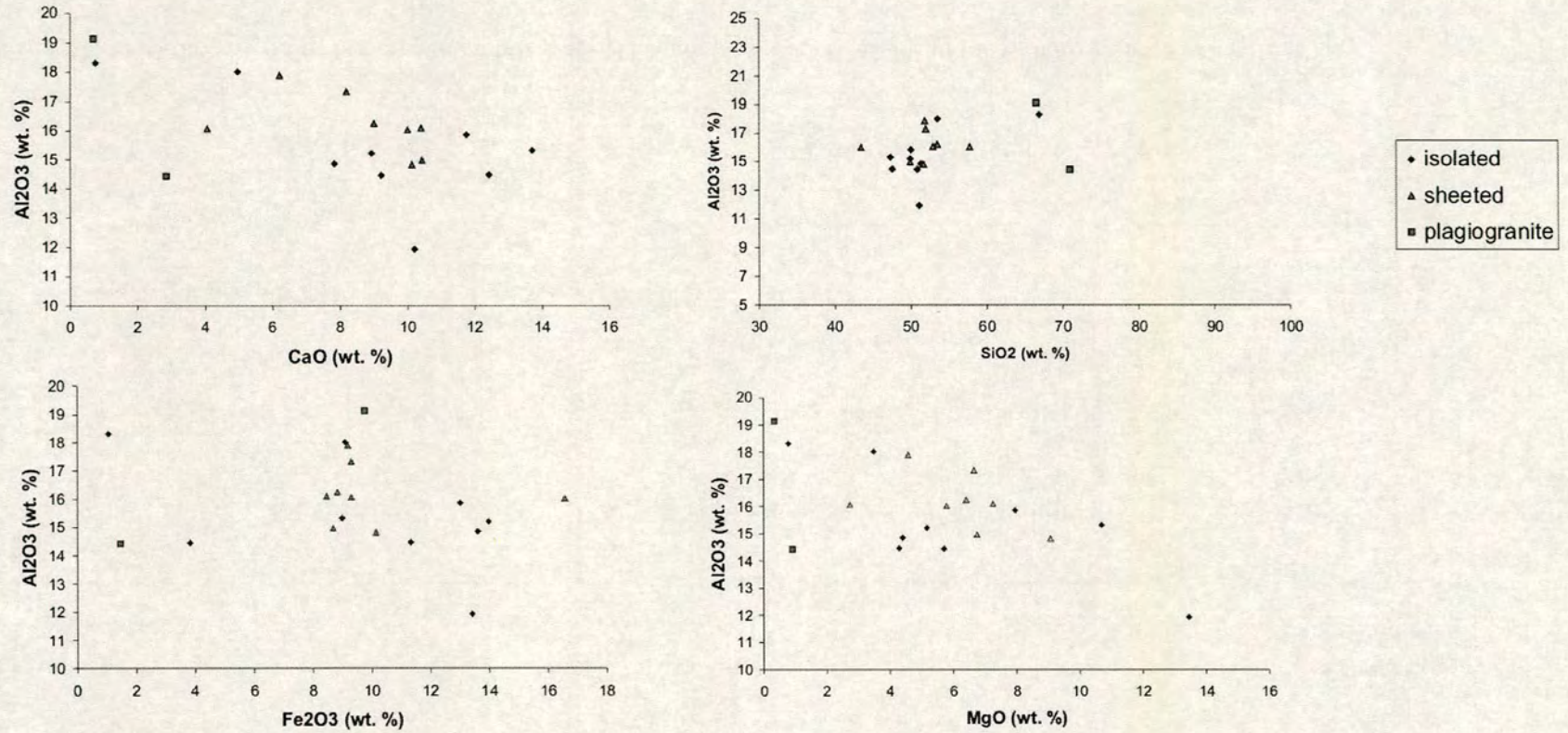


Figure 3.35. Variation diagrams to show variability of element mobility during alteration of the Refahiye Complex.

3.3.8.4 Tectonic discrimination

For investigations of tectonic processes the most meaningful classification of volcanic rocks is one based on the original tectonic setting of their eruption. Pearce and Cann (1973) defined the following four major groups of basalts by considering the major tectonic regimes:

1. Ocean floor basalts (diverging plate margins).
2. Volcanic arc basalts (converging plate margins).
3. Ocean island basalts (within-plate oceanic crust).
4. Continental basalts (within-plate continental crust).

In addition, basalts from ocean-floor and within-plate eruptive settings may be either tholeiitic or alkalic, while volcanic arc basalts are subdivided into low-K tholeiite, calc-alkali basalt and shoshonite (Peccerillo and Taylor 1976). Later workers used additional subdivisions (e.g. backarc). Many studies of the geochemistry of recent volcanic rocks from the major tectonic settings have been undertaken and suitable elements, which discriminate between samples from each magma type and which retain their discriminating power in metamorphosed and altered rocks have been identified (e.g. Pearce and Cann 1973; Winchester and Floyd 1979; Shervais 1982; Pearce 1982; Pearce 1983; Meschede 1986). Suitable elements for characterizing magma types must ideally:

- “Have a greater variation in concentration between samples of different magma types than between samples of the same magma type.” (Pearce and Cann 1973).
- “Be insensitive to secondary processes such as weathering and metamorphism.” (Pearce and Cann 1973).
- “Be easy to measure with good reproducibility of results.” (Pearce and Cann 1973).

Some ophiolites have been interpreted as emplaced backarc basin crust (e.g. Sarmiento, S. Andes, Dalziel 1974; Lachlan Orogen, Spaggari et al. 2003). When the Ti/Zr/Y diagram (Figure 3.36) was developed in 1973 there were insufficient data available for any chemical difference between basalts formed at mid-oceanic ridges and those occurring in subduction-related settings, e.g. backarc basins to be

established. Later workers (e.g. Weaver et al. 1979; Pearce 1982) began to identify geochemical differences between backarc volcanics and mid-ocean ridge basalt.

Ti, Zr and, Y are incompatible and immobile trace elements and, as such are useful in tectonic fingerprinting of ancient volcanic rocks (Cann 1970). The scaling factors (Ti/100, $Y*3$) serve to bring the points into the centre of the triangle. The Ti/Zr/Y diagram (Pearce and Cann 1973; Figure 3.36) shows compositional fields for ocean island and continental basalts, ocean-floor basalts, low-K tholeiites and calc-alkali basalts. On the Ti/Zr/Y diagram the isolated dykes and sheeted dykes analyzed from the Refahiye Complex plot in the fields of ocean floor basalts and low-potassium tholeiites (i.e. arc), with none in the within-plate field.

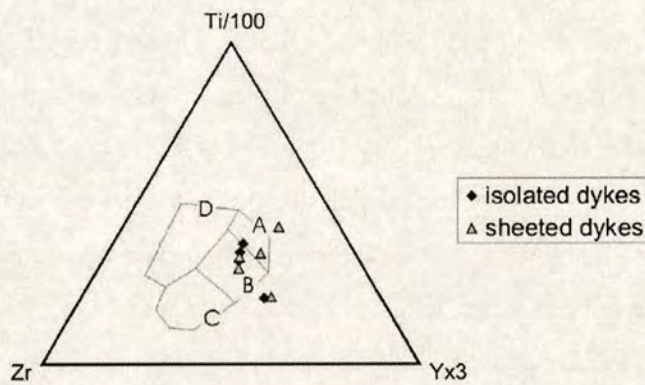


Figure 3.36. Isolated and sheeted diabase dykes from the Refahiye Complex plotted on the ternary Ti/Zr/Y discrimination diagram (Pearce and Cann 1973). Within-Plate basalts field D, ocean-floor basalts in field B, low-potassium tholeiites in fields A and B, calc-alkali basalts in fields C and B.

Island arc tholeiites are characterized by a low content of immobile incompatible trace elements for a given degree of fractionation (Pearce 1982). Discrimination diagrams which plot an index of fractionation (e.g. Cr, Ni) against an immobile but relatively compatible element (e.g. Ti, Y) can be useful for distinguishing between island arc tholeiite and MORB (e.g. Pearce 1975; Garcia

1978; Sharaskin et al. 1980). Cr and Y are compatible trace elements in garnet lherzolite and so their abundances in magma source regions are unaffected by mantle enrichment and depletion events (Pearce 1982). Therefore, Pearce (1982) postulated that most basaltic magmas were derived from a mantle source with primordial abundances of Cr and Y. This implies that variations of the abundances of Cr and Y in basalts result from differences in their partial melting and fractional crystallization histories. On a Cr/Y basalt discrimination diagram (Figure 3.37) volcanic arc basalts are well separated from mid-ocean ridge basalts. There is some overlap between the within-plate basalt, MORB and volcanic arc basalt fields.

In Figure 3.37 data from the Refahiye Complex plot roughly within the field of MORB. However, one sample has a lower Y content than MORB and falls in the volcanic arc field, while two samples show lower Cr values than MORB and fall in the within-plate basalt field. The low Cr values could possibly be explained by crystal fractionation.

It is generally agreed that Ti and Zr concentrations are insensitive to processes of alteration (Cann 1970). A simple Ti/Zr plot can be useful for discriminating basalts which are altered or metamorphosed (Pearce 1973). Figure 3.38 shows that analyses of basic dykes from the Refahiye Complex fall into two groups: ocean floor basalts and low-K tholeiites. This is consistent with the Ti/Zr/Y ternary plot (Figure 3.36).

An alternative diagram uses $\log \text{Ti}/\log \text{Zr}$ (Pearce 1981). The data again fall into two distinct groups, one close to the field for volcanic arc lavas and one well within the field of MORB (Figure 3.39).

Pearce (1983) showed that geochemical analyses of basalts from destructive plate boundaries can be subdivided into their upper mantle and subduction derived

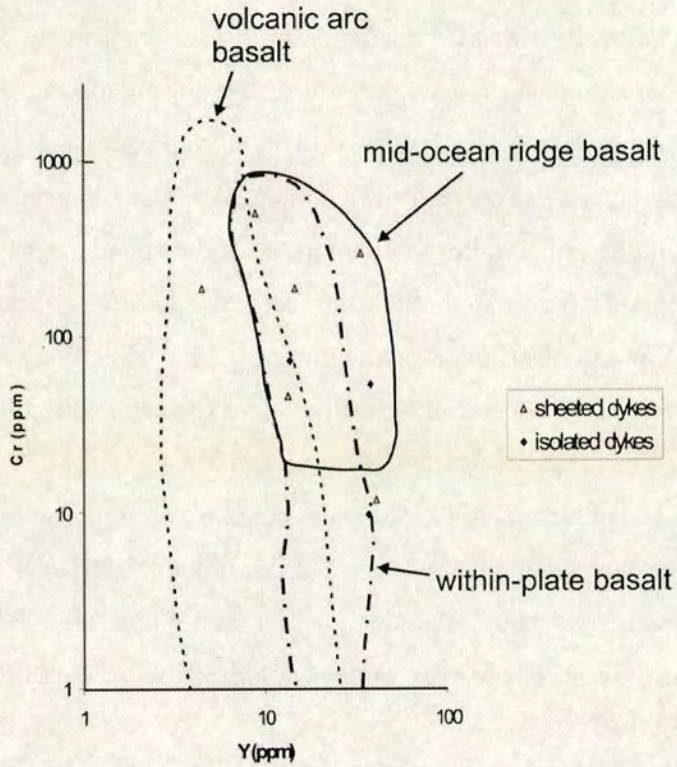


Figure 3.37. Isolated and sheeted diabase dykes from the Refahiye Complex plotted on the Cr-Y discrimination diagram (Pearce 1982).

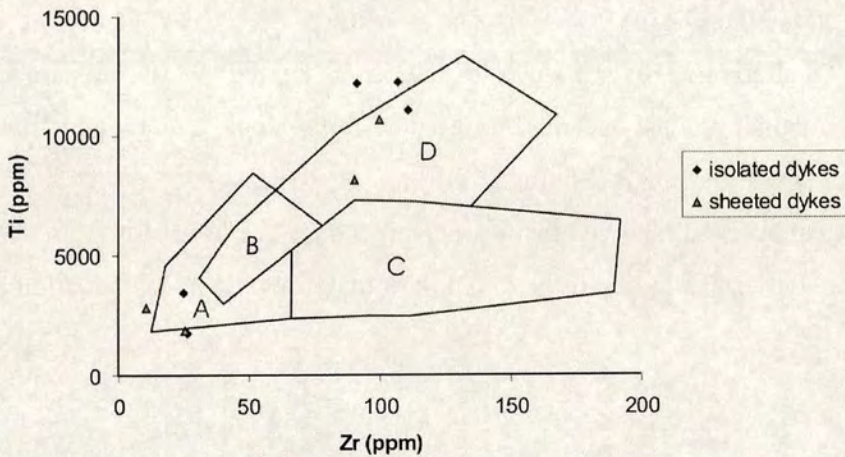


Figure 3.38. Isolated dykes and sheeted diabase dykes from the Refahiye Complex plotted on the Ti/Zr discrimination diagram (Pearce and Cann 1973). Ocean-floor basalts plot in fields D and B; low-potassium tholeiites in fields A and B, and calc-alkali basalts in fields C and B.

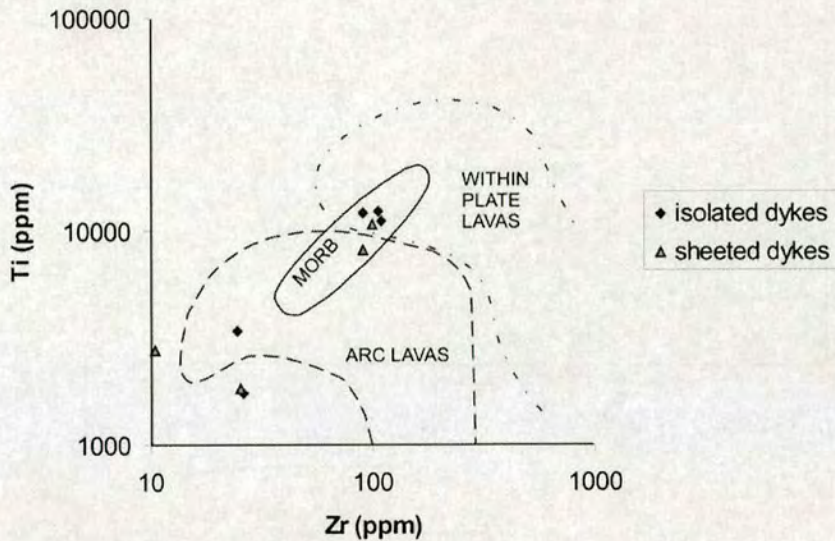


Figure 3.39. Isolated dykes and sheeted diabase dykes from the Refahiye Complex plotted on the log Ti/log Zr discrimination diagram (Pearce 1982). Ocean-floor basalts plot in fields D and B; low-potassium tholeiites in fields A and B, and calc-alkali basalts in fields C and B.

components. Rb, K, Ba, Th and Sr are slab-derived while Ta, Nb, Ce, P, Zr, Hf, Sm, Ti, Y and Yb originate in the mantle. A useful bivariate plot that separates these components is the Zr/Y against Zr diagram (Figure 3.40). Figure 3.40 uses Y as a normalizing factor to eliminate variations due to partial melting and fractional crystallization (Pearce 1983).

Analyses of basic dykes from the Refahiye Complex all lie within the compositional field of island arc basalts on Figure 3.40. The two clusters lie along a vector corresponding to either within-plate type enrichment or fractional crystallization. Figure 3.40 discriminates between continental and oceanic arcs but does not distinguish between the involvement of sub-continental lithospheric mantle or within-plate type enrichment, nor does it distinguish alkalic from tholeiitic compositions. However, Figure 3.36 shows that the analyses clearly do not show within-plate-type compositions.

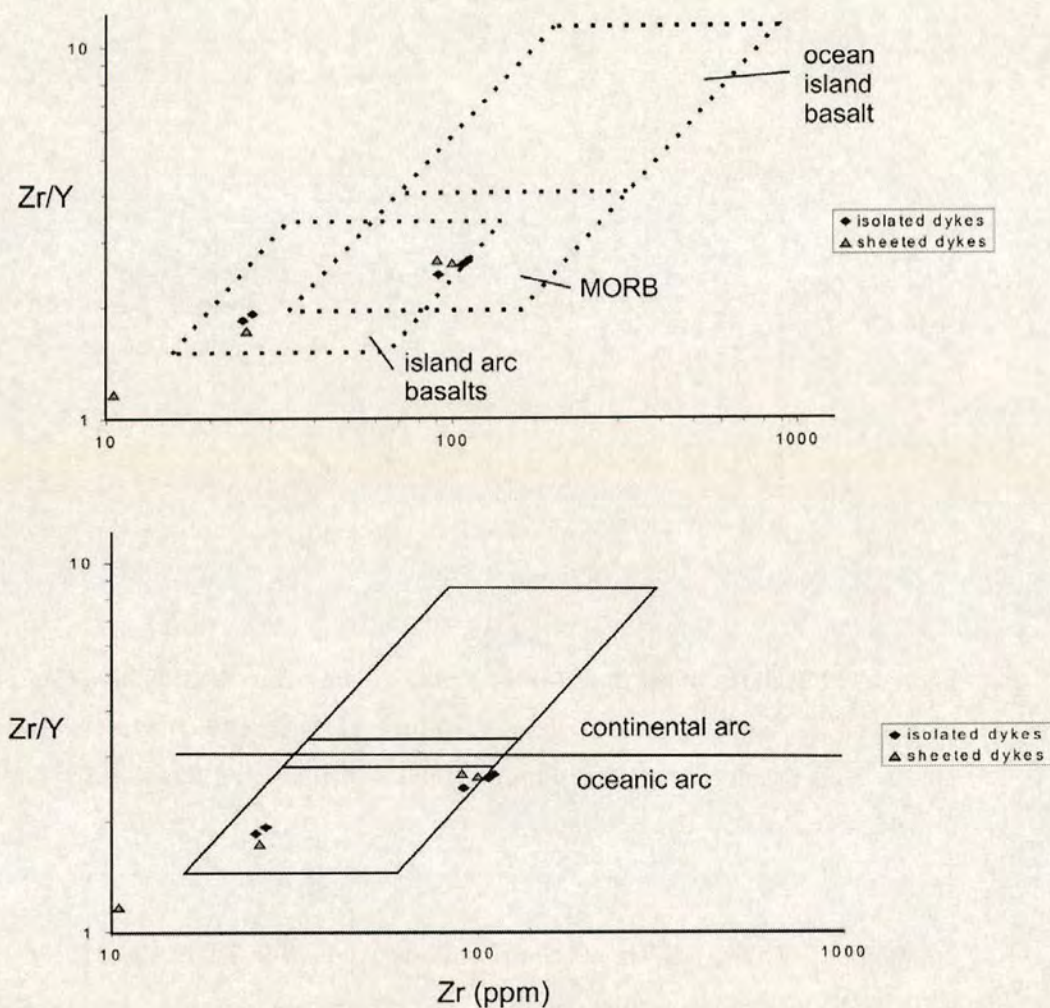


Figure 3.40. Isolated and sheeted diabase dykes from the Refahiye Complex plotted on the Zr/Y versus Zr discrimination diagram (Pearce and Norry 1979).

The bulk partition coefficient for vanadium in a crystallizing assemblage of liquid, pyroxene and magnetite varies by over two orders of magnitude as a function of oxygen fugacity (Lindstrom 1976; Shervais 1982). Because Ti is an immobile incompatible cation, Ti/V ratios are dependant upon the degree of partial melting and oxygen fugacity in the mantle. There is a generally coherent variation in V/Ti ratios between different major tectonomagmatic environments. High V/Ti ratios (20-50) are observed in basalts from mid-ocean ridges and ocean islands (Shervais 1982). Geochemical modeling suggests that these are consistent with 20-30% partial melting under relatively reducing conditions. Lower V/Ti ratios are observed from volcanic arc basalts and for a 20-30% partial melting require more oxidizing

conditions, consistent with melting of a mantle wedge overlying a devolatilizing, subducting lithospheric slab. However, magnetite fractionation strongly alters the Ti/V ratio and its role needs to be first assessed by plotting Ti against SiO₂ or FeO*/MgO.

Hydration, precipitation or leaching of other elements may increase the concentration of Ti and/or V. However, it has been shown that in most cases Ti and V behave coherently during seawater alteration and the ratio does not significantly change (Shervais 1982). Ti and V are stable over a wide range of metamorphic temperatures and water/rock ratios, with Ti/V being unaffected by chloritization or silicification (Shervais 1982).

On a bivariate plot of Ti against V (Figure 3.41) analyses of MORB are confined to ratios between 20 and 50 while alkali basalts and ocean islands have ratios generally higher than 50. Island arc tholeiites have Ti/V ratios ≤ 20 and there is a minor overlap with MORB compositions on the Ti/V diagram. Suites of arc tholeiite series rocks are distinguished from MORB as they lie along a steep vector (that coincides with the chondritic trend). Backarc basin basaltic rocks occupy a broad compositional field that overlaps both volcanic island arc and MORB compositions. These basalts tend to show less enrichment of Ti and V (Shervais 1982).

Data from the Refahiye Complex plot in two clusters. One is clearly an island arc tholeiite series while the other falls within the MORB and backarc basin compositional field. Because the fields for island arc tholeiite and MORB/backarc basins overlap the two groups of data display Ti/V ratios consistent with a backarc basin origin.

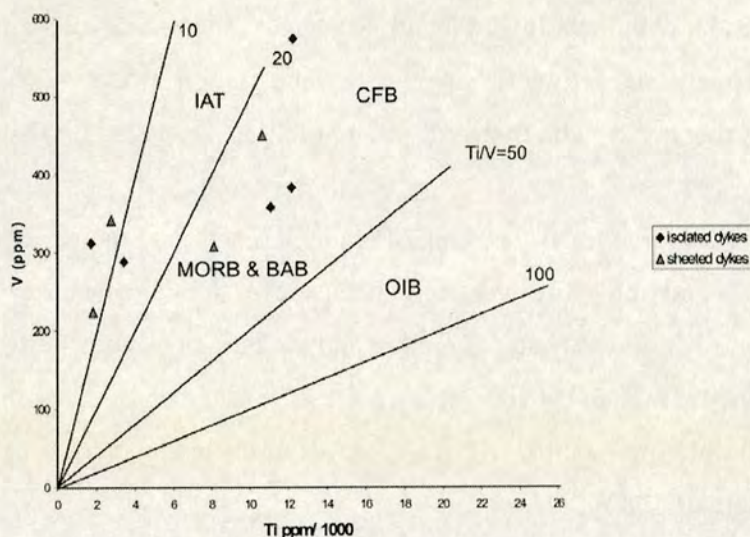


Figure 3.41. Isolated dykes and sheeted diabase dykes from the Refahiye Complex plotted on the V/Ti discrimination diagram (Shervais 1982).

Nb, Zr and Y are all immobile incompatible trace elements and thus useful for distinguishing magma types. Nb is particularly sensitive to mantle enrichment and depletion processes (Meschede 1986). The Nb/Zr/Y diagram (Figure 3.42) is only useful for distinguishing different types of tholeiites and not for alkalic compositions. The Nb/Zr/Y diagram is particularly useful for distinguishing continental tholeiites from normal mid-ocean ridge basalt.

Data from the Refahiye Complex, plotted on the Nb/Zr/Y diagram (Figure 3.42) fall in the MORB field.

Figure 3.43 uses Nb to distinguish between N-MORB and Icelandic (plume-type) basalt. This approach exploits the unusual behaviour of Nb during the melting processes responsible for depletion of the upper mantle (Fitton et al. 1997). This is the only diagram on which the sheeted dykes and isolated dykes seem to form individual groups. The sheeted dykes all plot just within the Icelandic basalt field, while the isolated dykes all plot below the Iceland array, having N-MORB compositions.

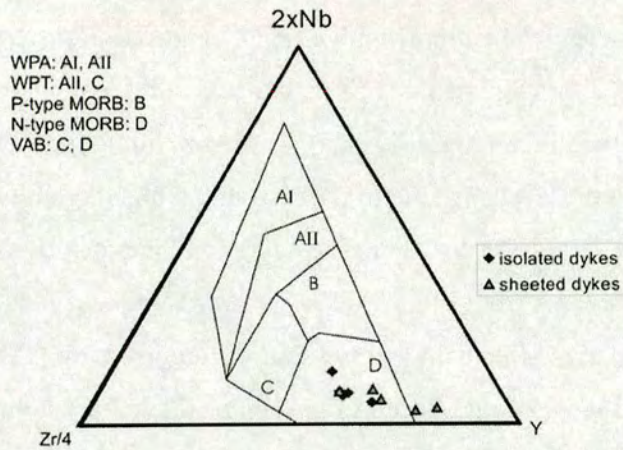


Figure 3.42. Isolated dykes and sheeted diabase dykes from the Refahiye Complex plotted on the Nb/Zr/Y discrimination diagram (Meschede, 1986). AI and AII = within-plate alkali basalt compositional field, B = plume-influenced MORB compositional field, C = within-plate tholeiite compositional field, D = N-type MORB and volcanic arc basalt.

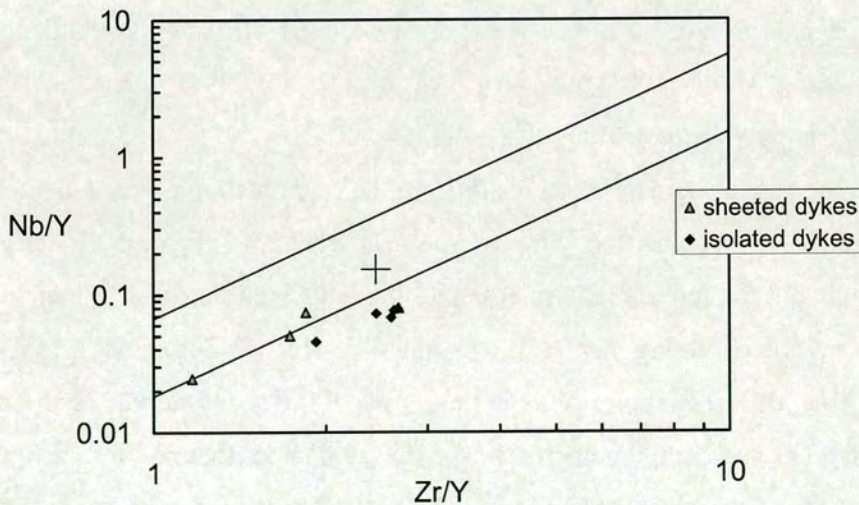


Figure 3.43. Nb/Y against Zr/Y variations (Fitton 1997) for basic isolated and sheeted dykes from the Refahiye Complex. Lines define the array for Icelandic basalts.

3.3.8.5 Multi-element plots.

Another way to compare the analyses of basalts from different settings is to plot their geochemical patterns with a typical mid-ocean ridge basalt as a normalizing factor (Figure 3.44). The elements in these plots are arranged according to their ionic potential (charge/radius). Large-ion lithophile elements (LILE; Sr, K, Rb, Ba) lie to the left hand side of the diagram, whilst high field strength elements (HFSE, Th to Cr) are to the right. The degree of incompatibility with 'fertile' garnet lherzolite decreases from Ba, Th, Ta, Nb towards the two ends of the plot. Pearce (1982) summarized the main features that distinguish basalts erupted in volcanic arc settings from those of mid-ocean ridge, Within-Plate, or 'anomalous' settings. Three characteristic features of volcanic arc basalts are as follows:

(1) Enrichment of Sr, K, Rb, and Ba (sometimes Th also) relative to the elements Ta to Cr. These elements are distinguished by their low ionic potential (charge/radius) and have a tendency to be mobilized by aqueous fluids either during subduction or subsequent metamorphism and alteration (Pearce 1982).

(2) Low abundances of elements with a high ionic potential relative to N-MORB tholeiite composition. This includes elements that are enriched during fractional crystallization (e.g. Th to Yb) and elements that are depleted during fractional crystallization (Cr) (Pearce 1982).

(3) Calc-alkaline basalts and shoshonites also display a selective enrichments of Th, Ce, P and Sm (Pearce 1982). These are associated with mature subduction zones (Saunders and Tarney 1984).

(4) Negative Nb anomaly.

The above characteristics result from the fractionation of trace elements which occurs in a subduction zone environment where melting or dehydration of the slab is thought to preferentially release mobile, incompatible, LILE, Th and Ce but not Nb into the overlying mantle wedge, and ultimately SSZ magmas. This fundamental differentiation results in the separation of a slab-derived component (SSZ magmas and continental crust) from the subducted oceanic lithosphere, i.e. the Residual Slab Component (Saunders et al. 1988). Nb fractionation can be explained by the stabilization of Ti-rich minor phases (sphene, rutile) within the basaltic oceanic crust. These phases may sequester Nb and Ta, whilst LILE (K, Rb, Ba, Th,

La, Ce, Pb) will preferentially enter the fluid phase and migrate into the overlying wedge (Saunders et al. 1988). The overlying mantle wedge is the source of ophiolitic, island-arc and calc-alkaline magmas, which are enriched in LILE's and thus show Nb and Ta depletion. The exact composition of the residual slab is unknown; however, it is likely to have high Nb and low LILE contents. It has been postulated that this residual slab component forms a major contribution to OIB and E-MORB (Hofmann and White 1982; Saunders et al. 1988).

Whole-rock geochemical analyses of samples from the Refahiye Complex are plotted on a multi-element diagram, (Figure 3.44). The analyses again, fall in two groups. One group of samples exhibits flat-lying patterns close to unity (i.e. the normalizing factor, N-MORB). The flat-lying patterns represent bulk chemical

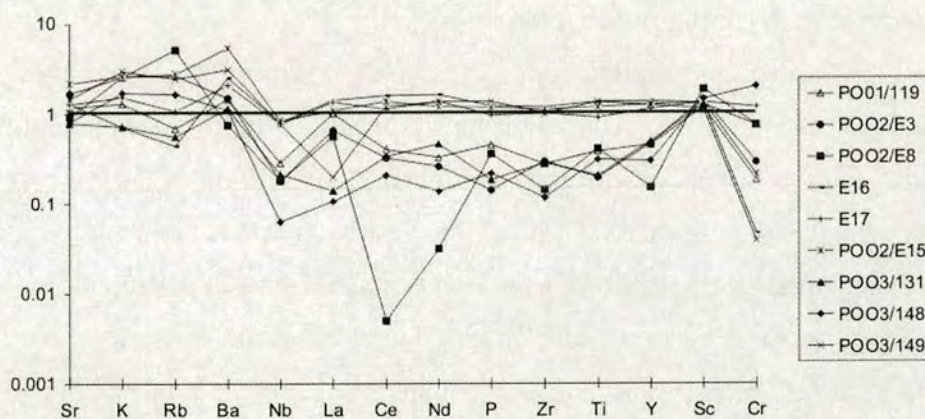


Figure 3.44. MORB-normalized multi-element abundances for unaltered basic dykes from the Refahiye Complex. Normalizing values: Sr = 120 ppm; K_2O = 0.15% ; Rb = 2.0 ppm; Ba = 20 ppm; Nb = 3.5 ppm; La = 3 ppm; Ce = 10 ppm; Nd = 8 ppm; P_2O_5 = 0.12% ; Zr = 90 ppm; TiO_2 = 1.5% ; Y = 30 ppm; Sc = 40 ppm; Cr = 250 ppm (Pearce 1973).

compositions similar to MORB, corroborating the MORB-like cluster of data points observed in the discrimination diagrams above (Figures 3.38 to 3.41). Samples PO01/119, PO02/E3, E8, PO03/131, and 148 show a depletion of the high field

strength (HFS) elements and slight enrichment of LILEs Sr, K, Rb and Ba. This latter group also shows a negative Nb anomaly. These are distinctive features of subduction-influenced basalt geochemical patterns. This group of samples corresponds to the cluster of volcanic-arc type basalts identified on the discrimination diagrams above (Figures 3.38 to 3.41). There seems to be no correlation between whether dykes are of Volcanic Arc Basalt (VAB) or MORB type and whether they occur as sheeted or as isolated dykes. There is no obvious pattern to the spatial distribution of VAB and MORB types.

3.3.8.6 Chromian spinel chemistry

Chromian spinel is an ubiquitous phase within the serpentinised harzburgite, occurring as vermicular intergrowths and 'amoeboid' grains interstitial to olivine and pyroxene. These spinels probably form during incongruent melting of 'fertile' peridotite to produce a calcic pyroxene-rich melt leaving an olivine and Cr spinel-rich residue (Dick and Bullen 1984).

Chrome spinel grains from five samples of serpentinised harzburgite from the Refahiye Complex were analysed using a Cameca SX100 electron microprobe at the School of GeoSciences, University of Edinburgh. For details of the systems operating conditions see Reed (1975). The instrument was fitted with five wavelength-dispersive spectrometers and operated with gun potential at 20 Kv. The probe current was measured in a Faraday cup of 20 nA and a focused beam was used. Standards used were a selection of Specpure metals, simple synthetic oxides crystals and simple silicates. Fe³⁺ concentrations were calculated stoichiometrically following the method of Droop (1987).

The ratios of Cr# ($\text{Cr} \cdot 100 / (\text{Cr} + \text{Al})$) and Mg# ($\text{Mg} \cdot 100 / (\text{Mg} + \text{Fe}^{2+})$) allow peridotites formed in a MOR-type setting to be discriminated from those formed in a SSZ-type setting (Dick and Bullen 1984). The main constituents of spinel (Mg, Fe^{2+}) (Cr, Al, Fe^{3+})₂O₄ behave differently during partial melting or crystallisation, with Cr and Mg partitioning into solid phases and Al into the melt (Dick and Bullen 1984).

Five samples of spinel-bearing serpentinised harzburgite collected from the Refahiye Complex were selected for microprobe analysis. Multiple analyses were made of the cores and rims of 12 or more individual spinel grains in each sample.

The data are shown on Figure 3.45. Of five samples from the Refahiye Complex, four (OEP1, OEP2, OEP4 and OEP5) fall within, or close to, the field of abyssal spinel peridotites, whereas one from the ophiolite (OEP3) exhibits a much higher Cr#. Samples OEP1, OEP3 and OEP5 were collected from a 3 km-long transect of a single peridotite thrust sheet. Where multiple grains were analysed from single samples, each sample falls clearly within one of the two petrogenetic types. A marked compositional variation is observed within the single thrust sheet, where several samples were analysed along strike. Such variation is not known within abyssal peridotites, but is observed in ophiolitic peridotites and is consistent with the variable depletion and enrichment trend found in chromites within peridotites dredged from backarc basins (e.g. Dietrich et al. 1978; Saunders and Tarney 1984; Barker et al. 2003).

Dick and Bullen (1984) divided Alpine peridotites into three types based on spinel compositions. Type I peridotites contain spinels with $Cr\# < 0.60$; type II peridotites are a transitional group covering the range of compositions of both type I and type III; and type III peridotites have $Cr\# > 0.60$. The ophiolitic peridotite of the Refahiye Complex is clearly a type II peridotite. Dick and Bullen (1984) showed that the analogous modern setting for type I peridotites is oceanic lithosphere formed at mid-ocean ridges. They infer a sub volcanic arc setting for type III peridotites and suggest a composite origin for the petrogenesis of type II peridotites. The most likely composite setting is a backarc basin.

3.3.9 Discussion: petrogenesis and tectonic setting

As is the case with other ophiolite complexes, the Refahiye Complex exhibits a petrologic association and structure resembling oceanic crust. Mafic/ultramafic cumulates attest to a fractionating basic magma body at depth, which is likely to have fed the sheeted diabase dykes, isolated diabase dykes and, plagiogranite dykes which occur higher in the pseudostratigraphy. However, the data presented in this chapter highlight considerable petrologic and geochemical differences between the Refahiye Complex and normal mid-oceanic lithosphere.

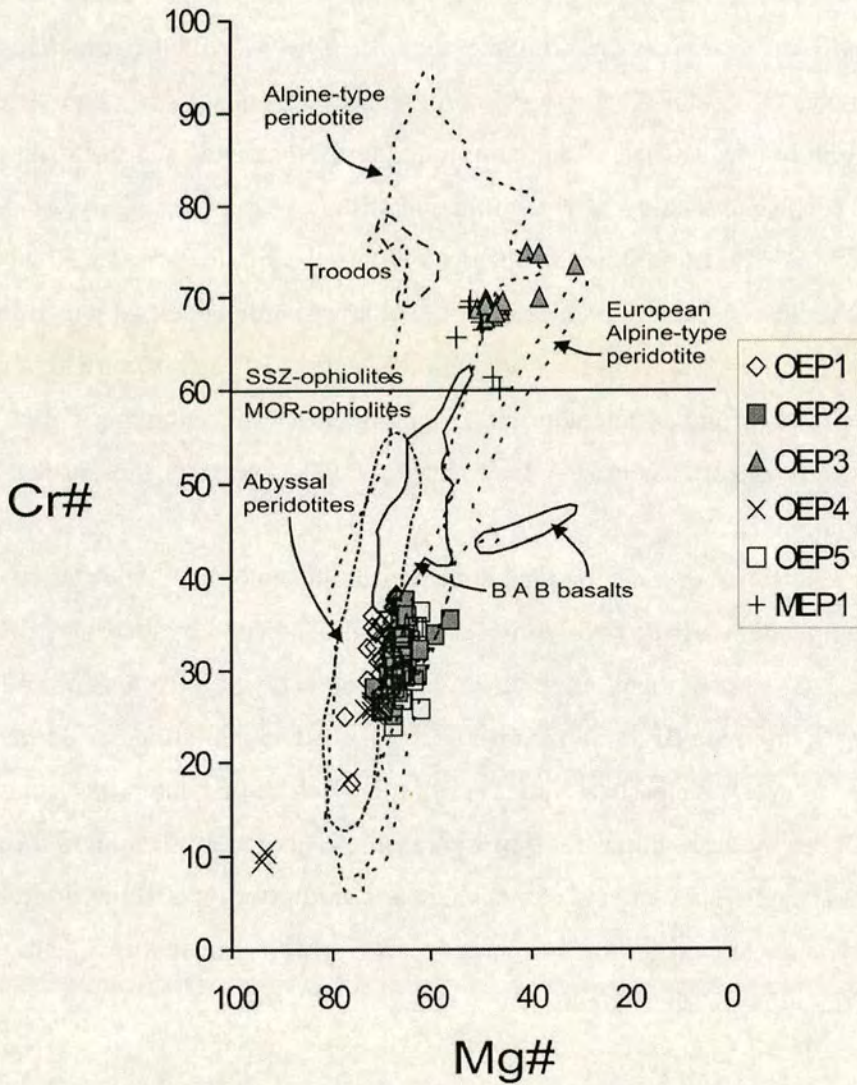


Figure 3.45. Cr# $((Cr \cdot 100)/(Cr + Al))$ versus Mg# $((Mg \cdot 100)/(Mg + Fe^{2+}))$ for spinels from peridotites in the Refahiye Complex, Eastern Pontides. Fields for Troodos, backarc basins (BAB) alpine-type peridotites, abyssal peridotites, and European alpine type peridotites are marked (Dick and Bullen 1984). Sample locations: OEP1, OEP3 and OEP5: Sakultan Geçedi; OEP2: Mercidiye; OEP4: Aktaş; MEP1: Avclar (see Figure 3.2).

The ultramafic rocks from the Refahiye Complex are clinopyroxene-poor harzburgites. Mineralogic and trace element characteristics of the harzburgites are

consistent with them being the mantle residue left after extraction of island-arc tholeiitic or boninitic type magmas (Pearce et al. 1992).

Geochemical patterns of relatively unaltered alkali basalts and basaltic andesites from the Refahiye Complex fall into two groups and, in addition to patterns lying close to N-MORB, display characteristics typical of volcanic arcs. The patterns may be explained in terms of four processes which are likely to act in combination at subduction zones (Pearce 1982). Oceanic crust is known to become hydrated during sea-floor metamorphism. The selective enrichment in incompatible elements of low ionic potential is thought to be due to the input of aqueous fluids from subducted oceanic crust into the overlying mantle wedge. This may also be explained by the addition of small amounts (<1% of the island arc basalt source) of subducted sediment to the mantle source region (Saunders and Tarney 1984). The low abundances of incompatible elements of high ionic potential may be modelled in terms of high degrees of melting, stabilization of residual oxide phases, or re-melting of previously depleted mantle (Pearce 1982). These processes are all likely to occur in a subduction zone environment (Pearce 1982).

When plotted on various basalt discrimination diagrams the samples again tend to fall into two groups. One group consistently plots in the fields of MORB or 'ocean-floor basalt', while another group plots in fields of low-K tholeiite, 'arc lavas', 'island arc basalts', island arc tholeiites or 'volcanic arc basalts'. The two geochemical groups do not appear to correspond to any spatial or structural pattern within the complex and there is no chemical distinction between the isolated and sheeted dykes.

The presence of metamorphic host rocks (schist, gneiss and marble) within the complex provides the most striking evidence that this unit was not formed in a mid-oceanic setting within a wide ocean, but is likely to have developed adjacent to a continental margin. Plagiogranite and diabase dykes intruding peridotites are fairly rare in ophiolites, but are seen in the Arakapas transform zone (Cyprus), and the Coast Range (New England). These occurrences have both been interpreted as leaky transform faults (Dilek 2003). Plagiogranites and rhyodacite also occur in *ensialic* marginal basins such as the Rocas Verdes marginal basin ophiolite (Stern and de Wit 2003) and the Bransfield Strait, but have not been recovered from *ensimatic* marginal

basins. Although no extrusives or sedimentary rocks are preserved within the complex the diabase dykes presumably fed surface eruptions (Dalziel 1974).

The geochemistry of the Refahiye Complex is transitional between that of MORB and volcanic arc basalts, a feature that is typical of supra-subduction zone ophiolites. Basalts retrieved from backarc basins also show this transitional geochemistry (Weaver et al. 1979). In backarc basins the high AH_2O combined with active extension gives rise to a high degree of melting and depletion of the source. These processes, together with localised enrichment of the source region in LILEs by fluids migrating from the slab may combine to produce the spectrum of MORB and volcanic arc magma types, as observed in both backarc basins and supra-subduction zone ophiolites. The degree of LILEs enrichment in supra-subduction zone ophiolites is thought to be dependant on the maturity of the adjacent subduction zone (Saunders and Tarney 1984).

Replacement of primary mafic minerals by serpentine and amphibole group minerals in basic and ultrabasic rocks from the Refahiye Complex is evidence of late-stage hydrothermal activity. Geochemical analysis of the samples reveals the preferential mobilization of LIL elements in the altered samples. Textural relationships indicate that this hydrous metamorphism was retrogressive and syn-deformational, post-dating all intrusive events in the Refahiye Complex.

3.3.10 Summary

The main exposure of the Refahiye Complex in the north is interpreted as a disrupted, but originally complete section of oceanic lithosphere and lithospheric upper mantle, of which the upper extrusive levels are not preserved. The metamorphic host rocks within the ophiolitic Refahiye Complex are comparable with the Upper Palaeozoic-Lower Mesozoic metamorphic basement of the Pontides (e.g. Doğankavak Unit; Topuz et al. 2004). The presence of igneous contacts between diabase dykes and their metamorphic host rocks, therefore, indicates that the ophiolite did not form in an open-ocean setting, but instead within a rifted continental margin.

The cross-cutting dykes are inferred to be related to the adjacent exposures of 100% sheeted dykes. They are unlikely to represent fragments of older dyke-rich T.

Ustaömer, pers comm. 2004). metamorphic basement, as exposed in some parts of the Pontides (e.g., Artvin region;

The petrology and geochemistry of the ophiolite have the characteristics of known backarc basins.

3.4 Late Mesozoic accretionary complex: Karayaprak Mélange

This ophiolitic mélange unit occurs at several different structural levels within the thrust stack, forming discrete slices, up to 4 km thick (Figure 3.46). Here the mélange is described in terms of lithological associations of blocks. Outcrops are generally bounded by north-dipping thrust faults or shear-zones (Figure 3.46). Outcrops of the Karayaprak Mélange become progressively larger and more abundant towards the south of the area. In the south, near Kemah (Figure 3.46), the mélange tectonically overlies the basinal Ayıkayası Formation (Section 3.2). The unit is unconformably overlain by Palaeocene-Eocene sedimentary rocks (Sipikör Formation; Figure 3.46) that postdate suturing, as seen in small exposures, both north and south of Erzincan (Section 3.7).

The mélange is a tectonised mixture of blocks and slices. The blocks range in size from several metres to > 2 km. Blocks are commonly tectonically juxtaposed, or are separated by scaly sheared serpentinite, fault breccia, gouge or mylonite. Less commonly, the blocks are olistoliths supported within a deformed sedimentary matrix, e.g. 1 km east of Kömür village (gr: İ42, 350199) (Figure 3.47). Two lithological associations are recognised within the Karayaprak Mélange;

- 1) basalt+radiolarian chert, pelagic limestone or mudstone.
- 2) basalt+massive limestone.

Other common components in the mélange include serpentinite, gabbro and diabase (ophiolitic association). Less common lithologies include volcanoclastic shale, lithoclastic sandstone, conglomerate and amphibolite (matrix association). Fissile, sheared serpentinite also occurs along shear zones and as a matrix to mafic and ultramafic blocks.

Pelagic carbonate blocks in the mélange yielded planktonic foraminifera (e.g. *Globotruncana linneiana* (D'ORBIGNY), *Archaeoglobigerina* sp., *Calpionella alpine* (LORENZ), *Calpionella elliptica* (CADISH) and calpionellids) of Early

Cretaceous (Berriasian) age (Prof. Izver Ongen, Prof. Kemal Taşlı and Prof. Nurdan İnan pers. comm. 2004; Appendix 1).

Recrystallised MnO (pyroleucite), haematite ore, Cu carbonate (malachite) and, leached silicate rocks are observed near the sheared contacts of the mélange. These rocks are indicative of SiO₂ and MnO mobilisation and suggest fluid-flow along major tectonic contacts.

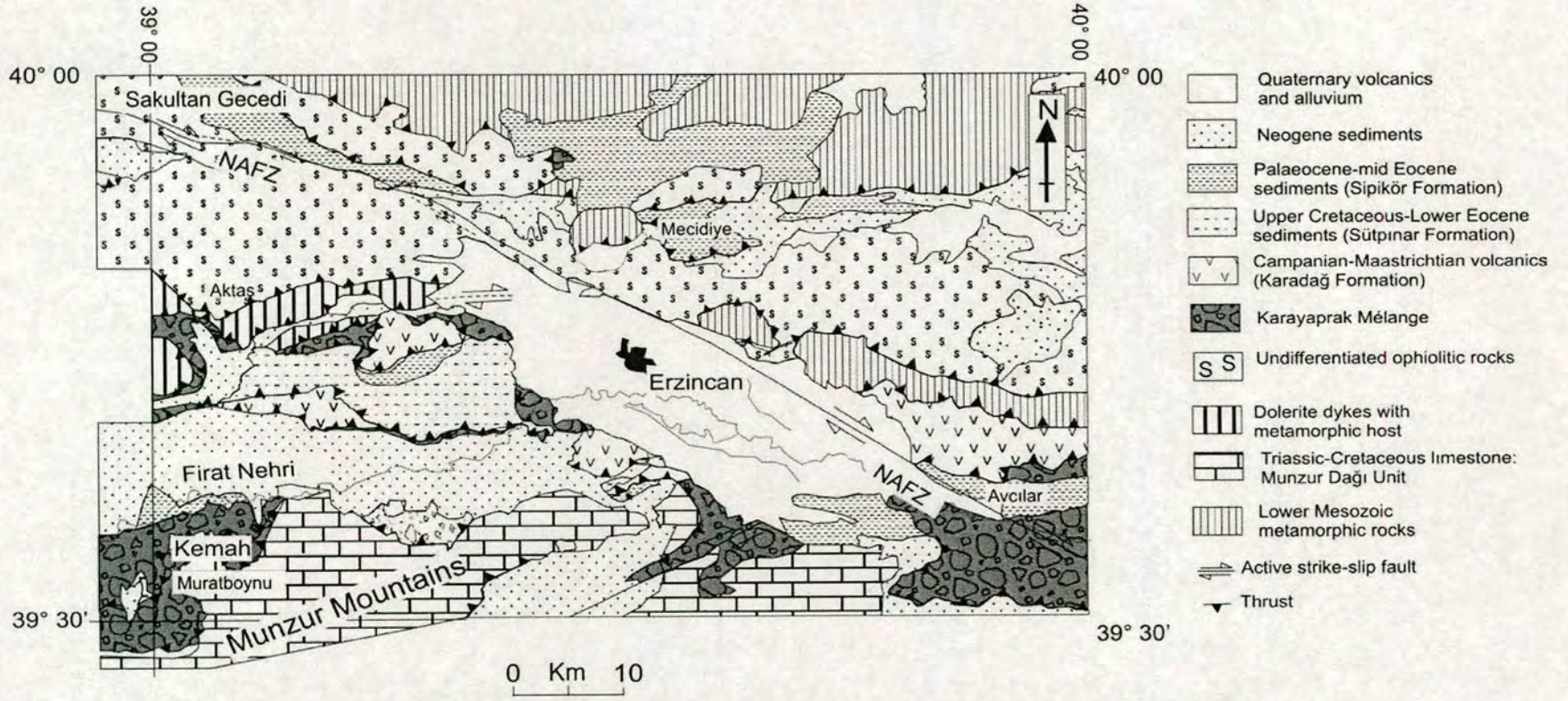


Figure 3.46. Simplified geological map of the Erzincan area showing outcrop of the Karayaprak Mélange.

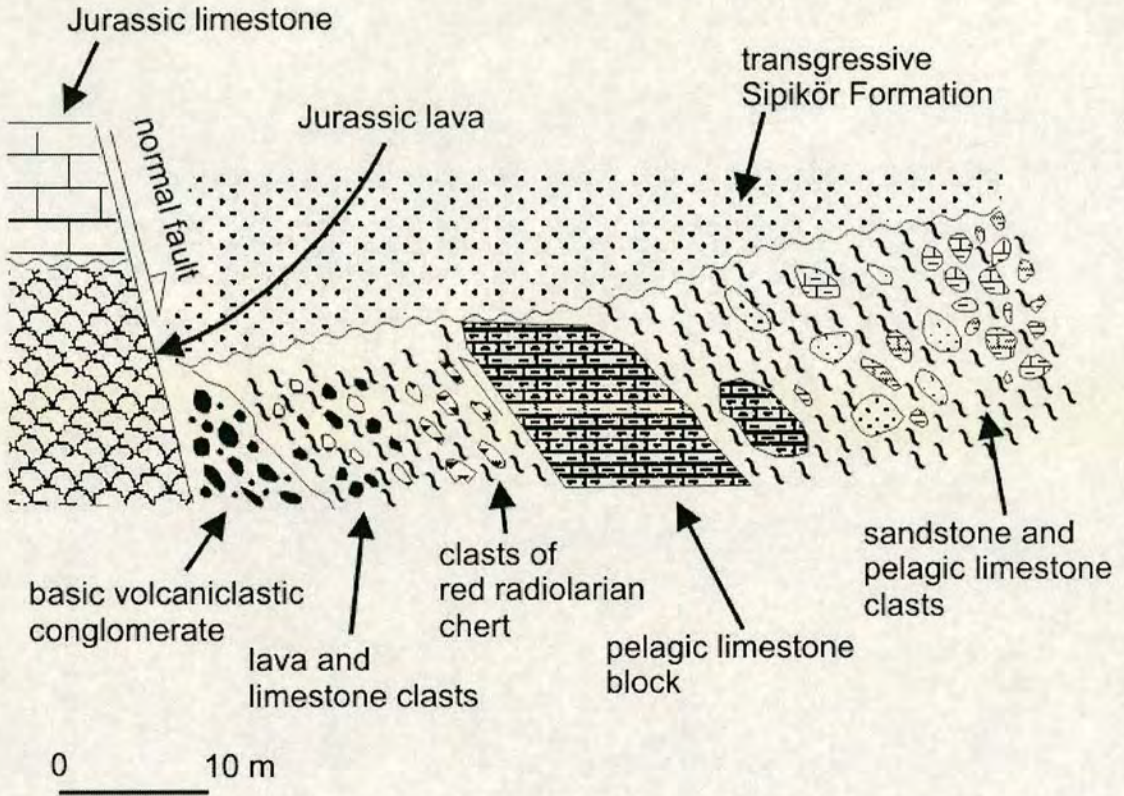


Figure 3.47. Sketch section at Kömür to show the olistostromal mélangé within the Karayaprak mélangé and its local field-relationships (gr: İ42, 350199).

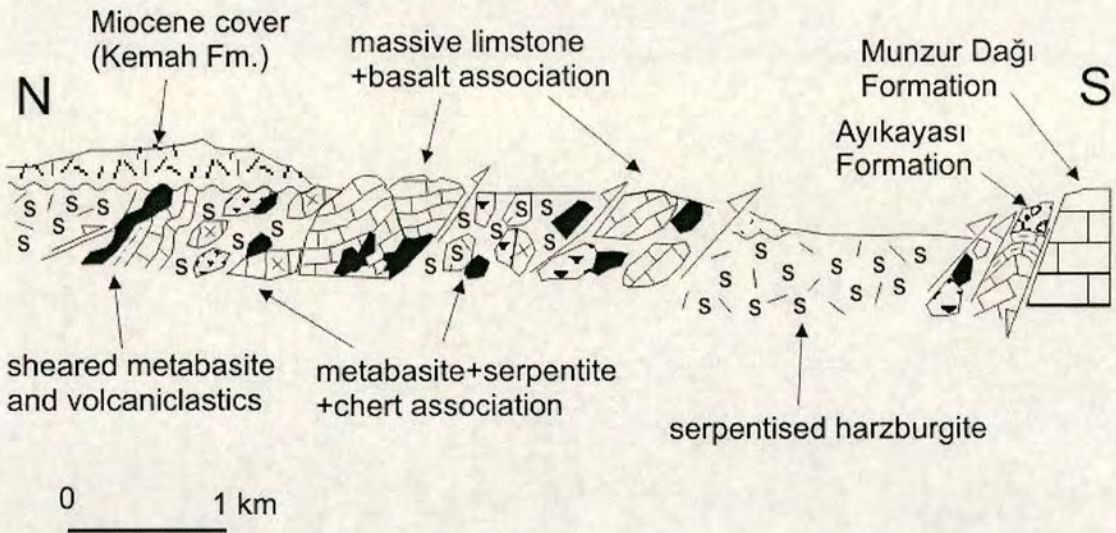


Figure 3.48. Section through outcrop of the Karayaprak Mélangé south of the River Euphrates near Muratboynu (gr: J41, 963731 - 985701).

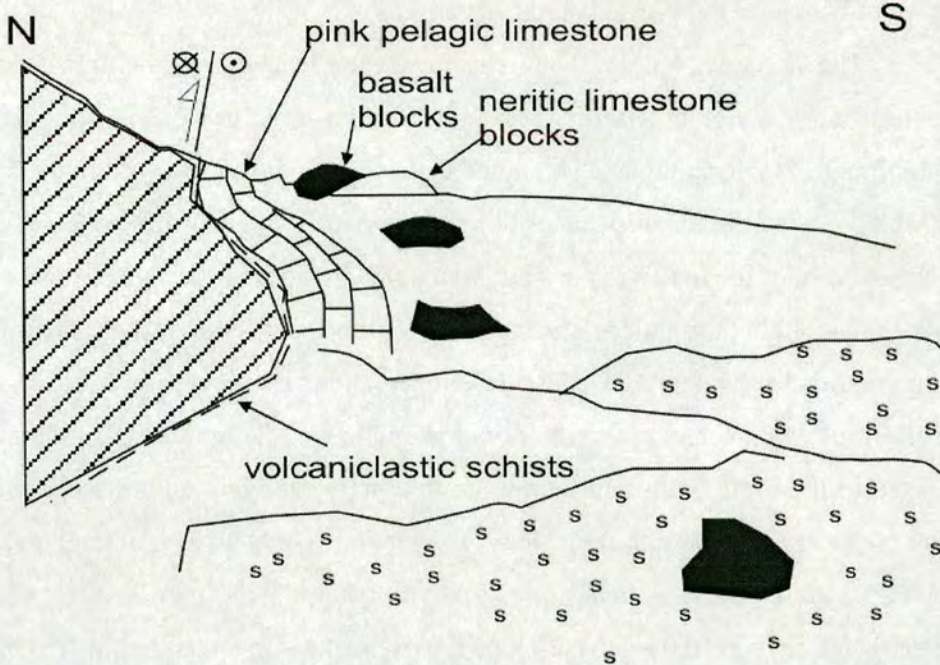


Figure 3.49. Field sketch showing outcrop of a serpentinite+basalt+neritic limestone association within the Karayaprak Mélange near Çardaklı (gr: İ43, 705884).

3.4.1 Structure

Within the mélange shear fabrics anastomose between blocks. Shear fabrics are observed within blocks and in the matrix. Limestone blocks within the mélange exhibit stylolites and tension gashes related to shearing.

The matrix of the mélange most commonly forms discrete zones of lithic crush-breccia or sheared serpentinite. More rarely scaly clay was observed in matrix-dominated horizons (e.g. seen ~20 km north of Erzincan at Kömür Village; gr: İ42, 362207).

Top-to-the-north shear fabric, commonly observed in the mélange is cut by top-to-the-south thrust faults. Top-to-the-north shear fabric is commonly folded and tilted. Orientation data for shear fabrics and fault planes in the Karayaprak mélange are shown in Figure 3.50.

E-W trending steeply inclined thrust faults and strike-slip faults (e.g. 70°N/070; 40°N/130) juxtapose the Karayaprak Mélange with other units, including the younger (Oligocene-Miocene;) sedimentary rocks to the south (exposed along the

Gülandere River ~10 km north of Kemah; Aktimur et al. 1995). These faults commonly exhibit a top-to-the-south shear fabric.

The structures observed in the Karayaprak Mélange, and their cross-cutting relationships are similar to structures described above (section 3.3.1) from the ophiolitic Refahiye Complex. The faults that separate the blocks within the mélange exhibit a range of kinematic senses likely to be related to localised motion of blocks. The structure of the mélange does not reveal the direction of subduction that was associated with its formation. The top-to-the-north shear fabric is correlated with the same fabric observed in the Refahiye Complex and is interpreted as a result of northwards emplacement of the Karayaprak mélange. The top-to-the-south faults that cut top-to-the-north faults and fabrics are interpreted as syn- and post-collisional. The major top-to-the-south faults that form tectonic contacts with other units, including the Tertiary Sivas basin (e.g. Aktimur et al. 1995), may have been reactivated since Tertiary deposition occurred. Strike-slip faults within the mélange may be related to pre-or syn-emplacement deformation and-or Neogene strike-slip tectonics of the North Anatolian Fault Zone.

3.4.2 Sedimentary and igneous petrography of the Karayaprak Mélange

3.4.2.1 Radiolarite-lava-diabase association

In thin section, the lava contains abundant randomly orientated, small (<0.5 mm) elongate plagioclase feldspar (An85%) set in a glassy groundmass. The basalt is non-vesicular and aphyric. Chlorite has completely replaced mafic phases (pyroxene and olivine?). other sections contain interlocking laths of plagioclase (An60%) with augite and pigeonite (<1 mm). Olivine is replaced by iddingsite; magnetite is also present. Much of the basalt is heavily altered and contains secondary epidote, sericite and chlorite. The radiolarite is red and, in thin section, is composed of microcrystalline silica. Radiolarians are commonly recrystallised. The basalt is homogenous and contains calcite veins.

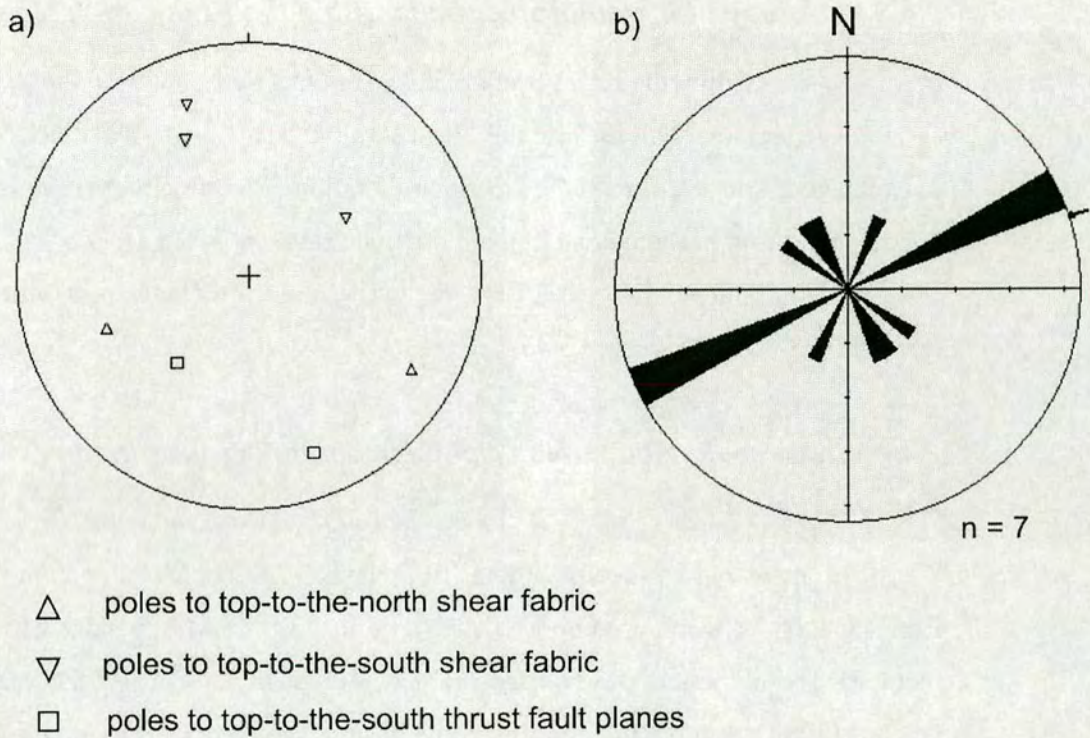


Figure 3.50. Structural data for the Karayaprak Mélange. a) equal-area plot (Lambert/Schmidt) showing orientation of faults and shear zones. b) rose diagram showing strike orientation of faults and shear zones.

3.4.2.2 Massive limestone-lava-volcaniclastic association

The massive limestone-lava-volcaniclastic association contains a coarse (<15 cm) sedimentary breccia (gr: I42, 2523501345) of limestone and lava clasts. The limestone and lava in the breccia are lithologically similar to the larger blocks. In thin section, the matrix of this breccia shows the limestone to be fine-grained, recrystallised limestone with fragmentary bioclasts. Clasts of lava are heavily weathered. Serpentinite clasts are also present. This lava-limestone breccia occurs within a block and is likely to have formed by redeposition of talus prior to accretion of the block into the mélangé.

3.4.3 Petrology of metamorphic rocks within the Karayaprak Mélange

Basalts within the Karayaprak mélange are metamorphosed to the assemblage: epidote±chlorite±calcite±sericite±albite. This greenschist facies assemblage is consistent with the sea-floor alteration of basaltic rocks, and is well documented from oceanic crust in the modern oceans (eg. Mottl 1983).

Amphibolite and greenschist were observed in the mélange near Muratboynu (gr: J41, 9635473130; Figure 3.46).

3.4.4 Whole-rock geochemistry of basic igneous rocks in the Karayaprak Mélange

Eighteen basic igneous samples from the Karayaprak Mélange in the Erzincan area were analysed by XRF (see section 3.3.8.1 and Appendix 1 for method). Ten of the samples had acceptable values of MgO+CaO (in the range 12-22 wt. %) and SiO₂ (< 56 wt. %) for unaltered basic igneous rocks. Among the 10 samples there is no correlation between the abundances of immobile Al and mobile major elements Si, Ca, Fe and, Mg (Figure 3.51), this indicates that mobilisation of these elements was due to alteration, weathering or metamorphism. By contrast, there is reasonable correlation between the abundances of immobile trace elements (Figure 3.52) suggesting they share a common parental magma. When plotted on the total alkalis versus silica rock classification diagram of LeMaitre et al. (1989) (Figure 3.53) the 10 samples exhibit basaltic compositions (1 sample is basaltic trachyandesite). Alteration and weathering are likely to have affected the concentration of K₂O, Na₂O and SiO₂ in the samples. However, the classification diagram based on trace element abundances (Figure 3.54) also shows the rocks to be of basaltic/andesitic composition and, therefore, suitable for use in geochemical tectonic discrimination. Plotted on the MORB-normalised 'spider diagram' (Figure 3.55) the patterns produced by all 8 of the samples have negative Nb anomalies and enrichment of the

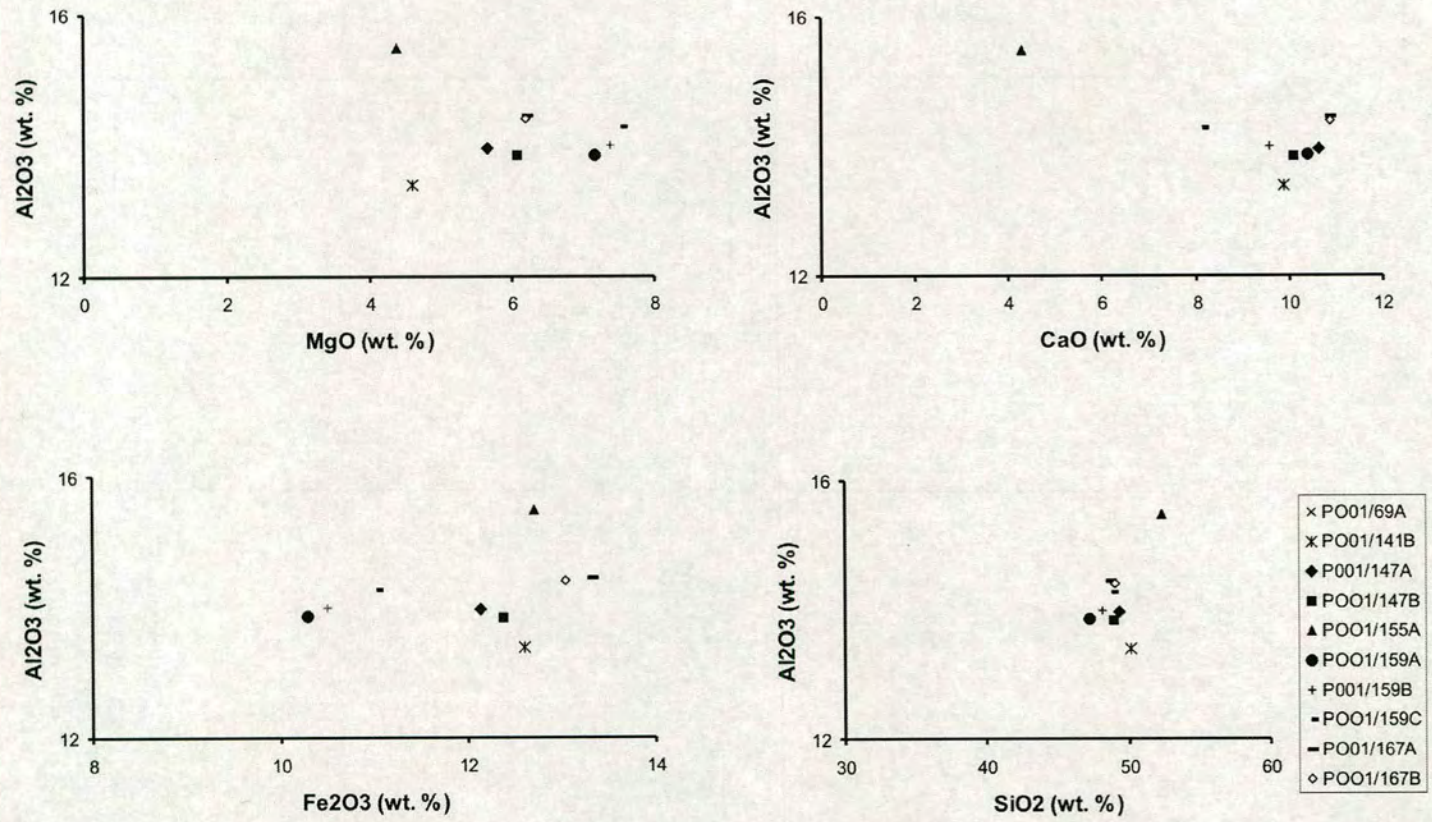


Figure 3.51. Variation diagrams (Harker 1909) of mobile major elements Si, Ca, Fe, Mg against relatively immobile Al for basic igneous rocks from the Karayaprak Mélange in the Erzincan area.

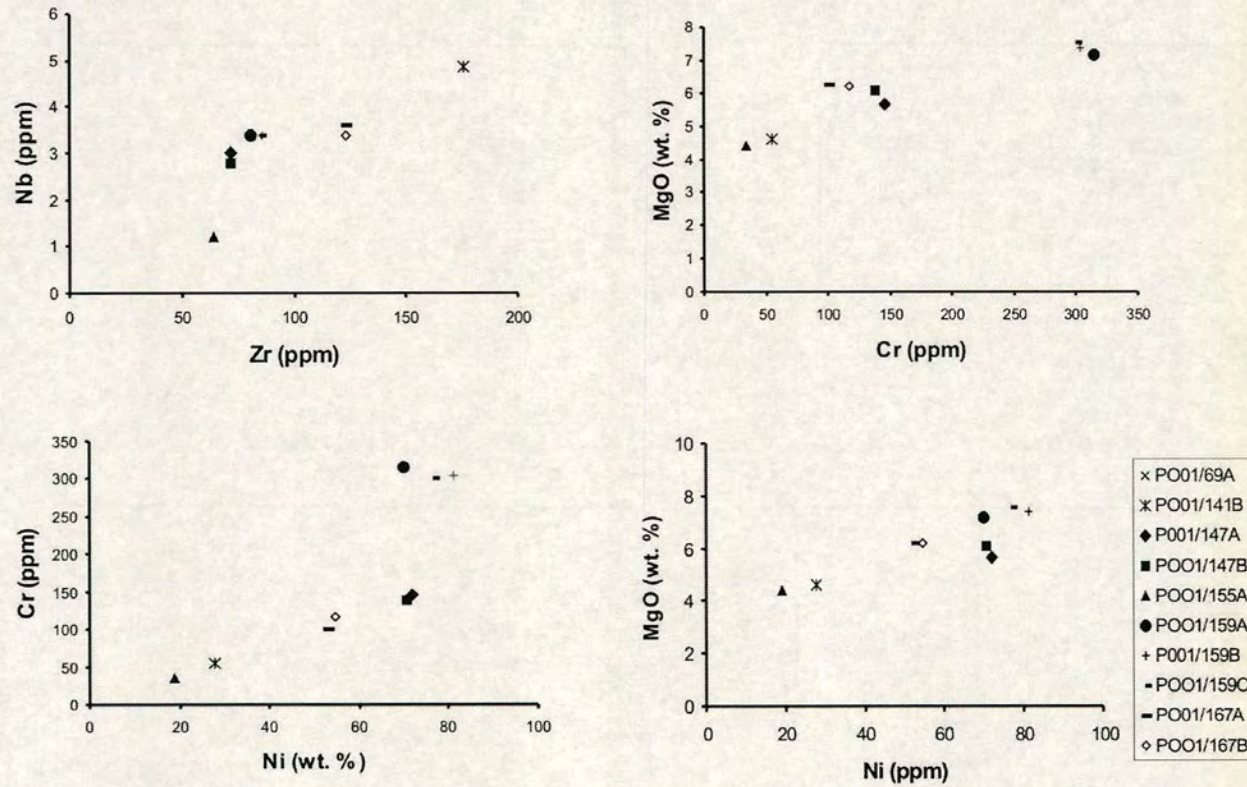


Figure 3.52. Variation diagrams (Harker 1909) of immobile trace elements for basic igneous rocks from the Karayaprak Mélange in the Erzincan area.

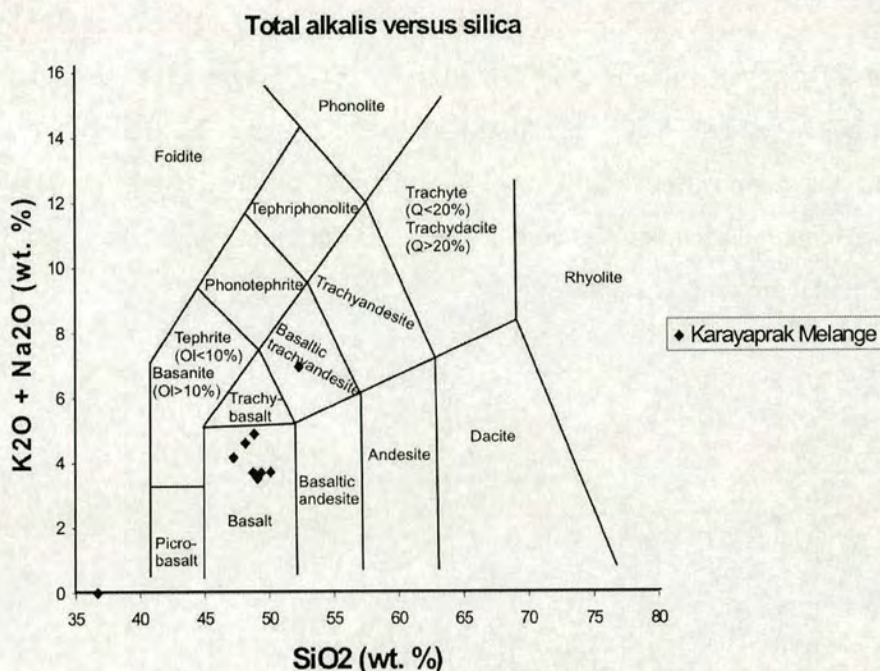


Figure 3.53. Samples from the Karayaprak Mélange plotted on the total alkalis versus silica rock classification diagram (LeMaitre et al. 1989).

mobile elements Sr, K, Rb and Ba relative to MORB. The mobile element enrichment is variable and may well be due to alteration and weathering. By contrast, the persistent negative anomaly of Nb, an immobile element, suggests a possible subduction influence on the source region (Pearce et al. 1973; Saunders et al. 1988).

However, the samples do not show a depletion of immobile incompatible elements (La, Ce, Nd, P, Zr) relative to MORB as would be expected of volcanic arc rocks (Pearce 1973). This may be due to the degree of magmatic evolution indicated by the andesitic-dacitic compositions of the samples. One sample (PO01 141B) exhibits a flat-lying pattern with no negative Nb anomaly (Figure 3.56). PO01 141B is more enriched in all the elements apart from Cr and K, consistent with a composition more evolved than MORB (Pearce 1973).

On the discrimination diagrams (Figure 3.57 to 3.63) the basalts fall within the compositional range for MORB (MORB, N-MORB or 'Ocean-Floor Basalts'). In

some of the diagrams the compositions of the samples from the Karayaprak Mélange overlap with the fields for 'Low Potassium Tholeiite'/'Arc Lavas'/'Island Arc Tholeiite'/'Volcanic Arc Basalt'/'Island arc Basalt' and the field for 'Within-Plate Lavas'. However, with the exception of the Ti-Zr-Y diagram (Pearce and Cann 1973; Figure 3.57) and the V-Ti diagram (Shervais 1982; Figure 3.62) all of the samples fall within the compositional field for MORB. In none of the diagrams do the samples show element enrichments characteristic of within-plate (i.e. oceanic island basalt) or continental arc eruptive settings.

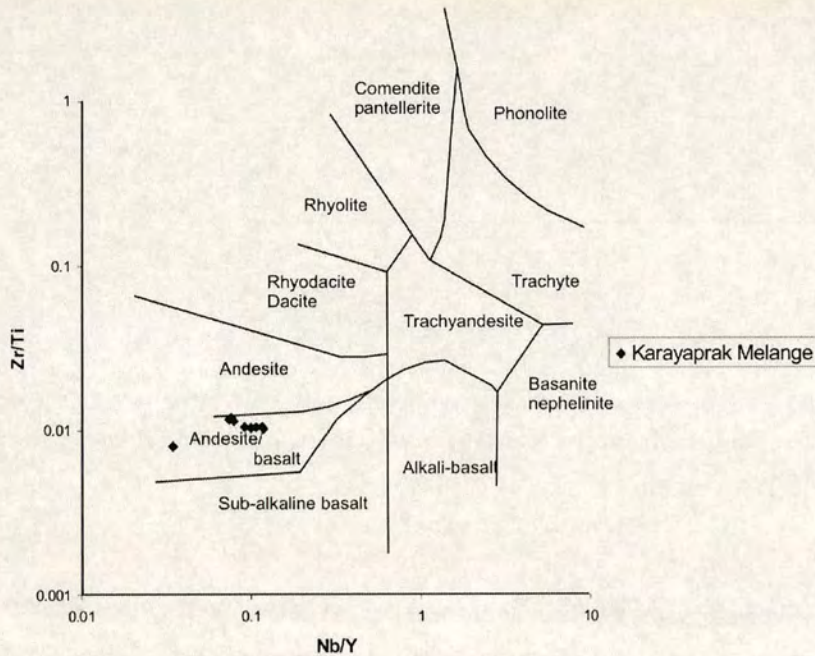


Figure 3.54. Samples from the Karayaprak Mélange plotted on the Zr/Ti versus Nb/Y rock classification diagram (Winchester and Floyd 1977).

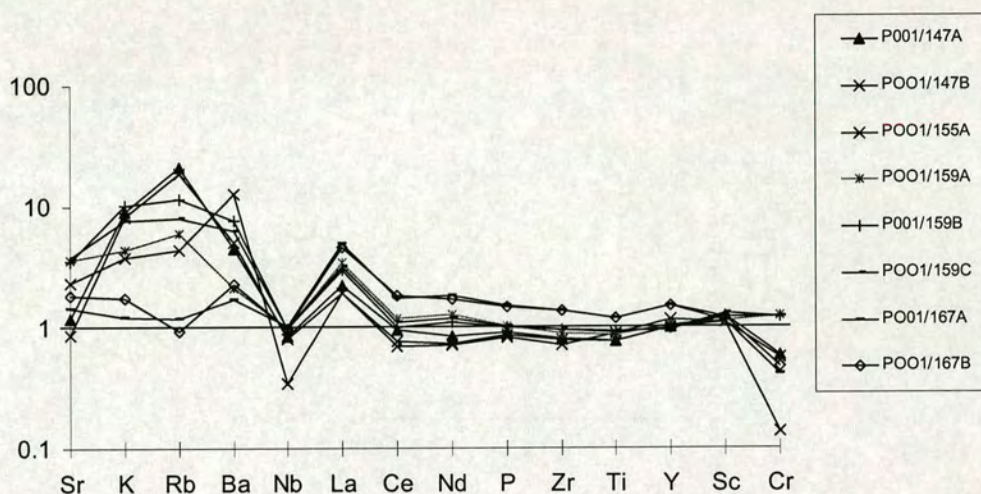


Figure 3.55. MORB-normalized multi-element abundances for igneous samples from the Karayaprak mélange with a -ive Nb spike. Normalizing values: Sr = 120 ppm; K₂O = 0.15% ; Rb = 2.0 ppm; Ba = 20 ppm; Nb = 3.5 ppm; La = 3 ppm; Ce = 10 ppm; Nd = 8 ppm; P₂O₅ = 0.12% ; Zr = 90 ppm; TiO₂ = 1.5% ; Y = 30 ppm; Sc = 40 ppm; Cr = 250 ppm (Pearce et al. 1984).

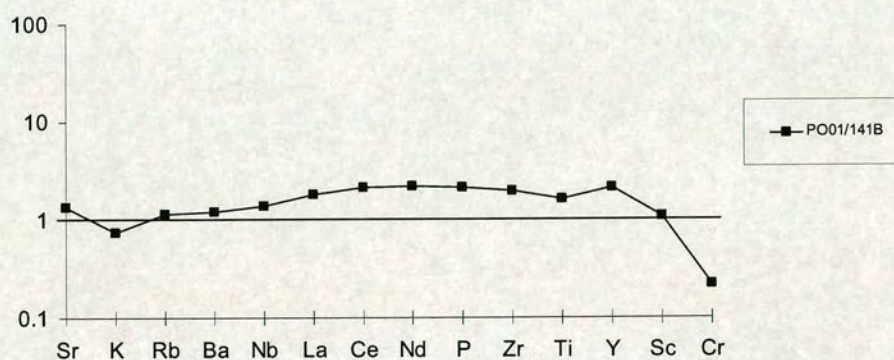


Figure 3.56. MORB-normalized multi-element abundances for one igneous sample from the Karayaprak mélange with a flat-lying pattern. Normalizing values: Sr = 120 ppm; K₂O = 0.15% ; Rb = 2.0 ppm; Ba = 20 ppm; Nb = 3.5 ppm; La = 3 ppm; Ce = 10 ppm; Nd = 8 ppm; P₂O₅ = 0.12% ; Zr = 90 ppm; TiO₂ = 1.5% ; Y = 30 ppm; Sc = 40 ppm; Cr = 250 ppm (Pearce et al. 1984).

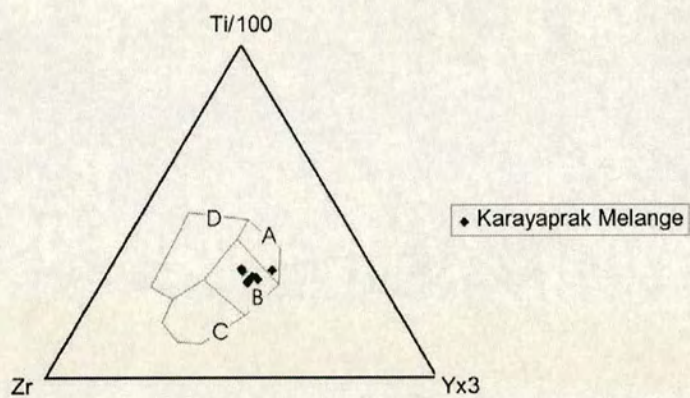


Figure 3.57. Basic igneous rocks from the Karayaprak M \acute{e} lange plotted on a discrimination diagram using Ti, Zr and Y (Pearce and Cann 1973). Within-plate basalts field D, ocean-floor basalts in field B; low-potassium tholeiites in fields A and B, calc-alkali basalts in fields C and B.

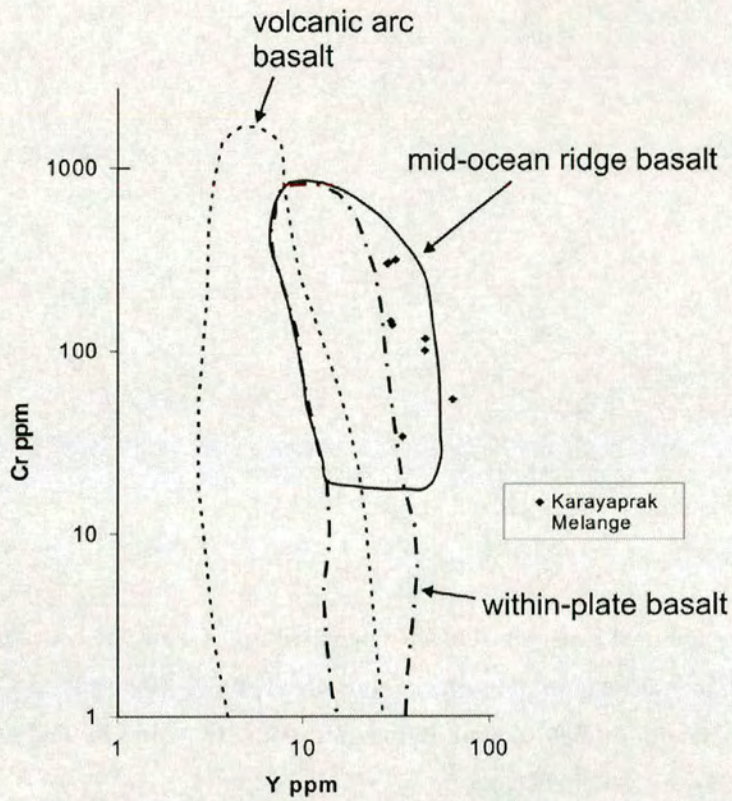


Figure 3.58. Geochemical analyses of basic igneous samples from the Karayaprak M \acute{e} lange plotted on a discrimination diagram based on Cr-Y covariations (Pearce 1982).

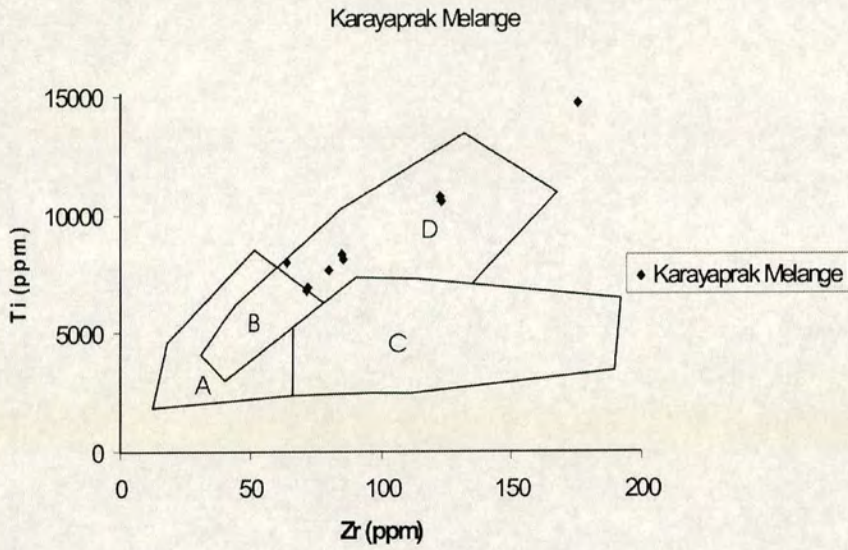


Figure 3.59. Geochemical analyses of basic igneous samples from the Karayaprak Mélange plotted on a discrimination diagram using Ti and Zr (Pearce and Cann 1973). Ocean-floor basalts plot in fields D and B, low-potassium tholeiites in fields A and B, and calc-alkali basalts in fields C and B.

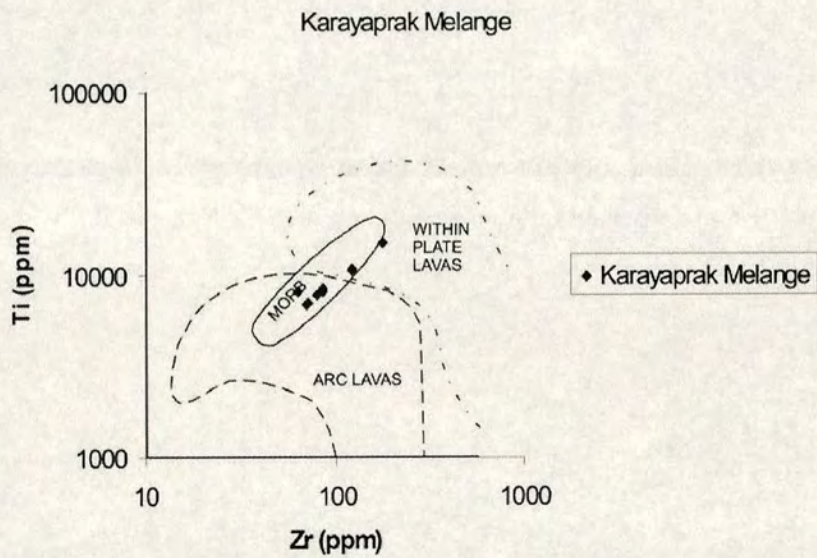


Figure 3.60. Basic igneous rocks from the Karayaprak Mélange plotted on the log Ti/log Zr Discrimination diagram (Pearce 1982). Ocean-floor basalts plot in fields D and B, low-potassium tholeiites in fields A and B, and calc-alkali basalts in fields C and B.

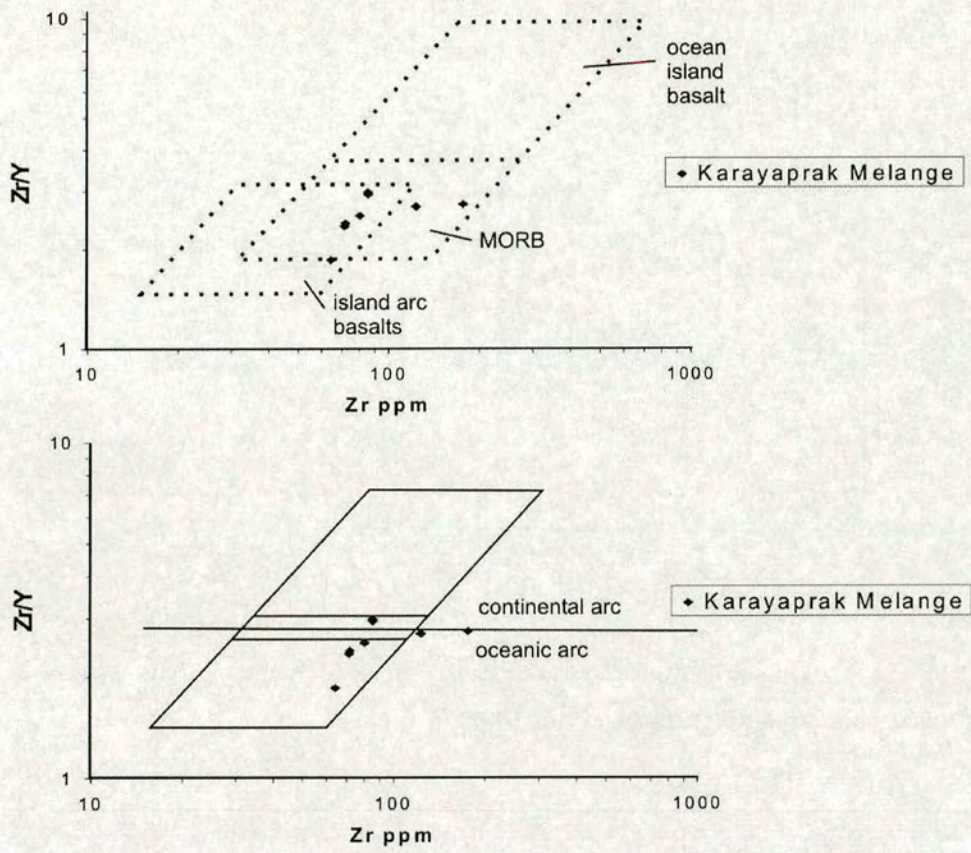


Figure 3.61. Basic igneous rocks from the Karayaprak M \acute{e} lange plotted on the Zr/Y versus Zr discrimination diagram (Pearce and Norry 1979).

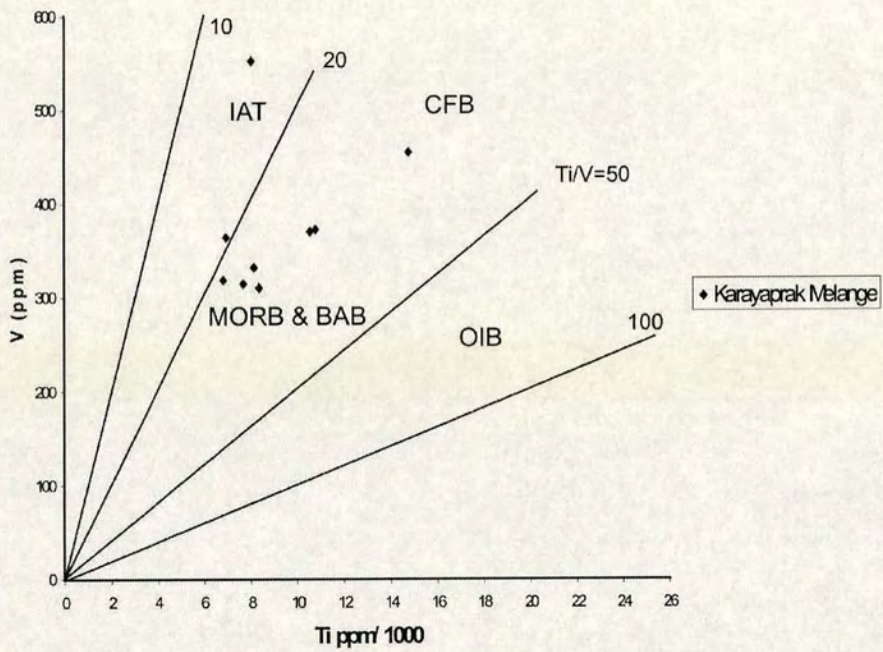


Figure 3.62. Basic samples from the Karayaprak Mélange plotted on the V/Ti discrimination diagram (Shervais 1982).

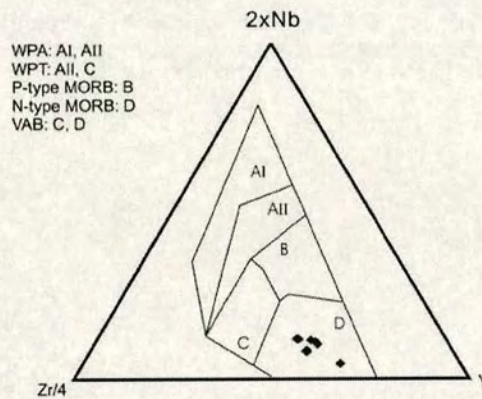


Figure 3.63. Basic rocks from the Karayaprak Mélange plotted on the Nb/Zr/Y discrimination diagram (Meschede 1986). AI and AII = within-plate alkali basalt compositional field; B = plume-influenced MORB compositional field; C = within-plate tholeiite compositional field; D = N-type MORB and volcanic arc basalt.

3.4.5 Timing and tectonic setting of the development of the Karayaprak Mélange

The presence of basalt interbedded with, and overlain by, neritic limestone indicates deposition above the CCD, possibly on a seamount. This association also contains coarse debris composed exclusively of basic lava and massive limestone. The chaotic debris-flow deposits may well represent mass wasting of a seamount prior to its inclusion into the *mélange* as it approached the trench. This process is occurring today at the Tonga trench (Capricorn Seamount; Clift et al. 1998) and also the Ijima seamount, Japan (Mohiuddin and Ogawa 1998.). By contrast, the lava-pelagic sediment association is interpreted as abyssal plain sedimentary rocks that accumulated on oceanic crust, of which only the highest levels were preserved by accretion into the *mélange*. In addition, other rock types, e.g. deformed blocks of volcanoclastic and polymict sedimentary rocks could represent accreted trench-fill sedimentary rocks. The predominance of igneous and hemipelagic sedimentary blocks over terrigenous clastic sedimentary rocks and, paucity of sedimentary matrix suggests that the accretionary wedge developed in an oceanic setting, remote from any potential supply of terrigenous sediment.

The massive limestone-lava-volcanoclastic association together with debrites and limestone talus suggests that volcanic seamounts were accreted at the trench. However, whole-rock basalt geochemistry supports a normal mid-oceanic spreading ridge eruptive setting for basalts within the *mélange*. The greater probability of magmatic evolution occurring during the petrogenesis of the volcanic seamount lavas could lead to a bias in the data (i.e. samples from the massive limestone-lava-volcanoclastic association were not useful in tectonic discrimination due to their more evolved compositions).

3.4.6 Summary

The Karayaprak Mélange is interpreted as an emplaced Cretaceous accretionary complex. Blocks within the The Karayaprak Mélange contain microfossils that indicate an Early Cretaceous age (e.g. Berriasian; 145.5-140.2 Ma; Gradstein et al. 2004). This reflects the age of the Neotethyan lithosphere that was being subducted during mélangé accretion. The Karayaprak Mélange contains two associations interpreted as; 1) Spreading ridge tectonic facies and; 2) Volcanic seamount tectonic facies (Robertson 1994). The Volcanic seamount facies contains angular lava and limestone talus which could have formed during collapse of a seamount as it approached the trench (i.e. before its inclusion into the accretionary wedge). The mélangé contains a relative paucity of terrigenous clastic sedimentary rocks and sedimentary matrix suggesting that the accretionary complex developed in an oceanic setting. Rare olistostromal levels are present within the mélangé.

Outcrop of the unit is more abundant toward the south of the suture zone i.e. south of the Refahiye Complex and the Karadağ Formation. This probably reflects the original position of the accretionary complex relative to the arc. The mélangé is thrust southward over the ?Permian-Upper Cretaceous Munzur Dağı Formation (carbonate platform) and the Upper Cretaceous (Turonian-Campanian; 93.5-70.6 Ma; Gradstein et al. 2004) Ayıkayası Formation (inferred flexural foredeep). The mélangé is unconformably overlain by Palaeocene-Eocene (65.5-33.9 Ma; Gradstein et al. 2004) sedimentary rocks (Sipikör Formation). The mélangé was emplaced southward between Turonian-Campanian time (93.5-70.6 Ma) and Palaeocene-Eocene time (65.5-33.9 Ma).

3.5 Emplaced oceanic volcanic arc: Karadağ Formation

The Upper Cretaceous Karadağ Formation contains a mixture of metamorphosed volcanic, intrusive and sedimentary rocks and exhibits dynamometamorphic textures and structures such as mylonitic and C-S fabrics. Exposures commonly exhibit abundant thrust faults and shear zones which indicate a polyphase deformation history.

The Karadağ Formation crops out as four large discontinuous thrust slices in the Erzincan area (individually up to 10 km long and $< \sim 3$ km thick) (Figure 3.64). Thrust slices of the Karadağ Formation are found at two structural levels within the south-vergent imbricate thrust stack. In some sections lava occurs as isolated flows within a sedimentary succession, while other sections are dominated by lava flows, with little or no sediment for thicknesses of several hundred metres. Southwest of Binkoç village (gr: İ43, 4236389247) *Globotruncana*-bearing pelagic limestones within the Karadağ Formation indicate that the unit is of Late Cretaceous age (I Ongen pers. comm. 2004). See Appendix 3; micropalaeontological data.

The lower-level slices of the Karadağ Formation were observed west of Erzincan at Karadağ, near Doğanbeyli (gr: İ42, 100950) and south of Erzincan at Karadağ, near Binkoç (gr: İ43, 385882) (note: there are three mountains named Karadağ, i.e. “Black Mountain” in the Erzincan area). These thick slices of volcanic and volcanoclastic rocks are thrust over Miocene sedimentary rocks that crop out to the south. The upper and lower boundaries of the unit are north-dipping thrust faults and shear-zones, e.g. observed near Gökkaya (Figure 3.65). However, near Doğanbeyli a vertically orientated tectonic contact was observed (Figure 3.66). West of Bahçeli (gr: İ42, 2478701428) and at Köhnemdağ the thick volcanic succession of the Karadağ Formation is thrust over a thin (~ 4 m) succession of recrystallised pink pelagic limestone.

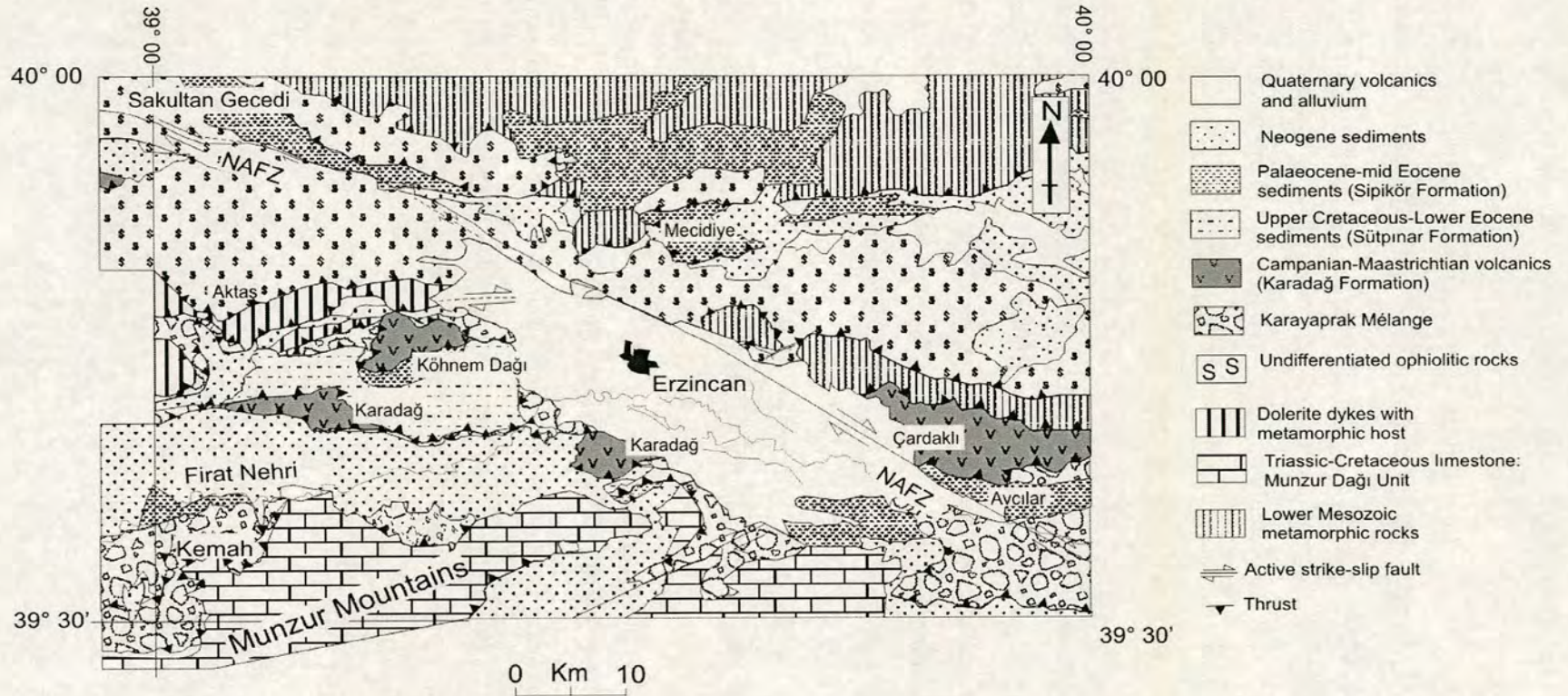


Figure 3.64. Map of the Erzincan area showing the outcrop of the Upper Cretaceous Karadağ Formation.

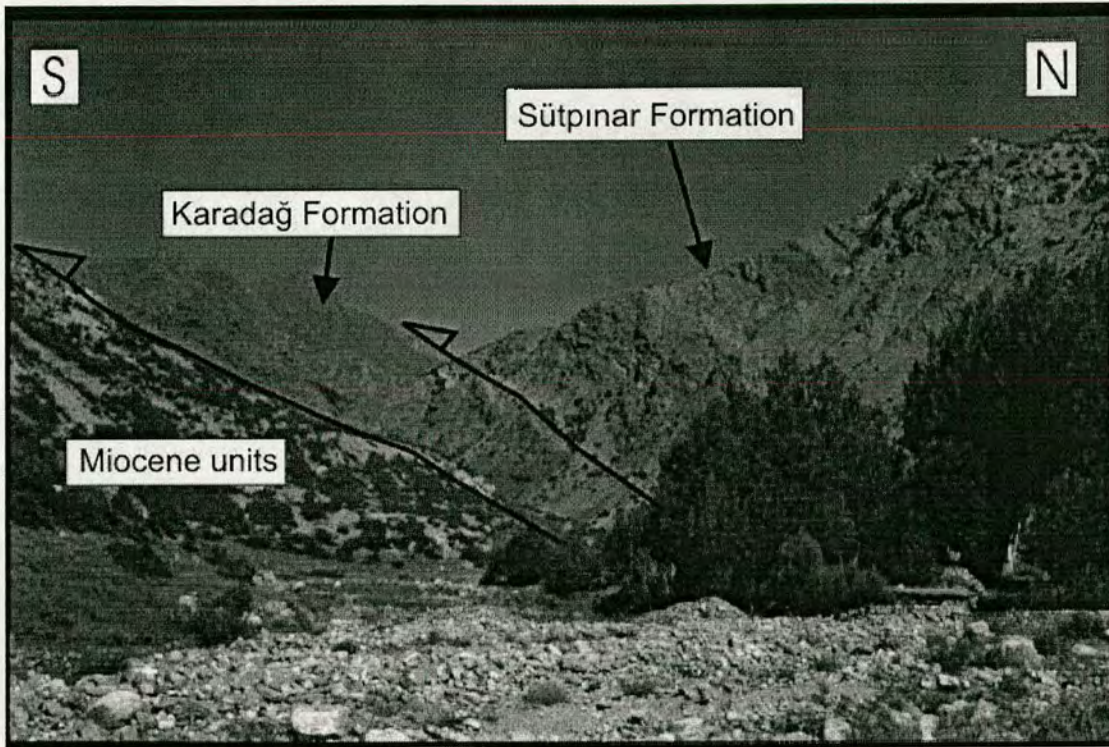


Figure 3.65. Photograph looking west from Gökkaya. The outcrop of the Upper Cretaceous Karadağ Formation ‘pinches out’. Both the upper and lower boundaries of the unit are north-dipping thrust faults.

Structurally higher slices of the Karadağ Formation crop out west of Erzincan at Köhnemdağ (gr: İ42, 177993) and east of Erzincan at Çardklı (gr: İ43, 692905) (Figure 3.64); these are again bounded by north-dipping thrust faults (Figure 3.64). The upper thrust slices of the Karadağ Formation are tectonically overlain by a thick (~4 km) slice of metamorphic basement. To the west of Erzincan these metamorphic rocks form part of the Upper Cretaceous ophiolitic Refahiye Complex (section 3.3.7; Figure 3.64).

In some sections lava occurs as isolated flows within a metasedimentary succession, while other sections exhibit little or no sediment over thicknesses of several hundred metres or more. Individual sections commonly exhibit a tectonically mixed succession of deformed meta-volcanic and meta-sedimentary rocks (Figure 3.67). Thick successions (i.e. >3km long) of 100% andesite are observed at Karadağ

(near Doğanbeyli; gr: I42, 100950) and at Karadağ, south of Binkoç (gr: I43, 395873).

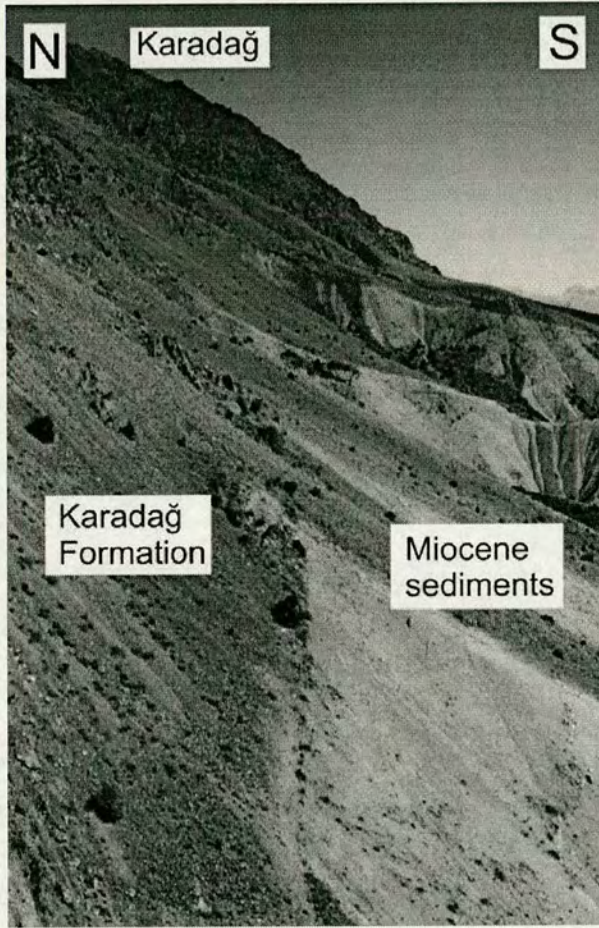


Figure 3.66. Photograph looking east towards Karadağ, 6 km east of Doğanbeyli to show the vertical tectonic contact between the Upper Cretaceous Karadağ Formation and Miocene sedimentary rocks.

3.5.1 Structure

The Karadağ Formation is bounded by sub-vertical and north-dipping thrusts (Figure 3.65 and 3.66). Structurally higher thrust slices (located in the northern part of the suture zone e.g. Çardaklı, gr: I43, 710880; Köhnamdağı, gr: I42, 180990) exhibit well-cleaved schistose metasedimentary rocks interbedded with massive

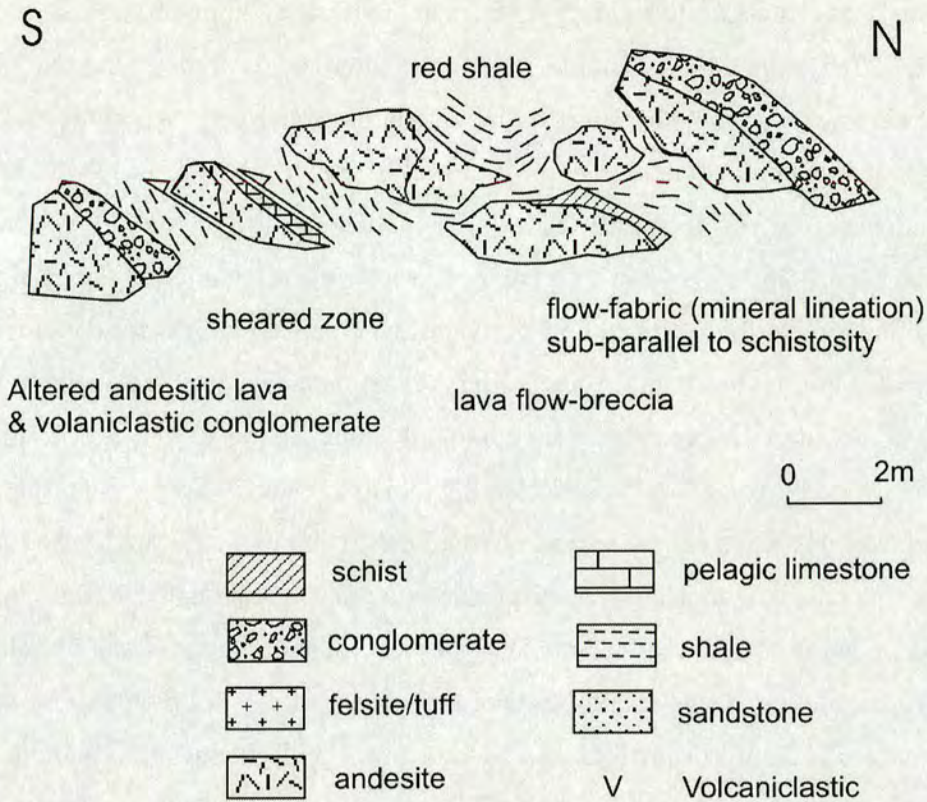


Figure 3.67. Field sketch of a section of the Karadağ Formation exposed at Köhnemdağı Yayla (gr: I42, 200005).

lavas. Cleavage is less well developed in the structurally lower thrust slices further south (e.g. Karadağ, gr: İI42, 390880; Karadağ, gr: İ42, 120940). Cleavage and bedding within the unit predominantly dip towards the north and are sub-parallel. Early structures (e.g. flow-bands in rhyolite, cleavage and schistosity) are folded, faulted

and sheared with a top-to-the-north sense of motion. Top-to-the-north structures are commonly cut by top-to-the-south structures. For example, at Köhnemdağı (gr: İ42, 180990) an andesitic lava flow is boudinaged within a mass of sheared volcanoclastic shale and schist (Figure 3.67). The andesite exhibits a south-dipping shear fabric (top-to-the-north; $60^{\circ}\text{S}/140$) which has been replaced by a north-dipping sinistral strike-slip shear fabric in the surrounding sheared metasedimentary rocks ($52^{\circ}\text{S}/110$).

The Karadağ Formation exhibits asymmetrical folds with long-limbs and axial surfaces inclined to the northwest and, short-limbs dipping steeply toward the south. These south-vergent structures fold the top-to-the-north shear fabric and

associated cleavage and bedding surfaces in the Karadağ Formation. At Berişerif (gr: İ41, 955151) small (wavelength ~15 cm) asymmetrical recumbent chevron folds fold the cleavage within the overturned limb of a larger south-vergent recumbent fold (facing direction not known). Short-limbs of the minor folds dip steeply to the southwest. The enveloping surfaces of the minor folds dip $35^{\circ}\text{NE}/040^{\circ}$ and their axial planes dip $35^{\circ}\text{SW}/045^{\circ}$. Figure 3.68a shows the orientation of the axial plane of a south-vergent fold. All bedding, cleavage and crenulation cleavage data for the Karadağ Formation are also shown. The fold axial plane is inclined gently towards the northwest. Cleavage planes are commonly not axial planar to the fold. However, crenulation cleavage is sub-parallel to the fold axial plane. This indicates that south-vergent folds represent the second phase of deformation in the Karadağ Formation, and that crenulation cleavage is axial planar to a second phase of folding. This second phase of deformation was south-vergent. In addition to folding by south-vergent folds, cleavage and top-to-the-north shear fabric is cut by top to the south thrust faults that form small duplex structures within the Karadağ Formation.

Steeply inclined and sub-vertical sinistral strike-slip faults were also observed within the unit. Their orientation ranged from 110 to 190.

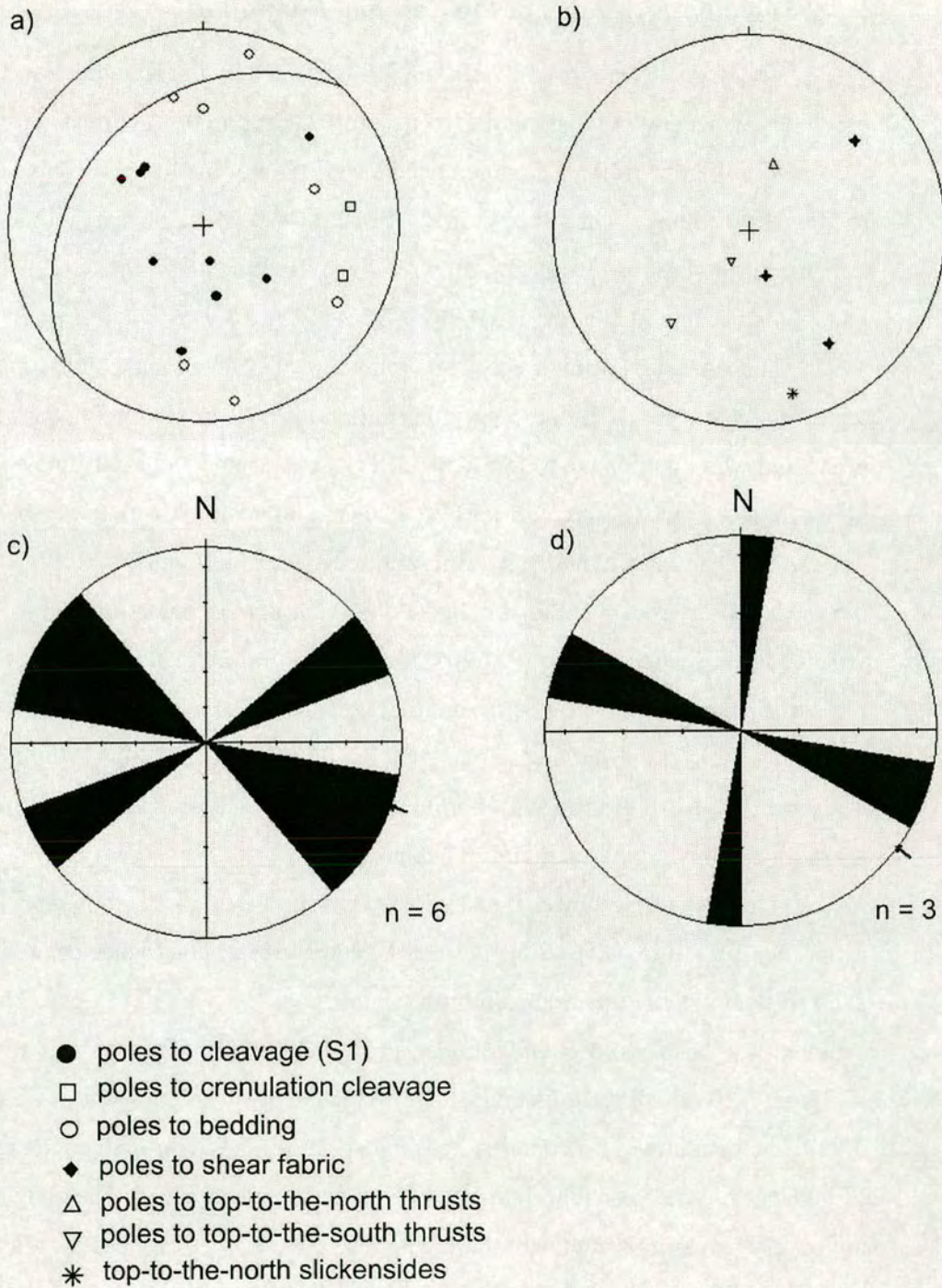


Figure 3.68. Structural data for the Karadağ Formation. a) equal-area plot (Lambert/Schmidt) showing bedding, cleavage and fold data; b) equal-area plot (Lambert/Schmidt) showing fault data; c) rose diagram showing strike orientations of thrust faults; d) rose diagram showing strike orientations of strike-slip faults.

3.5.2 Sedimentary facies of the Karadağ Formation

The degree of polyphase deformation exhibited by the Karadağ Formation precludes an accurate reconstruction of its entire stratigraphy. A composite log is presented in Figure 3.69 and a generalised description of the lithologies and relationships follows. The succession at Çardaklı (>1 km) displays a gradual transition from basic and andesitic flows and metasedimentary rocks to felsic metavolcanics and tuffite (gr: İ43, 6989290644; Figure 3.71).

The Karadağ Formation exhibits remnants of bedding and coarse-grained textures are preserved. Thin (<5 cm), discontinuous beds of alternating dark grey-green and white laminated, to thinly bedded (<1 cm), shale and sandstone occur between lava flows (Figure 3.70). These beds are intercalated with thinly-bedded (<1 cm) dark volcanoclastic mudstone, fine-grained calcareous and tuffaceous metasedimentary rocks and thickly bedded (~1-2 m) pale, coarse-grained volcanoclastic sandstone (Figure 3.70). Thin (~2m) turbiditic successions of regularly alternating beds (~4 cm) of dark and pale green/grey volcanoclastic pelite and psammite were observed (e.g. near Çardaklı gr: İ43, 6989290644; Figure 3.71). The succession also grained with purple and orange volcanic clasts of intermediate and acidic composition, including rare chert.

The structurally lower thrust slice, exposed further south, contains a lower proportion of pelitic metasedimentary rocks and a greater abundance of psammite and rudite in which dynamometamorphic fabrics are less-well developed. The sedimentary rocks (exposed at Gölpınar, gr: İ43, 3899391174) are mainly thick-bedded (<~10 m) coarse-grained (<40 cm) volcanoclastic conglomerates (Figure 3.72). The conglomerates contain sub-rounded, to sub-angular boulders and pebbles of feldspar-phyric, vesicular, purple and pink andesite and basalt. The conglomerates are poorly- containins abundant thickly bedded (<3 m), massive, coarse-grained (<20 cm) volcanoclastic conglomerates. The volcanoclastic conglomerates are matrix-supported, and poorly sorted with sub-rounded clasts. The matrix is dark and fine-sorted, lenticular bodies with erosive bases, interbedded with purple/pink, amalgamated, medium- to thickly bedded (< 5 m) and massive, coarse-grained (1 mm), angular, arkose. The arkose contains ~30% quartz, ~30% feldspar and, ~30%

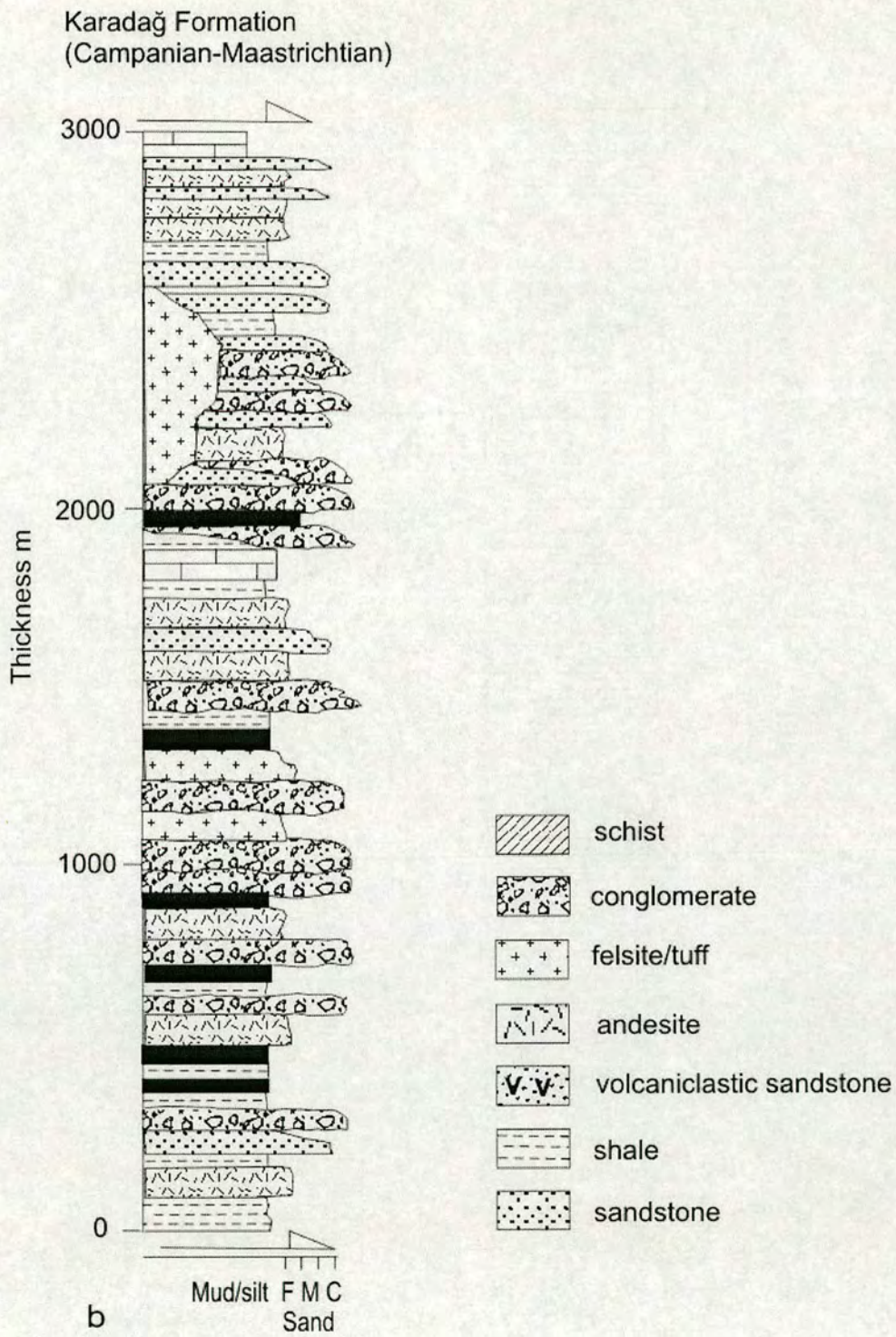


Figure 3.69. Composite log of the Karadağ Formation.

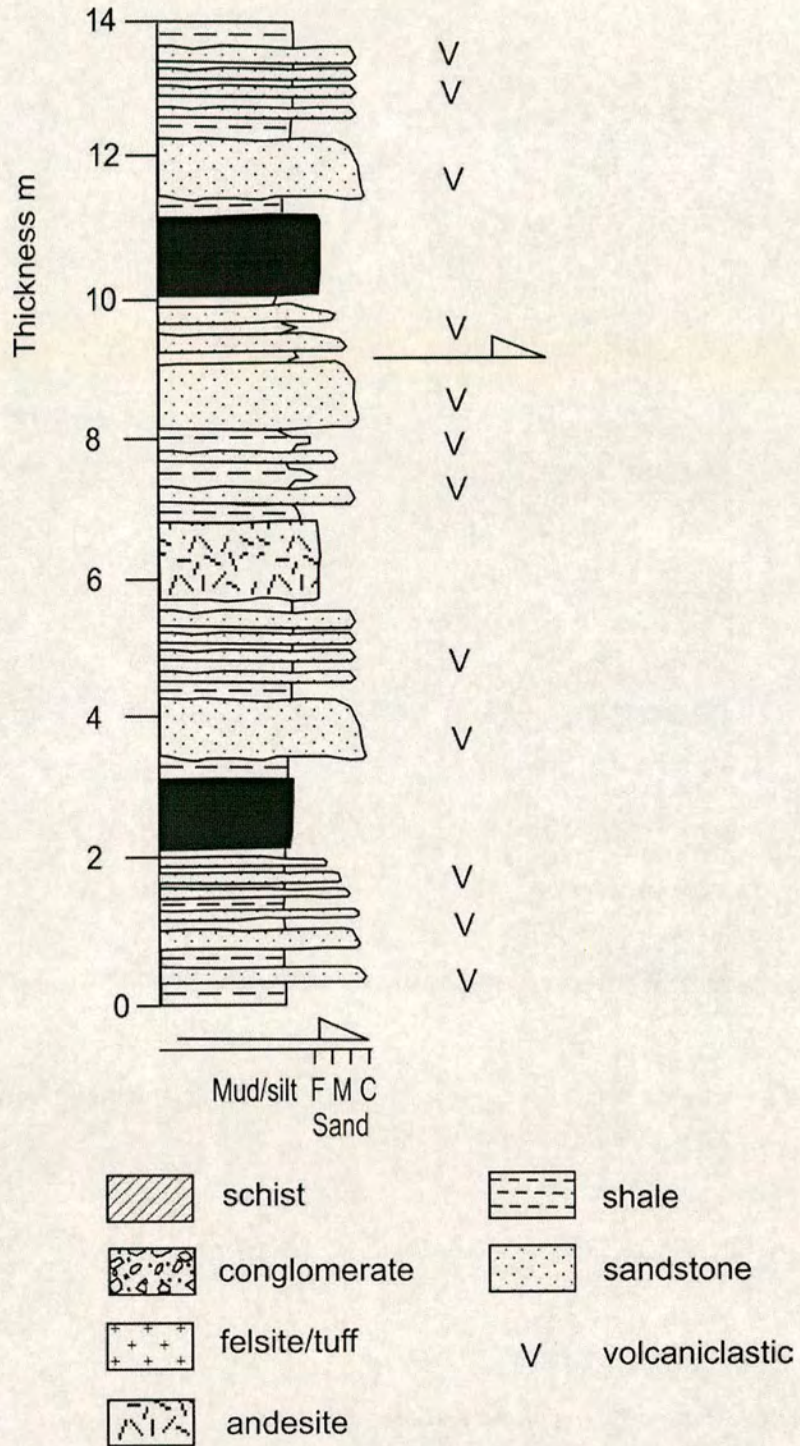


Figure 3.70. Log of part of the structurally higher thrust slice of the Karadağ Formation at Köhnemdağ (gr: İ42, 1968900455).

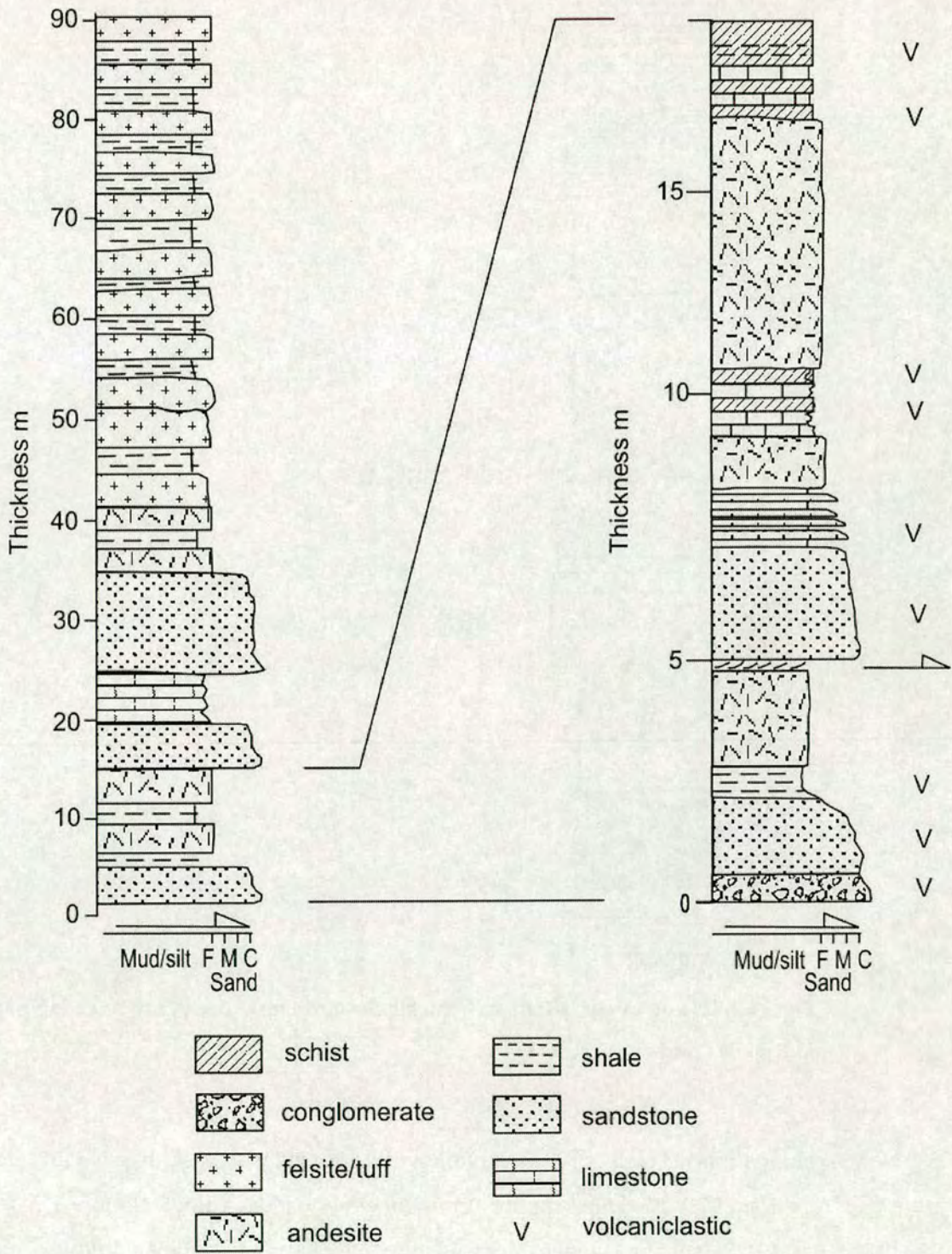


Figure 3.71. Log of part of the structurally higher thrust slice of the Karadağ Formation at Çardaklı (gr: İ43, 6989290644).

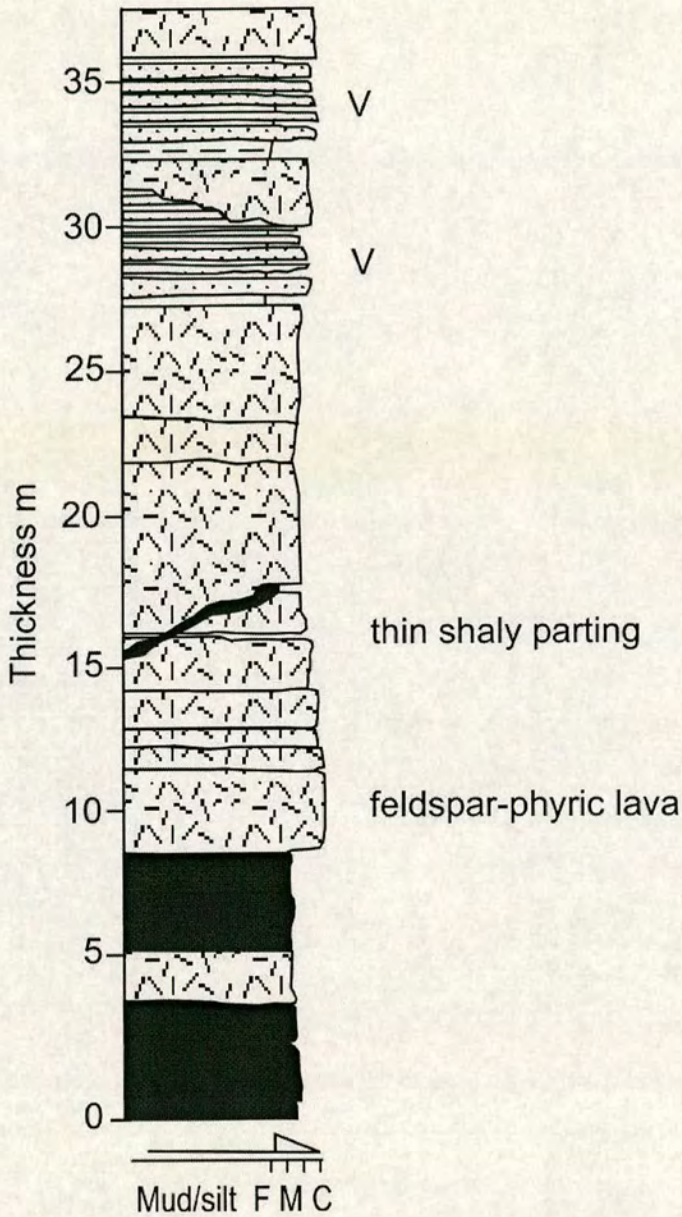


Figure 3.72. Log of part of the structurally lower thrust-slice of the Karadağ Formation at Binkoç (gr: İ43, 3899391174).

mafic grains. Thick (<10 m), irregular lenses of pale yellowish massive tuff are interbedded with the psammites, conglomerates and lava-flows (Figure 3.74).

Pelagic limestones interbedded with the lava and sedimentary rocks contain the age-diagnostic planktonic foraminifera, *Globotruncana sp.* and *Rugoglobigerina sp.* indicating that the unit is of Late Cretaceous age (Prof. Izver Ongen, Prof. Kemal Taşlı and Prof. Nurdan İnan pers. comm. 2004; see Appendix 1).

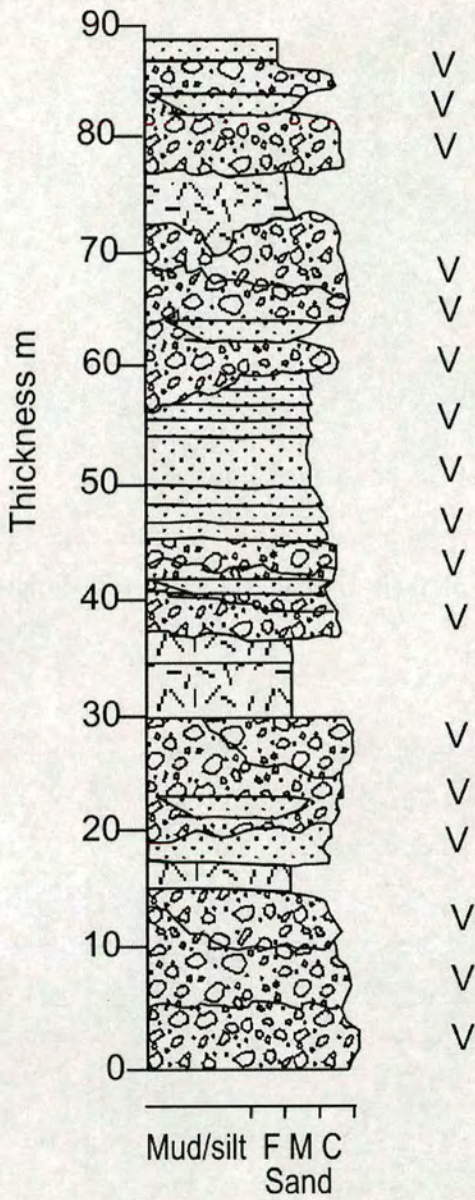


Figure 3.73. Log of part of the structurally lower thrust-slice of the Karadağ Formation at Gölpınar (gr: İ43, 3899391174).

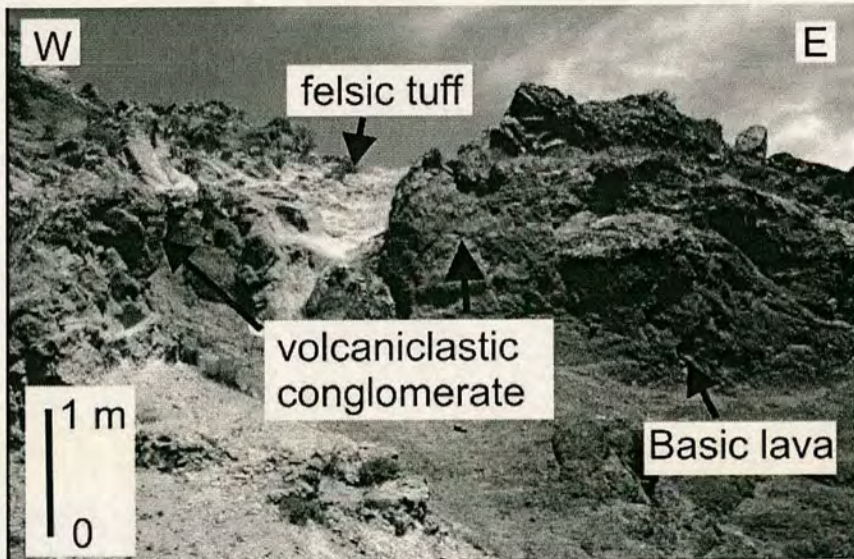


Figure 3.74. Photograph showing thick irregular bodies massive tuffite, volcaniclastic conglomerates and lava of interbedded with the Karadağ Formation at Gölpınar (gr: İ43, 3899391174).

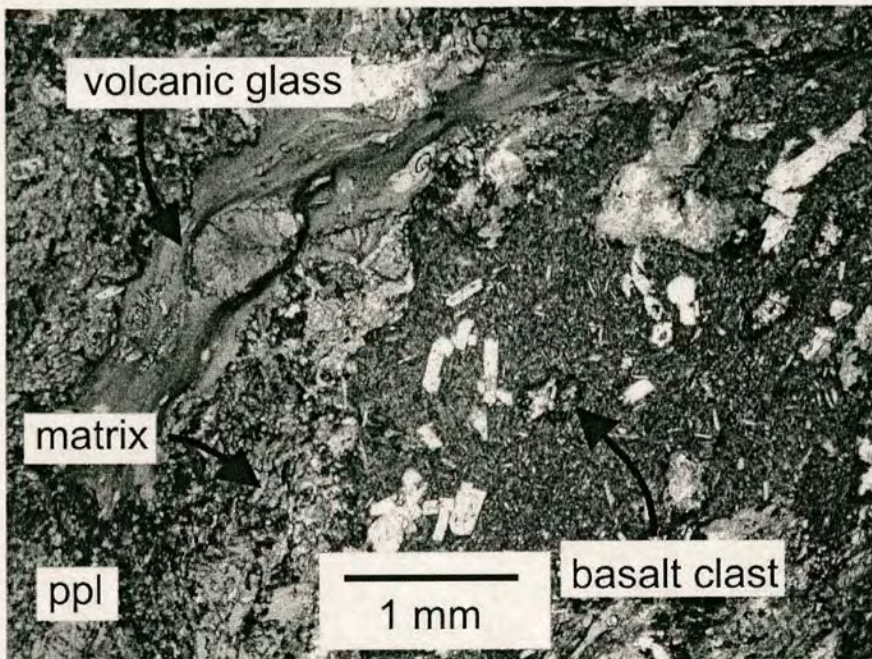


Figure 3.75. Photomicrograph of metamorphosed volcaniclastic conglomerate from the structurally lower thrust slice of the Karadağ Formation at Gölpınar (gr: İ43, 3899391174).

In thin section the pelitic volcanoclastic metasedimentary rocks exhibit millimetre-scale sedimentary lamination. Thin sections of coarse-grained metasedimentary rocks show a variety of volcanic clasts with a variety of primary igneous textures preserved. In some clasts plagioclase laths are randomly oriented, while others show a trachytic texture (Figure 3.75). Highly vesicular clasts and volcanic glass are also observed. Vesicles are filled with secondary minerals (e.g. epidote, zeolite or chlorite). Metamorphic mineral assemblages and textures are described below (section 3.5.4).

3.5.3 Igneous petrology of the Karadağ Formation

The Karadağ Formation contains basic, intermediate and felsic massive lava flows and sills. Feldspar-phyric andesitic flows comprise an estimated ~75% of the total igneous rocks within the Karadağ Formation. The other igneous rocks are basic flows and sills, rhyolitic flows and tuffs. In places, basic and intermediate flows are closely associated (Figure 3.70). Flow-banding was observed in the rhyolite. A varied degree of hydrothermal alteration is exhibited by the lavas. The porphyritic lavas contain the phenocrysts assemblage: plagioclase ± diopside ± olivine ± hornblende.

In thin section, porphyritic basic lava contains phenocrysts (60-70%) in a fine-grained or glassy matrix (30-40%). The most abundant phenocrysts phase (<50%) in the lavas is zoned plagioclase with twinned anorthite. The lath-shaped anorthite phenocrysts (<1mm long) are turbid and sericitised due to alteration. Rare large, zoned, equant highly altered feldspar crystals (<3mm) are also present in some sections. Large (<3 mm) euhedral, equant, zoned diopside (<25%), and brown/green anhedral hornblende (<10%, <2mm) are commonly also present. The diopside exhibits glomoporphyritic texture in some flows. Anhedral olivine phenocrysts (~10%, <2mm) were observed in some basic lavas, commonly replaced by iddingsite (Figure 3.76). An accessory opaque oxide (magnetite?) is ubiquitous. Secondary fibrous green chlorite + quartz fills vesicles and fractures. The lavas commonly exhibit vesicular and trachytic textures.

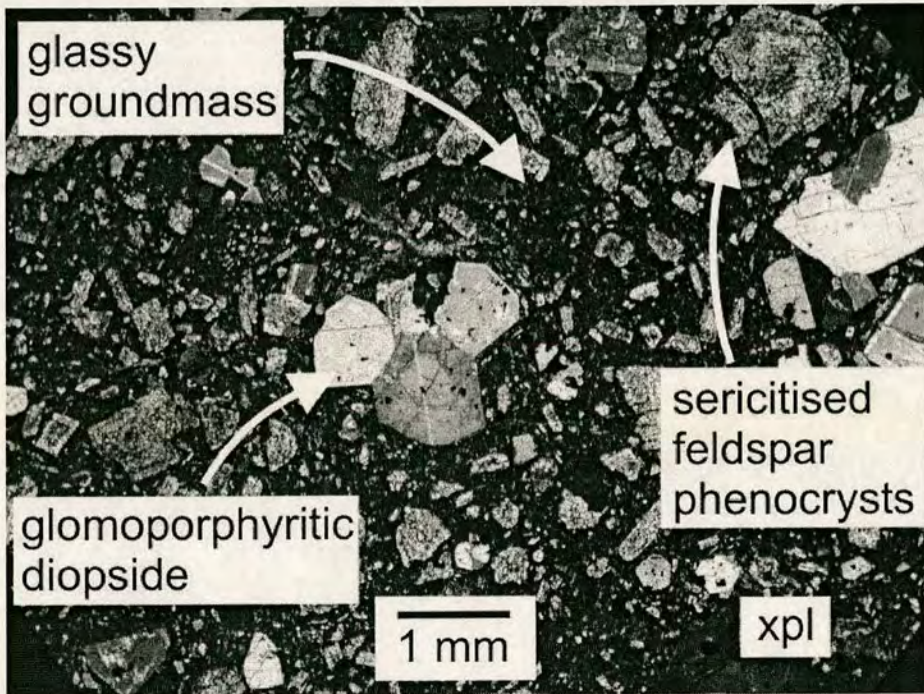


Figure 3.76. Photomicrograph of a typical basic lava from the Karadağ Formation showing glomoporphyritic diopside, sericitised feldspar and iddingsite pseudomorphs after olivine.

3.5.4 Metamorphism of the Karadağ Formation

Volcanic and volcanoclastic rocks of the Karadağ Formation contain the assemblage: epidote + chlorite + calcite + quartz \pm pyrite \pm sericite (Figure 3.77). Radiating blades of epidote fill amygdales and fractures. Coarsely crystalline (<0.5 mm) epidote also occurs in layers. In thin section, volcanoclastic schists show a fine-grained mylonitic fabric with metamorphic 'fish' composed of coarsely recrystallised quartz, and haematized pyrite porphyroblasts <1 mm within a matrix of sericite, fine-grained recrystallised quartz and chlorite (Figure 3.78). Coarse fibrous chlorite and sericite occur in pressure shadows around porphyroblasts. Fibrous masses of chlorite also fill fractures and cavities. Amygdales and fractures are commonly filled with zeolite or chlorite.

Shear-schistosity and mylonitic textures are observed in the fine- and coarse-grained metasedimentary rocks, as well as deformed andesitic lavas. The mineral

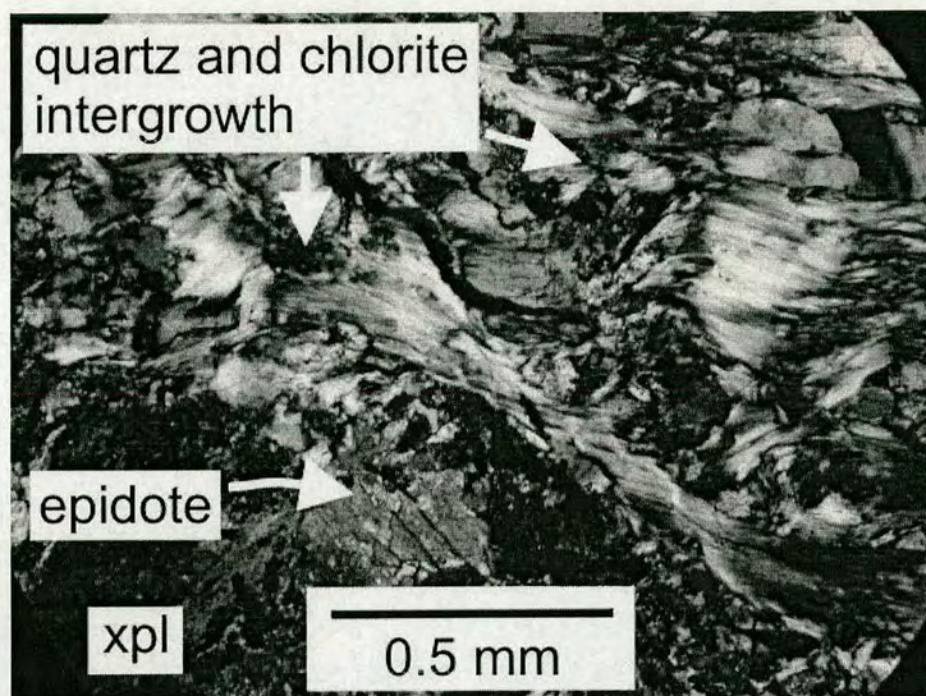


Figure 3.77. Photomicrograph of a typical volcaniclastic metasediment within the Karadağ Formation showing metamorphic quartz, epidote and chlorite.

assemblage and metamorphic textures exhibited by the Karadağ Formation indicate greenschist facies regional metamorphism.

3.5.5 Whole-rock igneous geochemistry of basic-intermediate lavas

Twenty eight lava samples from the Karadağ Formation were analysed for whole-rock major and trace element abundances by XRF (see 3.3.8 and Appendix 2 for method). The analytical results from 6 of these samples are used in the following geochemical determination of the petrogenesis and palaeotectonic setting of the unit. The results of the other 22 samples were not considered in the investigation due to having geochemical characteristics outside the natural range for unaltered basic igneous rocks, i.e. SiO_2 concentrations above 54% and/or $\text{MgO}+\text{CaO}$ outside the range 12-22% (Pearce 1973).

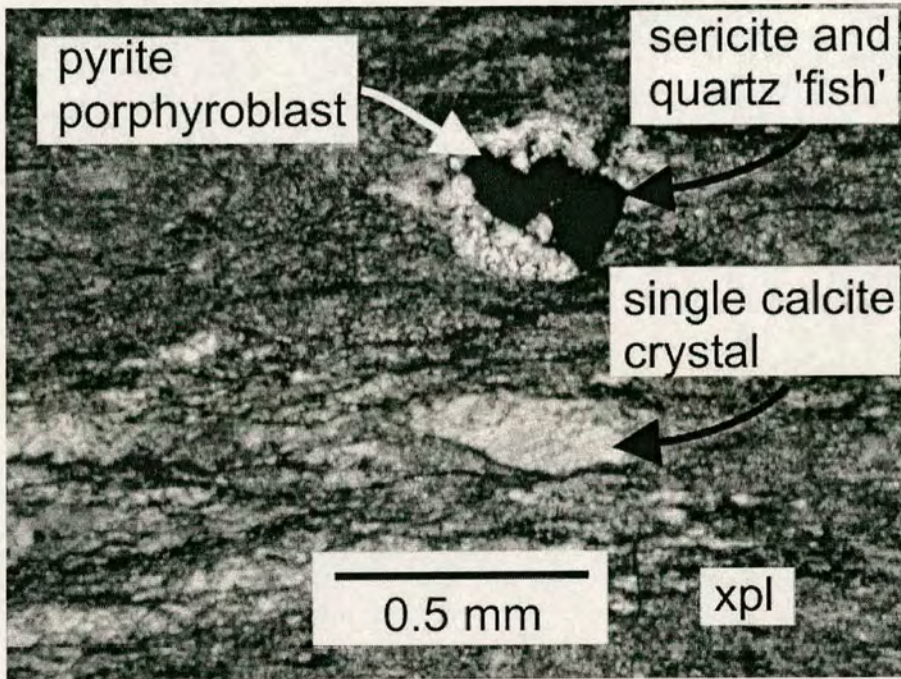


Figure 3.78. Photomicrograph of a volcanoclastic mylonite within the Karadağ Formation with pyrite and quartz 'fish'; sericite and chlorite are seen within pressure shadows.

Among the six remaining samples there is no clear correlation between the concentrations of the relatively 'immobile' element Al (Al_2O_3) and the potentially mobile elements Si, Ca, Fe and Mg (Figure 3.79). This suggests that the abundances of these elements in the samples were altered by post-magmatic processes (i.e. hydrothermal activity, metamorphism and/or weathering). However, variation diagrams of the immobile elements show good correlations (Figure 3.80) suggesting that the rocks represent different degrees of evolution of a single parental magma type.

A classification of the lava samples from the Karadağ Formation, based on $\text{K}_2\text{O} + \text{Al}_2\text{O}_3$ (total alkalis) versus silica suggests that the samples have basaltic to alkalic compositions and are suitable for tectonic discrimination. A classification based on immobile trace elements (Figure 3.82) shows the samples to comprise two groups. One group has a slightly more evolved

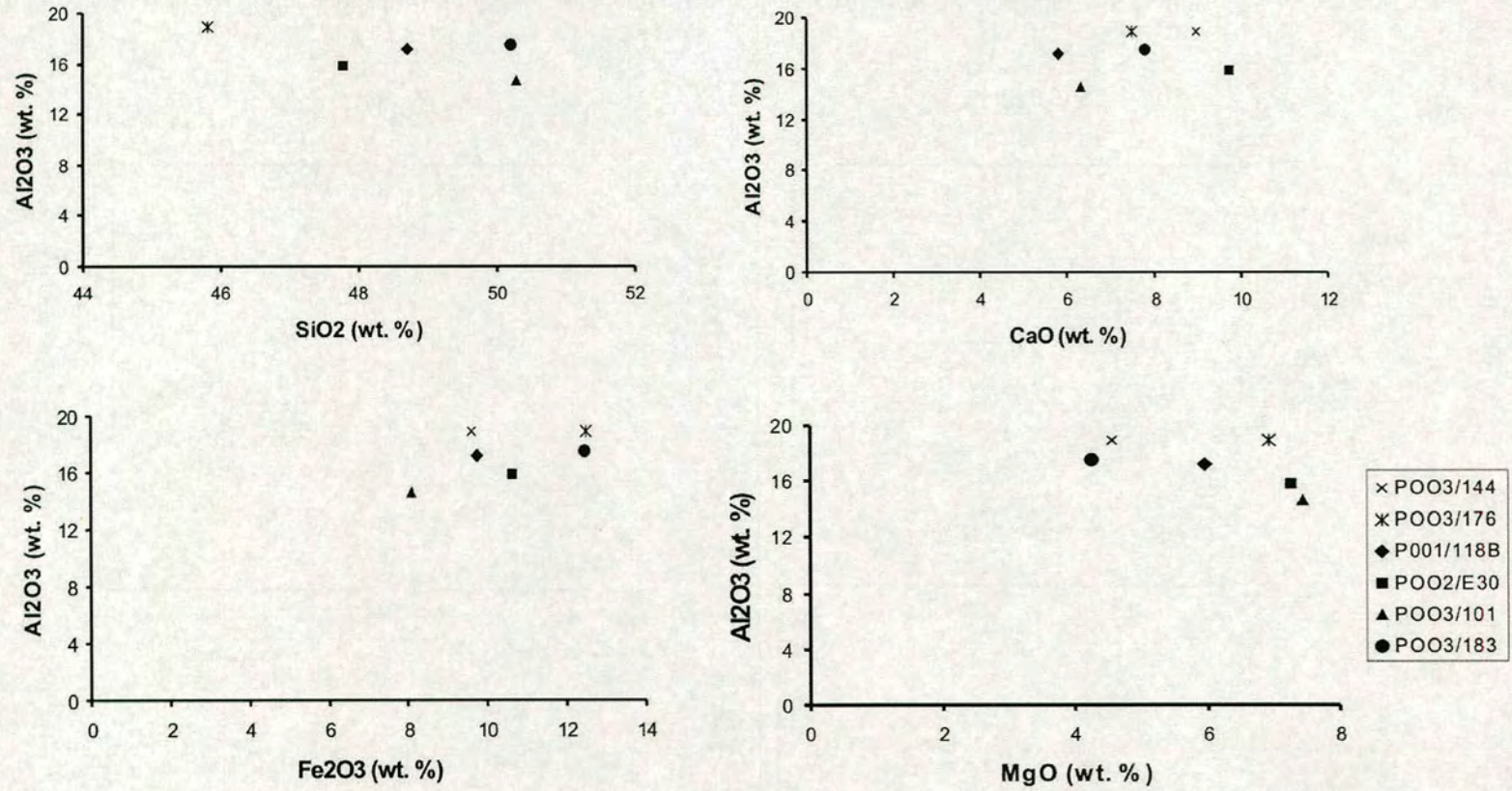


Figure 3.79. Variation diagrams of the mobile elements SiO₂, CaO, Fe₂O₃ and MgO against Al₂O₃ showing element mobility due to alteration of volcanic rocks in the Karadağ Formation.

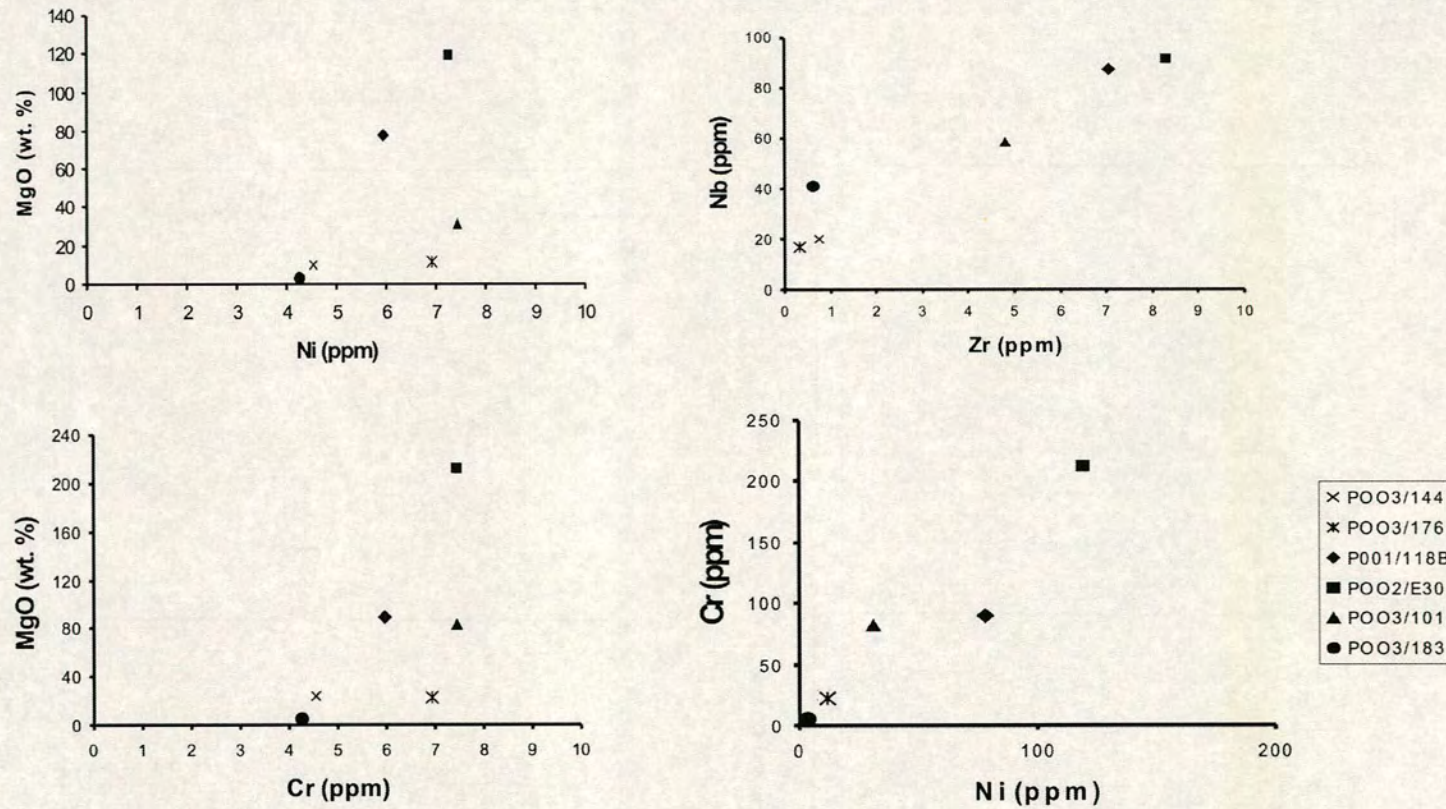


Figure 3.80. Variation diagrams of immobile trace elements in volcanic rocks of the Karadağ Formation.

composition than indicated by the total alkalis vs. silica plot (Figure 3.81). This group comprises basalts and andesites. Four of the samples of this less evolved group fall in the field that includes basalts (Figure 3.82). These four samples (PO03 144, PO02/E30, PO03 176, PO03/183) are the only analyses from the Karadağ Formation that are potentially useful for tectonic discrimination. However, since all of the lava samples are probably derived from a single parental magma type, data from these four samples are likely to be indicative of the petrogenesis and tectonic setting of the Karadağ Formation as a whole.

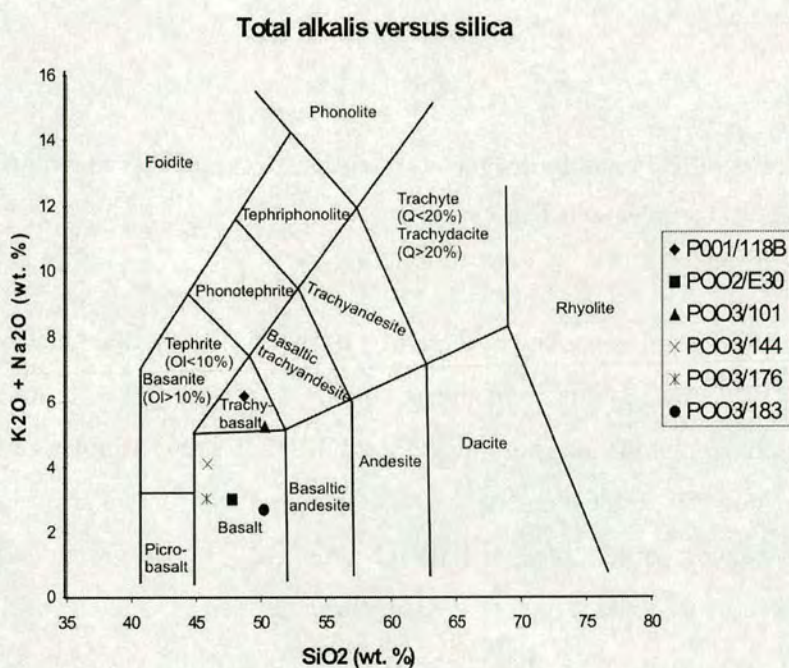


Figure 3.81. Analyses of basic and intermediate volcanic rocks from the Karadağ Formation plotted on the Total alkali-silica (TAS) diagram (Le Maitre et al. 1989).

Details of the basalt discrimination diagrams used here are given in section 3.3.8.4. When considered together, Figure 3.84 to 3.91 show that the four basic lava samples from the Karadağ Formation are both Volcanic Arc Basalts and, more precisely that they are Low-potassium tholeiites or, Island Arc Tholeiites.

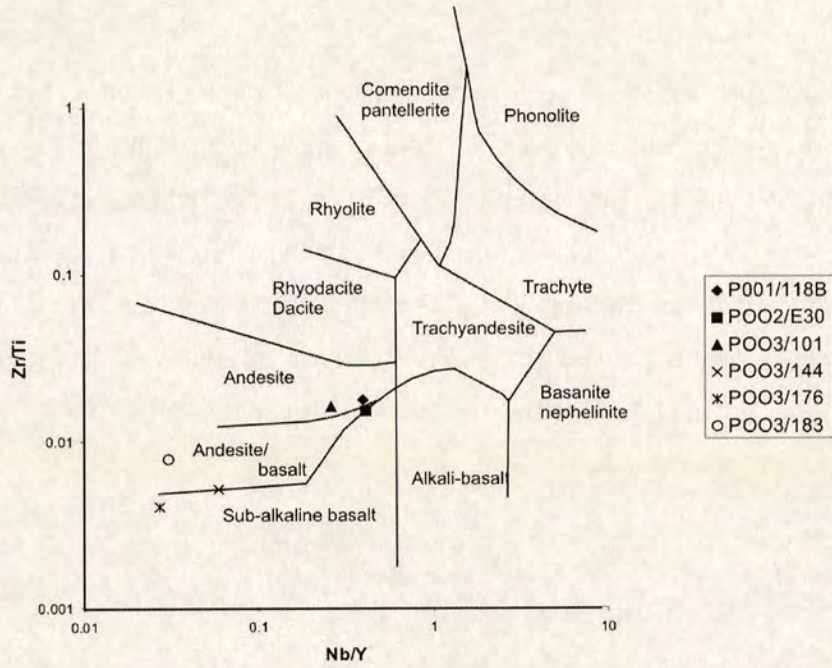


Figure 3.82. Classification of basic igneous intrusions from the Karadağ Formation using immobile trace elements (Zr/Ti versus Nb/Y).

It is also useful to consider the pattern of multi-element abundances for the six samples that have basaltic abundances of SiO₂, MgO and CaO. Figure 3.83 shows the multi-element abundances normalised to MORB. The four samples classified on the basis of immobile trace element abundances as basaltic show a clear depletion of the immobile incompatible trace elements (La, Ce, Nd, P and Zr) relative to MORB, whereas the more evolved samples show an enrichment of these elements. The depletion of these elements is characteristic of subduction-influenced petrogenetic environments (Pearce 1973). In the two intermediate samples the relative enrichment of these incompatible elements could be explained by crystal fractionation. These samples are petrogenetically related (Figure 3.80) and therefore it is unlikely that the enrichment of incompatible elements in the more evolved samples implies a different tectonic setting. All of the samples show a definite negative Nb anomaly and a relative enrichment of mobile large-ion lithophile elements (LILE; Sr, K, Rb, Ba). Both of these are typical features of basalts erupted above subduction zones (Pearce 1982).

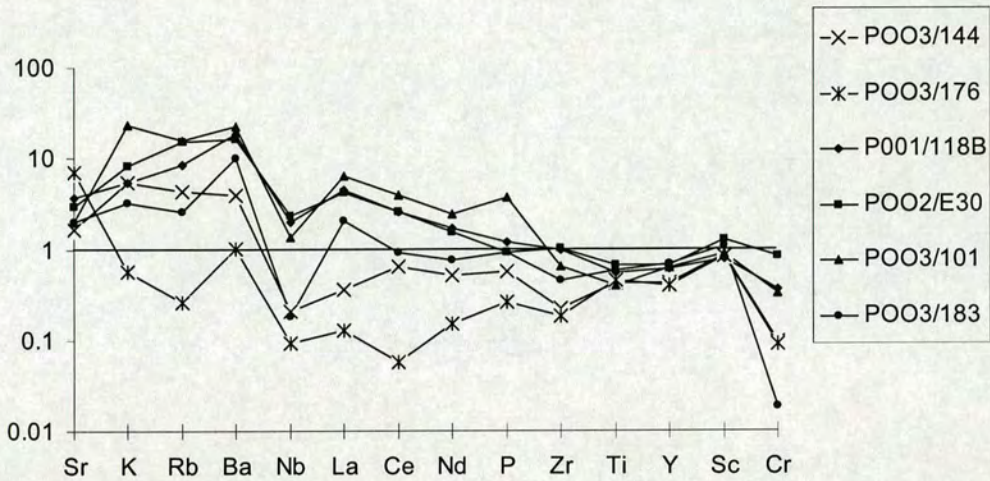


Figure 3.83. MORB-normalized multi-element abundances for basic and intermediate volcanic rocks from the Karadağ Formation. Normalizing values: Sr = 120 ppm; K_2O = 0.15% ; Rb = 2.0 ppm; Ba = 20 ppm; Nb = 3.5 ppm; La = 3 ppm; Ce = 10 ppm; Nd = 8 ppm; P_2O_5 = 0.12% ; Zr = 90 ppm; TiO_2 = 1.5% ; Y = 30 ppm; Sc = 40 ppm; Cr = 250 ppm.

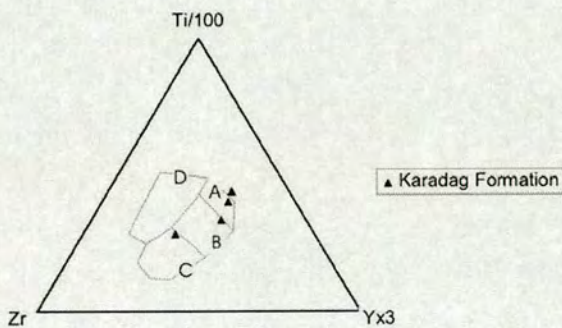


Figure 3.84. Basaltic lava samples from the Karadağ Formation plotted on the Ti, Zr and Y discrimination diagram (Pearce and Cann 1973). Within-plate basalts field D; ocean-floor basalts in field B; low-potassium tholeiites in fields A and B; calc-alkali basalts in fields C and B.

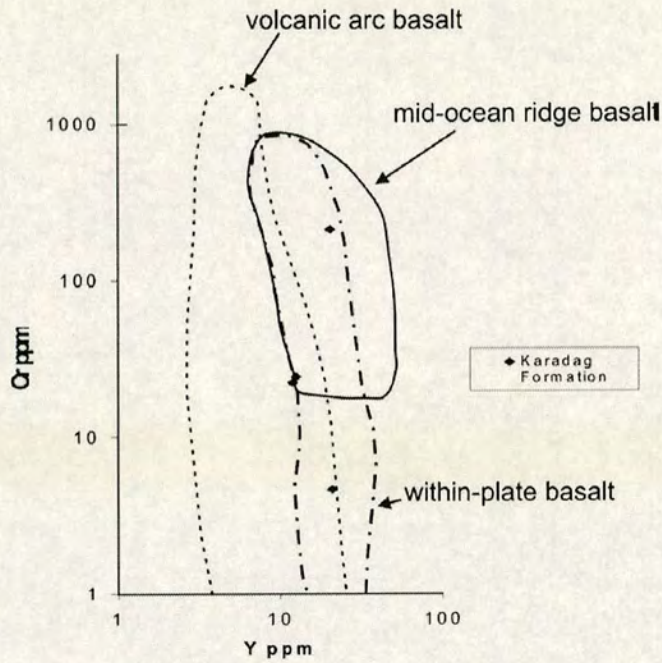


Figure 3.85. Geochemical analyses of two basic lava samples from the Karadağ Formation plotted on a discrimination diagram based on Cr-Y covariations (Pearce 1982).

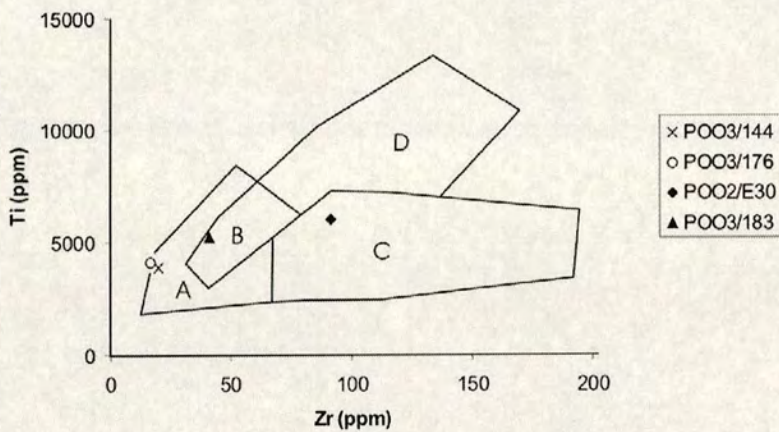


Figure 3.86. Geochemical analyses of basic lava samples from the Karadağ Formation plotted on a discrimination diagram using Ti and Zr (Pearce and Cann 1973). Ocean-floor basalts plot in fields D and B; low-potassium tholeiites in fields A and B, and calc-alkali basalts in fields C and B.

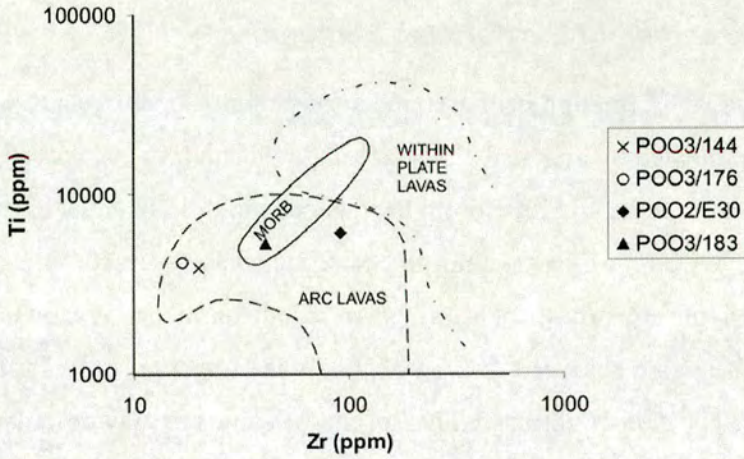


Figure 3.87. Basic lava from the Karadağ Formation plotted on the log Ti/log Zr discrimination diagram (Pearce 1982). Ocean-floor basalts plot in fields D and B; low-potassium tholeiites in fields A and B; and calc-alkali basalts in fields C and B.

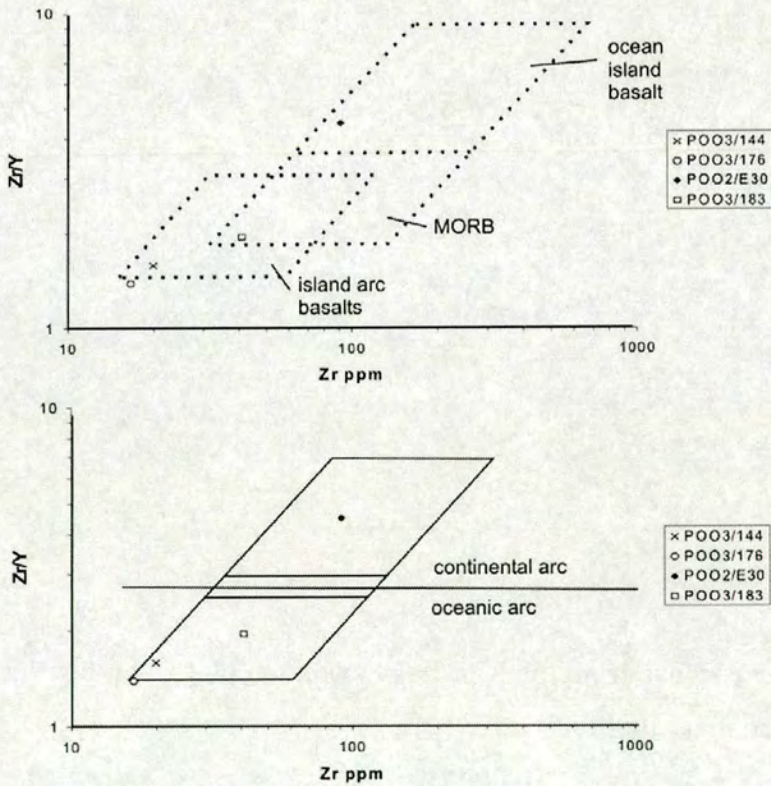


Figure 3.88. Basic lava samples from the Karadağ Formation plotted on the Zr/Y versus Zr discrimination diagram (Pearce and Norry 1979).

3.5.6 Tectonic setting of the Karadağ Formation

The Karadağ Formation is interpreted as part of an Upper Cretaceous volcanic arc, dominated by andesitic volcanics and volcanoclastic sedimentary rocks, with a pelagic microfauna and little or no terrigenous input. In contrast to the adjacent Refahiye Complex no metamorphic host rock was observed. This may suggest that this volcanic arc was not formed on rifted continental crust. However, as no plutonic bodies were observed it seems that only the upper portion of the arc has been preserved. The deeper, intrusive level of the volcanic arc may or may not have included a metamorphic host. The lower part of the arc has presumably been destroyed. The preservation of the upper part suggests that the lower part was not removed by post-emplacment erosion but tectonically, i.e. by subduction-erosion. This could suggest that at depth the subduction zone was erosive rather than accreting (Dewey 1980; Von Huene 1986; 1991, Clift et al. 2003).

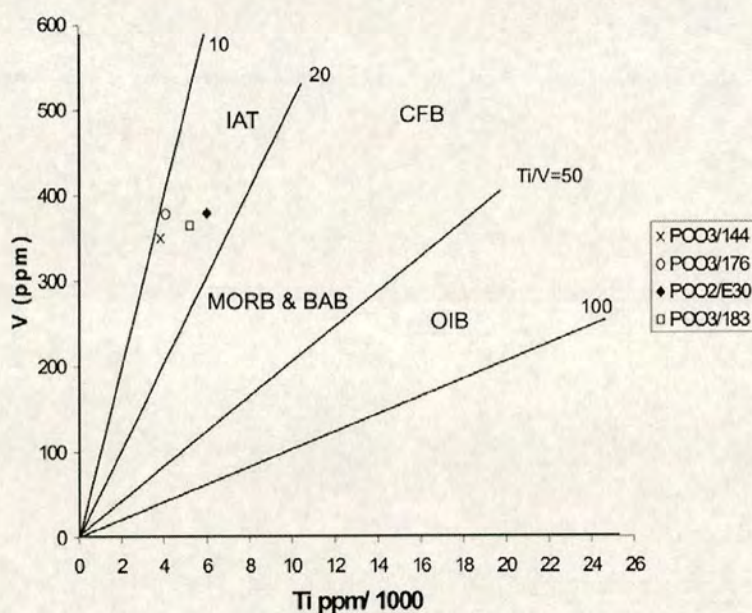


Figure 3.89. Basic lava from the Karadağ Formation plotted on the V/Ti discrimination diagram (Shervais 1982).

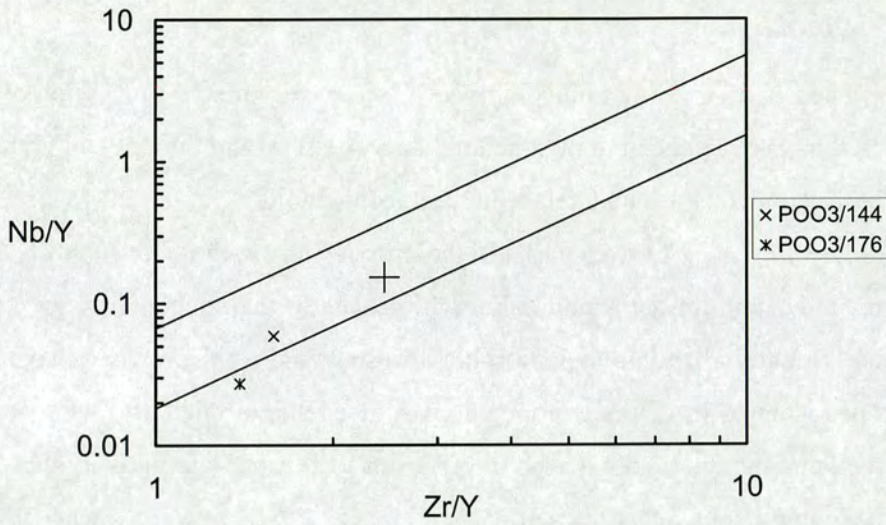


Figure 3.90. Nb/Y against Zr/Y for basic lava from the Karadağ Formation. Lines define the array for Icelandic basalts (Fitton et al. 1997).

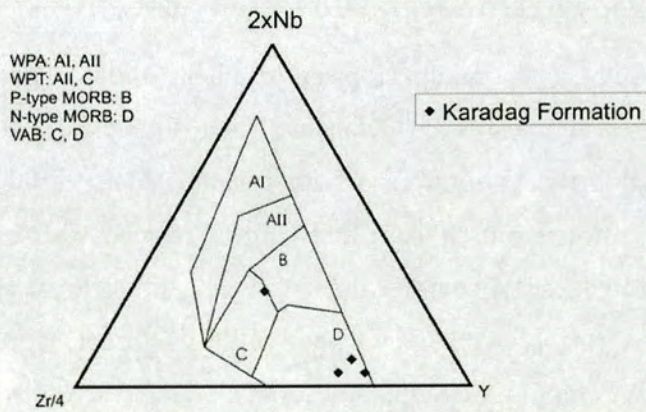


Figure 3.91. Basic lava samples from the Karadağ Formation plotted on the Nb/Zr/Y discrimination diagram (Meschede, 1986). AI and AII = within-plate alkali basalt compositional field; B = plume-influenced MORB compositional field; C = within-plate tholeiite compositional field; D = N-type MORB and volcanic arc basalt.

3.5.7 Summary

The Karadağ Formation comprises a tectonically mixed succession of deformed meta-volcanic and meta-sedimentary rocks ~3 km thick. Planktonic foraminifera indicate a Late Cretaceous age for the unit.

The presence of low-potassium tholeiite/island arc tholeiite supports a volcanic arc origin for the Karadağ Formation. The formation contains no terrigenous material and no metamorphic host rock and is thus likely to have developed isolated from any continental margin. Metamorphic host rocks may have been tectonically removed with the lower levels of the arc; alternatively the arc may have developed upon oceanic crust.

The Karadağ Formation is interpreted as an emplaced Upper Cretaceous volcanic arc. The inferred volcanic arc experienced north-vergent deformation related to its emplacement onto the Eurasian margin, followed by south-vergent deformation related to collision between the Taurides and Pontides.

3.6 Preserved forearc basin: Sütçinar Formation

The Sütçinar Formation crops out in a belt ~10 km wide extending west from the Erzincan Basin towards the Gülandere River (Figure 3.92). The pre-deformational thickness of the succession is estimated as ~1500 m. The Formation is sandwiched between thrust slices of the Upper Cretaceous Karadağ Formation and is thrust over Oligocene-Miocene sedimentary rocks of the Sivas Basin to the south. It is also unconformably overlain by Upper Tertiary sedimentary rocks near Dumanlı (gr: İ42, 0803294406). The Sütçinar Formation comprises a generally coarsening-upward succession of mixed carbonate and volcanoclastic sedimentary rocks.

Age-diagnostic species observed include *Globotruncanita stuarti* (DE LAPPARENT), *Globotruncana arca* (CUSHMAN), *Contusotruncana contusa* (CUSHMAN), *Globotruncana cf. ventricosa* (WHITE) (Prof. Izver Ongen, Prof. Kemal Taşlı and Prof. Nurdan İnan pers. comm. 2004). The assemblage indicates an Upper Cretaceous-Early Eocene age for the unit (see Appendix 1 for micropalaeontological data).

- The base of the Sütöinar Formation is everywhere a north-dipping thrust fault. The volcanoclastic lithologies present are similar to those of the Karadağ, (inferred) arc unit and it is likely that the two units were originally intergradational. The top of the Sütöinar Formation interdigitates with, and gradually passes into, the Palaeocene-Mid Eocene Sipikör Formation: e.g. west of Ballı Village (gr: İ42, 269007). The contact between the Sütöinar Formation and Sipikör Formation is cut by a north-dipping thrust near Yıldız Dağ (gr: İ42, 265992).

A composite log of the Sütöinar Formation is shown in Figure 3.93. The lowest part of the Sütöinar Formation exposed consists of an 800 m-thick coarsening-upward succession of thin- to medium-bedded, fine- to medium-grained calciturbidites and quartzofeldspathic sandstones with marly and shaly partings. This passes gradually upwards into a ~500 m-thick coarsening-upward succession of volcanoclastic shale and sandstone with thickly bedded, discontinuous volcanoclastic conglomerate lenses and rare andesitic lava flows. The volcanoclastic succession interdigitates with discontinuous coarse-grained, poorly sorted quartz-rich, polymict sandstone and conglomerate and thick (~50 m) lenses of massive fine-grained nummulitic limestone. The uppermost part of the succession is transitional with the overlying Sipikör Formation.

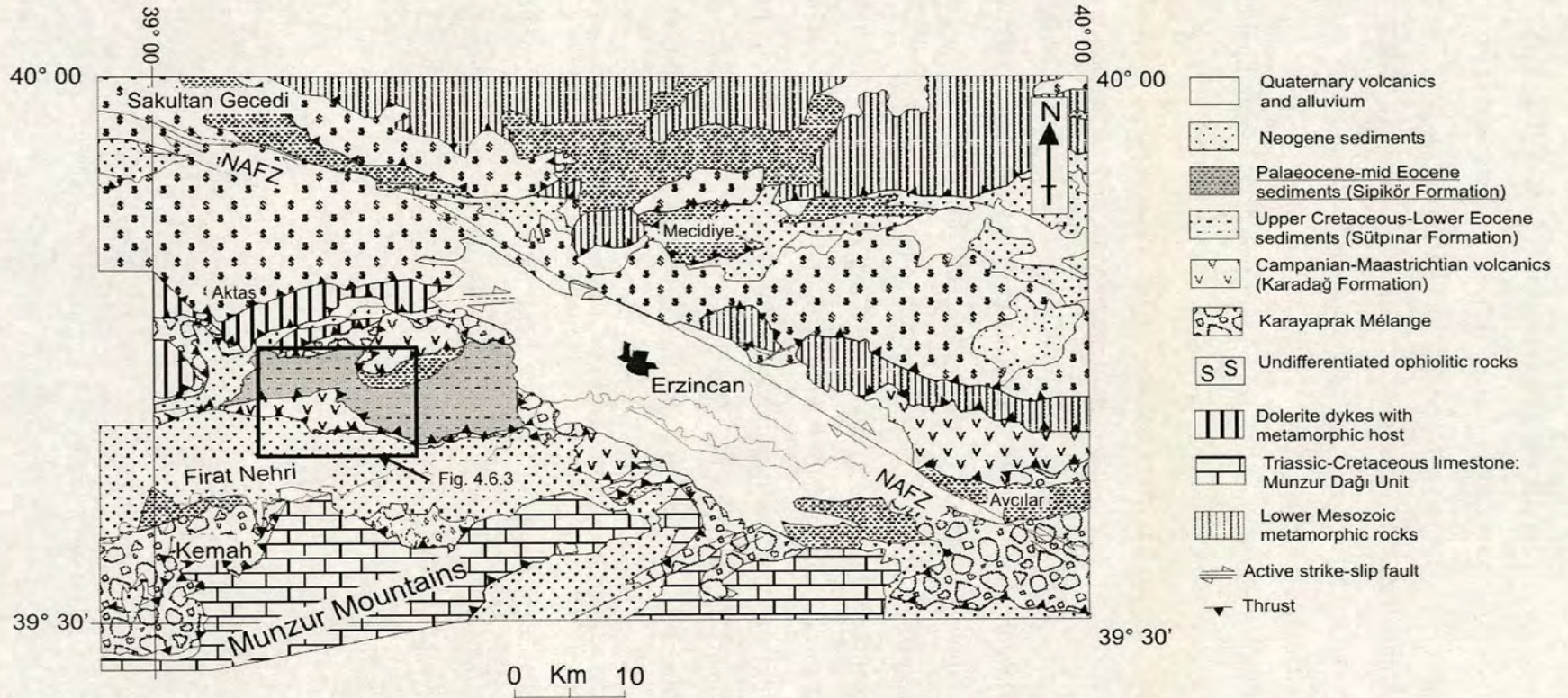


Figure 3.92. Map of the Erzincan area showing the outcrop of the Sütpinar Formation

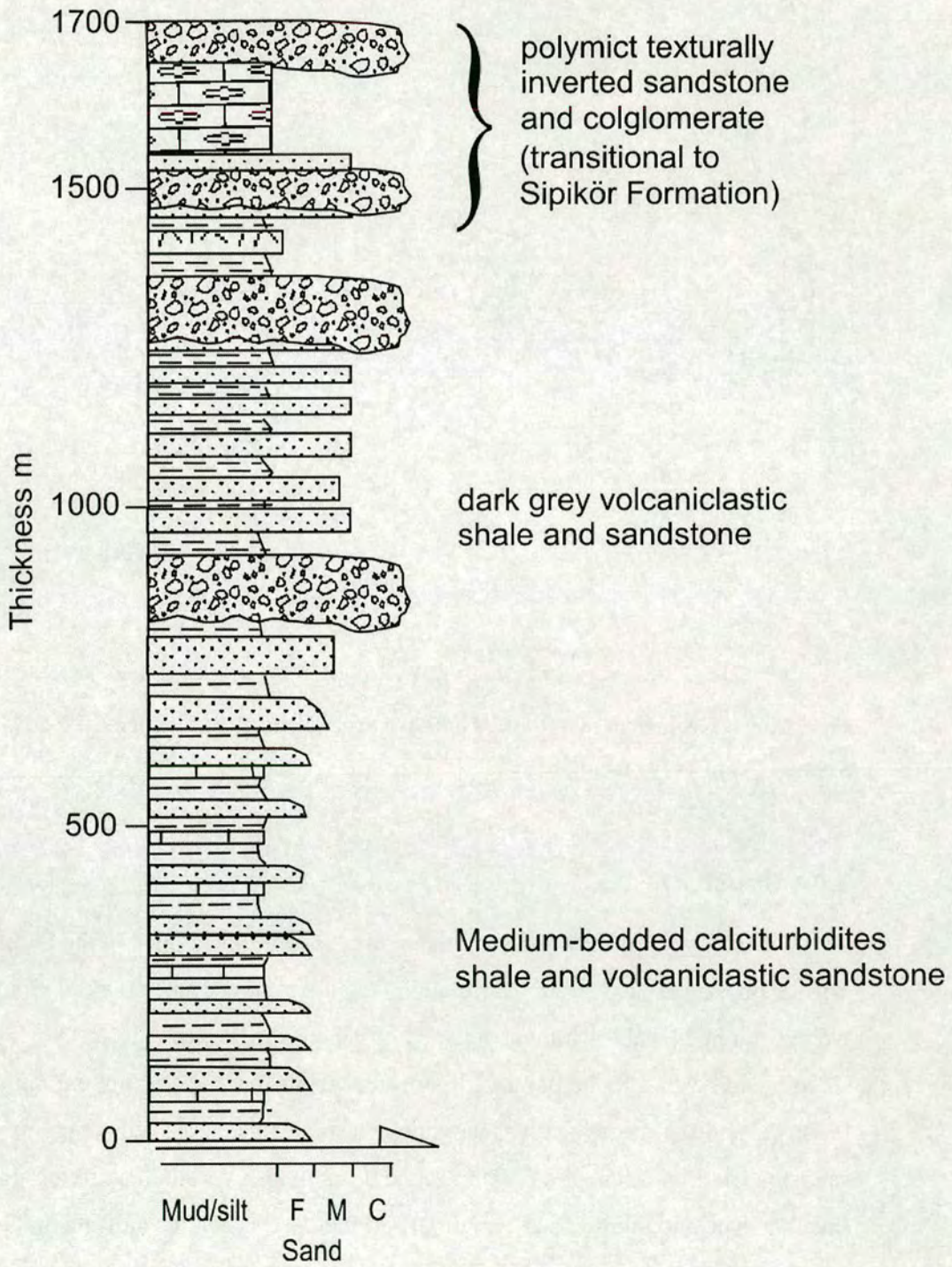


Figure 3.93. Composite sedimentary log of the Sütöpmar Formation.

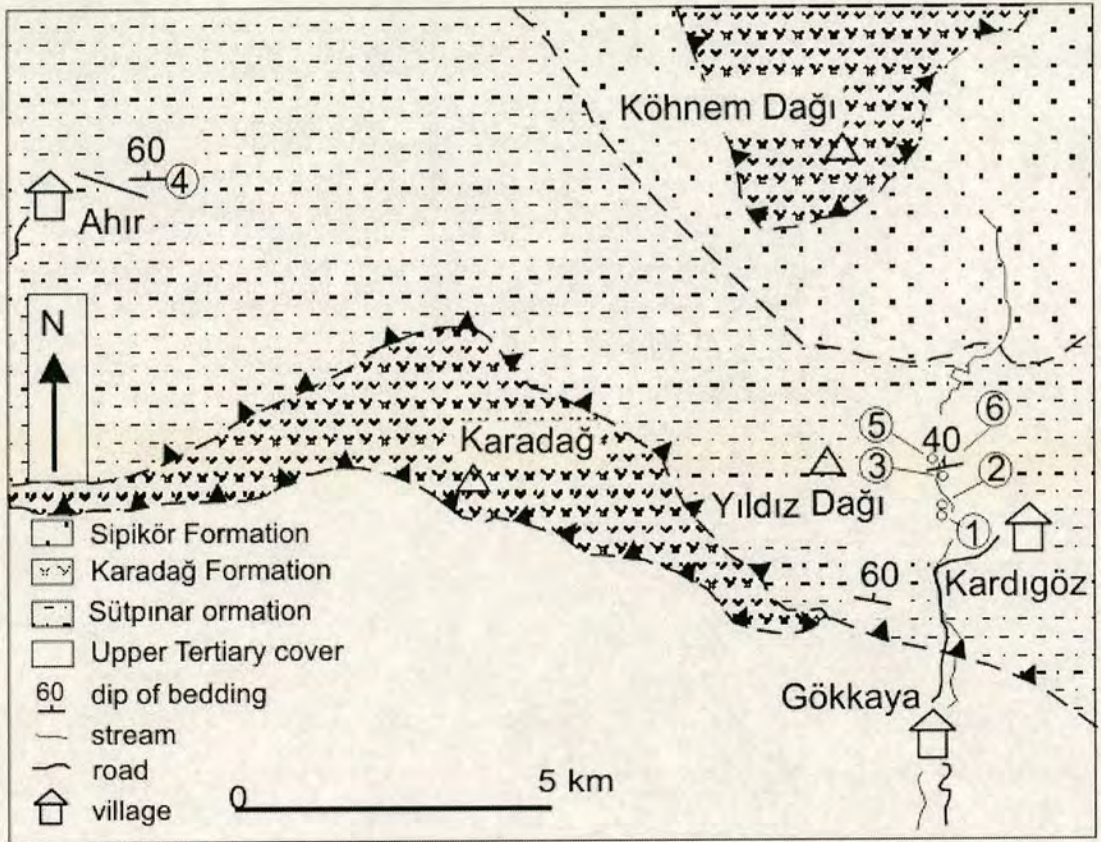


Figure 3.94. Geological map of the Gökkaya area to show the locations of logs 1-6. See Figure 3.92 inset for location.

3.6.1 Structure

Cleavage and schistosity are generally less well-developed in the Sütçinar Formation than in the Karadağ Formation (section 3.5.1). However, slaty cleavage is well developed locally within shaly and argillaceous rocks and dips $65^{\circ}\text{N}/040$. Bedding and cleavage dip dominantly toward the northwest. The unit exhibits top-to-the-north and top-to-the-south shear zones. In some exposures, beds of competent sandstone and limestone are boudinaged and imbricated within a matrix of highly sheared shale and mudrock. A variety of sedimentary structures indicate that beds are overturned in much of the unit and, indicate various local younging directions. Southward-younging beds commonly dip steeply to the north, whereas northward-younging beds commonly dip moderately to gently southward thus defining a north-vergent fold asymmetry within an overturned succession. However, the unit also

exhibits right-way-up beds and folds with opposed facing directions. Overturned beds are folded by asymmetrical recumbent south-facing north-vergent folds at Gökkaya (Figure 3.94 and 3.95) and at Cevizli (gr: İ42, 251014). North-facing north-vergent tight and close recumbent folds (wavelength 50 m) are exposed near Köhnemdağı (Figure 3.94 and 3.95). A wide variety of fold styles were observed including close to isoclinal, rounded and angular (chevron) folds on a variety of scales (wavelength <50 m). Disharmonic and polyclinal folds are developed locally. Fold orientations range from recumbent and horizontal to upright and steeply plunging.

The Sütçinar Formation exhibits top-to-the-north thrust faults, shear zones and folds. Top-to-the-north shear fabric dips $\sim 45^\circ$ toward the south at Bahçeli (gr: İ42, 251010). The top-to-the-north compressional structures are commonly cut by top-to-the-south compressional structures. At Gökkaya (Figure 3.94 and 3.95), a northward-younging (overturned) succession is folded by tight angular asymmetrical north-vergent folds. Fold axes are inclined $60^\circ\text{S}/070$. The same exposure exhibits a top-to-the-north duplex (thrust horses are individually ~ 20 m long). Low-angle top-to-the-south shear zones cut the top-to-the-north structures.

Minor asymmetrical chevron folds (wavelength 2 m) are seen within the limbs of a larger south-vergent recumbent fold near Gökkaya (Figure 3.94 and 3.95). Tight angular asymmetrical south-vergent folds and top-to-the-south thrust faults are exposed at Dumanlı on the road from Erzincan to Kemah. The top-to-the-south shear fabric dips moderately north, e.g. $50^\circ\text{N}/085$ at Ballı (gr: I42, 265016). South-vergent folding is also developed in the footwall of top-to-the-south thrusts that cut the top-to-the-north layer-parallel shear fabric. Structural data are shown in Figure 3.96.

The top-to-the-north deformational structures do not continue into the unconformably overlying Tertiary cover units (Kemah Formation; Aktimur et al. 1995). Major top-to-the-south thrusts place the Sütçinar Formation above the Tertiary units (e.g. at Gökkaya Figure 3.94 and 3.95).

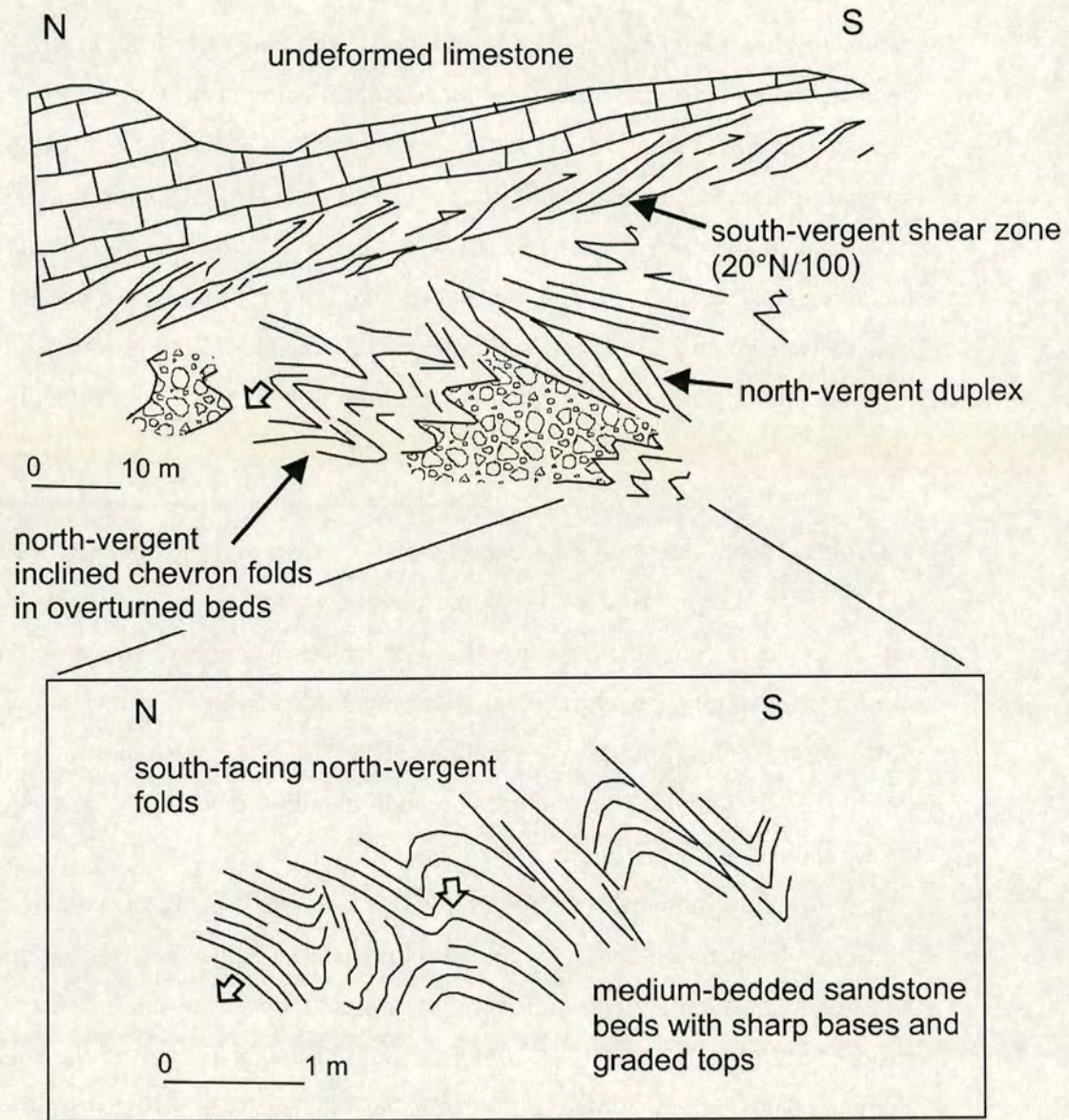
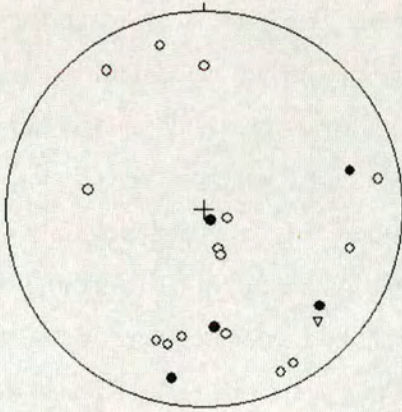
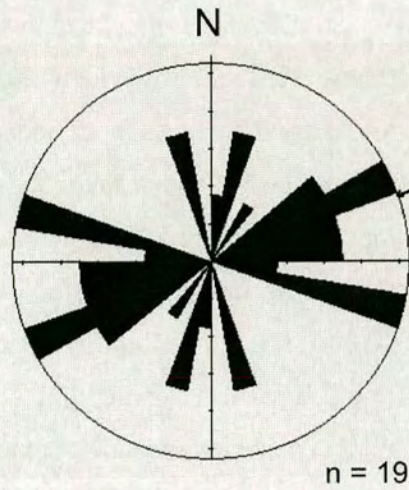


Figure 3.95. Field sketch showing structural relations within the Sütçinar Formation.

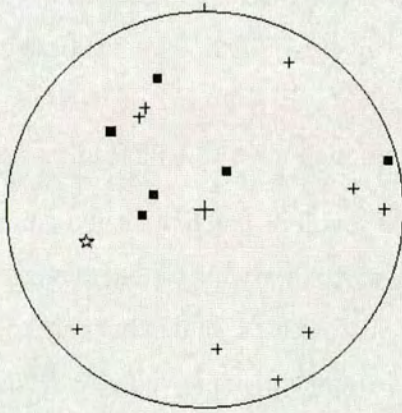
a) bedding and cleavage



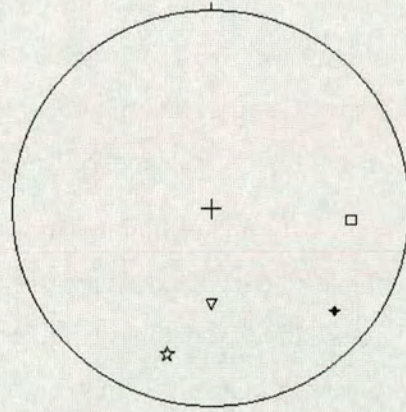
b) bedding planes



c) fold data



d) fault data



- | | |
|---------------------------------|---|
| ▽ top-to-the-north shear fabric | ■ pole to fold axial plane |
| ○ poles to bedding | ☆ stretching lineation |
| ● poles to cleavage | ◆ pole to fault plane (normal fault) |
| + plunge of fold axis | □ pole to fault plane (strike-slip fault) |

Figure 3.96. Structural data for the Sütçinar Formation. a) equal-area plot (Lambert/Schmidt) showing bedding and cleavage; b) Rose diagram showing strike orientations of bedding surfaces; c) equal-area plot (Lambert/Schmidt) showing fold data; d) equal-area plot (Lambert/Schmidt) showing fault data.

3.6.2 Sedimentary facies

The succession begins with buff-coloured sandy calciturbidites. These are thinly- and medium-bedded, medium- to fine-grained calcarenites and shaly to muddy limestones interbedded with fissile planar-laminated marly shale. The calcarenite beds have sharp bases with load-casts, graded bedding and, laminated tops and contain planktonic foraminifera of Late Cretaceous age (e.g. *Globotruncana* sp.). Sandstones near the base of the succession are thinly bedded (1-10 cm), fine- to medium-grained quartzo-feldspathic turbidites containing sub-rounded mafic-volcanic lithic clasts, feldspar and carbonate grains. Up-section, the thickness and abundance of quartzo-feldspathic sandstone beds increases at the expense of calcarenite. The lower part of the Sütüinar Formation is shown in Logs 1 and 2 (Figure 3.97 and 3.98); see Figure 3.94 for locations.

Thickly bedded, discontinuous, massive, coarse-grained sandstone beds with sharp bases, load casts and bioturbated tops appear ~500 m from the base of the exposed succession, interbedded with fissile grey shaly limestone. Nested discontinuous calcarenite lenses also interdigitate with the shale (Figure 3.99).

From ~500 m upwards the succession exhibits amalgamated medium- to thickly-bedded and flaggy grey, coarse-grained, fairly well-sorted, quartzo-feldspathic sandstones (Figure 3.100). The sandstones contain abundant rounded grains of quartz, feldspar, carbonate and sub-rounded, to angular, green and black volcanic lithoclasts. Some beds are quartz-rich, while others are more carbonate-rich. Graded-bedding is rare and scoured bases rarely seen. Thin- to medium-bedded (<15 cm), medium- to coarse-grained sandstones with fine tabular lamination, graded bedding, scoured bases and muddy calcareous tops were also observed. Shaly carbonate partings are present between some beds. The tops of some beds are bioturbated.

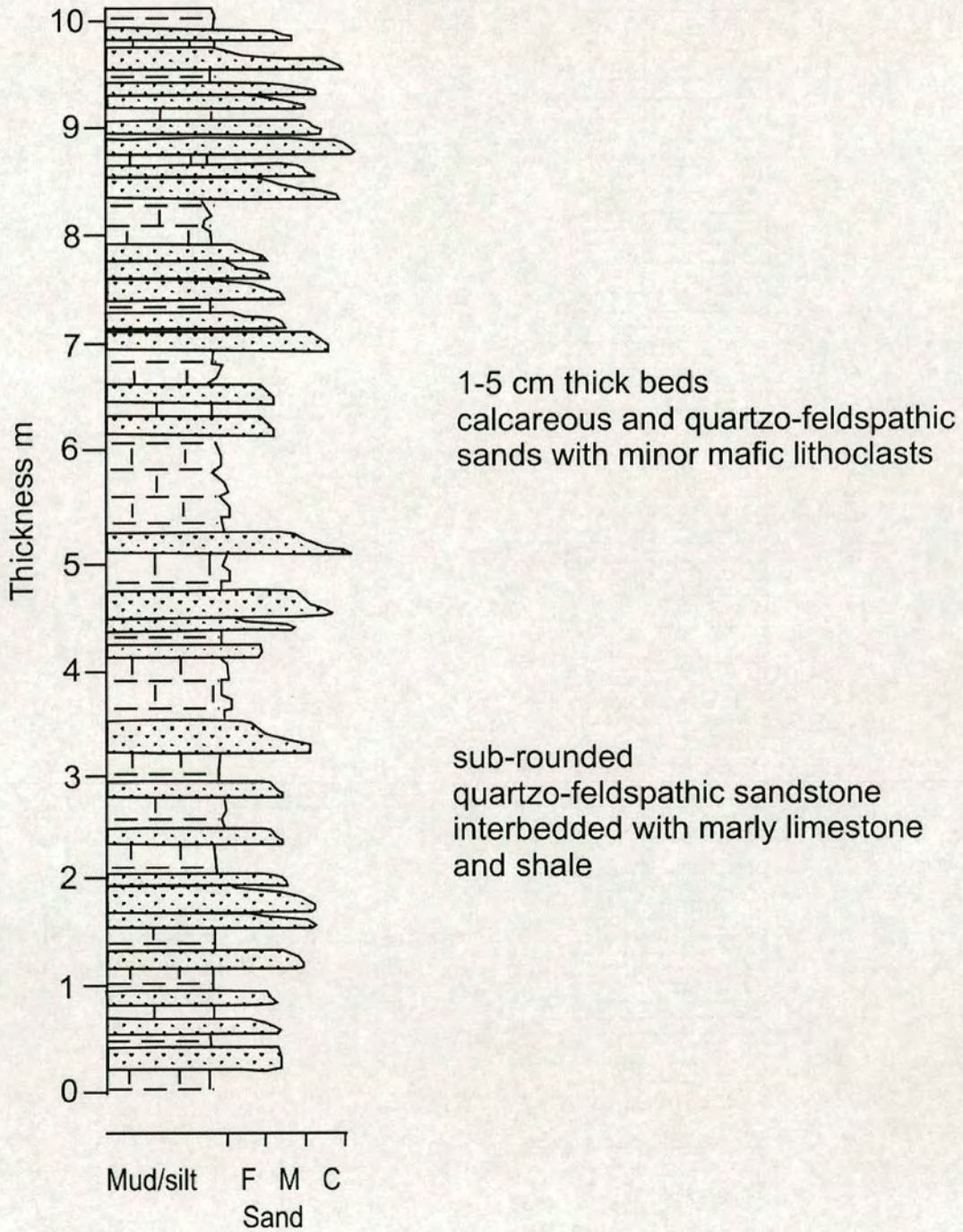


Figure 3.97. Log 1. Part of the Sütçinar Formation exposed near Gökkaya village (gr: İ42, 192937), representative of the lowermost part of the succession.

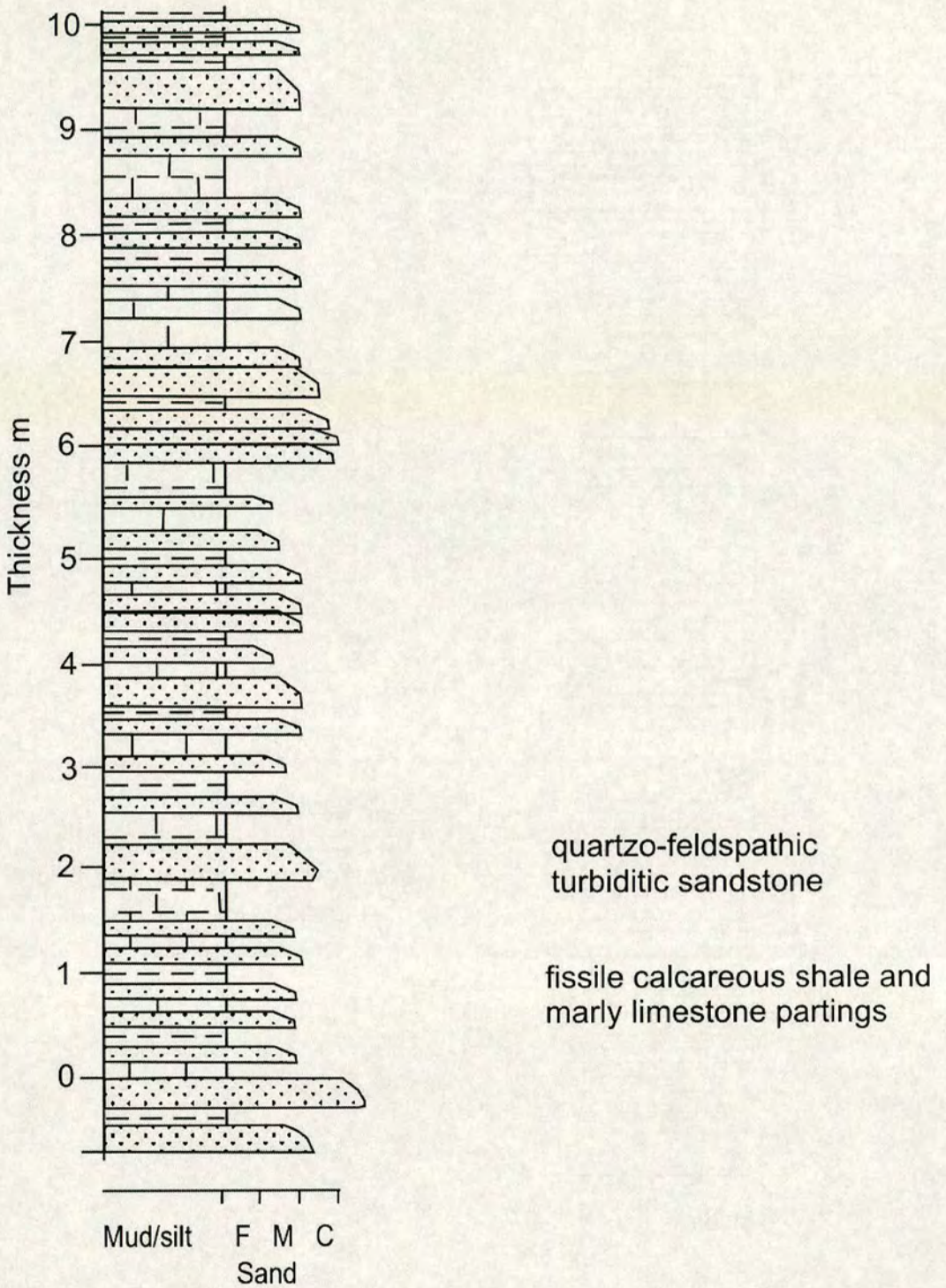


Figure 3.98. Log 2. Part of the Sütçinar Formation exposed 1 km north of Kardıgöz village (gr: İ42, 1920993817), representative of the lower levels in the succession.

The sandstones are associated with thick (~40 m) lenses of thickly bedded conglomerate (~3 m) and, thickly bedded massive sandstone and calcarenite beds (<20 m) (Figure 3.101). The thick lenses of conglomerate are grey, poorly sorted, matrix-supported and contain sub-rounded pebbles and boulders (<40 cm) of andesitic lava, basalt, rhyolite and, calcarenite in a matrix of sand and gravel. The conglomerate contains a greater diversity of lithoclasts up-section. The sandstones are medium- to coarse-grained and contain black, glassy, sub-rounded, to angular grains.

These coarse-grained sedimentary rocks interdigitate with fine-grained hemipelagic calciturbidite, shale and sandstone succession and continue to increase in abundance up-section. The sandstone and conglomerate beds interdigitate laterally with dark-grey, fine-grained siltstone and shale with rare, thin sandstone beds showing tabular bedding, planar- and cross-laminations and, slaty cleavage (~15 cm). Slump structures were observed in the surrounding thinly bedded shale. These coarse polymict sedimentary rocks are identical to those observed in the overlying Sipikör Formation where they are interbedded with thick lenses of massive, hard, fine-grained nummulitic limestone. Here they form part of a transitional succession in which they interdigitate with more texturally and compositionally mature sedimentary rocks typical of the Sütüinar Formation (Figure 3.102).

In thin section, the thinly bedded shaly limestones from the lower part of the succession are wackestones (clasts ~15%) containing angular to sub-angular clasts of feldspar, calcite, chloritised basalt, rare quartz and magnetite <0.25 mm. The matrix is shaly to muddy carbonate. Planktonic foraminifera and recrystallised radiolarians are present.

3.6.3 Sedimentary petrography

Coarse-grained calcarenite from the lowermost part of the succession are packstones (clasts ~95%) with angular to sub-angular clasts of calcite, wackestone, feldspar, chloritised basalt, volcanic glass, and large fragmentary foraminifera (~1 mm).

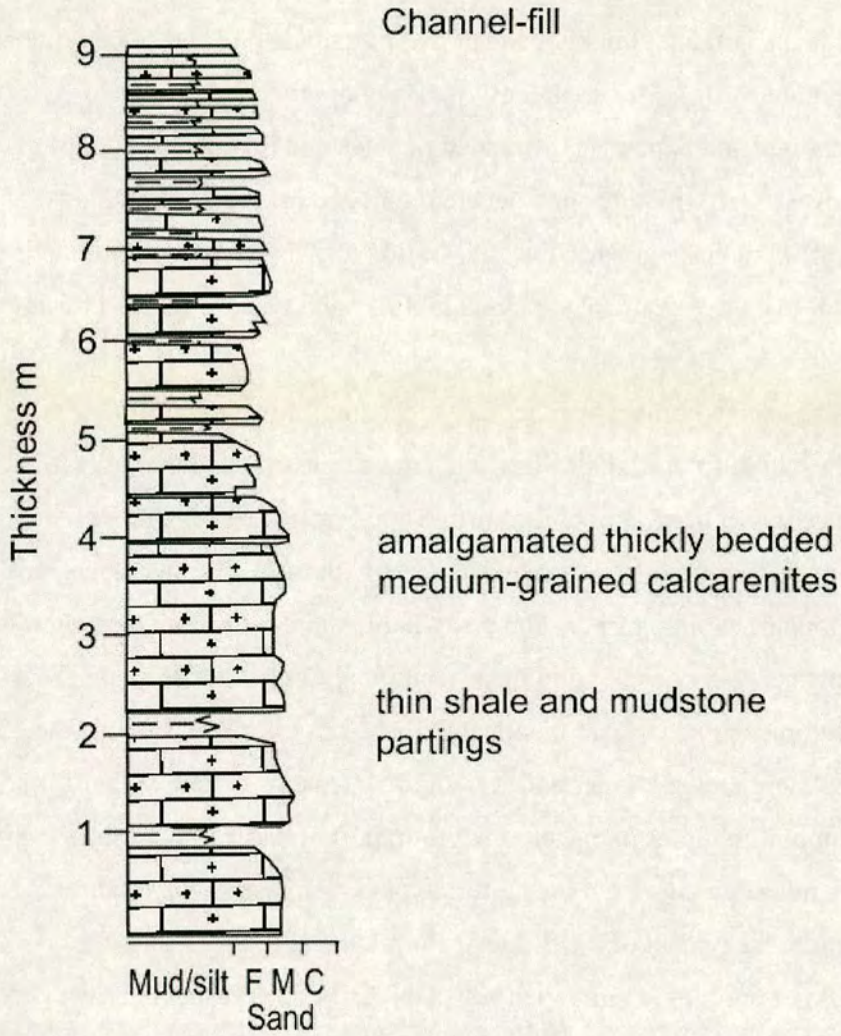


Figure 3.99. Log 3. Carbonate channel-fill within the lower part of the succession exposed north of Kardıgöz (gr: İ42, 1925494267).

Sandstones from the upper part of the succession are calcitic, arkosic, lithic arkoses and lithic wackes (clasts ~85%) containing abundant angular and sub-angular feldspar, and varying proportions of calcite, quartz, biotite, chloritised basalt, and fragmentary foraminifera. Volcanic quartz and feldspar becomes more abundant up-section.

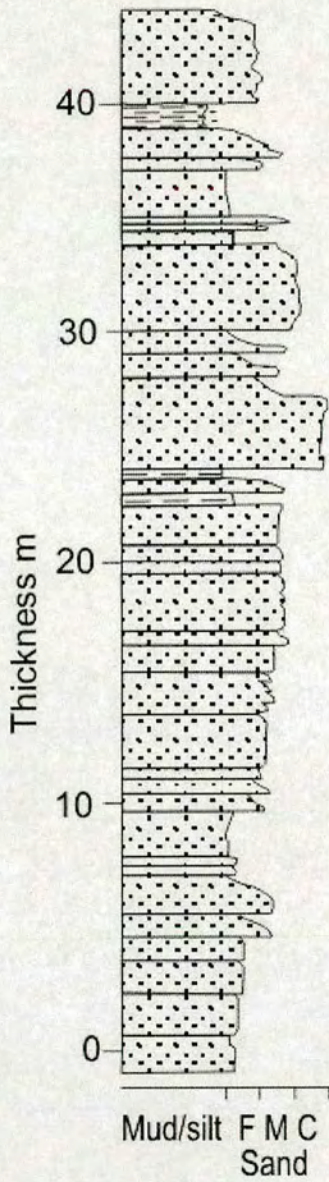


Figure 3.100. Log 4. Part of the Sütçınar Formation exposed east of Ahır village (gr: İ42, 0689198765), representative of overbank deposits found in the lower to middle parts of the succession.

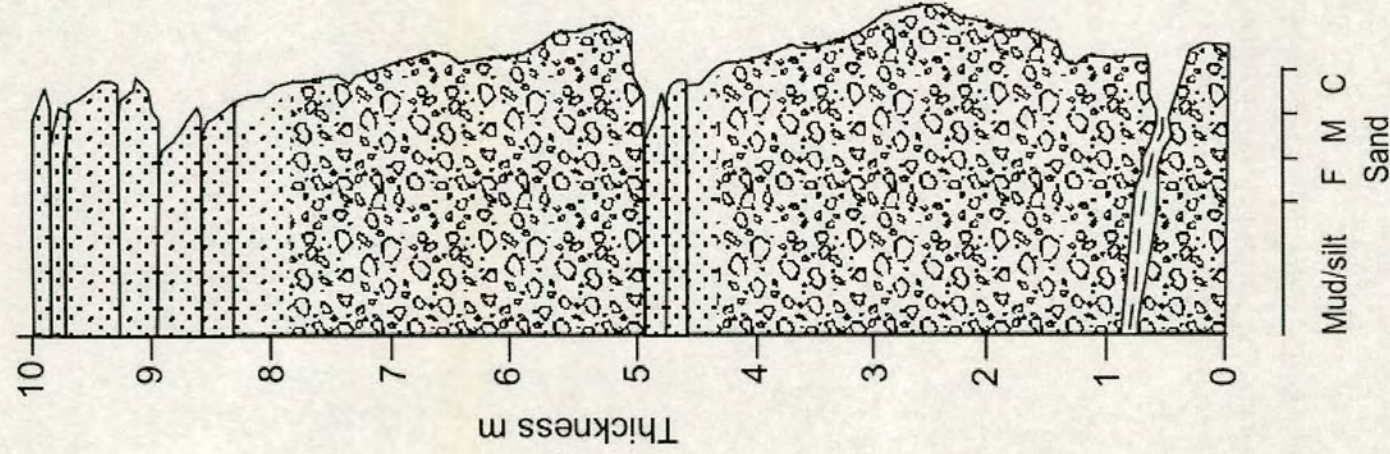


Figure 3.101. Log 5. A conglomerate channel deposit within the middle level of the Sütçü Formation (gr: İ42, 1918394508).

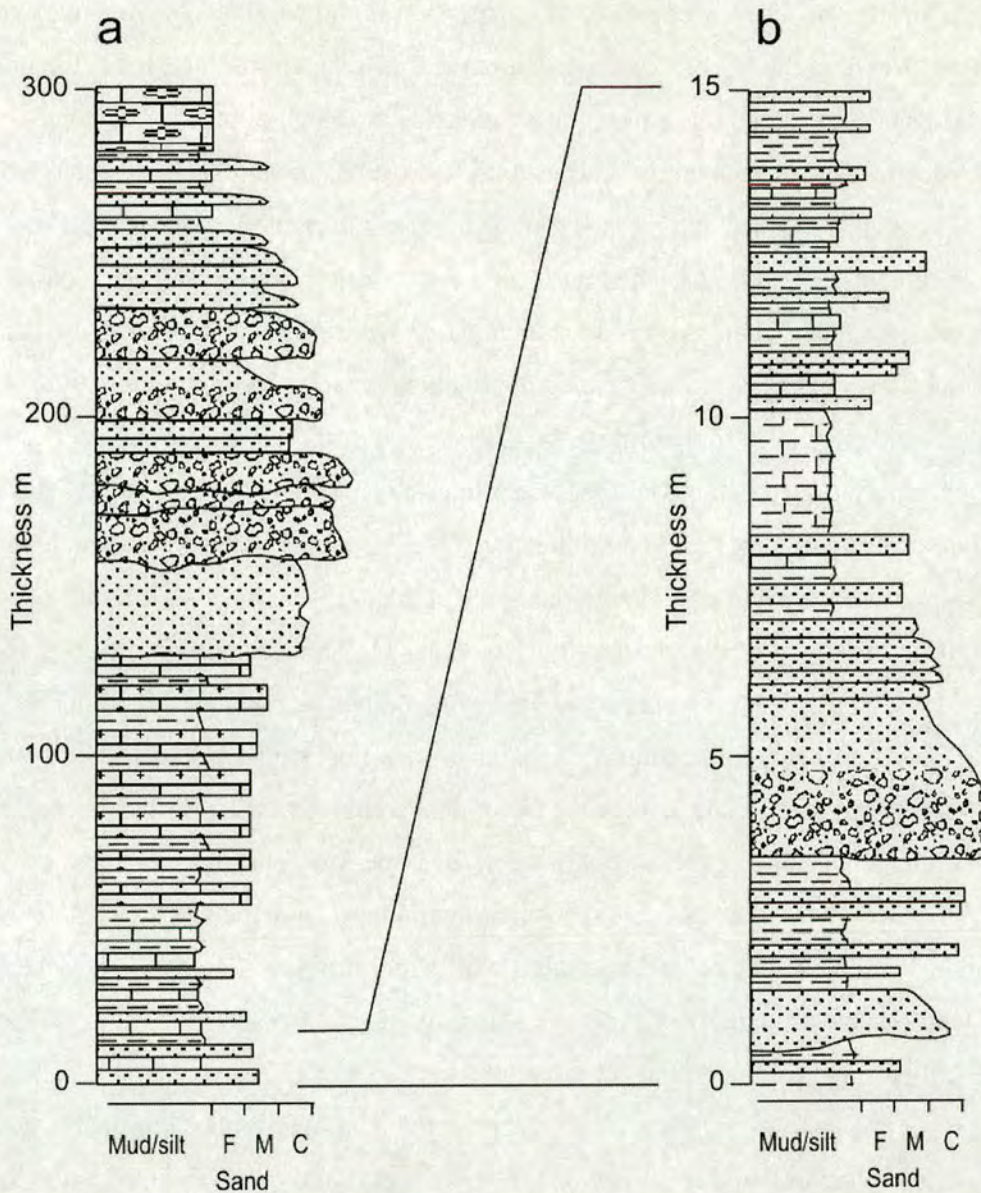


Figure 3.102. Log 6. Uppermost part of the Sütüinar Formation (transitional to the Sipikör Formation) showing a coarsening upward trend due to submarine fan progradation.

3.6.4 Environment of deposition and tectonic setting.

The lower part of the Sütüinar Formation contains silicious recrystallised radiolarians within carbonate wackestones suggesting a deep-water open marine setting but with deposition above carbonate compensation depth. the lower part of the succession is interpreted as 'distal' turbidites in a deep-water carbonate

environment. The lower part of the succession is comparable to sedimentary rocks deposited on the lower slopes of submarine fans (e.g. Crati, Italy, Ricci Luchi et al. 1984). The gradual up-section increase in clastic content, grain size and bed-thickness indicates a temporal transition to more 'proximal' submarine fan facies. The thickly-bedded and massive sandstones are interpreted as the product of sediment-gravity flows. The lenses of volcanoclastic conglomerate and coarse calcarenite and their associated amalgamated sandstones could represent channelised debris-flow deposits and associated overbank deposits. The immature texture suggests a low degree of sediment transport. The shale and fine sandstone observed at this level in the succession could represent inter-channel flats (Leeder 1982). The association of facies in the middle part of the Sütüpnar Formation is comparable with a mid-fan environment. The gradual replacement up-section of distal turbidites by more 'proximal' sediment-gravity flow deposits is consistent with the progradation of a submarine fan. The purely volcanic and carbonate composition of the Sütüpnar Formation, with no metamorphic grains or minerals, strongly suggests derivation from a purely volcanic source area and not a continental margin. The observation of a single andesitic lava flow observed in the uppermost part of the succession indicates the proximity of volcanism at the time of deposition of the unit. However, the low abundance of volcanic rocks within the succession suggests a low heat-flow setting and the paucity of sediment slump also structures also suggests that there was only limited local tectonic activity at the time of deposition.

The volcanoclastic lithologies present are similar to those of the Karadağ, inferred arc unit and it is likely that the two units were originally intergradational.

The unit is interpreted as an ancient prograding submarine fan that transported carbonate and volcanic-derived material into a basin, that on the basis of evidence from the adjacent tectono-stratigraphic units is interpreted as a forearc basin. A reduction of textural maturity also suggests an increase in depositional energy and source proximity.

3.6.5 Summary

The Sütöinar Formation contains foraminifera that indicate a Upper Cretaceous-Early Eocene age (83.5-48.6 Ma). The stratigraphic base of the formation is not exposed. The Sütöinar Formation comprises a 1500m thick, regressive succession of carbonate and volcanoclastic sedimentary rocks and passes conformably into the overlying Sipikör Formation.

Carbonate sediment was redeposited from a shelf-depth setting, rich in *Nummulites* sp. A carbonate shelf possibly fringed the inferred volcanic arc. The sedimentary rocks were redeposited in a deep-water open-marine environment by turbidity currents commonly within submarine channels. The regressive succession could be interpreted as a stratigraphic response to relative sea-level change or to progradation of a submarine fan. The unit contains no terrigenous material and a purely volcanic source area is inferred. The volcanoclastic lithologies present are similar to those of the Karadağ, inferred arc unit and it is likely that the two units were originally intergradational. The paucity of volcanic rocks indicates an environment with low heat-flow and there is little evidence for syn-sedimentary tectonism. Overall, the Sütöinar Formation is interpreted as a Upper Cretaceous-Lower Tertiary regressive fore-arc basin.

3.7 Syn-collisional sedimentation: Sipikör Formation

Figure 3.103 shows the outcrop of the Sipikör Formation in the Erzincan area. The thickness of the unit is variable. The unit is estimated to be >500 m thick to the south of Köhneındağ (gr: İ42, 199980). The succession is only ~10 m thick near Muratboynu (gr: J41, 963750). The Sipikör Formation lies conformably upon and, interdigitates with, the Upper Cretaceous Sütöinar Formation in the Köhneındağ area (Figure 3.103 and 3.93). The Sipikör Formation lies unconformably upon the Upper Cretaceous ophiolitic units (Refahiye Complex, Karadağ Formation and, Karayaprak Mélange) in the north and south of the area studied (eg. at Muratboynu, gr: J41, 963750, and Mecidiye, gr: İ43, 465125). The base of the unit is, therefore, likely to be diachronous. Lateral facies variations are observed within this unit. The microfauna present in the unit indicate a Palaeocene to Early Eocene age (65.5-48.6

Ma) (Prof. Izver Ongen, Prof. Kemal Taşlı and Prof. Nurdan İnan pers. comm. 2004; see Appendix 1 for micropalaeontological data).

3.7.1 Structure

Unlike older units, outcrops of the Sipikör Formation in the Erzincan area do *not* exhibit top-to-the-north compressional structures. Bedding generally strikes NE-SW (Figure 3.105).

The Sipikör Formation locally exhibits a pervasive top-to-the-south shear fabric at Muratboynu (south of Kemah; Figure 3.103). The shear fabric ‘flows’ around calcareous concretions in which age-diagnostic foraminifera are preserved (see above). Top-to-the-south shear fabric is not as widespread in the Sipikör Formation as in the Sütçinar Formation or the other Neotethyan units described above. 10 km south of Erzincan, at Giyabey Yürdü (gr: İ42, 399878), the Sipikör Formation unconformably overlies highly sheared serpentinite (either the ophiolitic Refahiye Complex or the Karayaprak Mélange). The strong shear fabric in the serpentinite does not continue into the Sipikör Formation. However, at Giyabey Yürdü the Sipikör Formation and its basal unconformity are folded into large steeply plunging, open to tight, rounded folds.

The Sipikör Formation exhibits top-to-the-south thrust faults and folds (Figure 3.104). At Mecidiye (~10 km north of Erzincan), top-to-the-south thrust faults imbricate the Sipikör Formation with the unconformably underlying ophiolitic Refahiye Complex. The Sipikör Formation exhibits a far a more simple structure than the polyphase-deformed Refahiye Complex below. The beds of the Sipikör

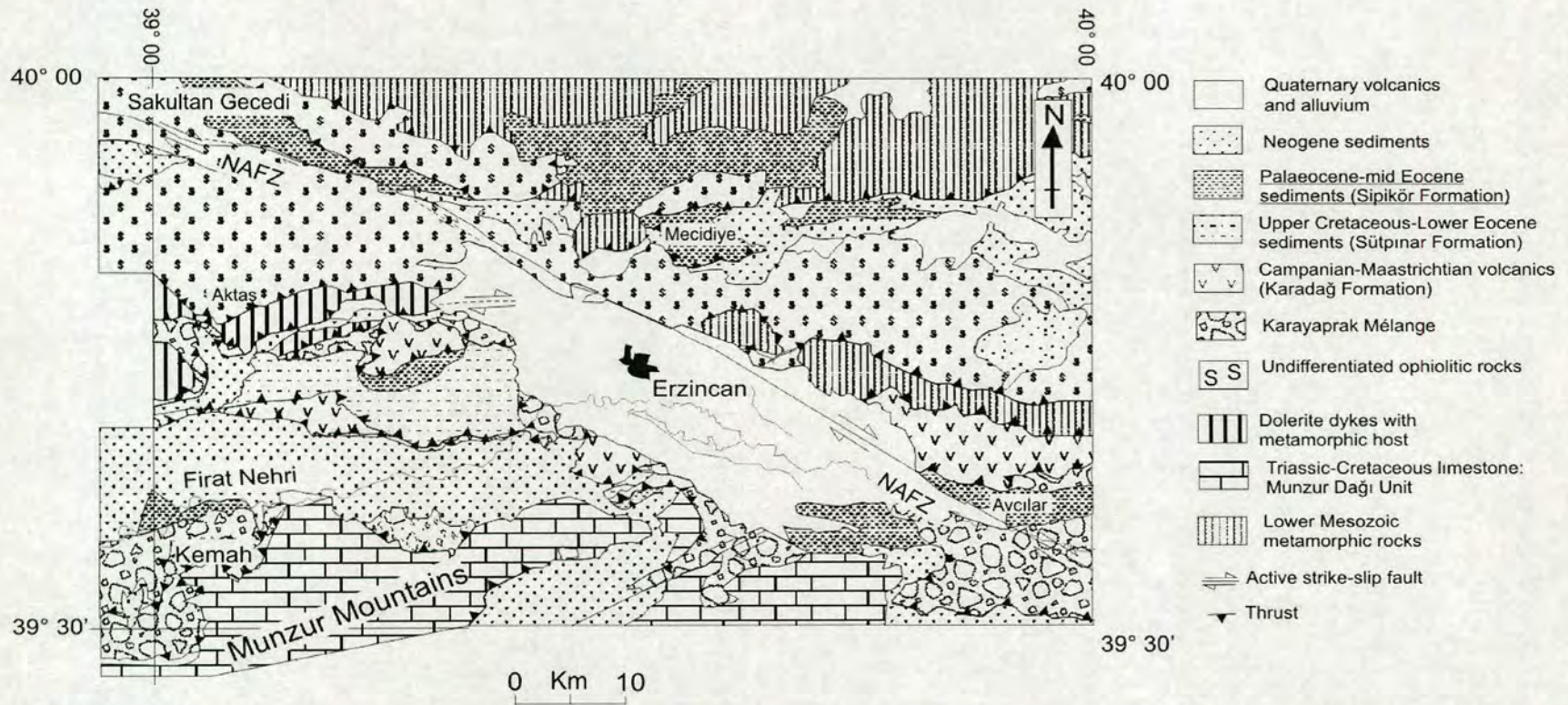


Figure 3.103. Map showing outcrop of the Sipikör Formation in the Erzincan area.

Formation are folded into a series of south-vergent asymmetrical recumbent close to tight parallel folds between thrust faults at Mecidiye. The folds have a wavelength of ~100m. North-dipping, top-to-the-south shear zones cut the succession at Köhnemdağı (Figure 3.94). At Komur, ~15 km northwest of Erzincan the Sipikör Formation is folded by upright open south-vergent asymmetrical folds with a wavelength >100 m.

These observations suggest that top-to-the-north deformation pre-dates deposition of the Palaeocene-Lower Eocene Sipikör Formation, locally at least, while later top-to-the-south deformation post-dates its deposition.

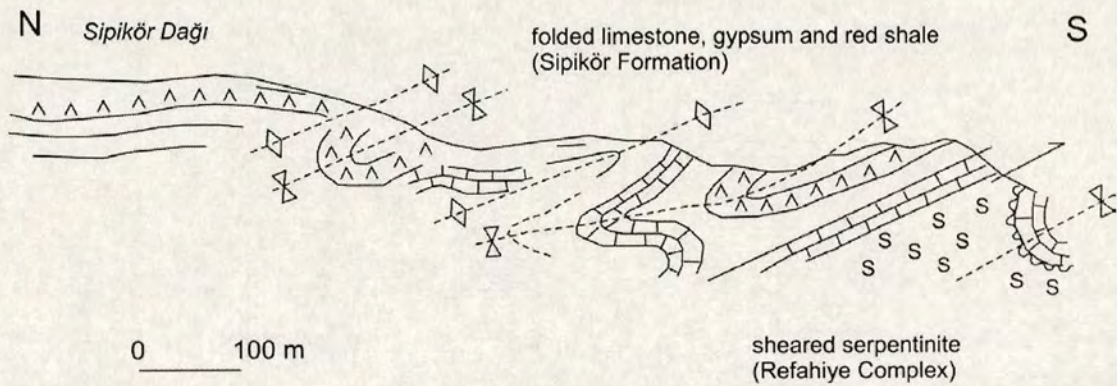


Figure 3.104. Field sketch at Sipikör Dağı (15 km north of Erzincan) showing structure of the Sipikör Formation.

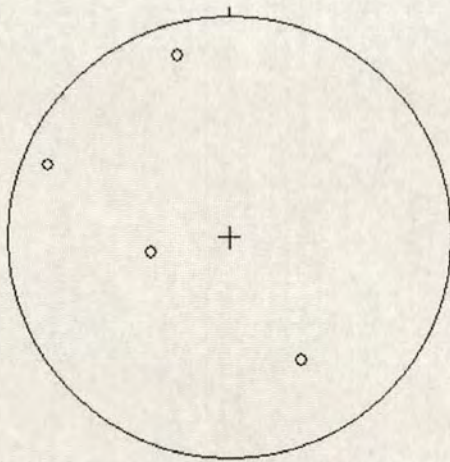


Figure 3.105. Equal-area lower hemisphere projection (Lambert/Schmidt) of poles to bedding for the Sipikör Formation.

3.7.2 Sedimentary facies

The Sipikör Formation exhibits lateral and vertical variations between a wide variety of sedimentary facies. Where the unit is conformable with the underlying Sütçinar Formation it begins with the appearance of polymict matrix-supported conglomerates together with homogenous, massive, fine-grained limestone containing (benthic) Nummulites (Figures 3.106 and 3.107), as observed south of Köhneşdağı (gr: İ42, 199980). The section at Köhneşdağı is deformed and four individual sedimentary logs were made in the area (Figures 3.106 to 3.108). It is unclear how they restore. The conglomerates and the limestone both form discontinuous thick (40 m) lenses. The conglomerate is associated with amalgamated, thickly bedded, massive calcareous sandstone and calcarenite. Individual conglomerate lenses fine upwards to cross-bedded sandstone and greywacke with laminated tops. Thick beds of massive and cross-bedded, coarse-grained sandstone contain abundant well-rounded quartz grains, feldspar and calcite. The sandstone also contains outsize clasts (rare pebbles) of recrystallised limestone, red chert and basalt. Rare thin beds of pelagic limestone, shale and siltstone are interbedded with sandstone and gravel. The top of the unit is removed by a north-dipping thrust fault in the Köhneşdağı area.

The Sipikör Formation exhibits a fining-upwards succession >80 m thick near Göltepe (gr: İ43, 439877; Figure 3.109). Here, the unit lies unconformably upon the Karadağ Formation and, is tectonically imbricated with younger (Miocene) sedimentary rocks. As at Köhneşdağı, the medium-bedded (~1 m) conglomerate contains basalt and limestone clasts, in addition to rudistic bivalves. Each conglomerate bed fines upwards to sandy limestone and marl. The first 30 m of the succession contains coarse angular lithoclasts, whereas the upper part of the succession is free of lithoclasts. Conglomerate and sandstone are gradually replaced by interbedded shale and nummulitic limestone.

The Sipikör Formation lies directly above the Karayaprak Mélange with an unconformable contact; exposed South of Muratboynu village near Kemah (Figure 3.103). The succession there is only ~10 m thick and is unconformably overlain by Oligocene-Miocene cover sedimentary rocks and volcanic rocks. The Sipikör

Formation there is a nodular micritic limestone with abundant nummulites, ~1 cm diameter and coarse shelly partings.

North of Erzincan, the Sipikör Formation exhibits lateral variation between two very different successions, both with an unconformable contact on the underlying Upper Cretaceous units. Unconformably on the Karayaprak Mélange there is a >50 m thick succession of dark grey sandstone and siltstone (Figure 3.110), exposed near Kömür village (gr: İ42, 3631220766). Greywacke with angular clasts (~1 mm) is composed of mafic igneous material, feldspar and red chert and contains benthic forams (~5 mm). The greywacke is interbedded with dark grey coarse-, medium- and fine-grained sandstone. The sandstone is well sorted and medium to thinly bedded.

A succession of clastic sedimentary rocks, carbonates, evaporite and conglomerate unconformably overlies part of the Refahiye Complex (Figure 3.111) exposed north of Erzincan, near Mecidiye (gr: İ43, 49731300). This succession begins with a thin (~2 m) matrix-supported conglomerate containing clasts of serpentinite, chloritised basic igneous rocks, feldspar and mafic mineral grains (ophiolite debris), set in a micritic matrix. This passes upwards into a poorly exposed fissile red siltstone (~20 m thick). The red siltstone passes into a generally coarsening-upwards succession of sandy limestones and evaporites (~60 m thick). The sandy limestones are fine- to coarse-grained packstones with shell fragments, foraminifera (including large (10 cm) nummulites), bivalves, echinoids and large (~2 m) sponges. The detrital content is present in varied concentration and consists of serpentinite, chloritised basic igneous rock, feldspar, quartz, spinel and chert. The limestones have a micritic matrix (<15%) and an isopachous sparry calcite cement in cavities and veins. Silty to marly interbeds separate the sandy limestones. A layer of anhydrite (~8 m thick) is found in the middle of the limestone succession. The anhydrite passes into >20 m thick succession of thickly bedded hard, massive, fine-grained, nummulitic limestone (similar to the thick lenses observed at Köhnemdağı) and thickly-bedded coarse-grained sandy limestones and calcarenites. The sandy limestones are coarse, shelly packstones/grainstones with mafic lithic clasts, oncoids, oolites, and feldspar in varying proportions and contain fragmented to whole shells.

The calcarenites are poorly-sorted containing quartz, chert and serpentinite clasts. Some whole shells are preserved, but, most are broken.

This carbonate succession is followed by lenses of red, polymict, poorly bedded and poorly sorted gravel. Both matrix-supported and clast-supported gravel is present. The gravel contains rounded, to angular, clasts of red chert, serpentinite, basalt, diabase and gabbro, set in a red silty matrix. The gravel beds interdigitate with thin beds of the red siltstone. White caliche horizons are present within the red siltstone and gravel.

3.7.3 Petrography of the Sipikör Formation

In thin section, the matrix of the basal conglomerate (at Mecidiye) is a micritic wackestone with sub-angular grains of clinopyroxene, serpentinite, amphibole (hornblende), feldspar, chloritised basalt; all of this is interpreted as ophiolitic detritus.

The limestones from near the base of the succession are oosparites (packstones) and oncoidal foraminiferal biomicrites (packstones). The biomicrite contains rare clasts of serpentinite, chloritised basalt, feldspar, quartz and spinel. An isopachous sparry calcite cement fills cavities and veins in the biomicrite. Foraminifera form the nuclei of oncoids.

Coarse shelly limestone in thin section is biomicritic packstone containing fragments of red algae, Nummulites, bryozoa, coral and bivalve. Rare sub-angular clasts of feldspar, chloritised basic lava, carbonated serpentinite and quartzite are present. (quartzite is coarsely polycrystalline with sutured grain boundaries and strained extinction patterns).

In thin section, the coarse-grained calcarenites are poorly sorted, angular, to sub-angular, and contain quartz, feldspar, basic lava, chert, calcite, quartzite, spinel and fragmentary bioclasts including echinoids, red algae, foraminifera and bivalves. Coarse-grained sandstone from near Kömür village is poorly-sorted, sub-rounded to angular with a micrite matrix and sparry calcite cement. Grain types include monocrystalline quartz, quartzite, chert, calcite, feldspar, opaque oxide (magnetite), clinopyroxene, carbonated serpentinite, chloritised and glassy basic lava, altered olivine (iddingsite), biotite, shell fragments, and whole Nummulites. Some sections

contain a much greater abundance of volcanic plagioclase and magnetite at the expense of other clast types.

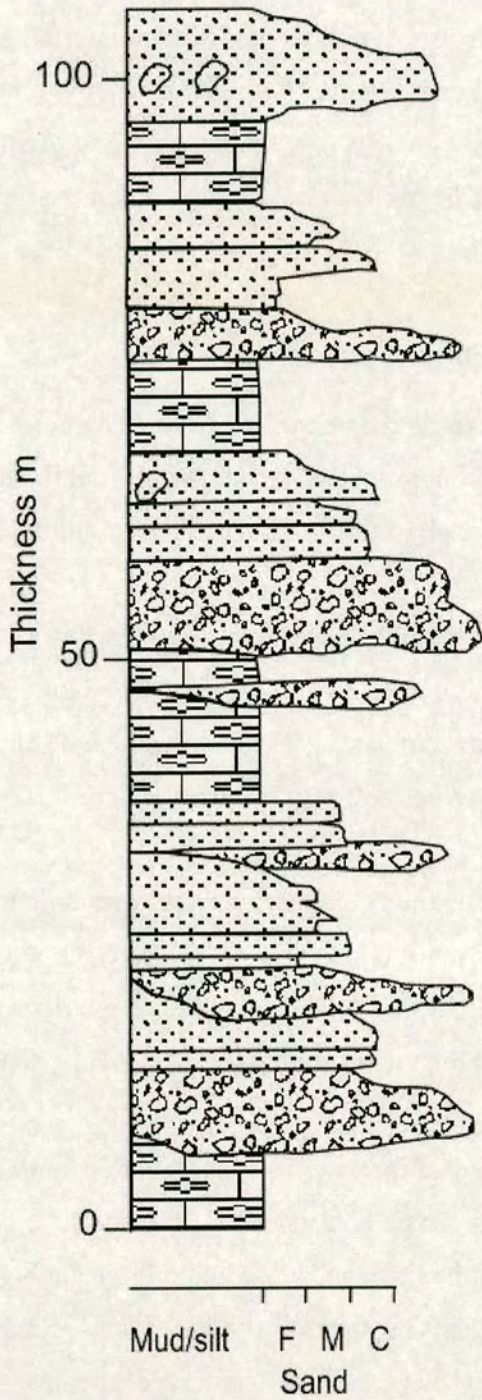


Figure 3.106. Sedimentary log of the Sipikör Formation exposed at Köhnemdağı (gr: İ42, 1963399176).

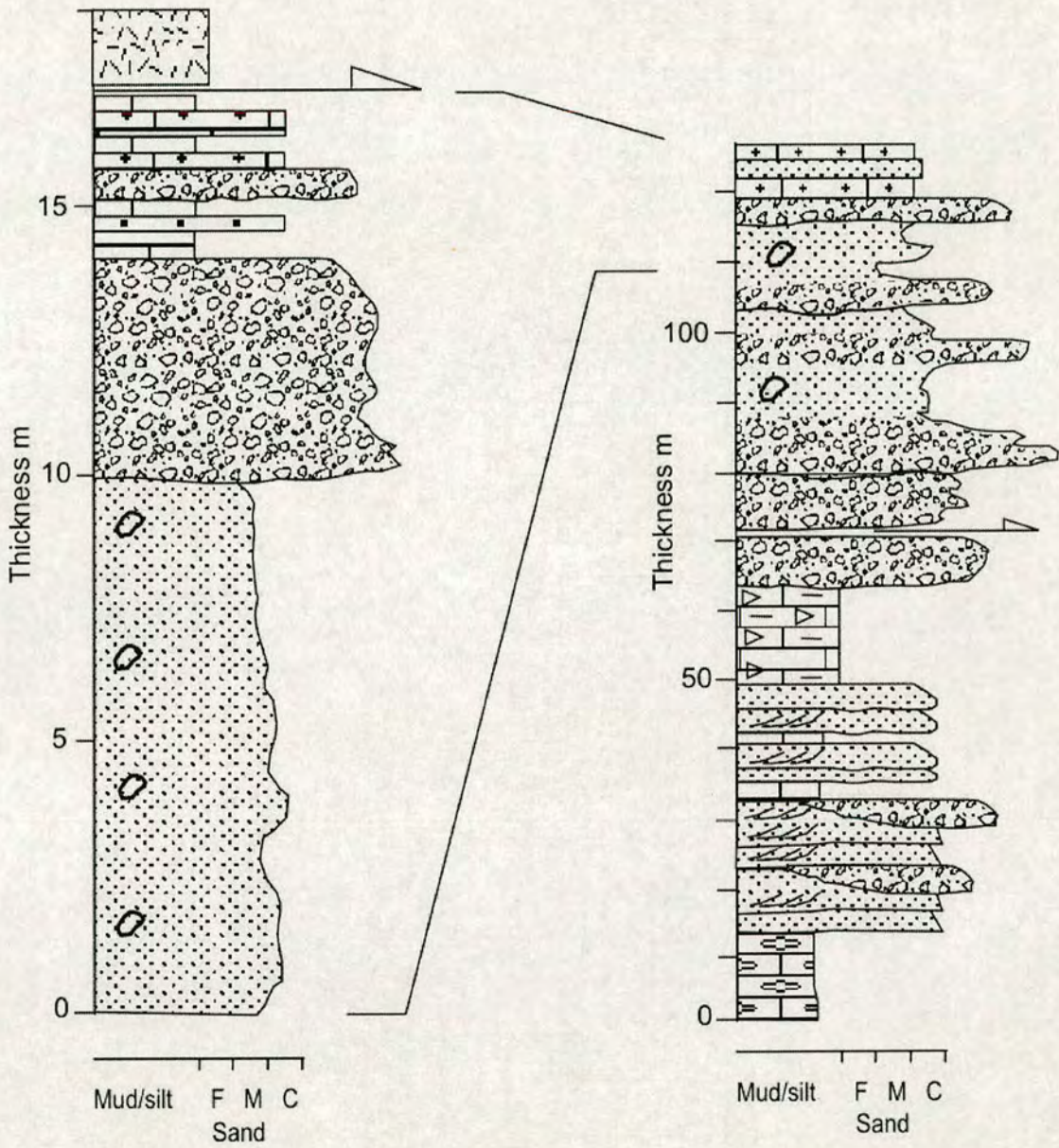


Figure 3.107. Sedimentary log of the Sipikör Formation exposed at Köhneddağı (gr: İ42, 1945299112).

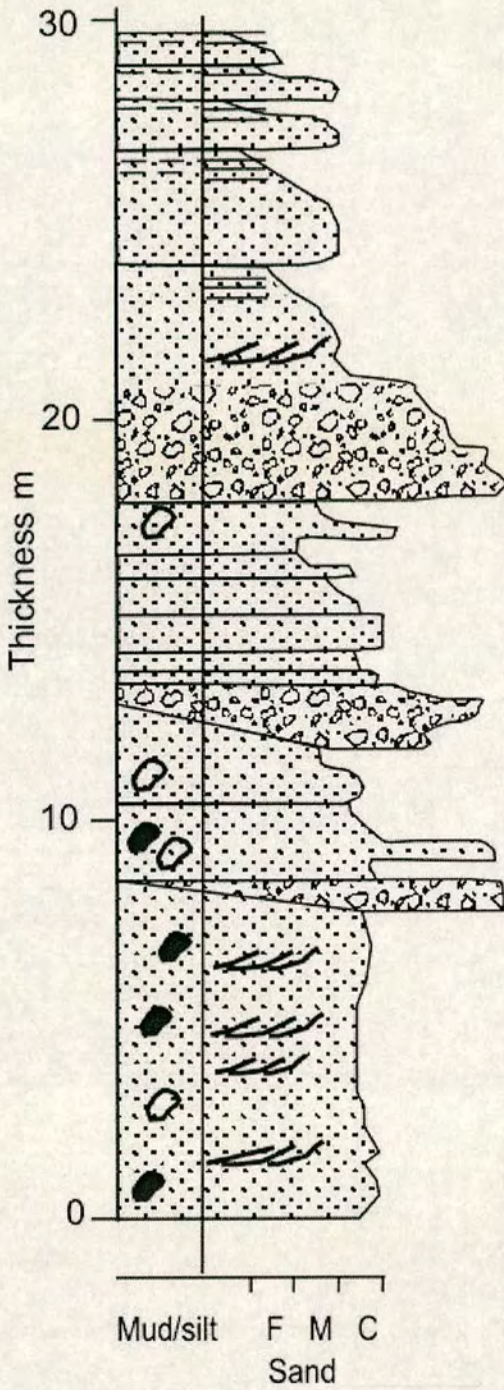


Figure 3.108. Sedimentary logs of the Sipikör Formation exposed at Köhneşdağı (gr: İ42, 1945299112).

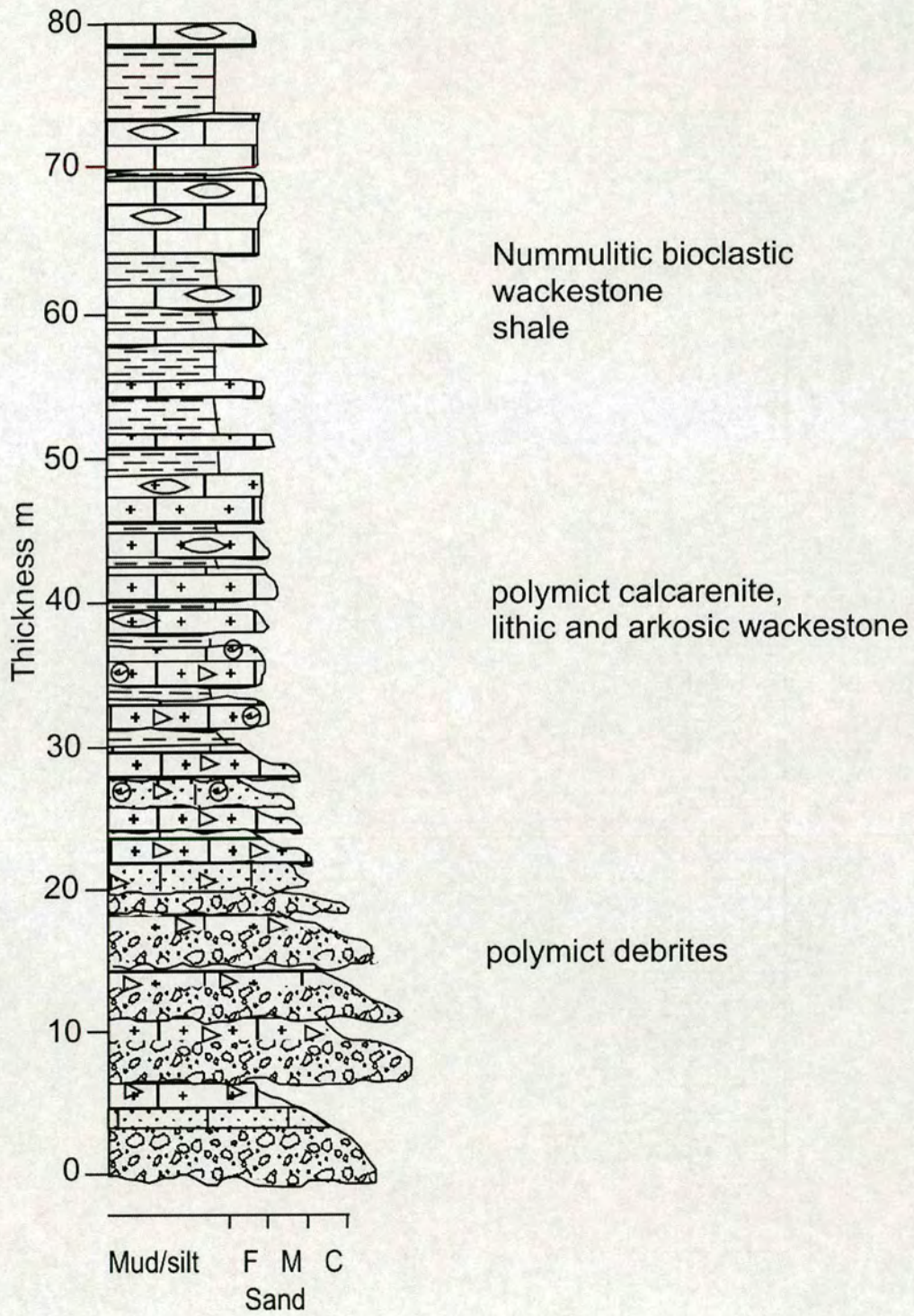


Figure 3.109. Sedimentary log of the Sipikör Formation exposed near Göltepe (gr: İ43, 439877) .

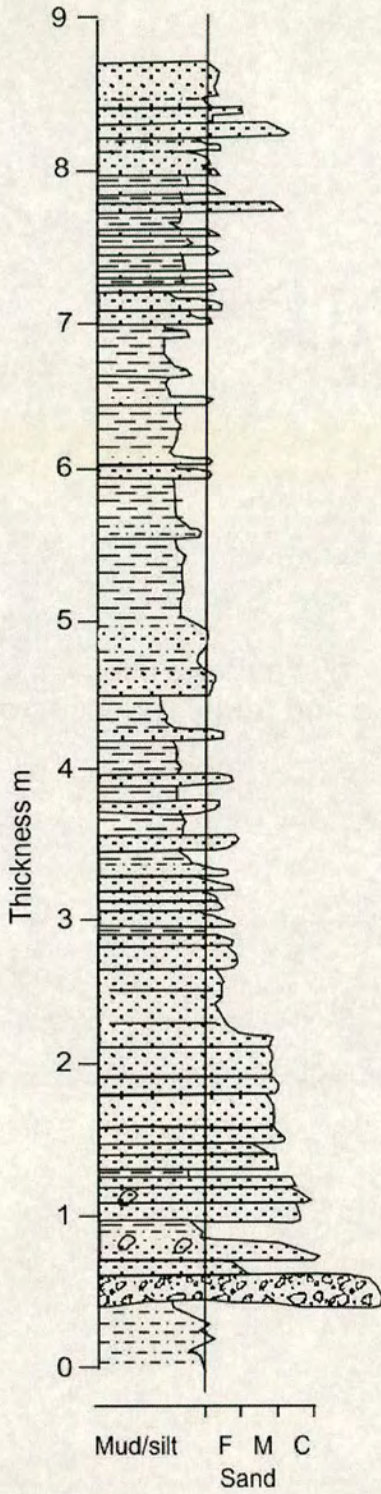


Figure 3.110. Sedimentary log of the Sipikör Formation exposed near Kömür (gr: İ42, 363120766).

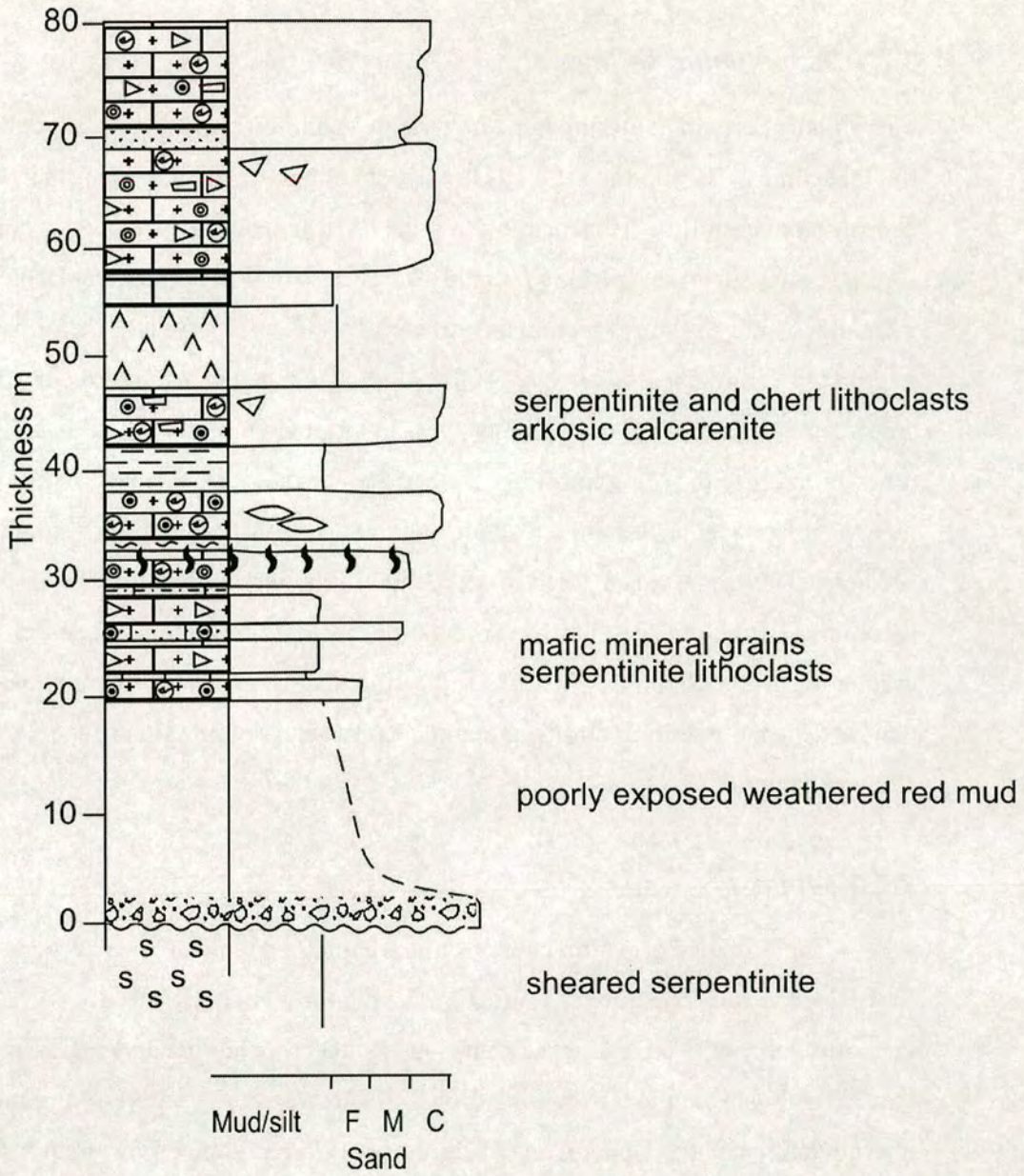


Figure 3.111. Sedimentary log of the Sipikör Formation exposed near Mecidiye (gr: İ43, 49731300).

3.7.4 Depositional setting

The Sipikör Formation accumulated in variable shallow-marine, lagoonal, deltaic, to fluvial settings. The mixture of well-rounded, to angular, grains is consistent with deposition in both fluvial and shallow-marine environments. The generally poorly sorted texture suggests reworking, mainly by gravity flows. This unit lacks the north-vergent tectonic structures seen in the structurally underlying units. The formation is interpreted as a transgressive cover of the suture zone, deposited after the northwards emplacement of the Upper Cretaceous units in latest Cretaceous (Late Maastrichtian) time, but prior to thrusting in Mid Eocene time. The unit rests unconformably above the Upper Cretaceous Refahiye Complex, Karadağ Formation and Karayaprak Mélange. Thus there was a break in deposition following northwards emplacement of these units. However, the Sütçinar Formation (inferred forearc basin) passes gradually into the Sipikör Formation, indicating that the forearc basin remained a marine depocentre during northward emplacement and deformation of the Neotethyan units.

3.7.5 Summary

The Sipikör Formation contains microfauna that indicate a Palaeocene to Early Eocene age. The Sipikör Formation is up to ~500 m thick and lies unconformably above the Upper Cretaceous mélange, ophiolitic and volcanic arc units (Refahiye Complex, Karadağ Formation). However, the Sipikör Formation interdigitates with the Upper Cretaceous-Lower Eocene Sütçinar Formation (inferred forearc basin).

The formation contains rounded continental-derived clasts in addition to ophiolitic lithoclasts derived from the Eurasian margin (Pontides) and the emplaced Neotethyan units. Faunal assemblages and sedimentary facies of the Sipikör Formation represent shallow-marine, lagoonal, fluvial and deltaic environments. The Sipikör Formation does not exhibit top-to-the-north compressional structures or a pervasive shear fabric as seen in the Upper Cretaceous Neotethyan units. Structural observations suggest that top-to-the-north deformation pre-dates deposition of the

Palaeocene-Lower Eocene Sipikör Formation in the Erzincan area. Top-to-the-south deformation post-dates its deposition.

The Sipikör Formation is interpreted as a syn-collisional basin that was deposited upon the Neotethyan units following their northward emplacement onto the Eurasian margin. The age of the Sipikör Formation constrains northward emplacement of the Neotethyan units to pre-Palaeocene and constrains the south-vergent deformation to post-Early Eocene.

3.8 Summary of main results from the Izmir-Ankara-Erzincan suture zone in the Eastern Pontides

The Ayıkayası Formation records the foundering (“pelagisation”) of the Munzur Platform and development of a foredeep during Turonian-Campanian time related to southward thrusting and emplacement of the Neotethyan ophiolitic nappes.

The Ayıkayası Formation is interpreted as a trench-margin collision facies and its tectonostratigraphic position is comparable to units of the same age found ~500 km southeast in the Taurides (Özer et al. 2004).

The Refahiye Complex is interpreted as a disrupted, but originally complete section of oceanic lithosphere and lithospheric upper mantle, of which the upper extrusive levels are not preserved. The petrology and geochemistry of the ophiolite have the characteristics of known back-arc basins. The metamorphic host rocks within the ophiolitic Refahiye Complex are comparable with the Upper Palaeozoic-Lower Mesozoic metamorphic basement of the Pontides (e.g. Doğankavak Unit; Topuz et al. 2004). The presence of igneous contacts between diabase dykes and their metamorphic host rocks, therefore, suggests that the ophiolite did not form in an open-ocean setting, but instead as a rifted continental margin. The cross-cutting dykes within the metamorphic rocks are inferred to be related to the adjacent exposures of 100% sheeted dykes. They are unlikely to represent fragments of older dyke-rich metamorphic basement, as exposed in some parts of the Pontides (eg. Artvin region; T. Ustaömer, pers comm., 2004).

The Karayaprak Mélange is interpreted as an emplaced Cretaceous accretionary complex. The Karayaprak Mélange contains two associations interpreted as; 1) Spreading ridge tectonic facies and; 2) Volcanic seamount tectonic

facies. Blocks within the The Karayaprak Mélange contain microfossils that indicate a Early Cretaceous age (e.g. Berriasian; 145.5-140.2 Ma; Gradstein et al. 2004). This reflects the age of the Neotethyan lithosphere that was being subducted at the trench. Blocks in the mélangé are dominantly ophiolitic lithologies and to a lesser extent terrigenous clastic sedimentary rocks, suggesting that the accretionary complex developed in an oceanic setting. Rare olistostromal levels are present within the mélangé. Outcrop of the unit is more abundant toward the south of the suture zone i.e. south of the Refahiye Complex and the Karadağ Formation. This probably reflects the original position of the accretionary complex relative to the inferred arc and backarc units (Yaylaçayı Formation and Kızılırmak Ophiolite respectively). The mélangé was emplaced southward over the Permian-Upper Cretaceous carbonate platform (Munzur Dağı Formation; Özgül and Türşücü 1984) and the Upper Cretaceous (Turonian-Campanian; 93.5-70.6 Ma; Gradstein et al. 2004) inferred flexural foredeep (Ayıkayası Formation) during Turonian-Campanian time (93.5-70.6 Ma). The mélangé is unconformably overlain by Palaeocene-Eocene (65.5-33.9 Ma; Gradstein et al. 2004) sedimentary rocks (Sipikör Formation). Northward emplacement of the mélangé, therefore, occurred before Palaeocene-Eocene time (65.5-33.9 Ma).

The Karadağ Formation is interpreted as an emplaced Upper Cretaceous volcanic arc. Planktonic foraminifera indicate a Late Cretaceous age for the volcanic arc unit. The formation contains no terrigenous material and no metamorphic host rock and is thus likely to have developed far from any continental margin. Metamorphic host rocks may have been tectonically removed with the lower levels of the arc. Alternatively the arc may have developed upon oceanic crust. The inferred volcanic arc experienced north-vergent deformation related to its emplacement onto the Eurasian margin followed by south-vergent deformation related to ongoing collision between the Taurides and the Pontides. The Upper Cretaceous-Lower Eocene (Campanian-Ypresian 83.5-48.6 Ma) Sütçinar Formation comprises a 1500m thick regressive succession of carbonate and volcanoclastic sedimentary rocks and passes conformably into the overlying Sipikör Formation. The sedimentary rocks of the Sütçinar Formation were redeposited in a deep-water open-marine environment by turbidity currents and in submarine

channels. The regressive succession of the Sütüinar Formation could be interpreted as a stratigraphic response to relative sea-level change or to progradation of a submarine fan. The Sütüinar Formation contains no terrigenous material and a purely volcanic and carbonate source area is inferred. The volcanoclastic lithologies present are similar to those of the Karadağ, inferred arc unit and it is likely that the two units were originally intergradational. The Sütüinar Formation is interpreted as an Upper Cretaceous-Lower Tertiary regressive fore-arc basin. The inferred forearc basin shallowed and deposition continued throughout the northward emplacement of Neotethyan units onto the Eurasian margin. The Eurasian basement, emplaced volcanic arc, ophiolite and accretionary *mélange* units were sources of sediment to the evolving basin.

Northward emplacement was followed by a marine transgression during Palaeocene-Early Eocene time (locally at least). Shallow-marine, carbonate lagoon, deltaic and fluvial depositional environments developed upon the emplaced Neotethyan ophiolitic and *mélange* units.

4 Tectonostratigraphy of the Central Pontides

In this chapter information for the Central Pontides is set out and discussed. The layout of the next two chapters follows that for the Eastern Pontides in the previous two chapters.

4.1 Introduction

A formal redefinition of the Upper Mesozoic-Lower Tertiary rocks of the Izmir-Ankara-Erzincan suture zone in the Central Pontides is presented here in order to provide a framework for sedimentological, geochemical and structural studies detailed in the subsequent chapters. The stratigraphy of the area has been modified in some way or other with each publication such that there is now considerable confusion regarding subdivisions, outcrop area and description. This problem is compounded by a severe lack of palaeontological and geochronometric data. In this chapter, the stratigraphy of the rocks of the Izmir-Ankara-Erzincan suture zone in the Central Pontides will be redefined in line with the International Stratigraphical Commission's guide to stratigraphical procedure (Murphy and Salvador 1994). The need for a stratigraphic revision reflects the history of geological research in the Central Pontides. This chapter summarises the major stratigraphic units, including the basement units as a background for the stratigraphic revision that follows. The revised stratigraphy provides the framework for the more detailed description of the Upper Cretaceous-Lower Tertiary units of the IAES suture zone in the remainder of the thesis. This chapter concludes by proposing the stratigraphic scheme adopted in this thesis in order to investigate the Upper Cretaceous-Lower Tertiary geology of the Izmir-Ankara-Erzincan Suture Zone in the Central Pontides.

4.2 Revised stratigraphy

The revised stratigraphy applies to the Upper Mesozoic-Lower Tertiary rocks of the suture zone and incorporates, with acknowledgements, previously published data. Previous stratigraphic nomenclature is retained as far as possible and the basis and methodology for this chapter is the same as that explained in chapter 2.3 for the

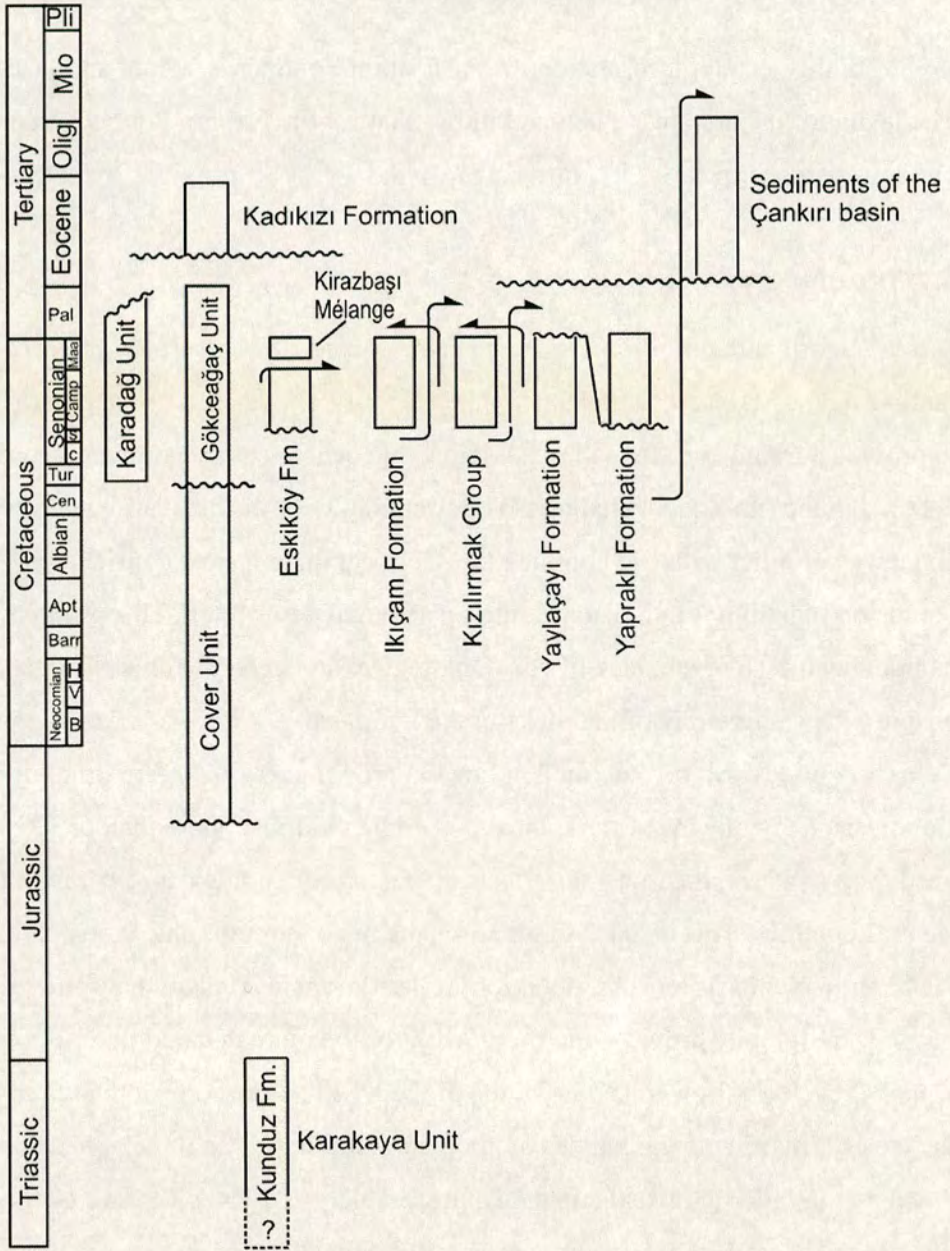


Figure 4.1. Revised stratigraphy of the Central Pontides.

Eastern Pontides. The revised tectonostratigraphy for the Central Pontides is shown in Figure 4.1.

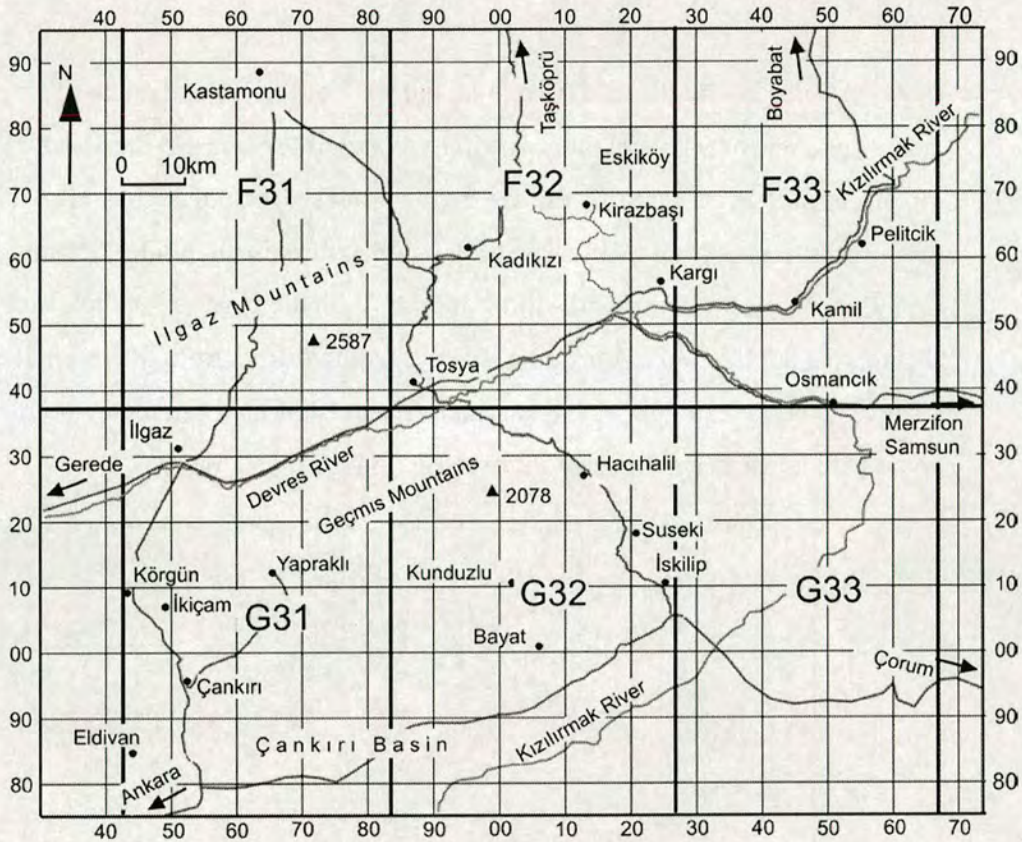


Figure 4.2. Geographical map of the Central Pontides to show locations referred to in the text. Turkish map numbers are shown.

4.2.1 Upper Cretaceous Kalecik Group

Synonymy. Ankara Mélange (Bailey and McCallian 1950); Kalecik Unit (Tüysüz and Dellaloğlu 1992); North Anatolian Ophiolitic Mélange (NAOM) (eg. Rojay 2001).

Name: The Kalecik Group was named informally by Tüysüz and Dellaloğlu (1992) after the town of Kalecik located 50km east of Ankara (outside the area studied here). Tüysüz (1990) further subdivided the Kalecik Unit to include the Kargı Group (named after the town of Kargı about 40km east of Tosya). The name Kargı Group was applied to outcrops of the Kızılırmak Ophiolite and the Kirazbaşı Mélange (sections 5.3 and 5.4) in this region but excludes any other Upper

Cretaceous volcanic and sedimentary associations. To avoid confusion this name has not been retained here.

Lithology: The Kalecik Group includes all of the diverse range of Upper Cretaceous-Palaeocene units present within the Izmir-Ankara-Erzincan suture zone in the Central Pontides area. These are divided into six main tectonostratigraphic units (Eskiköy Formation, Kirazbaşı Mélange, Kızılırmak Ophiolite, İkiçam Formation, Yaylaçayı Formation and Yapraklı Formation) described below (Chapter 5). Here, the application of the name Kalecik Group differs from the original usage by Tüysüz and Dellaloğlu (1992) as it includes an additional sedimentary unit, named here as the İkiçam Formation (see section 5.7).

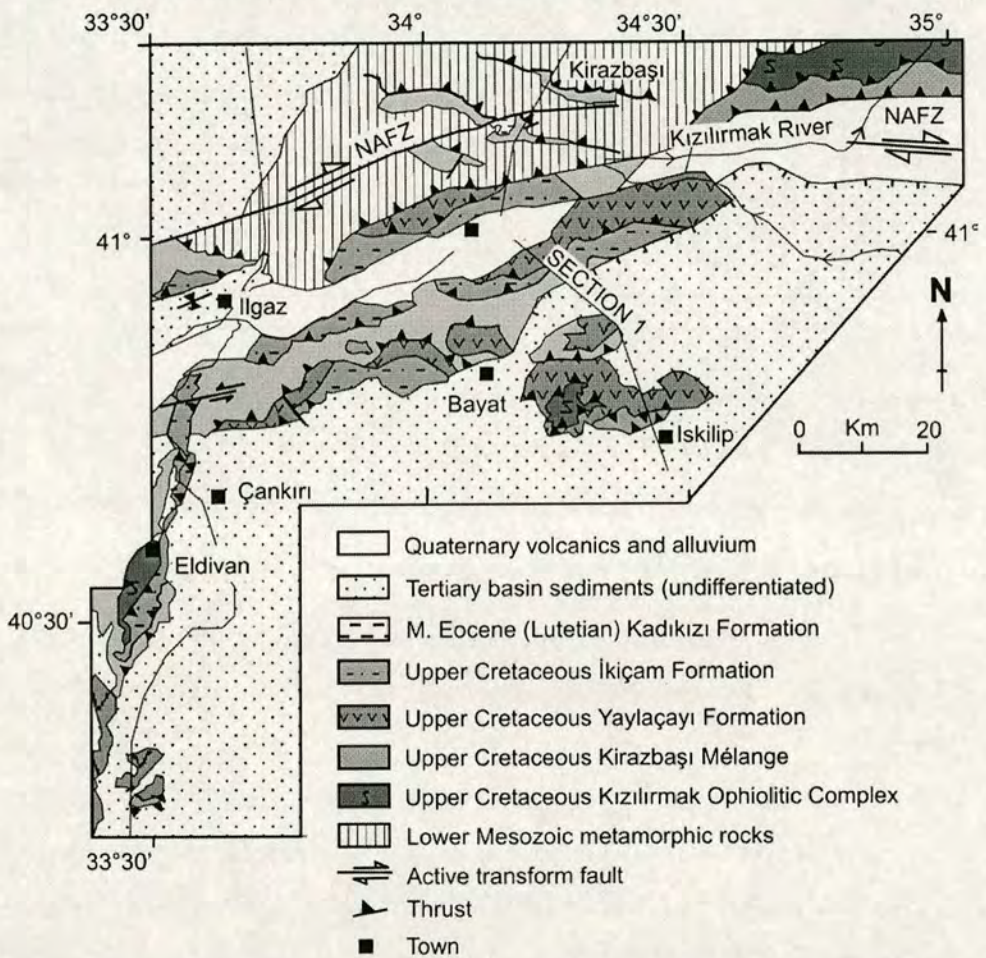


Figure 4.3. Geological map of the Central Pontides (Modified after Tüysüz, 1995). Line of section 1 (Figure 5.3) is shown. Eskiköy Formation and Yapraklı Formation not shown because of scale.

Lower and upper boundaries: The Kalecik Group is imbricated with the older Mesozoic metamorphic basement rocks and younger Tertiary sedimentary rocks (Figure 4.3) and its upper and lower contacts are commonly south-vergent thrusts. Individual units within the Kalecik Group may exhibit a distinctive relationship relative to older units that are not applicable to the Kalecik Group as a whole. For example, at Kirazbaşı the Mélange unconformably overlies schistose metamorphic basement rocks. Eocene and younger sedimentary rocks commonly rest unconformably on the Kalecik Group.

Thickness and lateral extent: The Kalecik Group is covered by the Tertiary sedimentary rocks of the Çankırı Basin along its southern edge, which cover its lower boundary and prohibit field study. The Kalecik Group crops out in a belt up to ~50km wide that extends beyond the studied area in the Central Pontides southwestwards toward Ankara and Izmir and southeastwards toward Çorum, Tokat and Erzincan (although nomenclature varies regionally).

4.2.2 Campanian Eskiköy Formation

Synonymy: Kirazbaşı Mélange (part of; Tüysüz, 1990).

Name: This unit is named after the village of Eskiköy near Kirazbaşı (Figure 4.2), located about 60km north east of Tosya. The Eskiköy Formation and its contact relations are well exposed 2km south of the village.

Lithology: The Eskiköy Formation begins with a thin (<10m) grey microcrystalline pelagic limestone that contains pelagic *Globotruncana* sp. of Campanian age (Tüysüz et al. 1988; Tüysüz 1990). This limestone passes upwards into a ~150m thick sheared, thrust and isoclinally folded section of clastic sedimentary rocks including shale, terrigenous turbiditic sandstones with shaly partings and poorly-sorted matrix-supported conglomerates that contain rounded

metamorphic quartz pebbles. Towards the top of the succession the sedimentary rocks are thrust imbricated with ophiolitic lithologies of the Kirazbaşı Mélange.

Lower and upper boundaries: At its base the Eskiköy Formation rests with angular unconformity upon the Eurasian schistose metamorphic basement (Kargı Complex; Ustaömer 1993) with a pisolitic bauxitic cap. At its upper boundary the unit is thrust imbricated with the Kirazbaşı mélange.

Thickness and lateral extent: The Eskiköy Formation is ~150m thick at the measured section 2km south of Eskiköy village (Figure 4.2). However, the pervasive shear fabric and isoclinal folding preclude reasonable estimation of the original stratigraphic thickness. Also, thrusting has removed an unknown thickness of strata from the top of the unit. The only locality where both upper and lower boundaries were observed is near Eskiköy village. The Eskiköy Formation is commonly observed in thin (eg. ~40m) thrust slices abundant within the more northerly outcrops of the Kirazbaşı mélange (eg. at Ödemiş near Ilgaz).

4.2.3 Upper Cretaceous-Lower Eocene Kirazbaşı Mélange: emplaced accretionary complex

Synonymy: Kirazbaşı Mélange (Tüysüz 1990); Anatolian Complex (Koçyiğit 1991); North Anatolian Ophiolitic Mélange (in part, Rojay 1993); “upper nape” of Kaecik Group (Tüysüz et. al. 1995); Kirazbaşı Mélange (Ustaömer and Robertson 1997);

Name: This Unit is named after the village of Kirazbaşı located about 60km north east of Tosya (Figure 4.2) where good exposure of its contact relations and internal structure are seen.

Lithology: The Kirazbaşı Mélange includes a pelagic limestone base passing up into shale and sandstone turbidites which are overlain by a tectonically deformed chaotic mixture of blocks of diverse size and lithology. The more commonly observed lithologies include serpentinised ultramafics, spilite or basalt, diabase,

radiolarian chert, pelagic and hemipelagic limestone; also mudstone, andesite, volcanoclastic sedimentary rocks, sandstone, neritic limestone, greenschist facies metavolcanics and metasedimentary rocks. Many of the blocks are likely to have been derived from the other Upper Cretaceous units described below. In the Merzifon region further east (outside the study area) the *mélange* is described as passing upwards conformably into coal-bearing deltaic and fluvial sandstones and conglomerates (Tüysüz et al. 1989, Yiğitbaş et al. 1990).

Lower and upper boundaries: In the type section, at Kirazbaşı, the base of the *mélange* is a grey pelagic limestone lying unconformably upon bauxitic mica-schist of the Upper Triassic Karakaya Complex. At its upper boundary the unit is unconformably overlain by Mid Eocene (Lutetian) and younger sedimentary rocks (eg. Kadıkızı Formation; section 5.8), as observed at Kadıkızı, about 30km north of Tosya (Figures 4.2 and 4.3). More commonly, individual outcrops of the unit are bound by south-vergent thrust faults.

Thickness and lateral extent: The Kirazbaşı *Mélange* crops out as several thrust slices occurring at all structural levels within the suture zone. Their outcrop covers >800 km² in the studied area. Thrust slices reach individual thicknesses of up to ~1km. Estimating the thickness of the Kirazbaşı *Mélange* in this region is made difficult by its intense internal polyphase tectonic deformation and poor internal stratification. In addition, the suture zone in the south of the region is buried beneath younger post-collisional sedimentary rocks of the Tertiary Çankırı basin. Excluding large-scale structural repetition the present thickness of the Kirazbaşı *Mélange* is estimated to exceed 6 km.

4.2.3 Campanian-Maastrichtian Kızılırmak Ophiolite

Synonymy: Kızılırmak Ophiolite (Tüysüz 1990; Tüysüz and Dellaloğlu 1995); Kızılırmak Ophiolite (Ustaömer and Robertson 1997).

Name: The Kızılırmak Ophiolite takes its name from the Kızılırmak River of northern Anatolia. In the Central Pontides good exposure is found along the Kızılırmak River valley near Pelitcik village (Figure 4.2).

Lithology: The Kızılırmak Ophiolite is a tectonically dismembered ophiolitic association that includes deformed serpentinitised hartzburgite, cumulate pyroxenite, isotropic and layered gabbro, deformed greenschist facies metabasaltic pillow lava, and rare epiophiolitic hemipelagic limestone, chert and mudstone.

Lower and upper boundaries: Both boundaries of this unit are south-vergent thrusts except where the upper boundary it an unconformity, with the unit being overlain by Eocene and younger sedimentary rocks.

Thickness and lateral extent: The present thickness of the Kızılırmak Ophiolite is estimated to be about 3.5km based on the measured section at Pelitcik. The unit crops out as three large thrust slices in the area studied (Figure 4.3). These thrust sheets are widely separated and are located at Pelitcik, near Kamil; Eldivan south of Çankırı, and north of Bayat, between Kunduzlu and Iskilip (Figure 4.2).

4.2.4 Campanian-Maastrichtian İkiçam Formation: emplaced marginal basin sedimentary rocks

Synonymy: Teşrekyayla Formation of the Memlik Group (Ankara region, Koçyiğit 1991); Upper Cretaceous-Palaeogene flysch (Ankara region, Rojay et al. 2001); “passive margin sediments of the Sakarya continent (Lias-Upper Cretaceous)” (Ankara and the Central Pontides regions, Tüysüz and Dellaloğlu 1995).

Name: The İkiçam Formation is named after the village of İkiçam (Figure 4.2) which is situated close to a relatively undeformed outcrop of much of the succession. Unlike Tüysüz and Dellaloğlu (1995) these sedimentary rocks are included within the Kalecik Group.

Lithology: The lower parts of the unit comprise thinly bedded (4cm) buff-coloured micritic to muddy limestones with thin grey pelitic schist partings. In the higher levels the succession comprises coarser grained and more texturally immature and compositionally varied terrigenous and volcanoclastic (turbiditic) sandstones and shales, commonly dominated by calcareous grains. These sedimentary rocks are accompanied by rare monchiquite sills, alkalic lava and basaltic pillow lavas. The İkiçam Formation laterally interdigitates with andesitic lava and coarse volcanoclastic conglomerates of the Yaylaçayı Formation. The İkiçam Formation represents a regressive deep-water slope facies with an increasing abundance of immature volcanic, ophiolitic and terrigenous sediment up-sequence together with minor contemporaneous basaltic-andesitic and alkalic magmatism.

Lower and upper boundaries: The lower boundary is a south-vergent thrust wherever observed. The upper boundary is commonly a thrust but the unit is also unconformably overlain by Eocene and younger sedimentary rocks of the Tertiary Çankırı Basin. The unit grades laterally into the Yaylaçayı and Yapraklı Formations.

Thickness and lateral extent: The İkiçam unit exceeds 3km measured thickness in the Korgun area but folding and thrusting give the unit a present thickness of more than 6km in places. Within the studied area the İkiçam Unit covers ~400 km² (Figure 4.3) and crops out as an elongate band within the imbricated suture zone (Kalecik Unit). The outcrop extends between Ankara and Tosya, and possibly further to the east and west. It predominantly crops out toward the northwest margin of the suture zone and at the higher structural levels within the Kalecik Group.

4.2.6 Campanian-Maastrichtian Yaylaçayı Formation: emplaced oceanic volcanic arc

Synonymy: Yaylaçayı Formation (Yoldaş 1982); Köşdağ Formation (Tüysüz 1990); Yaylaçayı Formation (Tüysüz and Dellaloğlu 1995).

Name: The Yaylaçayı Formation was first recognised and named by Yoldaş (1982). It is not known if the name refers to a specific locality. The name means simply “highland stream”. In 1990 a volcanic arc unit was mapped ~10 km south of Tosya and named the Köşdağ Formation by Tüysüz 1990. Then in 1995 Tüysüz mapped the Yaylaçayı Formation further south within the Izmir-Ankara-Erzincan Suture Zone near the Çankırı Basin. However, during this work it was found that there are sufficient similarities between the two units for them to be treated as a single unit.

Lithology: The Yaylaçayı Formation begins with basaltic pillow lavas passing gradually upwards into a succession of andesitic lava and coarse volcanoclastic conglomerate of intermediate composition. Felsic volcanics, intrusives and sulphide-mineralised tuff are present in lesser amounts. Stratigraphically higher levels of the Yaylaçayı Formation comprise volcanoclastic psammite and shale that grade into pale grey, thinly bedded shaly and micritic limestones. At higher structural levels, the Yaylaçayı Formation is metamorphosed to greenschist facies. The dominant lithologies are chloritic pelitic, volcanoclastic and metavolcanic schists and pelites containing epidote, talc, quartz, and albite.

Lower and upper boundaries: The lower boundary of the Yaylaçayı Formation is invariably a south-vergent thrust. The Formation is imbricated with the other units of the Kalecik Group, or younger sedimentary rocks (Figure 4.3). The upper boundary is commonly also a south-vergent thrust. Near the village of Yapraklı (Figure 4.2), the Yaylaçayı Formation is unconformably overlain by the Yapraklı Formation. Near Suseki and Hacıhalil, the Formation is unconformably overlain by mid-upper Tertiary and younger sedimentary rocks related to deposition in the Çankırı Basin.

Thickness and lateral extent: The unit is estimated to be over 4000 m thick. A less deformed outcrop near İskilip is estimated as ~1000 m thick.

The Yaylaçayı Formation is exposed fairly extensively within the Izmir-Ankara-Erzincan suture zone, covering ~500sq.km in the Central Pontides between Çankırı and Tosya. Outcrop of the Yaylaçayı Formation is concentrated in two zones: one at a lower structural level crops out along the south-eastern edge of the suture zone where it borders the Çankırı Basin; The other occurs at a higher structural level in the suture zone and crops out along its northern and western edges.

4.2.7 Campanian-Maastrichtian Yapraklı Formation: arc-derived sedimentary rocks

Synonymy: Yapraklı Formation (Birgili et al. 1975); Yapraklı Formation (Tüysüz and Dellaloğlu 1995).

Name: The Yapraklı Formation takes its name from the village of Yapraklı (Figure 4.2), where good exposure is easily accessible by road.

Lithology: The stratigraphically lower part the Yapraklı Formation consists of grey shales. These pass upwards into rudist-bearing, coarse-grained calcarenites, interbedded with volcanoclastic shales, thickly bedded glauconite-rich volcanoclastic sandstones, clast-supported conglomerates and coarse-grained debris-flow deposits. Abundant volcanic clasts are moderately rounded and andesitic in composition; the matrix is rich in feldspar and calcareous shell fragments.

Lower and upper boundaries: The Yapraklı Formation lies unconformably upon the Yaylaçayı Formation and is unconformably overlain by dacitic lava and tuff. The upper contact of the Yapraklı Formation is commonly thrust-faulted, being tectonically overlain by other units of the Kalecik Group.

Thickness and lateral extent: The section at Yapraklı is estimated to be ~500m thick before folding and thrusting. The main outcrop of the Yapraklı

Formation is located 1km north of Yapraklı village and covers an area of ~75sq.km (Figure 4.3).

4.2.8 Mid Eocene (Lutetian) Kadıkızı Formation: post-collisional neritic limestones and deltaic clastic sedimentary rocks

Synonymy: This unit has not been distinguished by previous workers. It may be correlative with parts of the Upper Cretaceous-Lower Tertiary Gökceğaç Unit of the Kastamonu-Boyabat basin to the north.

Name: The unit is named after the village of Kadıkızı where representative sections, with exposed contact relations, are accessible by road.

Lithology: Buff coloured, Nummulite-bearing calcarenites near the base pass upwards into less Nummulite-rich marls, shales and calcarenites. Lenticular bodies of lithoclastic polymict conglomerate and poorly sorted sandstone beds with plant debris are present in increasing abundance at higher stratigraphic levels.

Lower and upper boundaries: The Kadıkızı Formation lies unconformably above the Kirazbaşı Mélange in the area north of Tosya. The upper boundary of the Kadıkızı formation is commonly a south-vergent thrust fault which places various older units structurally above it. In the Kadıkızı area the unit is unconformably overlain by red-beds and alluvium of Plio-Quaternary to recent age.

Thickness and lateral extent: Based on mapping in the Kadıkızı area the Kadıkızı Formation is estimated as ~300m thick (with no structural repetition). Within the area studied here the outcrop of the Kadıkızı Formation is limited to the area near Kadıkızı village where it covers ~ 3sq.km.

4.3 Summary of tectonostratigraphy of the Central Pontides

Previously there has been no formal and comprehensive attempt to clarify the stratigraphy of the Upper Cretaceous rocks within the Neotethyan suture zone in the Central Pontides. As a basis for further discussion of the Upper Cretaceous-Lower

Tertiary rocks of the Izmir-Ankara-Erzincan Suture Zone in the Central Pontides this chapter has outlined a stratigraphic scheme that identifies six individual formations of Late Cretaceous-Early Tertiary age within the suture zone. In addition, a new formation of Mid Eocene age is proposed here: the Kadıkızı Formation. As it is the oldest unit unconformably overlying the ophiolitic *mélange* (Kirazbaşı *Mélange*), this unit is critical to the stratigraphic development of the suture zone. By contrast, a detailed consideration of the complex stratigraphy of the Tertiary sedimentary basins in the adjacent areas to the north and south (Çankırı and Kastamonu-Boyabat basins) is outside the scope of the project.

The lithostratigraphy presented here provides a meaningful basis for the analysis and interpretation of the suture zone presented in the following chapters of the thesis.

5 The Izmir-Ankara-Erzincan suture zone in the Central Pontides

5.1 Introduction

Six main tectonostratigraphic units of Late Cretaceous age were identified in the Central Pontides (Chapter 4). Each of these units is bounded by south-vergent thrusts and is unconformably overlain by Tertiary sedimentary rocks (Figures 5.1 to 5.3). In addition, unconformable mid Eocene sedimentary rocks (Lutetian; 48.6-40.4 Ma; Gradstein et al. 2004) provide a minimum age for north-vergent deformation in the region. This chapter presents new data from each of the Upper Cretaceous units and the oldest overlying unit (Eocene) and gives an interpretation of each.

5.2 The Eskiköy Formation: Trench-margin collision facies

The Eskiköy Formation (~150 m thick) crops out north of Tosya (Figure 5.4) and the best exposure of its contacts is found south of Eskiköy village (gr: F32, 130660). The unit rests with angular unconformity on a thin (~3 m) unit of pisolitic bauxite that caps the schistose metamorphic basement of the Pontides (Kargı Complex; Ustaömer and Robertson 1997) (Figure 5.5). The underlying bauxite is a dense, hard, metallic red, mica schist. Towards the top of the formation the sedimentary rocks are thrust-imbricated with ophiolitic *mélange* (Kirazbaşı *Mélange*; see section 5.4). The Eskiköy Formation is also exposed as thin (~40 m) thrust slices within outcrops of the *mélange* (e.g. at Ödemiş, near Ilgaz gr: F31, 459354).

5.2.1 Structure of the Eskiköy Formation

The Eskiköy Formation is tightly to isoclinally folded and cut by north- and south- dipping thrust faults (30-40°) and sub-vertical strike-slip shear-zones (Figure 5.5). Sedimentary structures (e.g. sharp bases and graded tops) and *Thalassinoides* sp. bioturbation at Eskiköy indicate that the unit is mostly the right-way-up but locally overturned and generally youngs southward. A pervasive north-vergent shear fabric is exhibited by argillaceous rocks within the unit. Small (<1 m wavelength)

north-vergent recumbent folds and duplex structures were also observed. Sandstone and limestone beds are commonly boudinaged. North-vergent shear zones commonly dip at $\sim 40^\circ\text{S}/040$ but various orientations were observed. The north-vergent structures are cut by the north-dipping thrusts and sub-vertical strike-slip faults. The north-vergent shear fabric is also folded by south-vergent folds (Figure 5.6). South-vergent folds are asymmetrical with longer limbs dipping northward $\sim 45^\circ$ and shorter limbs that are subvertical or overturned and dip steeply northwards (Figure 5.5-5.7). Axial planes dip to the northwest. Structural data from the unit are shown in Figures 5.8 and 5.9. The strike of bedding planes is generally between 040° - 060° . Sandstones, cherts and limestones are folded into parallel isoclines. Pelite and shale beds are folded into tight chevron folds (Figure 5.7). An open east-verging fold was observed locally. Sub-vertical strike-slip faults cut all of the structures mentioned above. Strike-slip faults within the unit are sub-vertical, strike 025° to 040° (Figures 5.8 and 5.9) and exhibit sinistral slickensides with slickensides plunging up to 45° towards the northeast and southwest.


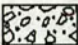

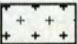
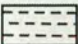
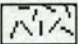
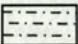
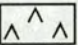


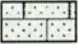
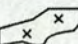
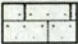
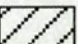
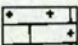
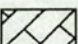
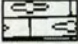
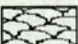
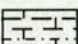
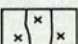
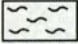
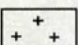

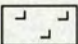
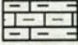
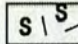
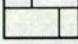
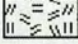
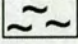
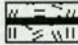
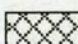
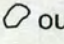

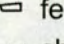

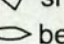
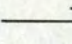
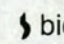
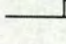
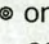
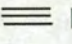
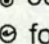
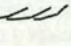


	schist		
	conglomerate		mudstone
	felsite/tuff/rhyolite		shale
	andesite		siltstone
	anhydrite		sandstone
	basalt		calcareous sandstone
	isolated diabase dyke		calcareenaceous sandstone
	schist or gneiss		calcarenite
	marble		nummulitic limestone
	pillow-lava		shaly/silty limestone
	diabase sheeted dykes		marl
	plagiogranite		chert
	cumulates (eg. dunite, pyroxenite)		pelagic limestone
	serpentinized harzburgite		neritic limestone
	isotropic gabbro		scaly clay
	layered gabbro		bauxite
	outsize clasts (pebbles/boulders)		younging direction/way-up
	feldspar grains		unconformity
	shell fragments		shear-zone
	benthic forams/nummulites		thrust fault
	bioturbation		planar lamination
	oncid		cross-bedding
	ooid		
	fossil (broken)		

Figure 5.1. Key to symbols used in maps, logs and cross sections unless indicated otherwise.

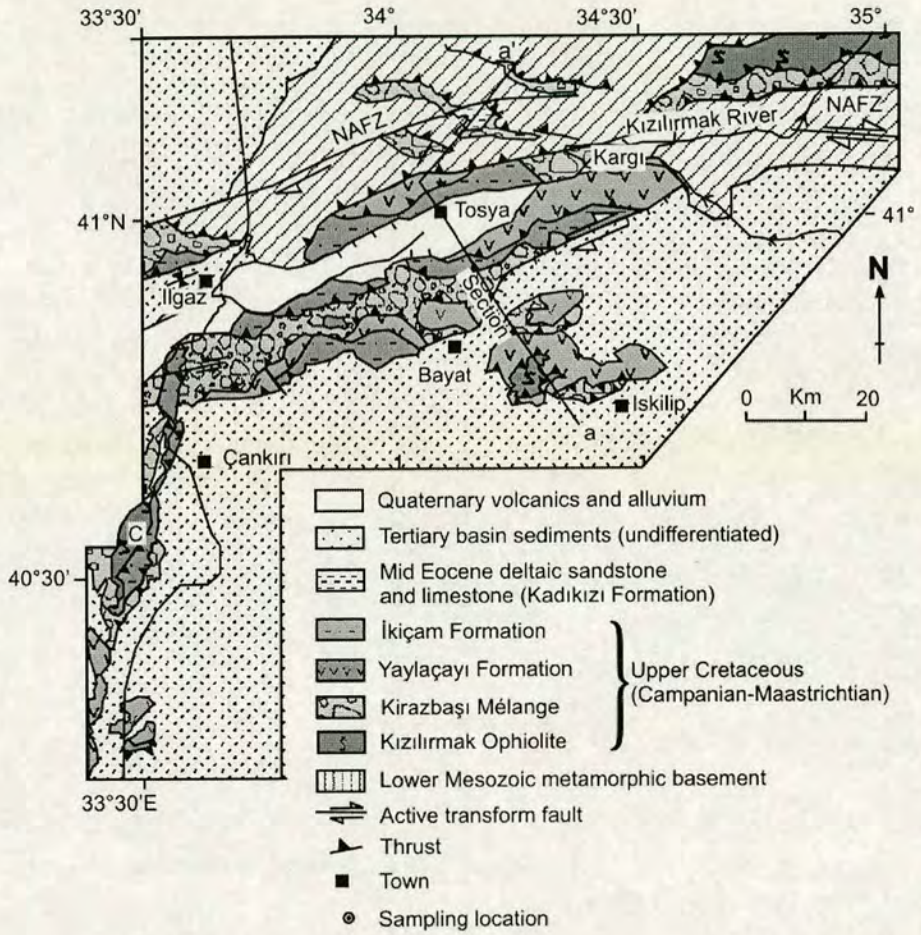


Figure 5.2. Geological map of the Izmir-Ankara-Erzincan suture zone in the Central Pontides. Shown is line of section (Figure 5.3).

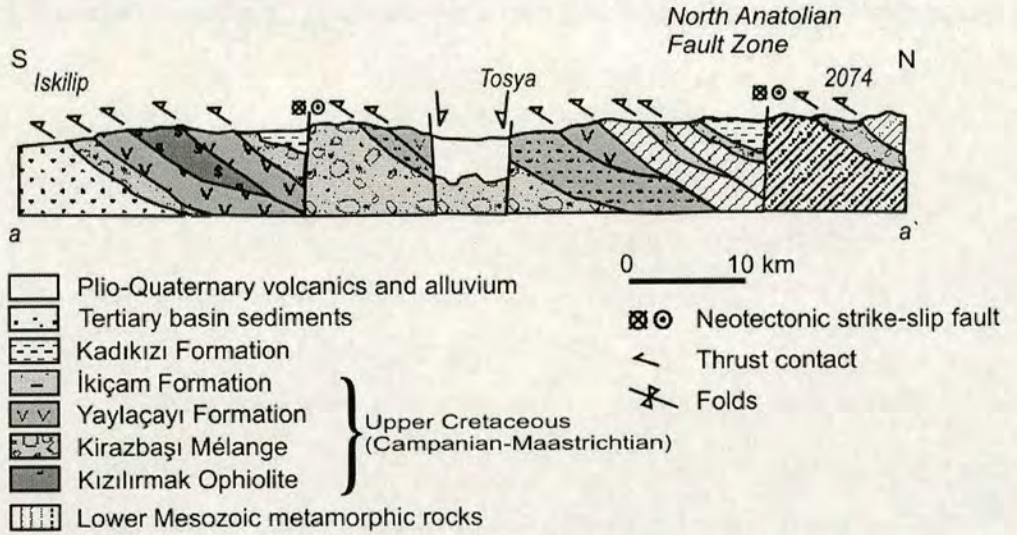


Figure 5.3. Simplified cross-section of the Izmir-Ankara-Erzincan suture zone in the Central Pontides.

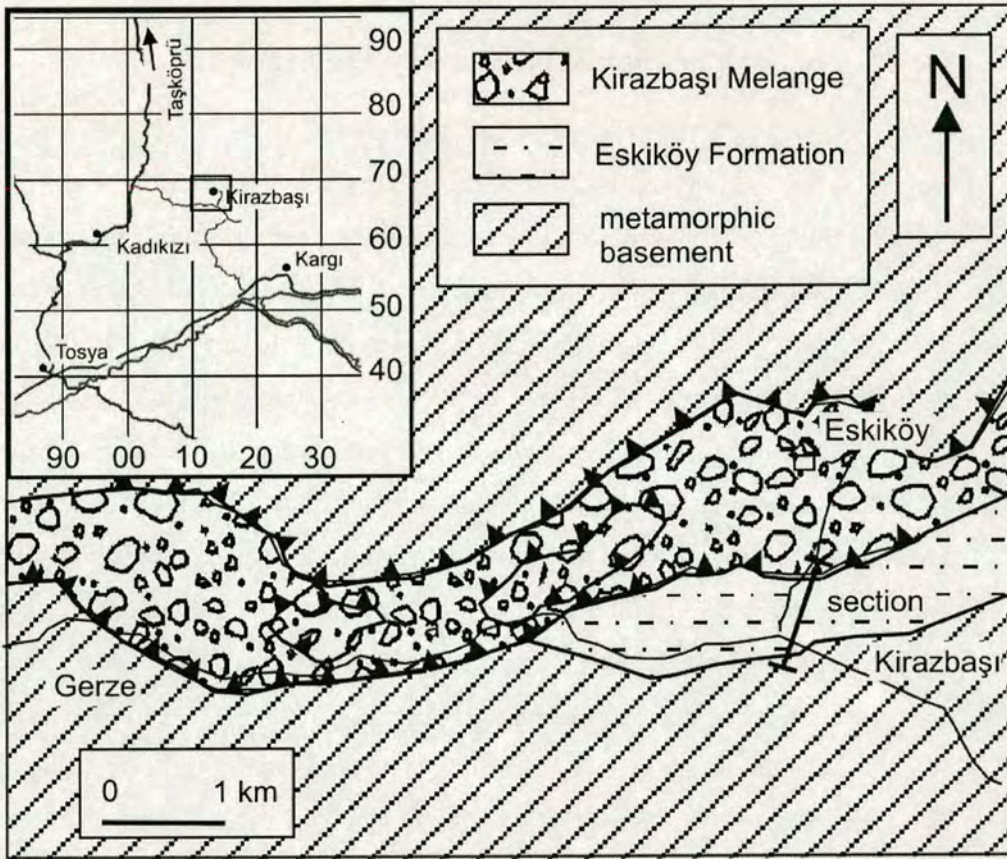


Figure 5.4. Geological map showing outcrop of the Eskiköy Formation. location of section shown (see Figure 5.5).

The pervasive north-vergent shear fabric, faults and small-scale folds within the unit are refolded by south-vergent folds and cut by north-dipping thrust faults that indicate top-to-the-south deformation. South-vergent deformational structures appear more pronounced at the northern end of the outcrop, at Eskiköy. These later top-to-the-south structures are in turn cut by the strike-slip shear zones. The Eskiköy Formation, therefore, records the relative timing of at least three distinct deformational events. The first deformation gave rise to a pervasive top-to-the-north fabric. These structures were then refolded by top-to-the-south deformation. Finally, there was a left-lateral strike-slip event probably related to the Neogene North Anatolian Fault Zone (Dhont et al. 1998).

5.2.2 Sedimentary facies of the Eskiköy Formation

The base of the Eskiköy Formation is marked by thick-bedded (<50 cm), grey, massive microcrystalline limestone, ~10 m thick (Figure 5.10). The limestone contains only planktonic foraminifera (e.g. *Globotruncana* sp.) of Campanian age (Tüysüz et al. 1988). The limestone passes upwards into sheared and isoclinally folded sandstones with shaly partings, ~150m thick, with rare lenses of matrix-supported conglomerate (<2 m). The sandstones are medium-bedded (<20 cm) and exhibit rare sole marks and *Thalassinoides* bioturbation (these features indicate that the sedimentary rocks locally young southwards, Figure 5.5). Individual sandstone beds have massive bases and fine upwards into laminated siltstone and/or mudstone. In addition, some beds exhibit parallel-laminated and/or cross laminated sand. Interbedded conglomerates have erosive bases and contain well-rounded clasts.

In thin section, the sandstones are seen to contain grains of polycrystalline quartz, schist and detrital white mica, indicating a metamorphic source (Figure 5.11). The sandstones also contain abundant clasts composed of recrystallised chert, mafic lava and serpentinite. The succession passes upwards into thin-bedded red shale, pelite and radiolarian chert, tectonically imbricated with sheared serpentinite and gabbro of the Kirazbaşı Mélange. The conglomerate contains pebbles (<5 cm) of paraquartzite and schist in addition to clasts of red radiolarian chert and basalt.

It is widely accepted that the Triassic schists underlying the Eskiköy Formation (Kunduz Unit) formed part of the Eurasian margin during Cretaceous time (Şengör and Yılmaz 1981; Tüyzüz 1990, 1999; Ustaömer and Robertson 1994, 1997; Yılmaz et al. 1997). The limestone unconformably overlying the bauxite contains only planktonic fauna (*Globotruncana fornicata* and *Globotruncana lapparenti*; Tüysüz 1990). The water depth inferred from their morphology is 'deep' i.e. thermocline or sub-thermocline (>700m; Stewart and Pearson 2000). The base of the Eskiköy Formation is, therefore, interpreted as a pelagic limestone succession representing open-marine deep-water carbonate deposition. The angular

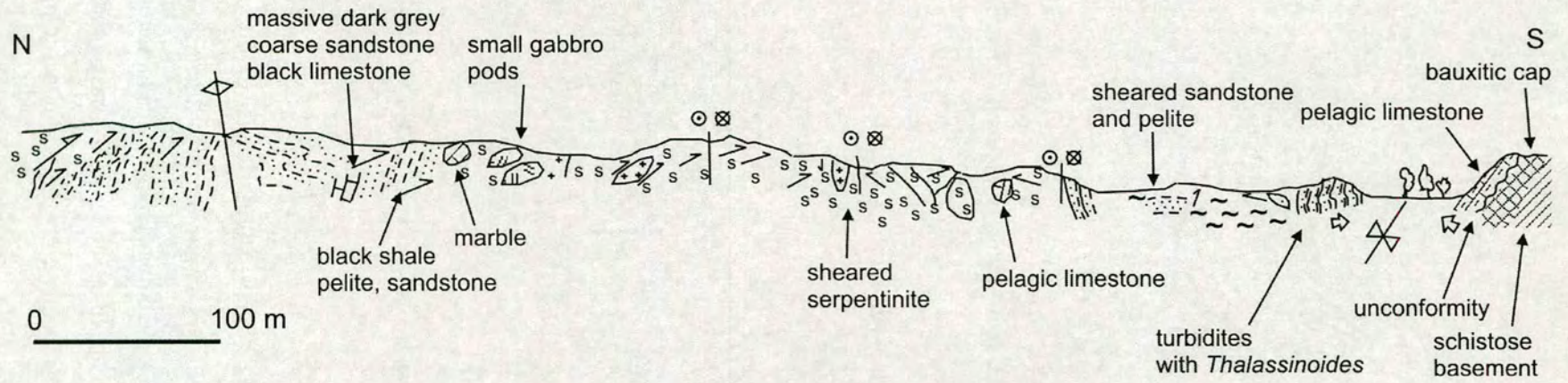


Figure 5.5. Road section at Eskiköy (see Figure 5.4 for location). For key to symbols see Figure 5.1.

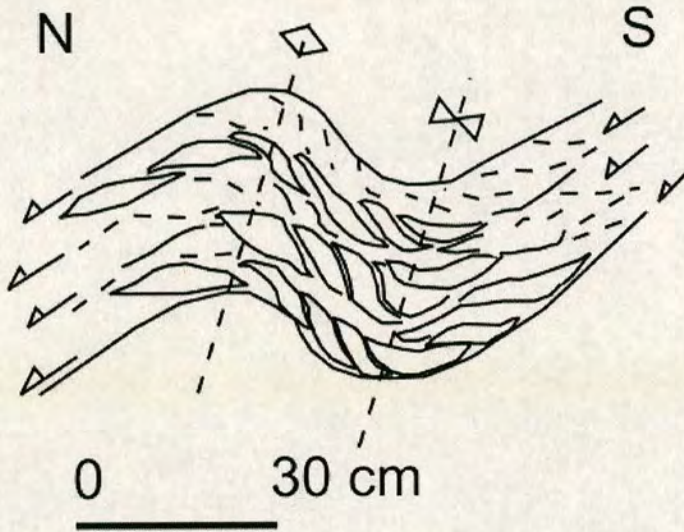


Figure 5.6. Field sketch showing top-to-the-north shear fabric folded by a south-vergent fold pair.

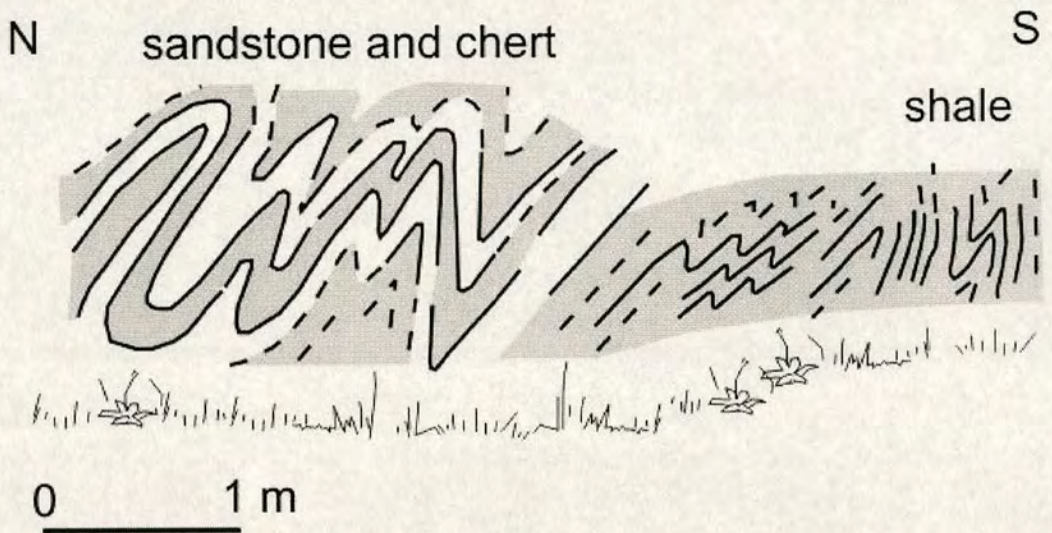


Figure 5.7. Field sketch showing tight to isoclinal folds in sandstone and chert, shale and fine-grained sandstone.

unconformity at the base of the Eskiköy Formation is interpreted to record subsidence of the Eurasian margin to form a foredeep during Campanian time (83.5-70.6 Ma), prior to tectonic emplacement of the allochthonous oceanic units from the south. The bauxitic 'cap' to the underlying Triassic schist indicates that the Pontide (Eurasian) margin was locally emergent and undergoing

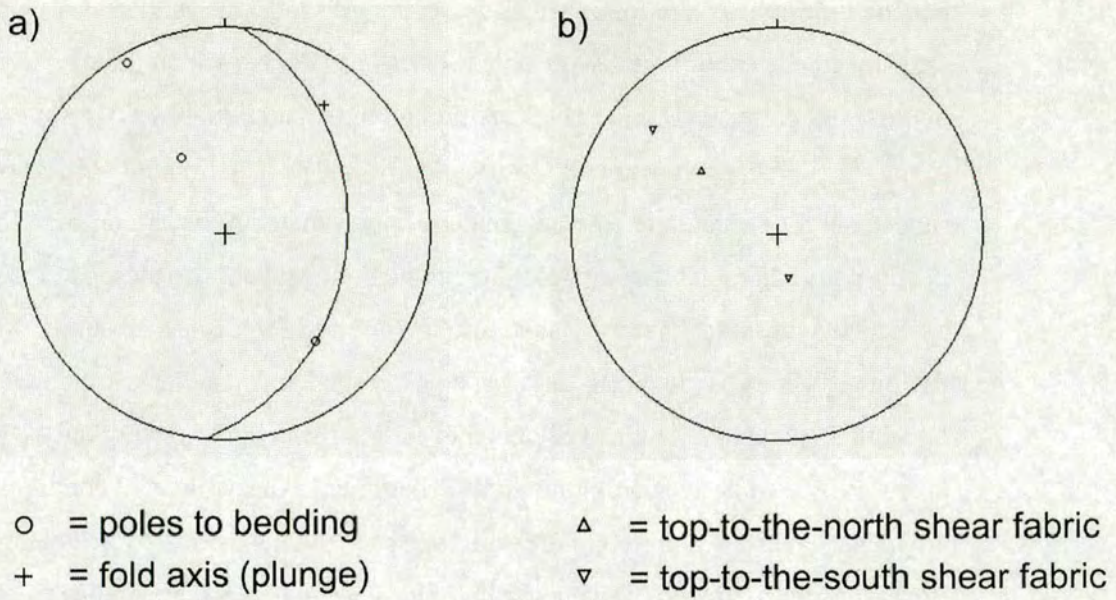


Figure 5.8. Lower hemisphere equal-area projection (Lambert/Schmidt) of structural data from the Eskiköy Formation. Great circle = measured fold axis.

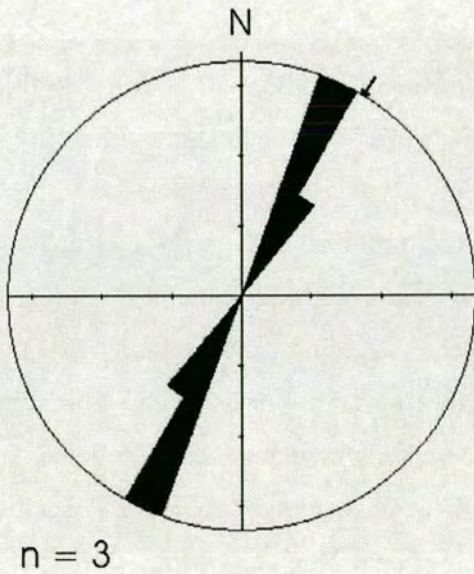


Figure 5.9. Rose diagram showing strike-slip fault plane orientations within the Eskiköy Formation.

tropical weathering before the transition to open-marine conditions during Campanian time. The lack of any basal conglomerate suggests an abrupt transition from terrestrial to open-marine conditions. Subsidence and initial deposition of

pelagic limestones were followed by deposition of sandstones and shales. Some sandstone beds exhibit the five 'Bouma' divisions (Ta-Te) which indicate deposition by turbidity currents (Bouma 1962). Although most individual beds do not exhibit all of the five divisions they are all observable in some beds within the succession. The sandstones also contain terrigenous material (muscovite and metamorphic lithoclasts) in addition to lithoclasts of an ophiolitic association and are therefore interpreted as terrigenous turbidites that were shed into the inferred foredeep. The source was the Pontide basement to the north that was being eroded and also the advancing Tethyan allochthonous units. Paraquartzite pebbles within the conglomerates were presumably also derived from the Pontide basement. The associated conglomerates are mainly matrix supported, indicating transport and deposition by sediment-gravity flows (or 'debris-flows'; Tucker 1982). Their well-rounded shape indicates abrasion of the terrigenous clasts in fluvial and/or beach environments before being redeposited into a deeper water setting by debris-flows.

5.2.3 Summary

The Eskiköy Formation, of Campanian age (83.5-70.6 Ma), records an abrupt change from tropical weathering of an emergent continental margin area to open-marine pelagic carbonate deposition, initially with little or no clastic input. Carbonate deposition was followed by deposition of turbidites derived from terrigenous and ophiolitic sources. Taking account of its tectono-stratigraphic position (i.e. unconformably above Eurasian basement and tectonically overlain by ophiolitic *mélange*) the Eskiköy Formation provides a record of subsidence of the Eurasian margin prior to the emplacement of accretionary *mélange*. It is likely that the subsidence of the Eurasian margin, and the deposition of the Eskiköy Formation were a direct result of the emplacement of ophiolitic units during the initial stages of the collision of oceanic and continental margin units. Therefore, the Eskiköy Formation is interpreted as a trench-margin collision facies (Robertson 1994). The Eskiköy Formation constrains the emplacement of the ophiolitic *mélange* to no older than Campanian (83.5-70.6 Ma).

Eskiköy Formation

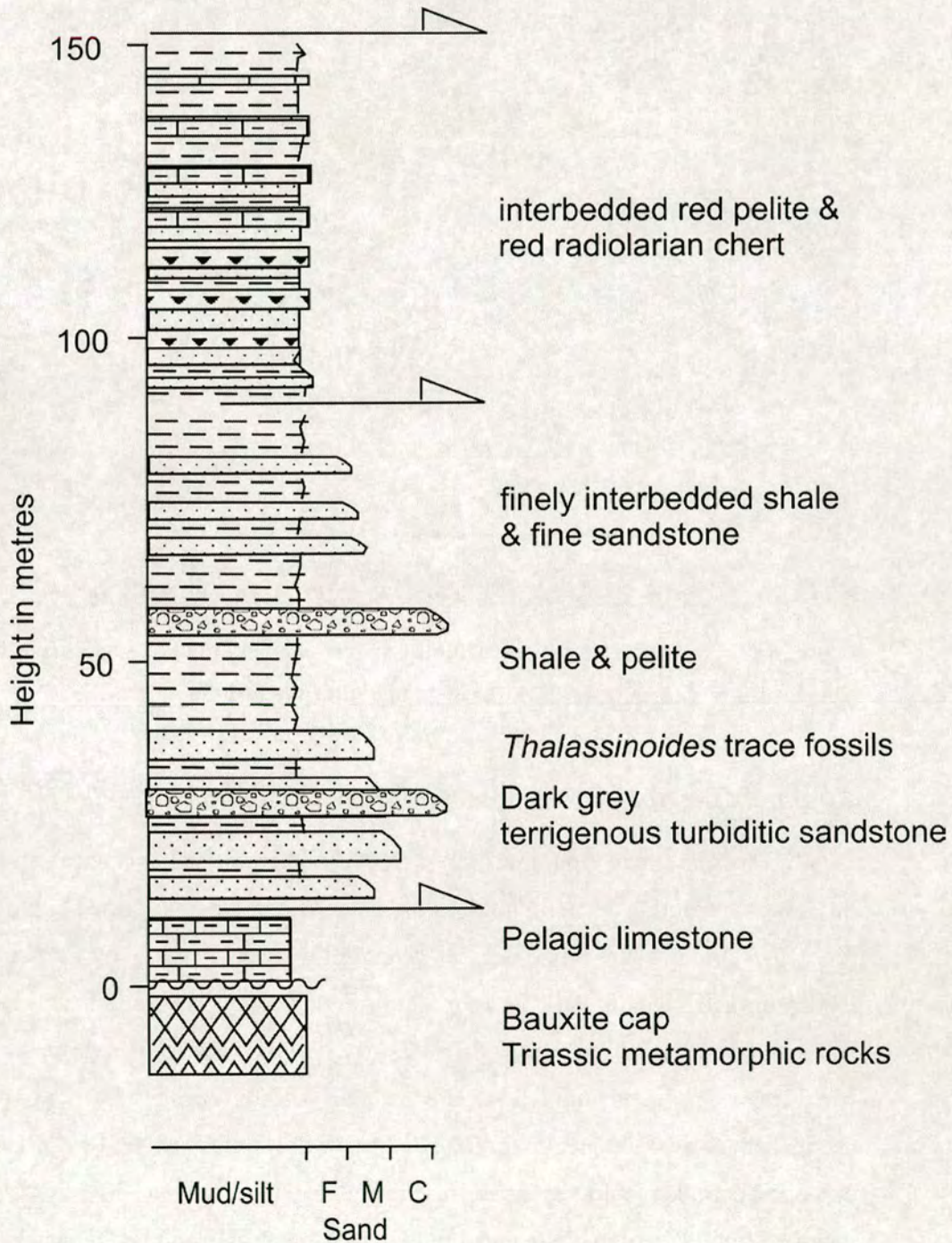


Figure 5.10. Log of the Eskiköy Formation. For key to symbols see Figure 5.1.

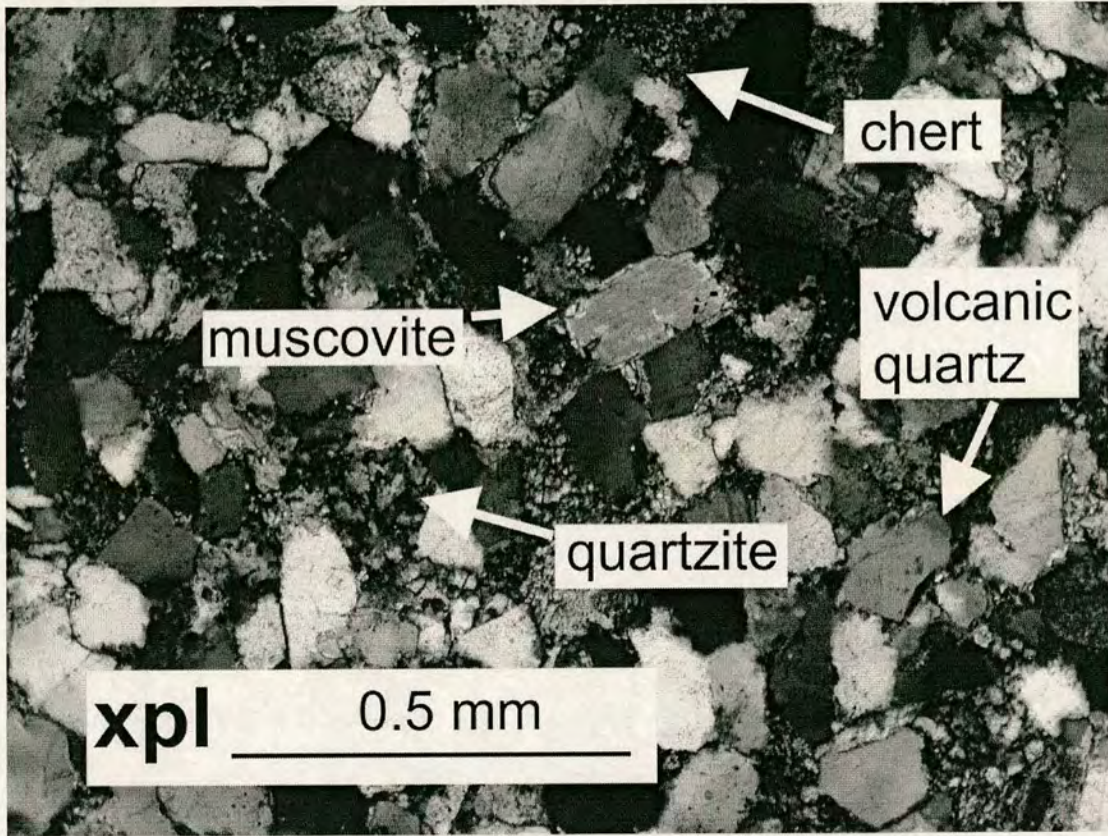


Figure 5.11. Photomicrograph of turbiditic sandstone from the Eskiköy Formation. Note grains of quartzite and muscovite of metamorphic origin.

5.3 Emplaced ophiolite slices: Kızılırmak Ophiolite

The Kızılırmak Ophiolite (Tüysüz 1990), ~3.5 km thick, occurs at several different structural levels within the suture zone. Outcrops of deformed ophiolitic rocks, 2-5 km thick, are found near Bayat and Eldivan, and also along the banks of the Kızılırmak River, at Pelitcik, near Kargı (Figure 5.12). The microfossils *Globotruncana lapparenti* BROTZEN, *G. tricarinata* QUERAU, *G. fornicata* PLUMMER are found within associated pelagic limestones and indicate a Campanian-Maastrichtian age for the Kızılırmak Ophiolite (Tüysüz 1990). The ophiolitic complex includes serpentinitised harzburgitic tectonite (~50% by area of outcrop), cumulate pyroxenite and dunite (~10%), isotropic and layered gabbro (~40%).

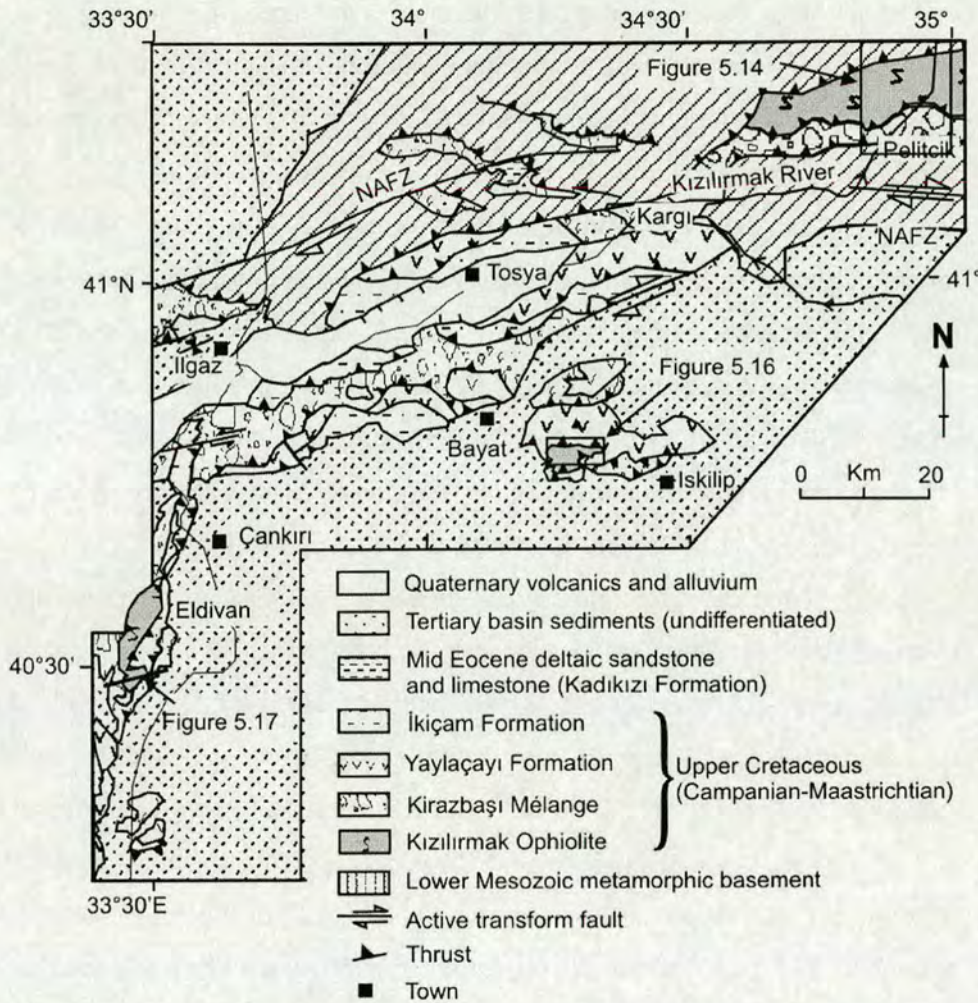


Figure 5.12. Geological map to show outcrop of the Kızılırmak Ophiolite. Locations of Figures 5.14 to 5.17 are shown.

5.3.1 Structure of the Kızılırmak Ophiolite

In the Central Pontides lithologies of ophiolitic association occur as tectonic slices and large blocks (<1 km) that exhibit primary structures e.g. small pods and lenses of chromite in harzburgite, cumulate mineral layering in gabbro; chilled margins of diabase dykes. The ophiolitic pseudostratigraphy is commonly disrupted by north- and south-dipping serpentinitic and mineralized shear zones (Figures 5.15 and 5.16). A relatively intact section crops out at Eldivan (Figure 5.17). Isolated dykes are uncommon in the Kızılırmak Ophiolite. No metamorphic sole is seen. At outcrop scale, the unit exhibits a pervasive north-vergent (south-dipping) shear fabric. Strike-slip faults and thrust faults dipping north and south cut the unit. To the

east of the Tosya Basin (Figure 5.12) the unit is tectonically juxtaposed by north-dipping (south-vergent) thrusts against metamorphic basement units of the Pontides (Figure 5.15). The unit is bounded above and below by south-vergent serpentinitic shear zones, up to ~100 m wide.

The harzburgite exhibits a foliation formed by the alignment of bastite (altered orthopyroxene) and alignment of aggregates of chromite grains. The S1 foliation in the harzburgite, measured at Pelitcik, dips $70^{\circ}\text{W}/175^{\circ}$ (Figure 5.18a). Measured strike directions of mineral layers in gabbro range between WNW-ESE and NNE-SSW, and dip steeply ($>40^{\circ}$) southwards at Pelitcik. At Eldivan, the layered gabbro dips to the north. Chilled margins of diabase sheeted dykes are steeply inclined to sub-vertical and strike E-W to NE-SW (Figure 5.18a).

The harzburgitic tectonite is commonly serpentinitised and pervasively sheared. The shear fabric has largely destroyed the primary foliation (described above). Many different orientations of serpentinitic shear fabric and a wide range of local kinematic directions were observed in the serpentinitised peridotite. These fabrics are probably the result of multiple deformations. Top-to-the-northeast thrusts and small (<50 cm) serpentinitic shear zones cut the S1 foliation in harzburgitic tectonite. An associated north-vergent shear fabric (S2) dips gently southward and commonly has destroyed the S1 foliation. Orientation and kinematic data for thrust faults in the Kızılırmak Ophiolite are shown in Figure 5.18b. Mafic/felsic mineral layers in gabbro are folded by open horizontal folds (wavelength ~2 m), with axes inclined $\sim 30^{\circ}$ towards the northeast and are cut by south-dipping shear zones that exhibit a top-to-the-north sense of motion. The shears form small-scale duplex structures in the layered gabbro (e.g. sigmoidal horses are <1 m long). Top-to-the-north thrust faults cut the layering and the fold axes. Chilled margins of diabase sheeted dykes are also cut by south-dipping thrusts and shear zones.

Top-to-the-north thrust faults and shear fabrics are commonly cut by north-dipping thrust faults with a top-to-the-south sense of motion. Thrust fault orientation and kinematic data are shown in Figure 5.18b. The Kızılırmak Ophiolite exhibits reidal shears dipping to the north and to the south.

Strike-slip shear zones and normal faults were observed cutting all of the structures mentioned above. Strike-slip faults cutting the Kızılırmak Ophiolite

exhibit dextral as well as sinistral slickensides. The orientations of dextral and sinistral strike-slip faults is shown in Figure 5.20. Kinematic data for sinistral strike-slip faults are shown in Figure 5.18c. The mean orientation of dextral strike-slip faults in the Kızılırmak Ophiolite is $\sim 90^\circ$ to the sinistral strike-slip faults. No cross-cutting relationships of the dextral faults were observed.

The orientations of primary structures (e.g. mineral layers in gabbro, sheeted dyke contacts) within the Kızılırmak Ophiolite show reasonable coherence. The foliation in harzburgite is interpreted as a mantle flow fabric. Its present sub-vertical orientation could be the primary mantle flow direction but more probably is the result of rotation during emplacement or later deformation (for example as seen in Oman (Girardeau et al. 2002)). With the exception of outcrops near Eldivan layering in the gabbro is orientated at a high angle relative to the foliation measured in the harzburgite at Pelitcik. The original orientation of the layering in the ophiolitic gabbros is not known. Therefore, the layered gabbro does not record how much rotation has occurred or how coherent the structure of the ophiolite is. The layers in the gabbro are orientated similarly to the sheeted dyke contacts (ie. steep to sub-vertical and striking NE-SW). If it is assumed that the ophiolite forms a coherent structural unit then the layers could represent crystallisation on the steep walls of a magma chamber. Tectonic rotation is more likely as layered gabbro does not usually form at steep angles (Dewey and Kidd 1977). The sub-vertical, to inclined, orientation of the sheeted dyke contacts indicates that the maximum final amount of tilting of the ophiolite is $\sim 46^\circ$ towards the southeast. If horizontal rotations of the ophiolite are assumed to have been small the strike of the sheeted dyke contacts suggest that the ophiolite was formed by roughly NNW-SSE spreading, and is indicative of a regional extensional palaeostress in roughly this orientation. The dyke contacts are roughly parallel to the strike of the suture zone and the current Eurasia-Anatolia plate boundary (the North Anatolian Fault Zone). Tectonic rotation to the present orientation is possible.

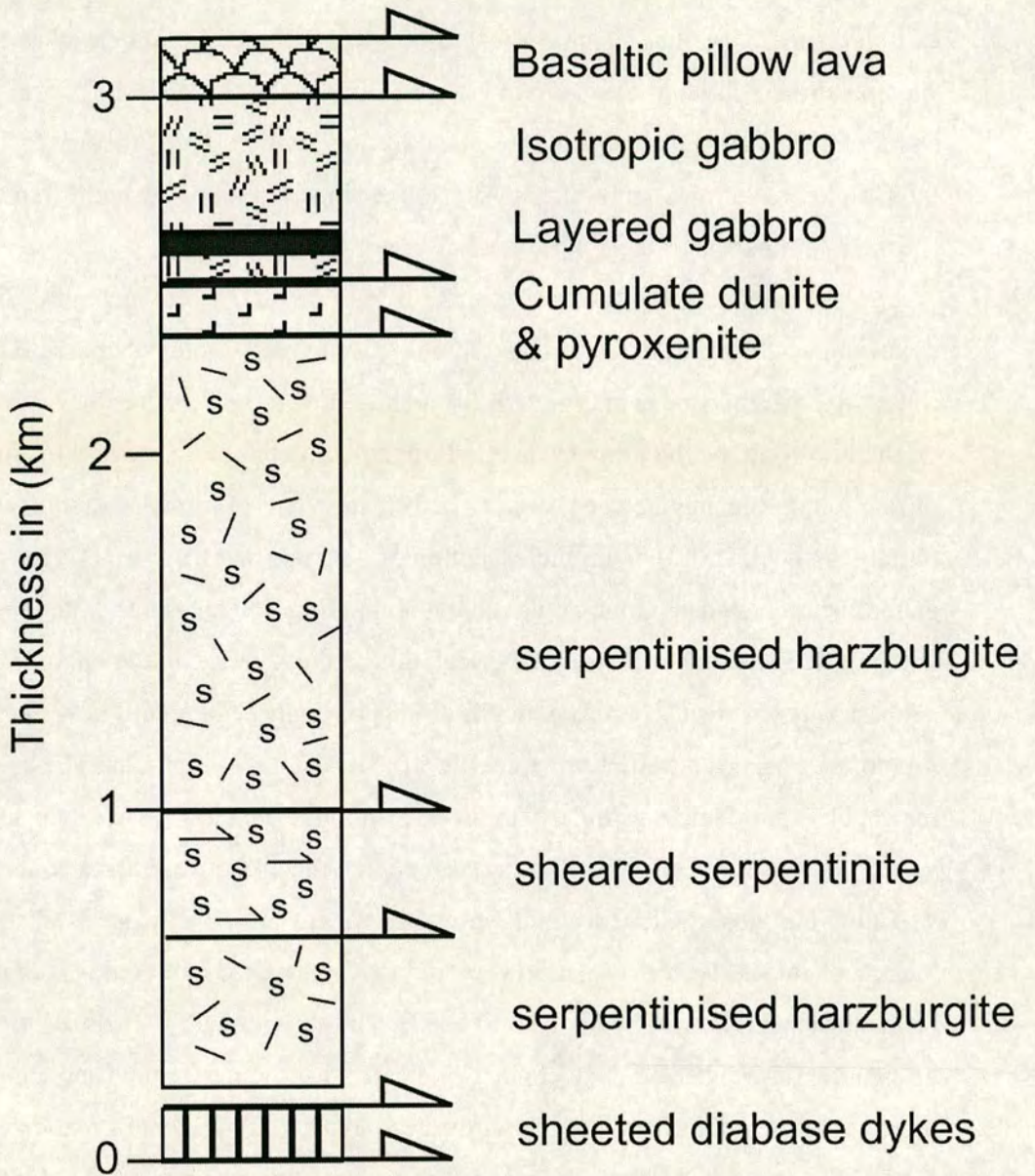


Figure 5.13. Log of the ophiolitic Kızılırmak Ophiolite exposed near Pelitcik (gr: F33, 569666). For key to symbols see 5.1.

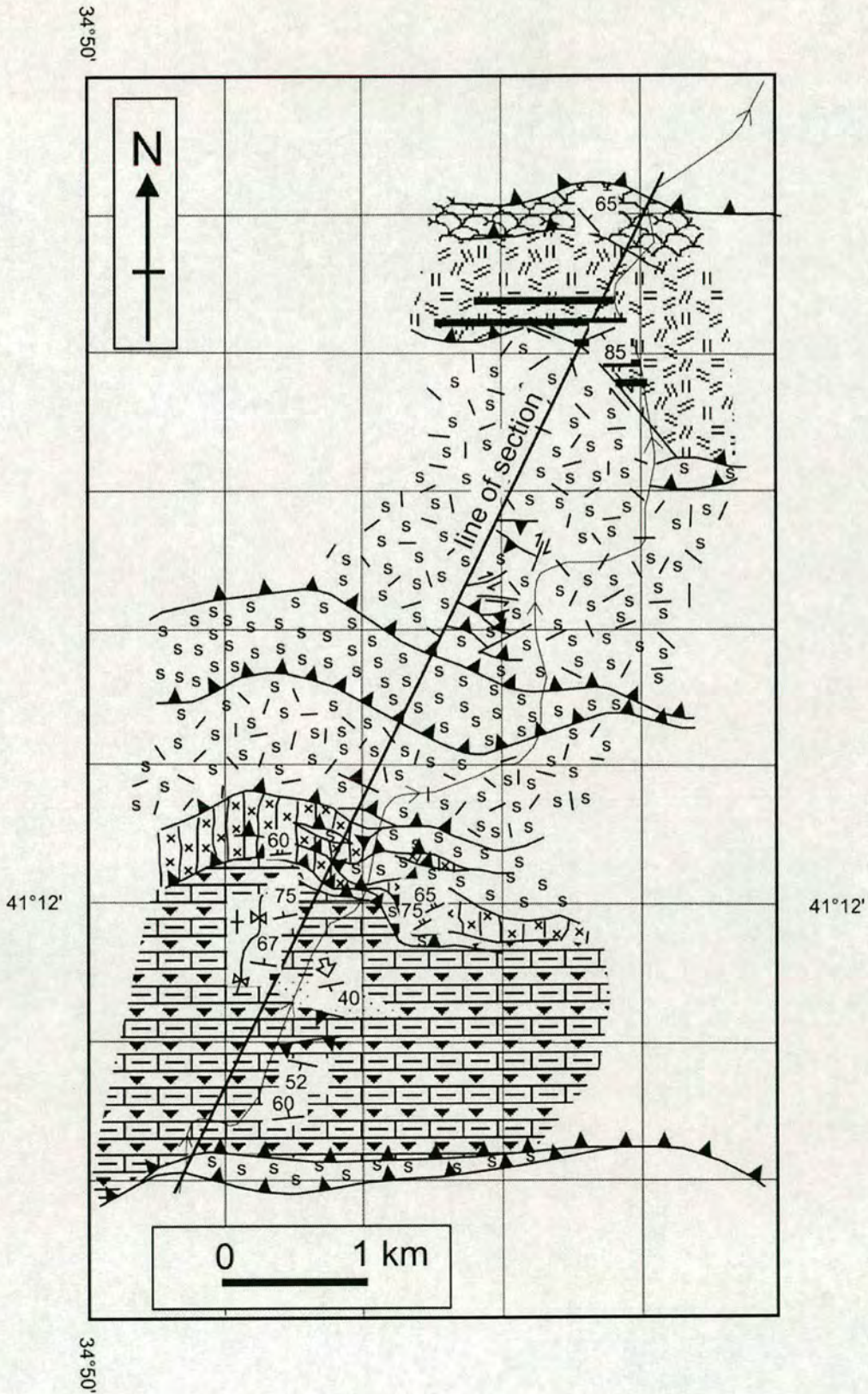


Figure 5.14. Geological map of the Pelitcik area. For key to symbols see Figure 5.1.

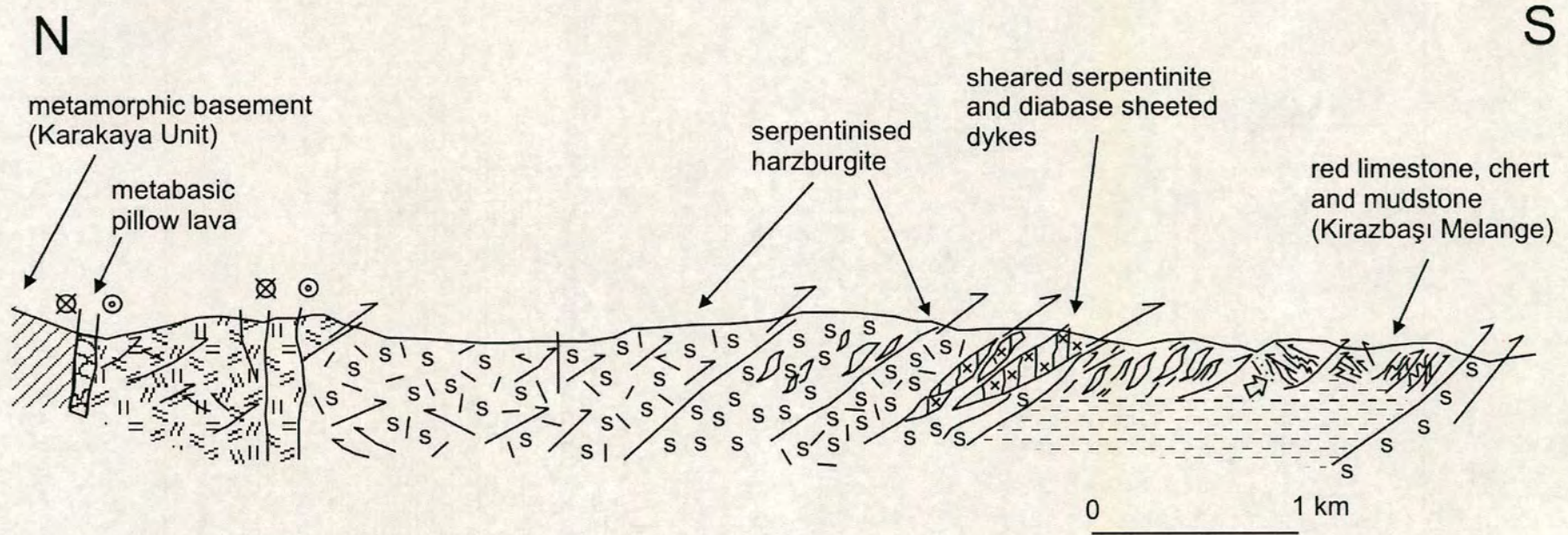


Figure 5.15. Cross-section at Pelitcik (see Figures 5.12 and 5.14). For key to symbols see Figure 5.1.

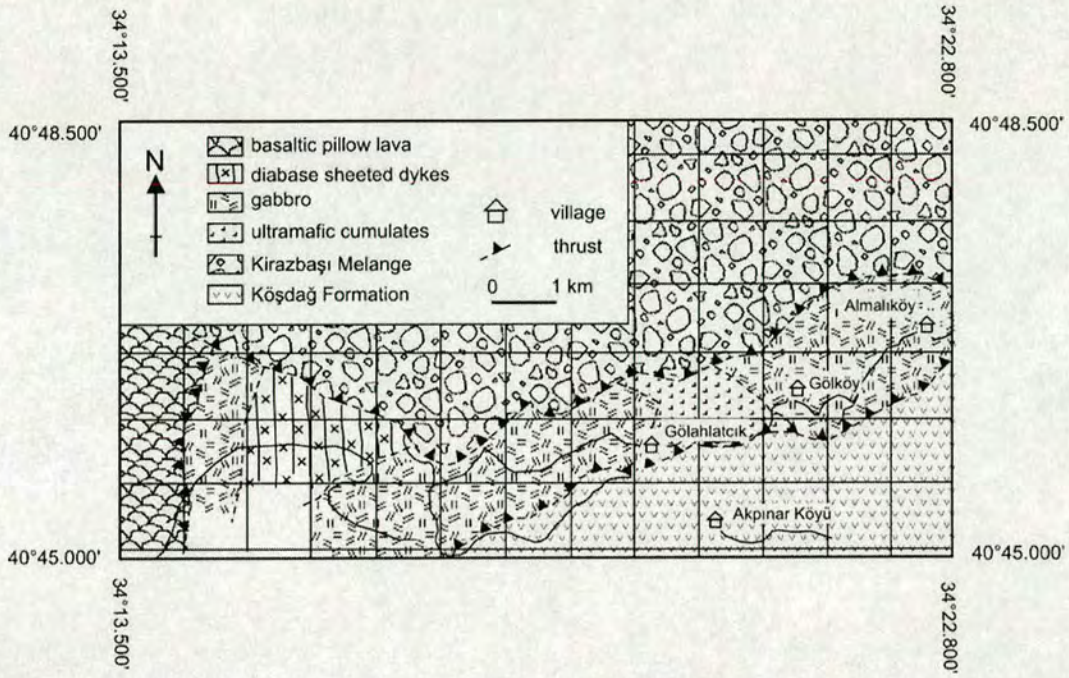


Figure 5.16. Geological map of the Kızılırmak Ophiolite East of Bayat.

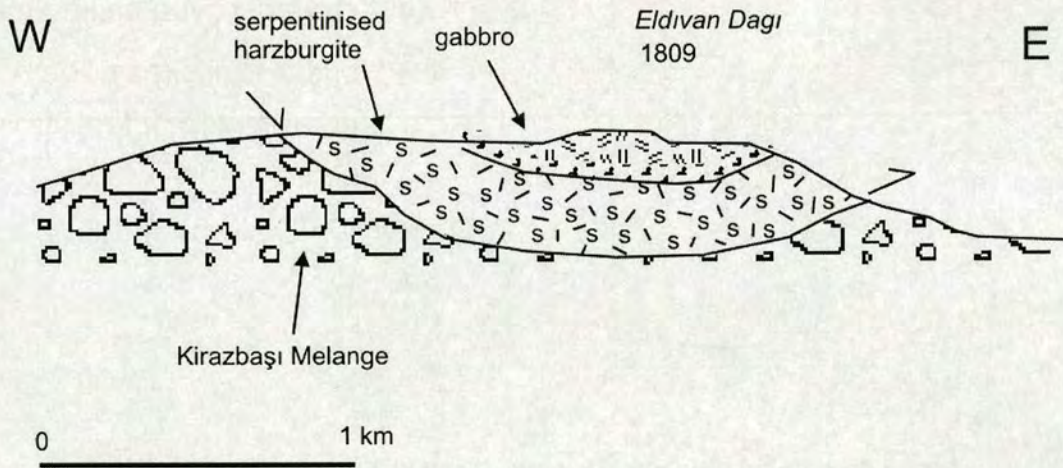
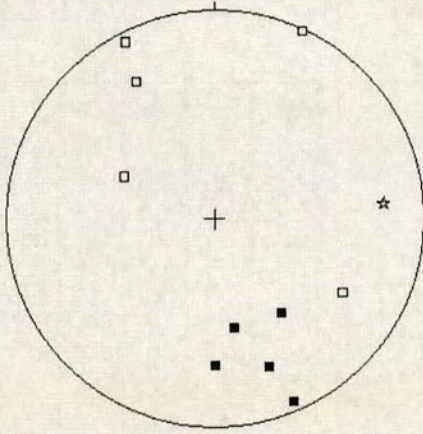
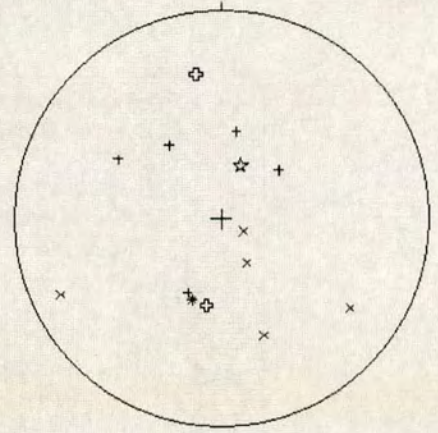


Figure 5.17. Cross-section of Eldivan Dağı (see Figure 5.12 for location).

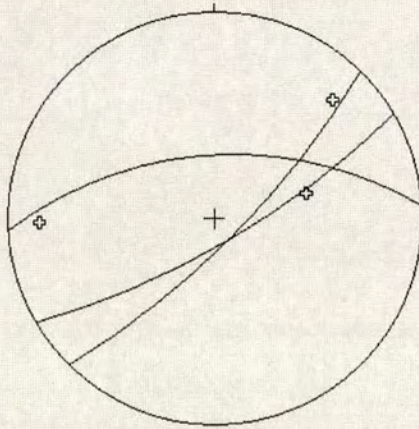
a) Ophiolite genesis



b) thrusts



c) sinistral strike-slip faults



- ☆ foliation in harzburgite
- layers in gabbro
- sheeted dyke chilled margins
- ⊕ sinistral slickensides
- + poles to top-N thrusts
- × poles to top-S thrusts
- ☆ top-S slickensides
- ⊕ top-N slickensides

Figure 5.18. Equal-area plots (Schmidt/Lambert) showing structural data from the Kızılırmak Ophiolite.

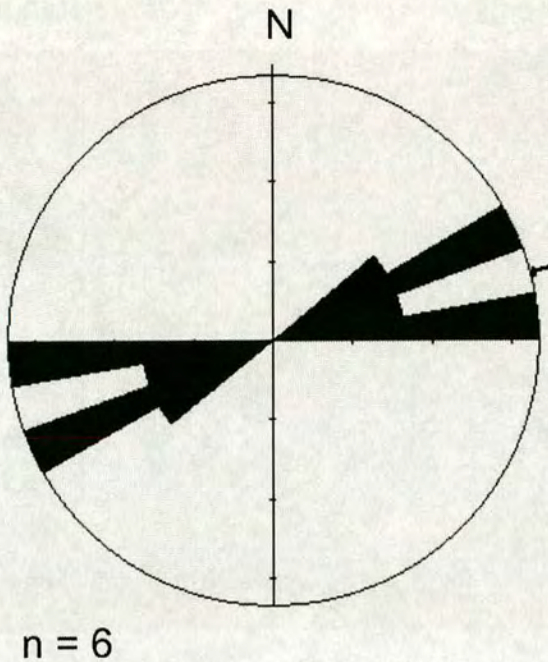
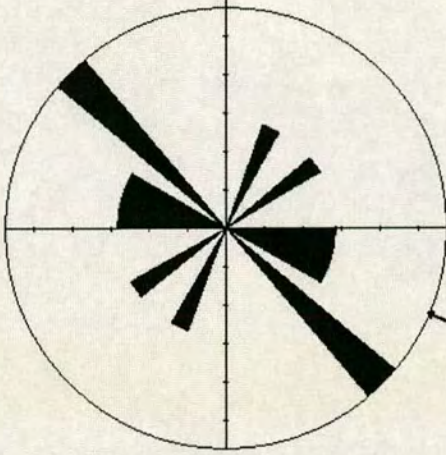


Figure 5.19. Rose diagram showing strike orientations for sheeted dykes within the Kızılrnak Ophiolite.

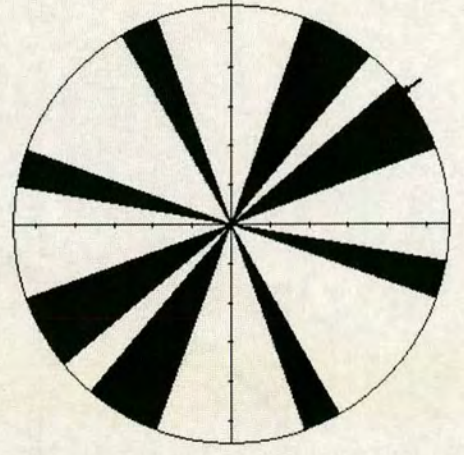
The earliest deformational structure observed is the foliation in harzburgite. This tectonic fabric is a common feature of harzburgite in ophiolites and is interpreted as a mantle flow fabric. The second deformational event gave rise to a top-to-the-north shear fabric and top-to-the-north thrusting. This is interpreted as the emplacement direction (Ustaömer 1993). A third deformational event produced top-to-the-south thrusting and imbrication of the ophiolite with the adjacent Eurasian basement and Neotethyan units. The final deformation produced the sub-vertical strike-slip faults that cut all of the other structures in the unit. D4 is related to plio-quadernary transform motion of the North Anatolian Fault Zone.

Dextral strike-slip faults are orientated $\sim 90^\circ$ to the sinistral strike-slip faults. Because of their NNW-SSE orientation it is unlikely that the dextral strike-slip faults are related to the North Anatolian Fault Zone which trends E-W in the Central Pontides (Dhont et al. 1998). The dextral faults are also normal to the strike of sheeted dyke contacts (i.e. the trend of the ancient spreading-ridge). Cross-cutting relationships were not observed for the dextral strike-slip faults. The dextral faults

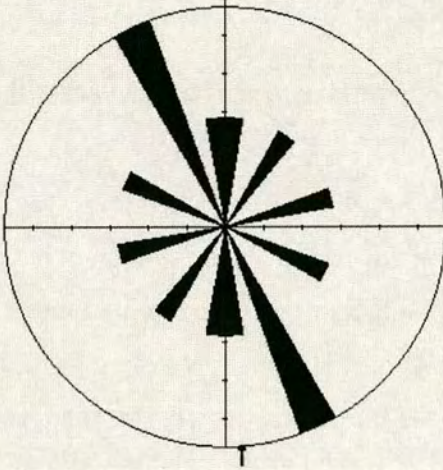
a) top-to-the-north thrust faults



b) top-to-the-south thrust faults



c) dextral strike-slip faults



d) sinistral strike slip faults

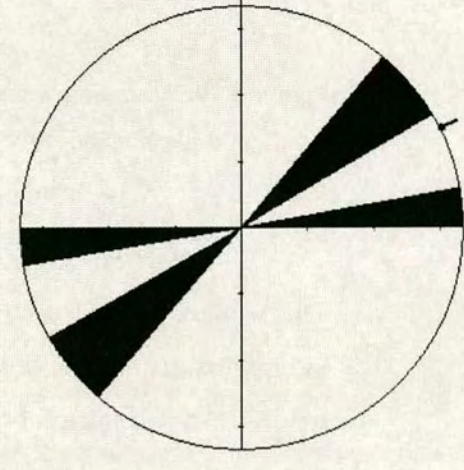


Figure 5.20. Rose diagrams showing strike directions of fault planes within the Kızılırmak Ophiolite.

may pre-date ophiolite emplacement and could represent the effects of oceanic transform-faulting. This suggestion is supported by the observation that the foliation measured in harzburgite (interpreted as a fabric pre-dating emplacement) is sub-parallel to the orientation of the dextral strike-slip fault planes.

5.3.2 Petrology of the Kızılırmak Ophiolite

Peridotites

Peridotites of the Kızılırmak Ophiolite are serpentinised harzburgites in which primary olivine and orthopyroxene (pigeonite) are almost completely replaced by mesh-textured serpentine and bastite, respectively. The harzburgite contains small (<1 mm) partially resorbed grains of chromite. The harzburgite preserves a coarse (<5 mm) primary igneous texture of interlocking crystals and exhibits a mineral foliation. Commonly, the serpentinised peridotite is highly sheared. Some serpentinitic shear zones are mineralised with dolomite, hydromagnesite and/or sepiolite. Fibrous, massive and botryoidal varieties of white sectile sepiolite are observed.

The primary mineralogy (orthopyroxene+olivine) and texture (coarse grained, S1 tectonite) support a lithospheric mantle origin for the serpentinised harzburgite. Their clinopyroxene-poor composition indicates that they are highly depleted in the incompatible elements as a result of a relatively high degree of partial melting or remelting of the mantle wedge (Saunders et al. 1988).

Sepiolite is a hydrous phyllosilicate known to occur as a secondary mineral associated with serpentine and which precipitates from alkali saline waters in arid environments (Jones and Galan 1988, Yalcin and Bozkaya 2004). The presence of dolomite ($\text{CaMg}(\text{CO}_3)_2$) indicates that carbonated fluids may have reacted with the Mg-rich ultramafic rocks along shear zones where permeability is greater (Allaby and Allaby 1990; Yalcin and Bozkaya 2004). The age of mineralization is not known.

Cumulates

Layered gabbro, lherzolite, dunite and pyroxenite are found exposed between outcrops of peridotite and isotropic gabbro near Eldivan, Pelitcik and Bayat (Figure 5.12). Layered gabbro exhibits centimetre-scale alternating fine- and coarse-grained (0.5 mm-7 mm) mafic and feldspathic layers (e.g. near Pelitcik, gr: F33,

5671967074). Thick (<4 m) mafic mineral layers, separated by thin (2-10 cm) feldspathic partings, are exposed in parts of the complex (e.g. near Gölahlatcık, gr: G32, 1163313602), while other exposures exhibit thick (<3 m) feldspathic layers with thin (~20 cm) mafic partings (e.g. near Kunduzlu, gr: G32, 0457812896; Figure 4.2). Orthopyroxene and olivine in the mafic layers are altered to bastite and iddingsite, respectively. Hornblende is also observed in some layers and is probably a secondary mineral after clinopyroxene. The dip of the mineral layering is varied but generally steep (e.g. 85°S/063 at Pelitcik, 75°N/060 at Gölahlatcık). The layers are cut by irregular veins of pegmatitic pyroxenite.

Isotropic gabbro

Gabbro and microgabbro are exposed in contact with cumulates near Eldivan, Bayat and Pelitcik (Figures 5.12, 5.16 and 5.17). The gabbro is light grey, massive, coarse to medium grained (~1 mm) and homogenous, containing ~50% feldspar and ~50% pyroxene. In thin section, the gabbro exhibits a granulitic texture of interlocking euhedral equant grains of plagioclase feldspar (with extinction angles up to 50° between twins, indicating a composition of anorthite 90%) and elongate grains of altered orthopyroxene (bastite; <1.5 mm long). Near Eldivan, a thick exposure (>200 m) of massive microgabbro (or diabase) without chilled margins is cut by rare thin (~30 cm) gabbroic dykes.

The mineralogy of the gabbro indicates that it formed by crystallization of a basaltic magma. The coarser grained gabbro may represent high-temperature slow crystallization at a deep crustal level, whilst the medium-grained gabbro probably crystallized more rapidly at a higher, cooler level in the crust. The crystallizing body of magma represented by the gabbro is interpreted as the source of melt for the diabase dykes above, and crystals for the cumulate layers beneath. As the gabbro crops out between cumulates and sheeted dykes it has retained its primary pseudostratigraphic position.

Diabase sheeted dykes

A thin slice (~200 m) of sheeted diabase dykes (individually ~40-50 cm thick) is well exposed near Pelitcik (Figures 5.14 and 5.15). The dyke chilled margins dip steeply to the northwest. In thin section, the dyke rocks are seen to contain primary plagioclase (<75%) and clinopyroxene (~25%) occurring in the groundmass and as phenocrysts. Orthopyroxene (commonly occurring as bastite) is seen in some samples. Secondary hornblende, epidote and chlorite are abundant. Thin sections show that the feldspars are albitised, sericitised and turbid with a decussate recrystallised texture.

The slightly porphyritic texture of the diabase dykes indicates that the magma underwent partial crystallisation prior to dyke injection. The assemblage of secondary minerals is the same as that observed in the ophiolitic Refahiye Complex (eastern Pontides) and indicates metamorphic reaction with seawater at approximately 200 to 450°C and 500-600 bars; compatible with sea-floor hydrothermal metasomatism of mid- to shallow-level oceanic crust (Elthon and Stern 1978; Mottl 1983).

5.3.3 Igneous Geochemistry of the Kızılırmak Ophiolite

5.3.3.1 Whole-rock geochemistry of basic igneous rocks

One sample of basaltic pillow lava and four samples of diabase dykes from the Kızılırmak Ophiolite were analysed by XRF for whole-rock major and trace-element geochemistry (see section 3.3.8 and Appendix 2 for analytical methods). All the samples have SiO₂ concentrations <54% and MgO+CaO between 12-22% and are, therefore, within the range of naturally occurring unaltered basic igneous rocks (Pearce 1973). Among the samples there are poor correlations between the concentrations of Al₂O₃, a relatively immobile element, and SiO₂, CaO, Fe₂O₃ or MgO (Figure 5.21), which are all potentially mobile during metamorphism, hydrothermal alteration and weathering (Loughnan 1969). The lack of any correlations suggests that the rocks were affected by alteration processes, corroborating the petrographic observations described above. Variations between pairs of elements known to be immobile (Figure 5.22; Loughnan 1969) show good correlations. This suggests that these samples are magmatically related and belong to

a co-magmatic suite. Furthermore, the concentrations of immobile elements were not significantly affected by post-magmatic geochemical processes.

Plotted on the total alkalis (K_2O+Na_2O) versus silica diagram (Figure 5.23; Le Maitre 1989) the samples of basaltic pillow lava and diabase sheeted dykes from the Kızılırmak Ophiolite are classified as basalts, with one basaltic andesite. K, Na and Si are all potentially mobile during alteration and so this classification is unreliable. A more useful classification for altered rocks can be achieved using the immobile elements: Zr, Ti, Nb and Y (Figure 5.24). Figure 5.24 shows that the rocks are basaltic to andesitic in composition and can therefore be used to discriminate between tectonic environments or petrogenetic provinces (which requires the use of basic igneous rock compositions for accurate determinations; section 3.3.8; Pearce and Cann 1973).

The tectonic discrimination diagrams are shown in Figures 5.25 to 5.31. On the Ti-Zr-Y diagram (Figure 5.25; Pearce and Cann 1973) two samples do not plot in any of the compositional fields. Three remaining samples plot within the compositional range for 'Ocean-Floor Basalts' or 'Low Potassium Tholeiites'. On the Cr/Y diagram (Pearce 1982; Figure 5.26) the samples all fall within the compositional field of MORB but with ambiguity regarding two samples because the fields of 'Within-Plate Basalt', 'Volcanic Arc Basalt' and MORB overlap. One sample is unambiguously MORB on the Cr/Y diagram. On all the other diagrams (Figure 5.27 to 5.31) the samples fall neatly into the compositional range that is transitional between MORB and 'Low Potassium Tholeiites'/'Arc Lavas'/'Island Arc Tholeiites'/'Volcanic Arc Basalts' based on Ti/Zr, Zr/Y versus Zr and Nb-Zr-Y ratios respectively (Figures 5.27 to 5.30). On the Zr/Y versus Zr diagram (which distinguishes between enriched (continental) and depleted (oceanic) volcanic arc basalts; Figure 5.29) the samples fall within the field for oceanic volcanic arcs. The N-MORB type basalts may have been erupted at a greater distance from the subduction zone than the basalts of island arc tholeiite type (Saunders and Tarney 1984; Pearce 1973, 1982; Bloomer 1995). basalt geochemistry is influenced by the distance of the backarc spreading centre from the trench in modern backarc basins (Saunders and Tarney 1984; Pearce 1982).

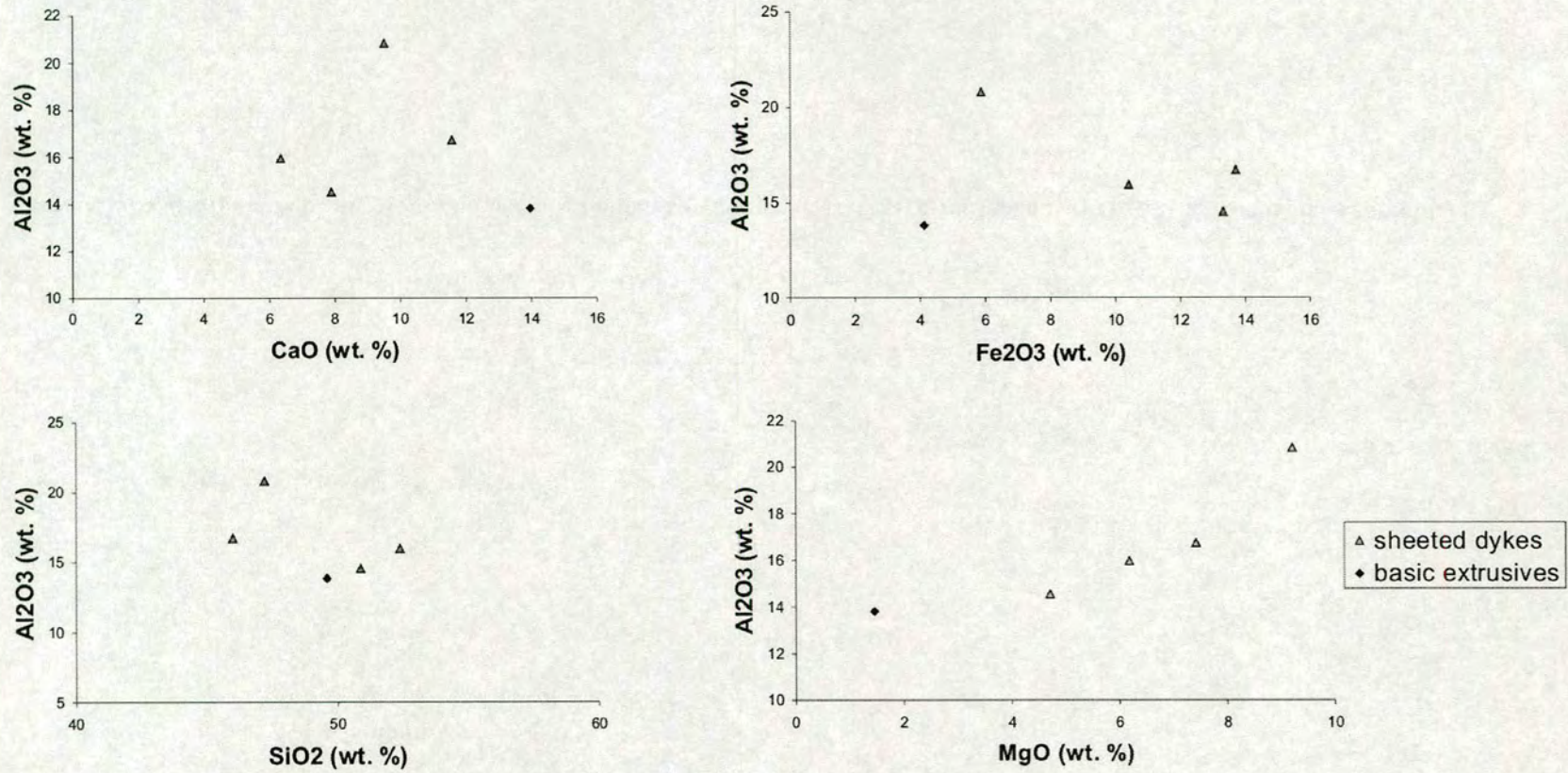


Figure 5.21. Variation diagrams of the mobile elements SiO₂, CaO, Fe₂O₃, and MgO against Al₂O₃ showing element mobility due to alteration of the basic igneous rocks of the Kızılrırmak Ophiolite.

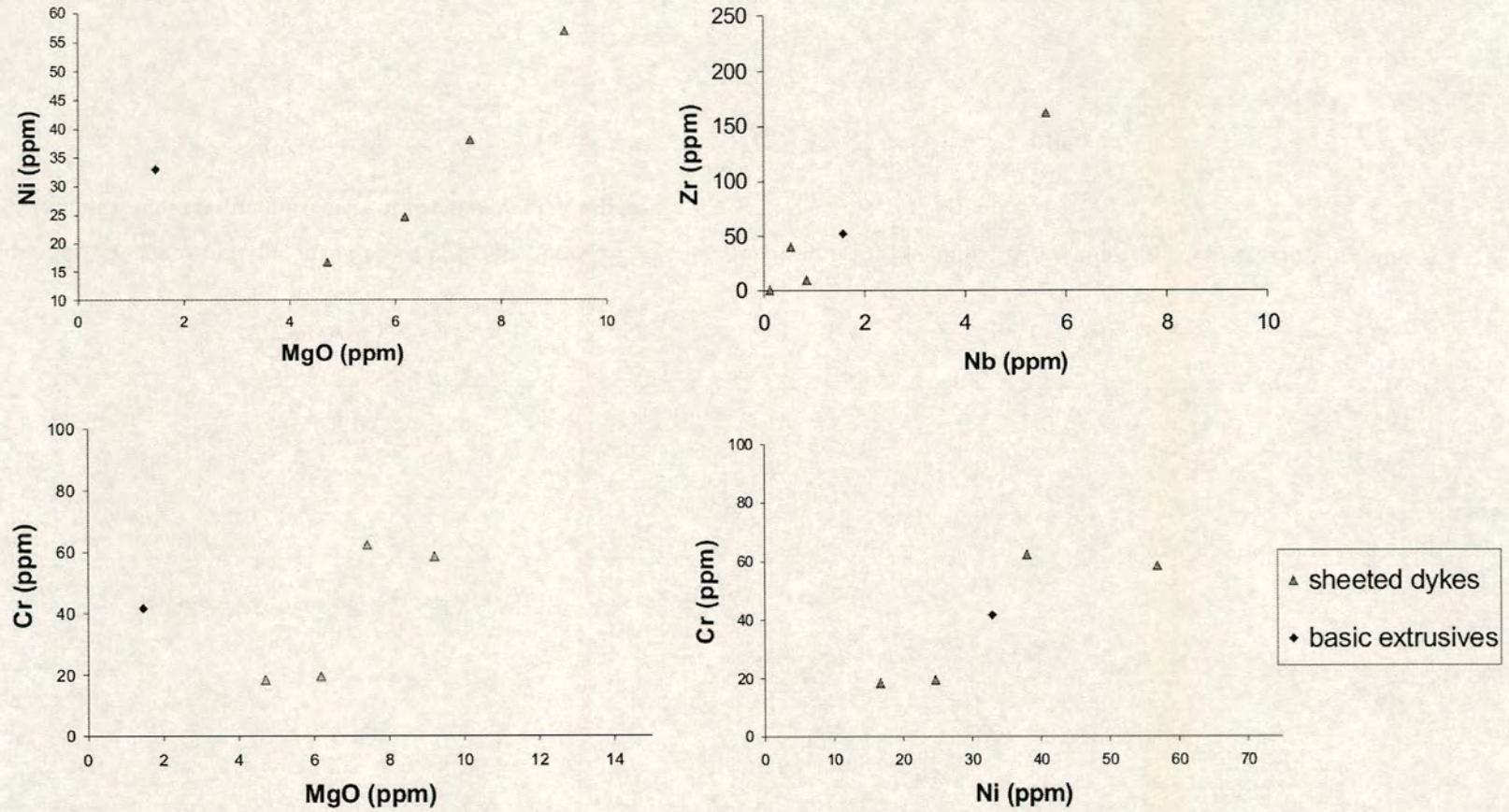


Figure 5.22. Variation diagrams of immobile trace elements in intrusive and extrusive igneous rocks of the Kızılrnak Ophiolite.

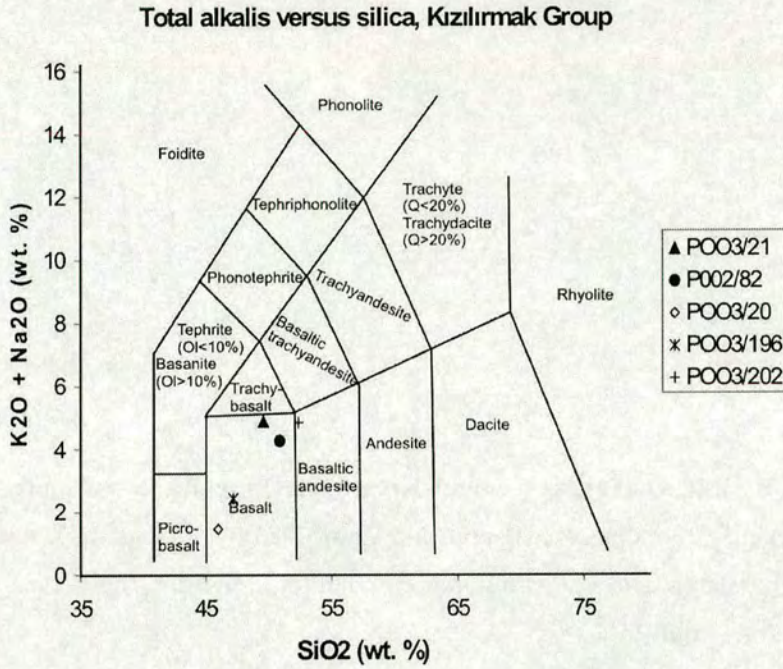


Figure 5.23. Analyses of intrusive and extrusive igneous rocks from the Kızılırmak Ophiolite plotted on the total alkali-silica (TAS) diagram (Le Maitre et al. 1989).

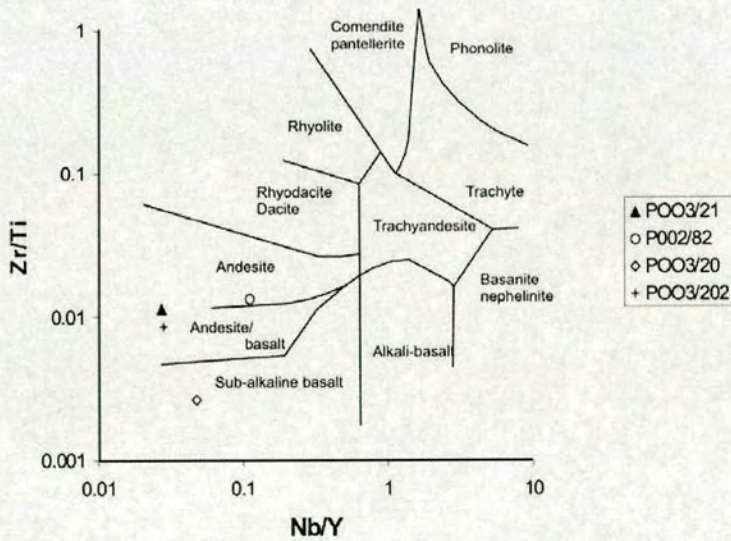


Figure 5.24. Classification of intrusive and extrusive rocks from the Kızılırmak Ophiolite using immobile trace elements Zr/Ti versus Nb/Y (diagram after Winchester and Floyd 1979).

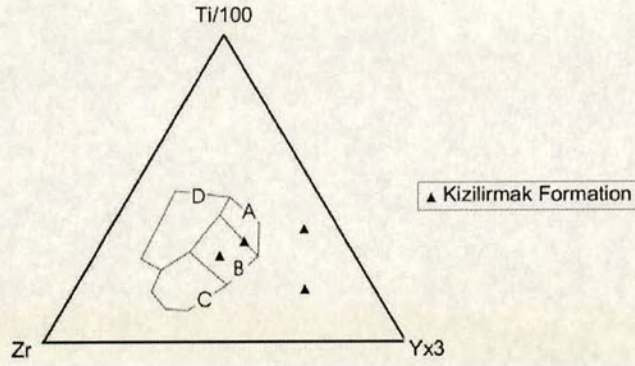


Figure 5.25. Basic igneous rocks from the Kızılırmak Ophiolite plotted on the ternary Ti/Zr/Y discrimination diagram (Pearce and Cann 1973). Within-plate basalts field D, ocean-floor basalts in field B, low-potassium tholeiites in fields A and B, calc-alkali basalts in fields C and B.

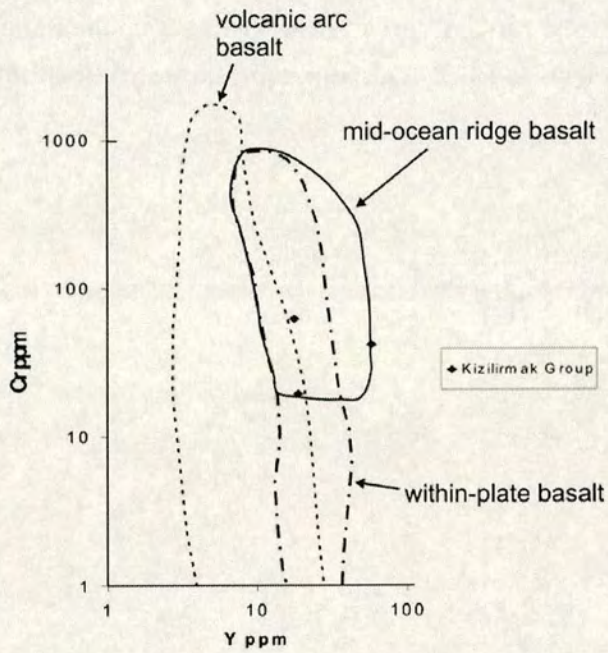


Figure 5.26. Basic igneous rocks from the Kızılırmak Ophiolite plotted on the Cr-Y discrimination diagram (Pearce 1982).

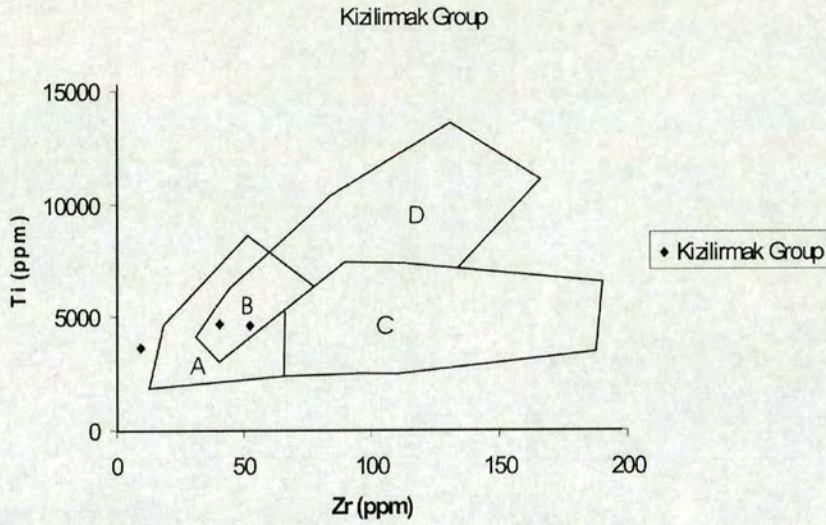


Figure 5.27. Basic igneous rocks from the Kızılırmak Ophiolite plotted on the Ti/Zr discrimination diagram (Pearce and Cann 1973). Ocean-floor basalts plot in fields D and B; low-potassium tholeiites in fields A and B, and calc-alkali basalts in fields C and B.

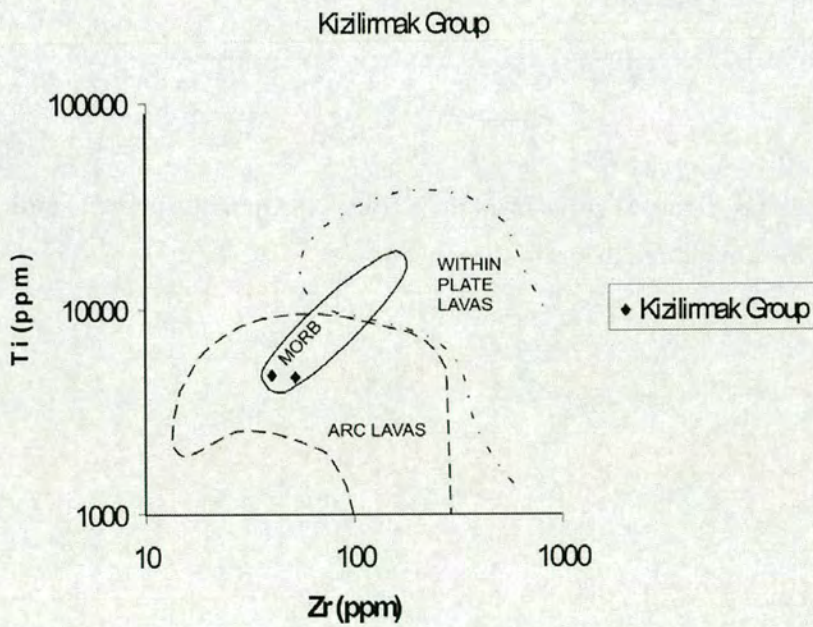


Figure 5.28. Basic igneous rocks from the Kızılırmak Ophiolite plotted on the log Ti/log Zr discrimination diagram (Pearce 1982).

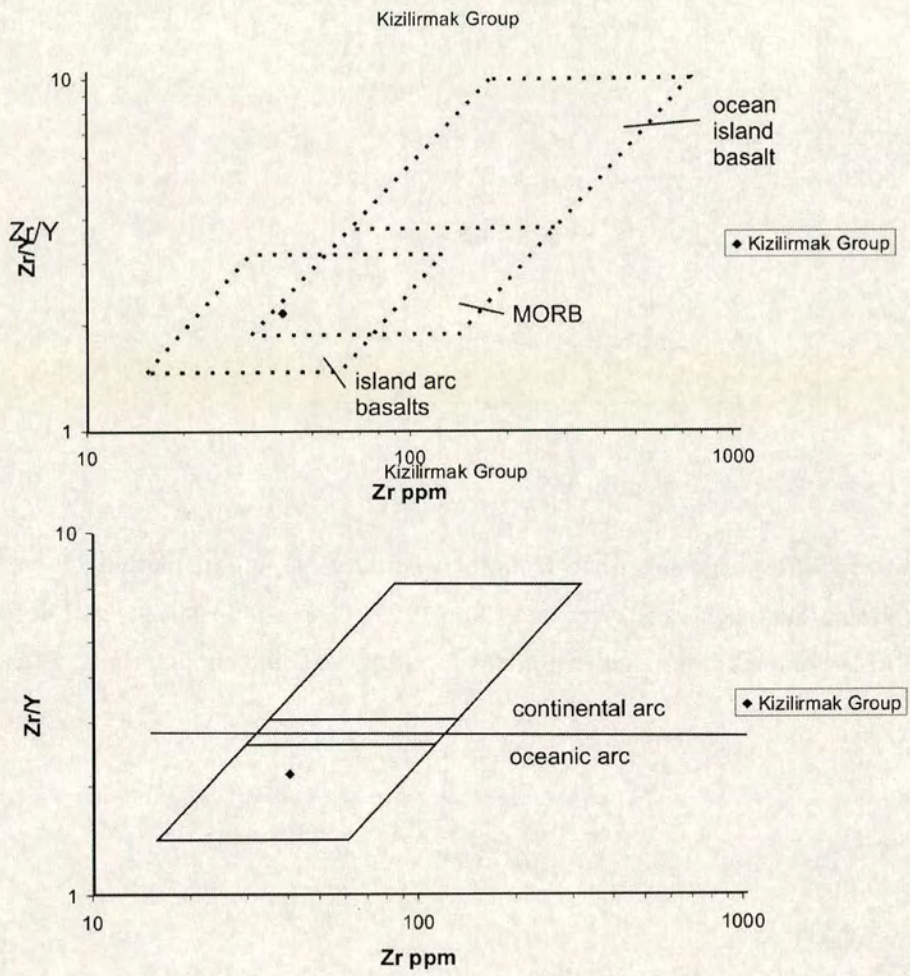


Figure 5.29. Basic igneous rocks from the Kızılırmak Ophiolite plotted on the Zr/Y versus Zr discrimination diagram (Pearce and Norry 1979).

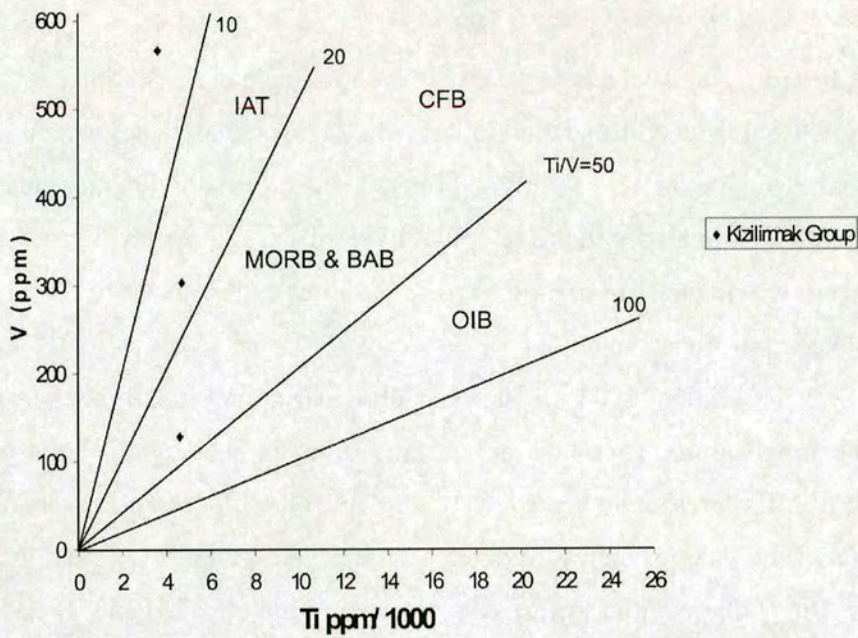


Figure 5.30. Basic igneous rocks from the Kızılırmak Ophiolite plotted on the V/Ti discrimination diagram (Shervais 1982).

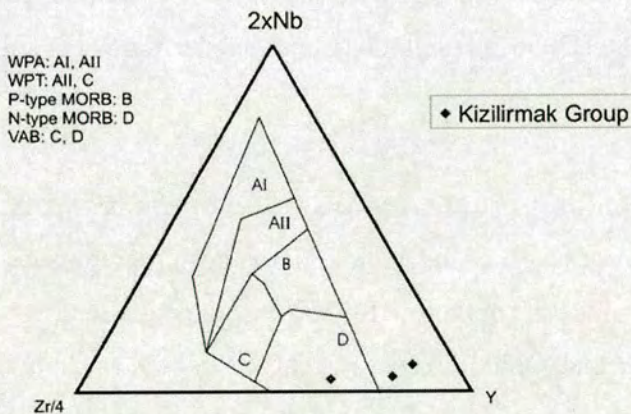


Figure 5.31. Basic igneous rocks from the Kızılırmak Ophiolite plotted on the Nb/Zr/Y discrimination diagram (Meschede 1986). AI and AII = within-plate alkali basalt compositional field, B = plume-influenced MORB compositional field, C = within-plate tholeiite compositional field, D = N-type MORB and volcanic arc basalt.

Chromian spinel chemistry

Chromite grains were analyzed within one sample of serpentinised harzburgite from the Kızılırmak Ophiolite (PO02/37; for analytical procedure see section 3.3.9 and Reed 1975). Cores and rims of seventeen individual chromian spinel grains were analysed in the sample. The results are shown in Figure 5.32. The analyses fall within the field of alpine type peridotites and are close to the abyssal peridotite compositional field.

Dick and Bullen (1984) divided ophiolitic peridotites into three types based on spinel compositions. Type I peridotites are similar to those found at mid-ocean ridges; Type III represent volcanic arc settings, and type II are transitional and the most likely candidate for their formation is in a backarc basin. Type I peridotites have low Cr# (<60) and plot towards the bottom of Figure 5.32. Type III peridotites plot at the top of the diagram (Cr# >60). Type II cover the full range of spinel compositions (Dick and Bullen 1984). The data from the Kızılırmak Ophiolite show that the sample cannot be a type III ophiolitic peridotite. It could be either type I or type II. This suggests the Kızılırmak Ophiolite represents either lithosphere formed at a mid-oceanic ridge or in a backarc setting. Analysis of a greater number of samples could clarify this result. Only one sample from the Kızılırmak Ophiolite was petrographically suitable.

5.3.4 Petrogenesis and tectonic setting of the Kızılırmak Ophiolite.

The lower levels of the ophiolitic pseudostratigraphy are preserved, dominantly. Unlike the ophiolitic Refahiye Complex in the Eastern Pontides (section 3.3), the Kızılırmak Ophiolite does not encompass metamorphic host rocks. The Kızılırmak Ophiolite is interpreted as a deformed, incomplete section of oceanic lithosphere of Campanian-Maastrichtian age, which could have formed in either a mid-oceanic ridge or a backarc setting. South-dipping thrusts and pervasive shear fabric confirm that the emplacement direction of the ophiolite was from the south-southwest towards the north-northeast, as suggested by Ustaömer (1993).

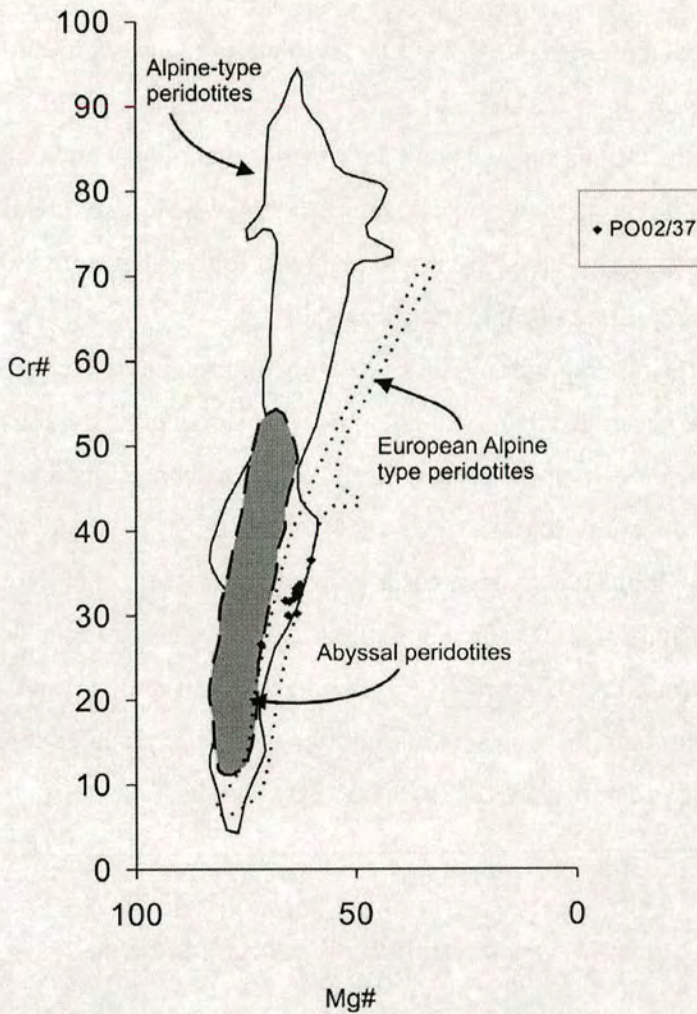


Figure 5.32. Cr# ($((Cr*100)/(Cr+Al))$) versus Mg# ($((Mg*100)/(Mg+Fe^{2+}))$) for spinels from peridotites in the Kızıllrmak Ophiolite, Central Pontides. Fields for alpine-type peridotites, abyssal basalts, and European alpine peridotites are marked (Dick and Bullen 1984). Sampling location; Pelitcik (gr: F33, 5633065332).

Geochemical studies indicate that the ophiolite represents lithosphere that formed in a tectonic-petrogenetic setting transitional between a mid-oceanic spreading centre and an oceanic volcanic arc. Comparison of the geochemical results with published analyses (Keller and Fisk 1992; Saunders and Tarney 1984; Shervais 1982; Pearce et al. 1984) suggests that the Kızıllrmak Ophiolite could have formed within a backarc basin setting.

5.3.5 Summary

The Kızılırmak Ophiolite is a ~3.5 km thick, relatively intact ophiolite of Campanian-Maastrichtian age (83.5-65.5 Ma; Tüysüz 1990). Coherency of ENE-WSW sheeted dyke orientations suggests that an oceanic spreading centre could have been orientated in this direction, and suggests regional NNW-SSE extensional palaeostress. Dextral strike-slip faults are orientated ~90° to the sheeted dykes (i.e. NNW-SSW) and may represent oceanic transform faulting.

Isolated diabase and plagiogranite dykes are uncommon in the Kızılırmak Ophiolite. Whole-rock basalt geochemistry and chromian spinel compositions indicate that the Kızılırmak Ophiolite represents either lithosphere formed at a mid-oceanic ridge or in a backarc setting.

The ophiolite exhibits a pervasive north-vergent shear fabric cut by top-to-the-south thrust faults and sinistral strike slip faults. The ophiolite was emplaced from south to north during Late Cretaceous (Campanian-Maastrichtian) time. Following emplacement onto the Eurasian margin, the ophiolite was later deformed by top-to-the-south thrust faults related to collision between the Tauride-Anatolide plate and Eurasia.

5.4 Late Mesozoic accretionary complex: Kirazbaşı Mélange

An ophiolitic *mélange* unit, the Kirazbaşı *Mélange* (Tüysüz 1990) crops out extensively within the suture zone and is distributed throughout several structural levels (Figure 5.33). North of Tosya, the Kirazbaşı *Mélange* is tectonically imbricated with older basement rocks. Samples collected from several of the blocks during this project contain age-diagnostic calcareous microfossils. These samples yielded ages ranging from Early Cretaceous (Albian) to Late Maastrichtian, based on the identification of *Pseudosiderolites vidali* DOUVILLE and *Rotalipora* sp. (Prof. Izver Ongen, Prof. Kemal Taşlı and Prof. Nurdan İnan, Pers. comm. 2004; see Appendix 1). Based on the biostratigraphic data (Appendix 1) a maximum age for the *mélange* accretion is suggested by the youngest known age of blocks in the *mélange* (i.e. Late Maastrichtian). The *mélange* is unconformably overlain by Eocene Nummulitic limestones and fluvio-deltaic sandstones (Kadıkızı Formation) that

postdate suturing (section 5.8). A minimum age of mélangé formation is indicated by the Eocene age of the unconformably overlying sedimentary rocks (Kadıkızı Formation; section 5.8). As noted above (section 5.2), in the north the mélangé tectonically overlies the Upper Cretaceous basinal Eskiköy Formation.

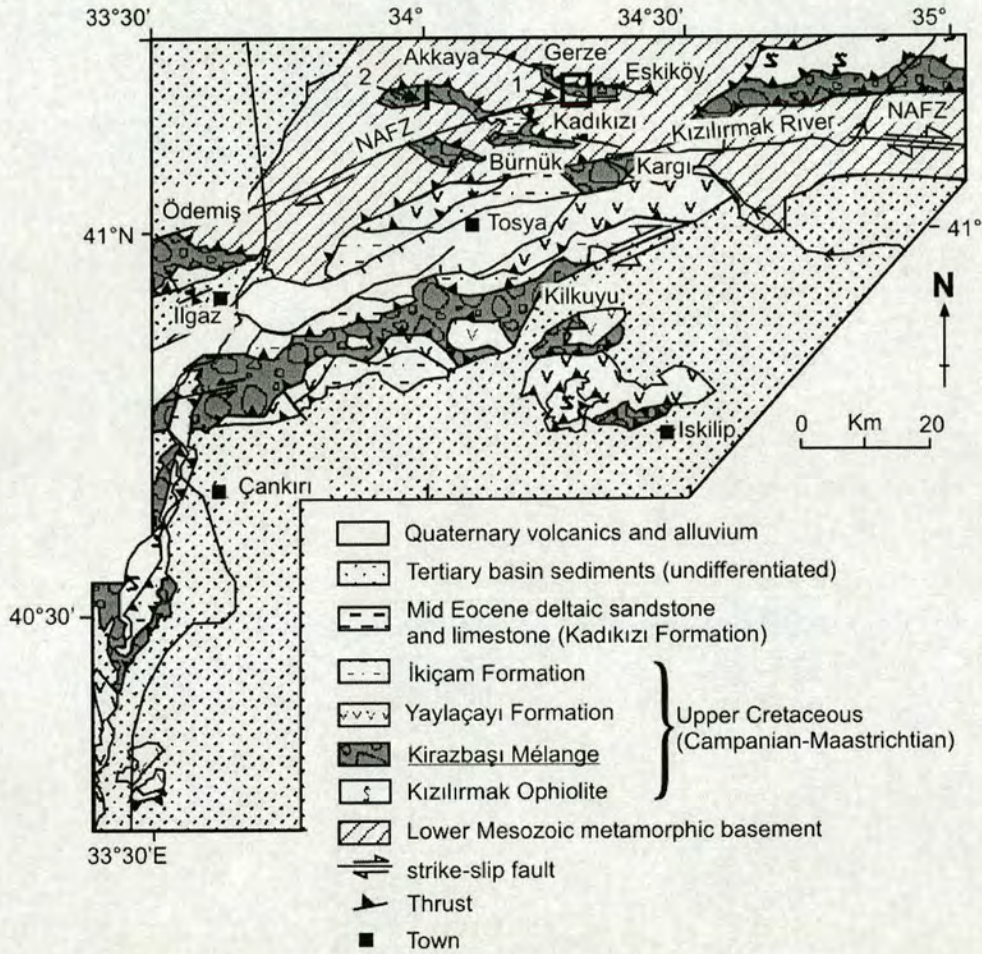


Figure 5.33. Simplified geological map showing outcrop of the Kirazbaşı Mélangé in the Central Pontides. 1 = map at Gerze (Figure 5.35); 2 = location of road section at Akkaya (Figure 5.34).

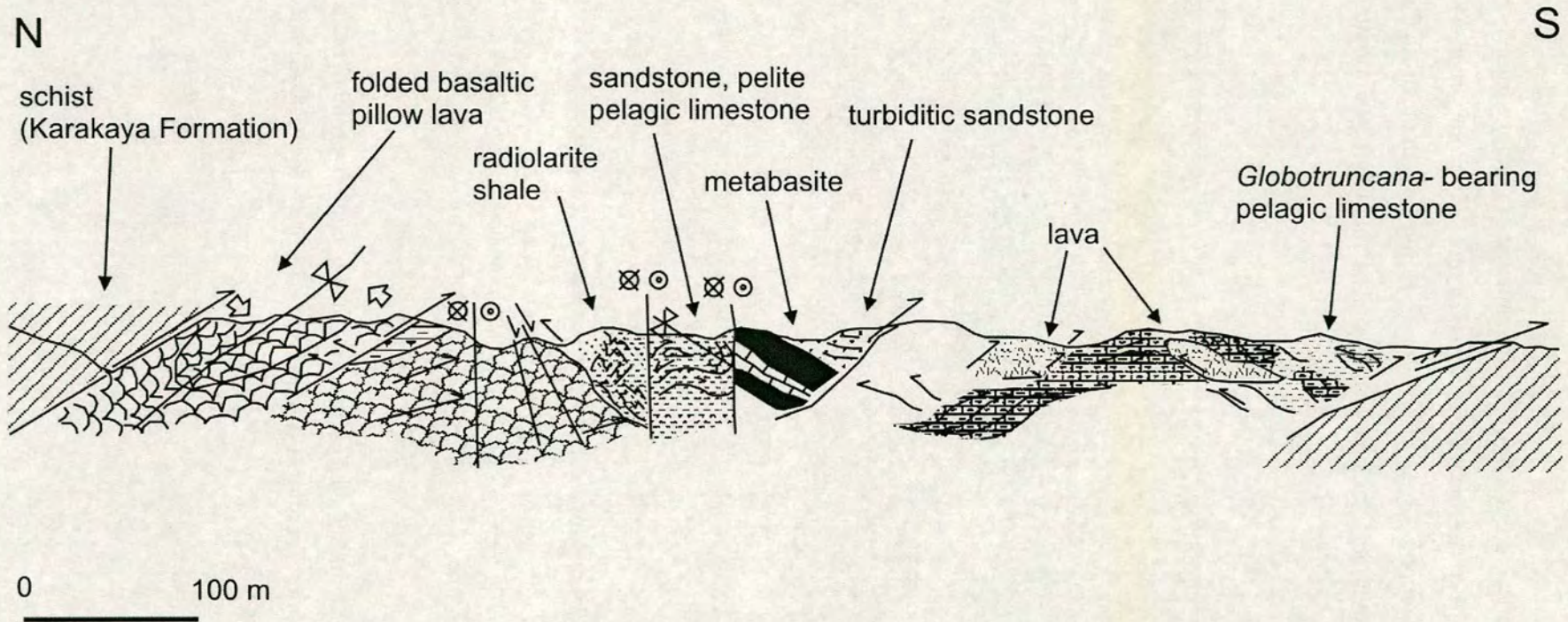


Figure 5.34. Road-section at Akkaya. See Figure 5.33 for location.

5.4.1 Structure of the Kirazbaşı Mélange

The Kirazbaşı Mélange contains blocks and slices ranging in size from <1 mm to >1 km. The blocks have sheared and faulted edges and are internally deformed at outcrop scale (Figure 5.34). The blocks are commonly tectonically juxtaposed or are separated by wide (<100 m) zones of sheared serpentinite or a brecciated muddy litharenitic matrix or fault gouge. The matrix is not bedded. Blocks are less commonly set in a scaly clay matrix or fault gouge.

Shear fabrics are concentrated in the matrix around the blocks but also are observed within blocks. A pervasive top-to-the-north shear fabric ($\sim 60^\circ\text{SE}/170$) is cut by top-to-the-south shear zones ($60^\circ\text{N}/040$). The top-to-the-north shear fabric is also folded by south-vergent asymmetrical upright folds (wavelength ~ 2 m).

A wide variety of fold geometries is observed within blocks of bedded sedimentary rocks, i.e. chert, mudstone and sandstone. Fold axes commonly exhibit a low angle of plunge. Vertical axes are less commonly present. Minor recumbent folds are common in blocks of ribbon chert. Upright open to tight, parallel folds and inclined tight chevron folds were observed. Kink bands in hemipelagic mudstone near Pelitcik (gr: F33, 541611) dip $45^\circ/070^\circ$. Small-scale recumbent asymmetrical folds commonly verge northwards.

The Kirazbaşı Mélange exhibits abundant thrust faults, normal faults and strike-slip faults. Some of the faults are confined to this unit. Others pass into adjacent units. Fault data are given below.

The Kirazbaşı Mélange exhibits a wide range of bedding and cleavage orientations within blocks (Figure 5.36a, b). Bedding and cleavage planes within the blocks rarely strike WNW-ESE. Pebbles within blocks of conglomerate are flattened in the cleavage plane. Bedding within the blocks is commonly orientated sub-parallel to cleavage. The mean strike direction of bedding is NE-SW. The mean strike direction of cleavage is NNE-SSW. Poles to cleavage planes (Figure 5.36b) are distributed around an axis trending roughly north-south. This direction is coincident with the mean strike direction of fold axes within blocks in the mélange (Figure 5.37c).

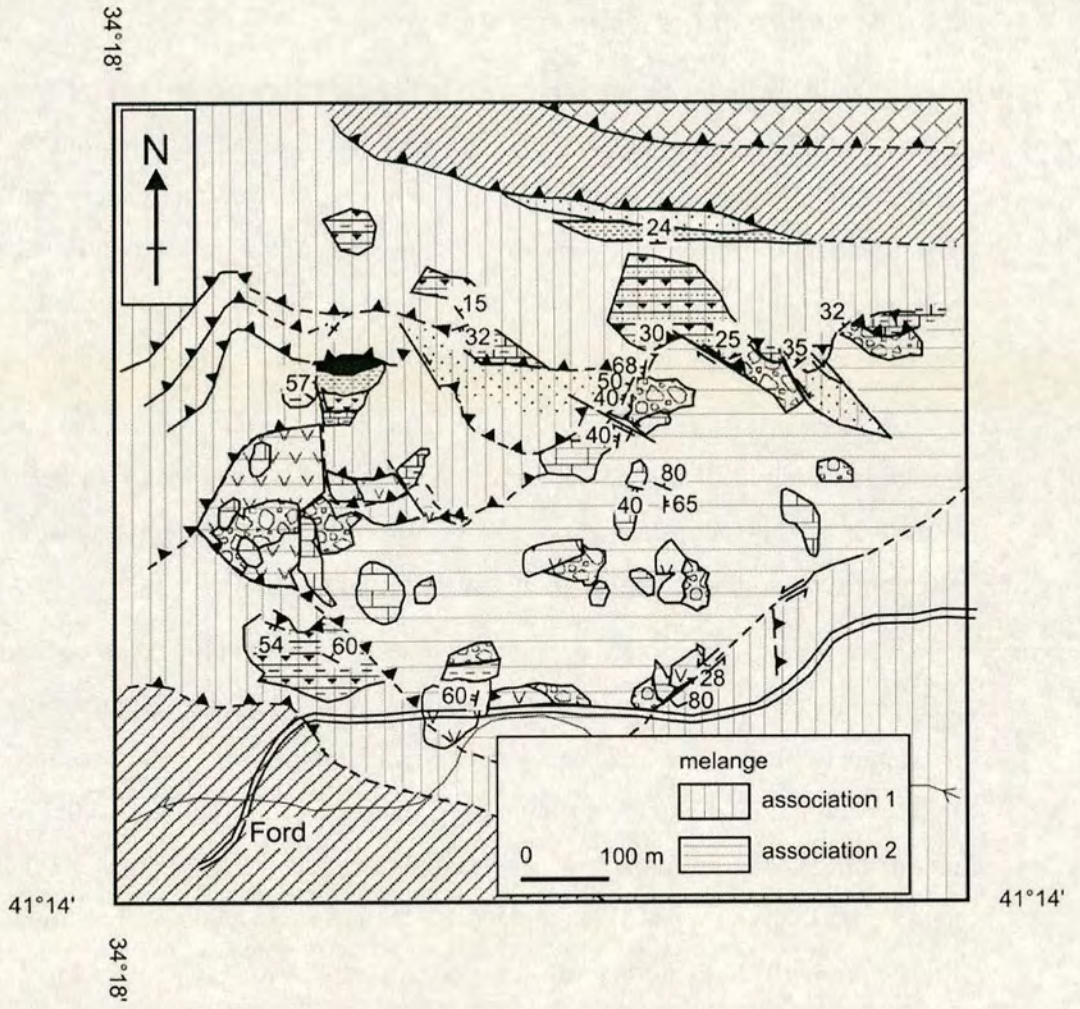


Figure 5.35. Detailed geological map of an outcrop of the Kirazbaşı Mélange at Gerze. See Figure 5.33 for location. see Figure 5.1 for key to symbols.

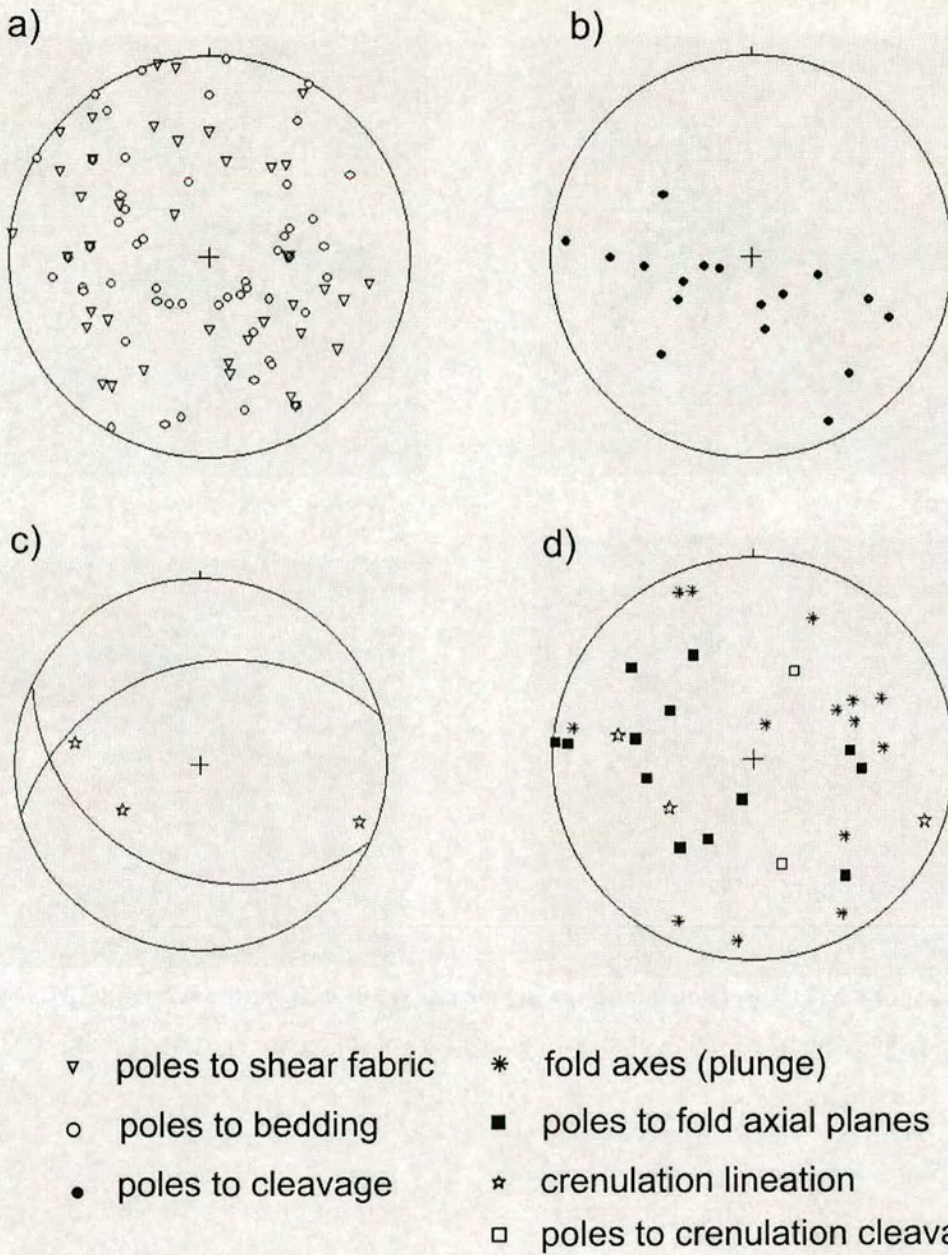


Figure 5.36. Structural data from the Kirazbaşı Mélange. a) poles to bedding and shear fabric; b) poles to cleavage; c) crenulation cleavage planes (great circles) and crenulation lineation; d) fold data.

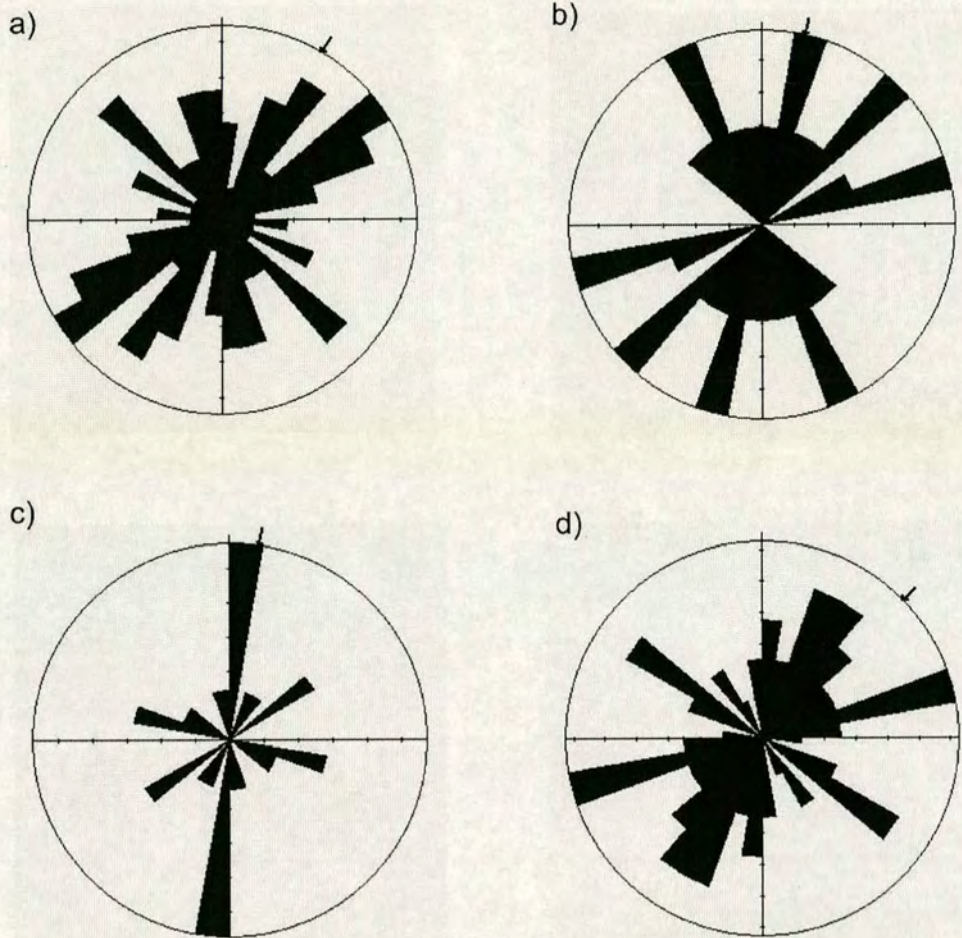
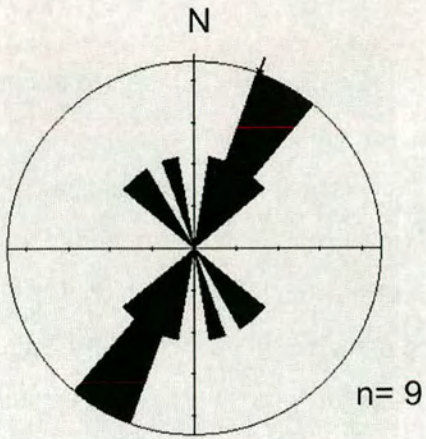


Figure 5.37. Rose diagrams showing structural data from the Kirazbaşı Mélange. a) strike of beds; b) strike of cleavage; c) strike of fold axial planes; d) strike of shear fabric.

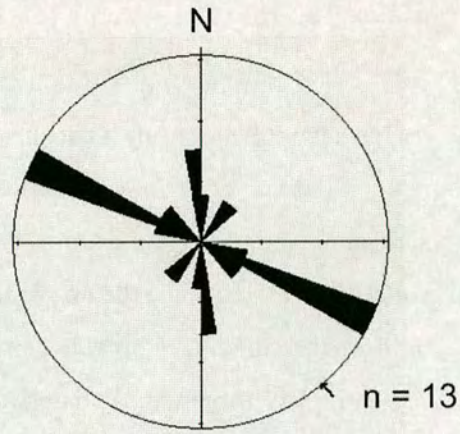
Crenulation cleavage observed in blocks of mica schist exhibits a range of orientations. The apparent irregularity of crenulation cleavage may illustrate the structural complexity of the *mélange* but also reflects a small dataset. Crenulation cleavage in blocks of mica schist could have been attained before inclusion in the *mélange*. Subsequent deformation within the *mélange* before, during, or after its emplacement would have rotated early structures. Shear fabric (measured in the matrix and in blocks) show a large range of orientations within the Kirazbaşı *Mélange* (Figures 5.36a and 5.37d). The mean strike of the shear fabric is NE-SW.

Faults orientation data are shown in Figure 5.38.

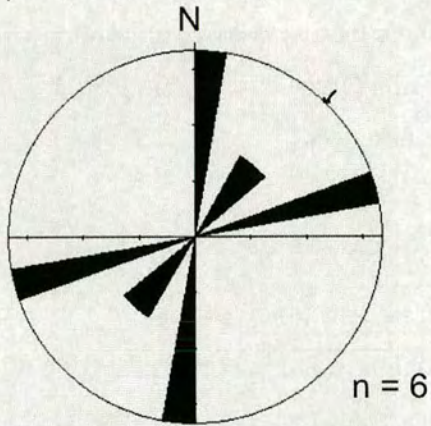
a) top-to-the-north thrusts



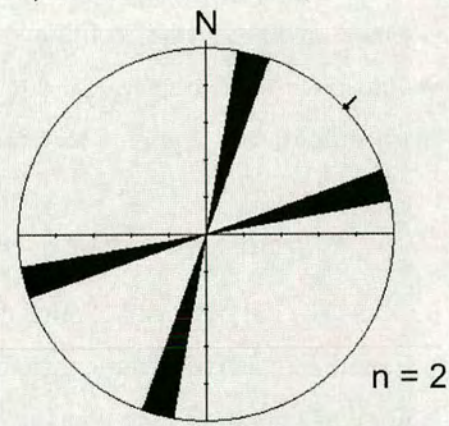
b) top-to-the-south thrusts



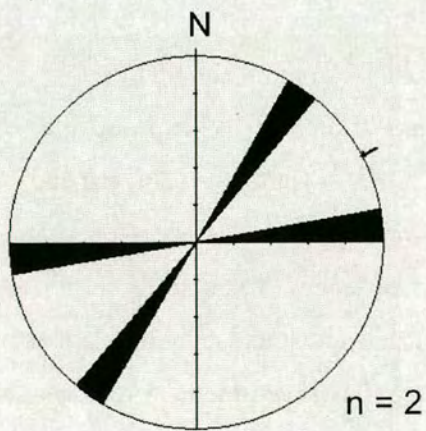
c) dextral strike-slip



d) sinistral strike-slip



e) normal faults



f) all faults

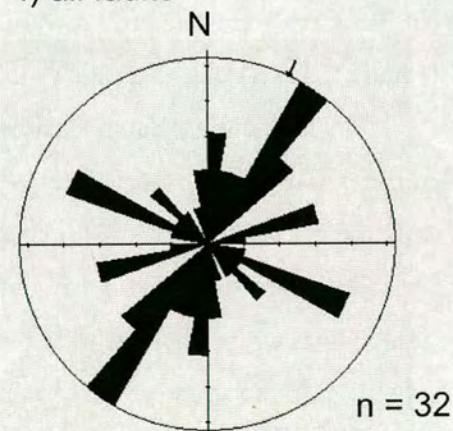


Figure 5.38. Fault plane orientations measured in the Kirazbaşı Mélange.

5.4.2 Sedimentary facies and igneous petrology of the Kirazbaşı Mélange

The most common lithologies in the mélangé are serpentinised ultramafic rocks, basalt/meta-basalt, andesite, diabase, red radiolarian chert, pelagic/hemipelagic limestone, shale, volcaniclastic and terrigenous quartzose sandstone and neritic limestone. The matrix is either sheared serpentinite, or a poorly sorted mixture of all of the above lithologies. In some localities scaly clay or deformed sedimentary breccia comprise the matrix of the Kirazbaşı Mélange, indicating a sedimentary “olistostromal” origin for some levels of the mélangé. The matrix and blocks in the mélangé form lithological associations which can be mapped (Figure 5.35), notably a chert+basalt+serpentinite±clastic sediment association (association 1; Figure 5.35); and a basalt+massive limestone +volcaniclastic sediment±andesite association (association 2; Figure 5.35). The two associations are commonly tectonically imbricated.

5.4.2.1 Radiolarite-basalt-serpentinite-clastic association

The Kirazbaşı Mélange contains an association consisting of blocks of serpentinite, altered basaltic lava, uralitic diabase and interbedded (~10 cm) red radiolarian chert, pelagic limestone and mudstone (association 1; Figure 5.35). Metabasite and chert blocks are generally most abundant in more southerly outcrops of the Kirazbaşı Mélange. Towards the north (Akkaya, Kadıkızı, Ödemiş, Bürnük; Figure 5.33) blocks of clastic sedimentary rock are more abundant.

The radiolarite-metabasite-clastic association is well exposed, e.g. 16 km north of Tosya, near Bürnük (gr: F32, 895549). Towards the southern end of the outcrop at Bürnük blocks of recrystallised red radiolarian ‘ribbon’ chert and chloritic metabasite are separated by serpentinitic shear zones. Vesicular basalt flows are interbedded with red chert. Rare blocks of mica-schist and psammite are also observed in the southern part of the outcrop. Clastic sedimentary rocks are abundant in the structurally higher northern part of the outcrop. The grain size of the clastic sedimentary rocks ranges from mudstone to sandstone. Dark grey arkose, calcareous siltstone and bedded micritic limestone are exposed north of Bürnük village. In

addition to clastic sedimentary rocks the *mélange* contains blocks of calcareous tuff interbedded with radiolarian micritic limestone, as seen north of Bürnük village.

The Kirazbaşı *Mélange* contains blocks (10-50 m long) of diabase, pillow lava and red pelagic limestone, for example ~5 km north of Ilgaz (Figure 5.33). This association contains slices of gabbro up to ~1 km long (seen between Çankırı and Ilgaz at Büyük Yayla; gr: G31, 602200; see Figure 5.33). Pillow lavas within this association are commonly aphyric and non vesicular. A block of basaltic pillow lava breccia with a red pelagic limestone matrix was also observed north of Ilgaz. Blocks of diabase (sheeted dykes with well-preserved chilled margins) were observed 13 km southeast of Ilgaz (near Yuvasaray (gr: G31, 640240) and also near Aşağıkaya; (gr: G31, 710270)). The diabase is uralitic and is locally associated with metabasalt, uralitic gabbro and ultramafic cumulates. These blocks are separated by zones of sheared serpentinite of varied thicknesses.

The structurally highest thrust slice of the Kirazbaşı *Mélange* is exposed at Kadıkızı, Kirazbaşı and at Akkaya (Figure 5.33). The *mélange* there contains interbedded mudstone, pelagic limestone (containing radiolarians) shale and sandstone, as seen for example at Akkaya, where the succession is in sheared contact with a large (<100 m long) block of pillow lava. A large slice (<500 m long) of sedimentary rocks within the *mélange*, exposed north of Kadıkızı, exhibits a succession (~40 m thick) of shale, micritic limestone, red mudstone, grey-buff chert and sandstone. The sandstone beds (up to 80 cm thick) are commonly graded and amalgamated. The sandstone is medium- to coarse-grained, moderately well-sorted, hard and quartzose. Glauconite and feldspar are present in minor amounts while lithoclasts and mud are negligible. Quartz grains are well-rounded. Blocks of sandstone and limestone within the *mélange* contain detrital mica flakes (seen ~6 km northwest of Ilgaz). A folded succession, estimated as >1 km thick (i.e. post-depositional thickness), consisting of red siliceous shale, mudrock, chert and pelagic limestone, is exposed near Kargı, at Pelitcik (Figure 5.14). The Kirazbaşı *Mélange* is tectonically imbricated with the Eskiköy Formation which contains very similar interbedded sandstone, shale and micritic limestone (e.g. at Kirazbaşı).

In southerly outcrops of the *mélange* association 1 (radiolarite-metabasite-clastic sedimentary rocks) is dominated by ophiolitic lithologies. These can be

reconstructed as an ophiolite pseudostratigraphy that resembles a section of oceanic lithosphere (Anonymous 1972). Sedimentary rocks include radiolarian chert and micritic limestone and mudstone. The fine-grained sedimentary rocks indicate low-energy environment of deposition and the fauna they contain (radiolaria) suggest that these represent deep-marine pelagic/hemipelagic sediments, comparable to sediments found in modern abyssal pelagic environments (Iijima et al. 1983). These sedimentary rocks are typical of those found within ophiolitic assemblages (i.e. epiophiolitic sedimentary rocks; Anonymous 1972).

The clastic sedimentary rocks in this *mélange* association, including arkosic sandstones, are interbedded with pelagic limestones and cherts and contain rare mica and well-rounded quartz grains. The well-rounded quartz grains indicate significant abrasion during transport, possibly by a large river. The source of the well-rounded quartz grains and the mica is interpreted to be the Cretaceous Eurasian margin to the north. The source of the arkoses was an area of volcanic rocks, possibly a volcanic arc related to the closure of Neotethys. In the Central Pontides no Cretaceous volcanic arc is seen to the north of the suture zone (i.e. no arc on the Cretaceous Eurasian margin). The volcanic source for the arkoses may have been located to the south of the Eurasian margin (i.e. an oceanic volcanic arc within Neotethys, as inferred from the Yaylaçayı Formation). Alternatively, the source could have been older volcanic rocks present on the Eurasian margin related to the Palaeotethyan history (Ustaömer 1993). The clastic sedimentary rocks are, therefore, interpreted as a continental margin association containing volcanic material. Ribbon chert, basaltic lava, diabase sheeted dykes, gabbro and serpentinite are more common further south and represent the upper- to mid-levels of oceanic lithosphere.

Massive limestone-lava-volcaniclastic association

The *mélange* includes an association of massive grey limestone, porphyritic and vesicular basalt, lava and related volcaniclastic sedimentary rocks (association 2; Figure 5.35). Intrusive and depositional contacts between the sedimentary rocks (including the massive limestone) and the basalt are commonly preserved. The volcaniclastic sedimentary rocks are mainly sandstones and coarse-grained matrix-supported conglomerates.

North of Ilgaz, the Kirazbaşı Mélange contains trains of large (<500 m) blocks or slices of massive fine-grained limestone. The limestone blocks commonly consist of redeposited breccia. Limestone blocks that have been weathered to create bauxite with a dark red metallic colour are well exposed north of Ilgaz on the Kastamonu road (Figure 5.33). This limestone also contains corals and colonial Upper Cretaceous rudist bivalves.

This mélange association comprises abundant blocks of volcanoclastic sandstone and conglomerate. The conglomerate is matrix supported and contains dark and pale sub-rounded basalt and andesite clasts, up to 1 m diameter. Clasts are feldspar-phyric (phenocrysts up to 4 mm long). The conglomerate is commonly schistose, has a green colour, and clasts that are flattened in the cleavage plane.

In addition to massive grey limestone, fine-grained sedimentary rocks in this mélange association include red mudstone and limestone containing rare outsize clasts of green altered basalt. Rare umber (i.e. metalliferous oxide sediment) was also observed.

Interstratified chert and lava were observed southwest of Çankırı near Eldivan (gr: H30, 394835). The chert is also interbedded with thin (<5 cm) beds of dark grey-black volcanoclastic sandstone. The sandstone interbeds are well-sorted, coarse- to medium-grained, well-rounded, moderately well sorted, graded and exhibit load casts (indicating that the block youngs to the north). Basaltic pillow lava and pillow disintegration breccia with a red micritic limestone matrix were also observed.

Mélange association 2 (massive limestone-lava-volcanoclastic sedimentary rock) contains large (<100 m diameter) blocks of picritic pillow lavas associated with coarse matrix-supported volcanoclastic conglomerate.

Association 2 is tectonically imbricated with association 1 (Figure 5.35). The rudistic fauna indicate a shallow-marine environment for the massive limestone blocks. The massive limestone-lava-volcanoclastic mélange association (association 2) is interpreted as a disrupted volcanic seamount facies. It is likely that seamounts were accreted into the ophiolitic mélange from the downgoing plate during subduction (see Chapter 6, Discussion).

5.4.3 Whole-rock geochemistry of basic igneous rocks in the Kirazbaşı Mélange

Twenty eight samples of relatively unaltered aphyric mafic lava and diabase were collected from the Kirazbaşı Mélange and analysed by X-ray fluorescence. For details of the method see section 3.3.8.

The variations between immobile element concentrations show poor correlations among the 28 samples (Figure 5.39). This suggests that the samples are not comagmatic and may represent a variety of petrogenetic sources. The mobile element concentrations also show weak correlations among the samples (Figure 5.40). This suggests that these elements have been mobilised during rock alteration processes (i.e. sea-floor hydrothermal metasomatism, regional metamorphism and weathering). Six of these samples also have SiO_2 and/or $\text{CaO} + \text{MgO}$ wt.% outside the range for naturally occurring basic lavas (ie. $\text{SiO}_2 < 54$ wt.%; $\text{CaO} + \text{MgO}$ between 12-22wt.%; Pearce 1973). Before plotting the dataset on tectonic discrimination diagrams (see 3.3.8 for explanation) the 28 samples were classified using the total alkalis/silica diagram (Figure 5.41; LeMaitre et al. 1989) and also using trace element ratios Zr/Ti and Nb/Y (Figure 5.42; Winchester and Floyd 1979). Twelve non-basaltic samples were removed.

The 16 remaining basaltic samples were plotted on a variety of tectonic discrimination diagrams (Figure 5.43 to 5.49). Among the tectonic discrimination diagrams the samples cover all of the fields, but not in every diagram. The MORB-compositional field overlaps with other compositional fields in many of the diagrams and in each diagram there is at least one sample that does not fall within the MORB or 'Ocean Floor Basalt' field. In none of the diagrams are any of the samples unambiguously 'Volcanic Arc Basalt', calc-alkali basalt, or 'Island Arc Tholeiite'. In five of the diagrams at least one sample falls unambiguously into the 'Ocean Island Basalt' or 'Within-Plate Basalt' field. The majority of the samples occupy the compositional fields for MORB or 'Ocean Floor Basalt' in most of the diagrams. In summary, the samples are interpreted to represent a mixture of 'Ocean Island Basalt'/'Within-Plate Basalt' and MORB/'Ocean Floor Basalt'. Although there is overlap between the fields of MORB and 'Volcanic Arc Basalt'/'Island Arc

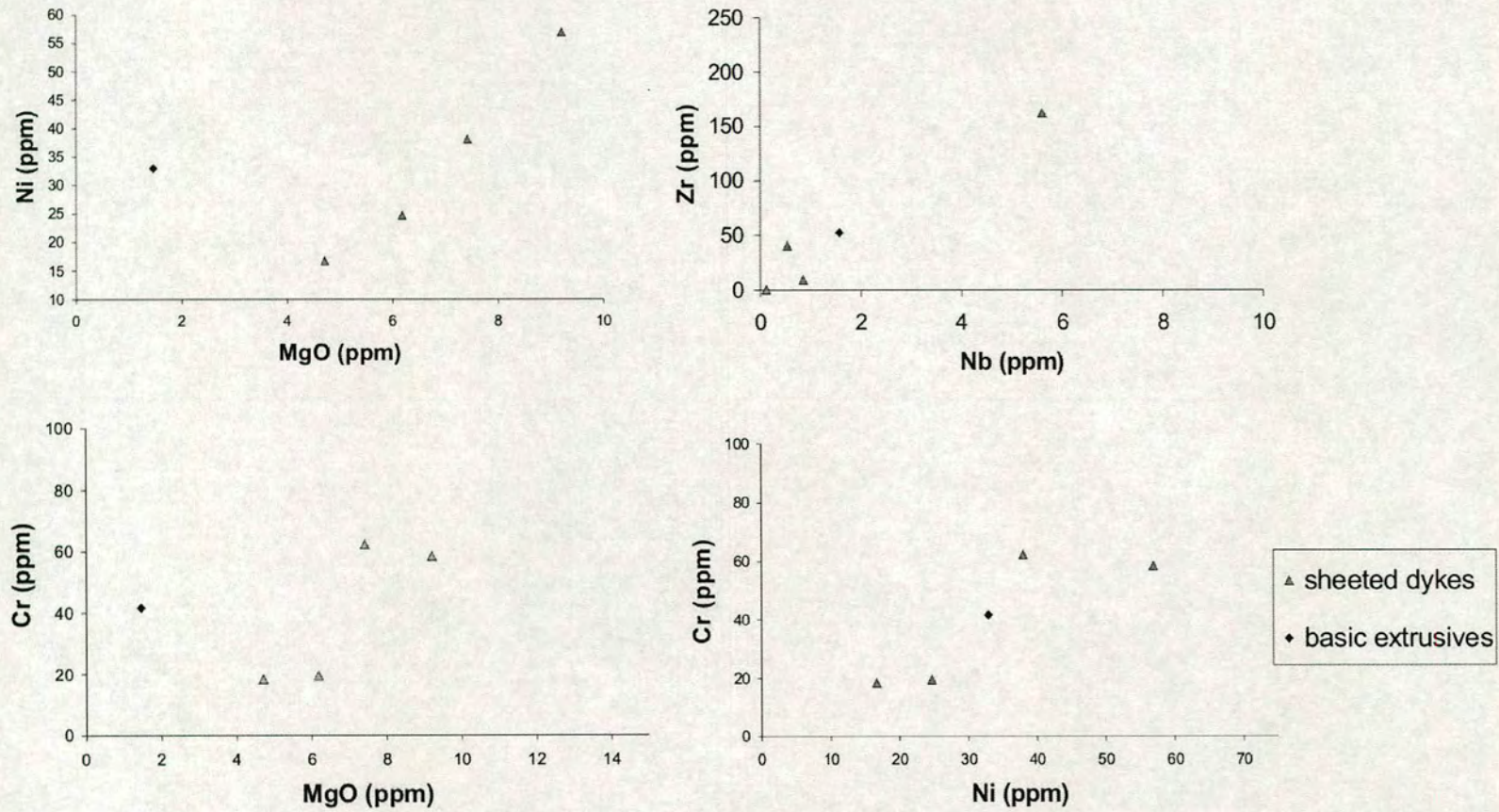


Figure 5.39. Variation diagrams of immobile trace elements for basic igneous rocks of the Kirazbaşı Mélange.

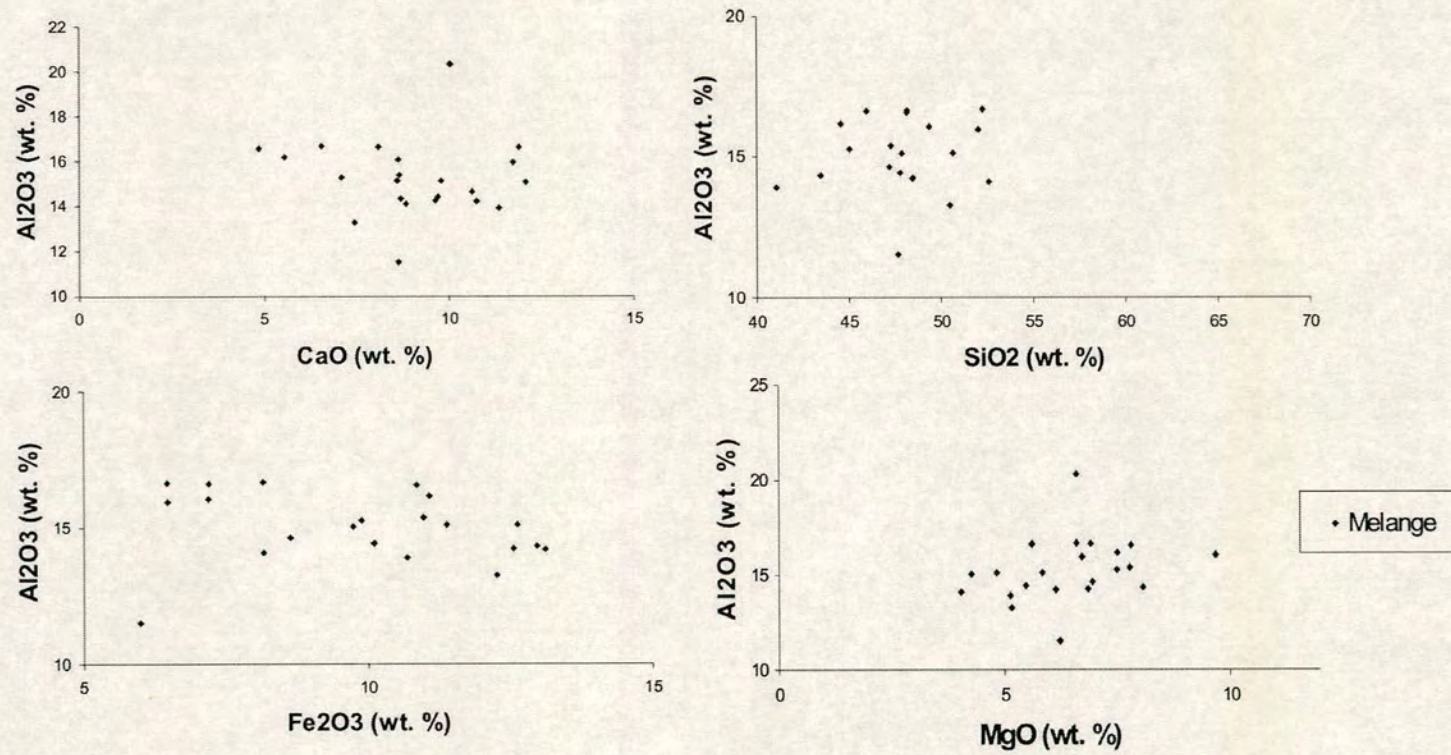


Figure 5.40. Variation diagrams of the mobile elements SiO₂, CaO, Fe₂O₃, and MgO against Al₂O₃ showing element mobility due to alteration of the basic igneous rocks of the Kirazbaşı Mélange.

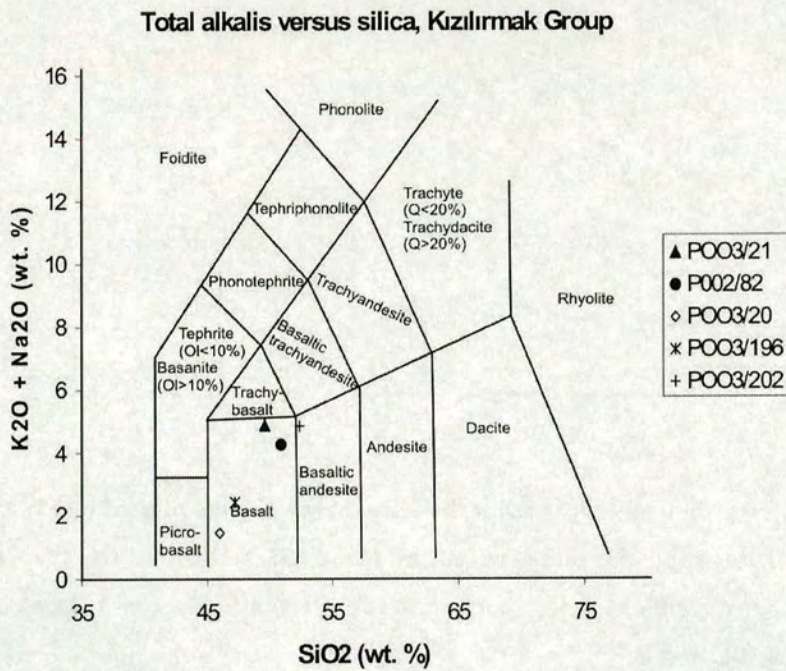


Figure 5.41. Analyses of basic igneous rocks from the Kirazbaşı Mélange plotted on the total alkali-silica (TAS) diagram (Le Maitre et al. 1989).

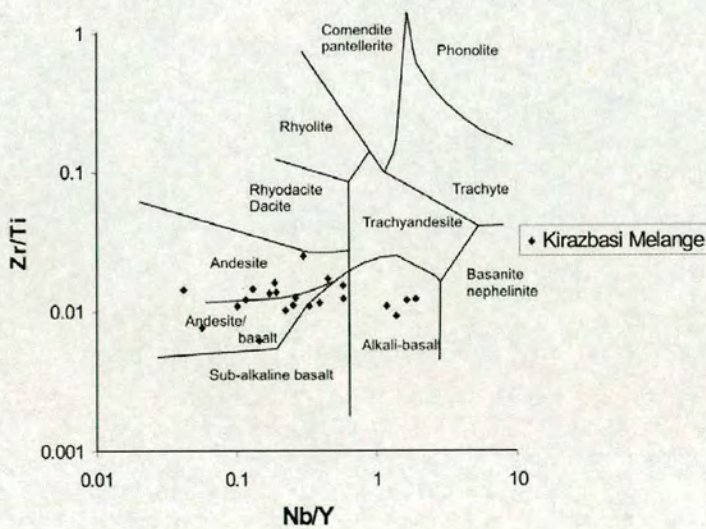


Figure 5.42. Classification of intrusive and extrusive rocks from the Kirazbaşı Mélange using immobile trace elements Zr/Ti versus Nb/Y (diagram after Winchester and Floyd 1979).

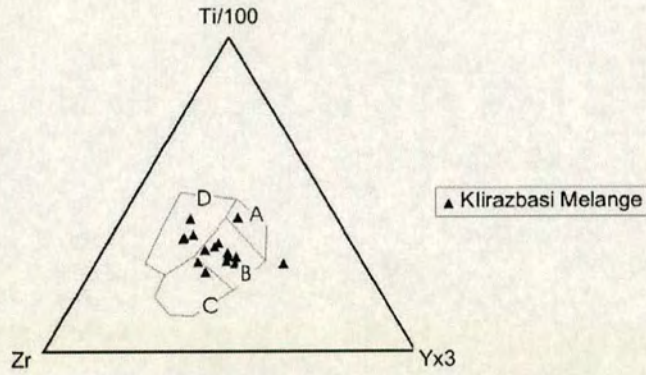


Figure 5.43. Basic igneous rocks from the Kirazbaşı Mélange plotted on the ternary Ti/Zr/Y discrimination diagram (Pearce and Cann 1973). Within-Plate basalts field D, ocean-floor basalts in field B, low-potassium tholeiites in fields A and B, calc-alkali basalts in fields C and B.

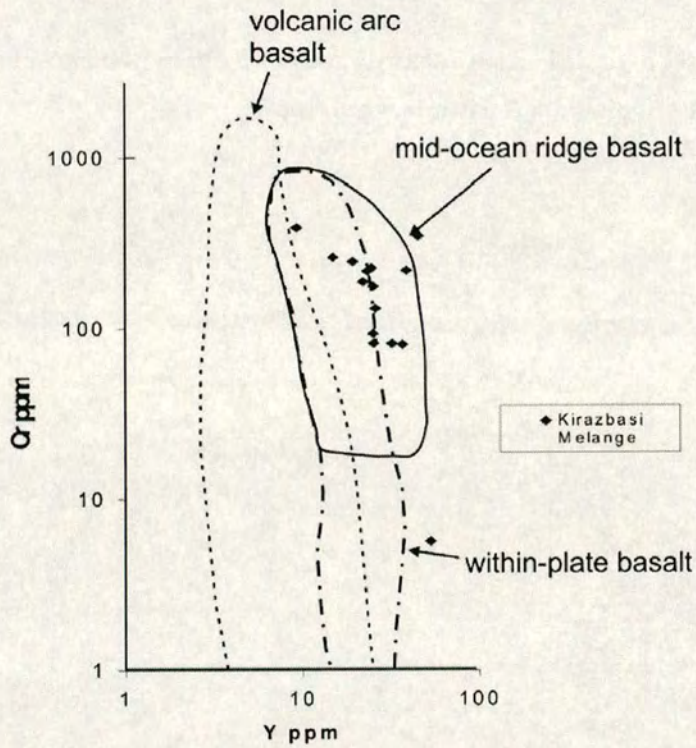


Figure 5.44. Basic igneous rocks from the Kirazbaşı Mélange plotted on the Cr-Y discrimination diagram (Pearce 1982).

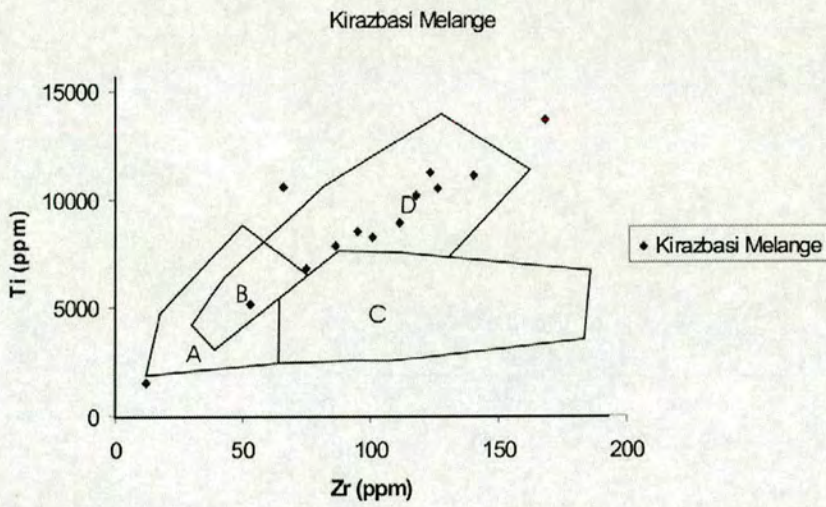


Figure 5.45. Basic igneous rocks from the Kirazbaşı Mélange plotted on the Ti/Zr discrimination diagram (Pearce and Cann 1973). Ocean-floor basalts plot in fields D and B; low-potassium tholeiites in fields A and B, and calc-alkali basalts in fields C and B.

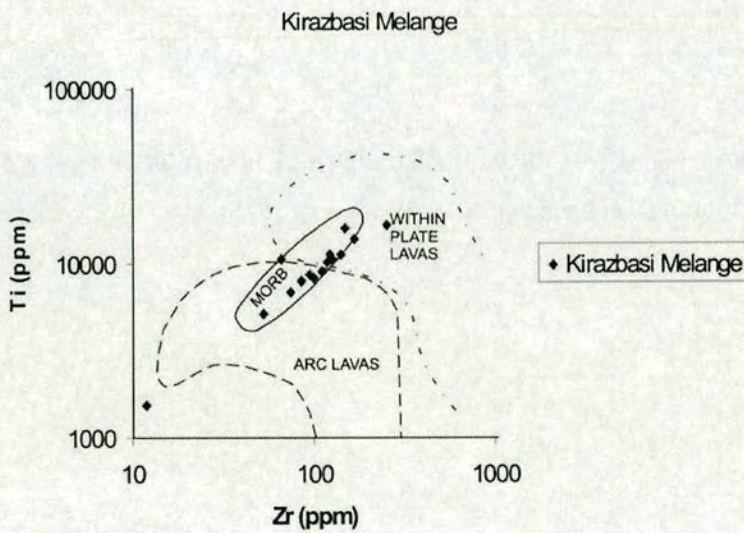


Figure 5.46. Basic igneous rocks from the Kirazbaşı Mélange plotted on the log Ti/log Zr discrimination diagram (Pearce 1982). Ocean-floor basalts plot in fields D and B; low-potassium tholeiites in fields A and B, and calc-alkali basalts in fields C and B.

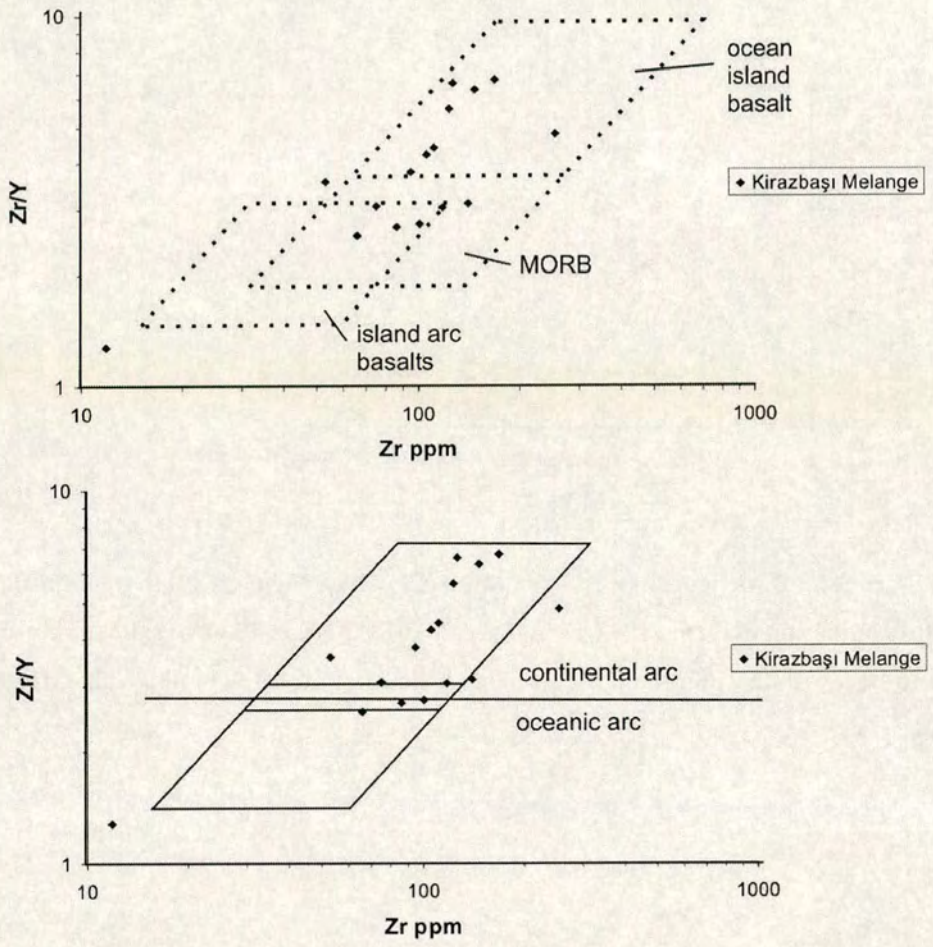


Figure 5.47. Basic igneous rocks from the Kirazbaşı Mélange plotted on the Zr/Y versus Zr discrimination diagram (Pearce and Norry 1979).

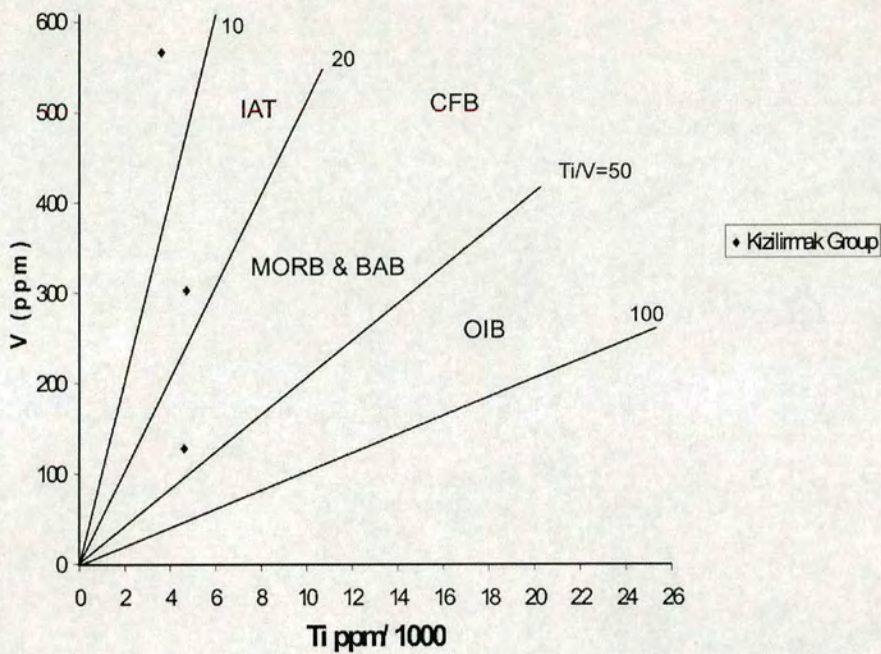


Figure 5.48. Basic igneous rocks from the Kirazbaşı Mélange plotted on the V/Ti discrimination diagram (Shervais 1982).

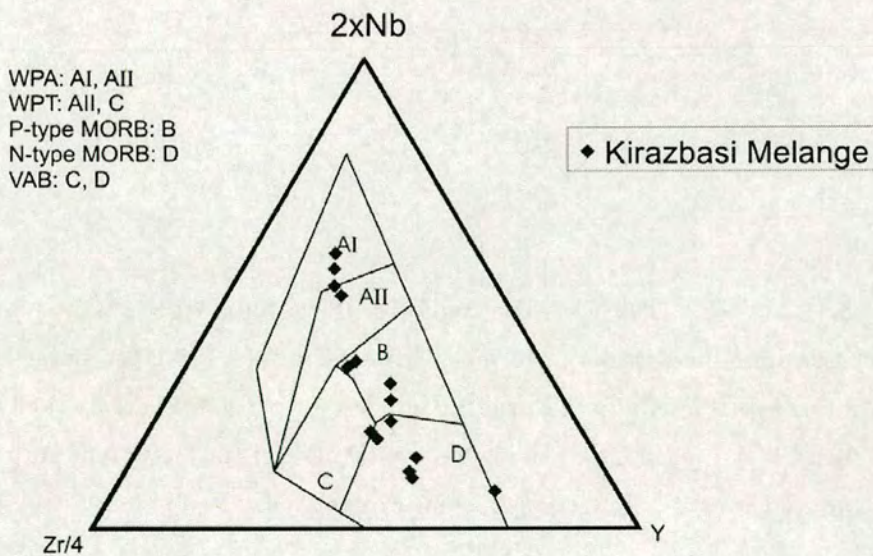


Figure 5.49. Basic igneous rocks from the Kirazbaşı Mélange plotted on the Nb/Zr/Y discrimination diagram (Meschede 1986). AI and AII = within-plate alkali basalt compositional field, B = plume-influenced MORB compositional field, C = within-plate tholeiite compositional field, D = N-type MORB and volcanic arc basalt.

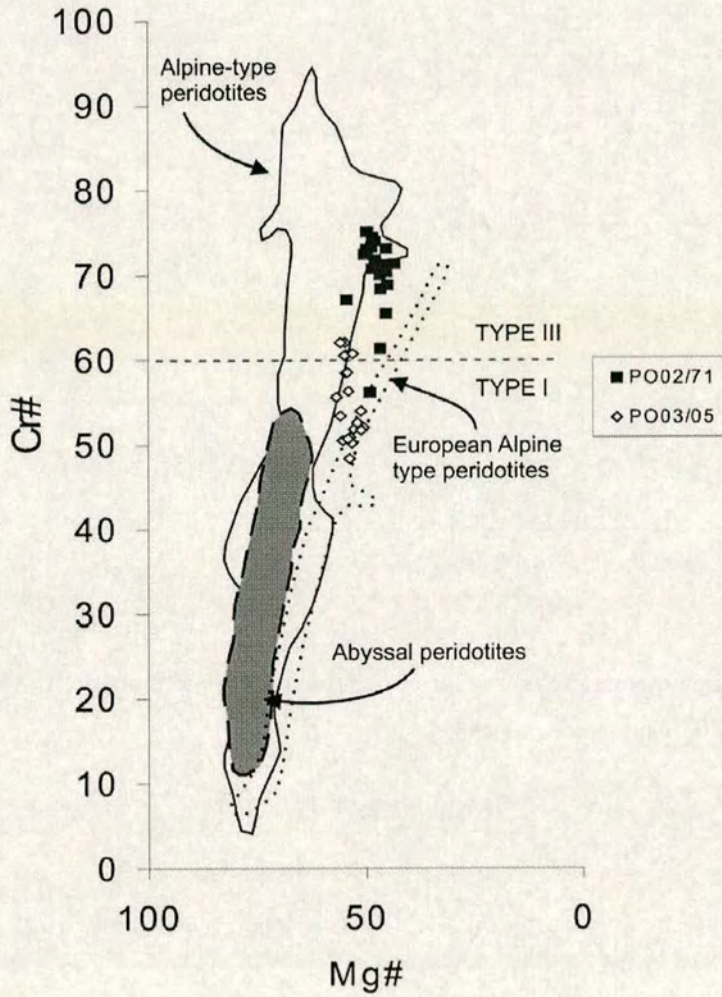


Figure 5.50. Cr# ($(Cr \cdot 100)/(Cr + Al)$) versus Mg# ($(Mg \cdot 100)/(Mg + Fe^{2+})$) for spinels from peridotites within the Kirazbaşı Mélange, Central Pontides. Fields for alpine-type peridotites, abyssal basalts, and European alpine-type peridotites are marked (Dick and Bullen 1984). Line at Cr# = 60 divides 'type I peridotites' from 'type II' peridotites (Dick and Bullen 1984). See section 3.3.9 for explanation.

Tholeiite' none of the samples are shown to be unambiguously of 'Volcanic Arc Basalt'/'Island Arc Tholeiite' composition

Two samples of peridotite from the Kirazbaşı Mélange were analysed by electron probe (see section 3.3.9 for method and explanation). Twenty chromite

grains were analysed from each sample. Figure 5.50 shows chromite compositions for the two peridotite samples from the Kirazbaşı Mélange. The samples are type II peridotites because their composition is intermediate between type I and type III peridotites (Dick and Bullen 1984). The peridotites within the Kirazbaşı mélange have compositions similar to those from backarc basins (Dick and Bullen 1984).

5.4.4 Age, petrogenesis and tectonic setting of the Kirazbaşı Mélange.

The mélange is interpreted as an accretionary complex that developed in response to northward subduction of Neotethys beneath the Pontides. However, the structure of the mélange may be related to emplacement and collisional processes and does not necessarily indicate the direction of subduction. Some of the blocks of basic igneous, volcanic and sedimentary rock were derived from Neotethyan oceanic lithosphere formed at a mid-ocean ridge (e.g. diabase, basalt, radiolarian chert), whereas others were derived from inferred seamounts (basalt-volcaniclastic sedimentary rocks-neritic limestone). Peridotite blocks were probably derived from supra-subduction zone lithospheric mantle. The dominance of oceanic-derived blocks over sedimentary matrix in most of the mélange suggests that the accretionary wedge may have developed in a sediment-starved setting, i.e. an oceanic, rather than a continental margin setting. However, the mélange contains blocks of terrigenous sediment interpreted as a continental slope facies. These blocks are much more common in the north of the area. Their lithology is similar to the Eskiköy Formation. They may have been progressively included into the mélange wedge as it moved, with the trench, northwards towards the continental margin. Alternatively the blocks could have been tectonically included in the mélange during northward backthrusting.

The mélange contains type II peridotites. These peridotites are harzburgites and are interpreted as blocks of lithospheric mantle (i.e. restite). The composition of the chromite grains indicates a degree of depletion through melt extraction that is intermediate between the highly depleted mantle thought to exist beneath volcanic arcs and the less depleted mantle at mid-oceanic spreading ridges (Dick and Bullen 1984). Type II peridotites are found in backarc settings (*ibid*). These blocks represent the lower part of the lithosphere. They are, therefore, unlikely to have been included

into the *mélange* from the downgoing slab. They could have been tectonically included from the overriding plate. Tectonic erosion of the overriding plate must have occurred.

Based on biostratigraphic data (Appendix 1) a maximum age for accretion of the *mélange* is suggested by the youngest known age of blocks in the *mélange* (i.e. Late Maastrichtian). A minimum age of *mélange* accretion and its emplacement is provided by the oldest overlying sedimentary rocks that do not exhibit north-vergent deformational structures; i.e. the Mid Eocene Kadıkızı Formation (section 5.8).

5.4.5 Summary

The Kirazbaşı *Mélange* contains blocks of Albian to Late Maastrichtian age (112-65.5 Ma). This range represents the age of the Neotethyan lithosphere that was subducted and provides a maximum age of *mélange* accretion (i.e. Late Maastrichtian). The Kirazbaşı *mélange* is interpreted as an accretionary complex that developed in response to northward subduction of Neotethys and contains two lithological associations; 1) a chert-basalt-serpentinite-clastic association that represents oceanic lithosphere with a terrigenous sedimentary cover; 2) a massive limestone-volcaniclastic association that represents a volcanic seamount facies.

Whole-rock geochemistry of basic igneous rocks from the Kirazbaşı Mélange indicates that the lavas have ‘within-plate’ and MORB compositions. Some of the samples have compositions that are ambiguous and could be either MORB or ‘Island Arc Tholeiite’. The Kirazbaşı mélange has a paucity of sedimentary matrix relative to blocks of ophiolitic association (e.g. peridotite, diabase, chert). This indicates a low degree of sediment accretion and/or deposition at the trench. The mélange could have formed in an oceanic setting, far away from the continental margin. Blocks of terrigenous sediment are common within the mélange in the north of the area while blocks of pelagic chert, sheeted dykes and gabbro are more common in the south. This could represent the original transition between the continental margin in the north and oceanic lithosphere to the south. The blocks of terrigenous sediment could have been progressively accreted into the mélange as it approached the continental margin. Alternatively the terrigenous sedimentary blocks could have been tectonically included during backthrusting.

The Kirazbaşı mélange exhibits a pervasive north-vergent shear fabric and top-to-the-north thrust faults. The top-to-the-north fabric could be related to northwards emplacement of the mélange onto the Eurasian margin. Top-to-the-south thrusts and shear-zones cut the top-to-the-north structures and juxtapose the mélange against various other units. top-to-the-south structures are interpreted as collision-related. The Kirazbaşı mélange is unconformably overlain by Mid Eocene sediments that locally do not exhibit north vergent structures.

5.5 Emplaced volcanic arc: Yaylaçayı Formation

Two major thrust slices of volcanic and volcanoclastic rocks, each up to ~4 km thick, occur at two different structural levels in the central Pontides (Figure 5.51, Figure 5.55). The lower thrust slice was first named the Yaylaçayı Formation by Yoldaş (1982). The presence of several species of *Globotruncana* (see Appendix 1) within interbedded sediments of the Yaylaçayı Formation indicates a Late Cretaceous (Campanian-Maastrichtian) age for this unit (Tüysüz et al. 1995; Prof. Izver Ongen, Prof. Kemal Taşlı and Prof. Nurdan İnan pers. comm. 2004). This lower thrust slice crops out at the northern edge of the Çankırı Tertiary Basin, near İskilip and Yapraklı (Figure 5.51). The lower thrust slice is not highly deformed or

metamorphosed (Figure 5.53) and exhibits primary sedimentary and igneous structures, e.g. well preserved pillows (Figure 5.54) and cross-laminations. The structurally higher thrust slice (Koşdağ Formation of Tüysüz 1990) crops out further north, near Tosya (Figure 5.51). This thick (4 km) thrust sheet exhibits dynamometamorphic fabrics which have largely destroyed the primary sedimentary and igneous structures. The upper thrust slice is mainly composed of tightly folded and thrust porphyroblastic greenschists (Figure 5.55).

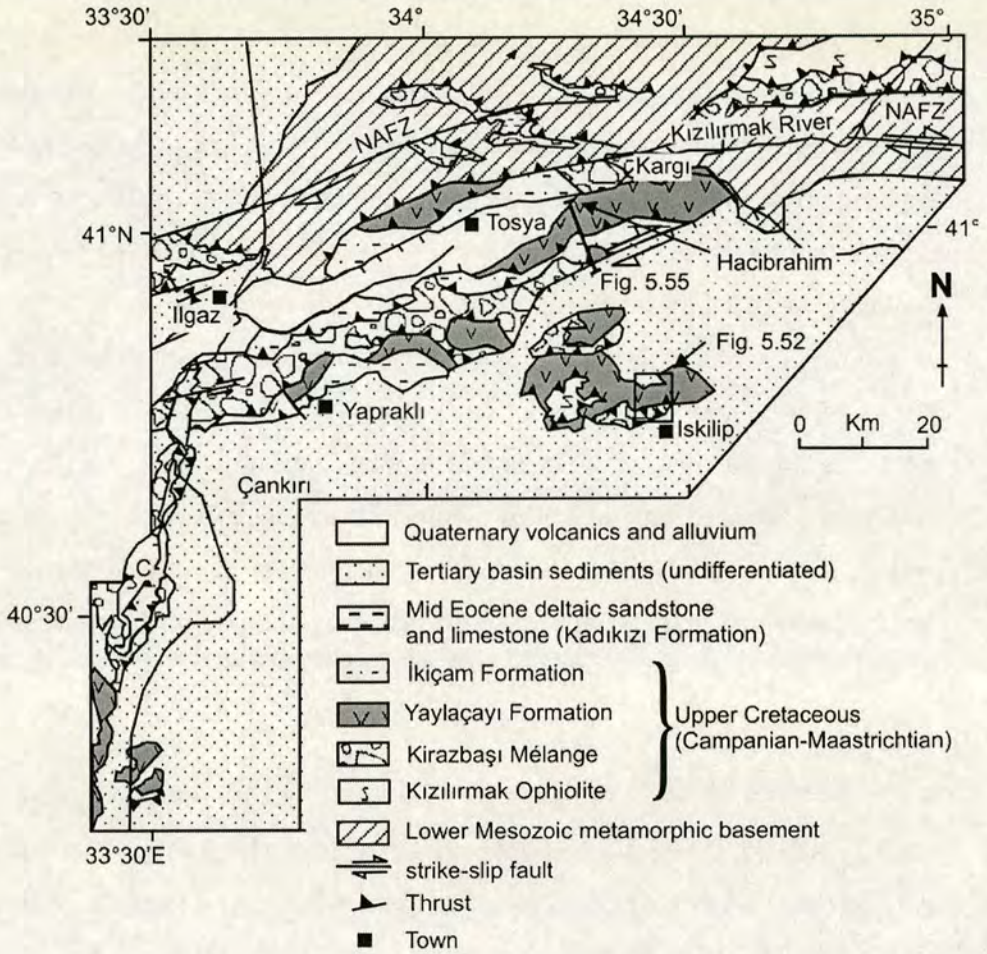


Figure 5.51. Simplified geological map of the Central Pontides showing the outcrop of the Yaylaçayı Formation (including the Koşdağ Formation of Tüysüz 1990).

5.5.1 Structure of the Yaylaçayı Formation

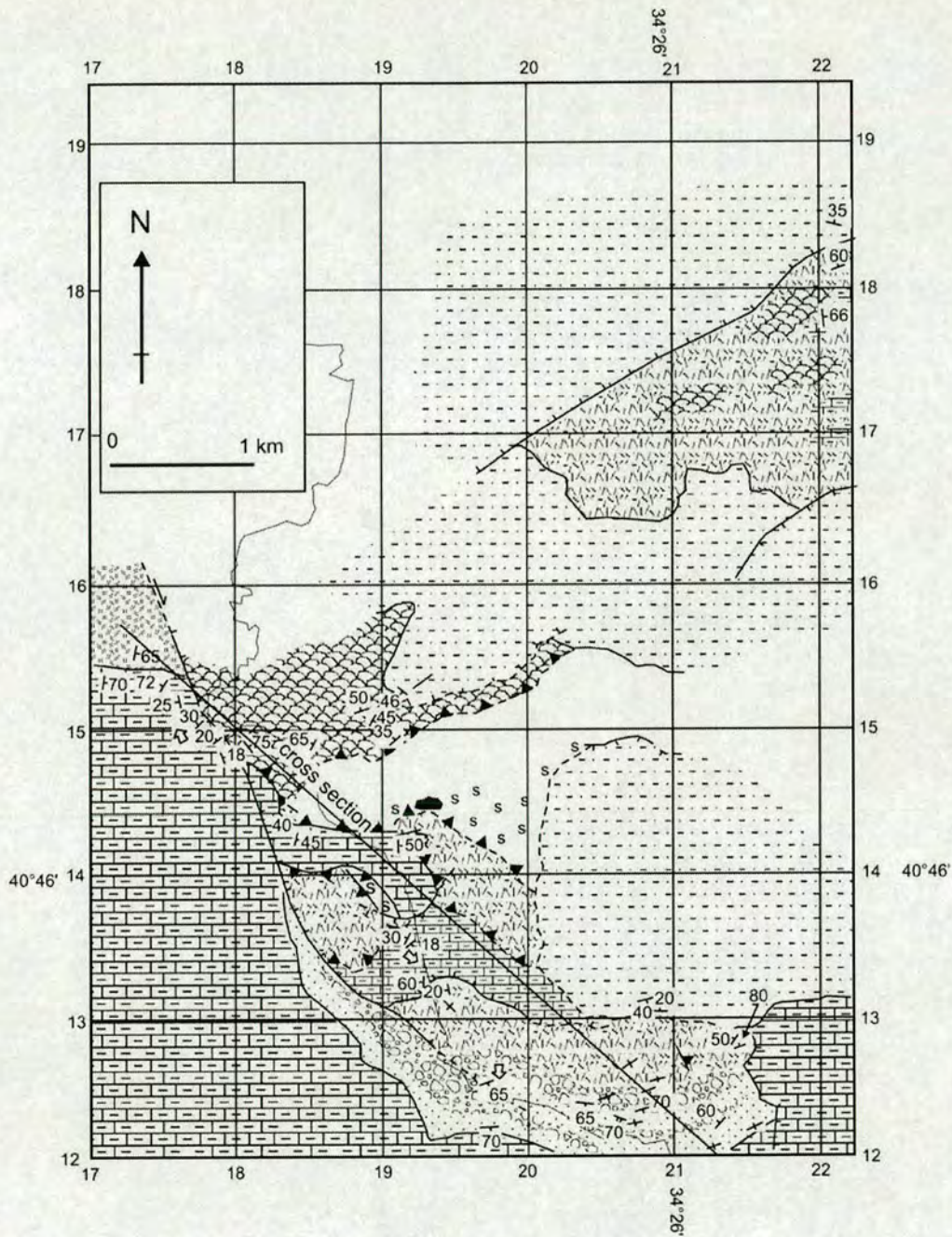


Figure 5.52. Geological map of the Yaylaçayı Formation in the Iskilip area. For location see Figure 5.51. For section a – a' see Figure 6.53. For legend see Figure 6.1.

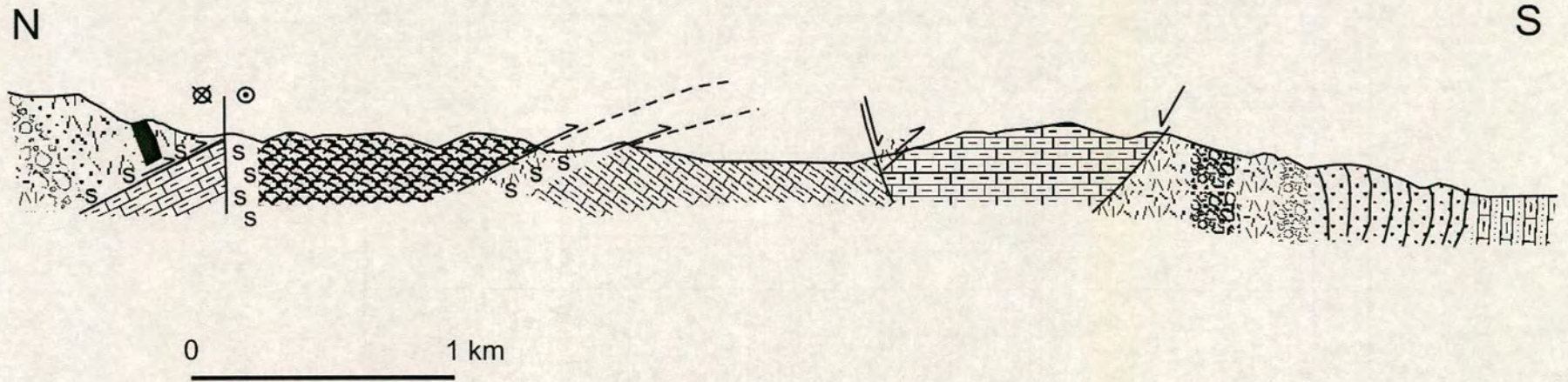


Figure 5.53. Cross-section through the Yaylaçayı Formation near Iskilip. See Figure 5.52 for location. For legend see Figure 5.1.

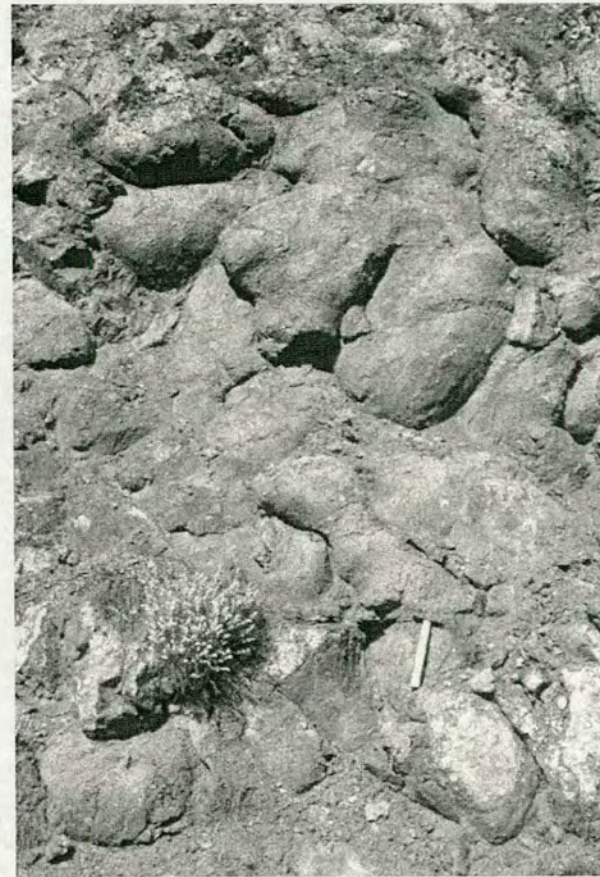


Figure 5.54. Photographs showing volcanic rocks in the stratigraphically lower part of the Yaylaçayı Formation near Iskilip. 1; andesitic debris-flow conglomerate. 2; pillow lava.

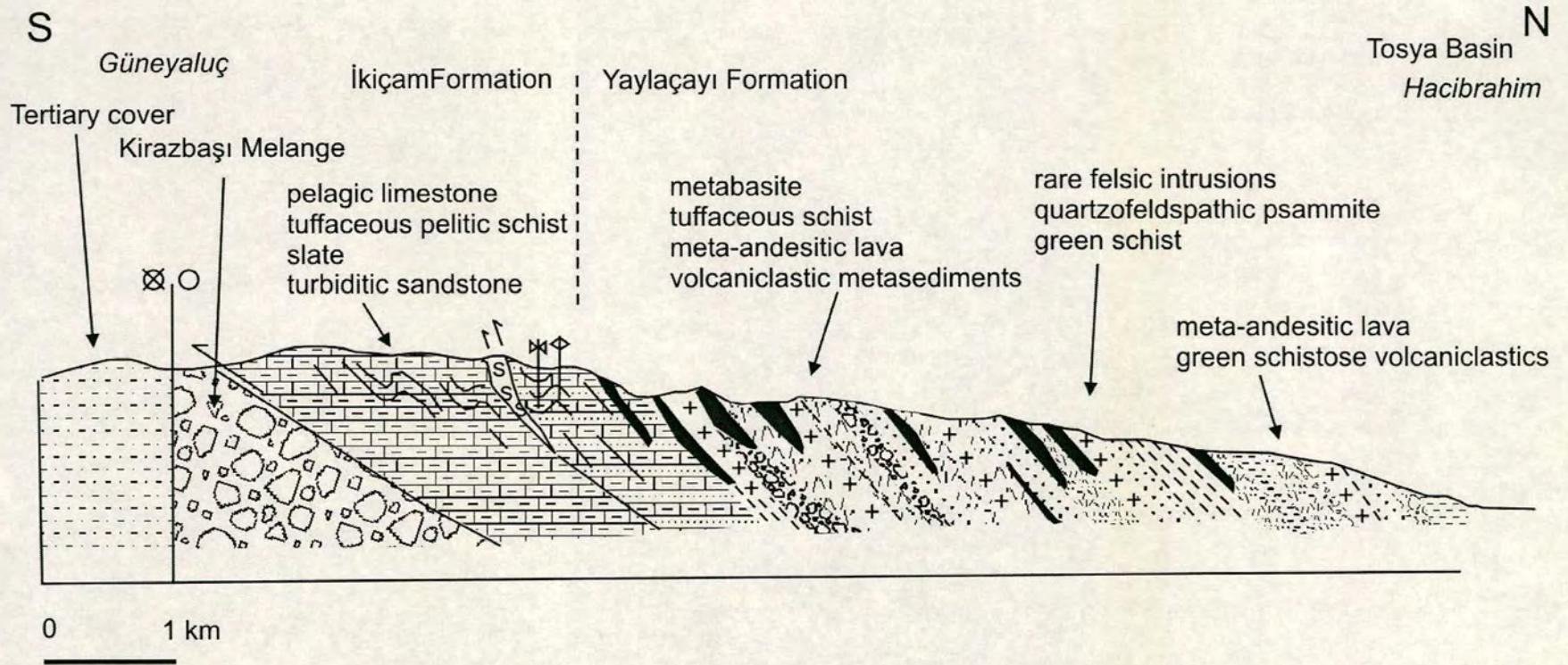


Figure 5.55. Cross-section through the Yaylaçayı Formation south of Hacibrahim (Koşdağ Formation of Tüysüz 1990; gr: F32, 0513344005).

The lower thrust slice of the Yaylaçayı Formation (exposed near Iskilip; Figure 5.51) is not well cleaved and does not exhibit a pervasive shear fabric or small-scale folding. The unit is folded and faulted on a large scale (fold wavelength >1 km) and cut by localised zones of strong shearing. Based on sedimentary structures and pillow morphology the unit youngs both to the northwest and to the southeast, due to folding. Beds are locally overturned with fold limbs that dip in either direction. This suggests that the large folds verge and face in both directions. However, the overall large scale structure is unclear. The structurally higher thrust slice, exposed ~10 km southeast of Tosya (Figure 5.51) is well cleaved and exhibits a strong dynamo-metamorphic fabric.

In the lower thrust slice limestone and sandstone beds locally form a small (individual thrust slices ~10 m thick) top-to-the-north duplex (Figure 5.53), as seen at the southern end of the section at Iskilip. These thrust-faulted beds occur within the south-dipping limb of a larger fold. Thin, top-to-the-north shear zones are seen in this part of the unit. Pillow lavas are folded into a recumbant northwest-facing syncline at the northern end of the Iskilip section. The steeply dipping short limb youngs northwards and the fold axial surface dips ~20° to the southeast. Cleavage planes generally dip moderately south (Figure 5.56a, b), sub-parallel to the south-dipping fold axial surface in the pillow lavas. This asymmetrical fold geometry suggests northwest vergence.

The upper thrust slice (Koşdağ Formation of Tüysüz 1990) exhibits a range of fold geometries. Pelitic schists exhibit recumbent polyclinal and disharmonic folds, in addition to north-vergent tight chevron folds ~10 km S of Tosya. Anastomosing conjugate kink bands, with a range of orientations (between subhorizontal and vertical) were observed in greenschist metavolcaniclastic sedimentary rocks.

In contrast to the lower thrust slice (exposed at Iskilip and Yapraklı), the structurally higher thrust slice (Koşdağ Formation of Tüysüz 1990), well exposed ~10 km southeast of Tosya, exhibits a pervasive shear fabric dipping northwest (e.g. 40°N/050). The upper thrust slice is schistose. The schistosity, cleavage and bedding are commonly sub-parallel (i.e. slaty cleavage) and dip to the northwest and to the southeast (Figure 5.55 and 5.57). Cleavage strikes NE-SW and has been folded

around upright sub-horizontal axes that trend NE-SW (F2). Pebbles in schistose volcanoclastic conglomerate are flattened in the S1 cleavage plane. Metavolcanic schists exhibit augen with long axes orientated $\sim 20^\circ$ to 240° .

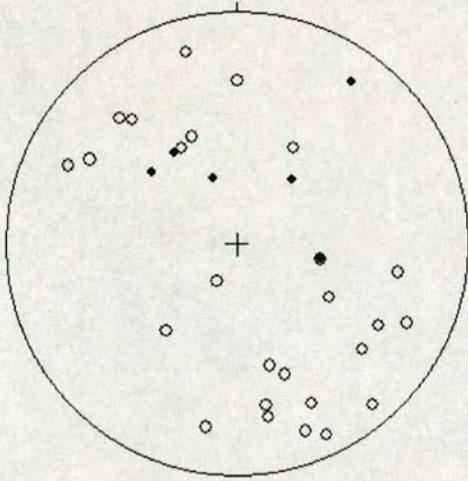
The dominant dip direction of cleavage and bedding is to the northwest since F2 folds are asymmetrical, verging southeast. Stretching lineations, crenulations, axes of augen and fold axes plunge gently to the northeast and southwest, i.e. roughly normal to the dominant dip azimuth of cleavage and bedding planes, and roughly parallel to the strike direction (045°).

In the lower thrust slice, top-to-the-south shear zones cut the volcanic section at Yapraklı (Figure 5.51), forming a duplex structure. Right way-up beds that dip and young southwards crop out in the southern part of the road section at İskilip (Figure 5.52, 5.53). The axis of a recumbent southeast-facing synclinal fold was measured $20^\circ\text{N}/185^\circ$ plunging 20° to 285° in this part of the section. Small-scale (wavelength < 2 m) south-vergent, south-facing, tight to open recumbent and inclined folds were observed in sandstones near İskilip. The fold axes there plunge at $\sim 10^\circ$ to 250° . Bedding planes strike NE-SW (Figure 5.56a, d). The strike of these beds is concordant with folding around NE-SW trending sub-horizontal fold axes Figure 5.56c. South-vergent folds were observed north of İskilip that fold top-to-the-north shear zones.

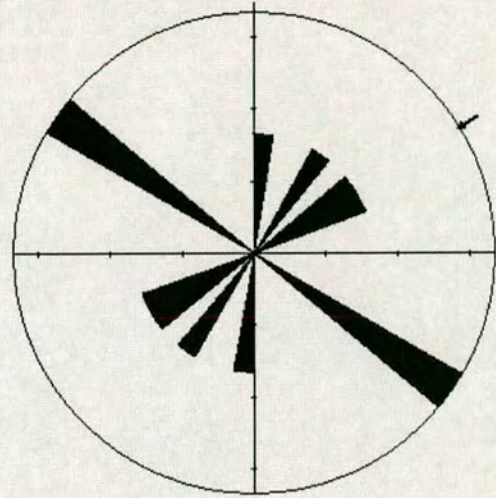
The section of the lower thrust slice near İskilip is cut by numerous shear zones, thrusts, strike-slip faults and normal faults. Figure 5.58 shows fault orientation data for the Yaylaçayı Formation. Thrust faults with top-to-the-north slickensides dip between 20° and 80° to the southeast and generally strike ENE-WSW. Thrusts exhibiting top-to-the-south slickensides dip at 45° to 50° towards the northwest and also strike ENE-WSW.

SOUTH

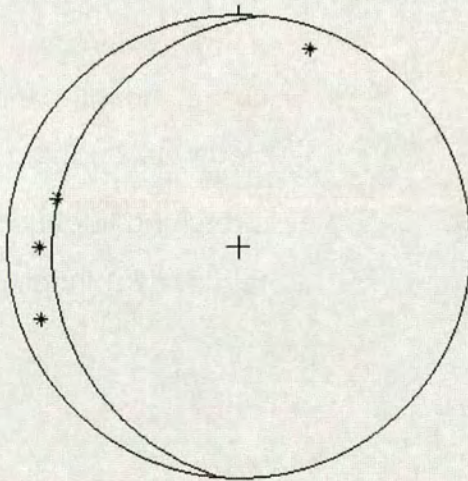
a) poles to bedding and cleavage



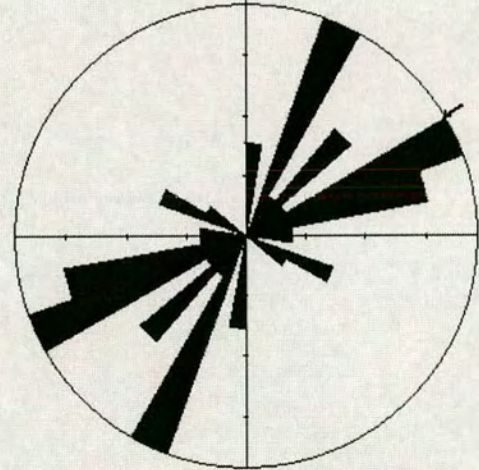
b) strike of cleavage



c) fold data



d) strike of bedding

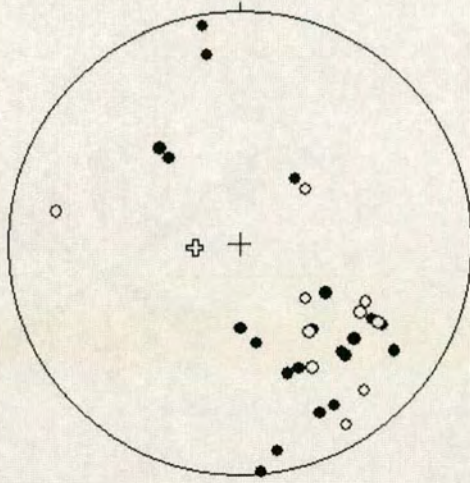


- poles to bedding
- poles to cleavage
- * fold axes (plunge)

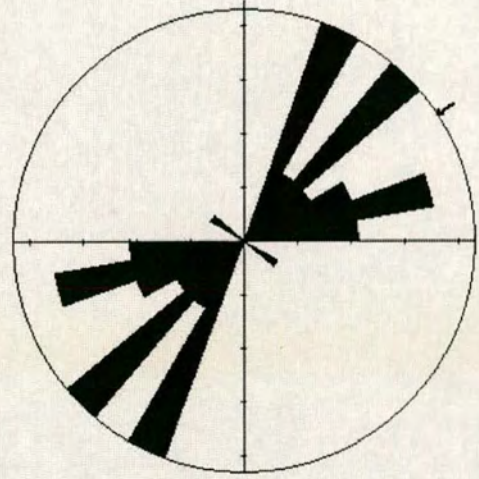
Figure 5.56. Structural data from the lower thrust sheet of the Yaylaçayı Formation.

NORTH

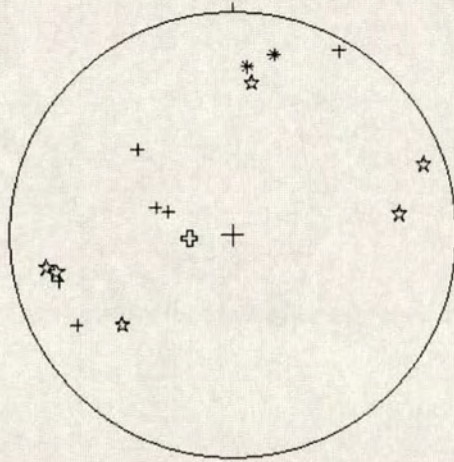
a) poles to bedding and cleavage



b) strike of cleavage



c) fold data



- poles to bedding
- poles to cleavage
- ☆ crenulation lineation
- ⊕ cleavage-bedding intersection
- + stretching lineation
- * fold axes (plunge)

Figure 5.57. Structural data from the upper thrust sheet of the Yaylaçayı Formation (Koşdağ Formation of Tüysüz 1990).

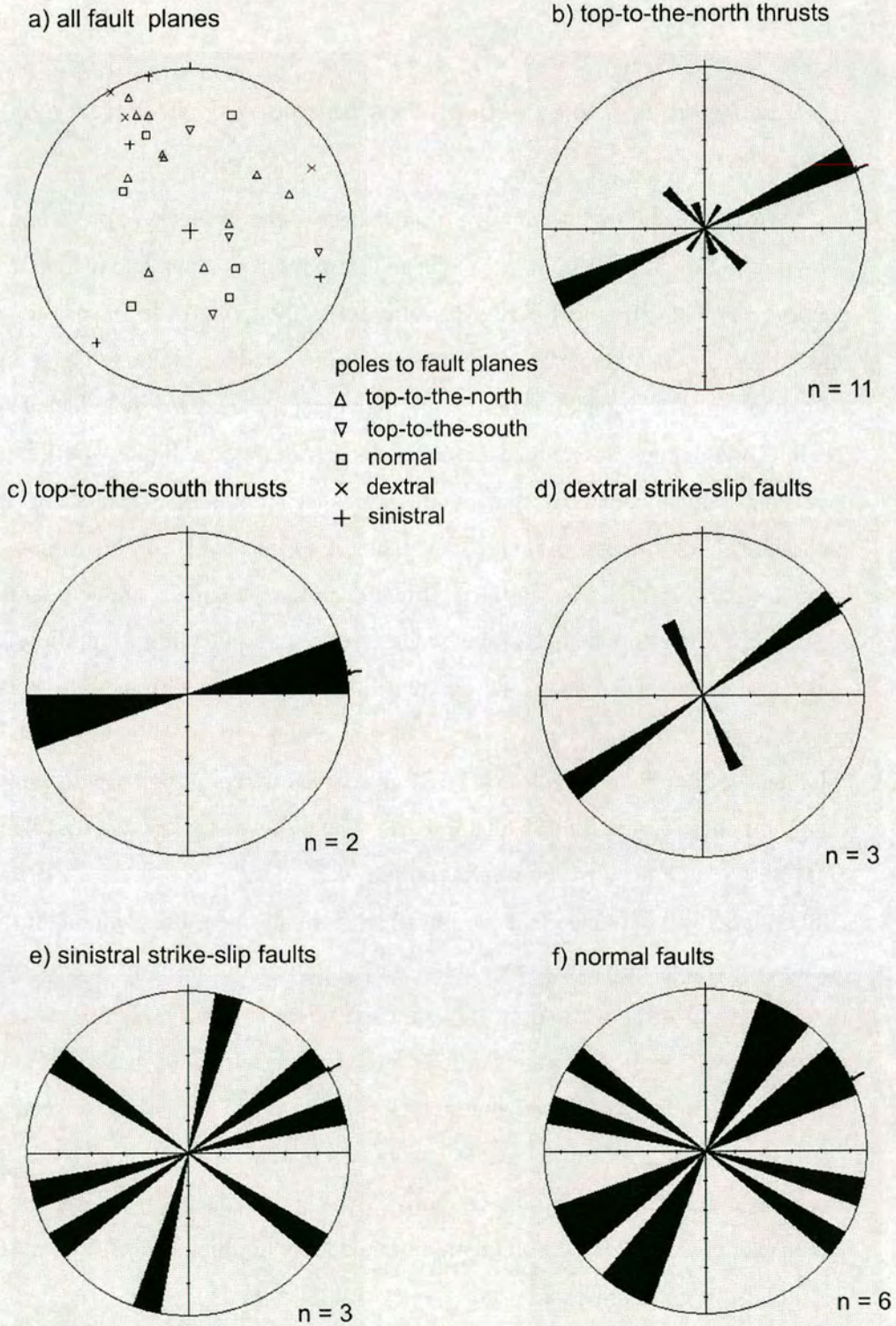


Figure 5.58. Fault data for the Yaylaçayı Formation (upper and lower thrust slices combined).

5.5.2 Sedimentary facies and igneous petrology of the Yaylaçayı Formation

A composite log of the lower thrust sheet of the Yaylaçayı Formation is shown in Figure 5.59. Within the Yaylaçayı Formation as a whole, volcanic rocks become magmatically more evolved stratigraphically upwards, from basaltic, to andesitic, then felsic (e.g. rhyodacite). Fine-grained sediments including chert, umber and micritic limestone are present between pillow lavas low in the succession. Texturally immature volcanoclastic sediments predominate at higher stratigraphic levels until the volcanoclastic succession grades into fine-grained sandstone, shale and micritic limestone, (~500 m thick) at the top of the sequence; this is then unconformably overlain by Tertiary sediments of the Çankırı Basin, near Iskilip.

The lower thrust slice of the Yaylaçayı Formation begins with pillow lavas and minor amounts (<5% by outcrop area) fine-grained inter-pillow sediments and passes gradually upwards into a very thick succession (up to 3500m apparent thickness) of dominantly andesitic lava and coarse matrix-supported volcanoclastic conglomerates (Figure 5.59, 5.60 and 5.61). The pillow lavas are mostly vesicular and feldspar and/or pyroxene-phyric. In thin section, the pillow lavas are seen to contain large (<2 cm long) feldspar phenocrysts (andesine-labradorite in thin section), glomoporphyritic diopside (<3 mm) and rare iddingsite pseudomorphs after olivine (<1 mm), set in a matrix of plagioclase feldspar laths and clinopyroxene. Trachytic and decussate textures are observed in the matrix. Amygdales contain zeolites and calcite. Deformed and metamorphosed felsic intrusions are seen in the upper thrust slice. Andesitic lava flows increase in abundance stratigraphically upwards at the expense of pillowed mafic flows. The andesitic flows contain large (<1 m) xenoliths of basic lava and are interbedded with thick (<3 m) lenses of volcanoclastic conglomerate.

The volcanoclastic conglomerates (present in both thrust slices) are thickly bedded (<3 m) and massive with scoured bases and lack sedimentary structures. The conglomerates exhibit a matrix-supported fabric with poorly sorted with sub-angular to sub-rounded clasts. Both the clasts and the matrix of the volcanoclastic

conglomerates are pale pink-purple in colour. The clasts are feldspar-phyric, vesicular and of intermediate composition (based on petrographic evidence). Felsic volcanics, intrusive rocks and altered tuff are present in lesser amounts. The conglomerates are interstratified with feldspar-phyric andesitic lava flows < 10 m thick and rare columnar-jointed basic lava flows. The lava and volcanoclastic sedimentary rocks become finer-grained and less abundant stratigraphically upwards, and grade into a lava-free volcanoclastic sandstone, shale and carbonate succession.

Stratigraphically higher levels are dominated by a sedimentary succession (< 300 m thick near İskilip) comprising volcanoclastic sandstone and shale, grading into pale grey, thinly bedded shaly, sandy and micritic limestones (Figure 5.62 and 5.63).

The volcanoclastic sandstones are dark grey-brown, medium to thickly bedded, coarse to fine-grained and moderately- to well- sorted. The grains are sub-angular and are composed of quartz, feldspar, mafic minerals and mafic volcanic lithoclasts. In thin section, some sandstones contain grains of pale pink, isotropic sodalite. Sedimentary structures include normally graded bedding, cross- and planar lamination, and load-casts with well-formed flames and lobes. Individual beds are commonly massive at the base and grade into thin laminated siltstone tops. These sedimentary structures represent the five 'Bouma' divisions that characterize the sedimentary deposits of turbidity currents (Ta-Te; Bouma 1962), although not all of the divisions are exhibited by each individual bed. Sandy limestones in the Yaylaçayı Formation contain sub-angular clasts of volcanogenic quartz, feldspar, pyroxene, olivine and biotite (<50% in total), in addition to calcite grains. Neither the sandstones nor the limestones contain muscovite, metamorphic quartz, or metamorphic lithoclasts. The absence of metamorphic detritus is confirmed in thin sections (Figure 5.64).

The stratigraphically highest levels of the formation are transitional to pelagic limestone in the İskilip area, whereas along strike, near Çankırı (Figure 5.51), the andesitic volcanic succession is unconformably overlain by a shallow-marine

Yaylaçayı Formation

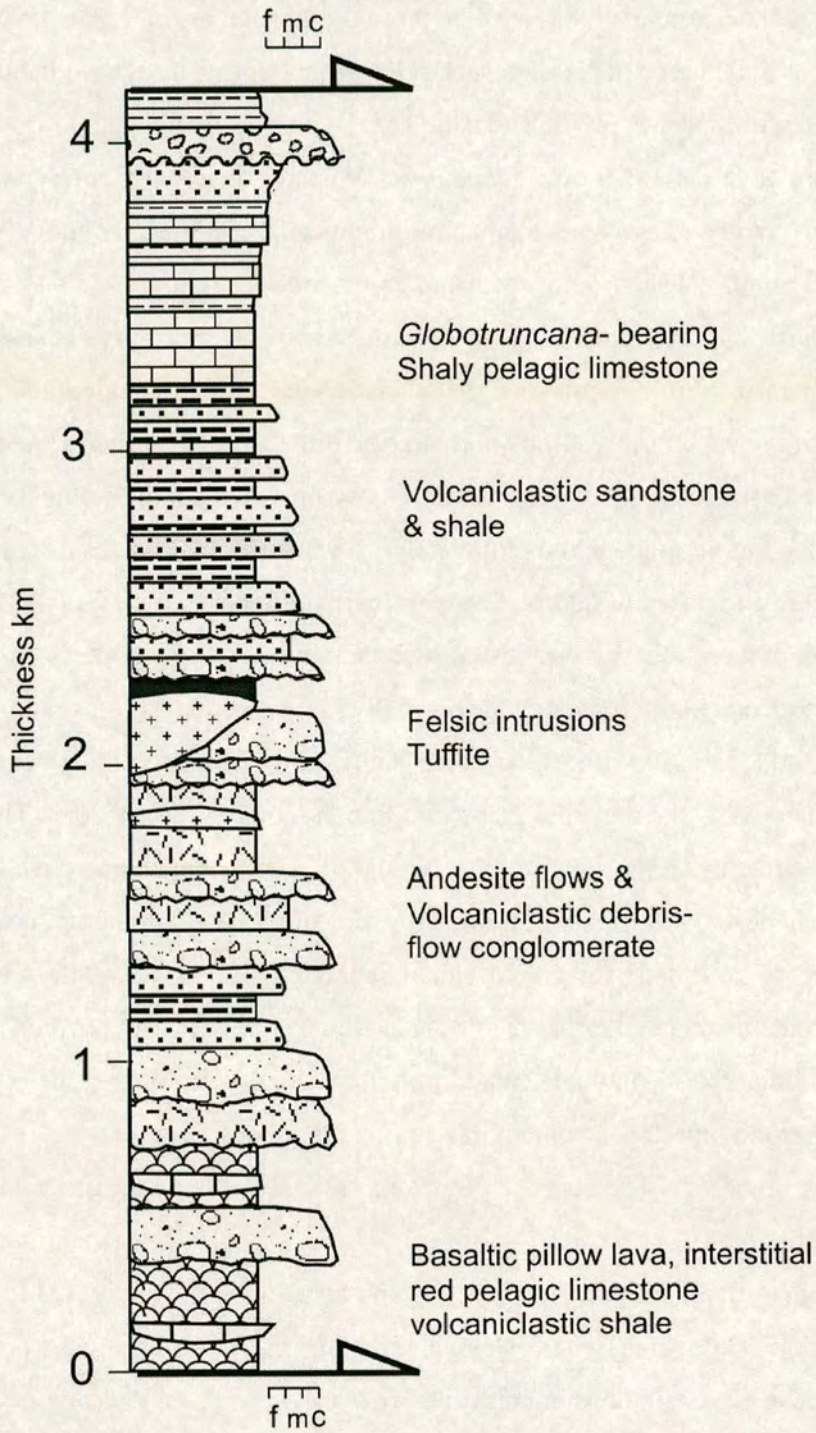


Figure 5.59. Composite log of the Yaylaçayı Formation (lower and upper thrust slices combined).

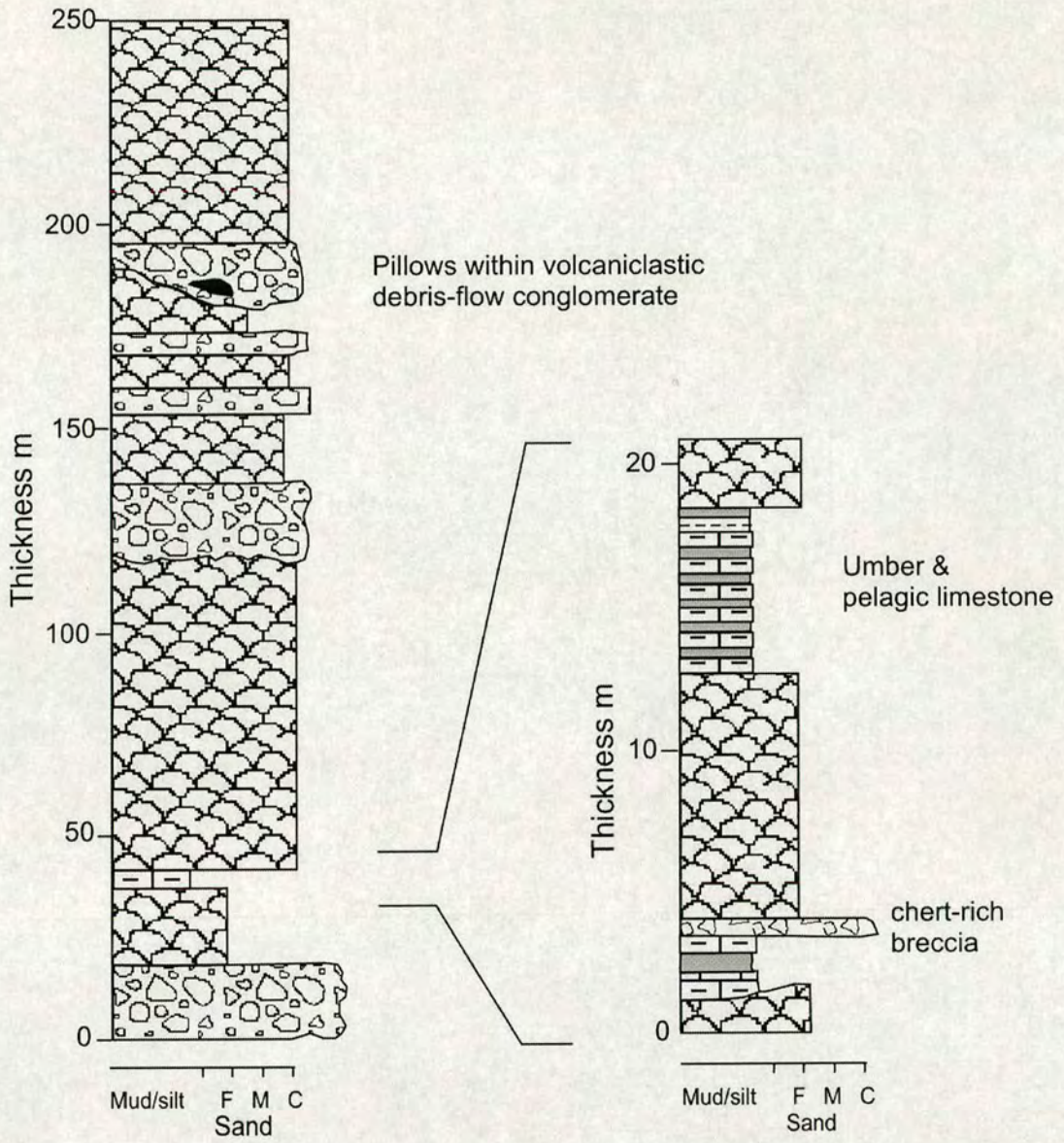


Figure 5.60. Measured log of the stratigraphically lowest part of the lower thrust slice of the Yaylaçayı Formation, exposed north of Iskilip (gr: G32, 1817514787).

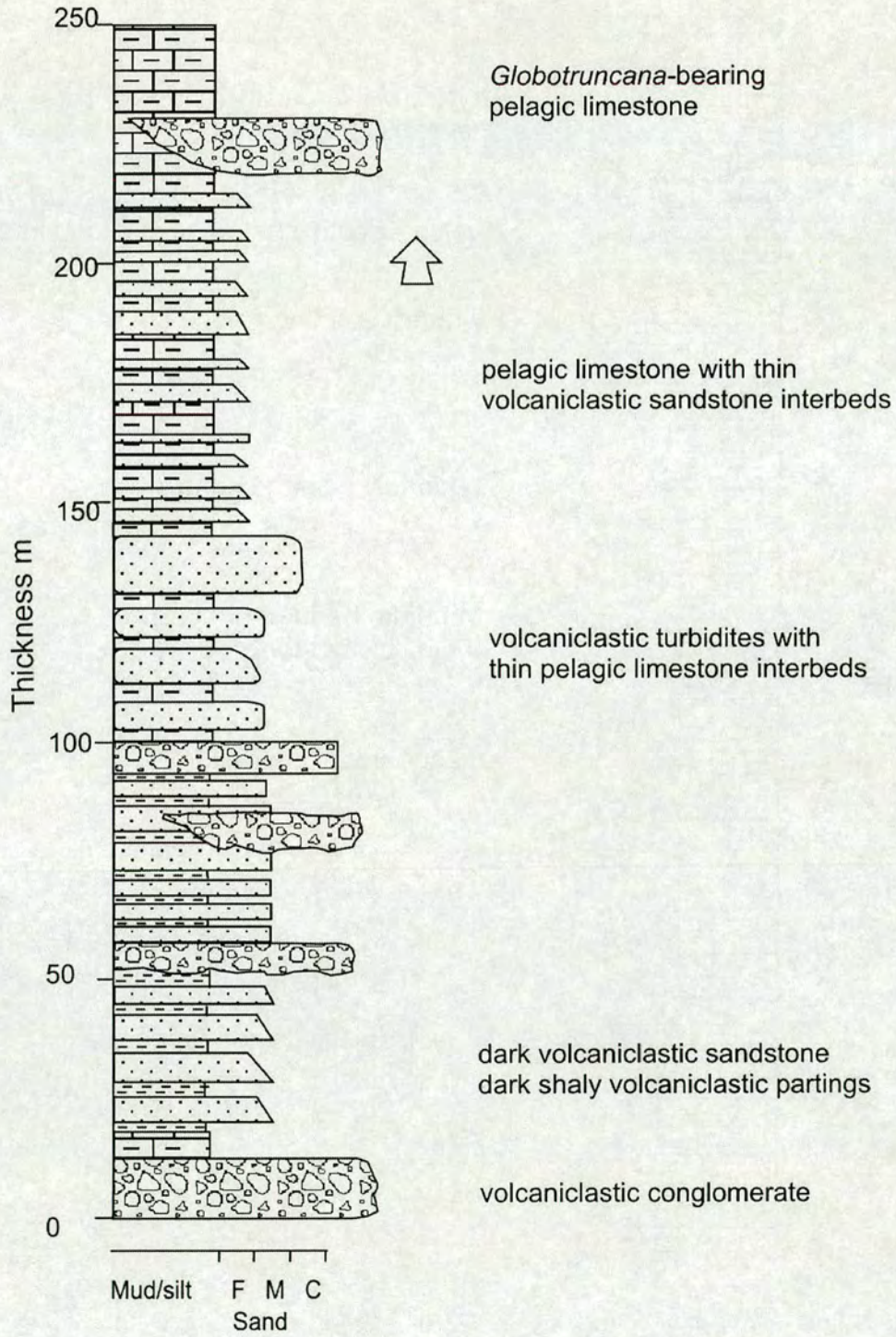


Figure 5.62. Measured log of part of the Yaylaçayı Formation exposed north of Iskilip (gr: G32, 2116711963).

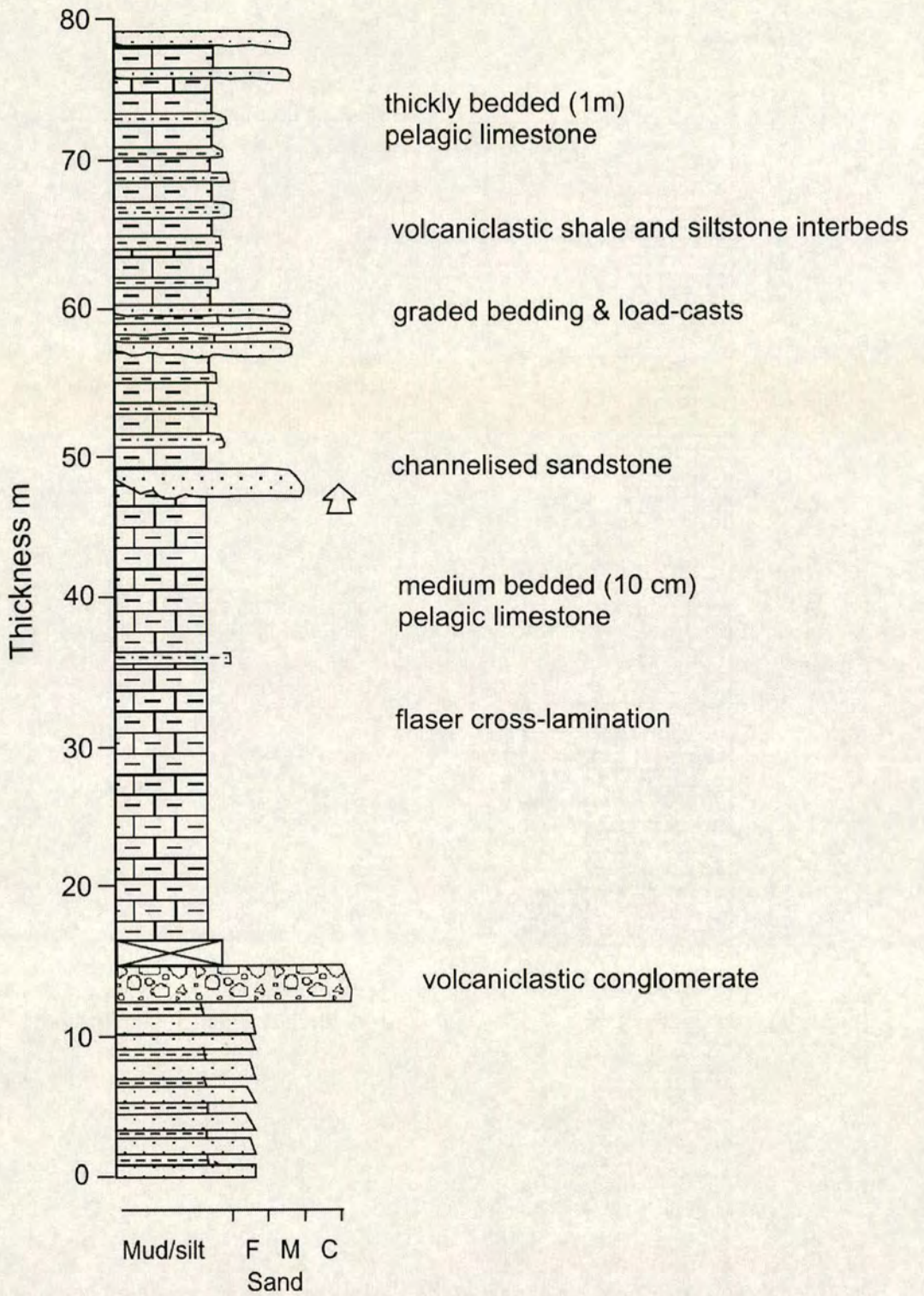


Figure 5.63. Measured log of part of the Yaylaçayı Formation exposed north of Iskilip (gr: G32, 2120011425).

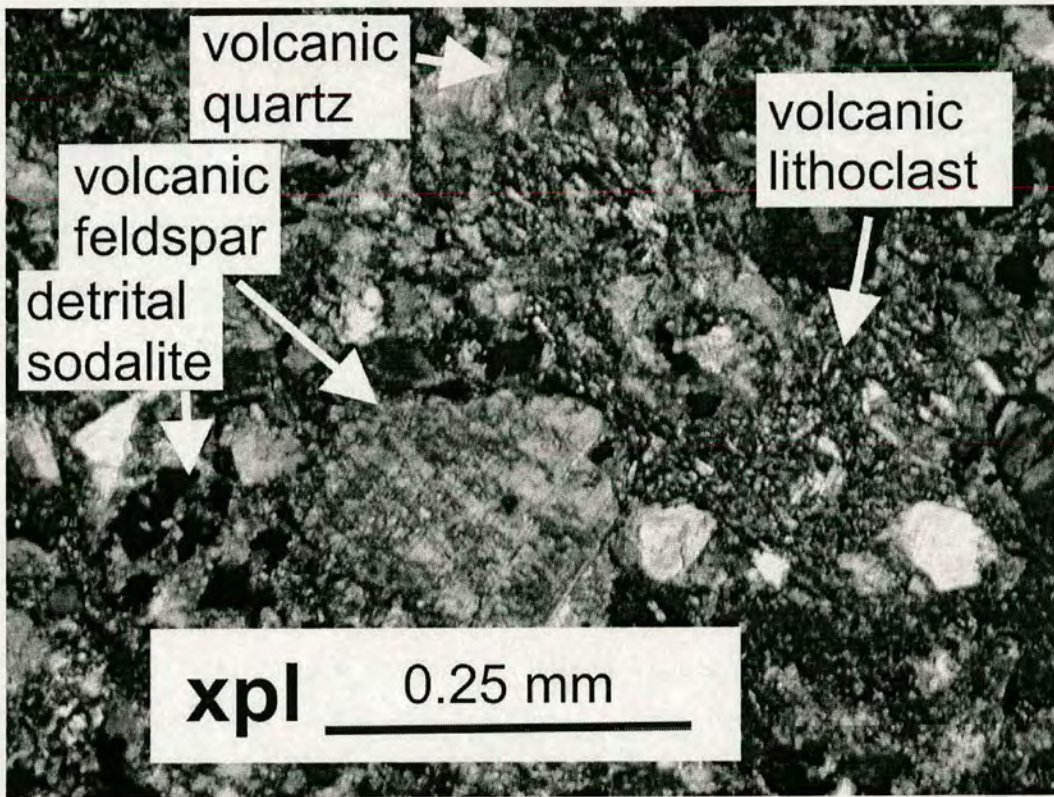


Figure 5.64. Photomicrograph of a typical volcanoclastic sediment from the Yaylaçayı Formation north of Iskilip. Note the absence of metamorphic detritus.

sedimentary cover (Yapraklı Formation; section 5.6). At high structural levels (i.e. the upper thrust slice exposed near Tosya) the dominant lithologies, chloritic pelite, schistose volcanoclastic and metavolcanic rocks, with a greenschist facies mineral assemblage (5.5.3). As a result of the strong shearing and internal deformation in the Tosya area details of the individual protolithologies are much less easy to recognise and interpret than in the much less deformed lower thrust slice (at Iskilip and Yapraklı).

5.5.3 Metamorphic petrology of the Yaylaçayı Formation

Rocks from both the upper and lower thrust slices of the Yaylaçayı Formation contain the assemblage epidote+chlorite+calcite+ quartz+albite+pyrite+zeolite. The metamorphic minerals are more abundant in the structurally higher parts of the unit. Metamorphic fabrics such as schistosity, lamination fabric, mylonite, pressure

solution and, crenulation cleavage, porphyroblasts, porphyroclasts and bearded 'fish' are much better developed in the structurally higher thrust slice exposed further north, e.g. along the banks of the Devrez River near Tosya (Figure 5.51).

5.5.4 Whole-rock igneous geochemistry of basic-intermediate lavas

Thirty four non-porphyritic, non-vesicular and petrographically fresh samples of mafic lava from the Yaylaçayı Formation were analysed by XRF for whole-rock abundances of major and trace elements (section 3.3.8 and Appendix 2 for analytical procedure). Fifteen of the samples fell within the acceptable range for naturally occurring unaltered basic igneous rocks ($\text{SiO}_2 < 54\%$, $\text{MgO} + \text{CaO} < 12-22\%$). These 15 samples are plotted on Harker diagrams showing the variation between immobile Al_2O_3 and the potentially mobile elements CaO, SiO_2 , Fe_2O_3 and MgO (Figure 5.65). Between the samples there are slight correlations between the abundances of the mobile elements and immobile Al_2O_3 . This suggests that the abundances of these elements have not been greatly affected by post-magmatic mobilisation during alteration, metamorphism or weathering of the Yaylaçayı Formation. Figure 5.66 shows Harker diagrams for pairs of relatively immobile elements in the samples from the Yaylaçayı Formation. With the exception of Ni/MgO there is a good correlation between the samples, suggesting that they belong to a comagmatic suite (e.g. Hall 1996).

The 15 samples with acceptable values for basic igneous rocks are classified using the total alkalis vs. silica diagram in Figure 5.67. The samples are seen to have basic compositions equivalent to tephrite, basanite, basalt, basaltic andesite, trachybasalt and foidite. A classification based on immobile trace elements (Figure 5.68) shows that in 8 of the samples the basic composition is a reflection of their primary igneous chemistry and not a result of element mobilisation during secondary processes. However, 7 samples are shown to have immobile element compositions indicative of intermediate (andesitic) primary rock compositions and are therefore not useful for tectonic discrimination (section 3.3.8).

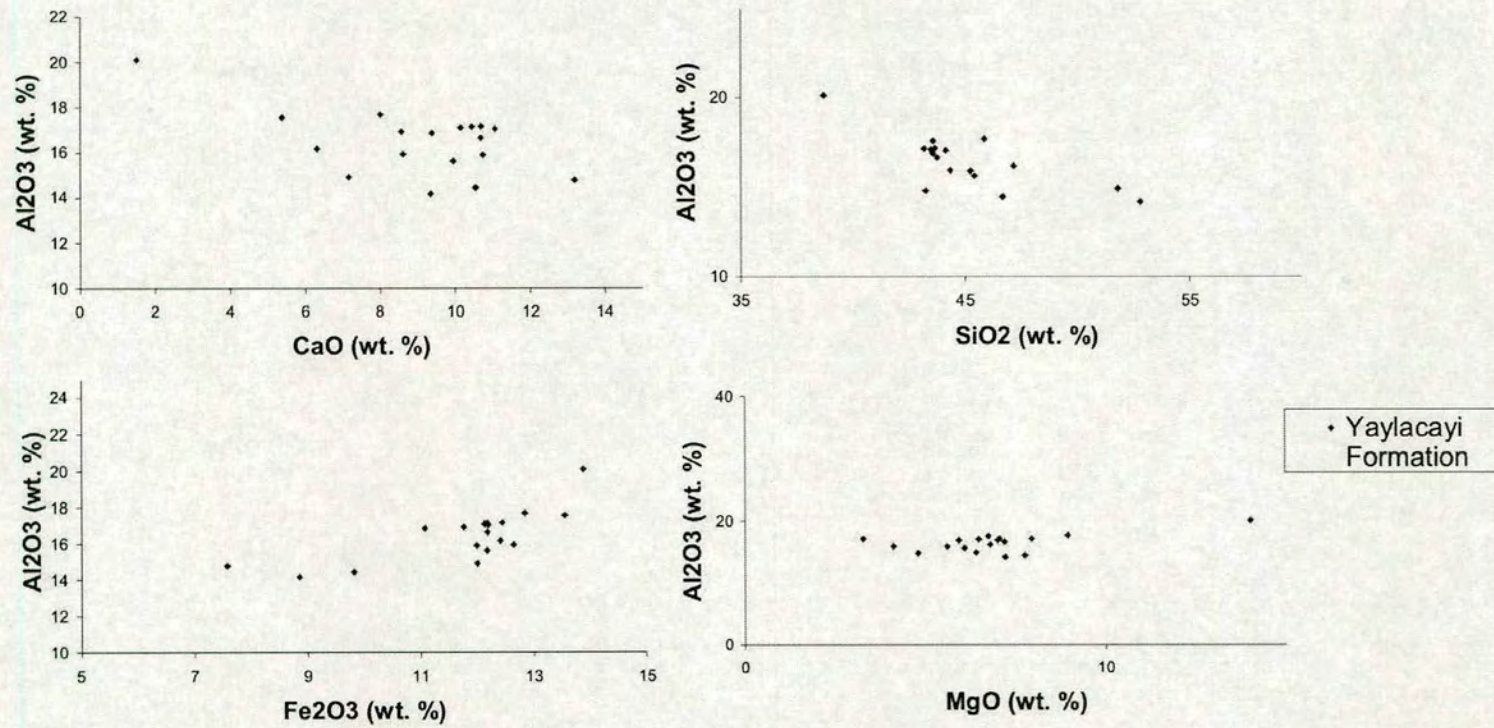


Figure 5.65. Harker diagrams showing variation between abundances of pairs of potentially mobile elements in 18 lava samples from the Yaylacayı Formation.

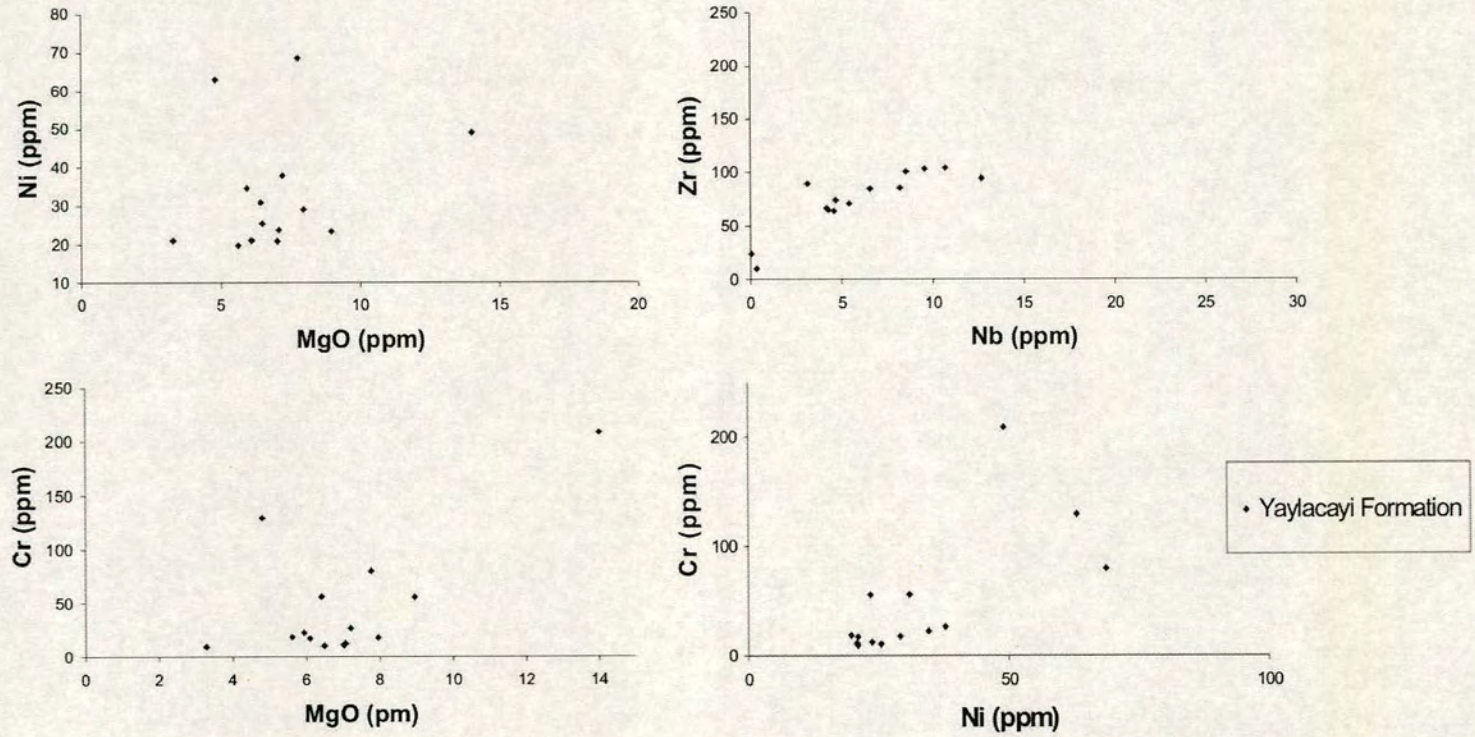


Figure 5.66. Harker diagrams showing variation between abundances of pairs of immobile elements in 18 lava samples from the Yaylacayı Formation.

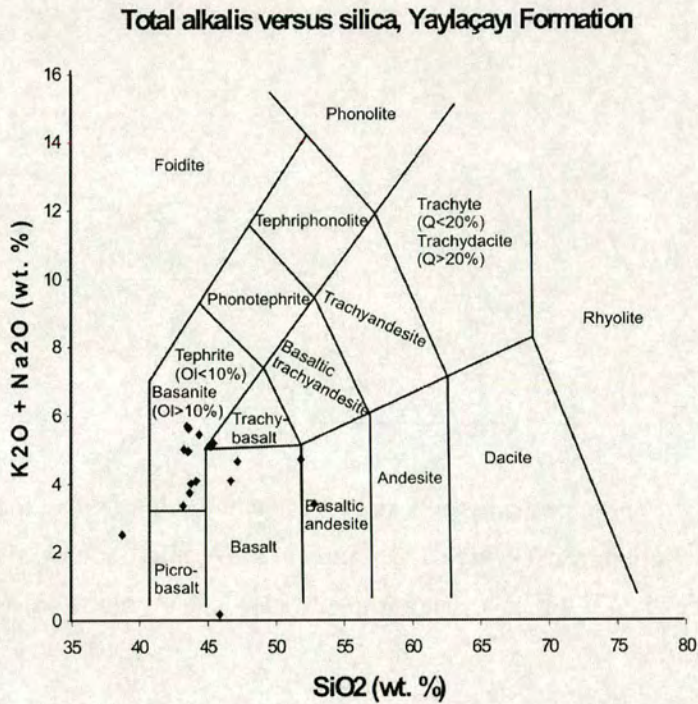


Figure 5.67. Samples from the Yaylaçayı Formation plotted on the total alkalis-silica rock classification diagram (Le Maitre et al. 1989).

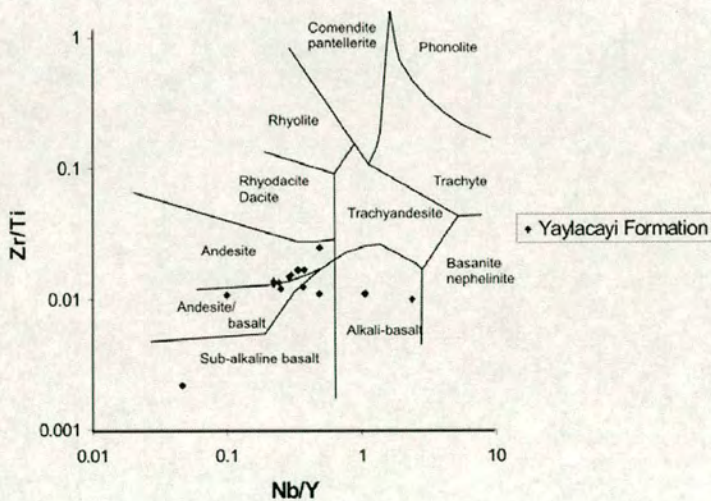


Figure 5.68. Classification of rock samples from the Yaylaçayı Formation using immobile trace element ratios Zr, Ti, Nb and Y (Winchester and Floyd 1977).

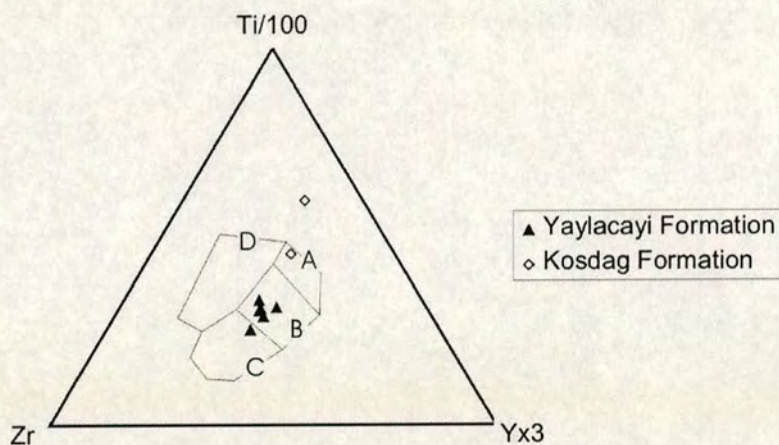


Figure 5.69. Basic igneous rocks from the Yaylaçayı Formation plotted on the ternary Ti/Zr/Y discrimination diagram (Pearce and Cann 1973). Within-plate basalts field D, ocean-floor basalts in field B, low-potassium tholeiites in fields A and B, calc-alkali basalts in fields C and B.

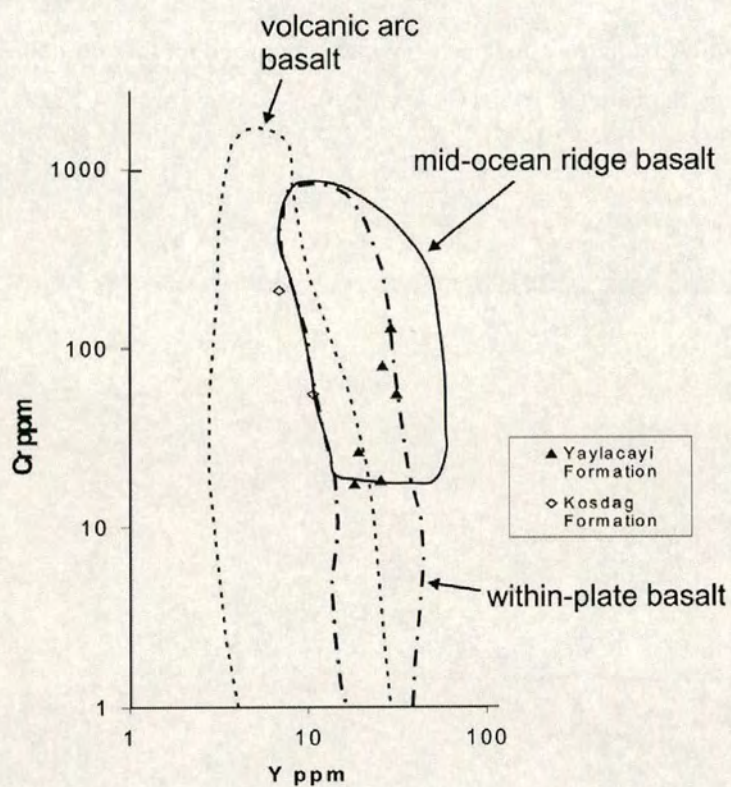


Figure 5.70. Basic igneous rocks from the Yaylaçayı Formation plotted on the Cr-Y discrimination diagram (Pearce 1982).

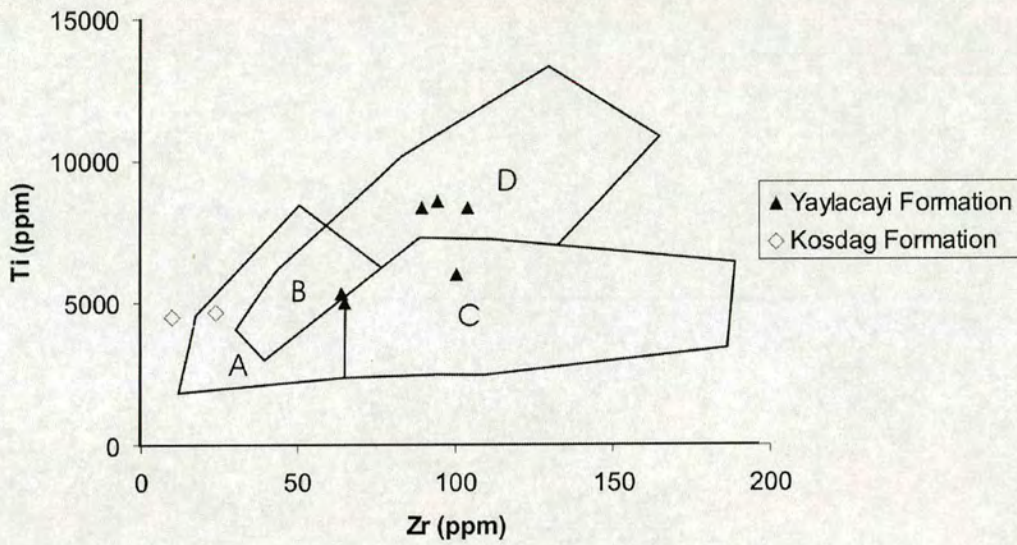


Figure 5.71. Basic igneous rocks from the Yaylacayi Formation plotted on the Ti/Zr discrimination diagram (Pearce and Cann 1973). Ocean-floor basalts plot in fields D and B; low-potassium tholeiites in fields A and B, and calc-alkali basalts in fields C and B.

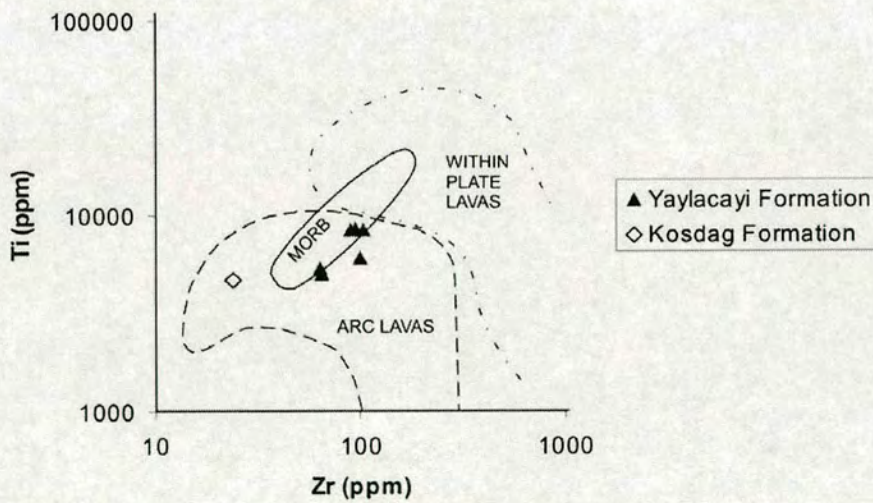


Figure 5.72. Basic igneous rocks from the Yaylacayi Formation plotted on the log Ti/log Zr discrimination diagram (Pearce 1982). Ocean-floor basalts plot in fields D and B; low-potassium tholeiites in fields A and B, and calc-alkali basalts in fields C and B.

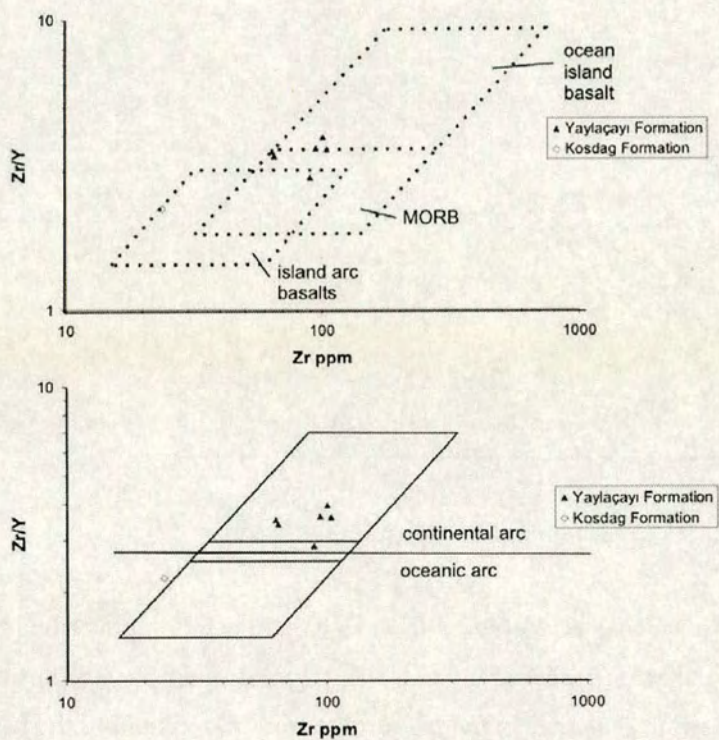


Figure 5.73. Basic igneous rocks from the Yaylaçayı Formation plotted on the Zr/Y versus Zr discrimination diagram (Pearce and Norry 1979).

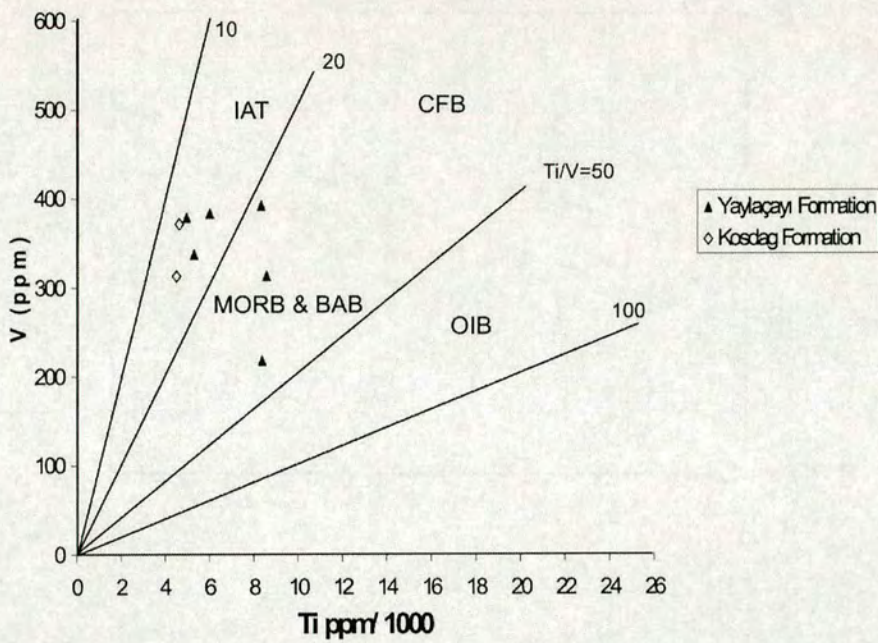


Figure 5.74. Basic igneous rocks from the Yaylaçayı Formation plotted on the V/Ti discrimination diagram (Shervais 1982).

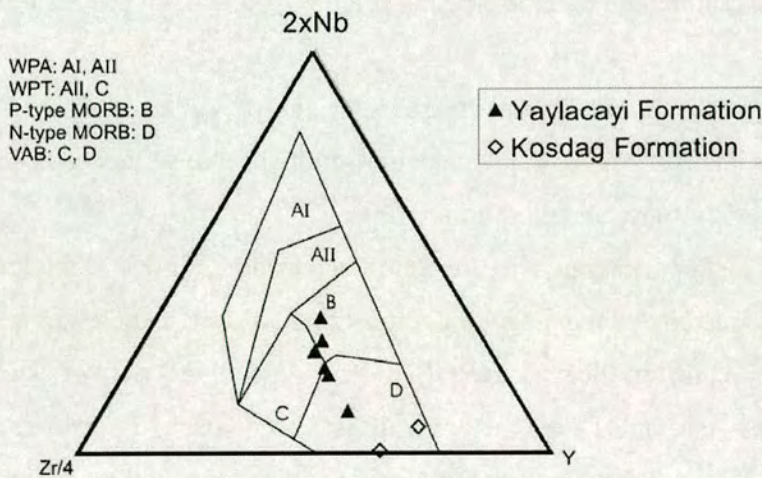


Figure 5.75. Basic igneous rocks from the Yaylaçayı Formation plotted on the Nb/Zr/Y discrimination diagram (Meschede 1986). AI and AII = within-plate alkali basalt compositional field, B = plume-influenced MORB compositional field, C = within-plate tholeiite compositional field, D = N-type MORB and volcanic arc basalt.

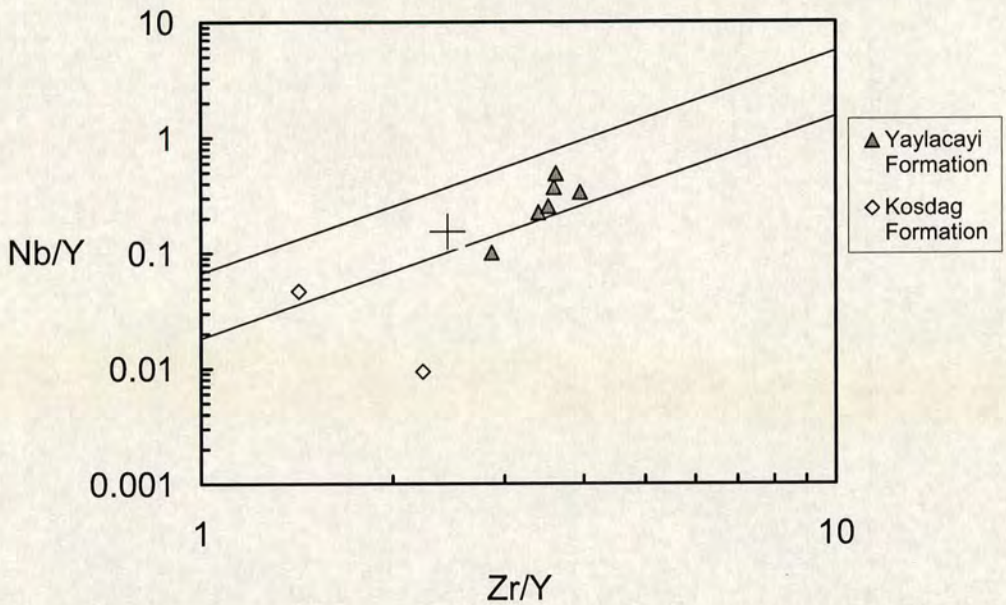


Figure 5.76. Nb/Y and Zr/Y variation in basalts from the Yaylacayı Formation. The parallel lines mark the range for Iceland data (Fitton et al. 1997).

The eight samples shown to have basic primary compositions are plotted on seven basalt discrimination diagrams below (Figure 5.69 to 5.75; see 3.3.8 for explanation).

In each of the discrimination diagrams the analyses give ambiguous results (i.e. the data points cover more than one compositional field). When considered together the diagrams are then more informative.

On the Ti-Zr-Y diagram (Figure 5.69; Pearce and Cann 1973) the group of samples as a whole covers the range of compositions for low-K tholeiites and calc-alkali basalts and most of the analyses fall in the compositional field of Ocean Floor Basalts. Of the two samples from the upper thrust slice (Koşdağ Formation of Tüysüz 1990) one has a low-potassium tholeiitic composition and the other is outside of the compositional range of any of the fields. The samples from the lower thrust slice are either ocean-floor basalts or calc-alkali basalts.

On the Cr-Y basalt discrimination diagram (Figure 5.70; Pearce 1982) the samples from the upper thrust slice (Koşdağ Formation of Tüysüz 1990) lie within

the compositional field for Volcanic Arc Basalts, the compositions of the other samples lie within the area of overlap between Within-Plate Basalts and MORB. However, all but one of the samples lie within the compositional field of MORB on this diagram.

On a linear plot of Ti/Zr (Figure 5.71; Pearce and Cann 1973) the samples from the lower thrust slice fall within the compositional range from ocean floor basalts and calc-alkali basalts, one sample from the upper thrust slice (Koşdağ Formation of Tüysüz 1990) is a low-K tholeiite and the other lies outside of the compositional fields. A logarithmic plot of the same Ti/Zr data shows that all the samples have compositions within the range for arc lavas however, four of the samples also fall within the compositional field for MORB (the samples with MORB compositions do not include either of the samples from the upper thrust slice. None of the samples have Within-Plate Lava compositions on this diagram.

On the Zr/Y vs. Zr diagram (Figure 5.73; Pearce 1983) the samples from the lower thrust slice of the Yaylaçayı Formation lie on the boundary between the compositional fields for Ocean Island Basalts and MORB. A sample from the upper thrust slice lies just inside the field for Island Arc Basalts. On this diagram, Ocean Island Basalts plot in the same field as continental arcs because Zr/Y ratio is a measure of within-plate enrichment and not alkalinity (Pearce 1983). With the exception of one sample, data from the Yaylaçayı Formation fall into the compositional field for continental arcs.

On the V/Ti diagram (Figure 5.74; Shervais 1982) the samples from the Yaylaçayı Formation plot in the compositional range for both Island Arc Tholeiites, MORB and backarc basins.

The ternary Nb/Zr/Y plot (Figure 5.75; Meschede 1986) shows the samples to have both Volcanic Arc Basalt and plume-influenced MORB compositions. The samples from the lower thrust slice are P-type MORB, Within-Plate Tholeiite or N-MORB. the samples from the upper thrust slice are N-MORB or Volcanic Arc Basalt.

Figure 5.76 shows the Nb/Y and Zr/Y variation for the basalts from the Yaylaçayı Formation. The lower diagonal line on Figure 5.76 divides Iceland data (ie. plume-influenced MORB) from 'normal' MORB (e.g. Southwest Indian Ridge,

East Pacific Rise, Reykjanes Ridge; Fitton et al. 1997). The samples from the lower thrust slice of the Yaylaçayı Formation (except one) and a single sample from the upper thrust slice fall within the Iceland array, (Koşdağ Formation of Tüysüz 1990). One sample that lies within the range for normal MORB could be due to sampling error in the field. One of these samples exhibits an unusually low Nb/Y ratio, even for MORB.

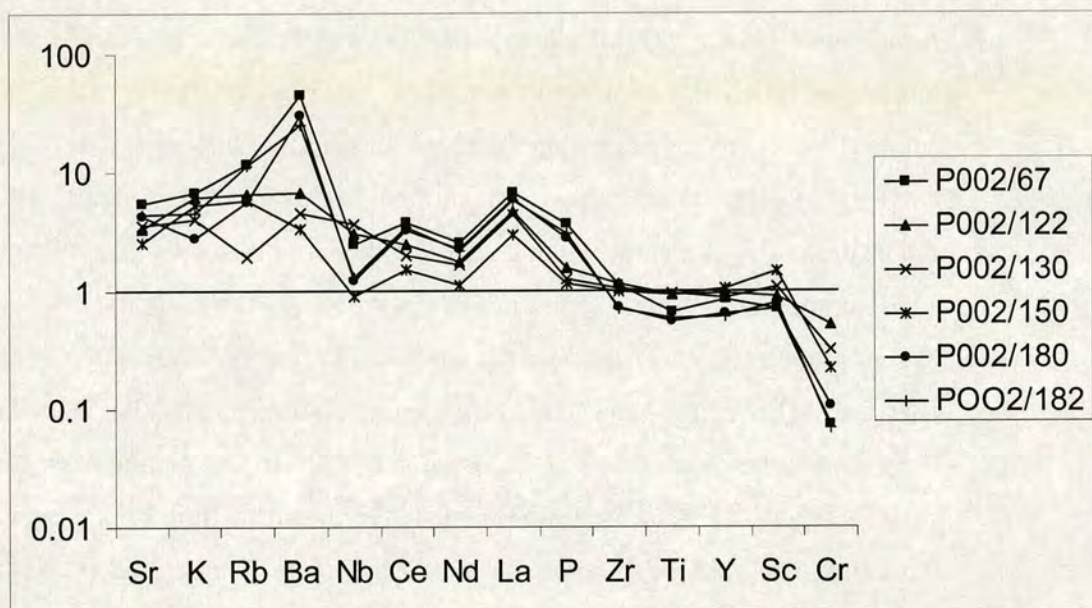


Figure 5.77. MORB-normalized multi-element abundances for unaltered basic dykes from the Yaylaçayı Formation. Normalizing values: Sr = 120 ppm; K₂O = 0.15% ; Rb = 2.0 ppm; Ba = 20 ppm; Nb = 3.5 ppm; La = 3 ppm; Ce = 10 ppm; Nd = 8 ppm; P₂O₅ = 0.12% ; Zr = 90 ppm; TiO₂ = 1.5% ; Y = 30 ppm; Sc = 40 ppm; Cr = 250 ppm (Pearce 1982).

A MORB-normalised multi-element (Figure 5.77) plot shows the variety of geochemical patterns that exist among the samples from the lower thrust slice of the Yaylaçayı Formation. The samples from the upper thrust slice i.e. the Koşdağ Formation of Tüysüz 1990) exhibit very low abundances of the mobile elements K, Ba and Nb. K and Ba may have been depleted during alteration or metamorphism. Nb is not mobile and its depletion in most of the samples is indicative of a subduction influence in the source region (Saunders et al. 1988). A subduction-

influenced mantle source is supported by the depletion of HFS elements (Zr-Cr). Sample PO02/130 and PO02/122 do not have a negative Nb anomaly and are not significantly depleted in any HFS elements. These samples show no evidence of a subduction influenced source. The other samples all have a negative Nb anomaly and are depleted in the HFS elements Zr, Ti, Y, Sc and Cr; in addition these samples are relatively enriched in the LFS elements K, Sr, Rb and Ba, suggesting a possible subduction influence on the mantle source.

Two samples of basaltic lava from the lower thrust slice of the Yaylaçayı Formation near Iskilip were analysed by Rojay (2001). These samples exhibited an enriched MORB geochemistry but with no subduction signature.

In summary, the basaltic rocks from the Yaylaçayı Formation exhibit a composite geochemistry, with volcanic arc, plume-influenced, MORB-like and possibly sub-continental mantle characteristics. Samples from the lower thrust slice show an enrichment trend which could indicate either a 'within-plate' or a sub-continental lithospheric mantle source. The samples from the upper thrust slice (Koşdağ Formation of Tüysüz 1990) show no such enrichment. The chemistry of samples from both slices indicates a subduction-influenced magma source. This apparently composite geochemistry could be explained by three possible scenarios: 1) rifting of an active continental margin, 2) plume-influenced intraoceanic subduction-related volcanism, or 3) 'historical contingency' of mantle geochemistry (which could apply to any of the signatures). This apparently composite geochemistry is considered further in chapter 6.

5.5.5 Discussion: age, petrogenesis and tectonic setting of the Yaylaçayı arc Unit.

The Yaylaçayı Formation (upper and lower slices combined) contains a high proportion of volcanoclastic and volcanic rocks of intermediate composition. The abundance of intermediate-evolved volcanic rocks is evidence that significant crystal fractionation has occurred. This degree of magmatic evolution suggests that a significant-sized volcanic arc edifice was constructed. The conglomerates have a matrix-supported fabric which is typical of the depositional products of debris-flows (Tucker 1982). They were derived from a purely volcanic (andesitic) source which is

inferred to be the volcanic arc edifice. An unconformity at the top of the succession (beneath the overlying Campanian-Maastrichtian Yapraklı Formation) indicates that the volcanic arc may have been locally emergent within the study area during deposition and eruption of the sedimentary and volcanic rocks of the Yaylaçayı Formation in Campanian-Maastrichtian time.

The volcanic activity ceased (locally, at least) and volcanoclastic sediments and limestones then accumulated around the volcanic edifice during Late Cretaceous (Campanian-Maastrichtian) times. The gradual passage from volcanic rocks (with coarse volcanoclastic debris-flows) to finer-grained volcanoclastic sediments and carbonates exhibited by the Yaylaçayı Formation records a waning of volcanism, or a switch in the locus of volcanism. The arc edifice was eroded following the cessation of volcanism. The sedimentary structures exhibited by the sandstone succession represent the five 'Bouma' divisions (T_a - T_e) and, thus, the sandstones are interpreted as the deposits of volcanoclastic turbidity currents (Bouma 1962). The volcanic and carbonate sediments contain no terrigenous material. The sediments are likely to have been derived solely from the volcanic and carbonate environments that are inferred to have been associated with the arc. The eruptive and depositional setting of the Yaylaçayı Formation was, therefore, probably remote from a continental margin (i.e. the Eurasian or Gondwanan margins). The fine-grained *Globotruncana*-bearing limestones at the top of the Campanian-Maastrichtian succession indicate a reduction in the supply of volcanoclastic material, possibly caused by a relative sea-level rise, or by complete denudation of the arc edifice. The grain-size and the fauna they contain indicate a deep-water environment (sub-thermocline, >700 m; Stewart and Pearson 2000). The limestones are interpreted as being pelagic in origin.

The geochemical investigations indicate an eruptive setting transitional between that of a volcanic arc, enriched (WPB) and MORB sources. The depletion of HFS elements (compatible elements in garnet lherzolite; Pearce 1982; Hall 1996), is characteristic of a subduction-influenced mantle source. In addition, the compositions of some of the lavas exhibit the characteristics of an enriched mantle source. This enriched source could be related to plume activity or, alternatively, could suggest that regions of sub-continental lithospheric mantle (e.g. garnet lherzolite) existed in the source region. The samples exhibit a transition from

enriched basalt (P-MORB) to island arc tholeiite; therefore, melting of a single enriched source could not have produced all of the samples. The source region is interpreted as spatially constrained enriched mantle (i.e. plume or sub continental), which has been influenced by subduction. The geochemistry is consistent with volcanism related to arc-rifting.

The formation as a whole is, therefore, interpreted as a fragment of a volcanic arc that formed remote from any supply of terrigenous sediment, possibly in a rifted arc or backarc setting. The inferred magma source included spatially limited sub-continental or plume-type lithospheric mantle. Magmatic activity ceased during the latest Cretaceous (Campanian-Maastrichtian) and was followed by deposition of volcanoclastic turbidites and pelagic carbonate around the flanks of an eroding arc edifice.

5.5.6 Summary

- The Yaylaçayı Formation contains microfossils that indicate a Campanian-Maastrichtian age for the unit.
- Fine-grained sediments including chert, umber and micritic limestone are present between pillow lavas low in the succession. Texturally immature volcanoclastic sediments predominate at higher stratigraphic levels. The volcanoclastic succession then grades into fine-grained sandstone, shale and micritic limestone, (~500 m thick) at the top of the sequence.
- Whole-rock geochemical analyses of basalts from the Yaylaçayı Formation show compositions comparable to modern volcanic arcs and MORB. Some samples also have enriched compositions.
- Northerly outcrops of the unit are schistose. The cleavage dips to the northwest and is folded by south-vergent folds. Top-to-the-north compressive structures are commonly cut by top-to-the-south structures. Later normal and strike-slip faults also cut the unit.

5.6 Volcanic arc cover: Yapraklı Formation

The oldest sedimentary cover unconformably overlying the Yaylaçayı Formation (Yapraklı Formation; Birgili et al. 1975) is exposed near Çankırı (Figure 5.78 and 5.79). The unit reaches ~500 m in thickness (Figure 5.80 and 5.82). A Late Cretaceous (Campanian-Maastrichtian; 85-71 Ma) age is indicated by the presence of planktonic foraminifera, including *Globotruncana linneiana* (D'ORBIGNY; Prof. Izver Ongen, Prof. Kemal Taşlı and Prof. Nurdan İnan, pers. comm. 2004, see Appendix 1). The formation begins with a thin basal conglomerate (~3 m), followed by grey volcanoclastic shales passing upwards into thick-bedded, coarse-grained calcarenites, volcanoclastic sandstones and conglomerates. The Yapraklı Formation is unconformably overlain by dacitic lavas and tuff of probable Late Eocene age, related to the Çankırı Basin that post-dates suturing (Kaymakçı 2000).

5.6.1 Structure of the Yapraklı Formation

Competent sandstone and limestone beds within the Yapraklı Formation are boudinaged within a less competent scaly clay matrix. Siltstone beds are well cleaved, whereas coarser grained clastic sedimentary rocks and limestones within the succession are not. Bedding planes mostly dip at moderate angles (~45°) southwards although locally sub-vertical and overturned steeply north-dipping beds are present. Abundant, well-preserved sedimentary structures (e.g. Bouma sequences) indicate that the unit youngs southwards and is dominantly the right way-up. The Yapraklı Formation, as exposed north of Yapraklı village, is folded into a large south-facing sub-horizontal recumbent syncline, gently inclined northwards (Figure 5.80). The large fold plunges gently southwest.

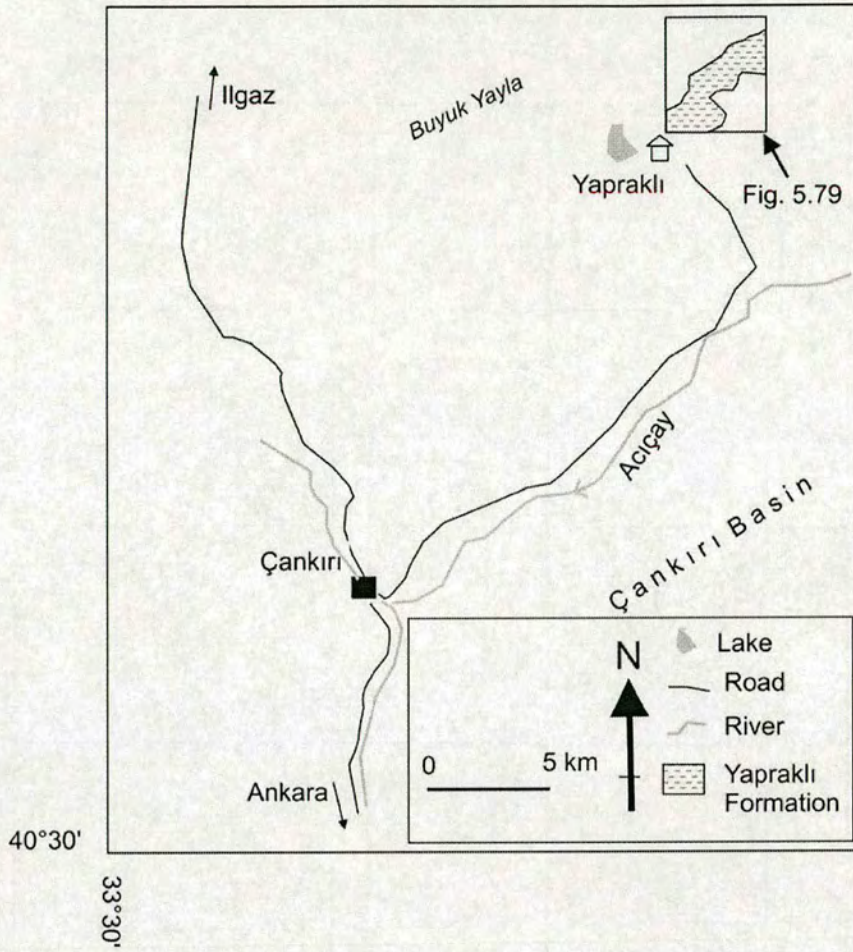


Figure 5.78. Map showing location of outcrop of the Yapraklı Formation.

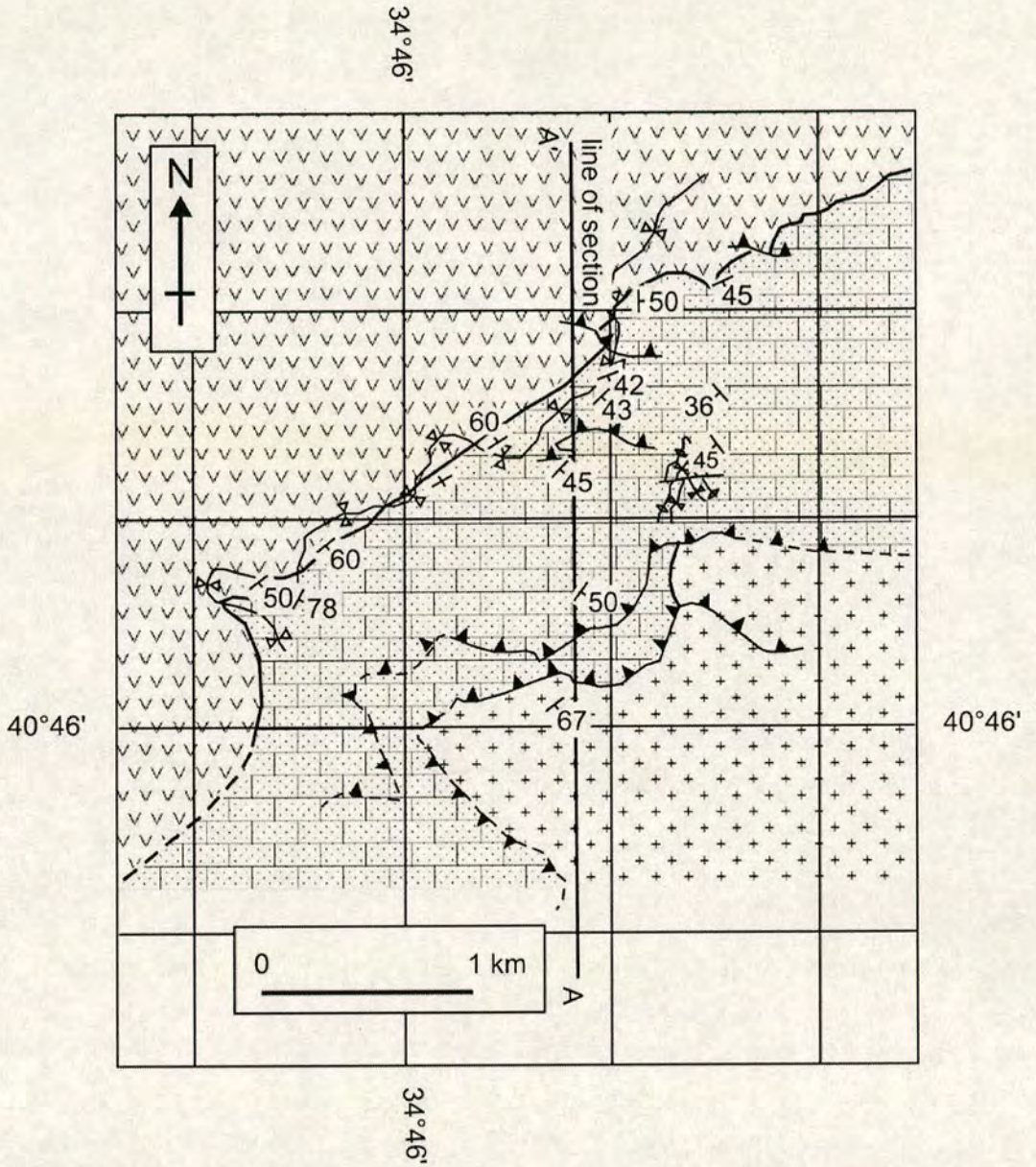


Figure 5.79. Geological map north of Yapraklı showing outcrop and contact relations of the Yapraklı Formation. For legend see Figure 5.1.

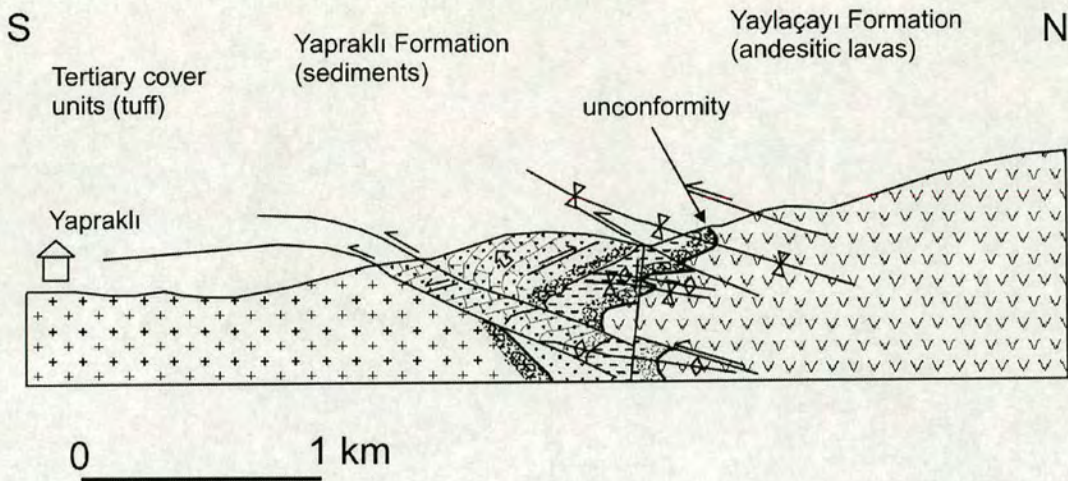


Figure 5.80. Geological section north of Yapraklı. See Figure 5.79 for location. For legend see Figure 5.1.

Measured structural data for the Yapraklı Formation are shown in Figure 5.81. The unit exhibits abundant shear zones with kinematic fabrics (p-foliation, Reidal shears) that indicate a top-to-the-north sense of motion. Top-to-the-north thrust faults and small duplex structures are also present. A pervasive shear fabric, sub-parallel to bedding, is observed in the fine-grained lithologies. These top-to-the-north compressional structures and fabrics are folded and cut by top-to-the-south compressional structures (e.g. small-scale folds, shear zones and thrusts) including the large fold described above. Top-to-the-south thrusts form small duplex structures.

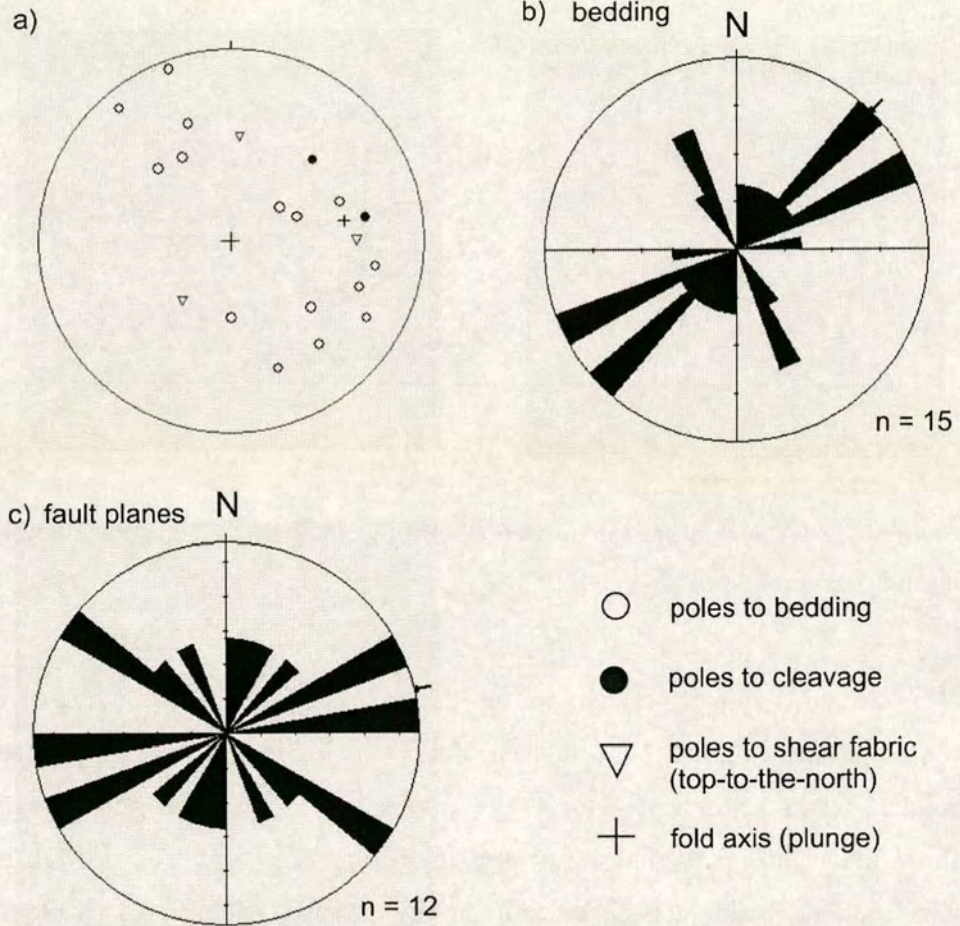


Figure 5.81. Structural data for the Yapraklı Formation.

South-vergent folds are cut by top-to-the-south thrusts (Figure 5.80).

All the above structures are cut by dextral and sinistral strike-slip faults.

Strike-slip faults trend NE-SW and E-W.

5.6.2 Sedimentary facies

The Yaylaçayı Formation begins with conglomerate and coarse-grained beds of sandy calcarenite (<1 m thick; Figure 5.82) containing fragmented rudistic bivalve shells, algae, bryozoa, benthic forams, mafic and ultramafic lithoclasts. In thin section, the calcarenite contains abundant detrital volcanogenic feldspar and quartz, bastite and chert. The conglomerate and sandy calcarenite unconformably overlie the

andesitic lava of the Yaylaçayı Formation (see section 5.5) and fill neptunian dykes (~15 cm wide) along the contact.

Shale facies: The calcarenite passes upwards into a thick (~200 m) homogenous succession of grey shale (Figure 5.82). The shale is fissile and poorly bedded. Lamination was observed in places.

Calcirudite facies: Stratigraphically above the shales are calcirudites and pebbly calcarenaceous sandstones (10-50% calcite grains; Tucker 1982; Figure 5.82). The calcirudites are massive, poorly sorted and matrix-supported, containing sub-rounded to well-rounded clasts, <5 cm (i.e. texturally inverted). The clasts are dominantly volcanoclastic (rhyodacite ~5%, chloritised basic lava ~5%, feldspar-phyric andesite ~90%) set in a grey-orange calcareous and arkosic sand-sized matrix. The beds form broad lenses (>30 m). The calcirudites grade upwards into amalgamated sandstones.

Amalgamated sandstones: Amalgamated sandstones form thick (~2 m) lenses. They are massive, coarse-grained and poorly sorted with sub-rounded to well-rounded grains, (also texturally inverted). These sandstones are again arkosic with outsize feldspar-phyric andesitic lithoclasts (<10) cm and contain large broken bivalve fragments.

Hybrid sandstones: sandy calcarenites and calcarenaceous sandstones. The succession becomes more calcareous towards the top, where amalgamated calcarenaceous sandstones (10-50% calcite grains) and sandy limestones (>50% calcite grains; definition of Tucker (1996) dominate the succession (Figure 5.82). In addition to sub-angular calcite grains and lithoclasts, these sandstones contain, well-rounded grains of quartz and glauconite (largely weathered to Fe-oxide, probably limonite). These calcareous sediments are thickly bedded (30 cm to 1 m) and contain coarse rudist shell fragments and rounded pebbles (<5 cm) of andesite. The beds exhibit graded bedding, trough- and planar cross-bedding and outsize imbricated clasts (pebbles) which yielded palaeocurrents (see section 5.83). Nodular concretions of haematite are seen locally.

In summary, the sediments of the Yapraklı Formation are poorly sorted with sub-angular, to well-rounded grains of mafic- and intermediate-composition volcanic rocks, quartz, feldspar, glauconite and abundant calcareous shell fragments

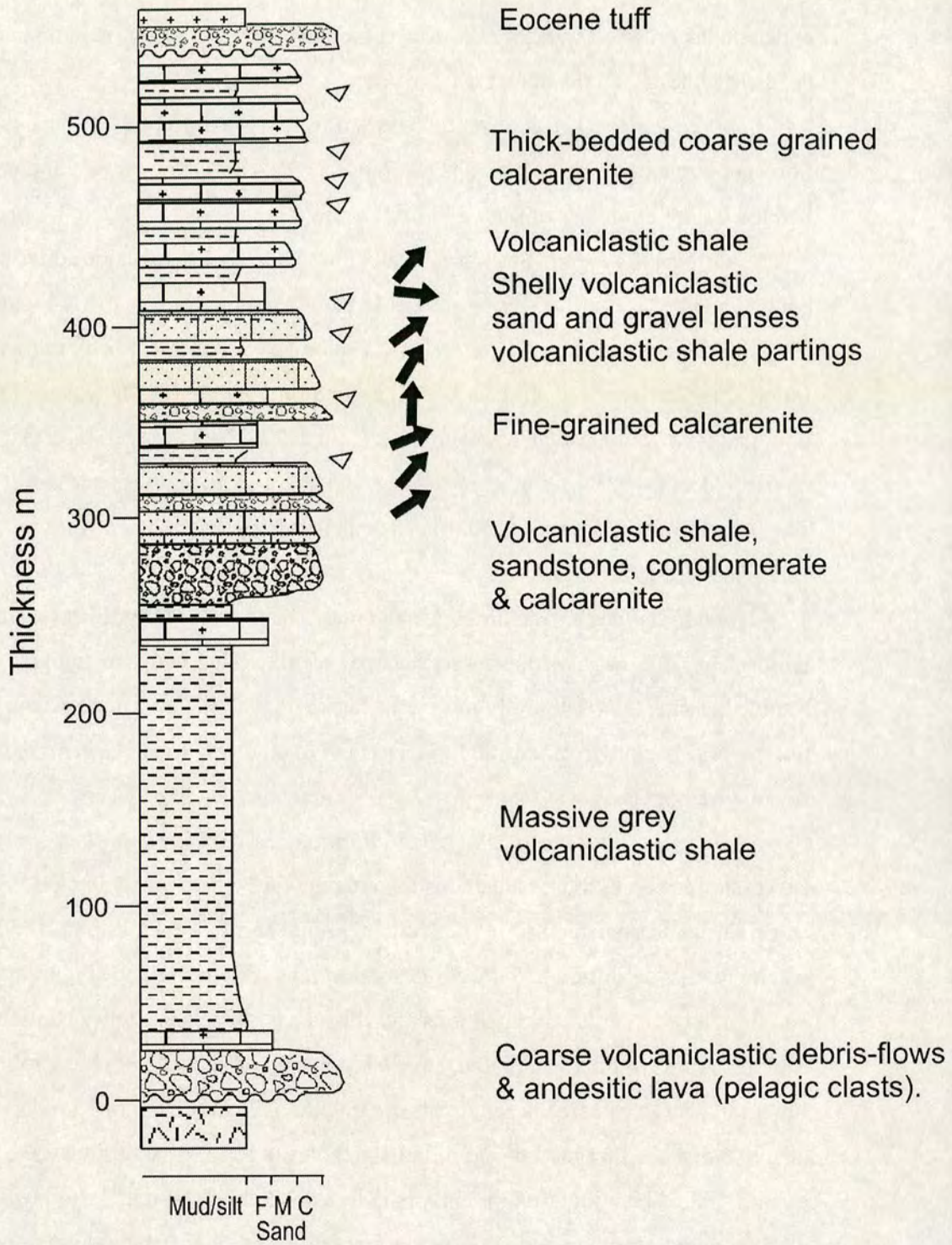


Figure 5.82. Composite log of the Yapraklı Formation.

(fragmented and whole rudist bivalves). Individual beds, up to 1.5 m thick, are commonly massive or graded and contain sub-rounded pebbles and boulders of feldspar-phyric andesite (up to 40 cm in diameter).

Palaeocurrent data

Twenty measurements of cross-laminations and pebble imbrication were taken from thickly bedded sandstones in the upper part of the succession. The data were stereographically corrected for angle of dip and the results are shown in Figure 5.83. The dip-corrected palaeocurrent directions are bimodal and dominantly towards the northeast.

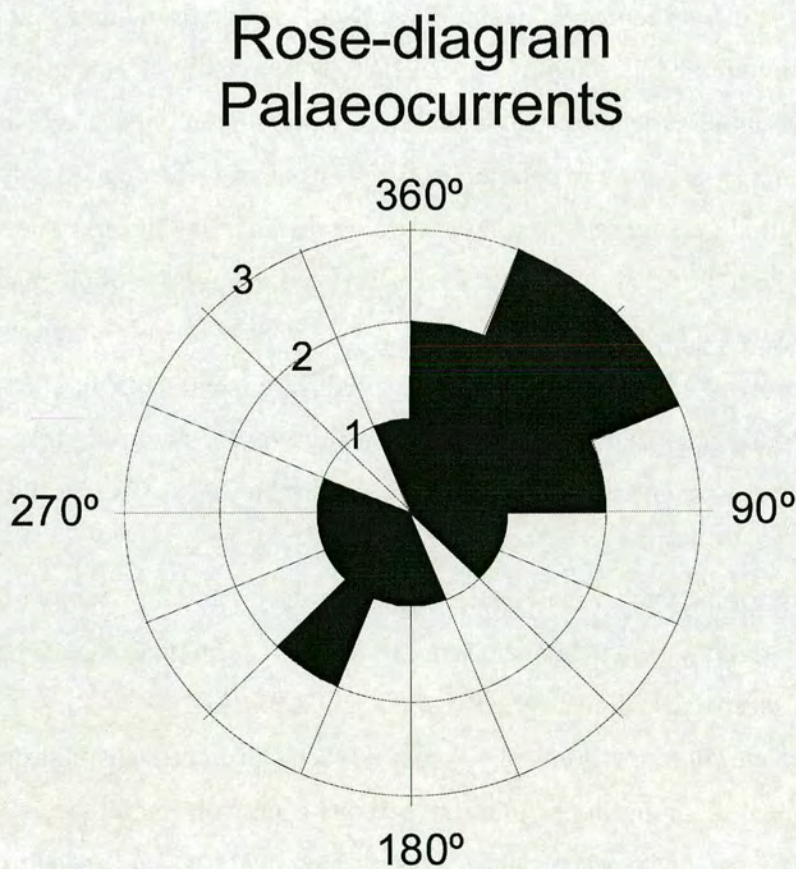


Figure 5.83. Dip-corrected palaeocurrent data from sandstone beds of the Yapraklı Formation measured from trough and planar cross-bedding and imbricated clasts (see text).

Depositional setting

The unconformable base of the succession and the thin basal conglomerate exposed in the type section indicate that at least localised erosion of the underlying arc-type unit (Yaylaçayı Formation) had taken place, possibly in a subaerial setting. This was followed by submergence and deposition of conglomerate and calcarenite containing marine fossils. The thin conglomeratic base is interpreted as a shoreface environment (Dickinson 1995; Boggs 1995) deposited during a marine transgression (that may have been localized). The transgression was followed by mudstone deposition, probably in an open-marine environment. The transition to mudrock is interpreted as an increase in water depth. The upward change from homogenous grey shales to coarser grained lithologies suggests that the source of volcanoclastic and carbonate material became more proximal. Whereas the fine-grained shaly partings suggest low-energy background conditions, the presence of well-rounded grains within the calcirudites suggests that they were abraided in a fluvial and/or beach environment (Pettijohn et al. 1987). However, the massive, poorly sorted, matrix-supported, texture suggests that the calcirudites were deposited rapidly by sediment-gravity flow processes (Tucker 1981). The inverted texture and lenticular bed morphology of the calcirudites suggests that they were redeposited from the shoreface by broad channelised debris-flows or submarine landslides (Reading 1978).

Because of the thick, broad lenticular bed geometry and the paucity of grain-size sorting or grading the amalgamated sandstones are interpreted as the deposits of grainflows or sheet-like sediment-gravity flows (Leeder 1982).

The calcirudites are followed by cross-bedded calcarenaceous sandstones which contain varied proportions of detrital carbonate and volcanic lithoclasts, including imbricated pebbles (i.e. outsize clasts). This suggests that the sediment source was partly a neritic carbonate environment and partly a denuding volcanic edifice. A neritic environment is supported by the presence of rounded quartz grains, rudists and glauconite (a green mica mineral that forms in modern oxidising shallow seas where decaying organic matter is present; e.g. Allaby and Allaby 1990). The graded and cross-bedding, clast imbrication and clast-supported fabric suggest that

the calcarenaceous sandstone beds were deposited by currents rather than sediment-gravity flows. The bimodal nature of the palaeocurrents suggests a tidal influence. The parallel and cross-laminated, and cross-bedded sandstones indicate that these sandstones could have been deposited in an upper shoreface environment (Tucker 1981; McLane 1995).

The transition between these three facies (shale-submarine fan/slope-shelf) could reflect either the normal migration of facies within this arc-apron environment; the progradation of sedimentary facies, or lowering of relative sea-level (Reading 1978). The lack of any terrigenous material (i.e. metamorphic grains) suggests that these sediments were isolated from the Eurasian margin. The measured palaeocurrent directions, although bimodal (i.e. tidal) are dominantly towards the northeast, i.e. towards the Eurasian margin from the arc. Assuming little horizontal tectonic rotation has occurred this could suggest that the Yapraklı Formation was deposited in a backarc position. Contemporaneous volcanic material (e.g. air-fall tuff) is absent, thus, this unit probably records reworking of arc-derived material after arc volcanism ended at least locally. Due to the presence of north-vergent structures and the limited clastic provenance the unit is inferred to have been deposited prior to Late Cretaceous tectonic emplacement onto the Pontides margin.

Previously this unit was interpreted together with the Yaylaçayı Formation as part of the volcanic arc succession (Tüysüz 1995). However, the presence of an important unconformity at the base of the Yapraklı Formation strongly suggests that the unit post-dates arc magmatism (at least locally). One possibility is that these sediments represent the base of an Upper Cretaceous forearc basin (e.g. Koçyiğit 1991). However, measured northward palaeocurrent directions appear to be more consistent with a backarc setting. This is discussed further in a regional tectonic context in Chapter 6.

5.6.3 Summary

The Campanian-Maastrichtian Yapraklı Formation is interpreted as a proximal (upper) submarine fan or slope facies (Nichols 1999) deposited following a marine transgression of the volcanic arc. Following initial transgression of the volcanic arc (Yaylaçayı Formation) the unit records a regression from inferred offshore to upper shoreface deposition. This could be either due to relative sea-level fall or progradation of the sediments. The shallow-water carbonate grains and shell fragments (e.g. rudists) were possibly derived from carbonate environments built upon or, around, the inferred volcanic arc edifices (represented by the Yaylaçayı Formation) in the area studied.

5.7 Preserved back-arc basin sediments: İkiçam Formation

The İkiçam Formation (>3000m thick) crops out extensively within the Izmir-Ankara-Erzincan Suture Zone near Çankırı and Tosya (Figure 5.84). The Formation occurs within the mid to upper structural levels of the imbricate thrust stack (Figure 5.3). A Late Cretaceous (Campanian-Maastrichtian) age is indicated by the presence of several species of Globotruncana (Prof. Izver Ongen, Prof. Kemal Taşlı and Prof. Nurdan İnan pers. comm. 2004; see Appendix 1). Microfossils present include Globotruncana arca (CUSHMAN), Heterohelicidae, Planomaliniidae and constrain the age of the İkiçam Formation to Campanian-Maastrichtian (83.5-65.5 Ma; Gradstein et al. 1004). The İkiçam Formation interdigitates with andesitic lava and coarse andesitic volcanoclastic conglomerates of the Upper Cretaceous Yaylaçayı Formation, as seen north of Tosya (Figure 5.84). The İkiçam Formation is unconformably overlain by Upper Eocene and younger sediments.

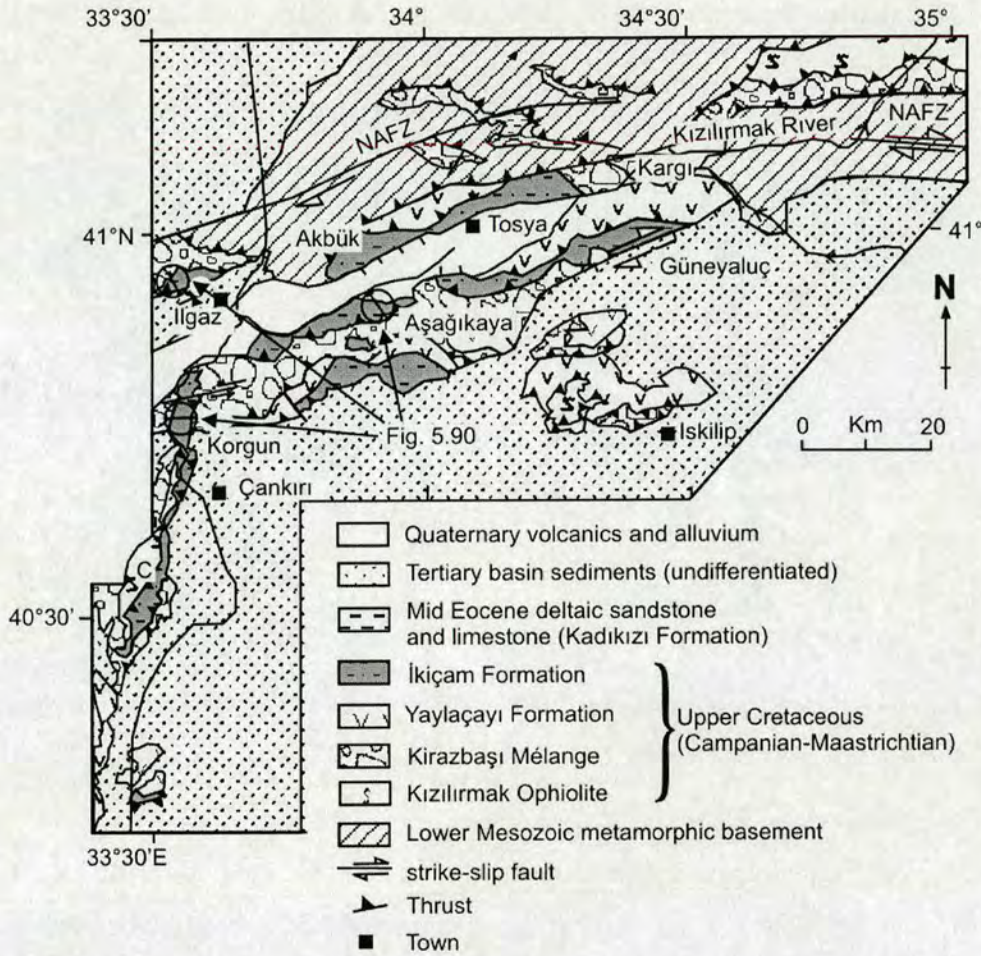


Figure 5.84. Simplified geological map of the central Pontides showing outcrop of the İkiçam Formation

5.7.1 Structure of the İkiçam Formation

The İkiçam Formation crops out within internally deformed, elongate fault-bounded slices (up to ~10 km long), unconformably overlain by Tertiary and younger cover sediments. Major thrusts and strike-slip faults (commonly containing serpentinite and/or carbonated serpentinite) juxtapose the İkiçam Formation with other units. Many of the major faults also cut the overlying Tertiary sediments. Outcrop of the unit straddles major strike-slip faults (e.g. Avsar fault, Tosya fault, Kargı Fault, Devrez Çay fault zone; Dhont et al. 1998) which are part of the active

North Anatolian Fault Zone, the current plate boundary between the Eurasian and Anatolian plates (Suzanne et al. 1990; Dhont et al. 1998). Estimates of finite

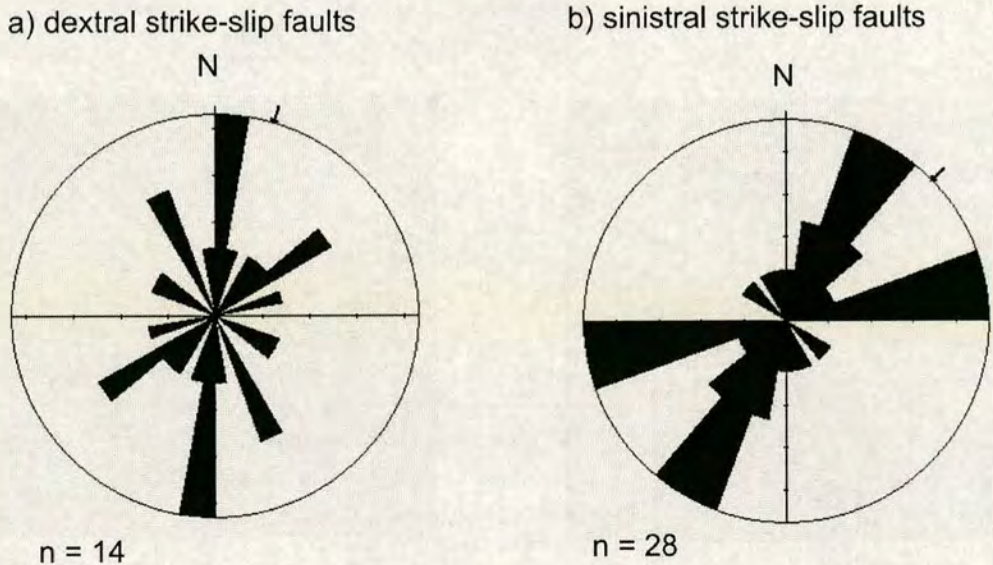


Figure 5.85. Rose diagrams showing measured strike orientations of strike-slip faults in the Central Pontides.

displacement along this fault zone range from 25 ± 5 km to 350 to 400 km (Barka 1992). Polyphased strike-slip deformation has resulted in both dextral and sinistral fault motions (Dhont et al. 1998). Measured strike orientations of strike-slip faults are shown in Figure 5.85. Large scale pre-Neogene structures of the İkiçam Formation are dissected and significantly offset by these Neogene strike-slip structures. The outcrops of the İkiçam Formation, therefore, occur within different tectonic blocks (i.e. South Tosya Block, North Tosya Block; Dhont et al. 1998) that may have been subject to independent rotations.

Sedimentary structures (graded bedding, load casts, bioturbation, cross-lamination) and cleavage-bedding relationships indicate a variety of younging directions and way-up within the unit. A continuous thick succession (<1000 m post deformational thickness) of overturned beds was observed in several localities between Tosya and Çankırı (e.g. Güneyaluç, Akbük, southeast of Ilgaz (near Yuvasaray village; gr: G31, 588231), northwest of Ilgaz (gr: G31, 460353), near Korgun and northwest of Çankırı (gr: G31, 464061); see Figure 5.84). Southeast of

Ilgaz (Yuvasaray) and at Akbük the overturned succession of sandstones forms a series of northward inclined downward-facing SW-plunging tight chevron folds

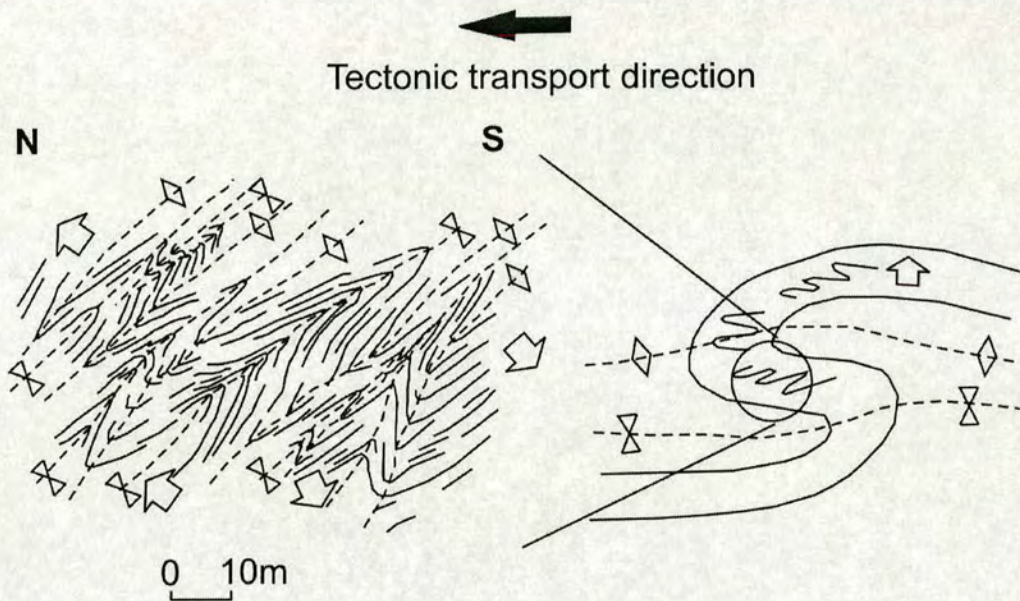


Figure 5.86. Field sketch of downwards-facing inclined tight asymmetrical chevron folds within the İkiçam Formation, observed southeast of Ilgaz near the village of Yuvasaray (gr: G31, 722394).

(Figures 5.86 and 5.87). Their asymmetry gives an apparent southwards vergence. However, because the beds are overturned and the folds are facing downwards to the north the structure is here interpreted to be part of the overturned limb of a northward verging nappe (Figures 5.86 and 5.87). Fold axes observed near Yuvasaray plunge dominantly to the west and poles to bedding lie in the ENE hemisphere of an equal-area projection (Figure 5.88a).

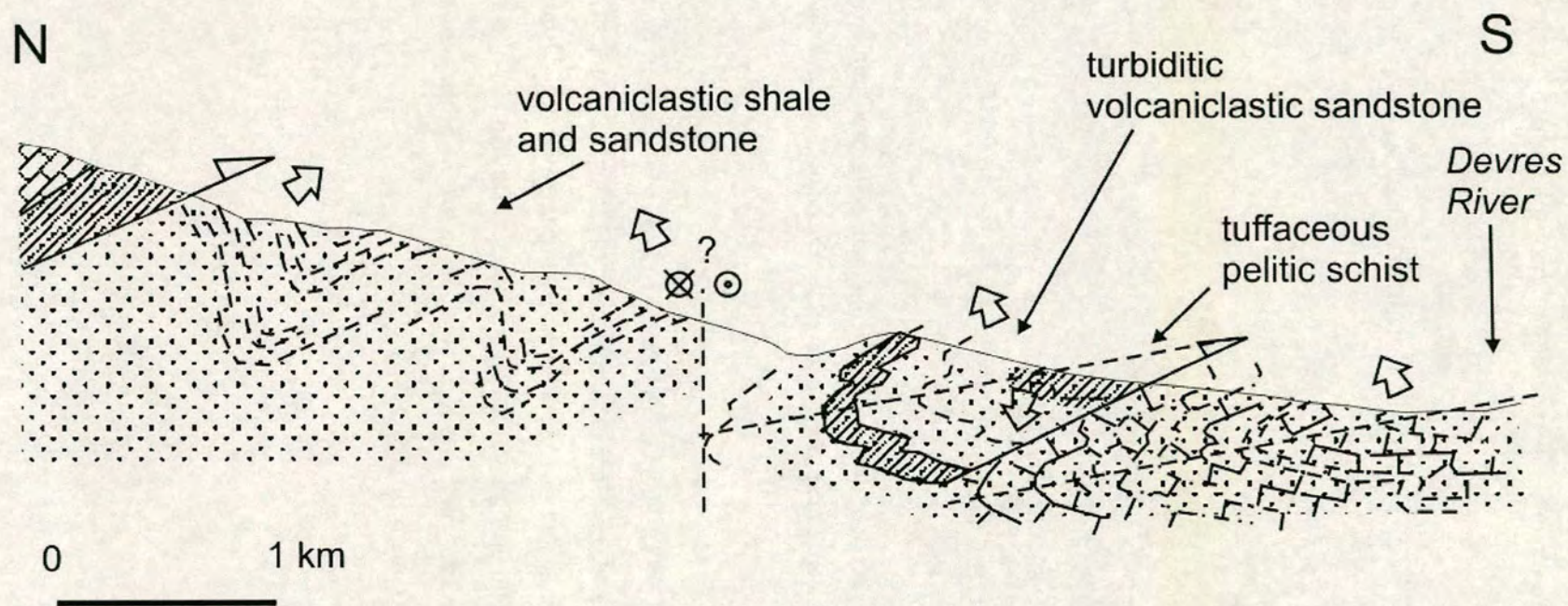
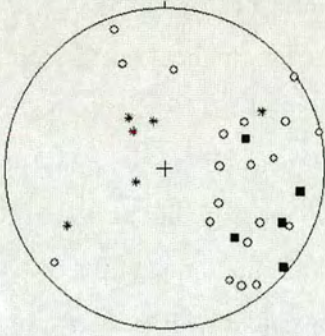
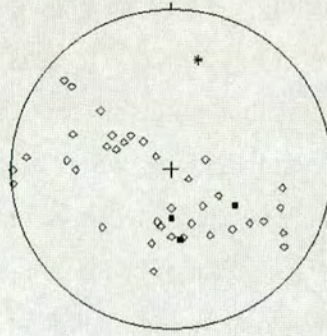


Figure 5.87. Generalised structural cross-section through the İkiçam Formation northwest of Akbük.

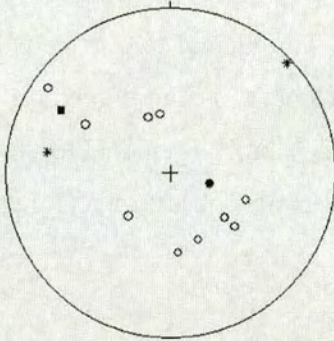
a) Yuvasaray



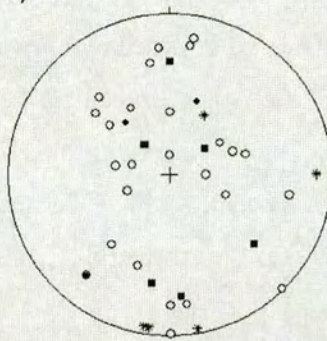
b) Akbük



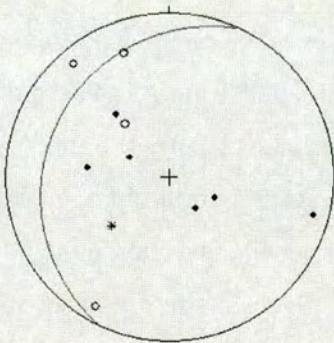
c) Ödemiş



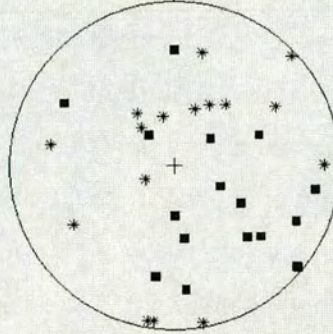
d) Ilıslık



e)



f)



- poles to bedding planes
- poles to fold axial planes
- * fold axes (plunge)

Figure 5.88. Equal-area (Schmidt/Lambert) plots of structural data collected from the İkiçam Formation at: a) Akbük; b) Yuvasaray; c) Ödemiş; d) Ilıslık; e) other localities. f) poles to all measured fold axial planes and plunge of all measured fold axes.

At Akbük, folds in sandstones of the İkiçam Formation are more rounded than at Yuvasaray and fold axes and cleavage are less steeply inclined northward, to sub-horizontal (Figure 5.87). The strike of measured recumbent north-dipping fold axial planes at Akbük range between 030° - 090° (i.e. NE-SW strike). The distribution of poles to bedding and the plunge of a minor fold measured in the field (Figure 5.88b) indicate that the folded structure at Akbük plunges to the northeast.

The distribution of bedding plane and fold orientation data for Akbük and Yuvasaray, as shown in Figure 5.88a and b are consistent with that for plunging inclined folds (Hobbs 1976, p. 180). Despite being located on different sides of a major strike-slip fault (i.e. the Avsar fault; Dhont et al. 1998), which has probably been active since Late Miocene time (Serravalian-Tortonian; McKenzie 1972) (11.61-13.65 Ma; Gradstein et al. 2004). The two localities exhibit downward-facing, northward-inclined, overturned folds. Both localities imply a regional top-to-the-north sense of motion. Similar overturned folds were also observed at Güneyaluç, Korgun, and 12 km northwest of Çankırı at Akçavakif (gr: G31, 464061) (Figure 5.84).

The İkiçam Formation commonly exhibits sedimentary structures that indicate an overall northward-younging direction for dominantly north-dipping right-way-up successions, as exposed at several localities, including the northern part of the cross-section at Akbük (Figure 5.87). Structural data from Akbük are shown in Figure 5.88b. Outcrops of the İkiçam Formation near Akbük less commonly exhibit steeply south-dipping beds or locally overturned, steeply north-dipping beds. The plunge of a minor fold measured 30° to 014° and pencil cleavage (in the nose of folds) is orientated $55^{\circ}\text{E}/020^{\circ}$. Measured axial surfaces in this area are typically inclined $37^{\circ}\text{N}/083^{\circ}$. In combination with south-vergent asymmetrical geometry of minor folds these observations indicate that the right-way-up succession forms a series of northward-inclined, southeast-facing southeast-vergent close chevron folds that plunge gently to the northeast. Large (wavelength >50 m) northward-inclined south-vergent, asymmetrical chevron folds are well exposed 5 km north of Tosya (on the Kastamonu road; Figure 5.84). Geometrically similar south-vergent structures were also observed in right-way-up successions of the İkiçam Formation south of Ilgaz near the village of Ilıslık (gr: G31, 597249), at Aşağıkaya, and 6 km northwest

of Ilgaz (near Ödemiş gr: G31, 460353) (Figure 5.84). Structural data from these localities are shown in Figure 5.88c, d and e. Fold data for the whole unit are shown in Figure 5.88f.

Overtured limestone beds of the İkiçam Formation near Güneyaluç (south of Tosya, gr: G32, 060360) exhibit a conformable transition (stratigraphically upwards) into the Yaylaçayı Formation.

A succession of interbedded calcarenite and pelite beds of the İkiçam Formation exhibiting a variety of styles of folding is exposed 10 km south of Ilgaz, near the village of Ilıslık (gr: G31, 597249). In the Ilıslık area, the unit exhibits parallel folds with wavelengths commonly ~10 m but ranging from <1 m to >40 m. Rounded and chevron folds are exposed with inter-limb angles ranging from open to tight and, with recumbent, inclined and upright axes ranging from sub-horizontal to sub-vertical. Polyclinal folds, box folds and kink bands were also observed. Structural data from this location are shown in Figure 5.88d. Fold axial surfaces are inclined to the north and also to the south. Measured plunge directions are both north and south. Fold axial surfaces in this area are not planar. Small-scale north-vergent asymmetrical folds were observed within the limbs of larger south-vergent folds. This outcrop (>2 km long) exhibits dominantly right-way-up bedding (as indicated by *Thalassinoides sp.* bioturbation, sole marks and graded beds). Only the short limbs of asymmetrical recumbent folds are overturned. Folds near Ilıslık exhibit northward and southward vergence and facing directions. This outcrop is located only 4 km west of Yuvasaray where the structures are overturned and face down to the north (as described above).

In addition to the folding described above, the İkiçam Formation commonly exhibits a strong shear fabric. Competent beds are commonly boudinaged within scaly-clay or form small-scale (~10 m) duplex structures. Top-to-the-north fabrics are commonly cut by top-to-the-south fabrics. Top-to-the-north shear fabrics are folded by south-vergent folds. The unit also exhibits discrete thrust faults that dip to the northwest and to the southeast. Measured strike orientations of thrust faults within the unit are shown in Figure 5.89.

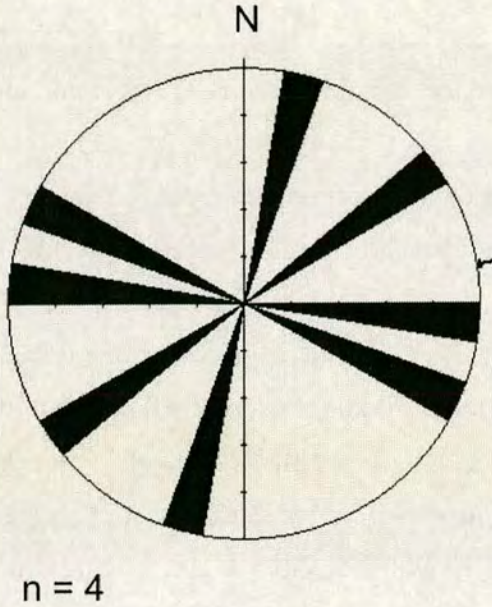


Figure 5.89. Rose diagram showing measured strike orientations of thrust faults within the İkiçam Formation.

The two different structural styles exhibited by the İkiçam Formation indicate apparently opposite senses of motion (ie. top-to-the-north and top-to-the-south). Some exposures exhibit folds with both top-to-the-north and top-to-the-south geometries; also non-planar axial surfaces suggest re-folding. The presence of small-scale north-vergent folds and shear fabrics within the limbs of larger south-vergent folds and within top-to-the south thrust duplexes suggests that north-vergent deformation preceded south-vergent deformation.

Outcrops of overturned north-vergent folds and outcrops of right-way-up south-vergent folds are separated by strike-slip faults of probable Neogene age. Therefore, the original structural relationship between the two fold geometries remains unclear.

5.7.2 Sedimentary facies and Igneous Petrology of the İkiçam Formation

The lower part (~2 km) of the formation comprises thinly bedded (beds <4 cm), buff-coloured, micritic, to muddy, limestones with thin grey pelitic schist partings and tuff (Figure 5.90). In thin section, these sediments are muddy and contain various species of *Globo truncana*. The morphology of some species can be

used as a guide to water depth. Within the Ikiçam Formation species of foraminifera were identified within individual samples (Appendix 1) that cover the full range of water depths (i.e. surface mixed layer-intermediate, sub surface mixed layer-deep, sub thermocline; Stewart and Pearson 2000; see Appendix 1). Surface mixed layer forms are less abundant; intermediate and deep forms are present in roughly equal abundance. Stratigraphically upwards, these sediments grade into cream-buff-coloured, well-bedded, normal-graded calcarenites containing volcanic lithoclasts (Figure 5.91). The calcarenites exhibit slump structures, convolute bedding and sole marks and have laminated shaly and marly tops. At higher stratigraphic levels the succession passes into medium-bedded (<50 cm), medium- to coarse-grained sericitic, and quartzo-feldspathic sandstones, and thinly bedded (<10 cm) volcanoclastic sandstones and shales. Individual sandstone beds exhibit erosive bases with load casts. The sericitic sandstones are massive near the base and some beds exhibit cross-lamination and laminated siltstone tops. These features represent the Bouma divisions of turbidites (Ta-Te; Bouma 1962). In thin section, the sandstones contain angular grains of volcanogenic quartz and feldspar. Some beds contain sericite, chert and polycrystalline (i.e. metamorphic) quartz grains. Rare schistose lithoclasts are present.

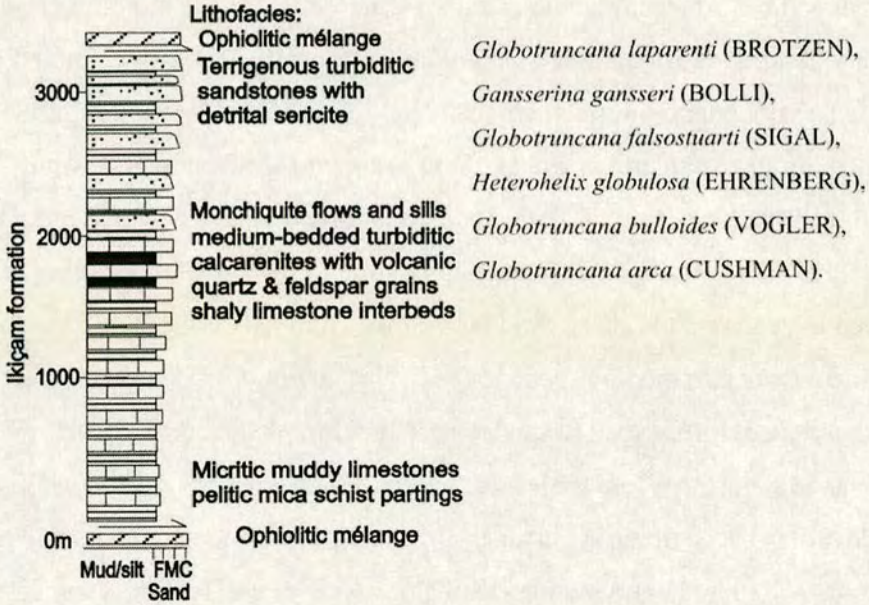
The sedimentary succession includes minor igneous sills, massive lava flows and rare pillow lavas. Olivine-, biotite- and hornblende-phyric flows (monchequite) are interbedded with calciturbidites, near Aşağıkaya (Figure 5.84). Their mineralogy indicates a potassium-rich magma composition. Basic lava flows and sills containing large (<2 cm) phenocrysts of biotite, analcite and salite (alkali pyroxene) are observed northwest of Tosya. These volcanic rocks are interbedded with coarse volcanoclastic debris-flows including boulders (<50cm) of sodalite- and amphibole-phyric basic vesicular lava, and volcanoclastic shales and sandstones of Late Cretaceous age (containing *Globotruncana*). The presence of analcite and salite indicates alkaline compositions (e.g. trachytic).

The unit locally interdigitates with volcanic and volcanoclastic rocks of the Yaylaçayı Formation.

Central Pontides

Log 1: Korgun and Aşağıkaya

Upper Cretaceous lower slope facies



Log 2: NW Ilgaz area

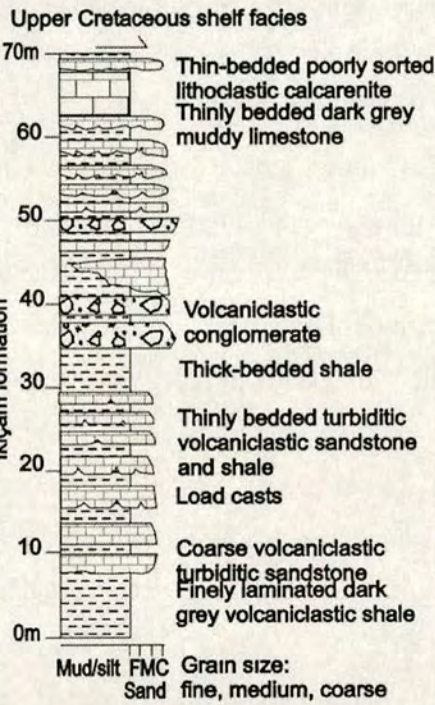


Figure 5.90. Composite (Log 1) and measured (Log 2) logs of the İkiçam Formation. For locations see Figure 5.84..

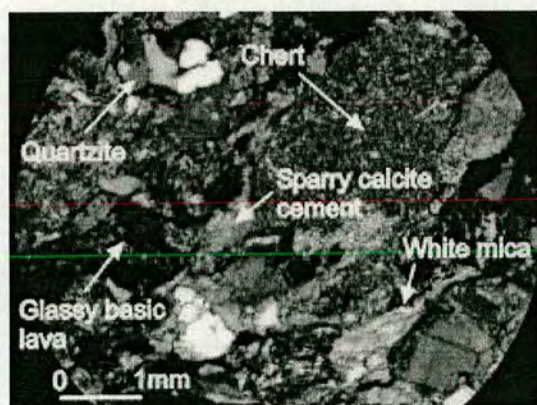


Figure 5.91. Photomicrograph of Upper Cretaceous sandstone from the İkiçam Formation: Note the presence of terrigenous (mica, quartzite), volcanic (lava) and biogenic clasts (chert).

5.7.3 Whole-rock igneous geochemistry of basic rocks within the İkiçam Formation

Ten non-porphyrific, non-vesicular and petrographically fresh samples of mafic lava from the İkiçam Formation were analysed by XRF for whole-rock abundances of major and trace elements (see chapter 3 and appendix 2 for analytical procedures). Four of the samples fall within the acceptable range for naturally occurring unaltered basic igneous rocks ($\text{SiO}_2 < 54\%$, $\text{MgO} + \text{CaO} < 12-22\%$; Pearce 1973). All ten samples are plotted on Harker diagrams showing the variation between immobile Al_2O_3 and the potentially mobile elements CaO , SiO_2 , Fe_2O_3 and MgO (Figure 5.92). Amongst the samples there is no correlation between the abundances of the mobile elements and immobile Al_2O_3 . This suggests that the abundances of these elements were affected by post-magmatic mobilisation during alteration, metamorphism or weathering of the İkiçam Formation. Figure 5.93 shows Harker diagrams for pairs of relatively immobile elements in the samples from the İkiçam Formation. There is a positive correlation between the variation of Ni and Mg, and between Zr and Nb. However, there is no clear relationship between the variation of Cr and Mg, or Cr and Ni. The lavas may represent more than one magma type.

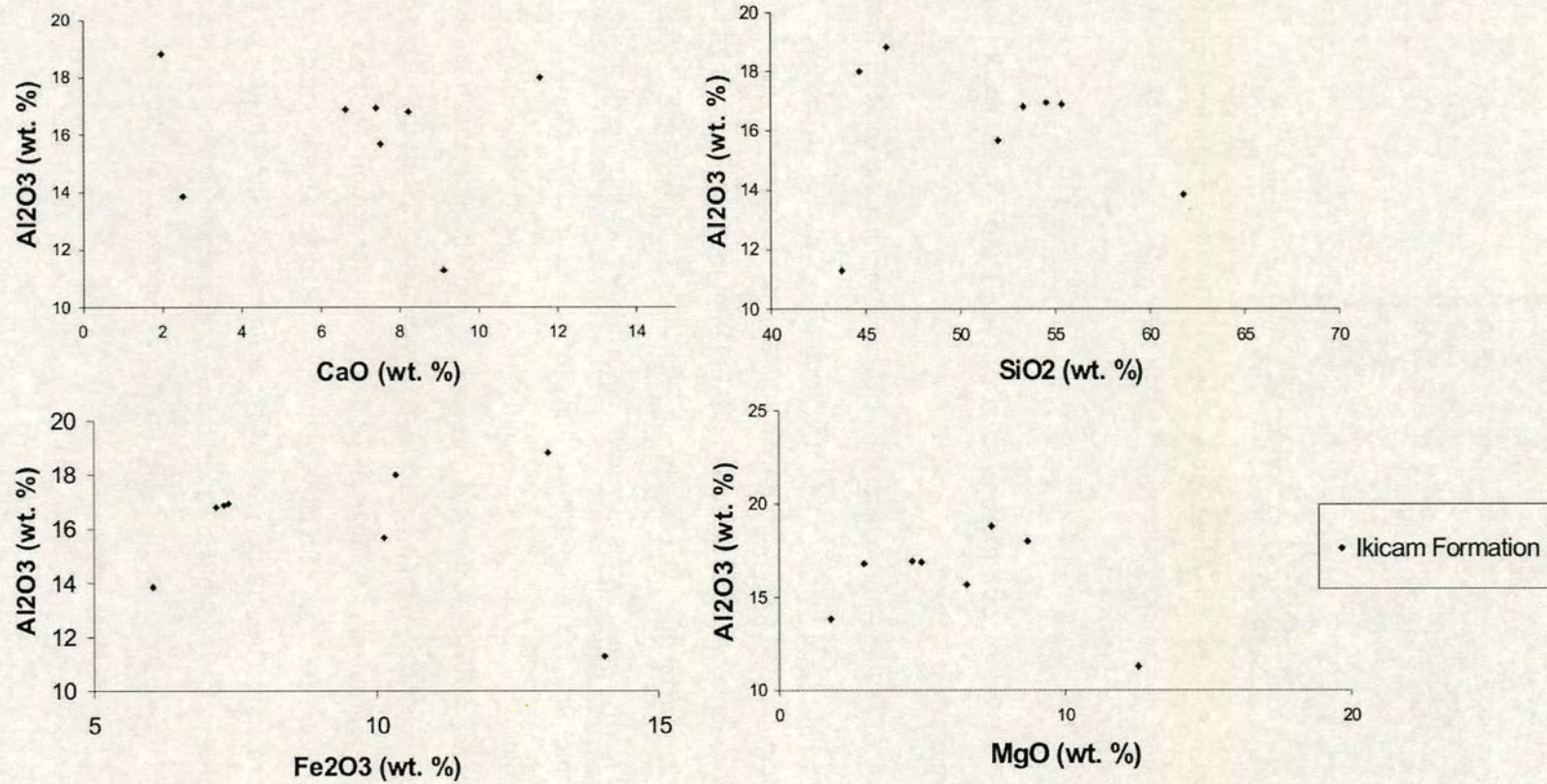


Figure 5.92. Harker diagrams showing variation between pairs of potentially mobile elements for samples from the İkiçam Formation.

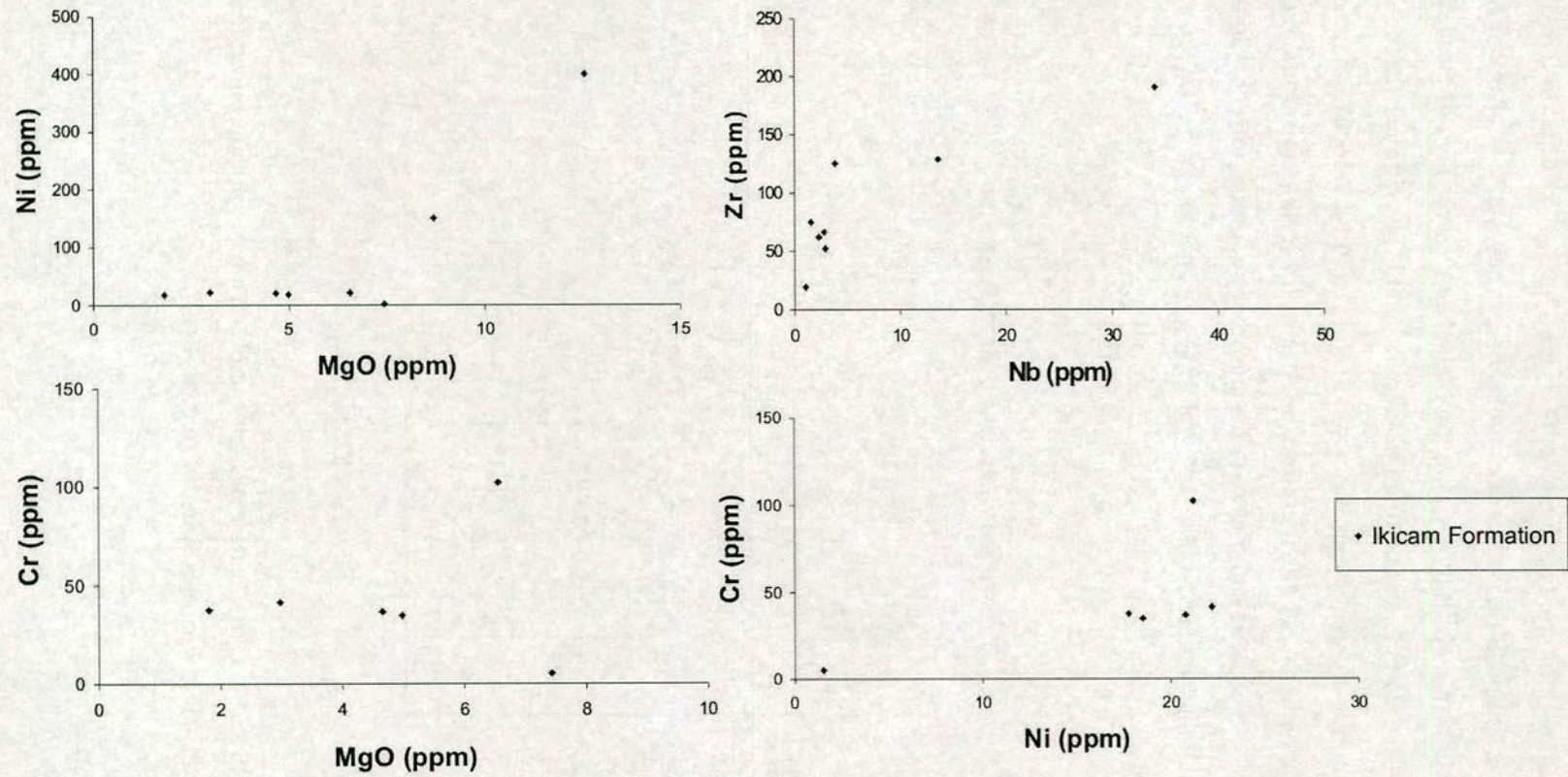


Figure 5.93. Harker diagrams showing variation between immobile elements for samples from the İkiçam Formation.

The ten samples are classified using the total alkalis vs. silica diagram in Figure 5.94. All but one of the samples have basic compositions. A classification based on immobile trace elements (Figure 5.95) shows that in five of the samples the basic composition is a reflection of their primary igneous chemistry and not a result of element mobilisation during secondary processes. Two of these samples have MgO+CaO outside the range 12-22 wt. % and five samples are shown to have immobile element compositions indicative of intermediate (andesitic) primary rock compositions and are, therefore, not useful for tectonic discrimination (section 3.3.8).

The three samples with basic primary compositions are plotted on seven basalt discrimination diagrams below (Figures 5.96 and 5.102; see section 3.3.8.4 for explanation).

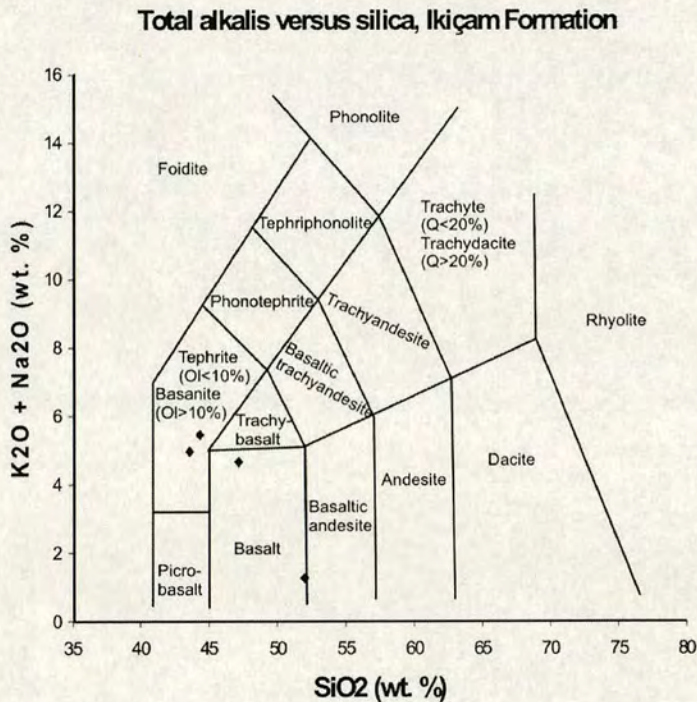


Figure 5.94. Classification of rock samples from the İkiçam Formation on the total alkalis-silica diagram (Le Maitre et al. 1989).

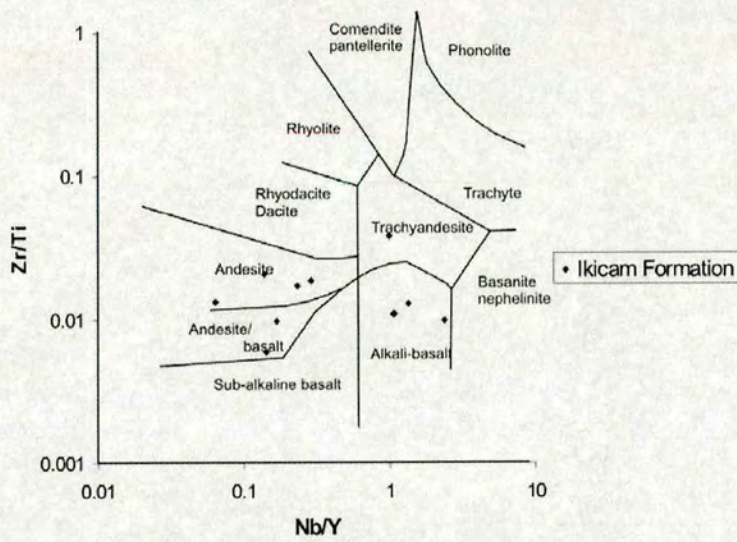


Figure 5.95. Classification of igneous rocks from the İkiçam Formation using immobile trace elements Zr, Ti, Nb and Y (Winchester and Floyd 1977).

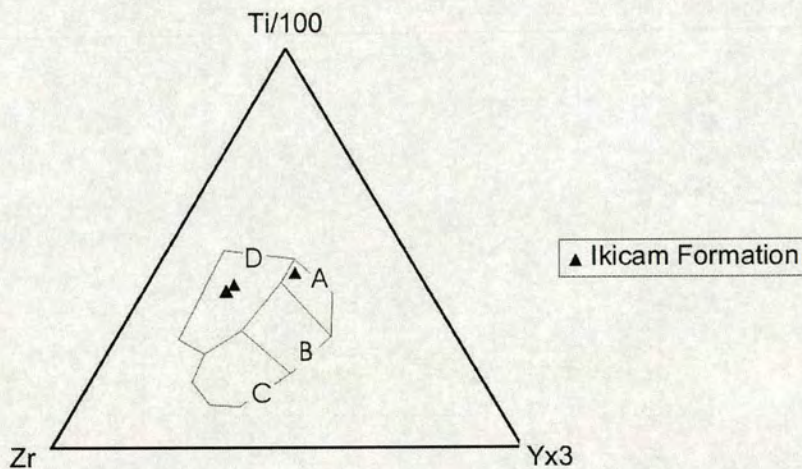


Figure 5.96. Basic igneous rocks from the İkiçam Formation plotted on the ternary Ti/Zr/Y discrimination diagram (Pearce and Cann 1973). Within-plate basalts field D, ocean-floor basalts in field B, low-potassium tholeiites in fields A and B, calc-alkali basalts in fields C and B.

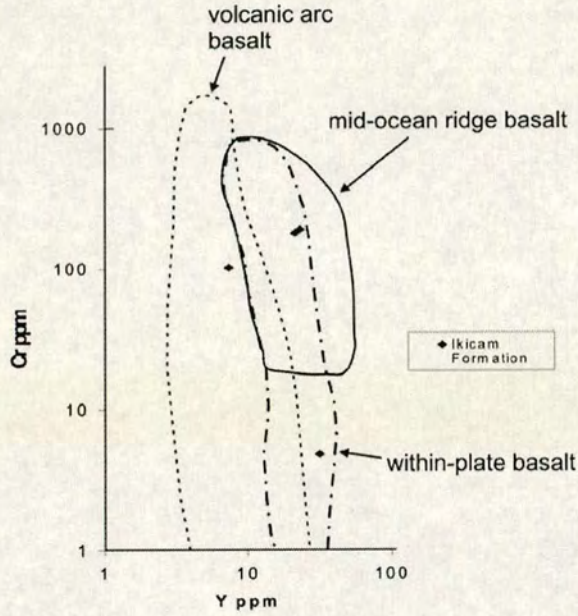


Figure 5.97. Basic igneous rocks from the İkiçam Formation plotted on the Cr-Y discrimination diagram (Pearce 1982).

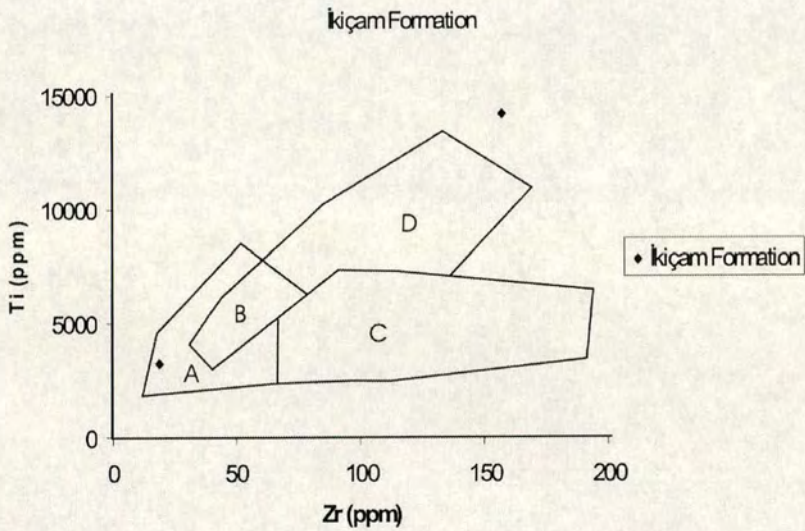


Figure 5.98. Basic igneous rocks from the İkiçam Formation plotted on the Ti/Zr discrimination diagram (Pearce and Cann 1973). Ocean-floor basalts plot in fields D and B; low-potassium tholeiites in fields A and B, and calc-alkali basalts in fields C and B.

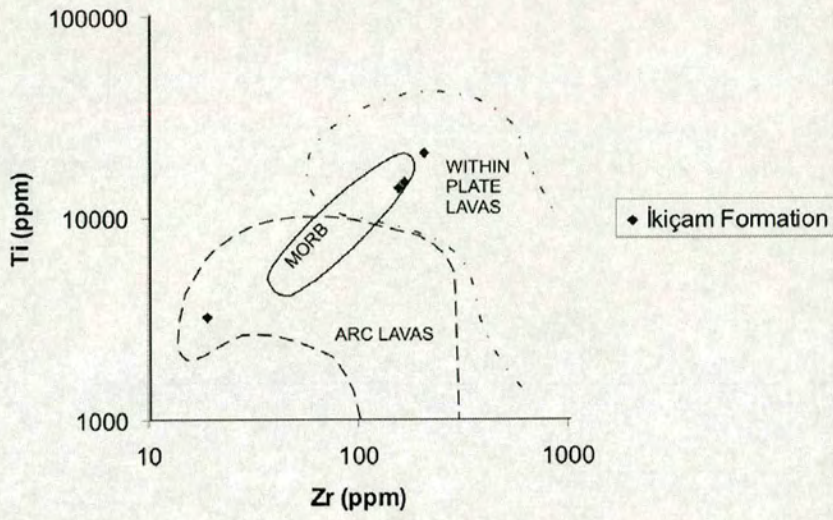


Figure 5.99. Basic igneous rocks from the İkiçam Formation plotted on the log Ti/log Zr discrimination diagram (Pearce 1982). Ocean-floor basalts plot in fields D and B; low-potassium tholeiites in fields A and B, and calc-alkali basalts in fields C and B.

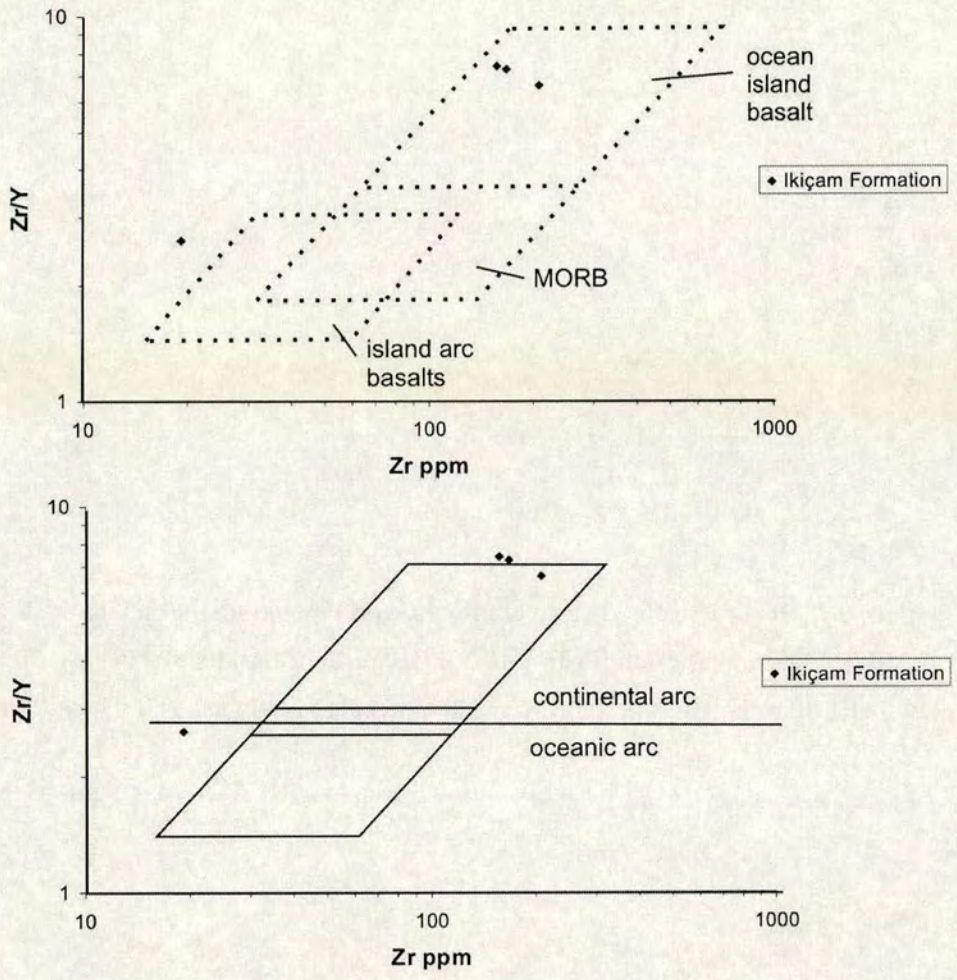


Figure 5.100. Basic igneous rocks from the İkiçam Formation plotted on the Zr/Y versus Zr discrimination diagram (Pearce and Norry 1979).

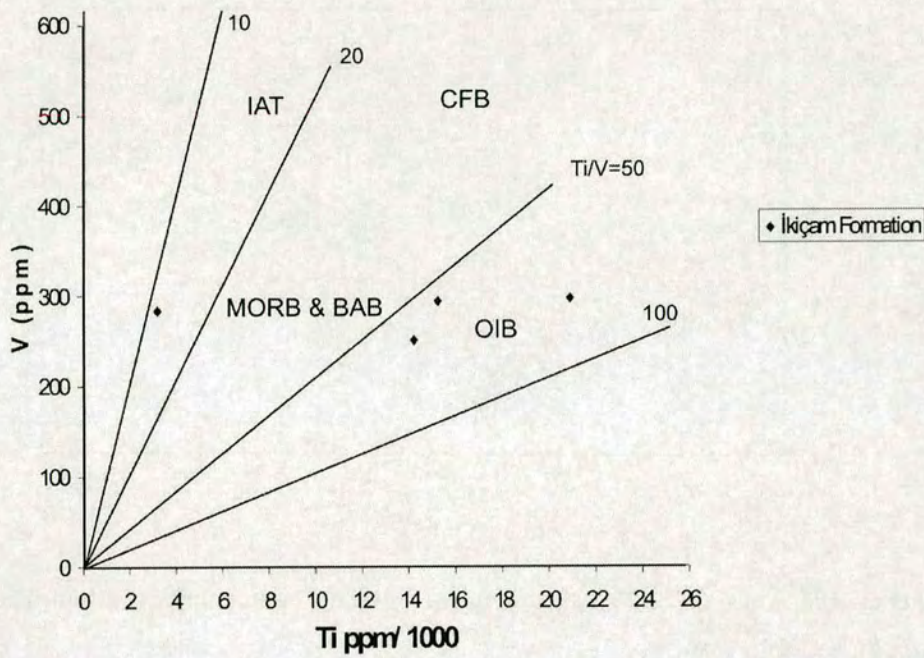


Figure 5.101. Basic igneous rocks from the İkiçam Formation plotted on the V/Ti discrimination diagram (Shervais 1982).

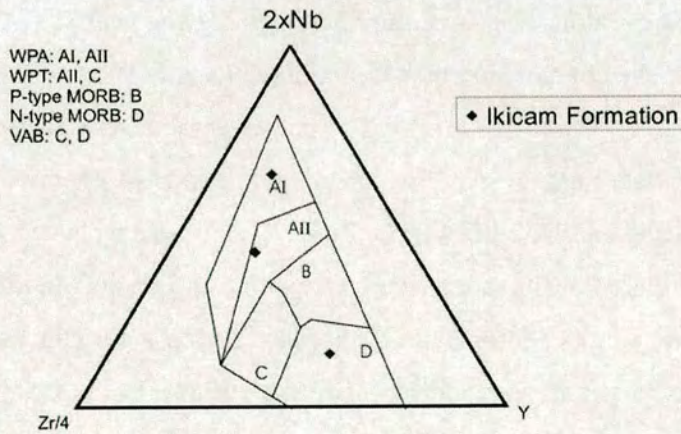


Figure 5.102. Basic igneous rocks from the İkiçam Formation plotted on the Nb/Zr/Y discrimination diagram (Meschede 1986). AI and AII = within-plate alkali basalt compositional field, B = plume-influenced MORB compositional field, C = within-plate tholeiite compositional field, D = N-type MORB and volcanic arc basalt.

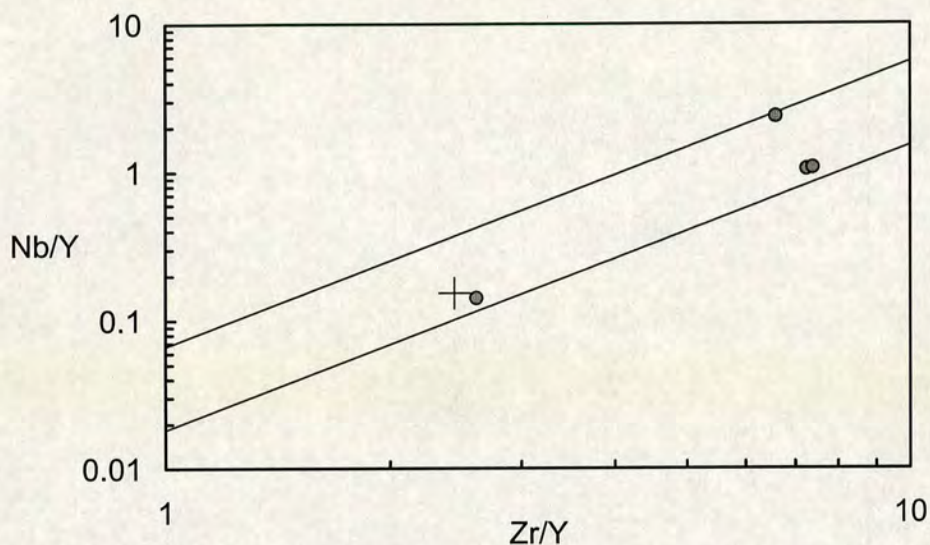


Figure 5.103. Nb/Y vs. Zr/Y variation for lavas from the İkiçam Formation. Diagram from Fitton et al. 1997.

On the Ti-Zr-Y ternary diagram (Figure 5.96; Pearce and Cann 1973) the samples are all 'Within-Plate Basalts' apart from one 'Volcanic Arc Basalt'. This is confirmed by the Cr/Y diagram (Figure 5.97; Pearce 1982) on which the composition of two of the Within-Plate Basalts overlaps with the compositional field for MORB. On the linear plot of Ti/Zr (Figure 5.98; Pearce and Cann 1973) the samples lie closest to the composition of 'Ocean Floor Basalt'. The logarithmic plot of Ti/Zr (Figure 5.99; Pearce and Cann 1973) shows agreement with the Cr/Y diagram i.e. 'Within-Plate Lava', (two of which are ambiguously either Within-Plate Lava or MORB) and one 'Arc Lava'. The Zr/Y vs. Zr diagram also confirms this. The three 'Within-Plate Basalts' are termed 'Ocean Island Basalts' on this diagram and plot in the same space as continental arcs because the Zr/Y enrichment is not a measure of alkalinity but of an enriched source (Pearce 1983). Both Ocean Island Basalts and Continental Arc Lavas could be derived from a similarly enriched source with the only difference being the presence or absence of a subduction component (Pearce 1983). The V/Ti plot (Figure 5.101; Shervais 1982) and the Nb-Zr-Y ternary diagram (Figure 5.102; Meschede 1986) are consistent with the results of the other discrimination diagrams. On these diagrams the three samples are 'Ocean Island

Basalts' or 'Within-Plate Alkali Basalt'. The Nb/Y vs. Zr/Y plot (Fitton et al. 1997) shows the lavas from the İkiçam Formation fall within the range of Icelandic basalts, i.e. plume-influenced MORB. Figure 5.104 shows that the MORB-normalised multi-element patterns of the basaltic samples from the İkiçam Formation do not exhibit any subduction component (eg. negative Nb anomaly, HFSE depletion). The samples do, however, exhibit an enrichment of Ti relative to Y, a distinctive feature of Within-Plate lavas (Pearce 1982).

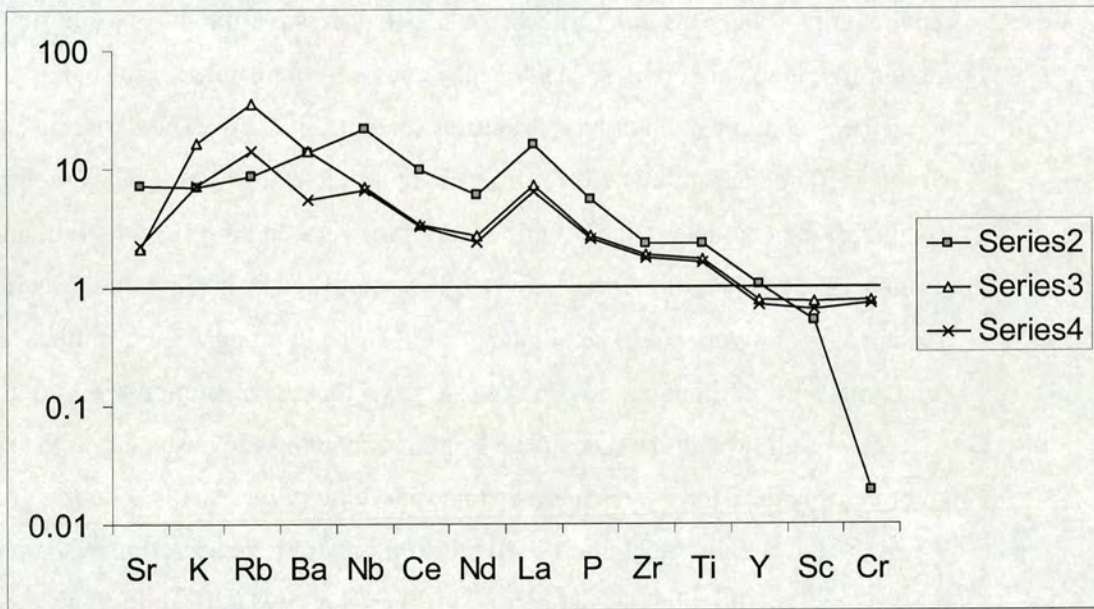


Figure 5.104. MORB-normalized multi-element abundances for unaltered basic dykes from the İkiçam Formation. Normalizing values: Sr = 120 ppm; K₂O = 0.15% ; Rb = 2.0 ppm; Ba = 20 ppm; Nb = 3.5 ppm; La = 3 ppm; Ce = 10 ppm; Nd = 8 ppm; P₂O₅ = 0.12% ; Zr = 90 ppm; TiO₂ = 1.5% ; Y = 30 ppm; Sc = 40 ppm; Cr = 250 ppm (Pearce 1973).

In summary the discrimination diagrams show that the three samples are 'Within-Plate Alkali Basalts'.

5.7.4 Environment of deposition and tectonic setting of the İkiçam Formation.

The İkiçam Formation begins with a muddy and tuffaceous limestone and pelitic facies which contain age-diagnostic, dominantly pelagic foraminifera (e.g. *Globotruncana*) that have a deep-water habitat (Stewart and Pearson 2000). This lowest facies in the succession contains no coarse-grained or texturally immature sediments and is interpreted as a deep-marine carbonate basin of Late Cretaceous age that contains distal volcanic tuff horizons. This facies is followed by thin- to medium-bedded calcarenites, sandy limestones and sandstones with shaly partings. These beds contain sedimentary structures (e.g. grading, cross-bedding, planar lamination) and commonly exhibit sole-marks such as load-casts. These sediments exhibit all the characteristic features of a turbidite succession (Bouma sequence; Bouma 1962). Some of the beds are rich in sericite and volcanic lithoclasts indicating a terrigenous provenance. The compositional variety amongst the turbidites (volcaniclastic, carbonate, terrigenous) suggests that the existence of a variety of sources of sediment to the basin. The Pontide metamorphic basement to the north is an obvious source for the terrigenous material. Fine polycrystalline quartz grains are interpreted as mainly meta-chert derived from pre-Jurassic accretionary complexes preserved in the Pontides (Ustaömer and Robertson 1997). In addition, the interfingering relations suggest that the volcaniclastic material was derived from an adjacent magmatic arc unit. The calciturbidites suggest that carbonate shelves were also a source for the turbidites. Deposition was accompanied by enriched within-plate type volcanism, together with sparse alkaline-peralkaline volcanism that could have been extension-related.

5.7.5 Summary

The Upper Cretaceous İkiçam Formation represents a volcanically active deep-water slope setting, with an increasing abundance of texturally immature volcanic and terrigenous sediments upwards. The unit contains deep-water and intermediate depth species of foraminifera. The İkiçam Formation interdigitates with the Upper Cretaceous Yaylaçayı Formation.

Deposition was accompanied by enriched within-plate type volcanism, together with sparse alkaline-peralkaline volcanism that was probably extension-related. Pillow lavas and sills within the succession are 'Within-Plate basalts' and 'Volcanic Arc Basalts'.

Early top-to-the-north shear fabric and folding is refolded by top-to-the-south folds and cut by top-to-the-south thrusts. The İkiçam Formation is interpreted as northward emplaced sedimentary deposits of a backarc basin (see Chapter 6).

5.8 Post-collisional sediments: Kadıkızı Formation

The Kadıkızı Formation (estimated >500 m thick; Figure 5.105) of Mid Eocene (Lutetian) age (from biostratigraphy) crops out north of Tosya (Figures 5.106 and 5.107) and comprises a succession of relatively undeformed sediments unconformably overlying the Kirazbaşı Mélange. The succession begins with Nummulitic limestones and then grades into calcarenites and shales. These sediments gradually pass stratigraphically upwards into lenticular conglomerate beds which then increase in abundance towards the top of the unit. Near the village of Kadıkızı, the Formation lies directly on the Kirazbaşı Mélange, which contains a variety of lithologies within large blocks. The base of the Kadıkızı Formation is exposed in a stream north of Kadıkızı village (gr: F32, 9525561941), where pale, fine-grained limestone unconformably overlies basalt (within the Kirazbaşı Mélange) and fills thin (3 cm) neptunian dykes. The base of the Kadıkızı Formation is also well exposed unconformably overlying a block of massive grey recrystallised fine-grained limestone (with patchy secondary chert nodules) within the Kirazbaşı Mélange, about 1 km west of Kadıkızı village. The unconformity surface is highly irregular suggesting that the underlying limestone block within the mélange may have been weathered prior to deposition of the Kadıkızı Formation. The Kadıkızı Formation is unconformably overlain by red, fissile Plio-Quaternary conglomerates.

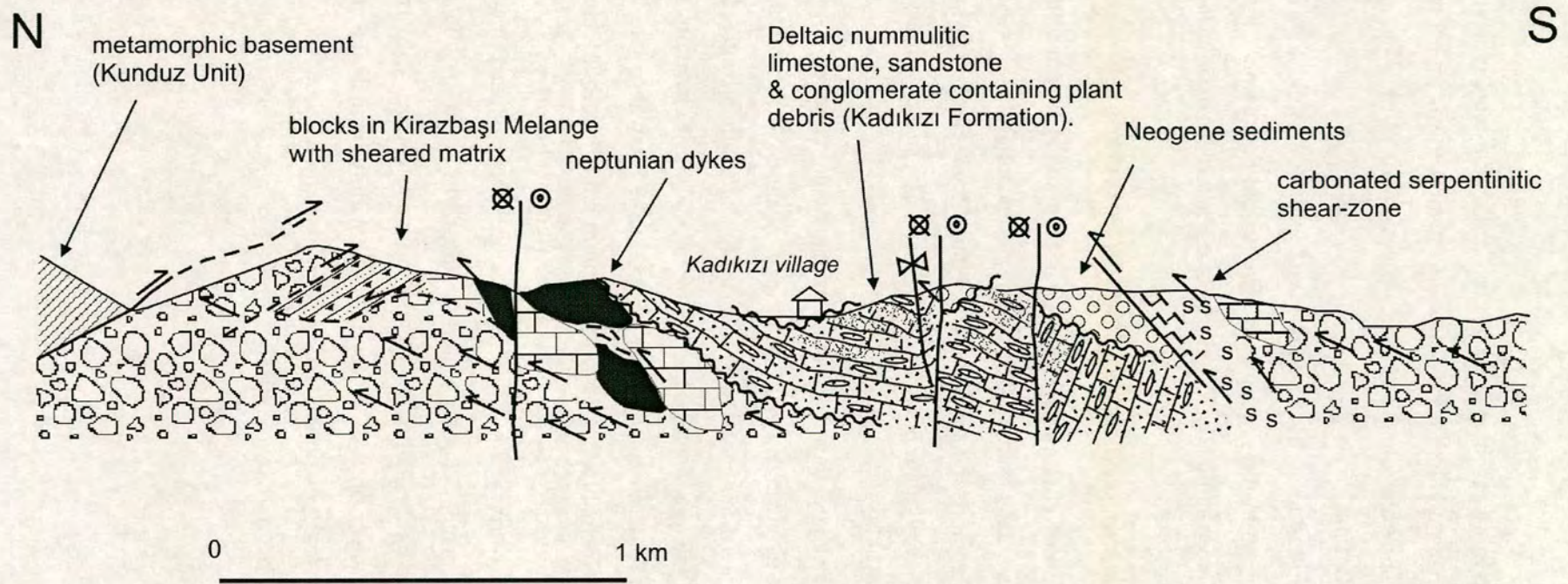


Figure 5.105. Cross section at Kadıkızı village showing the Eocene Kadıkızı Formation unconformably overlying the deformed Kirazbaşı Mélange.

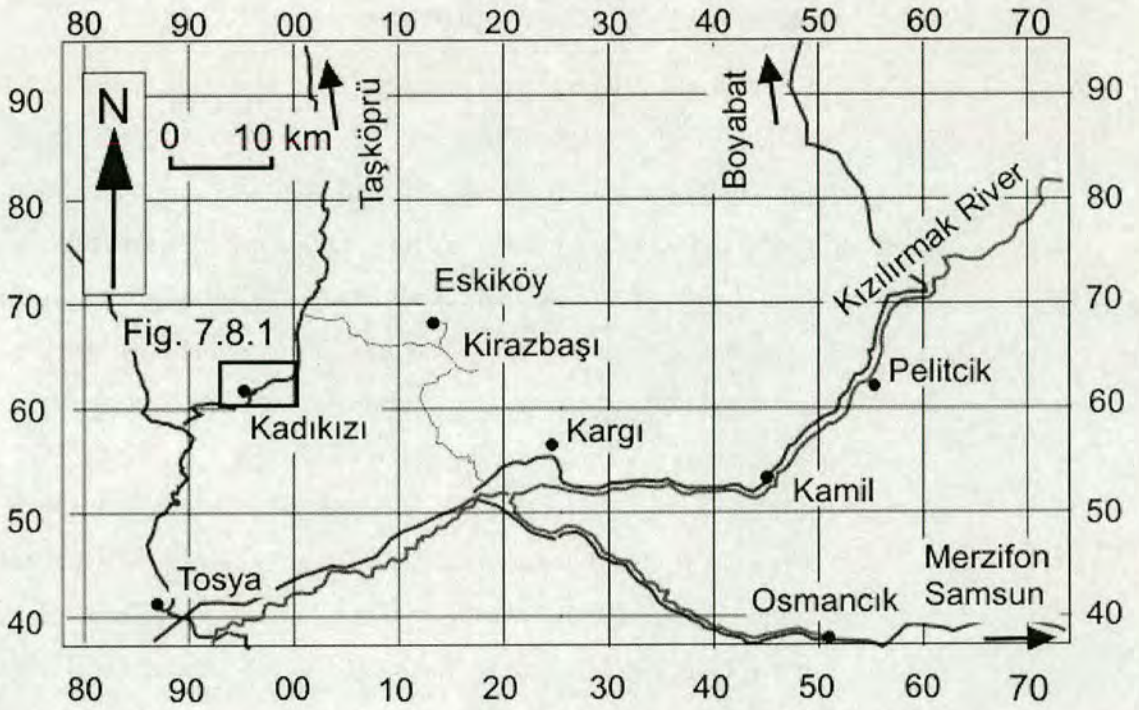


Figure 5.106. Map showing location of outcrop of the Kadıkızı Formation.

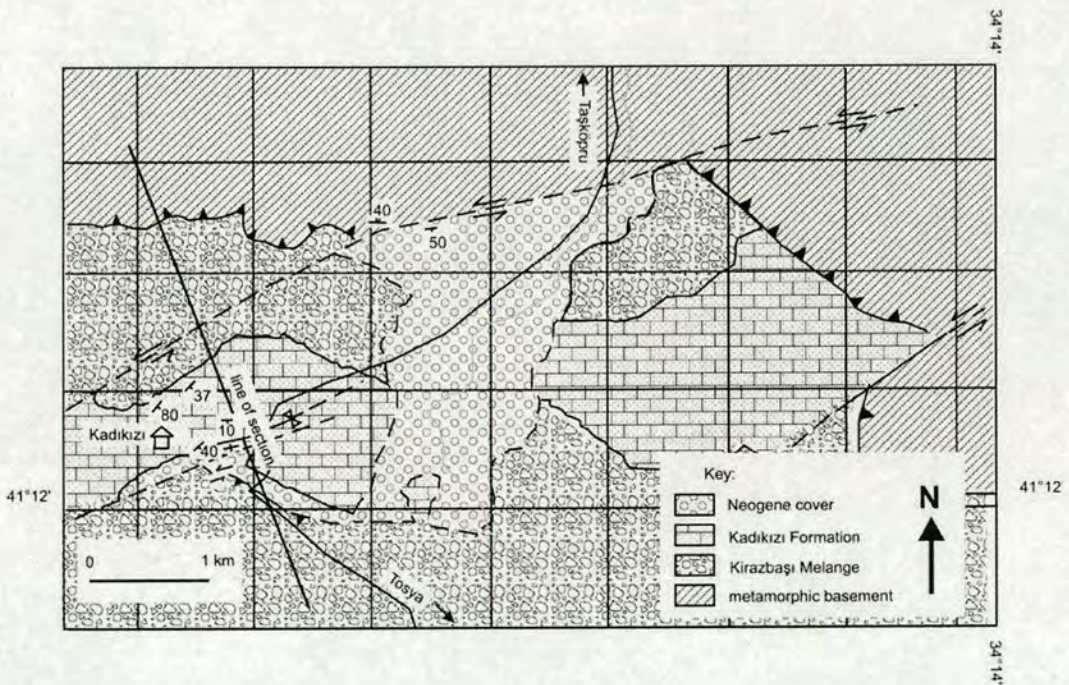


Figure 5.107. Geological map of the Kadıkızı area showing the outcrop of the Kadıkızı Formation, unconformably overlying the Kirazbaşı Mélange.

5.8.1 Structure of the Kadıkızı Formation

The Kadıkızı Formation crops out along the Tosya-Taşköprü road as part of an E-W trending, upright open syncline (wavelength >1 km) within a small elongate valley bounded by ENE-WSW trending strike-slip faults (Figures 5.105 and 5.107). These strike-slip faults cut the overlying Plio-Quaternary sediments and are part of the North Anatolian Fault Zone (Dhont et al. 1998). The valley is interpreted as a small pull-apart basin. The rocks of the Kadıkızı Formation are not well cleaved and the unit does not exhibit pervasive shear-fabric or small-scale folding. Only one minor fold was observed. This observed minor fold is open, inclined ($55^{\circ}\text{N}/100^{\circ}$) and gently plunging SW (30° to 245° ; Figure 5.108). The beds are the right way-up and most of the outcrop young southward. The large-scale upright synclinal axial plane shown on Figure 5.108 is inferred from measured bedding orientations. The inferred orientation is $75^{\circ}/140^{\circ}$ with a plunge of 8° to 225° . Because most rotation has affected the sub-vertical southern limb it is likely that this fold is north-vergent.

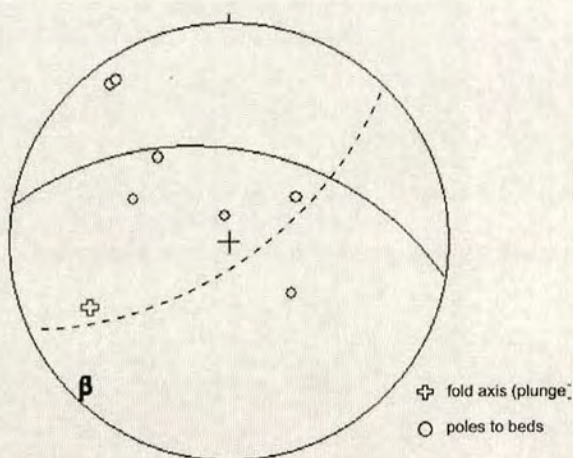


Figure 5.108. Lower hemisphere equal-area projection of structural data from the Kadıkızı Formation. Solid great circle marks the axis of a minor fold measured in the field. Dashed great circle marks the major fold axis inferred from bedding orientations. $\beta = 8^{\circ}$ to 225° .

Three faults were observed cutting the unit and were orientated $50^{\circ}\text{-}90^{\circ}/090^{\circ}$ and one at $90^{\circ}/010^{\circ}$. The faults exhibit low-angle slickensides (12° and 35°) that

define a top-to-the-north, dextral sense of motion. These faults also cut the unconformably overlying younger sediments.

5.8.2 Age and sedimentary facies of the Kadıkızı Formation

The Kadıkızı Formation comprises dominantly sandy bioclastic limestones containing abundant plant debris, large benthic *Nummulites sp.* and coarse shell fragments. The *Nummulites* constrain the age of this unit to Mid Eocene (48.6-40.4 Ma) (Prof. Izver Ongen, Prof. Kemal Taşlı and Prof. Nurdan İnan, Pers. comm. 2004; see Appendix 1). Their water depth habitat was in the range 20-100 m (Stewart and Pearson 2000). The formation begins with thin (~5 cm) graded beds of medium- to coarse-grained (<3 mm), poorly-sorted, pebbly litharenite composed of metamorphic clasts, quartz, mafic lithoclasts and pyrite. These graded sandstones exhibit (<20 cm) muddy micritic limestone tops (wackestone containing <50% sand grains) and contain detrital plant debris (lignite). The sandstone is interbedded with blueish grey silty marl.

The litharenites and marl are followed by thick bedded (<40 cm), massive, medium-grained and poorly sorted nummulitic calcarenites and calcareous quartzose sandstones, interbedded with laminated grey shale. The nummulitic calcarenite and calcareous quartzose sandstones dominate the mid levels of the succession. The calcarenite beds exhibit irregular bases and flat tops, which show that the unit is the right way-up stratigraphically, and that it locally youngs southwards (Figure 5.105). The sandstones are a light grey colour, well-bedded (beds <10 cm), medium- to poorly-sorted coarse-grained, nummulitic, quartz-rich calcareous arkoses. These sandstones are thinly bedded (2 mm – 5 cm), cross-bedded and laminated. They contain large bivalves, feldspar, white mica (up to 0.75 mm) and minor amounts of mafic lithoclasts and rare outsize clasts (~5 cm) of vein quartz.

The upper part of the succession comprises interbedded lenticular conglomerate bodies (~1 m thick) and laminated shale. The conglomerate contains large (<20 cm), well-rounded, spherical, clasts of quartz and, rollers and blades of mica schist (probably derived from the Kunduz unit) and vein quartz. The conglomerate beds are clast-supported, to locally matrix-supported, and exhibit clast imbrication. The long axes of clasts dip 30° east on gently southward-dipping

bedding planes, suggesting that Eocene palaeocurrents flowed towards the west. The conglomerate lenses have erosive bases. The abundance of conglomerate beds increases stratigraphically upwards.

5.8.3 Depositional setting

The irregular unconformity at the base of the formation indicates that the underlying Kirazbaşı Mélange was eroded before deposition of the Kadıkızı Formation. However, it is not clear whether the Kirazbaşı Mélange was subaerially exposed before deposition of the Kadıkızı Formation. The marine fauna present throughout the succession eg *Nummulites sp.* indicate that this is a marine succession deposited in a neritic environment (20-200 m; Stewart and Pearson 2000). The presence of plant material suggests sediment input was from nearby fluvial distributary channels (Nichols 1999).

Sandstones within the succession are interpreted as terrigenous litharenites and contain well-rounded clasts indicating abrasion in fluvial or shoreline environments while the low degree of sorting suggests that the sediment has been redeposited. Clast imbrication and graded bedding in the lower part of the formation indicates that the redeposition occurred from waning water currents (Tucker 1981).

The nummulitic calcarenites are coarse-medium grained. Together with the presence of large benthic *Nummulites* this suggests that the calcarenites probably also accumulated in a shelf-depth setting. Their calcareous composition indicates a relatively low lithoclastic input. The interbedded laminated shales could be interpreted as normal background sedimentation into which the thick bedded, massive calcarenites were redeposited from the carbonate shelf by dense sediment-laden currents (Leeder 1982).

Towards the top of the succession the calcarenite deposition is replaced by grey laminated shale and lenses of conglomerate. The clastic composition of the conglomerates indicates a metamorphic source region (i.e. they are terrigenous). The clasts were highly abraded in fluvial and/or beach environments. Together with their clast-supported fabric and clast imbrication this suggests they were redeposited by water rather than sediment-gravity flows. They have erosive bases into the shale. Their lenticular geometry therefore suggests that they were deposited in channels.

The shales contain no evidence for emergence (e.g. there are no rootlets or evaporites) and are interpreted as a product of marine or lacustrine deposition. Stratigraphically upwards the succession exhibits an increase in the grain size and abundance of metamorphic lithoclasts while the abundance of carbonate decreases. The terrigenous sandstone and conglomerate beds become lenticular towards the top of the succession. This suggests an increase in the proximity of the source of terrigenous material. The succession is regressive and records a transition from shallow carbonate shelf (<200 m; lower shoreface; McLane 1995) to proximal submarine fan or delta.

5.8.4 Summary

The Kadıkızı Formation, in the area studied, represents a shallow water (<200 m), proximal submarine fan or delta of Mid Eocene age (48.6-40.4 Ma) constructed directly upon the Upper Cretaceous Kirazbaşı Mélange. The presence of large benthic foraminifera *Nummulites sp.* indicate a Mid Eocene (Lutetian) age for the unit. The Kadıkızı Formation contains a variety of mafic lithoclasts and metamorphic terrigenous material. Because the Kadıkızı Formation is relatively undeformed at outcrop scale, and does not exhibit north-vergent deformational structures its age constrains the timing of early north-vergent collision-related deformation that is observed in the underlying Kirazbaşı Mélange and the other Upper Cretaceous units to pre-Mid Eocene.

5.9 Summary of the suture zone in the Central Pontides

In the north of the area, the Eskiköy Formation, of Campanian age (83.5-70.6 Ma), records an abrupt change from tropical weathering of an emergent continental margin area to open-marine pelagic carbonate deposition, initially with little or no clastic input. Carbonate deposition was followed by deposition of turbidites derived from terrigenous and ophiolitic sources. Taking account of its tectono-stratigraphic position (i.e. unconformably above Eurasian basement and tectonically overlain by ophiolitic *mélange*) the Eskiköy Formation records subsidence of the Eurasian margin prior to the emplacement of accretionary *mélange*. It is likely that the subsidence of the Eurasian margin, and the deposition of the Eskiköy Formation were a direct result of the emplacement of ophiolitic units during the initial stages of the collision of oceanic and continental margin units. Therefore, the Eskiköy Formation is interpreted as a trench-margin collision facies (Robertson 1994). It thus constrains the emplacement of the ophiolitic *mélange* to no older than Campanian (83.5-70.6 Ma).

The Kızılırmak Ophiolite is a ~3.5 km thick, relatively intact ophiolite of Campanian-Maastrichtian age (83.5-65.5 Ma; Tüysüz 1988, 1990). Coherency of ENE-WSW sheeted dyke orientations suggests that an oceanic spreading centre could have been orientated in this direction, and suggests regional NNW-SSE extensional palaeostress. Dextral strike-slip faults are orientated ~90° to the sheeted dykes (i.e. NNW-SSW) and may represent oceanic transform faulting. Isolated diabase and plagiogranite dykes are uncommon in the Kızılırmak Ophiolite. Whole-rock basalt geochemistry and chromian spinel compositions indicate that the Kızılırmak Ophiolite represents either lithosphere formed at a mid-oceanic ridge or in a backarc setting. The ophiolite exhibits a pervasive north-vergent shear fabric cut by top-to-the-south thrust faults and sinistral strike slip faults. Based on biostratigraphic data of Tüysüz (1988) the ophiolite is of Campanian-Maastrichtian age (83.5-70.6 Ma). The ophiolite was therefore emplaced from south to north during Late Cretaceous (Campanian-Maastrichtian) time.

The Kirazbaşı *Mélange* contains blocks of Albian to Late Maastrichtian age (112-65.5 Ma). This range represents the age of the Neotethyan lithosphere that was

subducted and provides a maximum age of *mélange* accretion (i.e. Late Maastrichtian). The *mélange* is interpreted as an accretionary complex that developed in response to northward subduction of Neotethys and contains two lithological associations; 1) a chert-basalt-serpentinite-clastic association that represents oceanic lithosphere with a terrigenous sedimentary cover; 2) a massive limestone-volcaniclastic association that represents a volcanic seamount facies. Whole-rock geochemistry of basic igneous rocks from the Kirazbaşı *Mélange* indicates that the lavas have 'within-plate' and MORB compositions. Some of the samples have compositions that are ambiguous and could be either MORB or 'Island Arc Tholeiite'. The *mélange* has a paucity of sedimentary matrix relative to blocks of ophiolitic association (e.g. peridotite, diabase, chert). This indicates a low degree of sediment accretion and/or deposition at the trench. The *mélange* could have formed in an oceanic setting, far away from the continental margin. Blocks of terrigenous sediment are common within the *mélange* in the north of the area while blocks of pelagic chert, sheeted dykes and gabbro are more common in the south. This could represent the original transition between the continental margin in the north and oceanic lithosphere to the south. The blocks of terrigenous sediment could have been progressively accreted into the *mélange* as it approached the continental margin. Alternatively the terrigenous sedimentary blocks could have been tectonically included during backthrusting. The *mélange* exhibits a pervasive north-vergent shear fabric that is cut by top-to-the-north thrust faults. The top-to-the-north fabric could be related to northwards emplacement of the *mélange* onto the Eurasian margin. Top-to-the-south thrusts and shear-zones cut the top-to-the-north structures and juxtapose the *mélange* against various other units. top-to-the-south structures are interpreted as collision-related.

The Yaylaçayı Formation contains microfossils that indicate a Campanian-Maastrichtian age for the unit. Fine-grained sediments including chert, umber and micritic limestone are present between pillow lavas low in the succession. Texturally immature volcaniclastic sediments predominate at higher stratigraphic levels. The volcaniclastic succession then grades into fine-grained sandstone, shale and micritic limestone, (~500 m thick) at the top of the sequence. Whole-rock geochemical

analyses of basalts from the Yaylaçayı Formation show compositions comparable to modern volcanic arcs and MORB. Some samples also have enriched compositions. Northerly outcrops of the unit are schistose. The cleavage dips to the northwest and is folded by south-vergent folds. Top-to-the-north compressive structures are commonly cut by top-to-the-south structures. Later normal and strike-slip faults also cut the unit.

The Campanian-Maastrichtian Yapraklı Formation is interpreted as a proximal (upper) submarine fan or slope facies (Nichols 1999) deposited following a marine transgression of the volcanic arc. Following initial transgression of the volcanic arc (Yaylaçayı Formation) the unit records a regression from inferred offshore to upper shoreface deposition. This could be either due to relative sea-level fall or progradation of the sediments. The shallow-water carbonate grains and shell fragments (e.g. rudists) were possibly derived from carbonate environments built upon or, around, the inferred volcanic arc edifices (represented by the Yaylaçayı Formation) in the area studied.

The Upper Cretaceous İkiçam Formation represents a volcanically active deep-water slope setting, with an increasing abundance of texturally immature volcanic and terrigenous sediments upwards. The unit contains deep-water and intermediate depth species of foraminifera. The İkiçam Formation interdigitates with the Upper Cretaceous Yaylaçayı Formation. Early top-to-the-north shear fabric and folding is refolded by top-to-the-south folds and cut by top-to-the-south thrusts. Deposition was accompanied by enriched within-plate type volcanism, together with sparse alkaline-peralkaline volcanism that was probably extension-related. Pillow lavas and sills within the succession are 'Within-Plate basalts' and 'Volcanic Arc Basalts'. The İkiçam Formation is interpreted as a backarc basin (see Chapter 6). A minimum age for accretion of the Kirazbaşı Mélange is provided by the Mid Eocene Kadıkızı Formation which are the oldest overlying sediments.

6 Discussion

6.1 Introduction

In this chapter key data from the Eastern Pontides and Central Pontides are compared and then discussed in the regional and global tectonic context.

6.1.1 Comparison of the Izmir-Ankara-Erzincan Suture Zone in the Eastern and Central Pontides.

In the Eastern Pontides the south Tethyan margin is represented by a thick carbonate succession that is interpreted as a stable carbonate platform; the Triassic-Upper Cretaceous Munzur Dağı Formation (Şengör and Yilmaz 1981, Özgül and Turşucu 1984). The top of the neritic carbonate succession passes conformably into a thin micritic limestone unit (Ayıkayası Formation Figure 6.1; section 3.2) which contains a pelagic microfauna of Campanian-Maastrichtian age (section 3.2, Özgül and Turşucu 1984). The upper levels of the Ayıkayası Formation contain conglomerates and sandstones with ophiolitic lithoclasts and pebbles of neritic carbonate. The obvious source for the limestone clasts is the Munzur Platform (Taurides) located to the south, while the ophiolitic lithoclasts are most likely to have been derived from the Izmir-Ankara-Erzincan Suture Zone to the north. The Ayıkayası Formation is interpreted as a trench-margin collision tectonic facies (Robertson 1994) and indicates a transition to deep-marine conditions during foundering of the south Tethyan margin ahead of ophiolitic nappes that were emplaced from the north (Özgül and Turşucu 1984). The same facies is observed in rocks of identical age 500 km southwest in the Taurides (Ozer et al. 2004) indicating roughly contemporaneous southward obduction of ophiolites onto the Tauride Platform. However, while ophiolites in the Munzur Mountains (Eastern extension of the Taurides) are likely to have been rooted in the Izmir-Ankara-Erzincan Suture Zone, those further southwest in the Taurides (e.g. Mersin) may have been rooted in a smaller south Tethyan ocean basin; the Inner Tauride Ocean (Clark and Robertson 2002).

In Central Anatolia ophiolites were emplaced southwards from the Izmir-Ankara-Erzincan Suture Zone onto the Kirşehir/Niğde massifs during Campanian-Maastrichtian time (Şengör and Yılmaz 1981; Floyd et al. 1998; Robertson 2004).

A very similar succession, also of Campanian age crops out in the Central Pontides to the north of the Izmir-Ankara-Erzincan Suture Zone (Eskiköy Formation; Figure 6.2; section 5.2). The base of the Eskiköy Formation is formed by a thin micritic limestone containing pelagic *Globotruncana* microfossils (Tüysüz et al. 1988, 1990; Ustaömer 1993; Yılmaz et al. 1997). The pelagic limestone passes upwards into turbiditic sandstone and shale containing ophiolitic and terrigenous material. However, in the Central Pontides the Eskiköy Formation lies directly upon the Palaeozoic-Early Mesozoic metamorphic basement of the Pontides (Tüysüz et al. 1988, 1990; Ustaömer 1993; Yılmaz et al. 1997). The terrigenous material and the ophiolitic lithoclasts observed within turbiditic sandstones of the Eskiköy Formation was presumably derived from the Pontides (Eurasian margin) to the north and the ophiolitic nappes advancing from the Izmir-Ankara-Erzincan Suture Zone to the south. The Eskiköy Formation records the development of a foredeep during northward emplacement of Neotethyan ophiolites onto the Eurasian margin in the Central Pontides during Campanian-Maastrichtian time (Ustaömer and Robertson 1997). This is roughly contemporaneous with the southward emplacement of ophiolites from the Izmir-Ankara-Erzincan Suture Zone and the Inner Tauride Ocean onto the south Tethyan margin in the Taurides (Ozer et al. 2004; Andrew and Robertson 2002). The volcanoclastic sediments within the succession could have been derived from a volcanic arc unit further south (the Koşdağ unit, interpreted as part of the Yaylaçayı arc; see below; Ustaömer and Robertson 1997). The volcanoclastic and terrigenous sandstones in the Eskiköy Formation are lithologically similar to parts of the İkiçam Formation and it is likely that the two units are intergradational.

The Refahiye Complex, of Cenomanian-Early Senonian age (Yılmaz 1985; Aktimur 1995) comprises an extensive thrust sheet of dominantly serpentinitised harzburgitic tectonite, ultramafic cumulates, gabbro and, a disrupted diabase sheeted dyke complex with screens of metamorphic host rocks (Figure 6.1; section 3.3). Thus, the Refahiye Complex exhibits the lower to mid-levels of a slice of oceanic-

type lithosphere. Whole-rock geochemistry of basic dykes and, chromite compositions show distinctive element enrichments transitional between supra-subduction zone (SSZ) and mid-ocean ridge basalt (MORB) compositions (section 3.3.8). The composite geochemistry of the Refahiye Complex is comparable to the composition of basaltic extrusive rocks from modern backarc basins (Weaver et al. 1979; Saunders and Tarney 1984). The metamorphic screens were first interpreted as parts of the Kirşehir Block (Kirşehir massif) tectonically emplaced into the ophiolite by the North Anatolian Fault Zone (Bergougnan 1975). However, the metamorphic rocks exhibit intrusive contacts with the sheeted dykes of the ophiolite (Yılmaz 1985). The metamorphic host rocks within the ophiolitic Refahiye Complex are comparable with the Upper Palaeozoic-Early Mesozoic metamorphic basement of the Pontides (e.g. Doğankavak Unit; Topuz et al. 2004). The cross-cutting dykes are inferred to be related to the adjacent exposures of 100% sheeted dykes. They are unlikely to represent fragments of older dyke-rich metamorphic basement, as exposed in some parts of the Pontides (e.g. Artvin region; T. Ustaömer, pers comm., 2004). The presence of igneous contacts between diabase dykes and their metamorphic host rocks, therefore, suggests that the ophiolite did not form in an

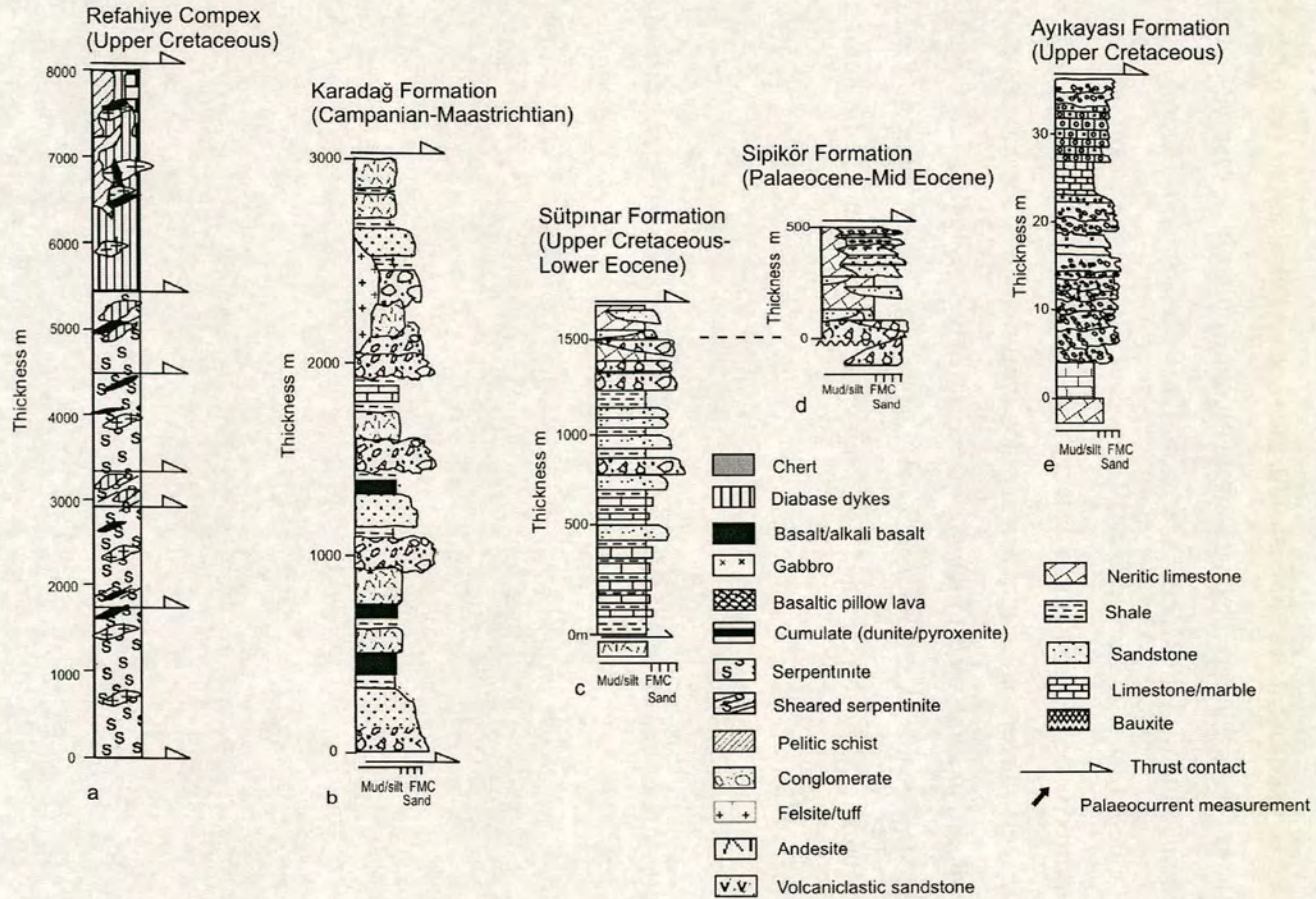


Figure 6.1. Composite logs of the units within the Izmir-Ankara-Erzincan Suture Zone in the Eastern Pontides.

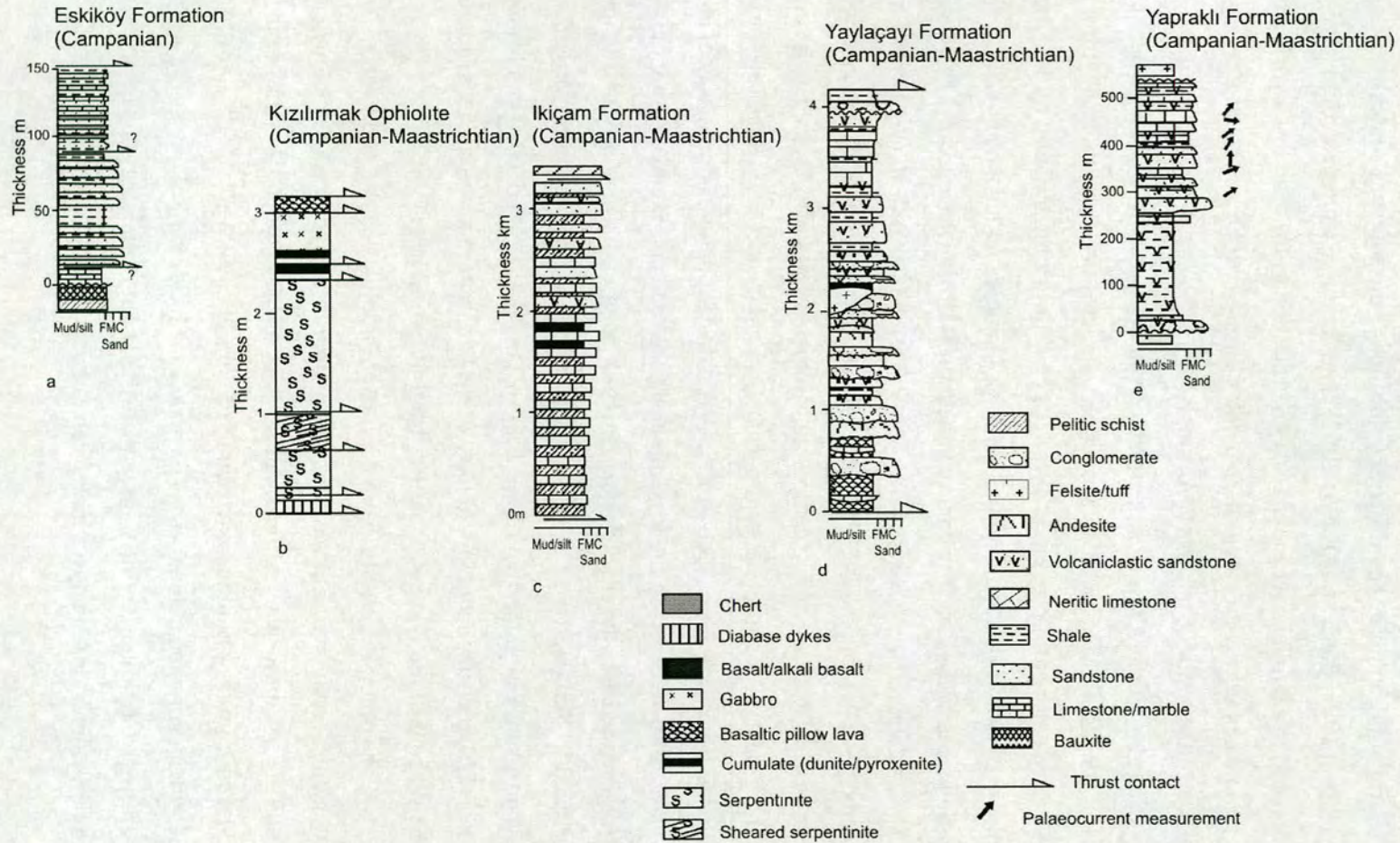


Figure 6.2. Composite logs of the units within the Izmir-Ankara-Erzincan Suture Zone in the Central Pontides.

intraoceanic setting, but instead within a rifted continental margin. Screens of metamorphic rocks have been used as evidence to support an autochthonous origin for the 'Rocas Verdes' ophiolites of the southern Andes, which are a classic example of a 'Cordilleran' ophiolite (cordilleran ophiolites of the southern Andes are described by Dalziel 1974, Stern and De Wit 2003). The Refahiye Complex could have originated in a similar way to the Rocas Verdes ophiolites. The Refahiye Complex was emplaced northwards onto the Pontides during Early Campanian-Early Maastrichtian time (Özgül 1981; Aktimur 1990, 1995).

In the Central Pontides the relatively intact Kızılırmak Ophiolite is thought to be of Campanian-Maastrichtian age based on microfossil assemblages within the associated epiophiolitic sedimentary rocks (Tüysüz 1990). Outcrop of the Kızılırmak Ophiolite is less extensive than the Refahiye Complex and isolated dykes and plagiogranite bodies are less common (section 5.30). The sheeted dykes trend ENE-WSW and subvertical dextral strike-slip faults trend NNW-SSE (i.e. normal to the sheeted dykes). It is possible that these orientations represent the original orientation of an oceanic-type spreading centre and associated transform faults. However, later tectonic rotation is entirely possible. Geochemical data indicate a backarc origin for the Kızılırmak Ophiolite (section 5.3.3). The discontinuous, lenticular geometry of the large thrust-slices and the high angle sheared contacts could indicate the role of strike-slip tectonics during emplacement of the ophiolite. Similar field relations are observed in southwest Turkey (Antalya Complex) where oblique convergence caused transpressional emplacement of the Tekirova Ophiolite (Woodcock and Robertson 1982). Oblique subduction could have played an important role in the tectonic development of the Izmir-Ankara-Erzincan Suture Zone.

The ophiolitic basalts from the Eastern Pontides have a composite geochemical character. Compositions are within the range for calc-alkaline and island arc basalts as well as for ocean floor basalts (section 3.3.8). The basalts analysed from the ophiolitic slices in the Central Pontides are of volcanic arc type but with an enriched component. The geochemistry of the Refahiye Complex and the Kızılırmak Ophiolite is consistent with a rifted continental margin backarc basin. Similar geochemical analyses have been obtained from a recent example of a rifted

backarc in the Bransfield Straits (section 6.3). In the Central Pontides the Kızılırmak ophiolite includes red shale and chert succession at the top of the section. Ustaömer and Robertson (1997) reported that these epiophiolitic sediments contain intercalated volcanoclastic sediments and interpreted them as being derived from the volcanic arc (Yaylaçayı Formation). This observation supports the geochemical evidence for genesis of the ophiolite within a backarc basin setting.

Extensive outcrops of *mélange*, dominantly composed of serpentinite, diabase, basalt, red radiolarite and pelagic limestone are exposed in the Eastern and Central Pontides (Karayaprak and Kirazbaşı *Mélanges* respectively; sections 3.4 and 5.4; Figure 6.3). The *mélange* in both areas contains two dominant associations interpreted as; 1) lithosphere formed at an oceanic spreading centre including basalt with N-MORB chemical characteristics and; 2) accreted volcanic seamounts with associated massive limestone and talus. The *mélange* is interpreted as an accretionary complex. Previous work has suggested that blocks in the *mélange* include limestones of Late Carboniferous, Permo-Triassic, and Late Jurassic-Cretaceous age (Yılmaz 1985; Koçyiğit 1990; Aktimur 1995; Rojay 1995). However, it has also been suggested that the *mélange* contains blocks of Campanian age and is, therefore, of Campanian or younger age (Yiğitbaş 1990; Yılmaz et al. 1997) Data obtained during this study indicate a Early Cretaceous maximum age for blocks within the *mélange*. This indicates the maximum age of oceanic lithosphere accreted during subduction and also indicates a maximum age for development of the accretionary complex. However, it is also possible that older oceanic crust existed but was not accreted.

During this study blocks of interbedded terrigenous sedimentary rocks, pelagic chert and mudstone were observed within the *mélange* in the north of the area in the Central Pontides where it is imbricated with metamorphic basement rocks (Kargı Complex; Tüysüz 1985, 1990). Ophiolitic blocks (e.g. gabbro, diabase sheeted dykes) were observed to be more abundant in the southern part of the suture zone. Yılmaz et al. (1997) noted that "The amount of the ophiolitic materials and thickness of the *mélange* slices within the imbricated pile show an apparent increase toward the south". Research in the Tokat and Çankırı areas led to the suggestion that two separate *mélange* belts exist in the Pontides representing two separate Upper Cretaceous subduction-accretion complexes (Rojay 1995; Tüysüz 1995). An

alternative interpretation was that mélangé development began in an oceanic setting in the south and progressed northwards towards the Eurasian margin (Yılmaz et al. 1997).

The northwards emplacement of ophiolitic mélangé onto the Eurasian margin in the Central Pontides is constrained by the oldest overlying sediments that do not exhibit a north-vergent deformational structure (Kadıkızı Formation), which are of Lutetian age (48.6-40.4 Ma; section 5.8).

In the Eastern Pontides there is little exposure of accretionary mélangé (Karayaprak mélangé) to the north of Erzincan (section 3.40). This may be due to deeper erosion locally related to Neogene transpressional tectonics, rather than reflecting any differences between the central and eastern Pontides in terms of the Late Cretaceous development of the suture zone. Where the Karayaprak Mélangé was observed north of Erzincan it exhibited a scaly clay matrix and is interpreted as a deformed sedimentary mélangé (olistostromal mélangé). The Karayaprak Mélangé in the Eastern Pontides exhibits a pervasive north-vergent shear fabric and north-vergent thrust faults. The north-vergent structures in the mélangé are also seen in all the Upper Cretaceous units of the suture zone and are interpreted to be related to their northward emplacement. The Karayaprak Mélangé is transgressively overlain by Palaeocene-Eocene sedimentary rocks that lack north-vergent deformational structures (Sipikör Formation; section 3.7). In addition, the Sipikör Formation does not occur as blocks in the mélangé and, therefore, the timing of northward emplacement of the accretionary mélangé from the Izmir-Ankara-Erzincan Suture Zone in the Eastern Pontides is constrained by the age of the Sipikör Formation. Bergougnan (1975) first named the Sipikör Formation and mapped it as Thanetian (Upper Eocene: 58.7-55.8 Ma). However, the Sipikör Formation appears to have a diachronous transgressive base and is intergradational with the Campanian-Lower Eocene Sütçinar Formation. North of Erzincan where the Sipikör Formation lies unconformably upon the Karayaprak Mélangé it contains large benthic foraminifera (*Nummulites*) of Eocene age. This is the same locality which was mapped by Bergougnan as Thanetian (Upper Eocene). Northward emplacement, therefore, occurred before the Late Eocene (58.7 Ma; Gradstein et al. 2004). Where the Sipikör Formation unconformably overlies the Karayaprak Mélangé south of Erzincan, near

the Munzur Mountains (e.g. at Muratboynu; section 3.7) it contains benthic foraminifera of Late Palaeocene-Lower Eocene age (i.e. 58.7-48.6 Ma; see appendix 1). Southward emplacement of mélangé from the Izmir-Ankara-Erzincan Suture Zone, therefore, occurred prior to Late Palaeocene time (>58.7 Ma).

An intraoceanic origin for the mélangé in the southern part of the suture zone is supported by the dominance of pelagic and ophiolitic lithologies over clastic or terrigenous sediments. Tectonic erosion of the overriding plate is suggested by the presence of harzburgitic blocks in the mélangé that may have been derived from the overriding SSZ plate.

In both the Central Pontides and Eastern Pontides the Izmir-Ankara-Erzincan Suture Zone includes two slices of an inferred Upper Cretaceous volcanic arc unit (Figures 6.1 to 6.3, sections 3.5 and 5.5). These two thick lozenge-shaped slices of dominantly volcanic and volcanoclastic rocks have been previously identified in the Central Pontides and interpreted as intraoceanic volcanic arcs (Koşdağ volcanic arc in the north and Yaylaçayı volcanic arc in the south; Tüysüz 1990, 1995). These two units in the Central Pontides are here treated together and interpreted as two thrust slices of a single volcanic arc unit.

In the eastern Pontides a >2000 m thick succession of spilitic basalt, andesite and pyroclastic rocks of Lutetian age (Karadağ Volcanics) was mapped within the Izmir-Ankara-Erzincan Suture Zone by Koçyiğit (1990). Biostratigraphic data obtained during this project suggest that this unit, here named the Karadağ Formation, is of Late Cretaceous age (Appendix 1). In addition, the lithological characteristics, field relations, metamorphic assemblage and structural style exhibited by the unit suggests that this unit is correlative with the Cretaceous-Palaeocene Karadağ Basalt Member mapped ~20 km further west by Aktimur et al. (1995). These characteristics also suggest that the Karadağ Formation is correlative with the volcanic arc unit in the Central Pontides (Yaylaçayı Formation).

The Karadağ Formation in the Eastern Pontides and the Yaylaçayı Formation in the Central Pontides exhibit many similarities in terms of structural position, metamorphism, structure, stratigraphy and lithology (sections 3.5 and 5.5). Basalts from the volcanic arc units in both areas have compositions of island-arc and calc-alkali basalts, indicating a common volcanic arc origin (sections 3.5.5 and 5.5.4).

Neither of the units contain terrigenous material. Together with pelagic microfossils (e.g. *Globotruncana*) within shaly limestones that are interbedded with the lavas this indicates an open-marine extrusive setting isolated from a continental margin. In the Central Pontides the volcanic arc unit exhibits a locally unconformable volcanoclastic sedimentary cover (Yapraklı Formation; section 5.6) deposited in shallow-marine conditions and which lacks terrigenous material. The Yapraklı Formation is interpreted as a proximal arc debris apron. Palaeocurrent directions are towards the northeast assuming no horizontal tectonic rotation.

The inferred volcanic arc units (Karadağ Formation in the Eastern Pontides and the Yaylaçayı Formation in the Central Pontides) both show intergradational relationships with thick successions of Upper Cretaceous sedimentary rocks. The Yaylaçayı Formation appears to pass laterally into the İkışam Formation near the base.

In the Eastern Pontides the Karadağ Formation interdigitates with the Sütüpnar Formation which crops out to the south (section 3.6). The Sütüpnar Formation was previously mapped as Maastrichtian flysch and Upper Cretaceous-Palaeocene sandstone, conglomerate, clay and limestone (Koçyiğit 1990; Aktimur et al. 1995 (Çerpacindere Formation)). Biostratigraphic data obtained during this study indicate a Campanian-Early Eocene depositional age (83.5-48.6 Ma) for the Sütüpnar Formation. The stratigraphic base of the formation is not exposed. The unit comprises a 1500 m thick regressive succession of carbonate and volcanoclastic sedimentary rocks and passes conformably into the overlying Sipikör Formation (section 3.6.3). Carbonate sediment was redeposited from a carbonate shelf rich in *Nummulites* sp. which could have fringed the inferred volcanic arc. The sediments were redeposited into a deep-water open-marine environment by turbidity currents and submarine channels. The regressive succession could be interpreted as a stratigraphic response to relative sea-level change or the progradation of a submarine fan. No terrigenous material is present and a purely volcanic source area is inferred. The paucity of volcanic rocks indicates tectonic setting with a low heat-flow. The Sütüpnar Formation is interpreted as a Campanian-Lower Eocene regressive fore-arc basin.

The inferred volcanic arc unit in the Central Pontides (Yaylaçayı Formation) is intergradational with a thick sedimentary succession, which was mapped for the first time during this study and named the İkiçam Formation (section 4.2.5). The İkiçam Formation occurs within the mid to upper structural levels of the imbricate thrust stack (section 5.7). A Late Cretaceous (Campanian-Maastrichtian) age is indicated by the presence of several species of *Globotruncana* (Prof. Izver Ongen, Prof. Kemal Taşli and Prof. Nurdan İnan pers. comm. 2004; see Appendix 1) and is unconformably overlain by Upper Eocene and younger sedimentary rocks of the Tertiary Çankırı Basin. Much of the unit is overturned. The İkiçam Formation contains volcanogenic and terrigenous material, which increases in abundance stratigraphically upwards. In addition, the sediments appear to become more coarser-grained stratigraphically upwards. These observations indicate an increasing proximity or exhumation of volcanic and terrigenous sediment sources. Deposition was accompanied by enriched within-plate type volcanism, together with sparse alkaline-peralkaline volcanism that was possibly extension-related. Pillow lavas and sills within the succession have 'Within-Plate basalt' and 'Volcanic Arc Basalt' geochemical characteristics. The evidence for contemporaneous volcanism indicates high heatflow in the sedimentary basin and the presence of slump structures suggests that the basin was tectonically active. These observations, together with the presence of volcanic and terrigenous material can be contrasted with the data from the Sütçü Formation in the Eastern Pontides and indicate a different tectonic setting for the İkiçam Formation (sections 3.6 and 5.7). The İkiçam Formation is interpreted as an emplaced backarc basin deposit.

In the Central and the Eastern Pontides Tertiary sedimentary rocks (Mid Eocene Kadıkızı Formation and Palaeocene-Eocene Sipikör Formation) transgressively overlie the ophiolites and ophiolitic mélangé units (sections 3.7 and 5.8). The Palaeocene-Eocene Sipikör Formation in the Eastern Pontides is intergradational with the inferred Campanian-Lower Eocene forearc basin (Sütçü Formation). The Kadıkızı Formation in the Central Pontides and the Sipikör Formation in the Eastern Pontides both exhibit a similar association of shallow-marine clastic deltaic, carbonate lagoonal, and terrestrial fluvial facies and were constructed directly upon the Upper Cretaceous accretionary mélangé (Kirazbaşı

Mélange and Karayaprak Mélange respectively). The Kadıkızı Formation and the Sipikör Formation contain a variety of mafic lithoclasts and metamorphic terrigenous material. Both of these formations lack north-vergent deformational structures and, therefore, constrain the timing of north-vergent deformation observed in the underlying mélangé and the other Upper Cretaceous units of the Izmir-Ankara-Erzincan Suture Zone to pre-Mid Eocene.

Adjacent units

Any tectonic interpretations need to take account of several adjacent units. The evolution of the Eurasian continental margin is documented by the relatively autochthonous Pontide basement to the north. In the Eastern Pontides, Cretaceous-Eocene calc-alkaline volcanic rocks (up to 4 km thick) are exposed ~50 km north of the suture zone. These volcanic rocks are traditionally interpreted as part of a continental margin volcanic arc related to northward subduction of the northern Neotethys ocean (Şengör and Yılmaz 1981; Robertson and Dixon 1984; Akıncı 1984; Yılmaz et al. 1997; Okay and Şahintürk 1997). However, it was recently suggested that the Lower Tertiary Eastern Pontide arc might relate to southward subduction of Mesozoic oceanic crust within the Black Sea region to the north (Bektaş et al. 1999). This model has been opposed by other workers (e.g. Yılmaz et al. 1997; Okay and Şahintürk 1997). Subduction-related volcanism in the Pontides began at the Late Coniacian-Santonian boundary (Yılmaz et al. 2003). These volcanic rocks are overlain by Campanian pelagic limestones (Akıncı et al. 1984), and, in turn, are overlain by high-K andesites that continued into the Eocene (Bektaş et al. 1999). No volcanic arc is present north of the Izmir-Ankara-Erzincan Suture Zone in the Central Pontides.

The lower part of the Galatean Volcanic Province, known as the Saraçköy Volcanic Suite is located about 80 km southwest of the area studied in the Central Pontides. This suite was radiometrically dated at 76.4 ± 2.4 Ma (Late Campanian; Koçyiğit et al. 2003; based on two K-Ar rock dates of uncertain accuracy), and inferred to represent the rifting of an Upper Cretaceous forearc in a nascent extensional backarc setting. This was surprising since most of the Galatian Volcanic Province represents syn- to post-collisional magmatism of Oligocene-Miocene age.

The Saraçköy Volcanic Suite is similar in terms of both geochemistry and age to basalts within the Campanian-Maastrichtian Ikiçam and Yaylaçayı Formations. However, the Saraçköy volcanic suite is subaerial in contrast to the deep-marine setting of the Ikiçam and Yaylaçayı Formations and may have originated in a southerly (distal) setting, possibly by supra-subduction zone rifting of an Upper Cretaceous forearc (Koçyiğit *et al.* 1999). However, the Saraçköy Volcanic Suite could also be correlative with the Ikiçam or Yaylaçayı Formations, possibly related to trench-retreat (rollback) and southward migration of the arc during latest Cretaceous time.

Kilometre-thick sedimentary basins of latest Cretaceous to mid Eocene age (e.g. Haymana-Polatlı region, near Ankara (e.g. Koçyiğit 1991) have in the past been interpreted as fore-arc basins related to northward subduction of Neotethys that persisted until mid Eocene time (Görür *et al.* 1984). However, there is little regional evidence of steady-state subduction after latest Cretaceous time, and it is possible that the Haymana-Polatlı Basin and other parts of the Central Anatolian Basin complex developed in a setting of incipient collision (“soft collision”) prior to suture tightening (“hard collision”) during late Eocene time (Clark and Robertson 2003, 2005).

6.1.2 Structure of the Izmir-Ankara-Erzincan Suture Zone

In both the Eastern and Central Pontides each of the Upper Cretaceous units occupies a distinct structural position within the suture zone (Figure 6.3). The ophiolitic units in both the Central and Eastern Pontides occur towards the top of the south-vergent thrust stack. An exception is relatively small exposures in the south of the Eastern Pontide region, which could represent large tectonic blocks within the mélangé. In both areas the inferred volcanic arc unit forms two thrust slices towards the middle of the thrust stack (Figure 6.3). The uppermost slice is more highly deformed than the lower slice. Metamorphic minerals and textures are better developed in the upper slice of the arc, although the same greenschist facies mineral assemblage is present in both slices of the arc. The ophiolitic mélangé occurs throughout the thrust stack in both regions. Ophiolitic detritus is more abundant and the mélangé appears to be thicker towards the south within the suture zone, at a

lower structural level within the south-vergent imbricate thrust stack (Yılmaz et al. 1997). In the Central Pontides, thrust slices of the thick Upper Cretaceous, inferred marginal basin unit (İkiçam Formation) mainly occur towards the top of the structural pile. By contrast, the Upper Cretaceous sediments (Yapraklı Formation) that unconformably overlie the inferred arc unit (Yaylaçayı Formation) occur at a lower level in the thrust stack. The thick Upper Cretaceous, inferred fore-arc basin succession in the Eastern Pontides (Sütpınar Formation), is also located at a low- to mid-level in the thrust stack, where it is tectonically imbricated with the volcanic arc unit and Tertiary post-collisional basin sediments.

Schistosity and highly strained gneissose banding is seen in the metamorphic basement rocks within the Refahiye Complex (section 3.3.7). A variety of deformational structures (e.g. folds, tension gashes, stylolites) seen within blocks in the *mélange* are cut by faults that separate the blocks and by the shear fabric observed in the matrix, which commonly gives a top-to-the-north sense of motion. Within the ophiolites, a foliation and lineation are observed in serpentinised hartzburgitic tectonite (sections 3.3.1 and 3.3.2). In the Eastern Pontides this foliation dips to the north. In the Central Pontides the foliation is sub-vertical and strikes roughly N-S. The foliation in the peridotites is cut by faults and shear zones that indicate various kinematic directions.

North-vergent thrust duplexes and a pervasive top-to-the-north shear fabric are observed in all of the Upper Cretaceous units within the suture zone. North-vergent asymmetrical folds exhibiting a variety of styles were also observed. Asymmetrical folds that appear to verge southwards were observed in overturned sedimentary successions. Way-up structures show that these folds locally face downwards and to the north and are interpreted as part of an inverted limb of a large north-vergent fold structure that has been dissected by later thrusts and strike-slip faults.

The north-vergent structures are widespread and are commonly cut by top-to-the-south thrusts and shear zones. North-vergent shear fabrics are seen to be folded and faulted by later top-to-the-south structures. North-vergent shear is commonly preserved within north-dipping thrust horses of top-to-the-south duplex structures.

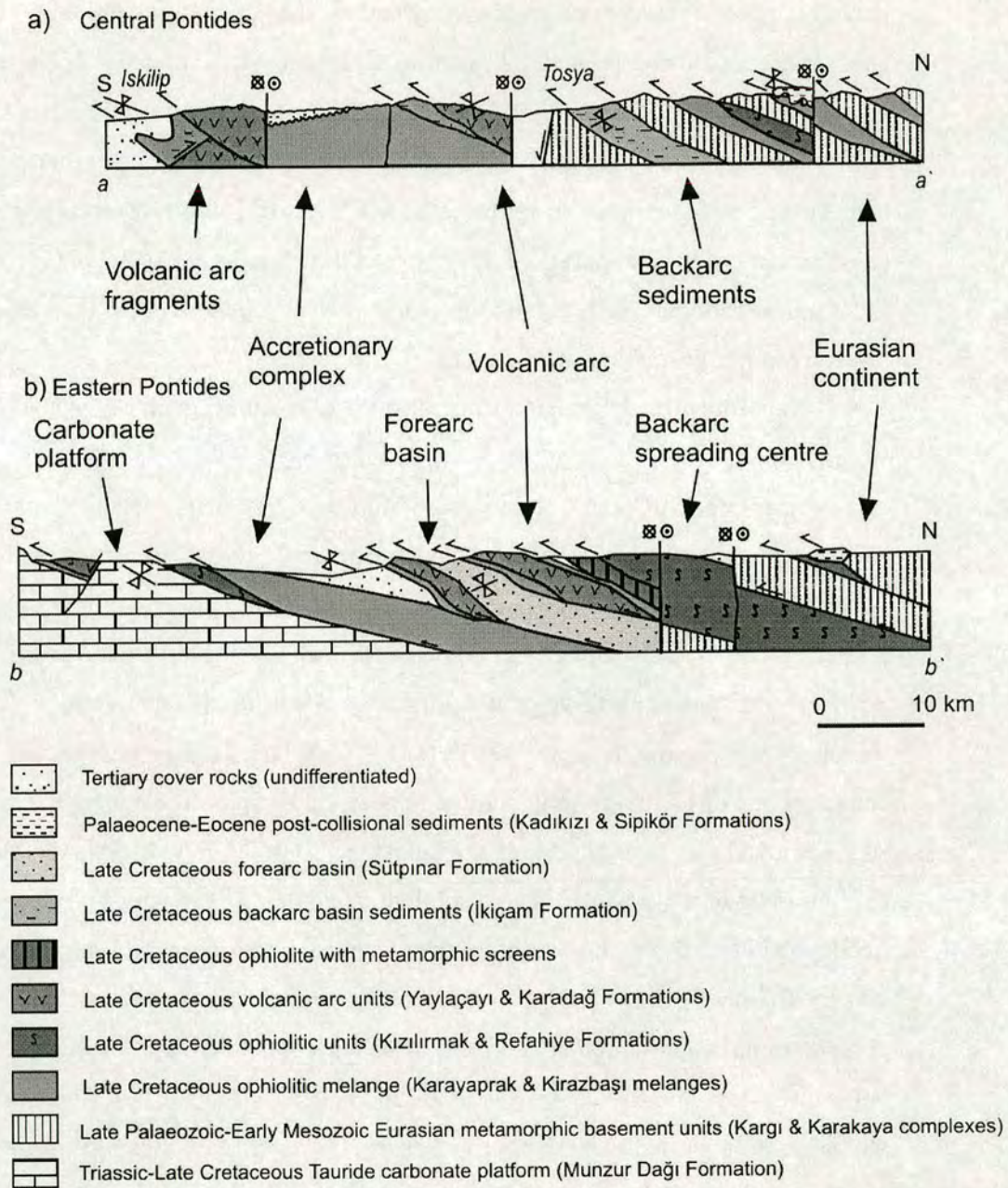


Figure 6.3. Interpretative cross-sections of the Izmir-Ankara-Erzincan Suture Zone in the Central and Eastern Pontides.

The mid Eocene rocks of the Sipikör and Kadıkızı Formations lie unconformably above the Upper Cretaceous mélange, ophiolitic and volcanic arc units of the Izmir-Ankara-Erzincan Suture Zone and do not exhibit pervasive shear-fabric, strong folding or related cleavage (sections 3.7.1 and 5.8.1). Because the Sipikör and Kadıkızı Formations are relatively undeformed at outcrop scale, and do

not exhibit north-vergent deformational structures they constrain the timing of early north-vergent collision-related deformation evidenced by the underlying Upper Cretaceous units to being pre-mid Eocene. The Sipikör Formation exhibits a far a more simple structure than the polyphase-deformed Refahiye Complex below. The beds of the Sipikör Formation are folded into a series of south-vergent asymmetrical recumbent close to tight parallel folds between thrust faults at Mecidiye (Figure 3.3). Later top-to-the-south deformation therefore post-dates deposition of the Palaeocene-Eocene Sipikör Formation.

Subsequently, dextral and sinistral strike-slip faults cut all of the above structures.

In summary, Upper Cretaceous ophiolites, accretionary *mélange*, volcanic arc and associated forearc and backarc basin sedimentary successions of the Izmir-Ankara-Erzincan Suture Zone all exhibit pervasive north-vergent deformational fabrics related to their emplacement onto the Eurasian margin from the south. This emplacement-related north-vergent deformation is constrained by overlying sediments to a pre-mid Eocene age (48.6-37.2 Ma). The north-vergent deformation is contemporaneous with the southward emplacement of ophiolitic *mélange* onto the south Tethyan margin in the Munzur Mountains, Taurides and Central Anatolia (Kırşehir/Niğde massifs). North and south directed deformation appear to have overlapped in time. South-vergent thrusting and folding occurred within the Izmir-Ankara-Erzincan Suture Zone after mid Eocene time. The post-Eocene south-vergent compressional deformation is interpreted as a regional collision-related event ('hard collision'; Clark and Robertson 2002, 2005). Post-Early Eocene north-vergent structures are reported from northern areas of the Eastern Pontides (Robinson et al. 1995; Rojay 1995). These structures may relate to deformation of the Black Sea province to the north. Deformational fronts are likely to have migrated. However, the units within the Izmir-Ankara-Erzincan Suture Zone clearly record an early pre-mid Eocene north-vergent compression and a later post mid Eocene south-vergent compression. Although south-vergent thrusts cut mid Eocene and younger strata the intensity of south-vergent deformation in the Upper Cretaceous rocks appears to be greater than is observed in the Eocene and younger strata. Pre-Eocene south-vergent deformation is therefore likely to have also occurred.

All of the above structures were transacted by strike-slip faults related to the Neogene North Anatolian Fault Zone.

6.1.3 Summary of comparisons

The IAES in the Central and the Eastern Pontide regions is composed of Upper Cretaceous-Lower Tertiary units that record the development of an accretionary complex, a rifted volcanic arc (with fore-arc basin), and a backarc basin (with sedimentary cover) during Campanian-Maastrichtian time (83.5-65.5 Ma). Ophiolites were emplaced southwards and northwards from the Izmir-Ankara-Erzincan Suture Zone during Campanian-Maastrichtian time. North-vergent deformation predates deposition of shallow-marine and fluvio-deltaic sediments during Late Palaeocene (Thanetian; 58.7-55.8) to Mid Eocene (Lutetian; 48.6-40.4 Ma) times. Structural data indicate that northward emplacement-related deformation occurred prior to south-vergent regional re-imbrication. South-vergent thrusts cut Eocene cover rocks, however, reactivation of pre-Eocene north-dipping thrusts is possible.

The above comparisons indicate that there are sufficient similarities between the Upper Cretaceous-Early Tertiary tectonostratigraphy of the Central and Eastern Pontides, ~400 km apart, to suggest that both originated in a similar overall tectonic setting along strike from each other (~600 km).

6.2 Tectonic evolution of the northern Neotethyan Ocean

6.2.1 Alternative models

A simple tectonic model (Figure 6.4a), as envisaged by Şengör and Yılmaz 1981, invoked a single N-dipping subduction zone consuming MOR-type Neotethyan oceanic lithosphere; this could generate the eastern Pontide volcanic arc and also provide a mechanism for southward ophiolite genesis as lithosphere was either trapped or newly formed behind the trench in a forearc location. Southward emplacement could have occurred during arc-trench collision. The main problems, however, are the lack of a viable mechanism to emplace the ophiolites and related units northwards onto the Eurasian margin and the lack of a continental margin

volcanic arc north of the suture zone in the Central Pontides (Ustaömer and Robertson 1997).

A second model for the Central Pontides (Figure 6.4b) involved two contemporaneous subduction zones, one beneath the Pontide margin as in Figure 6.4a, and another within the Neotethyan Ocean to the south, although its polarity was not specified (Tüysüz 1990); thus, the implications of this model for ophiolite emplacement are unclear. One problem with this model is the observed lack of Late Cretaceous arc volcanism north of the Izmir-Ankara-Erzincan Suture Zone in the Central Pontides (Ustaömer and Robertson 1997).

A third model (Figure 6.4c) postulated a reversal of subduction direction (Okay and Şahintürk 1997): the SSZ ophiolites were generated above a south-dipping subduction zone and emplaced northwards onto the Pontides as a result of trench-margin collision during Cenomanian-Turonian (~93 Ma); subduction then flipped to consume remaining oceanic crust northwards beneath the Eurasian margin, creating the eastern Pontide magmatic arc. The main problems here are that the Neotethyan Kızılırmak Ophiolite and Refahiye Complex and the inferred backarc basin unit (İkiçam Formation) occur to the north of the volcanic arc units within the suture zone in a structurally higher position. This model would, therefore, imply that the ophiolites represent the lithospheric basement of the intraoceanic forearc. However, geochemical and sedimentological data obtained during this study suggest that the ophiolites and associated thick sedimentary successions represent backarc basin lithosphere. Biostratigraphic data from the foredeep succession (Eskiköy Formation; inferred trench-margin collision facies) on the Pontides, to the north of the Izmir-Ankara-Erzincan Suture Zone and also in the Taurides to the south (Ayıkayası Formation) suggest that northward emplacement onto the Pontide basement did not significantly predate emplacement onto the Munzur Platform to the south, as suggested by this model. Okay and Şahintürk's (1997) model also suffers from the lack of any volcanic arc in the Central Pontides and the fact that Upper Cretaceous volcanic rocks are not seen overlying the ophiolite in the Eastern Pontides.

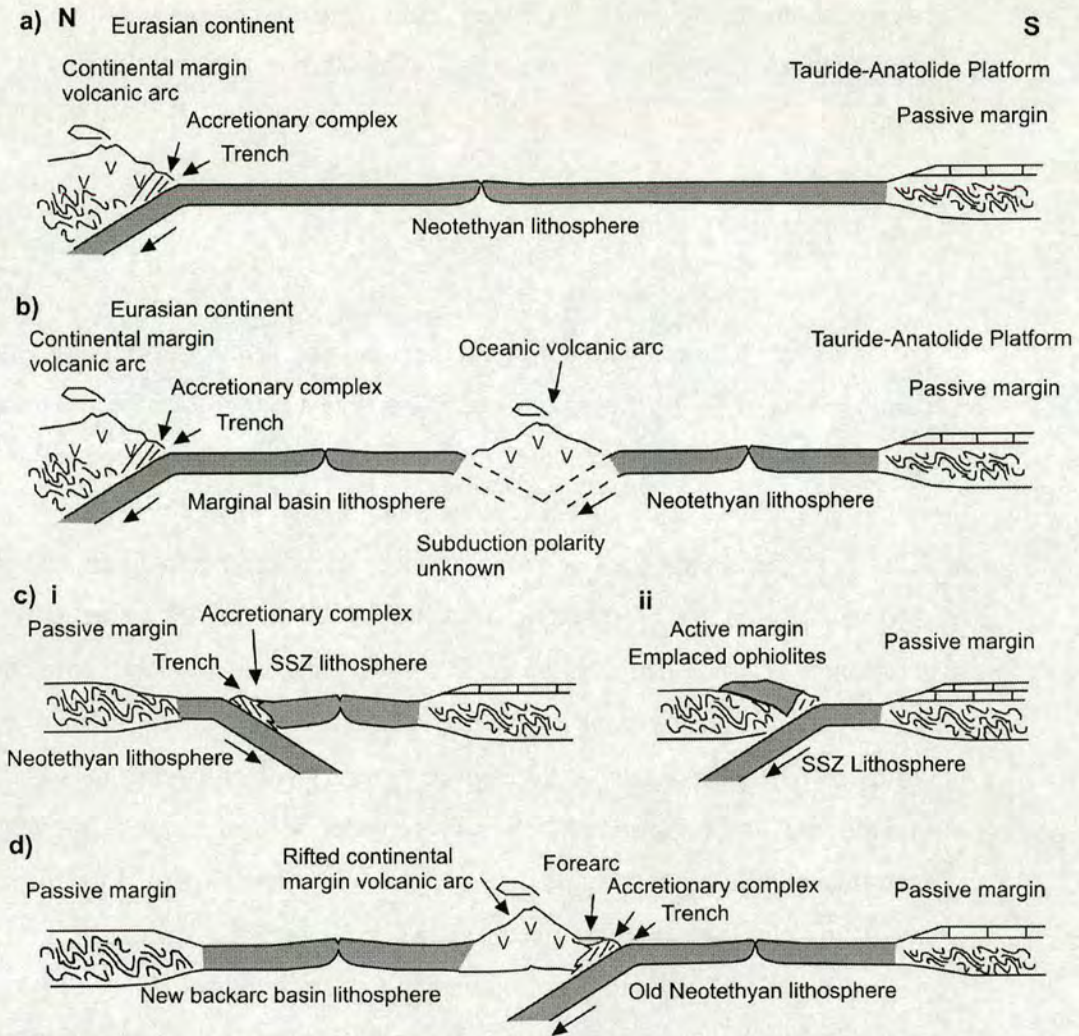


Figure 6.4. Alternative tectonic models for the Late Cretaceous-Early Tertiary development of the Izmir-Ankara-Erzincan Suture Zone. a) single north-dipping subduction model with a single continental margin arc (Bergougnan 1975; Yılmaz 1980; Koçyiğit 1991; Rojay 1995); b) double subduction model with continental and intraoceanic arcs (Tüysüz 1990, 1995); c) trench-margin collision model with subduction polarity reversal (Okay and Şahintürk 1997); d) single subduction zone model with slab rollback (Ustaömer and Robertson 1997; Koçyiğit et al. 1999).

In a further alternative (Figure 6.4d), Neotethyan oceanic crust was subducted northward related to opening of a marginal basin; this basin later collapsed and ophiolites were emplaced northwards onto the Pontide margin (Ustaömer and Robertson 1997). However, the timing was not clearly specified and the relationship

between continental collision, northwards emplacement and southwards emplacement of ophiolites from the Izmir-Ankara-Erzincan Suture Zone was not known.

6.2.2 Proposed new model

The interpretation which best fits the new data obtained during this study is shown in Figure 6.5a. Northward subduction is seen as initiating adjacent to the Eurasian margin, leading to the construction of a marginal volcanic arc in the Eastern Pontides during Late Coniacian-Santonian time (Yilmaz et al. 2003). The lack of volcanism in the Central Pontides could reflect locally strike-slip dominated oblique convergence (similar to present day Costa Rica or California; Ustaömer and Robertson 1997). Alternatively, the northernmost arc (located on the continental margin in the East) may have been located offshore in the Central Pontides, related to an irregular palaeogeography of the Pontide margin (with embayments and promontories), low angle subduction as in the andes or the arc trending at an angle (rather than parallel) to the Pontide margin. A backarc basin rifted along the south-Eurasian margin within the Pontide basement, explaining the inclusions of metamorphic rocks within the ophiolite in the Eastern Pontides. This extension could have been caused by trench retreat/slab rollback. (Figure 6.5b-c). Accretionary mélange and ophiolites were emplaced southwards when the subduction trench collided with the Tauride continental margin (Munzur Platform) in Campanian-Maastrichtian time (83-65 Ma; Figure 6.5d). At roughly the same time the marginal basin, located to the north, is assumed to have subducted southwards to explain the northward ophiolite emplacement onto the Pontide basement. This is compatible with seismic tomographic studies that have revealed a large S-dipping high-Q body beneath the region (Koulakov et al. 2002). However, evidence from other parts of the Pontides point to a much later northward thrusting event, i.e. during Palaeocene to Early Eocene time (Okay and Şahintürk 1997) or even post-Mid Eocene time (Rojay 1995). It is possible that the front of north-vergent deformation migrated northwards during early collision. Finally the entire thrust stack was re-imbricated southwards

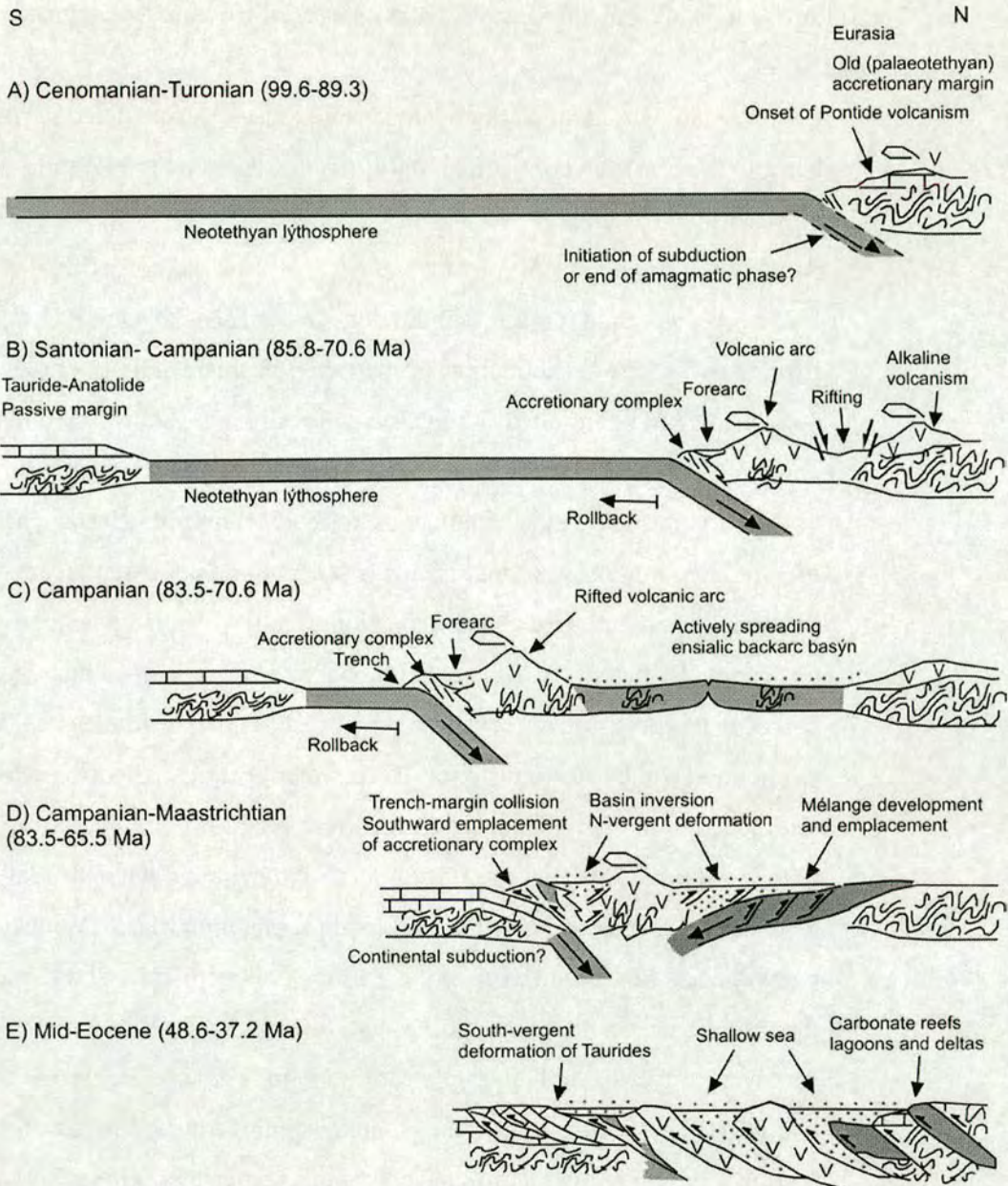


Figure 6.5. Favoured model for the Late Cretaceous-Early Tertiary development of the Izmir-Ankara-Erzincan Suture Zone.

during pervasive thick-skinned continental collision after mid Eocene time (Figure 6.5e).

The following Late Cretaceous-Early Tertiary stages of tectonic development are envisaged:

1. Cenomanian-Turonian: Neotethyan oceanic crust was subducted northwards beneath the Eurasian continental margin, represented by the Pontide metamorphic basement.
2. Santonian-Campanian: A volcanic arc was constructed, bordering the Eurasian continental margin. Subduction zone roll-back triggered backarc rifting, giving rise to subduction-influenced volcanism and minor alkaline volcanism. With continued subduction zone retreat, a backarc marginal basin opened, floored by oceanic crust and overlain by redeposited terrigenous, volcanoclastic and pelagic sedimentary rocks. Metamorphic basement was incorporated into the marginal basin crust during rifting. Arc volcanism continued in an outboard oceanic location, removed from any source of terrigenous sediment. A frontal accretionary prism developed that was composed of pelagic sediments, oceanic crust (e.g. serpentinite) and detached seamounts (e.g. basalt-limestone). Deep-water pelagic and volcanoclastic sediments accumulated in an associated fore-arc basin.
3. Late Maastrichtian: The Tauride continent (Munzur and Kirsehir Platforms) reached and then collided with the Pontide subduction trench. With continued convergence the leading edge of the Tauride continent entered the trench and the accretionary complex, ophiolites and fore-arc basin were thrust southwards over the collapsed platform margin. The fore-arc basin shallowed and filled. This collision, in turn, triggered southward subduction of the marginal basin creating additional accretionary *mélange*. This subduction zone then collided with the Pontide margin and the ophiolite and *mélange* were thrust northwards onto the Eurasian margin.
4. Palaeocene-Early Eocene: Subduction halted; the former fore-arc basin completely filled, with the accumulation of shallow-marine and non-marine sediments. The emplaced oceanic units were also transgressed by shelf-depth carbonates (Nummulitic limestones). There is no record of subduction continuing in the Central and Eastern Pontides during this time. Northward thrusting during this time is reported from other areas in the north of the

Pontides but is not recorded in the areas studied here, suggesting northward migration of the deformation front following initial collision.

5. Mid Eocene: Suture tightening resulted in crustal thickening and southward imbrication of the entire accretionary allochthon to produce the present-day S-vergent thrust stack.
6. Oligo-Miocene: The suture zone was largely emergent during Oligocene time then was transgressed by shallow-water carbonates during the Miocene. Plio-Quaternary time saw left-lateral displacement of segments of the suture zone by up to 80 km in both the Central and Eastern Pontides along the North Anatolian Fault Zone.

6.3 Modern and ancient examples of comparable tectonic processes.

The Pontide units described here can usefully be compared with a range of modern and ancient convergent margin settings, including accretionary prisms, arcs and backarc basins. The *mélange* is comparable to accretionary *mélanges*, specifically those associated with ophiolite emplacement e.g. Upper Cretaceous *mélange*, Oman (Searle and Cox 1999) or retreating active continental margins e.g. Franciscan Complex, U.S.A. (e.g. Cloos 1982; Robertson 2002). The inferred arc units are comparative to the Dras-Kohistan arc (Robertson and Degnan 1994; Clift et al. 2002) and the associated Shyok backarc basin formation in the Himalayas (Robertson and Collins 2003). However, the Dras-Kohistan arc appears to have formed in a more oceanic setting.

Specific comparisons can also be made with several modern backarc basins (e.g. Japan Sea; Bransfield Straits, S Atlantic), and also ancient backarc basins (e.g. Western USA; Eastern Mediterranean and Southern Andes).

Eastern Mediterranean examples are relevant in view of their proximity and value for regional synthesis. The Upper Palaeozoic-Early Mesozoic Küre marginal basin in the Central Pontide “basement” (Figure 6.6) opened by rifting of the Eurasian continental margin in response to inferred northward subduction (Ustaömer and Robertson 1991, 1997), and later collapsed by southward underthrusting when a small rifted continental fragment (Kargı Complex) arrived at the trench prior to Late Jurassic time (Figure 1.10). During its emplacement the Küre backarc ophiolite was

dismembered and is preserved as thrust sheets and detached blocks within an accretionary complex. The ophiolitic extrusives are of near-MORB composition, with a small negative Nb anomaly (Ustaömer and Robertson 1999).

In addition, further west, in northern Greece, the Guevgueli ophiolite rifted along the Eurasian margin during Mid-Late Jurassic time (Bébien et al. 1989; see Robertson 2002 for review). This ophiolite retains primary magmatic contacts with metamorphic country rocks that are correlated with the Eurasian basement. The ophiolitic extrusives are mainly of MORB-type but locally show a minor subduction influence. The backarc ophiolite was bordered on its oceanic side by a rifted continental fragment, capped by a Jurassic magmatic arc (Brown and Robertson 2003).

In detail, the Guevgueli ophiolite in northernmost Greece formed during Jurassic time above an eastward subducting Almopias (Vardar) ocean as a backarc basin adjacent to the Serbo-Macedonian margin (Brown and Robertson 2002). The ophiolite, together with a volcanic arc unit (Paikon Massif) are preserved within the Vardar suture zone as relatively autochthonous units (Robertson 2004). The Guevgueli ophiolite and the Paikon Massif exhibit contact metamorphism with adjacent continental crust of the Serbo-Macedonian zone, ruling out an intraoceanic origin (Brown and Robertson 2002). The Vardar suture forms a Lower Tertiary west-vergent thrust stack. Ophiolites were emplaced westwards from the Vardar oceanic basin during Late Jurassic time due to trench-margin collision (Brown and Robertson 2002). It is unclear when the Vardar oceanic basin finally closed (during Late Cretaceous-Early Tertiary time). Strike-slip tectonics associated with oblique convergence played a role in the preservation of the Guevgueli ophiolite (Bebien et al. 1982).

The Guevgueli ophiolite appears to have formed in a similar tectonic setting (during Jurassic time) as the Refahiye Complex and Kızılırmak Ophiolite of the Pontides. The Jurassic Paikon Massif is comparable to the Upper Cretaceous volcanic arc units in the Pontides (Karadağ and Yaylaçayı Formations) in terms of the tectonic setting of its formation. However, the Jurassic ophiolites and volcanic arc units of the Vardar suture zone could be of Corilleran type if their emplacement pre-dates final closure of the Vardar ocean. However, these ophiolites do not appear

to have been tectonically obducted and the timing of final closure of the Vardar ocean is uncertain. Therefore, it is unclear how the mode of their emplacement compares to that of the Upper Cretaceous ophiolites in the Pontides which were emplaced during collision between the Karadağ-Yaylaçayı arc and the Tauride-Anatolide platform in latest Cretaceous time.

The Guleman, Berit and, Ispendere ophiolites in southeast Turkey formed in a southerly strand of Neotethys above a north-dipping subduction zone. These SSZ ophiolites were accreted to the northern active margin of southern Tethys during latest Cretaceous time (Hall 1976; Aktaş and Robertson 1984). Upper Cretaceous arc-related plutons cut the ophiolites and the Tauride Platform, indicating that southern Neotethys continued to subduct northwards after their emplacement (Yazgan and Chessex 1991; Parlak et al. 2001). Their mode of emplacement is not yet well documented. It is generally believed that the southerly Neotethys was subducted northward, so that their emplacement onto the northerly active margin may require a model similar to the Cordilleran model exemplified by the Rocas Verdes ophiolites of the Andes (section 6.3) as their emplacement appears to pre-date final closure of the south Neotethyan Ocean (Yilmaz 1993; Robertson 1998; Parlak et al. 2001). Therefore, it appears that the mode of their emplacement is not related to collision and is not comparable to the Upper Cretaceous ophiolites in the Pontides.

The closest example of ophiolite emplacement onto a northerly active Tethyan margin during arc-continent collision in a similar way to the Upper Cretaceous ophiolites of the Pontides is the Triassic to Lower-Mid Jurassic Küre Complex and Çangaldağ arc, located in the Central Pontides north of the main Izmir-Ankara-Erzincan Suture Zone. The Küre Complex comprises a thrust-imbricated stack of siliciclastic sedimentary rocks and slices of dismembered ophiolite (Ustaömer and Robertson 1997). The ophiolite can be reconstructed as a sequence beginning with serpentinitised peridotite at the base, overlain by layered cumulate gabbros, isotropic gabbro, 100% sheeted dyke complex, pillows and, hemipelagic sedimentary rocks (Ustaömer and Robertson 1997). Associated sedimentary rocks include black shales. The immobile element geochemistry of

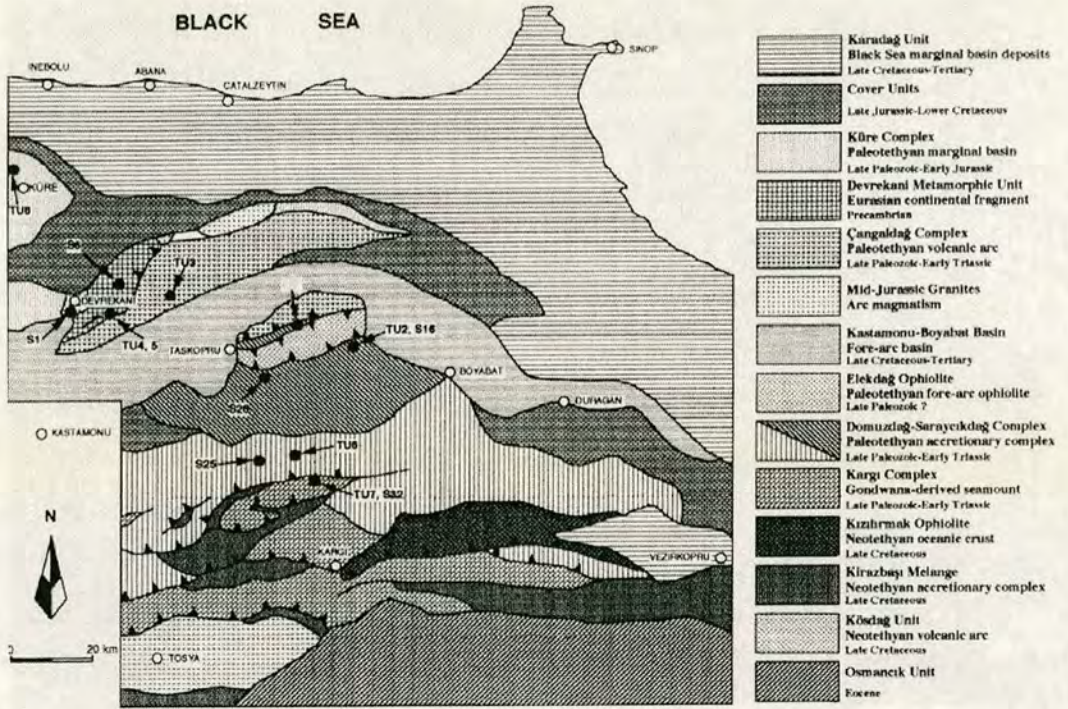


Figure 6.6. Simplified geological map of the northern Central Pontides, showing the main tectonic units (modified after Tüysüz 1990; Ustaömer and Robertson 1997).

the basalts indicates MOR and island-arc tholeiite (IAT) compositions implying a supra-subduction zone eruptive setting (Ustaömer and Robertson 1997). $Cr\#$ ($Cr/(Cr + Al)$) ratio of chrome spinels is >0.60 , which also indicates a suprasubduction zone setting (Ustaömer and Robertson 1997). Sedimentary rocks depositionally overlying the Küre ophiolite include black shales, volcanoclastic sedimentary rocks and terrigenous sandstones interpreted as the northern sedimentary apron of a related volcanic arc unit located to the south (Çangaldağ arc; Ustaömer and Robertson 1997).

Shear zones and thrusts within the Küre Complex mainly dip southward and indicate north-vergent overthrusting. North-vergent, north facing tight, asymmetrical folds, also indicate top-to-the-north compressive deformation (Ustaömer and Robertson 1997). These structures are related to northward emplacement of the Küre Complex during Late Jurassic time (Ustaömer and Robertson 1997).

The Çangaldağ arc and the Küre ophiolite are interpreted as a volcanic arc and backarc, respectively that developed through rifting of the Eurasian active

margin above a north-dipping subduction zone, which consumed Palaeotethyan oceanic lithosphere during Late Palaeozoic-Early Mesozoic times (Ustaömer and Robertson 1997). A small rifted continental fragment or non-volcanic seamount overlain by carbonate platform and slope sedimentary rocks (Kargı Complex) collided with the trench during Late Permian to earliest Triassic time (Ustaömer and Robertson 1997). This collision caused the Küre marginal basin to subduct southwards beneath the Çangaldağ arc between Early Triassic and Late Jurassic time (Ustaömer and Robertson 1997). Following closure of the Küre marginal basin the Eurasian margin stabilised. Deformation was followed by development of a passive margin carbonate platform (Figure 1.10; Şengör and Yılmaz 1981; Yılmaz et al. 1997).

In this model final emplacement of the Küre backarc ophiolite in the Late Jurassic occurred ~90 m.y. later than the inferred accretion of the Kargı continental seamount at the trench. In contrast, the Upper Cretaceous ophiolites in the Pontides (Refahiye Complex and Kızılırmak Ophiolites) were emplaced synchronously with the collision of the volcanic arc with the Tauride-Anatolide platform in Campanian-Maastrichtian time. This suggests a much more delayed process of final ophiolite emplacement onto the Eurasian margin as a response to blocking of the trench during the Triassic-Jurassic than in the Late Cretaceous. A possible reason is that pre-Jurassic events were associated with only partial closure of Tethys, whereas the Late Cretaceous tectonics relate to final closure of Tethys and onset of continental collision.

Circum-Pacific examples are especially relevant. In the western USA the Jurassic Josephine marginal basin rifted along a pre-existing accretionary margin, similar to the Pontides, during Mid-Late Jurassic time. The backarc basin was bordered on its oceanward side by an active arc (Chetco arc). The backarc crust was overlain by mainly terrigenous, but locally volcanoclastic, sediments (Galice). This marginal basin closed, oceanwards, beneath the arc, resulting in the emplacement of the oceanic basement as the Josephine ophiolite (Harper 1984).

Of particular interest is the Rocas Verdes mafic complex (Sarmiento and Tortuga ophiolites) of Late Jurassic to Early Cretaceous age in southern Chile (Dalziel et al. 1974; Weaver 1979; Keller and Fisk 1992; Stern and de Wit 2003).

This comprises discontinuous exposures of deformed gabbros, sheeted dykes and pillow basalts (>3 km thick), interpreted as deformed and uplifted (but relatively autochthonous) marginal basin crust. The pillow basalts are overlain by cherts in addition to tuffs and clastic sediments that were derived from the Mesozoic magmatic arc to the southwest and the continental platform to the northeast (Dalziel et al. 1974; Stern and De Wit 2003). The ophiolites overlie a metamorphic basement, similar to the Eurasian basement in the Pontides, composed of previously accreted units. The Andean ophiolites formed between Palaeozoic basement to the east and the roots of a Lower Cretaceous andesitic arc to the west (Patagonian Batholith). The ophiolitic rocks locally intrude metamorphic basement, supporting an intra-continental rift origin (Dalziel et al. 1974). Deformational structures within the Andean ophiolites indicate eastward displacement, towards the continental interior. N-MORB normalised trace-element patterns from the ophiolitic basalts (Sarmiento and Tortuga) show an enrichment in large ion lithophile elements (LILE) relative to high field strength elements (HFSE) and a negative Nb anomaly, suggestive of a subduction influence. However, Th, Ce or P peaks, indicative of calc-alkaline magmatism, are absent. On the Zr-Ti/100- Y*3 diagram (Pearce and Cann 1973) these basalts plot in the combined ocean-floor, island-arc and calc-alkaline basalts field.

A model of formation and emplacement of the Rocas Verdes ophiolitic complex is shown in Figure 6.7. The formation of the Patagonian batholith, located at the southwestern edge of the Rocas Verdes Basin, was contemporaneous with the formation of the ophiolites and represents a rifted magmatic arc equivalent to the volcanic arc units in the Izmir-Ankara-Erzincan Suture Zone. However, the batholith appears to have no large plutonic equivalent in the Izmir-Ankara-Erzincan Suture Zone. This could be due to lack of preservation, perhaps related to subduction erosion or collision-related processes, or it could indicate that a mature magmatic arc never developed in the north Neotethyan Ocean, indicating that subduction proceeded to a more mature stage in the Andes than in the Izmir-Ankara-Erzincan Suture Zone. In the southern part of the Rocas Verdes Complex basalts of the Tortuga ophiolite have a MORB-like geochemistry (Keller and Fisk 1992; Stern and de Wit 2003). This indicates that a wider backarc basin (>100 km) developed in

the south than in the north (Stern and de Wit 2003). The Rocas Verdes Complex is, therefore, interpreted as “remnants of the progressive stages of development of oceanic-type crust in a continental backarc extensional tectonic environment” (Stern and de Wit 2003). The northern Rocas Verdes ophiolites (Sarmiento Complex) that may represent a narrow backarc rift exhibit abundant plagiogranites and trondjhemites, whereas the southerly ophiolites (Tortuga Complex) that apparently developed into a wide rifted basin lack these units (Stern and de Wit 2003). Similarly, in the Pontides, the Refahiye Complex in the east exhibits abundant plagiogranites together with metamorphic host rocks while the ophiolites further west in the Central Pontides (Kızılırmak Ophiolite) do not. This may indicate that backarc rifting was more extensive in the Western Pontides during the Late Cretaceous.

Closure and uplift of the basin occurred during mid Cretaceous compression with top-to-the-east vergence (i.e. toward the continental interior; Figure 6.7; Halpern 1973; Cunningham 1995). This appears to be comparable to the mechanism of emplacement inferred for ophiolites in the Pontides (Figure 6.5). However, the mid Cretaceous compressive event in the Andes was not associated with any continental collision and the Pacific plate still continues to subduct eastwards beneath the Andes. The Rocas Verdes ophiolites are a classic example of a Cordilleran-type ophiolite.

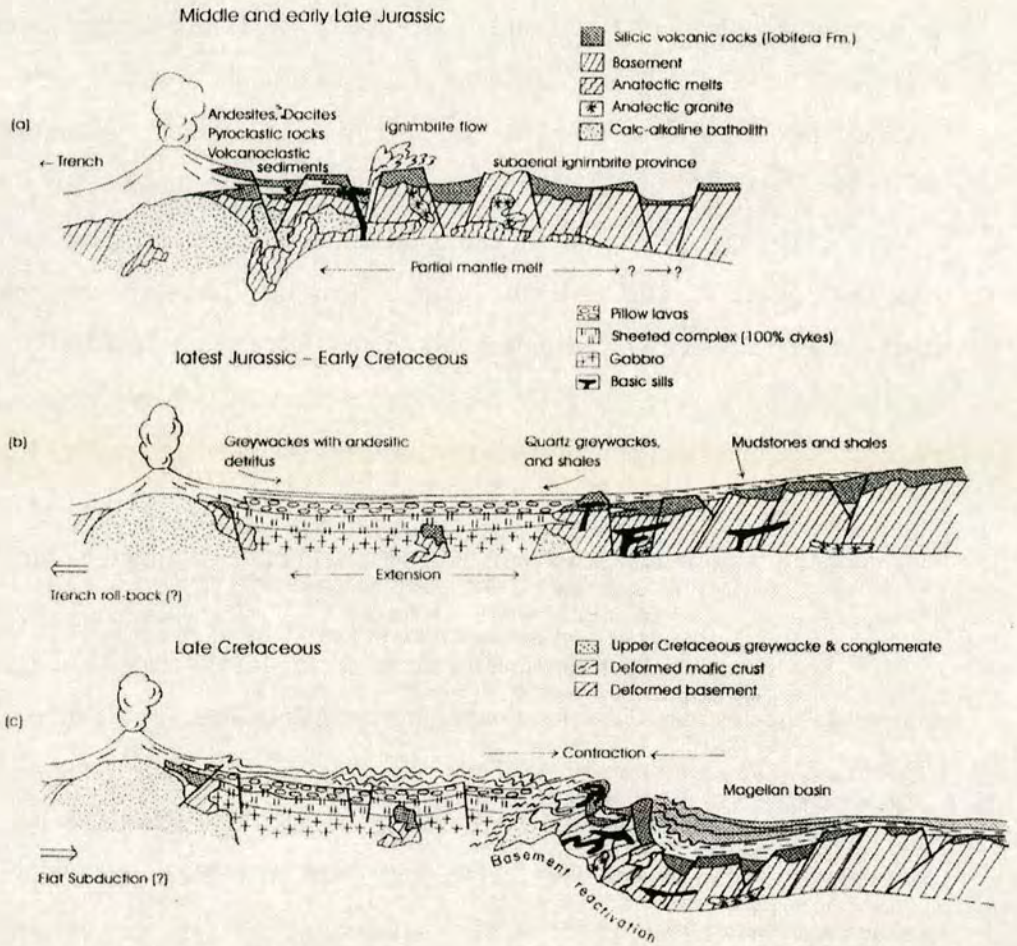


Figure 6.7. Sequential sections showing the Mid-Jurassic to Late Cretaceous formation and collapse of the Rocas Verdes backarc basin (after Dalziel (1974), Bruhn et al. (1978) and de Wit and Stern (1978, 1981, 2003).

The suggested causes of emplacement of the Rocas Verdes ophiolite are varied. They include flattening of the angle of subduction as a result of either ridge subduction or a global increase in spreading and convergence rates (de Wit 1977; Dalziel 1986; Stern et al. 1991). The northeast-vergent overthrusting of the Rocas Verdes Complex, in addition to deepening of the Magellan forearc basin to the northeast and thick turbidite sequences within the Magellan Basin support a model in which the Rocas Verdes backarc basin was subducted westwards beneath the volcanic arc (Gealey 1980). If this was the case, then north-vergent emplacement-related structures in the Pontides could imply that the Upper Cretaceous backarc

basin was subducted southwards beneath the volcanic arc during emplacement (Figure 6.5).

One of the best exposed modern-day intra-continental marginal basins is the Bransfield Strait, South Atlantic. This is inferred to have formed by supra-subduction zone extension of the Antarctic continental margin and the development of a backarc spreading centre (Barker 1982). The arc magmatism is exposed on the South Shetland Islands, where the oldest extrusive rocks are mostly low-K, high-alumina basalts, basaltic andesites and low-silica andesites of Aptian age (Keller and Fisk 1992). Cogenetic gabbros, tonalites and granodiorites are also exposed. Most samples dredged from the centre of the Bransfield Strait are olivine (Fo_{82} to Fo_{85})- and plagioclase (An_{73} to An_{85})-phyric, vesicular basalts (Keller and Fisk 1992). Normalised trace element patterns of the basalts show an enrichment in LILE relative to HFSE and a negative Nb anomaly. On the Zr-Ti/100- Y^*3 tectonic discrimination diagram (Pearce and Cann 1973) the Bransfield Strait basalts plot in the combined field of ocean-floor, island-arc and calc-alkaline basalts. The basalts from Bransfield straits are transitional between island arc and ocean ridge basalts and, are geochemically similar to the samples from the Pontide ophiolites (sections 3.3.8.4 and 5.3.3).

In summary, the ancient and modern backarc marginal basins, summarized above, show some similarities with the proposed tectonic model for the Central and Eastern Pontides (Figure 6.5). One difference, however, is that the backarc rifting appears to have taken place along the southern periphery of the Eurasian Margin, rather than further inboard, as there is no evidence of any preserved rifted continental margin units (c. f. S Andes). However, the roots of the Upper Cretaceous volcanic arc are not exposed and it is possible that any rifted continental crust was removed by subduction-erosion or during collision. Tectonic erosion is also suggested by the presence of harzburgitic blocks in the mélange that may have been derived from the overriding SSZ plate.

Oceanic subduction zones may either retreat (roll-back) towards the ocean (i.e. Mariana-type subduction; Uyeda and Kanamori 1979; Uyeda 1982) associated with an extensional stress field in the upper plate, or advance towards the hinterland, resulting in compression of the margin. Intra-oceanic trench retreat can accommodate

the opening of backarc basins (e.g. Mariana and Lau Basins). Several “retreating accretionary orogens” characterise the Western Pacific region; e.g. Mariana (Karig 1971); Sea of Japan (Uyeda 1982); Scotia Sea (Saunders and Tarney 1979), and the Bransfield Straits (Dalziel et al. 1974; Keller et al. 1992). Oceanward roll-back of a subduction zone lying adjacent to a continental margin can similarly accommodate opening of an intra-continental backarc basin (e.g. S Andean ophiolites). The S-Andean marginal basin is inferred to have been inverted and deformed during mid-Cretaceous time without physical collision with any other units. This deformation possibly took place in response to a flattening of the angle of subduction (de Wit 1977), and/or an increase in seafloor spreading rates during the opening of the South Atlantic in mid-Cretaceous time (Rabinowitz and La Breque 1979; Dalziel 1986).

A change from a retreating orogen to an advancing one could be triggered by various factors including; 1) changes in the properties of and/or forces acting upon the subducting lithospheric slab and a subsequent change to its angle of descent (Karig 1971; Uyeda 1982; Royden 1993); 2) changes in large-scale relative plate motions (Dalziel 1974; Smith *in press*); 3), lateral mantle flow (Flower 2003), or 4) motion of the continental plate toward the trench (Uyeda 1979; Saunders and Tarney 1984). In the case of the Pontides, the inferred backarc rifting can be related to slab retreat as the north Neotethys was consumed beneath the Eurasian active margin. The northward emplacement can be related to collision of the Tauride continental margin (Kırşehir and Munzur Dağı units) with an inferred north-dipping subduction zone during latest Cretaceous time (~70 to 65.5 Ma) since the two events were roughly synchronous (Figure 6.5). In the Pontides the northward ophiolite emplacement was determined by the presence of an intraoceanic arc, which collided with the Taurides. Continued convergence resulted in northwards emplacement of the backarc rather than southwards emplacement of the volcanic arc over the Taurides.

6.4 Wider implications

6.4.1 Role of the volcanic arc: Experimental work on preservation of volcanic arcs.

It has been observed that suture zones commonly do not contain remnants of an oceanic volcanic arc (Boutelier et al. 2003). Thermo-mechanical analogue experiments have been used to investigate the preservation potential of intra-oceanic volcanic arcs during collision (Boutelier et al. 2003). The absence of preserved volcanic arc rocks within many suture zones may indicate amagmatic subduction (e.g. flat subduction in Chile), or that ocean basins were too small to lead to mature subduction and significant arc magmatism (Stampfli et al. 1998; O'Brien 2001). Boutelier et al. (2003) argue that, since oceanic subduction typically involves the formation of volcanic arcs their absence in many suture zones could imply that they have a low preservation potential. Numerical modelling and experimental results have simulated arc subduction (Chemenda et al. 2001; Tang et al. 2003; Boutelier et al. 2003). Subduction of the whole arc plate is shown to occur when an extensional subduction regime (i.e. 'Mariana type'; Uyeda 1979) goes into compression following the arrival of a continental margin at the trench (Boutelier et al. 2003). Transfer of compressional stress across the plate boundary leads to failure in the vicinity of the failed backarc spreading centre (Boutelier et al. 2003). In their experiments, the arc plate was then partially or completely subducted beneath the backarc. Boutelier et al. (2003) established that the arc may be partially or completely subducted depending on the size, density and strength of the arc crust, with thick, low density arc crust being more resistant to subduction.

The thermo-mechanical analogue experiments did not result in collapse of the backarc beneath the arc, as is inferred for the Late Cretaceous evolution of the Pontides. In the experiments subduction of the arc plate occurred, whereas the model proposed for Pontides, based on field observations, involves southward subduction of the backarc plate (Eurasian plate; Figure 6.5); a feature shared with the observation-based model for emplacement of the Jurassic Küre marginal basin complex in the

Pontides and, some models for 'Cordilleran' ophiolite emplacement, as applied to the Rocas Verdes ophiolites of the southern Andes (Chile; e.g. Gealey 1980).

6.4.2 Role of the volcanic arc during early collision: continental subduction, 'hard' and 'soft' collision.

In the proposed model for the evolution of the Izmir-Ankara-Erzincan Suture Zone collision of the volcanic arc (Yaylaçayı and Karadağ Formations) with the Tauride-Anatolide Platform resulted in closure of the backarc basin and northward emplacement of ophiolites during Campanian-Maastrichtian time (Figure 6.5). Roughly synchronous development of foredeep basins on both the southern and northern margins of northern Neotethys (Taurides and Pontides, respectively) can be related to the emplacement of ophiolitic units northwards and southwards from the Izmir-Ankara-Erzincan Suture Zone during Campanian-Maastrichtian time. These foredeep basins are interpreted as trench-margin collision facies, reflecting the arrival of the continental margin at a trench, and, therefore, represent the initial closure of Neotethys in latest Cretaceous time (at least in these areas). However, regional post-mid Eocene south-vergent deformation is associated with collisional deformation. This implies a gap of at least 15 m.y. between initial closure of Neotethys and the onset of thick-skinned deformation resulting from continental collision. The initial closure of Neotethys during latest Cretaceous time was accompanied by extensional sedimentary basin development in some areas (e.g. Ulukışla Basin, southern Turkey; Clark and Robertson 2002, 2005). The term 'soft collision' has been applied to this early oceanic closure (Clark and Robertson 2002), which is expressed in the Pontides as pervasive north-vergent folding and thrusting event of Campanian-Maastrichtian age. The later, Eocene phase of regional south-vergent thrusting and folding has been termed 'hard collision' (Clark and Robertson 2002). Thick-skinned 'hard' collision caused large-scale south-vergent reimbrication in the Pontides in post mid Eocene time.

The arrival of continental lithosphere at a subduction trench does not necessarily immediately cause collisional deformation. Regard et al. (2003) distinguish an important phase of continental subduction from the onset of continental collision. Ultrahigh-pressure metamorphic minerals (e.g. coesite),

indicating pressures of ~30-35 kbar within metamorphosed sedimentary successions that were deposited on former continental margins reinforce the idea of continental subduction (e.g. Chopin 1984; Ernst and Liou 2000). Blueschists in northwest Turkey (Okay 1984) indicate that high-pressure low-temperature metamorphism of continental crust occurred during closure of Tethys. The collisional process can be defined as the onset of shortening, by development of folds and thrusts, which initiates when horizontal compressional stress overcomes the strength of the lithosphere (Regard et al. 2003; Davy and Cobbold 1991). Where the contact between the two colliding plates was preceded by subduction of oceanic lithosphere, the horizontal compressional stresses must also overcome the slab-pull force if the lithospheric slab is still attached (Regard et al. 2003). Laboratory experiments were used to investigate the controls on the onset of collision (Regard et al. 2003). The results suggest that when the continental plate enters the trench there is no immediate tectonic or morphological response (Regard et al. 2003). Collisional deformation, marked by surface shortening and rapid shallowing of the trench, occurs when the trench begins to lock (Regard et al. 2003). Regard et al. (2003) showed that locking of the trench is controlled by the balance between slab-pull forces and compressive stresses (forced convergence). The implications of these results are that the amount of continental crust that will be subducted before the onset of continental collision occurs (i.e. 'hard collision') depends on the forces acting on the slab, the properties of the slab and, the convergence rates. These forces relate to slab break-off, deformation and phase changes. Another important implication of this is the size of the slab, i.e. the amount of oceanic lithosphere subducted prior to arrival of the continental margin at the trench. These processes have implications for the timing of oceanic closure relative to the timing of collisional deformation. In Turkey, this time lag appears to be ~15 m.y..

However, other factors could influence the time between 'soft' and 'hard' collision, for example irregular continental margins between the Kirşehir/Nigde massifs and the Pontides and Taurides, localised strike-slip controlled extrusion tectonics or development of transtensional/extensional basins in response to the adjustment of geometrically irregular microplates during early collision (Clark and Robertson 2002).

6.4.3 Ophiolites and orogenesis: local vs. global controls?

Ophiolites were generated and emplaced in great abundance within discrete brief intervals of geological time (e.g., Early Ordovician, Mid Jurassic, Late Cretaceous, Late Eocene). No equivalent process is known to be occurring on this scale today and there is no certain modern analogue for such extensive ophiolite development and emplacement (Robertson 2002, 2004). The creation and emplacement of ophiolites seems to occur in temporal pulses and many workers have related this to specific phases of drastic plate boundary reorganisation, or the generation of Large Igneous Provinces (e.g. Dilek 2003; Smith 2004; Robertson 2002). Therefore, ophiolites appear to present a challenge to uniformitarianism. Are ophiolites indicative of some drastic global tectonic event or can their emplacement be controlled only by local tectonic processes?

The 'Cordilleran' emplacement of ophiolites in the southern Andes during the mid Cretaceous was not a response to collision or terrane accretion (e.g. Dalziel 1974). Instead, the cause of emplacement of these ophiolites has been variously related to a change in global spreading rates and opening of the South Atlantic (Dalziel 1981), the action of mantle diapirs (Stern and de Wit 2003), variations in the properties of the downgoing slab with time, or spreading ridge subduction (Dalziel 1981, 1986; de Wit and Stern 1981; Storey and Alabaster 1991). Dalziel et al. (2000) suggested that plumes rising from the deep mantle could have caused flattening of the subducting lithospheric plate. Stern and de Wit (2003) noted that the backarc extension that led to development of the Rocas Verdes ophiolites overlapped in time with the major tectono-magmatic events in southwest Gondwana that led to the formation of Large Igneous Provinces (LIPs).

Similarly, Smith (2004) notes that ophiolite creation and emplacement can be related to the motions of the surrounding continents and compares the timing of opening of the North Atlantic with the timing of ophiolite formation and emplacement in the Eastern Mediterranean region. At ~75 Ma (Campanian) a change of relative plate motion between Afro-Arabia and stable Europe took place from roughly transform to convergent (Klitgord and Schouten 1986; Srivastava et al. 1990, Smith 2004). This was followed by a phase of very little motion until ~50 Ma (Early

Eocene), after which convergence continued. Smith (2003) argues that the Cretaceous-Early Tertiary motion between Africa and stable Europe could have close linkages with ophiolite formation and emplacement in the Mediterranean region.

Many authors have noted that where plate convergence rates are smaller than the rate of subduction, extension occurs in the upper plate (e.g. Karig 1971; Molnar and Atwater 1978; Dewey 1980; Uyeda 1981). This may eventually lead to supra-subduction zone spreading or the development of an arc-backarc system. This relationship is of primary significance for the mode of subduction, orogenesis and ophiolite development (Molnar and Atwater 1978; Uyeda 1981; Royden 1993; Regard et al. 2003).

Also, increased plate convergence rates have been attributed to the cause of ophiolite emplacement, particularly for Cordilleran-type ophiolites and as an explanation for the non-uniformitarian record of ophiolites in Earth history (e.g. de Wit 1977; Dalziel 1986; Stern et al. 1981; Robertson 2004).

The very slow rate of convergence between Afro-Arabia and stable Europe during latest Cretaceous-Early Eocene time (Smith 2004) coincides with the formation of many SSZ Neotethyan ophiolites, including the Refahiye Complex and Kızılırmak Ophiolite in addition to the volcanic arc units within the Izmir-Ankara-Erzincan Suture Zone. The negative buoyancy of old Neotethyan lithosphere is likely to have caused the rate of slab descent to exceed the regional convergence rate, causing slab roll-back and extension in the upper plate as has been inferred for Pacific regions and from experimental data (e.g. Molnar and Atwater 1978; Dewey 1980; Regard et al. 2003; Royden 2003).

When considering the trench-margin collision model for ophiolite emplacement, which is applicable to most Eastern Mediterranean ophiolites, it would appear fortuitous that the timing of drastic global plate motion reorganisation should be contemporaneous with the arrival of several continental margins at oceanic trenches. In the case of the Upper Cretaceous Refahiye Complex and Kızılırmak Ophiolite it appears that collision between the oceanic volcanic arc and the Anatolide-Tauride continent was contemporaneous with northward emplacement. The oceanic arc-passive margin collision could be seen as a local phenomenon controlling ophiolite emplacement. However, the apparent synchronicity of this event

with the emplacement of other ophiolites onto south- and north-facing margins of Tethyan ocean basins throughout the region suggests some larger scale control.

In summary, it seems likely that ophiolite genesis occurred by SSZ spreading in Campanian-Maastrichtian time related to trench retreat during a period of very slow convergence between ~75 and ~50 Ma (Campanian-Eocene; Smith 2004). This was shortly followed by the arrival of the margins of continental blocks within Tethys at several oceanic trenches during latest Cretaceous (Maastrichtian) time. The apparent synchronicity of this event ('soft collision') suggests that the various oceanic basins were of roughly equal width and were consumed at a similar rate. Later, during the Eocene there was a rapid increase in the convergence rate between Afro-Arabia and Europe (Livermore and Smith 1984). This led to the regional southward thrust imbrication ('hard collision').

In summary, because emplacement of Upper Cretaceous ophiolites in the Pontides was related to the arrival of the Tauride-Anatolide margin at the trench they cannot be considered as ideal 'Cordilleran' ophiolites. Their emplacement may not require a global-scale process of drastic plate motion reorganisation.

6.4.4 Future work

The model proposed here relies on the precise timing of events. More biostratigraphic data combined with isotopic dating of intrusive and extrusive rocks from the various units (Refahiye Complex, Kızılırmak Ophiolite, Karadağ, İkiçam and Yaylaçayı Formations) could better refine the stratigraphy and timing of events and lead to a better understanding of the processes.

A more detailed combined stratigraphic and structural investigation could test the interpretations of the thick sedimentary successions related to the volcanic arc (Sütpınar and İkiçam Formations). Combined with detailed provenance studies of heavy mineral grains the development of the suture zone during collision could be more confidently understood.

The *mélange* units (Karayaprak *Mélange* and Kirazbaşı *Mélange*) contain a wealth of information about the Neotethyan lithosphere and the timing and tectonic environment of its subduction, which remains to be fully explored. Lithological association mapping of the *mélange* could help to establish whether there was one or

two subduction zones as proposed by Tüysüz (1990). Was a separate accretionary complex formed during closure of the backarc basin or was all of the mélangé derived from Neotethys? If the mélangé represents a single accretionary complex, how did it become imbricated with both continental margins and the volcanic arc?

Comparable areas are found in Central Anatolia (e.g. Rojay 1995; Özden et al. 1998). North of Sivas; south-verging thrust slices of Cenomanian-Turonian ophiolitic mélangé crop out between the Pontides to the north and the Taurides to the south (Özden et al. 1998). In addition to ophiolitic mélangé the thrust belt in the Sivas area contains units derived from the Northern Neotethys and from the margins of adjacent plates (Tekelidağ Mélangé, Mermer Formation, Tokuş Formation and Kızılalan units; Özden et al. 1998). The Mermer Formation, described by Özden et al. (1998) comprises a volcanic and volcanoclastic succession with intercalated carbonates of Late Cretaceous age and may be comparable to the volcanic arc units within the Izmir-Ankara-Erzincan Suture Zone in the Eastern and Central Pontides.

7 Conclusions

Northward subduction of Neotethys was probably initiated during Coniacian-Santonian time (~85.8 Ma) as evidenced by the earliest arc-related volcanism in the Pontides (Yılmaz et al. 2003). No continental margin arc developed in the Central Pontides north of the Izmir-Ankara-Erzincan Suture Zone, perhaps due to oblique convergence or flat subduction.

Trench-retreat (slab roll-back) caused southward migration of the magmatic front and SSZ extension during Campanian-Maastrichtian time (~83.5-65.5 Ma), probably related to slow convergence between Afro-Arabia and stable Europe, and led to formation of the Kızılırmak Ophiolite and Refahiye Complex. Geochemistry of basic igneous rocks from the Kızılırmak Ophiolite and Refahiye Complex supports a backarc basin eruptive setting. Geochemical analyses from the volcanic arc units in the Eastern and Central Pontides (Karadağ and Yaylaçayı Formations) supports a volcanic arc origin.

Thick sedimentary successions accumulated in deep-water environments in the backarc and forearc regions. Accretionary mélangé developed above a north-dipping subduction zone during the Late Cretaceous isolated from a continental margin.

The southern margin of Eurasia subsided during Campanian time to form a flexural foreland basin. Slices of the backarc lithospheric plate, together with accretionary mélangé were emplaced northwards over the Eurasian margin at this time. This deformational event led to north-vergent folding and thrusting of all the units within the Izmir-Ankara-Erzincan Suture Zone.

The southern margin of northern Tethys (Tauride-Anatolide Platform) subsided during latest Cretaceous (Maastrichtian) time as it collided with the trench. Ophiolitic mélangé was emplaced southward over the Tauride-Anatolide platform at this time. Shallow marine and fluvial deposition followed in Palaeocene-Mid Eocene time directly upon the amalgamated deformed Neotethyan units. South-vergent thrusting and folding reimbricated all the units after Mid Eocene time due to renewed regional compression.

Data collected during this study support a model for the tectonic assembly of the Izmir-Ankara-Erzincan Suture Zone which involves emplacement of ophiolites onto the active continental margin of Eurasia during latest Cretaceous time, contemporaneous with arc-trench collision (a regional scale tectonic event). Therefore, the Neotethyan ophiolites in the Pontides do not fit the typical 'Tethyan' or 'Cordilleran' ophiolite models. Both regional and global tectonic processes contributed to the genesis and emplacement of these ophiolites.

References:

Adamia, S.H.A., Lordkipanidze, M.B. & ve Zakariadze, G.S. 1977. Evolution of active Continental margin as exemplified by the Alpin history of Caucasus. *Tectonophysics*, **40**,183-199.

Adamia, S.H.A., Chkhotuma, T., Kekelia, M., Lordkipanidze, M. & Shavishvilli, I. 1981. Tectonics of Caucasus and adjoining regions: implications for the evolution of the Tethys Ocean. *Journal of Structural Geology*, **3**, 437-447.

Akıncı, Ö.T. 1984. The Eastern Pontide volcano-sedimentary belt and associated massive sulphide deposits. In: Robertson, A.H.F. & Dixon, J.E. (Eds.), *The Geological Evolution of the Eastern Mediterranean Region*. Geological Society London Special Publications, **17**, 415-428.

Aktaş, G. & Robertson, A.H.F. 1984. The Maden Complex, SE Turkey: evolution of a Neotethyan continental margin. In: Dixon, J.E. & Robertson, A.H.F. (Eds.), *The Geological Evolution of the Eastern Mediterranean. Special Publication*, Geological Society of London, **17**, pp375– 402.

Aktimur, H.T., Tekirli, M.E., Yurdakul, M.E. 1990. Geology of the Sivas-Erzincan Tertiary basin. *Bulletin of Mineral Research Exploration*, **111**, 21-30.

Aktimur, H.T., Yurdakul, M.E., Sariaslan, M., Göksel, M. & Keçer, M. 1995. Geology of Erzincan region and petrology of Quaternary volcanic rocks. In: Erler et al. (Eds.) *Geology of the Black Sea Region*. General Directorate of Mineral Research and Exploration and Chamber of Geological Engineers. pp82-90.

Akyürek, B., Bilginer, E., Çatal, E., Dager, Z., Soysal, Y. & Sunu, O. 1979. Eldivan-Şabanözü (Çankırı) dolayında ofiyolit yerleşmesine ilişkin bulgular. *Jeoloji Mühendisliği*, **9**, 5-11.

Allaby, A. & Allaby, M. 1990. Dictionary of Earth Sciences (2nd edition), Oxford.

Andrew, T. & Robertson, A.H.F. 2002. The Beyşehir-Hoyran-Hadim Nappes: genesis and emplacement of Mesozoic marginal and oceanic units of the northern Neotethys in southern Turkey. *Journal of the Geological Society of London*, **159**, 529-543.

Anonymous, 1972. Penrose field conference on ophiolites: *Geotimes*, **17 (12)**, 24–25.

Ashcroft, W.A. 1972. Crustal Structure of the South Shetland Islands and Bransfield Strait. *British Antarctic Survey Scientific Reports*, **66**.

Atalay, Z. 1999. The palaeographic evolution of the Sivas Tertiary basin (W-SW Sivas). *Bulletin Mineral Research and Exploration (Ankara, Turkey)*, **76**, 153-173.

Ataman, G. 1972. Ankara'nin güneydoğusundaki granitik granodiyoritik kütlerlerden Cefalık Dağı'nın radyometrik yaşı hakkında ön çalışma. *Hacettepe Fen Mühendislik Bilimleri Dergisi*, **2**, 44–49.

Audley-Charles, M.G. 1981. Geochemical problems and implications of large-scale overthrusting in the Banda Arc-Australian margin collision zone. In: McClay, J. R. & Price, N. J. (Eds.), *Thrust and Nappe Tectonics*, Geological Society of London Special Publication, **9**, 407-416.

Bailey, E.M. & McCallien, W.J. 1950. Serpentine lavas, the Ankara Melange and the Anatolian Thrust. *Transactions of the Royal Society of Edinburgh*, **62**, 403-442.

Barker, P.F. 1982. The Cenozoic subduction history of the Pacific margin of the Antarctic Peninsula: Ridge crest-trench interactions. *Geological Society of London Journal*, **139**, 787-801.

Barker, D.H.N., Christeson, G.L., Austin Jr., J.A. & Dalziel, I.W.D. 2003. Backarc basin evolution and cordilleran orogenesis: insights from new ocean-bottom seismograph refraction profiling in Bransfield Strait, Antarctica. *Geological Society of America Bulletin*, **31** (2), 107-110.

Bébién, J. 1982. L'association ignée de Guevgueli (Macédoine, Grèce). Expression d'un magmatisme ophiolitique dans une déchirure continentale. Thèse, Nancy, 467 p.

Bébién, J., Dubois, R. & Gauthier, A. 1986. Example of ensialic ophiolites emplaced in a wrench zone: Innermost Hellenic ophiolite belt (Greek Macedonia). *Geology*, **14**, 1016-1019.

Beccaluva, L., Coltorti, M., Giunta, G. & Siena, F. 2004. Tethyan vs. Cordilleran ophiolites: a reappraisal of distinctive tectono-magmatic features of supra-subduction complexes in relation to the subduction mode. *Tectonophysics*, **393** (1-4), 163-174.

Bektaş, O., Şen, C., Atıcı, Y., Köprübaşı, N. 1999. Migration of Upper Cretaceous subduction-related volcanism towards the back-arc basin of the Eastern Pontide magmatic arc (NE Turkey). *Geological Journal*, **34**, 95-106.

Best, M.G. 2003. *Igneous and Metamorphic Petrology*. Second edition. Blackwell. p.463.

Bergougnan, H. 1975. Relations entre les edifices pontique et taurique dans le Nord-Est de l'Anatolie. *Bulletin de la Société Géologique de France*, **7**, XVII, No.6, 1045-1057.

Birgili, Ş., Yoldaş, R. & Ünalın, G. 1975. Çankırı-Çorum havzasının jeolojisi ve petrol olanakları. *MTA Enst. Rep.*, 5621.

Bloomer, S.H., Taylor, B., MacLeod, C.J., Stern, R.J., Fryer, P., Hawkins, J.W. & Johnson, L. 1995. Intrusive volcanic rocks in Western Pacific forearcs. In: Taylor, B.

& Natland, J. (Eds.). *Active Margins and Marginal Basins of the Western Pacific Geophysical Monograph*, pp.1-30

Boggs, S. 1995. *Principles of Sedimentology and Stratigraphy*. Prentice Hall, New Jersey.

Boudier, F., Ceuleneer, G., Nicolas, A. 1988. Shear zones, thrusts and related magmatism in the Oman ophiolite: initiation of thrusting on an oceanic ridge. *Tectonophysics*, **11**, 275-296.

Bouma, A.H. 1962. Sedimentology of some flysch deposits: A graphic approach to facies interpretation: Amsterdam, *Elsevier*, 168p.

Boutelier, D., Chemenda, A. & Burg, J.-P. 2003. Subduction versus accretion of intra-oceanic volcanic arcs: insight from thermo-mechanical analogue experiments. *Earth and Planetary Science Letters*, **212**, 31-45.

Bozkurt, E. & Mittwede, S.K. 2001. Introduction to the geology of Turkey - A synthesis. *International Geology Review*, **43** (7), 578-594.

Brongniart, A. 1813. Essai d'une classification minéralogique des roches mélangées. *Journal des Mines*, **34** (199), 5-48.

Brown, S. 1997. The geological evolution and regional significance of the Mesozoic to Tertiary Paikón Massif, Northern Greece. PhD Thesis (*unpublished*), University of Edinburgh.

Brown, S.A.M. & Robertson, A.H.F. 2003. Sedimentary geology as a key to understanding the tectonic evolution of the Mesozoic-Early Tertiary Paikón Massif, Vardar suture zone, N Greece. *Sedimentary Geology* **160**, 179-212.

- Bruhn, R.L., Stern, C.R. & De Wit, M.J. 1978. Field and geochemical data bearing on development of a Mesozoic volcano-tectonic rift zone and back-arc basin in southernmost South-America. *Earth Planetary and Science Letters*, **41** (1), 32-46.
- Brunn, J.H. 1954. Les eruptions ophiolitiques dans le Nord-Ouest de la Grece: leurs relations avec l'orogenese. *Nineteenth International Geological Congress Algiers*, **17**, 19-27.
- Cann, J. R. 1970. Rb, Sr, Y, Zr and Nb in some ocean-floor basaltic rocks. *Earth and Planetary Science Letters*, **10**, 1.
- Capedri, S., Venturelli, G., Bocchi, G., Dostal, J., Garuti, G. & Rossi, A. 1980. The geochemistry and petrogenesis of an ophiolites sequence from Pindos, Greece. *Contributions to Mineralogy and Petrology*, **74**, 189-200.
- Casey, J.F. & Dewey, J.F. 1984. Initiation of subduction zones along transform and accreting plate boundaries, triple-junction evolution, and forearc spreading centres; implications for ophiolitic geology and obduction. In: Gass, I. G., Lippard, S. J. & Shelton, A. W., (Eds.), *Ophiolites and Oceanic Lithosphere*, Geological Society of London Special Publication, **13**, 269-290.
- Çelik, Ö. & Delaloye, M. 2003. Origin of the ophiolites related metamorphic rocks and their post-kinematic mafic dyke swarms in the Antalya and Lycian ophiolites. *Geological Journal*, **38**, 235-256.
- Chemenda, A.I., Hurpin, D., Tang, J.-C., Stefan, J.-F. & Buffet, G. 2001. Impact of arc-continent collision on the conditions of burial and exhumation of UHP/LT rocks: experimental and numerical modelling. *Tectonophysics*, **342**, 137-161.
- Chopin, C. 1984. Coesite and pure pyrope in high-grade blueschists of the western Alps: a first record and some consequences. *Contributions to Mineralogy and Petrology*, **86**, 253-274.

Chorowicz, J., Dhont, D. and Gündoğdu, N. 1999. Neotectonics in the eastern North Anatolian fault region (Turkey) advocates crustal extension: mapping from SAR ERS imagery and Digital Elevation Model. *Journal of Asian Earth Sciences*, **21**, 511-532.

Çiner, A., Kosun, E. & Deynoux, M. 2002. Fluvial, evaporitic and shallow-marine facies architecture, depositional evolution and cyclicity in the Sivas Basin (Lower to Middle Miocene), Central Turkey. *Journal of Asian Earth Science*, **21** (2), 147-165.

Clark, M.S. & Robertson, A.H.F. 2002. The role of the Early Tertiary Ulukışla Basin, southern Turkey in suturing of the Mesozoic Tethys ocean. *Journal of the Geological Society of London*, **159**, 673-690.

Clift, P.D. & Dixon, J. E. 1998. Jurassic ridge collapse, subduction initiation and ophiolite obduction in the southern Greek Tethys. *Eclogae Geologicae Helveticae*, **91**, 128-139.

Clift, PD, MacLeod CJ, Tappin, D.R., Wright, D.J. & Bloomer, S.H. 1998. Tectonic controls on sedimentation and diagenesis in the Tonga Trench and forearc, southwest Pacific. *Geological Society of America Bulletin*, **110** (4), 483-496.

Clift, P.D., Hannigan, R., Blusztajn, J. & Draut, A.E. 2002. Geochemical evolution of the Dras-Kohistan Arc during collision with Eurasia: Evidence from the Ladakh Himalaya, India. *The Island Arc*, **11**, 255-273.

Clift, P.D., Pecher, I., Kukowski, N. & Hampel, A. 2003. Tectonic erosion of the Peruvian forearc, Lima Basin, by subduction and Nazca Ridge collision. *Tectonics*, **22** (3), 7-1-16.

Cloos, M. 1982. Flow melange, numerical modelling and geological constraints on the origin of the Franciscan Complex, California. *Bulletin of the Geological Society of America*, **93**, 330-345.

Collins, A. 1997. Tectonic evolution of the Lycian Taurides. PhD thesis *Unpublished*, University of Edinburgh.

Collins, A. & Robertson, A.H.F. 1998. Processes of Late Cretaceous to Late Miocene episodic thrust-sheet translation in the Lycian Taurides, southwestern Turkey. *Journal of the Geological Society of London*, **155**, 759-772.

Cox, J., Searle, M. & Petersen, R. 1999. The petrogenesis of leucogranite dykes intruding the northern Semail ophiolite, United Arab Emirates: field relationships, geochemistry and Sr/Nd systematics. *Contributions to Mineralogy and Petrology*, **137**, 267-287.

Cunningham, W.D. 1995. Orogenesis at the southern tip of the Americas-the structural evolution of the Cordillera Darwin metamorphic complex, southernmost Chile. *Tectonophysics*, **244** (4), 197-229.

Dalziel, I.W.D. 1986. Collision and Cordilleran Orogenesis: an Andean perspective. In: Coward, M. P. & Ries, A. C. (Eds.), *Collision Tectonics*, Geological Society of London Special Publication, **19**, 389-404.

Dalziel, I.W.D., de Wit, M.J. & Palmer, K.F. 1974. Fossil marginal basin in the southern Andes. *Nature, London*, **250**, 291-294.

Dalziel, I.W.D., Lawver, L.A. & Murphy, J.B. 2000. Plumes, orogenesis, and supercontinental fragmentation. *Earth and Planetary Science Letters*, **178**, 1-11.

Davy, P. & Cobbold, P.R. 1988. Experiments on shortening of a 4-layer model. *Tectonophysics*, **188**, 1-25.

Dercourt, J., Zonenshain, L.P., Ricou, L.E., Kazmin, V.G., Le Pichon, X., Knipper, A.L., Grandjacquet, C., Sbertshnikov, I.M., Geysant, J., Lepvrier, C., Perchersky, D.H., Boulin, J., Sibuet, J.-C., Savostin, L.A., Sorokhtin, O., Westphal, M., Bazhrnov, M.L., Lauer, J.-P. & Biju-Duval, B. 1986. Geological evolution of the Tethys belt from the Atlantic to the Pamirs since the Lias. *Tectonophysics*, **123**, 241-315.

Dercourt, J., Ricou, L.E. & Vrielynck, B. (Eds.), 1992. Atlas Tethys Paleoenvironmental Maps, Beicip-Franlab.

Dercourt, J., Ricou, L.E. & Vrielynck, B. (Eds.), 1993. Atlas Tethys Paleoenvironmental Maps, Beicip-Franlab.

Dewey, J.F. 1976. Ophiolite Obduction. *Tectonophysics*, **31**, 93-120.

Dewey, J.F. 1980. "Episodicity, Sequence and Tectonic Style at Convergent Plate Boundaries" In: Strangeway, D.W. (Ed.), *The Continental Crust and its Mineral Deposits*, Geological Association of Canada Special Paper, **20**, pp.553-573.

Dewey, J.F., Pitman, W.C., Ryan, W.B.F. & Bonin, J. 1973. Plate tectonics and evolution of the Alpine system. *Geological Society of America Bulletin*, **84**, 3137-3180.

Dewey, J.F. & Kidd, W.S.F. 1977. Geometry of plate accretion. *Geological Society of America Bulletin*, **88**, 960-968.

De Wit, M.J. 1977. The evolution of the Scotia Arc as a key to the reconstruction of Gondwanaland. *Tectonophysics*, **37**, 53-81.

De Wit, M.J. & Stern, C.R. 1978. Pillow talk. *Journal of Volcanology and Geothermal Research*, **4**, 55-80.

De Wit, M.J. & Stern, C.R. 1981. Variations in the degree of crustal extension during the formation of a back-arc basin. *Tectonophysics*, **72**, 229-260.

Dhont, D., Chorowicz, J., Yürür, T. & Köse, O. 1998. Polyphased block tectonics along the North Anatolian Fault in the Tosya basin area (Turkey). *Tectonophysics*, **299**, 213-227.

Dick, H.J.B. & Bullen, T. 1984. Chromian spinel as a petrogenetic indicator in abyssal and alpine-type peridotites and spatially associated lavas. *Contributions to Mineralogy and Petrology*, **86**, 54-76.

Dickinson, W. 1995. Forearc Basins. In: Busby, C.J. & Ingersoll, R.V. (Eds) *Tectonics of Sedimentary Basins*, pp. 238.

Dietrich, V., Emmermann, R., Oberhänsli, R. & Puchelt, H. 1978. Geochemistry of basaltic and gabbroic rocks from the West Mariana basin and the Mariana trench. *Earth and Planetary Science Letters*, **39**, 127-144.

Dilek, Y., Thy, P., Hacker, B. & Grundvig, S. 1999. Structure and petrology of Tauride ophiolites and mafic dyke intrusions (Turkey), implications for the Neotethyan ocean. *Geological Society of America Bulletin*, **111**, 1192-1216.

Dilek, Y. 2003. Ophiolite pulses, mantle plumes and orogeny. In: Dilek, Y. & Robinson, P.T. (Eds.). *Ophiolites in Earth History*. Geological Society of London Special Publications, **218**, 9-19.

Dilek, Y. & Harris, R. 2004. Continental margins of the Pacific Rim: introduction. *Tectonophysics*, **392** (1-4), 1-7.

Elthon, D. & Stern, C. 1978. Metamorphic petrology of the Sarmiento ophiolite complex, Chile. *Geology*, **6**, 464-468.

Erickson, S.G. 1993. Sedimentary loading, lithospheric flexure, and subduction initiation at passive margins. *Geology*, 21, 2; 125-128.

Ernst, W.G. & Liou, J.G. 2000. Overview of UHP metamorphism and tectonics in well-studied collisional orogens. In: Ernst, W.G. & Liou, J.G. (Eds.), *UHP metamorphism and Geodynamics in collision-type orogenic belts*. Geological Society of America, Boulder Colorado, pp.3-19.

Erol, O. 1954. Köroglu Isik daglari volkanik kütlelerinin orta bölümleri ile Beypazari Ayas arasindaki Neojen havzasinin jeolojisi hakkında rapor: *Ankara, General Directorate for Mineral Research and exploration (MTA)*. Report no. 2279.

Fitton, J.G. & Dunlop, H.M. 1985. The Cameroon line, West Africa, and its bearing on the origin of oceanic and continental alkali basalts. *Earth and Planetary Science Letters*, 72, 23-38.

Fitton, J.G., James, D., Kempton, P.D., Ormerod, D.S. & Leeman, W.P. 1988. The role of lithospheric mantle in the generation of Late Cenozoic basic magmas in the Western United States. *Journal of Petrology*, 29, 131-149.

Fitton, J.G., Saunders, A.D., Norry, M.J., Hardarson, B.S. & Taylor, R.N. 1997. Thermal and chemical structure of the Iceland plume. *Earth Planetary Science Letters*, 153 (3-4), 197-208.

Fitton, J.G., Saunders, A.D. Larsen, L.M., Hardarson, B.S. & Norry, M.J. 1998. Volcanic rocks from the southeast Greenland margin at 63°N: composition, petrogenesis and mantle sources. *Proceedings of the Ocean Drilling Program, Scientific Results*, 152, 331-350.

Flower, M.F.J. 2003. Ophiolites, historical contingency, and the Wilson cycle. In: Dilek, Y. & Newcomb, S. (Eds.), *Ophiolite Concept and the Evolution of Geological Thought*. The Geological Society of America Special Paper, **373**, 111-136.

Floyd, P.A., Yaliniz, M.K. & Goncuoglu, M.C. 1998. Geochemistry and petrogenesis of intrusive and extrusive ophiolitic plagiogranites, Central Anatolian Crystalline Complex, Turkey. *Lithos*, **42** (3-4) 225-241.

Garcia, M.O. 1978. Criteria for the identification of ancient volcanic arcs. *Earth Science Reviews*, **14**, 147-165.

Gass, I.G. 1968. Is Troodos Massif of Cyprus a fragment of Mesozoic Ocean floor? *Nature*, **220**, 5262.

Gass, I.G., Neary, C.R., Plant, J., Robertson, A.H.F., Simonian, K.O., Swewing, J.D., Spooner, E.T.C., & Wilson, R.A.M. 1975. Comments on the "Troodos ophiolitic complex was probably formed in an island arc" by A. Miyashiro. *Earth and Planetary Science Letters*, **25**, 236-238.

Gealey, W.K. 1980. Ophiolite obduction mechanisms. In: Panayiotou, A. (Ed.), *Ophiolites, Proceedings International Ophiolite Symposium, Cyprus*. Cyprus Geological Survey, Nicosia, 228-243.

Girardeau, J., Monnier, C., Launeau, P. & Quatrevaux, F. 2002. Kinematics of mantle flow beneath a fossil Overlapping Spreading Center: The Wuqbah massif case, Oman ophiolite. *Geochemistry Geophysics Geosystems* **G³**, **3**, no.7.

Glennie, K.W., Boeuf, M.G.A., Hughes Clarke, M.W., Moody-Stuart, M., Pilaar, W.F.H. & Reinhardt, B.M. 1973. Late Cretaceous nappes in the Oman Mountains and their geologic significance. *American Association of Petroleum Geologists Bulletin*, **57**, 5-27.

Glennie, K.W. 2000. Cretaceous tectonic evolution of Arabia's eastern plate margin: a tale of two oceans. In: Alsharhan, A.S. & Scott, R.W. (Eds.), *Middle East Models of Jurassic/Cretaceous Carbonate Systems*. Special Publication-Society of Economic Paleontologists and Mineralogists, **69**, 9-20.

Göncüoğlu, M.C. 1986. Geochronologic data from the southern part (Niğde area) of the Central Anatolian Massif. *Maden Tetkik ve Arama Dergisi*, **105/106**, 83–96.

Görür, N., Oktay, F.Y., Seymen, I. & Sengör, A.M.C. 1984. Palaeotectonic evolution of the Tüzgölü Basin Complex, central Turkey. In: Dixon, J.E., Robertson, A.H.F. (Eds.), *The Geological Evolution of the Eastern Mediterranean*. Geological Society of London Special Publication, **17**, 81-96.

Görür, N. & Tuysuz, O. 2001. Cretaceous to miocene palaeogeographic evolution of Turkey: Implications for hydrocarbon potential. *Journal of Petroleum Geology*, **24** (2), 119-146.

Gradstein, F.M., Ogg, J.G., Smith, A.G., Agterberg, F.P., Bleeker, W., Cooper, R.A., Davydov, V., Gibbard, P., Hinnov, L., House, M.R., Lourens, L., Luterbacher, H-P., McArthur, J., Melchin, M.J., Robb, L.J., Shergold, J., Villeneuve, M., Wardlaw, B.R., Ali, J., Brinkhuis, H., Hilgen, F.J., Hooker, J., Howarth, R.J., Knoll, A.H., Laskar, J., Monechi, S., Powell, J., Plumb, K.A., Raffi, I., Röhl, U., Sadler, P., Sanfilippo, A., Schmitz, B., Shackleton, N.J., Shields, G.A., Strauss, H., Van Dam, J., Veizer, J., van Kolfschoten, T.H. & Wilson, D. 2004. *A Geologic Time Scale 2004*. Cambridge University Press, 589p

Hall, R. 1976. Ophiolite emplacement and the evolution of the Taurus suture zone, South-east Turkey. *Geological Society of America Bulletin*, **87**, 1078–1088.

Hall, A. *Igneous Petrology* (second edition). Longman. 1996.

- Halpern, M. 1973. Regional geochronology of Chile South of 50°S Latitude. *Geological Society of America Bulletin*, **84**, 2407-2422.
- Harker, A. 1909. *The Natural History of Igneous Rocks*. New York. Macmillan, 384pp.
- Harris, R. 1992. Peri-collisional extension and the formation of Oman-type ophiolites in the Banda Arc and Brooks Range. In: Parson, L.M., Murton, B.J. & Browning, P. (Eds.), *Ophiolites and their modern oceanic analogues*. Special Publication Geological Society of London, **60**, pp.301– 325.
- Hobbs, B.E., Means, W. D. & Williams, P. E. 1976. *An Outline of Structural Geology*, John Wiley & Sons, Inc, 571p.
- Hofmann, A.W. & White, W.M. 1982. Mantle plumes from ancient oceanic-crust. *Earth Planetary Science Letters*, **57** (2), 421-436.
- Holland, C.H. *et al.* 1978. *A guide to stratigraphical procedure*. Geological Society of London Special Report, No. 10.
- Hopson, C.A., Pallister, J.S. 1980. Semail ophiolite magma chamber:1. Evidence from gabbro phase variation, internal structure and layering. In: Panayiotou, A. (Ed.), *Ophiolites, Proceedings of the International Ophiolite Symposium, Cyprus, 1979*. Cyprus Geological Survey Department, pp. 402–404.
- Iijima, A., Hein, J.R. & Siever, R. (Eds), 1983. *Siliceous Deposits in the Pacific Region*. Elsevier, Amsterdam, 472 pp.
- Jones, B.F. & Galan, E. 1988. Sepiolite and Palygorskite. In: Bailey, S. W. (Ed.) *Hydrous Phyllosilicates (exclusive of micas)*. Mineralogical Society of America, *Reviews in Mineralogy*, **19**.

Judd, J.W. 1886. Report on a series of specimens of the deposits of the Nile delta. *Proceedings of the Royal Society*, **39**, 213–227.

Juteau, T. 1979. Ophiolites des Taurides: essai sur leur histoire océanique. *Revue de Géologie Dynamique et de Géographie Physique*, **22**.

Juteau, T. 1980. Ophiolites of Turkey. In: Rocci, G. (Ed.), *Ofioliti, Special Issue Tethyan Ophiolites: 2. Eastern Area*, pp.199– 237.

Karig, D.E. 1971. Origin and development of the marginal basins in the Western Pacific. *Journal of Geophysical Research*, **76**, 2542-2561.

Kaymakçı, N. 2000. Tectono-stratigraphical evolution of the Çankırı Basin (Central Anatolia, Turkey). PhD Thesis (*Unpublished*), ITC Universiteit Utrecht.

Keller, R.A. & Fisk, M.R. 1992. Quaternary marginal basin volcanism in the Bransfield Strait as a modern analogue of the southern Chilean ophiolites. In: Parson, L. M., Murton, B. J. & Browning, P. (Eds.), *Ophiolites and their Modern Oceanic Analogues*. Geological Society of London Special Publication, **60**, 155-169.

Klitgord, K.D. & Schouton, H. 1986. Plate kinematics of the central Atlantic. In: Vogt, P.R. & Tucholke, B.E. (Eds.), *The Western North Atlantic region, Volume M: Geology of North America, Boulder, Colorado*. Geological Society of America, 351-378.

Koçyiğit, A., Özkan, S. & Rojay, B. 1988. Examples from the fore arc basin remnant at the active margin of Northern Neo-Tethys: emplacement age of the Anatolian Nappe. *METU Journal of Pure and Applied Sciences*, **21**, 183-210.

Koçyiğit, A. 1990. Structural relationships of three suture zones to the west of Erzincan (NE Turkey): Karakaya, Inner Tauride and Erzincan sutures. *8th Petroleum*

Congress of Turkey Turkish Association of Petroleum Geologists UCTEA Chamber of Petroleum Engineers. 152-161.

Koçyiğit, A. 1991. An example of an accretionary forearc basin from northern Central Anatolia and its implications for history of subduction of Neo-Tethys in Turkey. *Geological Society of America Bulletin*, **103**, 22-36.

Koçyiğit, A., Winchester, J.A., Bozkurt, E. & Holland, G. 2003. Saraçköy volcanic suite: implications for the subductional phase of arc evolution in the Galatean Arc Complex, Ankara, Turkey. *Geological Journal*, **38**, 1-14.

Koulakov, I., Tychkov, S., Bushenkova, N. & Vasilevsky, A. 2002. Structure and dynamics of the upper mantle beneath the Alpine-Himalayan orogenic belt, from teleseismic tomography. *Tectonophysics*, **358**, 77-96.

Kurtman, F. 1961. Sivas-Divriği arasındaki sahanın jeolojisi ve jipsli seri hakkında müşahedeler. *Maden Tektik ve Arama*, **56**, Ankara.

Larson, R.L. & Pitman, W.C., 1972. World-Wide correlation of Mesozoic magnetic anomalies and its implications. *Bulletin of the Geological Society of America*, **83**, 3645p.

Leeder, M.R. 1982. *Sedimentology Process and Product*, Chapman & Hall, London.

Le Maitre, R.W., Bateman, P., Dudek, A., Keller, J., Lameyre, J., Le Bas, M.J., Sabine, P.A., Schmid, R., Sorensen, H., Streckeisen, A., Woolley, A.R. & Zanettin, B. 1989. *A Classification of Igneous Rocks and Glossary of Terms: Recommendations of the International Union of Geological Sciences Subcommission on the Systematics of Igneous Rocks*. Oxford: Blackwell Scientific. London. Edinburgh, 183p.

Lindstrom, D.J. 1976. Experimental study of the partitioning of the transition metals between clinopyroxene and coexisting silicate liquids. PhD dissertation, University of Oregon, p188 (unpublished).

Lippard, S.J., Shelton, A.W. & Gass, I.G. 1986. The ophiolite of Northern Oman. *Memoir-Geological Society of London*, **11**, pp178.

Loughnan, F.C. 1969. *Chemical Weathering of the Silicate Minerals*. American Elsevier, New York.

Martinez, F. & Taylor, B. 1996. Backarc spreading, rifting, and microplate rotation, between transform faults in the Manus basin. *Marine Geophysical Researches*, **18** (2-4), 203-224.

McDonough, W.F. & Sun, S. 1995. The composition of the Earth. *Chemical Geology*, **120**, 223-253.

McKenzie, D. 1972. Active tectonics of the Mediterranean region. *Geophysical Journal Royal Astronomical Society*, **30**, 109-185.

McLane, M. 1995. *Sedimentology*, Oxford University Press, Oxford.

Meschede, M. 1986. A method of discriminating between different types of mid-ocean ridge basalts and continental tholeiites with the Nb-Zr-Y diagram. *Chemical Geology*, **56** (3-4), 207-218.

Mohiuddin, M.M. & Ogawa, Y. 1998. Late Paleocene-middle Miocene pelagic sequences in the Boso Peninsula, Japan: New light on northwest Pacific tectonics. *The Island Arc*, **7** (3), p301.

Molnar, P., & Atwater, T. 1978. Inter-arc spreading and Cordilleran tectonics as alternates related to the age of the subducted lithosphere. *Earth Planetary and Science Letters*, **41**, 330-340.

Moore, E.M. & Vine, F.J. 1971. The Troodos Massif, Cyprus and other ophiolites as oceanic crust: evaluations and implications. *Philosophical Transactions of the Royal Society of London A*, **268**, 433-466.

Mottl, M.J. 1983. Metabasalts, axial hot springs, and the structure of hydrothermal systems at mid-ocean ridges. *Geological Society of America Bulletin*, **94**, 161-180.

Murphy, M.A. & Salvador, A. 1994. International Stratigraphic Guide – an abridged version. International Subcommittee on Stratigraphic Classification of the International Union of Geological Sciences, International Commission on Stratigraphy.

Nichols, G. 1999. *Sedimentology and Stratigraphy*, Blackwell Science Ltd, pp355.

Nicolas, A. 1989, *Structures of ophiolites and dynamics of oceanic lithosphere: Dordrecht, Netherlands*, Kluwer Academic Publishers.

Nicolas, A. & Le Pichon, Z. 1980. Thrusting of young lithosphere in subduction zones with special reference to the structures in ophiolite peridotites. *Earth and Planetary Science Letters*, **46**, 97-406.

Niu, Y., O'Hara, M.J. & Pearce, J.A. 2003. Initiation of Subduction Zones as a Consequence of Lateral Compositional Buoyancy Contrast within the Lithosphere: a Petrological Perspective. *Journal of Petrology*, **44, **5**, 851-866.**

Noiret, G., Montigny, R. & Allegre, C.J. 1981. Is the Vourinos complex an island arc ophiolites? *Earth and Planetary Science Letters*, **56**, 375-386.

O'Brien, P. 2001. Subduction followed by collision: Alpine and Himalayan examples. *Physics of Earth and Planetary Interiors*, **127**, 277-291.

Okay, A.I. & Monié, P. 1997. Early Mesozoic subduction in the Eastern Mediterranean: Evidence from Triassic eclogite in northwest Turkey. *Geology*, **25** (7), 595-598.

Okay, A.I. & Şahintürk, Ö. 1997. Geology of the Eastern Pontides. In: Robinson A. G. (Ed.) *Regional and Petroleum Geology of the Black Sea and Surrounding Region*. American Association of Petroleum Geologists Memoirs, **68**, 291-311.

Okay, A.I. & Tüysüz, O. 1999. Tethyan sutures of northern Turkey, In: Durand, B., Jolivet, L., Horvath, F. & Seranne, M. (Eds.) *The Mediterranean Basins: Tertiary Extension within the Alpine Orogen*. Geological Society of London Special Publications, **156**, 475-515.

Okay, A.I., Tansel, I. & Tüysüz, O. 2001. Obduction, subduction and collision as reflected in the Upper Cretaceous-Lower Eocene sedimentary record of western Turkey. *Geological Magazine*, **138** (2), 117-142.

Önen, A.P. 2003. Neotethyan ophiolitic rocks of the Anatolides of NW Turkey and comparison with Tauride ophiolites. *Journal of the Geological Society of London*, **160**, 947-962.

Osozawa, S., Takeuchi, H. & Koitabashi, T. 2004. Formation of the Yakuno ophiolite; accretionary subduction under medium-pressure-type metamorphic conditions. *Tectonophysics*, **393**,(1-4), 197-219.

Ozer, E., Koc, H. & Ozsayar T.Y. 2004. Stratigraphical evidence for the depression of the northern margin of the Menderes-Tauride Block (Turkey) during the Late Cretaceous. *Journal of Asian Earth Sciences*, **22**, (5) 401-412.

Özgül, N. 1981. Munzur dağlarının jeolojisi. *MTA Report*, **6995**, (unpublished), Ankara.

Özgül, N. & Turşucu, A. 1984. Stratigraphy of the Mesozoic carbonate sequence of the Munzur Mountains (Eastern Taurides). In: Goncolu (Ed.) *Geology of the Tauride Belt International Symposium*, 173-180.

Pallister, J.S. & Hopson, C.A. 1981. Samail ophiolite plutonic suite: field relations, phase variation, cryptic variation and layering, and a model of a spreading ridge magma chamber. *Journal of Geophysical Research*, **8**, 2593– 2644.

Parlak, O., Kozlu, H., Delaloye, M. & Hoek, V. 2001. Tectonic setting of the Yüksekova ophiolite and its relation to the Baskil magmatic arc within the southeast Anatolian orogeny. *Fourth International Turkish Geology Symposium*, Cükurova University, Adana, Turkey Abstract, p.233.

Parson, L.M. & Murton, B.J. 1992. Ophiolites and their modern oceanic analoges. In: Parson, L. M., Murton, B. J. & Browning, P. (Eds.), *Ophiolites and their Modern Oceanic Analogues*. Geological Society Special Publication **60**, 1-2.

Pearce, J.A. 1973. Some relationships between the geochemistry and tectonic setting of volcanic rocks: PhD Thesis (*unpublished*) University of East Anglia.

Pearce, J.A. 1975. Basalt geochemistry used to investigate past tectonic settings on Cyprus. *Tectonophysics*, **25**, 41-67.

Pearce, J.A. 1982. Trace element characteristics of lavas from destructive plate boundaries. In: Thorpe, R. S. (Ed.) *Andesites*, J. Wiley, 525-548.

- Pearce, J.A. 1983. Role of the Sub-continental Lithosphere in Magma Genesis at Active Continental Margins. In: Hawkesworth C. J. & Norry, M. J. *Continental basalts and mantle xenoliths*. Nantwich: Shiva.
- Pearce, J.A. & Cann, J.R. 1973. Tectonic setting of basic volcanic rocks determined using trace element analysis. *Earth and Planetary Science Letters*, **19**, 290-300.
- Pearce, J.A., Alabaster, T., Shelton, A.W. & Searle, M.P. 1981. The Oman ophiolite as a Cretaceous arc-basin complex: evidence and implications. *Philosophical Transactions of the Royal Society of London A*, **300**, 299–317.
- Pearce, J.A., Lippard, S.J. & Roberts, S. 1984. Characteristics and tectonic significance of supra-subduction zone ophiolites. In: Kokelaar, B.P., Howells, M.F. (Eds.), *Marginal Basin Geology*. Geological Society of London Special Publications, **16**, pp.77-89.
- Pearce, J.A. & Norry, M.J. 1979. Petrogenetic implications of Ti, Zr, Y, and Nb variations in volcanic-rocks. *Contributions to Mineral Petrology*, **69** (1), 33-47.
- Pearce, J.A., Van der Laan, S.R., Arculus, R.J., Murton, B.J., Ishii, T., Peate, D.W. & Parkinson, I., 1992. Boninite and harzburgite from ODP Leg 125 (Bonin-Mariana forearc): A case study of magma genesis during the initial stages of subduction. *Proceedings of Ocean Drilling Program, Scientific Results*, **125**, 623-659.
- Peccerillo, A. & Taylor, S.R. 1976. Geochemistry of Eocene calc-alkaline volcanic rocks from the Kastamonu area, Northern Turkey. *Contributions to Mineralogy and Petrology*, **58**, 63-81.
- Pettijohn, F.J, Potter, P.E. and Siever, R. 1987. *Sand and Sandstone*. Springer-Verlag, New York.

Pickett, E.A., Robertson, A.H.F. & Dixon, J.E. 1995. The Karakaya Complex, NW Turkey: a Palaeotethyan accretionary complex. In: Erler, A., Ercan, T., Bingöl, E. & Orcen, S. (Eds.), *Geology of the Black Sea Region: Proceedings of an International Symposium on the Geology of the Black Sea Region, September 7–11, 1992, Ankara, Turkey*. MTA, Ankara, pp.11–18.

Pickett, E.A. & Robertson, A.H.F. 1996. Formation of the Late Palaeozoic–Early Mesozoic Karakaya Complex and related ophiolites in NW Turkey by Palaeotethyan subduction–accretion. *Journal of the Geological Society of London*, **153**, 995–1009.

Pickett, E.A. & Robertson, A.H.F. 2005. Significance of the volcanogenic Nilüfer Unit and related components of the Triassic Karakaya Complex for Tethyan subduction/accretion processes in NW Turkey. In: Okay, A.I. & Göncüoğlu, C.M. (Eds.) *Turkish Journal of Earth Sciences*, Special Issue commemorating Okan Tekeli.

Rabinowitz, P.D. & La Breque, J. 1979. The Mesozoic South Atlantic Ocean and evolution of its continental margins. *Journal of Geophysical Research*, **84**, 5973–6002.

Reading, H.G. (Ed.) 1978. *Sedimentary Environments and Facies*, Blackwell Scientific Publications, pp.557.

Reed, S.J.B. 1975. *Electron Microprobe Analysis*. Cambridge University Press.

Regard, V., Faccenna, C., Martinoid, J., Bellier, O. & Thomas, J.-C. 2003. From subduction to collision: control of deep processes on the evolution of convergent plate boundary. *Journal of Geophysical research*, **108**, 13-1 – 13-16.

Ricci Luchi, F., Colella, A., Gabianelli, G., Rossi, S. & Normark, W.R., 1984. The Crati submarine fan, Ionian sea. *Geo-Marine Letters*, **3**, 71-78.

Riccou, L.-E. 1971. Le croissant ophiolitique peri-arabe: une ceinture de nappes mises en place au Cretacé supérieur. *Revue Géographique Physique et Géologique Dynamique*, **13**, 327-349.

Robertson, A.H.F. 1987. The transition from a passive margin to an Upper Cretaceous foreland basin related to ophiolite emplacement in the Oman Mountains. *Geological Society of America Bulletin*, **99**, 633-653.

Robertson, A.H.F. 1994. Role of the tectonic facies concept in orogenic analysis and its application to Tethys in the Eastern Mediterranean region. *Earth Science Reviews*, **37**, 139-213.

Robertson, A.H.F. 1998. Mesozoic–Tertiary tectonic evolution of the Easternmost Mediterranean area; integration of marine and land evidence. In: Robertson, A.H.F., Emeis, K.C., Richter, K.-C., & Camerlenghi, A. (Eds.), *Proceedings of the ODP. Scientific Results*, **160**, pp723–782.

Robertson, A.H.F. 2002. Overview of the genesis and emplacement of Mesozoic ophiolites in the Eastern Mediterranean Tethyan region. *Lithos*, **65**, 1-67.

Robertson, A.H.F. 2004. Development of concepts concerning the genesis and emplacement of Tethyan ophiolites in the Eastern Mediterranean and Oman regions. *Earth Science Reviews*, **66**, 331-387.

Robertson, A.H.F., Awadallah, S.A.M., Geraubo, S., Lackschewitz, K.S., Monteleone, B.D., Sharp, T.R. & other members of The Shipboard Scientific Party, 2001. Evolution of the Miocene-Recent Woodlark Rift Basin, SW Pacific, inferred from sediments drilled during the Ocean Drilling Program. In: Wilson, R.C.L., Whitmarsh, R.B., Taylor, B. & Froitzheim, N. 2001. *Non-volcanic Rifting of Continental Margins A comparison of Evidence from Land and Sea*. Geological Society of London Special Publications, **187**, 335-372.

Robertson, A.H.F. & Collins, A.S. 2002. Shyok Suture Zone: late Mesozoic-Tertiary evolution of a critical suture zone separating the oceanic Ladakh arc from the Asian continental margin. *Journal of Asian Earth Sciences*, **20**, 309-351.

Robertson, A.H.F. & Degnan, D.J. 1994. The Dras arc Complex: lithofacies and reconstruction of a Late Cretaceous oceanic volcanic arc in the Indus Suture Zone, Ladakh Himalaya. *Sedimentary Geology*, **92**, 117-145.

Robertson, A.H.F. & Dixon, J.E. 1984. Introduction: aspects of the geological evolution of the Eastern Mediterranean. In: Dixon J.E. & Robertson A.H.F. (Eds.), *The Geological Evolution of the Eastern Mediterranean*. Geological Society of London Special Publications, **17**, 1-74.

Robinson, A.G., Banks, C.J., Rutherford, M.M. & Hirst, J.P.P. 1995. Stratigraphic and structural development of the eastern Pontides, Turkey. *Journal of Geological Society of London*, **152**, 861-872.

Rojay, B. 1993. PhD Thesis (*unpublished*), Middle East Technical University.

Rojay, B. 1995. Post-Triassic evolution of the Central Pontides: Evidence from Amasya region, Northern Anatolia. *Geologica Romana*, **31**, 329-350.

Rojay, B., Yalınız, K.M. & Altınır, D. 2001. Tectonic implications of some Cretaceous Pillow Basalts from the North Anatolian Ophiolitic Mélange (Central Anatolia-Turkey) to the evolution of Neotethys. *Turkish Journal of Earth Sciences*, **10**, 93-102.

Rollinson, H. 1993. *Using geochemical data: evaluation, presentation and interpretation*. Wiley & Son. New York. 352pp.

Royden, L.H. 1993. The tectonic expression of slab pull at continental convergent boundaries. *Tectonics*, **12** (2), 303-325.

Sartorio, D. 1988. *Southern Tethys biofacies*. Agip. (Milan, Italy).

Saunders, A.D. & Tarney, J. 1984. Geochemical characteristics of basaltic volcanism within back-arc basins. In: *Marginal Basin Geology*. Geological Society of London Special Publications, **16**, 59-76.

Saunders, A.D., Norry, M.J. & Tarney, J. 1988. Origin of MORB and chemically depleted mantle reservoirs: trace element constraints. *Journal of Petrology*, Special Lithosphere Issue, 415-445.

Schandl, E.S. & Wicks, F.J. 1993. Carbonate and associated alteration of ultramafic and rhyolitic rocks at the Hemingway Property, Kidd Creek volcanic complex, Timmins, Ontario. *Economic Geology*, **88**, 1615-1635.

Searle, M.P. & Malpas, J. 1980. Structure and metamorphism of rocks beneath the Semail ophiolites of Oman and their significance in ophiolites obduction. Transactions of the Royal Society of Edinburgh. *Earth Sciences*, **71**, 247-262.

Searle, M.P. & Malpas, J. 1982. Petrochemistry and origin of sub-ophiolite metamorphic rocks in the Oman Mountains. *Journal of the Geological Society of London*, **139**, 235-248.

Searle, M.P. & Cox, J. 1999. Tectonic setting, origin and obduction of the Oman ophiolite. *Geological Society of America Bulletin*, **111**, 104-122.

Şengör, A.M.C., Yılmaz, Y. & Ketin, I. 1980. Remnants of a pre-Late Jurassic ocean in northern Turkey: fragments of Permian-Triassic Paleo-Tethys? *Geological Society of America Bulletin*, **91**, 599-609.

Şengör, A.M.C. & Yılmaz, Y. 1981. Tethyan Evolution of Turkey: a plate tectonic approach. *Tectonophysics*, **75**, 181-241.

Şengör, A.M.C., Yılmaz, Y. & Sungurlu, O. 1984. Tectonics of the Mediterranean Cimmerides: nature and evolution of the western termination of Palaeo-Tethys. In: Dixon, J.E. & Robertson, A.H.F. (Eds.), *The Geological Evolution of the Eastern Mediterranean*. Special Publication Geological Society of London, **17**, pp. 77–112.

Seymen, I. 1981. Kaman (Kırşehir) dolayında Kırşehir Masifi'nin stratigrafisi ve metamorfizması. Türkiye Jeoloji Kurumu Bülteni, **24** (2), 101–108.

Sharaskin, A.Y., Dobretsov, N.L., & Sobolev, N.V. 1980. Geochemistry and timing of the marginal basin and arc-magmatism of the Phillipine Sea. *Philosophical Transactions of the Royal Society of London*. A **300**, 287-297.

Shervais, J.W. 1982. Ti-V plots and the petrogenesis of modern and ophiolitic lavas. *Earth Planetary and Science Letters*, **59** (1), 101-118.

Shipboard Scientific Party, 2004. Site 1268. In Kelemen, P.B., Kikawa, E., Miller, D.J., et al., *Proc. ODP, Init. Repts.*, 209, 1-171 [Online]. Available from World Wide Web:http://www.odp.tamu.edu/publications/209_IR/VOLUME/CHAPTERS/IR209_03.PDF. [Cited 09.05.2005]

Smith, A.G., 2004. Are N Atlantic hot-spots and N Atlantic continental break-up related to Tethyan ophiolite creation and emplacement? In: Chatzipetros, A.A. and Pavlides, S.B. (Eds.), *Proceedings of the 5th International Symposium on Eastern Mediterranean Geology*, **1**, 288-289.

Smith, A.G. *The Royal Society of London Special Publications*, (in press).

Spaggari, C.V., Gray, D.R. & Foster, D.A. 2003. Tethyan- and Cordilleran-type ophiolites of eastern Australia: implications for the evolution of the Tasmanides. In: Dilek, Y. & Robinson, P.T. (Eds.), *Ophiolites in Earth History*. Geological Society of London Special Publications, **218**, 517-539.

Srivastava, S.P., Roest, W.R., Kovacs, L.C., Oakey, G., Levesque, S., Verhoef, J. & Macnab, R. 1990. Motion of Iberia since the Late Jurassic: results from detailed aeromagnetic measurements in the Newfoundland Basin. *Tectonophysics*, **184**, 229-260.

Stampfli, G., Mosar, J., Faure, P., Pillecuit, A. & Vannay, J.-C. 2001. Permo-Mesozoic evolution of the western Tethys real: the Neotethys East Mediterranean basin connection, In: Ziegler, P., Cavazza, W., Robertson, A.H.F. & Crasquin-Soleau, S. (Eds.), *Peri-Tethys Memoir no. 5 Peri-Tethyan Rift/Wrench Basins and Passive Margins*. Memoirs du Museum National D'Histoire Naturelle, p.51-10.

Steinmann, G. 1927. Die ophiolithischen Zones in der Mediterranean Kettengebirger. *Congres de Geologie Internationale, 14th Session. Madrid*, 577-637.

Stern, C.R., & de Wit, M.J. 2003. Rocas Verdes ophiolites, southernmost South America: remnants of progressive stages of development of oceanic-type crust in a continenyal margin back-arc basin. In: Dilek, Y & Robinson, P.T. (Eds.), *Ophiolites in Earth History*. Geological Society of London Special Publications, **218**, 665-683.

Stern, C.R., Mohenseni, P.P. & Fuenzalida, R. 1991. Petrochemistry and tectonic significance of Lower Cretaceous Barros Arrana Formation basalts, southernmost Chilean Andes. *Journal of South American Earth Sciences*, **4**, 331-342.

Stewart, D.R.M. & Pearson, P.N. 2000. PLANKRANGE: A database of planktonic foraminiferal ranges [Online]. University of Bristol. Available from: <http://palaeo.gly.bris.ac.uk/Data/plankrange.html>

Storey, B.C. & Alabaster, T. 1991. Tectonomagmatic controls on Gondwana break-up models: evidence from the proto-Pacific margin of Antarctica. *Tectonics*, **10**, 1274-1288.

Suess, E. 1909. Das Antlitz der Erde. *Vienna F. Tempsky*, S. 789.

Suzanne, P., Lyberis, N., Chorowicz, J., Nurlu, M., Yurur, T. & Kasapoglu, E. 1990. Geometry Of The North Anatolian Fault From Landsat-Mss Images. *Bulletin De La Societe Geologique De France*, **6** (4), 589-599.

Tang, J.-C., Chemenda, A.I., Chery, J., Lallemand, S. & Hassani, R. 2003. Compressional subduction regime and arc continent collision: combined experimental and numerical modelling. *Geological Society of America Special Paper*.

Taylor, R.N., Murton, B.J. & Nesbitt, R.W. 1992. Chemical transects across intra-oceanic arcs: implications for the tectonic setting of ophiolites. In: Parson, L.M., Murton, B.J. & Browning, P. (Eds.), *Ophiolites and their Modern Oceanic Analogues*. Geological Society of London Special Publication, **60**, 117-132.

Tekeli, O. 1981. Subduction complex of pre-Jurassic age, northern Anatolia, Turkey. *Geology*, **9**, 68-72.

Thomas, C., Livermore, R. & Pollitz, F. 2003. Motion of the Scotia Sea Plates. *Geophysical Journal International*, **155**, 789-804.

Topuz, G., Altherr, R., Satur, M. & Schwartz, W.H. 2004. Low-grade metamorphic rocks from the Pular complex, NE Turkey: implications for the pre-Liassic evolution of the Eastern Pontides. *International Journal of Earth Science*, **93**, 72-91.

Tucker, M.E. 1981. *Sedimentary Petrology*. Blackwell Science.

Tucker, M.E. 1996. *Sedimentary Rocks in the Field*, John Wiley, Chichester, pp150.

Tüysüz, O. 1990. Tectonic evolution of a part of the Tethyside orogenic collage: the Kargı Massif, northern Turkey. *Tectonics*, **9**, 141-160.

Tüysüz, O. 1993. Karadeniz'den Orta Anadolu' ya bir jeotravers: Kuzey Neo-Tetis' in tektonik evrimi (A Geotransverse from Black Sea to Central Anatolia: tectonic evolution of Neotethys). *Turkish Association of Petroleum Geologists Bulletin*, **5**, 1-33.

Tüysüz, O. 1999. Geology of the Cretaceous sedimentary basins of the Western Pontides. *Geological Journal*, **34** (1-2), 75-93.

Tüysüz, O. & Dellaloğlu, A.A. 1992. Çankırı havzasının tektonik birlikleri ve havzanın tektonik evrimi, Türkiye. *Petroleum Kongresi Bildirileri*, **9**, 333-349.

Tüysüz, O., Dellaloğlu, A.A. & Terzioğlu, N. 1995. A magmatic belt within the Neo-Tethyan suture zone and its role in the tectonic evolution of northern Turkey. *Tectonophysics*, **243**, 173-191.

Tüysüz, O., Yigitbaş, E. & Serdar, H.S. 1988. Vezirköprü-Boyabat dolayının jeolojisi, *TPAO Raporu*, **55**.

Tüysüz, O., Yiğitbaş, E. & Serdar, H.S. 1989. Orta Pontidlerin güney kesiminin jeolojisi. Turkish Petroleum Company, Internal Report 2596, 291.

Ünalın, G., Yüksel, V., Tekeli, T., Gönenç, O., Seyirt, Z. & Hüseyin, S. 1976. Haymana-Polath yöresinin (GB Ankara) Üst Kretase-Alt Tersiyer stratigrafisi ve paleocoğrafik evrimi. *Geological Society of Turkey Bulletin*, **19** (2), 159-176.

Underwood, M., Ballance, P. & Clift, P. 1995. Sedimentation in forearc basins, trenches, and collision zones of the western Pacific: A summary of results from the Ocean Drilling Program. In: Taylor, B. & Natland, J. Eds. *Active Margins and Marginal Basins of the Western Pacific*. American Geophysical Union Monograph **88**, 315-54.

- Ustaömer, T. 1993. Pre-Late Jurassic tectonic-sedimentary evolution of North Tethys: Central Pontides, N Turkey. PhD thesis (*unpublished*), University of Edinburgh.
- Ustaömer, T. & Robertson, A.H.F. 1994. Late Palaeozoic marginal basin and subduction–accretion: evidence from the Palaeotethyan Küre Complex, Central Pontides, N. Turkey. *Journal of the Geological Society of London*, **151**, 291–305.
- Ustaömer, T., Robertson, A.H.F., 1997. Tectonic-sedimentary evolution of the north Tethyan margin in the Central Pontides of northern Turkey. In: Robinson, A.G. (Ed.), *Regional and Petroleum Geology of the Black Sea and Surrounding Region*. Memoir-American Association of Petroleum Geologists, **68**, 255-290.
- Ustaömer, T. & Robertson, A.H.F. 1999, Geochemical evidence use to test alternative plate tectonic models for pre-Upper Jurassic (Palaeotethyan) units in the Central Pontides, N. Turkey. *Geological Journal*, **34**, 25-54.
- Uyeda, S. 1982. Subduction zones: an introduction to comparative subductology. *Tectonophysics*, **81**, 133-159.
- Uyeda, S. & Kanamori, H 1979. Back-arc opening and the mode of subduction. *Journal of Geophysical Research*, **84**, 1049-1061.
- Vine, F.J. & Matthews, D.H. 1963. Magnetic anomalies over oceanic ridges. *Nature*, **189**, 947-949.
- Vogt, J.H.L. 1921. The physical chemistry of the crystallization and magmatic differentiation of igneous rocks. *Journal of Geology*, **29**: 318-350; 426-443; 515-539; 627-649.
- Von Huene, R. 1986. To accrete or not to accrete, that is the question. *Geologische Rundschau*, **75**, 1-15.

Weaver, S.D., Saunders, A.D., Pankhurst, R.J. & Tarney, J. 1979. A geochemical study of magmatism associated with the initial stages of back-arc spreading. The Quaternary volcanics of Bransfield Strait, from South Shetland Islands. *Contributions to Mineralogy and Petrology*, **68**, 151-169.

Whitney, D.L. & Hamilton, M. 2004. Timing of high-grade metamorphism in central Turkey and the assembly of Anatolia. *Journal of the Geological Society of London*, **161** (5), 823-828.

Wicks, F.J. & O'Hanley, D.S. 1988. Serpentine minerals: structures and petrology. In: Bailey, S. W. (ed.) *Hydrous Phyllosilicates (exclusive of micas)*. *Mineralogical Society of America, Reviews in Mineralogy*, **19**,

Wilson, R.A.M. 1959. The geology of the Xeros-Troodos area: Cyprus. *Memoir-Geological Survey Department 1*, 1-136.

Winchester, J.A. & Floyd, P.A. 1977. Geochemical discrimination of different magma series and their differentiation products using immobile elements. *Chemical Geology*, **20**, 325-343.

Woodcock, H.H., Robertson, A.H.F. 1982. Wrench and thrust tectonics along a Mesozoic–Cenozoic continental margin: Antalya Complex, SW Turkey. *Journal of the Geological Society of London*, **139**, 147–163.

Woodcock, H.H., Robertson, A.H.F. 1985. The structural variety in Tethyan ophiolite terranes. In: Gass, I.G., Lippard, S.J. & Shelton, A.W. (Eds.), *Ophiolites and Oceanic Lithosphere*, Special Publication Geological Society of London, **13**, pp.321– 332.

Yalcin & Bozkaya 2004. Ultramafic-rock-hosted vein sepiolite occurrences in the Ankara ophiolitic melange, central Anatolia, Turkey. *Clays and clay minerals*. **52** (2), 227.

Yalınz, M.K., Floyd, P.A., Göncüođlu, M.C. 1996. Supra-subduction zone ophiolites of Central Anatolia: geochemical evidence from the Sarikaraman Ophiolite, Aksaray, Turkey. *Mineralogical Magazine*, **60**, 697–710.

Yazgan, E. & Chessex, R. 1991. Geology and tectonic evolution of Southeastern Taurides in the region of Malatya. Turkish Association of Petroleum Geologists Bulletin, **3**, 1-42.

Yiđitbař, E., Tüysüz, O. & Serdar, H.S. 1990. Orta Pontidlere Üst Kretase yařlı aktif kıta kenarının jeolojik özellikleri. *Türkiye 8. Petrol Kongresi. Bildiriler*, 141-151.

Yılmaz, A. 1985. Basic geological characteristics and structural evolution of the region between the Upper Kelkit Creek and the Munzur Mountains. *Bulletin of the Geological Society of Turkey*, **28**, 79-92.

Yılmaz, Y. 1993. New evidence and model on the evolution of the southeast Anatolian orogen. *Geological Society of America Bulletin*, **105**, 251–271.

Yılmaz, Y., Tüysüz, O., Yiđitbař, E., Can Genç, ř., & řengör, A.M.C. 1997. Geology and tectonic evolution of the Pontides, In: Robinson, A.G., (Ed.), *Regional and Petroleum Geology of the Black Sea and Surrounding Region: American Association of Petroleum Geologists Memoir*, **68**, 183-226.

Yılmaz, C., řen, C. & Özgür, S. 2003. Sedimentological, palaeontological and volcanic records of the earliest volcanic activity in the Eastern Pontide Cretaceous volcanic arc (NE Turkey). *Geologica Carpathica*, **54**, (6), 377-384.

Yoldaş, R. 1982. Tosya (Kastamonu) ile Bayat (Çorum) arasındaki bölgenin jeolojisi. Ph.D. Thesis, İstanbul Üniversitesi, 311pp.

Young, D.A. 2003. N.L. Bowen, H.H. Hess, and ultramafic rocks; perspectives on ophiolites before plate tectonics. In: Dilek, Y. (Ed.) *Ophiolite concept and the evolution of geological thought*. Special Paper - Geological Society of America, **373**, 55-63.

Appendix 1: Biostratigraphy

Part 1: Preliminary determinations

Rock samples containing planktic and benthic microfossils were collected from the relevant units in the field areas for palaeontological analysis. The aim of this work was primarily biostratigraphic, i.e. to determine the ages of the relevant units. Secondly, the microfossils provide information about the environment of deposition, principally water-depth.

Rock samples were cut into thin-sections and analysed by transmitted-light petrographic microscope for fossil content. The samples were commonly strongly recrystallised with fossils too poorly preserved for accurate determination.

More than 100 photomicrographs were made of the well-preserved fossils in the slides and an attempt was made to identify each microfossil and assign a preliminary age to each sample and to each stratigraphic unit. This preliminary data is presented here with a selection of the photomicrographs.

1 Central Pontides

Kirazbaşı Mélange

(Sample) PO02 23. (Location) Sıvar (N Tosya). Limestone block.

Globotruncana sp.

PO02 26. Akkaya (N Tosya, CP). Limestone block.

Globotruncana sp.

Amphistegina sp.

Praeglobigerina sp., Upper Cretaceous



file no. 25. *Globotruncana*-type microfossil in PO02 26.

PO03 204. Kunduzlu (NE Bayat).

Field description: thin-bedded pale shaly pelagic *globotruncana?*-bearing limestone interbedded with basaltic rudistic volcanoclastic debris-flow deposits and basaltic pillow-lavas.

Globotruncana.

PO02 228. Soğanlar (N Tosya).

Field description: Pelagic limestone.

Globotruncana-type and siliceous radiolarians in carbonate matrix.

PO02 231. Soğanlar (N Tosya).

Field description: shaly limestone.

Globotruncana or *Marginotruncana*.

PO02 255. Karanlıkdere Yayla (SE Tosya).

Field description: Limestone.

Siliceous radiolarians in micrite. Some replaced by calcite.

Marginotruncana, Maastrichtian.

Borelis melo? (Miocene!), or *Pseudolituonella?*, U. Cenomanian.

PO02 262. Akkaya (N Tosya).

Field description: Pelagic limestone.

Globotruncana/Marginotruncana-type.

PO02 76. Eldivan (SW Çankırı).

Field description: Pelagic limestone.

Globotruncana

Marginotruncana.

PO02 85. Eldivan (SW Çankırı).

Field description: Limestone.

Eoruperita? Eocene.

Morozovella, Eocene.

Praeglobotruncana? *Rotalipora?* *Cenomania*.

PO02 86. Eldivan (SW Çankırı).

Field description: Limestone and replacement chert.

Praeglobotruncana? *Cenomanian*.

Morozovella aequa, Uppermost Palaeocene-Lowermost Eocene.

PO02 66. Korgun (N Çankırı).

Field description: limestone.

Planomalina buxordi? U. Albian. *Tincinella?* Albian. *Conicospirillina?* *Berriasian*.

Eoruperita? U. Eocene.

Morozovella, Palaeocene-Eocene.

Globotruncana.

PO02 68. Yapraklı (NE Çankırı).

Field description: Limestone.

Amphistegina?

PO02 23. Sıvar (N Tosya).

Field description: Pelagic limestone.

Globotruncana-type.

PO02 26. Akkaya (N Tosya).

Field description: Limestone.

Globotruncana-type.

PO02 36. Saraycık (NE Kargı, CP).

Field description: shale and mudstone.

Globotruncana.

İkiçam Formation

PO03 218. Yukarıberçin (N Tosya).

Field description: volcanoclastic turbiditic sandstone with coarse feldspathic interbeds,

Petrographic description: poorly-sorted angular calcareous quartzofeldspathic sandstone/greywacke.

Angular small non-diagnostic planktonic forams.

Globotruncana-type. Santonian-Maastrichtian, Basin facies.

Globotruncana, ? Santonian-Maastrichtian, Basin facies.

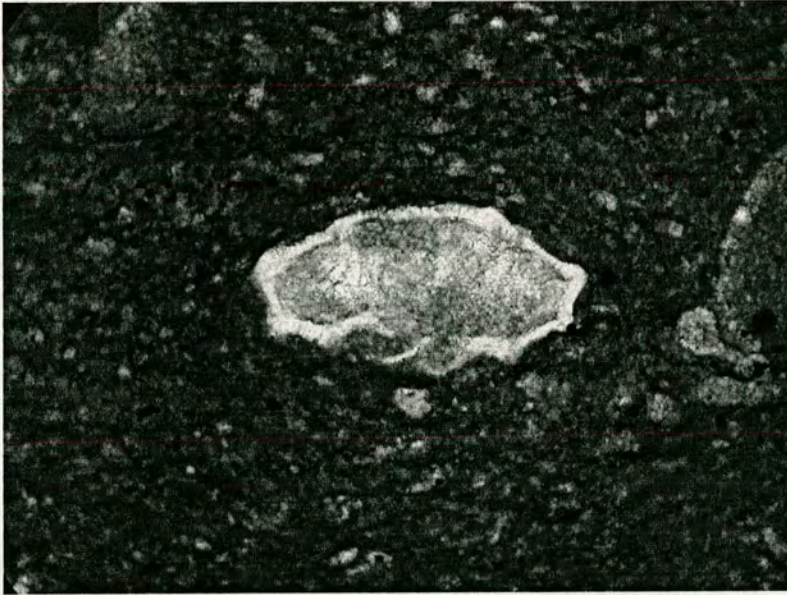
PO03 211. Yukarıberçin (NW Tosya).

Field description: Hard fine shaly volcanoclastic limestone, slaty cleavage. Interbeds of dark volcanoclastic sandstone and conglomerate. Associated with rudistic volcanoclastic debris-flow deposits.

well-preserved U. Cretaceous(?) planktonic forams of *Globotruncana*-type.

Planktonic foram (*Globotruncana*?)

Globotruncana.linneina (?) Campanian?



file no. 145

PO02 33. Aşağıkaya (SW Tosya).

Field description: Calciturbidite (with lavas).

Marginotruncana, Coniacian-Santonian?

PO02 193. Çukurban Yayla (SE Tosya).

Field description: Calcareous volcanoclastic sandstone.

Globotruncana or *Marginotruncana*? U. Turonian-Lower Coniacian.

Globotruncana or *Marginotruncana*? U. Turonian-Lower Coniacian.

PO02 197. Ekincik (N Tosya).

Field description: shale.

Globotruncana.

Marginotruncana, U. Turonian-Lower Coniacian.

Heterohelicidae, Mid-Upper Maastrichtian.

PO02 198. Ekincik (N Tosya).

Field description: shale.

Heterohelicidae & *Marginotruncana*?

Glootruncanidae, Maastrichtian.

PO02 218. Ilıslık (SW Tosya).

Field description: silty pelagic limestone.

Petrographic description: coarse fragmenary bioclasts in micrite matrix.

Heterohelicidae, Globotruncana, Milliolidae, Amphistegina, algae.

PO02 72. Ilıslık (SW Tosya).

Stratigraphic unit: Köşdağ sediments Unit.

Field description: Limestone.

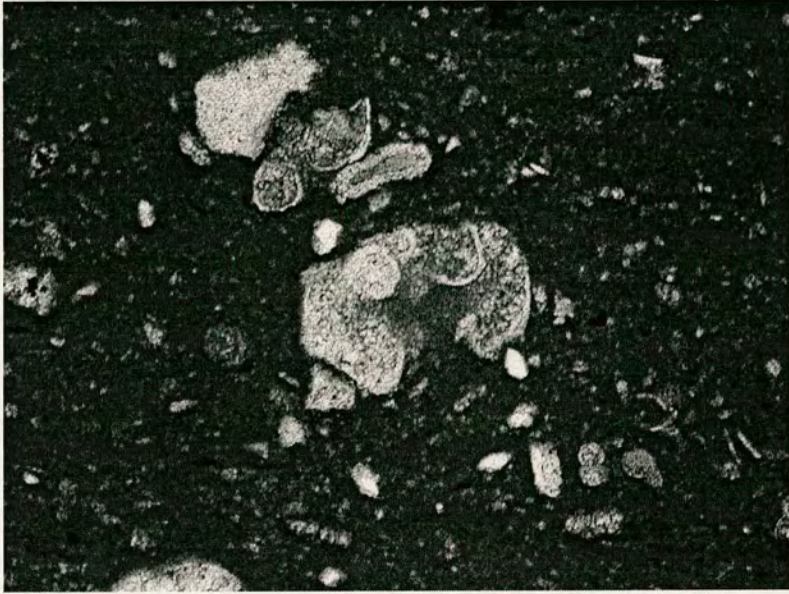
Marginotruncana?

PO02 51. Ekincik (N Tosya).

Field description: Mudstone.

Heterohelicidae.

Globotruncana gansseri and another, Maastrichtian.



file no. 30. *Gansserina gansseri* (BOLLI) in PO02 51.

Yaylaçayı Formation

PO02 10. Seki (N Iskilip).

Field description: Limestone.

Globo truncana.



file no. 20. *Globo truncana* sp. in PO02 12

PO02 12. Seki (N Iskilip).

Field description: Red limestone.

Globo truncana.

Marginotruncana.

Whiteinella.



file no. 21. *Globotruncana* in PO02 12.

PO02 129. Seki (N Iskilip).

Field description: Pelagic limestone.

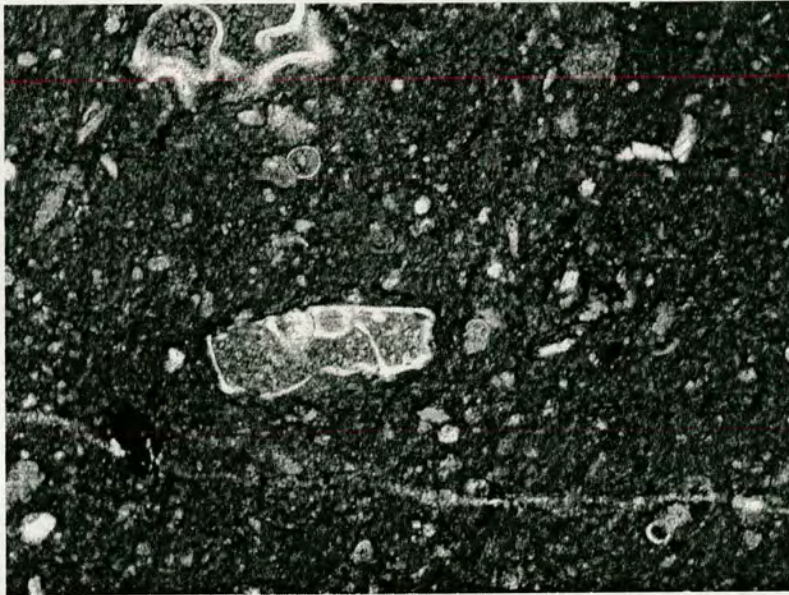
Globotruncana.

PO02 143. Iskilip

Field description: Limestone.

Globotruncana stuarti, Maastrichtian.

Marginotruncana.



file no. 47. *Globotruncana stuarti* (LAPPARENTI) in PO03 143.

PO02 145. Iskilip

Field description: Limestone.

Praeglobotruncana? Cenomanian.

Marginotruncana, Coniacian-Santonian.

Marginotruncana, Coniacian-Santonian.



file no. 28. Recrystallised *Globotruncana*-type microfossils in PO02 45.

PO02 45. Hacibrahim (E Tosya).

Field description: shale.

Recrystallised *Globotruncana*-type.

Yapraklı Formation

PO02 173. Yapraklı (NE Çankırı).

Field description: Limestone.

Globotruncana.

Kadıkızı Formation

PO02 226. Kadıkızı (N Tosya,).

Field description: numulitic limestone.

Nummulites, Eocene.

Discocyclina, Mid, Eocene.

PO02 227. Kadıkızı (N Tosya).

Field description: Numulitic limestone.

Nummulites, *Discocyclina*, *Milliolidae* and *Heterohelicidae*.

2 Eastern Pontides

Aykayası Formation

PO03 69. Muratboynu (S Erzincan).

Field description: calcirudite (matrix).

Petrographic description: coarse peloidal/oncoidal calcarenite packstone with angular lithiclasts of radiolarian chert and deformed radiolarian micritic limestone.

Benthic Miliolina and large forams.

Debarina hahounerensis, Lower Aptian, or *Ovalveolina reicheli*, U. Aptian.

Pseudolituonella reicheli? Upper Cenomanian.

PO03 68. Muratboynu (S Erzincan).

Field description: massive pelagic limestone with *Globo truncana*.

Petrographic description: fine micrite with rare bioclasts.

?Jurassic *Positova*, benthic Miliolinid (shallow water facies).

Globo truncana.

Karayaprak Mélange

PO03 90. Çerpaçın Yayla, (W Erzincan).

Field description: Pink pelagic limestone associated with lavas.

Petrographic description: sheared fossiliferous micritic limestone.

dateable planktic forams.

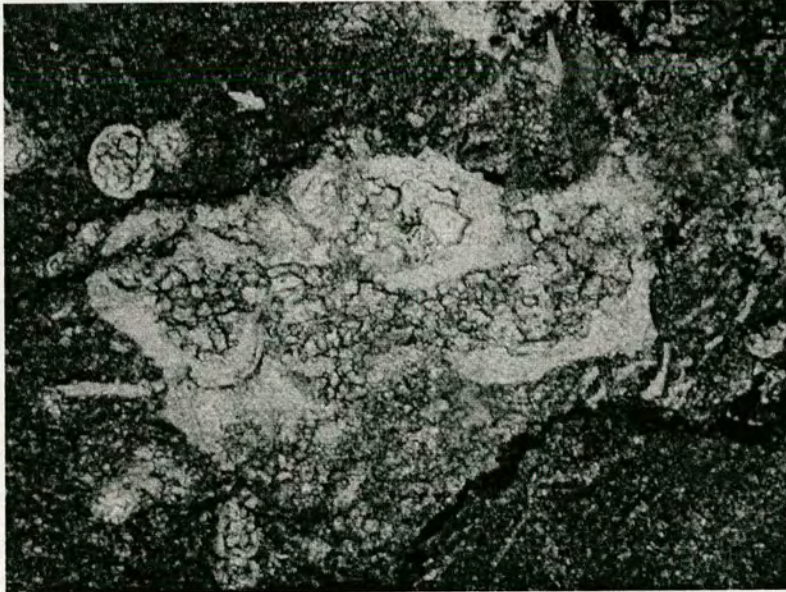
Globo truncanidae, Maastrichtian, Basin facies.

Heterohelicidae, Maastrichtian, Basin.

Morozovella Subbotinae, Lower Eocene, Basin facies.

Globo truncana, Maastrichtian.

Globo truncanidae?, Turonian?



file no. 91. *Globo truncana linneiana* in PO03 90

PO03 38. Ballı (W Erzincan).

Field description: pink pelagic limestone.

Petrographic description: fine-grained deformed micritic bioclastic marble.

Marginotruncana?

Globigerinelloides, Albian-Maastrichtian.

Karadağ Formation (Late Cretaceous

PO03 115 Bilkoç (S Erzincan).

or Köşdağ/Yaylaçayı arc Unit.

Field description: Pink calcareous schist and pelitic schist associated with arc volcanics.

?palaeocene planktonic Globigerinids.

Tincinella or *Planomalina*, Albian, Basin facies.

Globigerinid, Upper Albian.

Sakesaria, Upper Palaeocene.

Sütpınar Formation

PO03 30. Çevizli (W Erzincan).

Field description: fossiliferous calciturbidites.

Petrographic description: wackestone.

Pithonella Ovalis, Coniacian.

Globotruncana. (maastrichtian?).



file no. 70. *Globotruncana stuarti* (DE LAPPARENT) in PO03 30.

PO03 116. Bilkoç (S Erzincan).

Field description: Nummulitic Limestone unconformable on Late Cretaceous calcareous schist (115).

Upper Palaeocene-Lower Eocene planktonic forams

Nummulites (& *amphistegina*), Mid Eocene.

Morozovella (?*velascoensis*), Upper Palaeocene.

Assilina, Lower Eocene.

Eoruperita, U. Eocene.

Assilina?/*Amphistegina*?

Amphistegina?

Alveolina, Mid Eocene.



file no. 105. *Amphistegina* sp. in PO03 116.

PO03 117. Gıyabey Yurdu (S Erzincan).

Field description: Coarse algal bioclastic limestone with benthic forams u/c on mélange. Same lithology as PO03 135.

rhodoliths, pecten, bryozoan bioclasts.

Lepidocyclina, Upper Oligocene? Upper slope/shelf edge facies.

PO03 121. Gıyabey Yurdu (S Erzincan).

Field description: Nummulitic calcarenite with siliceous clasts.

Nummulites, Mid Eocene.

Morozovella?

Euoperita, Upper Eocene.



file no. 119. *Nummulitidae euoperita* in PO03 121.

PO03 138. Ahır (W Erzincan).

Field description: Shaly limestone.

Petrographic description: very fine pelagic limestone.

Rotalipora.

PO03 139b. Ahır (W Erzincan).

Lower Tertiary Globigerinids.

PO03 139c. Ahır (W Erzincan).

Field description: very fine pelagic limestone.

Globigerinidae. Lower Tertiary

PO03 153. Gökkaya (SW Erzincan).

Field description: Pelagic limestone with turbiditic sandstone interbeds.

Reworked large (shallow-facies) forams and pelagic forams, U. Palaeocene-Lower Eocene.

Planorotalites, U. Palaeocene.

Mozorovella spinulosa?, Mid Eocene.

valvulininae, Eocene.

Eoruperita?/*melobesia*? U. Eocene



file no. 123: *Mozorovella aragonensis* (NUTALL) in PO03 153



file no, 122. Globigerinidae in PO03 153

PO03 155. Gökkaya (SW Erzincan).

Field description: Pelagic limestone with shale/siltstone and thin turbiditic sandstone interbeds.

U. Palaeocene-Lower Eocene Planktonic deep-water *Globotruncana*.

Planktic Morozovella, *Globigerinathika* or *Planorotalites*? U. Palaeocene.

Melobesiae, U. Eocene?

PO03 156. Gökkaya (SW Erzincan).

Field description: Nummulitic limestone.

Well preserved diagnostic Eocene forams.

Euoperita or *Operculina*? U. Eocene?

Praerhapydionina (Lower Palaeocene)? Or *Operculina* (Eocene)?

Amphistegina, Eocene-Oligocene.



file no. 130: *Amphistegina* in PO03 156

PO03 175. Gökkaya (SW Erzincan)

Field description: Fine pelagic limestone with thin interbeds of dark volcanoclastic shale, shaly limestone and turbiditic quartzofeldspathic calcarenite.

Petrographic description: sheared, rediposited pelagic sediment.

Palaeocene-Eocene(?) planktonic forams.

Globotruncana.

PO03 57. Gıyabey Yurdu (S Erzincan).

Field description: coarse bioclastic wackestone with bivalve fragments, forams (nummulites-type and *globotruncana*).

Petrographic description: fossiliferous touchstone, micritic matrix.

Benthic & planktic Forams, detrital fragments, milliolinids.

Amphistegina.

Glomalveolina. Primaeva. Palaeocene.

Morozovella, Palaeocene-Eocene.

PO03 99. Çerpaçin Yayla, (W Erzincan).

Petrographic description: fossiliferous micritic lst.

Large benthic forams, non-age determinative miliolinids indicate open shelf facies.

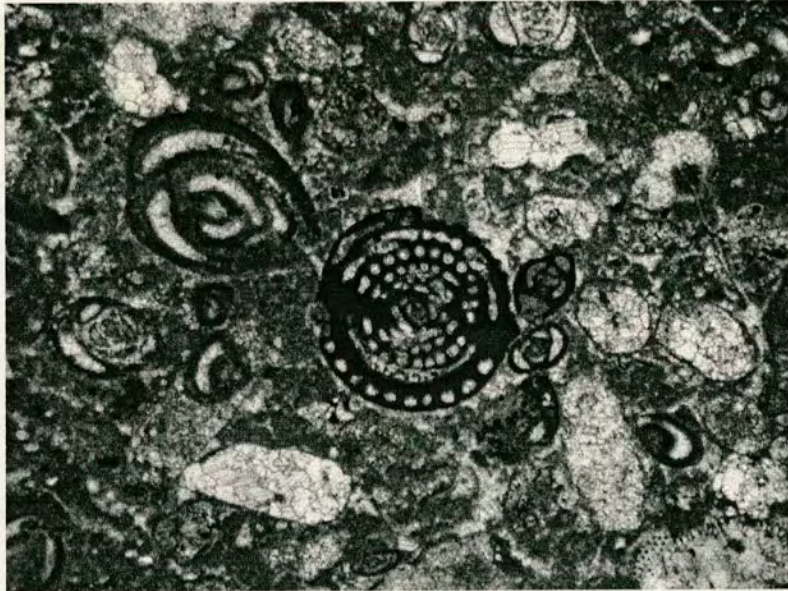
Dateable planktonic forams.

Borelis melo, Mid Miocene, or *Alveolina*, Palaeocene.

Coskinolina, Palaeocene-Early Eocene, Inner shelf facies.

Planorotalites?

Heterohelix, Maastrichtian.



file no. 96. *Boris melo* in PO03 99

PO03 86 Bahçeli (W Erzincan).

Field description: pelagic globotruncana-bearing limestone.

Petrographic description: micrite.

Lower cretaceous Calpionellids, radiolarians.

Stomiospaera sphaerica or *Calcisphaerula innominata*, Lower Turonian.

Pithonella ovalis, Coniacian.

Sipikör Formation

PO01 79. Muratboynu (SW Erzincan).

Field description: Pseudoconglomeratic nodular limestone.

Nummulitic

Euoperita U. Eocene.

PO01 81. Muratboynu (SW Erzincan).

Field description: fossiliferous mudstone.

Amphistegina, miliolidae, dendritina (mid-miocene), algae, coral, bryozoa.

Miliolidae (Aptian-Oligocene)

Lower-Mid Eocene form? Inner shallow platform facies.

Valvulininae (cf. *Discorinopsis*), Eocene, Inner shallow platform facies.

Dendritina, Mid-Upper Eocene, Inner shallow platform facies.

Alveolina, Mid Eocene, Inner shallow platform facies.



file no. 7. *Alveolina* in PO01 81.

PO01 152a. Muratboynu (SW Erzincan).

Field description: Pseudoconglomeratic nodular limestone unconformable on melange.

Petrographic description: bioclastic wackestone.

benthic forams, palaeocene-Eocene shallow-water facies.

Ranikothalia, Miscellanea or *Saudia Labyrinthica* GRIMSDALE, Upper Palaeocene, Upper slope/shelf edge facies.

Globotruncana, Campanian-Maastrichtian, Slope/basin facies.

Globotruncana and *Ranikothalia*, Campanian, Basinal facies.

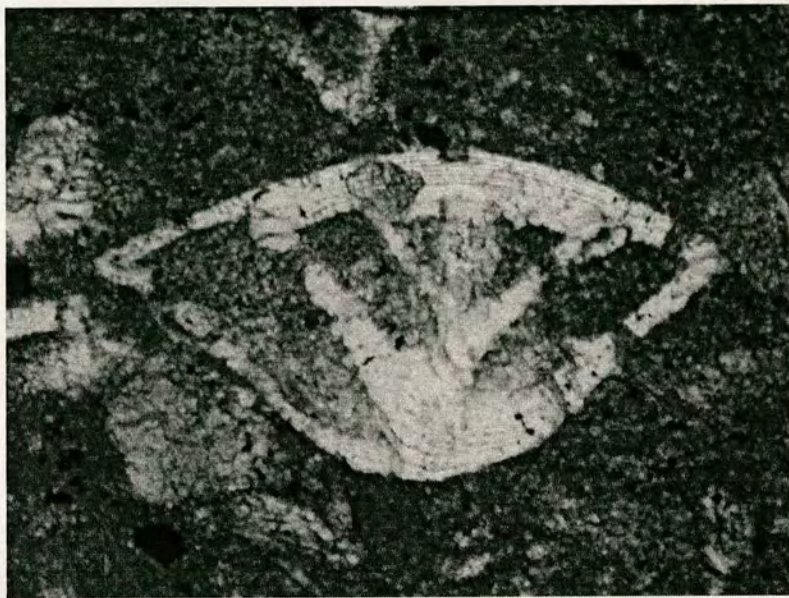
Nummulites? Or *Alveolina*, Lower Eocene-Mid Eocene, Slope facies.

Amphistegina, *Discoyclina*, *lithothanium* or *Lithophyllum?* Eocene, Slope facies.

Morozovella spinulosa, Mid Eocene, Basin/slope facies.



file no. 10. *Globotruncana* in PO01 152a.



file no. 12. *Amphistegina* in PO01 152a.

PO01 152b. Muratboynu (SW Erzincan).

Field description: Pseudoconglomeratic nodular limestone unconformable on melange.

Petrographic description: bioclastic wackestone.

benthic forams, palaeocene-Eocene shallow-water facies.

Turborotalia, Upper Eocene, OR *Planorotalites* or *Morozovella*? Mid Palaeocene, Planktonic.

Spiroclypeus or *Pellatispira*? And *Zezzazata*. Upper Eocene.

Millioliidae, Aptian-Oligocene.

Amphistegina, Mid Eocene-Pleistocene.

Globigerinacea, *Globorotalidae* or *Palorotalites pusilla pusilla*, Mid Eocene, Planktonic.



file no. 17. *Amphistegina* in PO01 152b.



file no. 14. ?*Turborotalia* in PO01 152b.

PO03 135. Baltaşı (W Erzincan).

Field description: Coarse algal bioclastic limestone with benthic forams. Same lithology as PO03 117)

algae. Indicates shallow water.

Globigerinidae.

PO03 53. Gıyabey Yurdu (S Erzincan).

Field description: *Nummulitic* calcarenite.

Petrographic description: coarse bioclastic touchstone, micritic matrix.

Fallotella? Palaeocene.

Pithonella? coniacian.



file no. 74. *Pitholella ovalis* in PO03 53.

PO03 56. Gıyabey Yurdu (S Erzincan).

Field description: bioclastic calcarenite.

Petrographic description: coarse bioclastic wackestone, micritic matrix.

Eoruperita, U. Eocene.

Nummulite. Eocene.

PO03 59. Göltepe (S Erzincan).

Field description: foraminiferal massive calcarenite w. nummulites and globotruncana?

Petrographic description: wackestone.

algae, pelagic and benthic forams, ?Miocene.

Heterohelicidae? Maastrichtian.

Pithonella ovalis, Albian-Santonian

Large benthic foram.

Coskinolina? Palaeocene?

PO03 61. Göltepe (S Erzincan).

Field description: limestone (soft grey micrite).

Petrographic description: micritic limestone.

Globotruncana type.

1 *Pithonella ovalis*, Albian-Cenomanian?

2 *globotruncana*?

PO03 61. Göltepe (S Erzincan).

Field description: limestone (soft grey micrite).

Petrographic description: micritic limestone.

Globotruncana type.

1 *Pithonella ovalis*, Albian-Cenomanian?

2 *Globotruncana*?

PO03 62. Göltepe (S Erzincan).

Field description: Eocene nummulitic calcarenite.

Petrographic description: fractured/sheared recrystallised wackestone.

Miliolinids & algae.

PO03 187. Kömür (N Erzincan).

Field description: grey volcanoclastic sandstone with foraminifer.

Petrographic description: Volcanoclastic sandstone.

small planktonic forams in matrix. Large Palaeocene-Eocene forams.

Favusella Washitensis (in clast), Lower Cenomanian.

Victoriella? (matrix) U. Eocene.

Nummulites, Eocene.

Planktonic, Eocene?

clast of chert.

clast of chert.

Turborotalia cerroazulensis cocoaensis? Upper Eocene.

Appendix 1: Biostratigraphy

Part 2: Determinations from Drs. K Tasli and N. Inan (Mersin University, Turkey).

1 Central Pontides

Kirazbaşı Mélange (Albian-U maastrichtian)

PO02 68 (Yapraklı) Upper Maastrichtian

Pseudosiderolites vidali (DOUVILLE), oblique section, Upper Maastrichtian.

Fig.1H.

Bryozoa, algae

PO02 85 (Eldivan) Albian-Cenomanian

Rotalipora sp., subaxial section, Albo-cenomanian. Fig. 1 C.

PO02 86 (Eldivan) Albian

Ticinella sp., axial section, Albian, Fig 1 D.

İkiçam Formation (U Cret (Campanian-Maastrichtian))

PO02 51 (Ekincik) Maastrichtian

Globotruncana linneiana (D'ORBIGNY)

Gansserina gansseri (Bolli),

Contusotruncana fornicata (PLUMMER)

Operculina complanata (DEFRANCE) LUTETIAN, Fig. 2 C.

Orbitoclypeus sp., Lutetian, Fig. 2 F.

Planomaliniidae

Heterohelicidae

PO02 72 (Ilısk)

Radiolaria, no marker fossil

PO02 197 (Ekincik) Campanian-Maastrichtian (Mersin)

Globotruncana linneiana (D'ORBIGNY)

Planomaliniidae

Heteroheliciidae

PO03 211 (Yukarıberçin) Campanian-Maastrichtian

Globotruncana arca (CUSHMAN)

Planomaliniidae

Heteroheliciidae

Yaylaçayı Formation (Campanian-Maastrichtian)

PO02 111 (İskilip) Campanian-Maastrichtian

Globotruncana arca (CUSHMAN)

Globotruncana linneiana (D'ORBIGNY)

Pseudotextularia sp.

Planomaliniidae

PO02 118 (İskilip) Campanian-Maastrichtian

Globotruncana linneiana (D'ORBIGNY)

Pseudotextularia sp.

Archaeoglobigerina sp.

Planomaliniidae

PO02 143 (İskilip) Campanian-Maastrichtian

Globotruncana arca (CUSHMAN)

Globotruncana linneiana (D'ORBIGNY)

Globotruncana bulloides VOGLER

PO02 197 (Ekincik) Campanian-Maastrichtian

Globotruncana linneiana (D'ORBIGNY)

Planomaliniidae

Heteroheliciidae

Yapraklı Formation (U Cretaceous)

PO02 166 (Yapraklı) Upper Cretaceous

Archaeoglobigerina sp.

Pithonella ovalis (KAUFMANN)

Rotaliidae

Kadıkızı Formation (U Eocene)

PO02 226 (Delibey) U Eocene (Priabonian)

Nummulites incrassatus DE LA HARPE

Nummulites striatus BRUGUIERE)

Discocyclina seunesi DOUVILLE

Operculina sp.

Assilina sp.

Miliolidae

2 Eastern Pontides

(Ayıkayası Formation?) (Late Cretaceous?)

PO03 69 (Muratboynu, Ayıkayası Formation) Cretaceous

Fossils are reworked

Charentia? sp. (Cretaceous)

Siphovalvulina sp. (Jurassic-Cretaceous)

Rotaliidae

Dasycladacean and Codiacean algae

Echinoderm debris Fossils are reworked

PO03 86 (Bahçeli) Berriasian (pelagic limestone block age)

Calpionella alpina LORENZ

Calpionella elliptica CADISH Fig. A, B.

Radiolaria

PO03 90 (Çerpaçindere Yayla pink pelagic limestone) Campanian-Maastrichtian

Globotruncana linneiana (D'ORBIGNY)

Archaeoglobigerina sp.

Heterohelicidae

Planomaliniidae

Karayaprak Mélange (Late Cretaceous)

PO03 68 (Muratboynu) Lower Cretaceous? platform limestone.

Vercorsella? sp.

Miliolidae (*Pyrgo* and *Quinqueloculina*)

Ostracoda

Gastropoda

PO03 38 (Ballı) Campanian-Maastrichtian pink pelagic limestone block in melange

Globotruncana linneiana (D'ORBIGNY)

Planomaliniidae

Heterohelicidae

Karadağ Formation (Late Cretaceous (?L Turonian-Maastrichtian)(Campanian-Maastrichtian)

PO03 115 (Binkoç) Lower Eocene?

Eponides sp.

Morozovella sp.

Globigerina sp.

Pelecypoda fragments

Echinoderm debris

Sütpınar Formation (Upper Cretaceous-Lower Eocene/?mid Eocene)

PO03 138 (Ahr) Maastrichtian

Globotruncanita stuarti (DE LAPPARENT)

Globotruncana arca (CUSHMAN)

Contusotruncana contusa (CUSHMAN)

P003 139B (Ahr) Lower-Middle Palaeocene

Planorotalites compressa (PLUMMER)

"*Subbotina*" *pseudobulloides* (PLUMMER)

Globigerinidae

PO03 153 (Gökkaya, mid) Lower Eocene

Discocyclina sp.

Nummulites sp.

Rotalia sp.

Planktic foram.: *Morozovella* gr. *subbotinae* (MOROZOVA)

Morozovella gracilis (BOLLI)

Globigerina sp.

Bryozoa

Echinoderm debris

Ostracoda

PO03 175 (Gökkaya, mid-upper) Upper Cretaceous

Globotruncanidae

Textularia sp.

Bryozoa
Echinoderm debris
Shell fragments

Sipikör Formation

PO01 152A (Muratboynu) Lower (?) EOCENE

Sphaerogypsina globula (REUSS)

Rotalia trochidiformis LAMARCK

Idalina sinjarica GRIMSDALE

Ophthalmidium sp.

Eponides sp.

Nummulites sp.

Bryozoa

Gastropoda

Echinoderm debris

Ostracoda

Coral

Dasycladacean alga

PO01 79 (Muratboynu) Lower (?) Eocene

Gyrodinella magna (LE CALVEZ) lower Eocene, Fig. 2 B.

Ophthalmidium sp.

Eponides sp.

Orbitolites sp.

Triloculina sp.

Nummulites sp.

Orbitolites sp.

Sphaerogypsina sp.

Bryozoa

Gastropoda

Echinoderm debris

Ostracoda

Coral

PO01 81 (Muratboynu) Lower (?) Eocene

Sphaerogypsina globula (REUSS) Fig. 2 D.

Sphaerogypsina carteri SILVESTRI

Asterigerina rotula KAUFMANN Fig. 2 E.

Alveolina ellipsoidalis SCHWAGER

Operculina sp.

Nummulites sp.

Triloculina sp.

Orbitolites sp.

Morozovella sp.

Bryozoa

Gastropoda

Echinoderm debris

Ostracoda

Coral

Dasycladacean alga

PO03 116 (Binkoç) Lower (?) Eocene

Sphaerogypsina globula (REUSS)

Sphaerogypsina carteri SILVESTRI

Lockhartia haimei DAVIES

Nummulites millecaput BOUBEE

Nummulites striatus (BRUGUIERE)

Alveolina pasticillata SCHWAGER

Alveolina ellipsoidalis SCHWAGER

Assilina sp.

Eponides sp.

Coralline alga

Echinoderm debris

PO03 156 (Gökkaya) Upper Palaeocene (Thanetian)

Idalina sinjarica GRIMSDALE

Ophthalmidium sp.

Quinqueloculina sp.

Triloculina sp.

Textularia sp.

Rotalia sp.

Dasycladacean alga

Ist:

Nummulitidae Eocene Fig. 128.

Milliolidae, Fig, 129.

Amphistegina, Eocene-Oligocene, Fig. 130.

PO03 62 (Göltepe) Upper Palaeocene (Thanetian)

Idalina sinjarica GRIMSDALE

Alveolina sp.

Coral: *Litharaeopsis subbepithecata* (OPPENHEIM)

Echinoderm debris

Coralline alga

PO03 135 (Baltaş) no marker fossil (?) Cretaceous-Tertiary

Bryozoa

Echinoderm debris

Coralline algae,

PO03 99 (Çerpaçın Yayla) U Palaeocene (Thanetian)

Idalina sinjarica GRIMSDALE Fig. 1 J.

Coskinolina (Coskinon) rajkae HOTTINGER and DROBNE Fig 1. I.

Ophthalmidium sp.

Spirolina sp.

Alveolina (Glomalveolina) sp. Fig. 1 J.

PO03 156 (Gökkaya) Upper Palaeocene (Thanetian)

Idalina sinjarica GRIMSDALE

Ophthalmidium sp.

Quinqueloculina sp.

Triloculina sp.

Textularia sp.

Rotalia sp.

Dasycladacean alga

PO03 187 (Kömür) Eocene

Nummulites cf. striatus (BRUGURIERE)

Discocyclina sp.

Operculina sp.

(Reworked clasts of radiolarite and wackestone with globigerinids)

PO03 30 (Çevizli) Campanian-Maastrichtian

Contusotruncana fornicata (PLUMMER)

Globotruncanita stuarti (DE LAPPARENT)

Globotruncana bulloides VOGLER

Globotruncana linneiana (D'ORBIGNY)

Planomaliniidae

Echinoderm debris

Shell fragments

Kemah Formation (Oligocene-Mid Miocene)

PO03 59 (Göltepe) Lower Miocene

Miogypsina mediterranea BRÖNNIMANN

Gypsina sp.

Textularia sp.

Coral
Echinoderm debris
Coralline alga

PO03 53 (Giyabey Yurdu) Lower Miocene
Miogypsina mediterranea BRÖNNIMANN
Miogypsina cf. irregularis (MICHELOTTI) Fig. 2 H.
Textularia sp.
Coralline alga: *Amphiroa cf. propria* (LEMOINE)
Echinoderm debris
Bryozoa

PO03 51 (Giyabey Yurdu) Maastrichtian
Globotruncana linneiana (D'ORBIGNY)
Gansserina gansseri (BOLLI) Fig. 1 G.
Contusotruncana fornicata (PLUMMER) Fig. 1 F.
Planomalinidae
Heterohelicidae

PO03 56 (Giyabey Yurdu) Lower Miocene
Miogypsina cf. irregularis (MICHELOTTI)
Gypsina sp.
Bryozoa
Echinoderm debris
Coralline algae:
Archaeolithothamnium johnsoni MASTRORILLI
Ethelia alba PFENDER

PO03 57 (Giyabey Yurdu) Lower Miocene
Borelis melo (REICHEL) Lwr Miocene, Fig. 2 I.
Amphistegina cf. lessoni (D'ORBIGNY)
Miogypsina irregularis (MICHELOTTI)

Miogypsina mediterranea BRÖNNIMANN Lwr. Miocene, Fig. 2 J.

Asterigerina rotula (KAUFMANN)

Miogypsinoidea cf. dehaartii (VANDER VLERK)

Gypsina sp.

Quinqueloculina sp.

Peneroplis sp.

Dentritina sp. Lwr. Miocene, Fig. 2 K.

Gastropoda

Coralline alga

PO03 117 (Giyabey Yurdu) Lower Miocene

Miogypsina cf. irregularis (MICHELOTTI)

Miogypsina mediterranea BRÖNNIMANN

Miogypsina cf. antillae (CUSHMAN)

Miogypsinoidea cf. dehaartii (VANDER VLERK)

Operculina cf. complanata (DEFRANCE)

Lepidocyclina sp.

Elphidium sp.

Miliolidae

Algae:

Amphiroa cf. piopria (LEMOINE)

Archaeolithothamnium johnsoni MASTROLI

Appendix 1: Biostratigraphy

Part 3: Determinations by Prof. Izver Onen (Istanbul University).

PO01 81. Muratboynu (SW Erzincan).

Amphistegina, miliolidae, dendritina (mid-miocene), algae, coral, bryozoa.

Miliolidae (Aptian-Oligocene), *Triloculina* sp.

Valvulininae (cf. Discorinopsis), Eocene, Inner shallow platform facies.

Alveolina, Mid Eocene, Inner shallow platform facies.

PO01 152a. Muratboynu (SW Erzincan).

Ranikothalia, *Miscellanea* or *Saudia Labyrinthica* (GRIMSDALE), Upper Palaeocene, Upper slope/shelf edge facies.

Globotruncana cf. ventricosa (WHITE) Campanian-Maastrichtian, Slope/basin facies.

Globotruncana and *Ranikothalia*, Campanian, Basinal facies.

Nummulites Or *Alveolina*, *Morozovella aragonensis*, Lower Eocene-Mid Eocene, Slope facies.

Amphistegina, *Discocyclus*, *lithothanum* or *lithophyllum*? Eocene, Slope facies.

Morozovella spinulosa, *Pseudohastigerina* sp., Mid Eocene, Basin/slope facies.

PO01 152b. Muratboynu (SW Erzincan).

4 (fig.17) Amphistegina, Mid Eocene

Morozovella aragonensis (Nuttall)

Morozovella formosa formoso (Bolli)

Nummulites sp.

Operculina sp.

Peneroplis sp.

Lenticulina sp.

Soritidae

Ostracoda

PO02 10. Seki (N Iskilip, CP).

Stratigraphic unit: Yaylaçayı Formation.

Field description: Limestone.

Petrographic description:

Fossil content:

Globotruncana sp.

Globotruncana sp.

PO02 12. Seki (N Iskilip, CP).

Globotruncana.

Marginotruncana.

Whiteinella.

Abathomphalus mayaroensis (Bolli) Upper Maastrichtian

Globotruncana falsostuarti Sigal

Globotruncanidae, *Rugoglobigerina* sp.

Globotruncana linnerana (d'Orbigny)

Globotruncana sp.

Hedbergella sp.

Globotruncanita cf. stuarti (de Lapp.)

Globotruncanella sp.

Globigerinelloides sp.

Rugoglobigerina sp.

PO02 23. Sıvar (N Tosya, CP).

Globotruncana-type.

PO02 26. Akkaya (N Tosya, CP).

Globotruncana-type.

Cretaceous

Hedbergellidae

PO02 33. Aşağıkaya (SW Tosya).

Marginotruncana, Coniacian-Santonian?

Rotalidae fragments, echinoderm debris, no marker fossil

PO02 45. Hacibrahim (E Tosya).

recrystallised *Globotruncana*-type.

PO02 51. Ekincik (N Tosya).

Heterohelicidae?

Globotruncanidae, *Gl. cf. lapparenti* (BROTZEN) Santonian-Maastrichtian

Gansserina gansseri (BOLLI) and *Gl. cf. falsostuarti sigal*

PO02 66. Korgun (N Çankırı).

Tincinela or Rotalipora (Upper Cenomanian)

No marker fossil

PO02 68. Yapraklı (NE Çankırı, CP).

Amphistegina, Bryozoa, algae

PO02 72. Ilıslık (SW Tosya, CP).

Globotruncanidae, *Radiolaria* Upper Cretaceous.

PO02 76. Eldivan (SW Çankırı, CP).

Globotruncanidae

PO02 85. Eldivan (SW Çankırı, CP).

Nummulites sp. Eocene.

Morozovella sp. Palaeocene?

Globotruncana cf. falsostuarti Sigal, *Radiolaria*, Maastrichtian.

Amphistegina sp., Eocene

PO02 86. Eldivan (SW Çankırı, CP).

Rugoglobigerina

Planorbulina sp.?

PO02 129. Seki (N Iskilip, CP).

Globotruncana cf. *aegyptiaca* NAKKADY, *Rugoglobigerina* sp. (Maastrichtian).

Radiolaria

Gastropoda and Ammonoidea shell (fragments)

Cadosina sp. ?

Stomiosphaera sp. ?

Stomiosphaera cf. *wanneri* BORZA

PO02 143. Iskilip (CP).

Globotruncana stuarti, Maastrichtian, *Globotruncanita* sp., *Gl. lapparenti*,

Globotruncanita stuarti (de LAP.) BROTZEN

PO02 145. Iskilip

Globotruncana bulloides (VOGLER)

Globotruncana arca (CUSHMANN)

Globotruncana linneiana (D'ORBIGNY)

Globotruncana lapparenti (BROTZEN)

Gansserina gansseri (BOLLI)

Globotruncana sp.

Globigerinelloides sp.

Rugotruncana sp.

Heterohelix globulosa (EHRENBERG).

PO02 166

Globotruncana sp., *Gl. linneiana* (D'ORBIGNY), Santonian-Campanian

PO02 173

Globotruncanita sp.

PO02 197. Ekincik (N Tosya).

Globotruncanidae Upper Cretaceous

PO02 198. Ekincik (N Tosya).

Heterohelix globulosa (EHRENBERG)

Glootruncana bulloides (VOGLER) Campanian-Maastrichtian.

Rosita cf. fornicata (PLUMMER)

Globotruncanella sp.

Globotruncana aegyptiaca NAKKADY

Abathomphalus sp.

Heterohelix sp.

PO02 226. Kadıkızı (N Tosya, CP).

Globotruncana bulloides VOGLER, Campanian-Maastrichtian

Discocyclina, Mid, Eocene.

Discocyclina sp., *Amphistegina* sp., algae, Eocene

PO02 227. Kadıkızı (N Tosya, CP).

Nummulites sp., *Discocyclina cf. discus* (RUTIMEYERI), *Discocyclina* sp.,

Milliolidae. Mid Eocene.

PO02 228. Soğanlar (N Tosya, CP).

Discocyclina sp. *Nummulites* sp., *Assilina* sp., *Verneuillinidae* EOCENE
pelagic forams, radiolarian.

PO02 231. Soğanlar (N Tosya, CP).

Radiolaria

PO02 255. Karanlıkdere Yayla (SE Tosya, CP).

Globotruncanidae?

PO02 262. Akkaya (N Tosya, CP).

Globotruncana sp..

Radiolaria (recrystallised)

Globigerinidae

Planorotallites sp.

PO03 30. Çevizli (W Erzincan).

Pithonella Ovalis, Cretaceous.

Globotruncanita stuarti (DE LAPPARENT)

PO03 38. Ballı (W Erzincan).

Maastrichtian

Globotruncana lapparenti (BROTZEN)

priariehilensis (PESSAGNO) Maastrichtian

PO03 53. Gıyabey Yurdu (S Erzincan).

Pithonella ovalis (KAUFMANN)

Verneullinidae

Lithophyllum sp.

PO03 57. Gıyabey Yurdu (S Erzincan).

Amphistegina sp., *Lithophyllum sp.*, Eocene.

Glomalveolina? *Alveolina sp.*, *Bullalveolina sp.*, *Miogyopsina sp.* Upper Oligocene-Lower Miocene.

Milliolidae, *Cibicides sp.*

PO03 59. Göltepe (S Erzincan).

Planorbulina sp. (Palaeocene-Eocene)

Pithonella ovalis? Albian-Santonian

algae

Verneullinidae, *Planorbulinidae?* (Eocene).

PO03 61. Göltepe (S Erzincan).

Pithonella ovalis, Albian-Cenomanian

globotruncana

PO03 68. Muratboynu (S Erzincan).

Upper Cretaceous pelagic forams

PO03 69. Muratboynu (S Erzincan).

Radiolaria

PO03 86 Bahçeli (W Erzincan).

Stomiospaera sphaerica or *Calcisphaerula innominata*, Lower Turonian.

Pithonella ovalis, Cretaceous.

PO03 90. Çerpaçın Yayla, (W Erzincan).

Globotruncana cf. linneiana (D'ORBIGNY) Santonian-Maastrichtian

Globotruncana sp. Maastrichtian

Rugoglobigerina sp. (Maastrichtian)

PO03 99. Çerpaçın Yayla, (W Erzincan). Mid Miocene.

Borelis melo, Mid Miocene.

Miliolidae, Palaeocene?-Early Eocene? Inner shelf facies.

Verneuillinidae

PO03 115 Bilkoç (S Erzincan).

Globotruncana sp. Upper Cretaceous

Rugoglobigerinid sp. Upper Cretaceous

Pelagic forams.

PO03 116. Bilkoç (S Erzincan).

Nummulites (& *Amphistegina*), *Assilina* sp., Mid Eocene.

Morozovella? (?*velascoensis*), *M. Simulatis* (SCHWAPER) Upper Palaeocene.

Assilina, Lower Eocene. *Nummulites* sp.,

Rotalidae, *Soritidae*

PO03 117. Gıyabey Yurdu (S Erzincan).

Miogypsinidae

Miogypsina spp.

Miogypsina cf

algae, Upper Oligocene-Lower Miocene

PO03 121. Gıyabey Yurdu (S Erzincan).

Discocyclina cf. discus (Rutimiyeri)

Discocyclina sp.

Nummulites sp.

Assilia sp.

Amphistegina sp.

Discocyclina marthae (Schlumberger)

PO03 135. Baltaş (W Erzincan).

Truncorotaloides cf. rohri (Brönnimann&Bermudez)

Acarinina sp.

Globigerina sp.

Rugoglobigerina sp.

Globotruncanidae

Upper Cretaceous

PO03 152. Gökkaya (SW Erzincan).

Stratigraphic unit: Çerpaçin member (near base), Çerpaçindere Formation.

Field description: thin-bedded shaly-muddy limestone with fissile shale partings.

Petrographic description:

Fossil content: Not dateable in thin section. No planktonic forams.

1 Siliceous radiolarians in calcareous micrite. Indicating Siliceous productivity and carbonate deposition above CCD in unrestricted open ocean.

PO03 153. Gökkaya (SW Erzincan).

Planorotalites? U. Palaeocene.

Mozorovella aragonensis (NUTALL), Mid Eocene.

Acarina sp. Eocene.

PO03 155. Gökkaya (SW Erzincan).

Globigerina

Acarinina sp.

PO03 156. Gökkaya (SW Erzincan).

Nummulitidae

Miliolidae

PO03 166. Çeltek (Sivas).

Pithonella ovalis KAUFMANN

Ostracoda

PO03 175. Gökkaya (SW Erzincan)

Planorotalites sp. Palaeocene-Eocene

PO03 187. Kömür (N Erzincan).

Pithonella ovalis (Turonian)

Pseudohastigerina sp.

Radiolaria, Nummulitidae (Eocene)

Turborotalia sp.

PO03 211. Yukarıberçin (CP, NW Tosya).

Globotruncana arca (CUSHMAN)

Heterohelicidae

Appendix 2. Whole-rock geochemistry analytical procedure.

X-Ray Fluorescence Analysis (XRF): sample preparation and analytical method

The particular method described here has been developed by Dodie James and Godfrey Fitton and incorporates procedures specified by de Jongh (1973), Govindaraju (1994), Jochum *et al.* (1990), Norrish & Hutton (1969) and Reynolds (1963).

Samples were analyzed for 10 major and 15 trace elements at Edinburgh University using a Phillips PW2404 wavelength-dispersive, sequential X-ray fluorescence spectrometer fitted with a Rh anode end-window X-ray tube.

Sample Preparation for Major-element Analysis

Major element concentrations were measured on fused glass discs prepared by a method similar to that of Norrish & Hutton (1969). Powdered rock samples were dried in an oven at 110°C overnight. A nominal, but precisely weighed, 0.9g of each sample was ignited for 20 minutes in a Pt-5%Au crucible at 1100°C to determine loss on ignition (LOI). Loss on ignition was calculated from the measured mass change and expressed as a percentage of the un-ignited sample mass.

The remaining ignited powder was mixed thoroughly with a borate flux (Johnson Matthey Spectroflux® 105), using a 5:1 (flux/sample) dilution calculated on the basis of the sample mass before second ignition, and then fused in a muffle furnace for 20 minutes at 1100°C. Spectroflux® contains 47% lithium tetraborate ($\text{Li}_2\text{B}_4\text{O}_7$), 37% lithium oxide (Li_2O) and 16% lanthanum oxide (La_2O_3) as a heavy absorber.

After fusion the crucible is reweighed and weight loss due to adsorbed moisture from the flux was made up by the accurate addition of extra flux. While fusing for the second time over a Meker burner the mixture in the crucible was swirled thoroughly to ensure homogeneity. The molten material was cast into a graphite plate and pressed into a thin disc by lowering an aluminium plunger onto the globule. The casting operation was carried out on a hotplate at 220°C and the glass disk was allowed to anneal at this temperature for 5 minutes before cooling.

B sample preparation for trace element analysis

Approximately 8g of powdered rock sample was mixed with 8 drops of binding agent (2% aqueous solution of polyvinyl alcohol). The mixture was placed in a tapered aluminium pellet cup inside a steel mold. A polished tungsten carbide disc was placed on top of the powder and the whole assembly compressed at 8 tons using a hydraulic press to form a 40-mm diameter pellet.

C Calibration

The spectrometer was calibrated for major- and trace-element analysis using international standard samples. The concentrations of Nb and Zr used in the calibrations were those given by Jochum *et al.* (1990). The concentrations of major elements and all other trace elements were those recommended in the compilation of “working values” by Govindaraju (1994). Instrumental settings used for both calibration standards and routine samples are given in table 1 below.

D Interference and matrix corrections

Analytical lines were chosen to provide high intensity with minimal interference from other elements. Line overlap factors were calculated using the international standards used in the calibrations and, in addition, synthetic standards for trace-element overlaps. The synthetic standards were prepared from pure oxide mixtures of basalt and granite composition, spiked with stoichiometric trace-element compounds. The mixtures were fused, ground, and pressed into pellets as above. Line overlap corrections were applied for Rb on Y, Sr on Zr, Y on Nb, Ti on V and Ba, V on Cr, Cr on Ce and Nd, Ce on Nd, Ca on Sc, Sc on Ba. For major elements, corrections were applied for Ca on Mg, Ti, and P, and Mg on Na.

The use of flux containing a heavy absorber (La_2O_3) for major-element analysis produces glass discs with a relatively constant matrix composition. However, linearity of calibration lines was improved by correcting the intensities of major-element lines for matrix effects using theoretical alpha coefficients (de Jongh, 1973) calculated on-line. The coefficients were calculated to allow for the volatile components in the sample which were replaced by flux. Analytical totals should,

therefore, be 100% less the measured LOI. The intensities of five trace-element lines (Rb, Sr, Y, Zr, and Nb) were corrected for matrix effects by using the count rate from the RhK α Compton scatter line as an internal standard (Reynolds, 1963). All other trace-element intensities were corrected for matrix effects using theoretical alpha coefficients based on major-element concentrations measured on the powder pellets at the same time.

Because the background around the wavelength of NbK is curved, linear interpolation between two background positions can introduce significant error at low concentrations. Instead, the background correction was calculated by fitting a third-order polynomial to background count rates measured at four positions, two either side of the peak. Long counting times (500 s at the peak and 500 s in total at the background positions) were used in order to improve precision in the determination of Nb. Each sample was analysed three times and the average value taken. A LiF220 analysing crystal was used in the determination of Zr to give better wavelength dispersion and hence reduce overlap of the SrK peak on ZrK.

Precision and accuracy

Analytical precision is a function of reproducibility. Reproducibility has two aspects to consider; 1) the ability of the spectrometer to reproduce results from repeated analysis of a single sample, 2) the ability of the analyst to manufacture samples of a particular material which give the same results when analysed. For major elements, instrument reproducibility is better than sample reproducibility, but for trace elements it is similar to, or worse than, sample reproducibility.

Accuracy is a measure of the absolute quality of the analysis and is more difficult to estimate. To some extent accuracy depends on the quality of the calibration. This can be assessed by comparing the measured standard values with those of Govindaraju (1994) and can be quantified as the root mean square deviation (rmsd), expressed in wt.% or ppm, of the calibration data about the regression line. For major-elements precision and accuracy are very similar but for trace-elements precision is much better than accuracy. This probably reflects the accuracy of the values recommended for the standards used in trace-element calibrations. Inter-laboratory agreement on standard values is much better for major elements than for

trace elements. Reproducibility (σ) and accuracy (rmsd) data were obtained by preparing five glass discs from a single rock sample (PO01/42) and measuring each five times. The results appear in Table 2.

Table 2. Reproducibility (standard deviation σ) and accuracy (rmsd) data.

	SiO ₂	Al ₂ O ₃	Fe ₂ O ₃	MgO	CaO	Na ₂ O	K ₂ O	TiO ₂	MnO	P ₂ O ₅	LOI	Total
PO01/42A	47.99	16.09	12.82	2.89	7.96	3.06	1.332	1.699	0.139	0.205	5.07	99.26
PO01/42A	47.96	16.11	12.84	2.91	7.94	3.08	1.326	1.697	0.138	0.205	5.07	99.28
PO01/42A	47.96	16.12	12.82	2.89	7.92	3.06	1.330	1.700	0.137	0.206	5.07	99.21
PO01/42A	47.93	16.13	12.83	2.91	7.95	3.11	1.332	1.697	0.140	0.206	5.07	99.31
PO01/42A	47.97	16.10	12.82	2.92	7.94	3.06	1.328	1.700	0.139	0.205	5.07	99.25
PO01/42B	48.11	15.84	12.82	2.90	7.94	3.05	1.323	1.698	0.140	0.206	5.00	99.03
PO01/42B	48.11	15.87	12.83	2.92	7.96	3.09	1.324	1.705	0.140	0.205	5.00	99.15
PO01/42B	48.13	15.91	12.80	2.92	7.95	3.06	1.319	1.697	0.140	0.203	5.00	99.13
PO01/42B	48.14	15.82	12.81	2.88	7.96	3.07	1.322	1.706	0.141	0.202	5.00	99.05
PO01/42B	48.13	15.86	12.83	2.91	7.95	3.04	1.322	1.697	0.139	0.201	5.00	99.08
PO01/42C	48.35	15.93	12.92	2.92	8.00	3.08	1.333	1.713	0.142	0.206	5.05	99.64
PO01/42C	48.38	15.93	12.92	2.95	7.99	3.06	1.331	1.707	0.140	0.209	5.05	99.67
PO01/42C	48.39	15.96	12.92	2.93	8.00	3.07	1.337	1.717	0.142	0.206	5.05	99.72
PO01/42C	48.44	16.02	12.93	2.91	7.98	3.13	1.325	1.716	0.140	0.204	5.05	99.85
PO01/42C	48.42	15.98	12.92	2.94	8.01	3.09	1.332	1.718	0.140	0.206	5.05	99.81
PO01/42D	48.17	16.03	12.86	2.90	7.95	3.07	1.329	1.705	0.137	0.208	6.24	100.60
PO01/42D	48.20	16.00	12.89	2.92	7.96	3.10	1.330	1.704	0.138	0.206	6.24	100.69
PO01/42D	48.20	15.95	12.87	2.92	7.96	3.03	1.329	1.719	0.140	0.208	6.24	100.57
PO01/42D	48.21	16.00	12.89	2.92	7.98	3.08	1.327	1.712	0.139	0.207	6.24	100.71
PO01/42D	48.23	15.97	12.88	2.93	7.97	3.09	1.331	1.709	0.140	0.207	6.24	100.70
PO01/42E	48.41	16.09	12.85	2.88	7.83	2.97	1.307	1.675	0.137	0.200	5.03	99.38
PO01/42E	48.48	16.00	12.85	2.88	7.83	3.06	1.313	1.674	0.135	0.205	5.03	99.46
PO01/42E	48.51	16.06	12.87	2.89	7.84	2.95	1.310	1.676	0.139	0.204	5.03	99.48
PO01/42E	48.48	16.05	12.85	2.88	7.84	3.02	1.316	1.677	0.138	0.202	5.03	99.48
PO01/42E	48.53	16.06	12.88	2.90	7.83	3.03	1.307	1.681	0.137	0.205	5.03	99.59

	<u>instrument reproducibility</u>		<u>sample reproducibility</u>		<u>accuracy</u>
	mean	σ	mean	σ	r.m.s.d
SiO ₂	46.62	0.0275	48.2332	0.2095	0.22
Al ₂ O ₃	15.463	0.0302	15.9952	0.0985	0.12
Fe ₂ O ₃	12.4301	0.0107	12.8608	0.043	0.05
MgO	2.8111	0.0132	2.9088	0.0186	0.08
CaO	7.6711	0.0103	7.9376	0.0622	0.05
Na ₂ O	2.9575	0.028	3.0604	0.0362	0.06
K ₂ O	1.2802	0.0028	1.3246	0.0089	0.02
TiO ₂	1.6428	0.0038	1.7	0.0149	0.01
MnO	0.1344	0.0011	0.1391	0.0017	0.01

P2O5	0.1982	0.0015	0.2051	0.0022	0.01
LOI	5.1097		5.278	0.5384	
Total	96.3182	0.062614	99.6427	0.6153	

Appendix 3. XRF Data.

Refahiye Complex

Sample	POO1/47/48	POO1/53	POO1/119	POO2/E3	POO2/E8	POO2/E15	E16	E17	E19	E20
SiO2	43.38	50.84	53.47	50.02	51.95	49.90	47.55	49.91		57.74
Al2O3	0.80	14.45	16.25	15.86	17.33	15.21	14.47	14.97		16.07
Fe2O3	8.65	13.41	9.71	9.76	9.30	13.01	13.97	11.32		8.68
MgO	45.28	5.71	6.41	7.96	6.66	5.17	4.29	6.75		2.73
CaO	0.35	9.22	9.00	11.75	8.19	8.93	12.42	10.43		4.06
Na2O	-0.01	3.30	2.79	2.11	3.64	3.77	3.02	3.05		7.07
K2O	0.00	0.24	0.19	0.39	0.39	0.40	0.11	0.23		0.41
TiO2	0.05	1.85	0.57	0.29	0.61	1.78	2.04	1.36		1.27
MnO	0.12	0.22	0.16	0.17	0.16	0.21	0.22	0.19		0.16
P2O5	0.01	0.19	0.05	0.02	0.04	0.14	0.15	0.12		0.12
LOI	1.40	0.98	0.91	1.92	1.34	0.91	1.16	1.12		1.63
Total	100.03	100.41	99.52	100.25	99.61	99.42	99.40	99.44		99.93
Zn	50	96	74	80	67	93	105	89	38	52
Cu	7	63	72	23	123	35	71	70	11	6
Ni	2770	51	40	30	41	34	33	83	10	0
Cr	2948	100	46	72	188	53	12	296	27	5
V	13	358	288	312	318	450	574	308	232	180
Ba	5	38	29	30	15	109	51	42	73	57
Sc	5	42	47	57	75	54	53	54	44	51
Nb	0	3	1	1	1	3	3	3	2	3
Zr	0	111	25	27	13	100	107	90	43	64
Y	-2	42	13	14	5	38	41	34	14	28
Sr	-3	130	141	200	110	260	154	153	287	199
Rb	0	2	1	5	10	6	1	2	17	8
La	3	6	3	2	2	3	4	4	4	2
Ce	-3	17	4	3	0	14	16	11	8	10
Nd	1	14	3	2	0	10	13	11	4	5

Appendix 3. XRF Data.

Refahiye Complex

Sample	POO3/27	POO3/29	POO3/74	POO3/122	POO3/127B	POO3/131	POO3/148	POO3/149	POO3/151
SiO2	43.45	66.91	47.30	51.84	47.67	52.91	51.65	51.32	51.07
Al2O3	16.03	18.31	15.32	17.89	15.08	16.10	14.82	14.85	11.93
Fe2O3	16.57	1.06	8.98	9.18	9.67	8.46	10.14	13.60	8.83
MgO	5.79	0.79	10.69	4.58	6.50	7.26	9.08	4.40	13.45
CaO	10.00	0.75	13.71	6.20	14.25	10.40	10.13	7.83	10.20
Na2O	2.99	10.77	1.06	3.75	2.62	2.67	2.34	4.43	1.65
K2O	0.03	0.32	0.08	1.70	0.31	0.11	0.26	0.45	0.17
TiO2	2.48	0.19	0.54	0.82	1.20	0.31	0.46	2.03	0.38
MnO	0.18	0.01	0.16	0.19	0.17	0.15	0.18	0.25	0.15
P2O5	0.01	0.05	0.01	0.18	0.13	0.02	0.03	0.16	0.03
LOI	1.91	0.24	2.17	3.27	0.01	1.09	1.11	0.41	1.69
Total	99.44	99.40	100.01	99.60	97.60	99.48	100.19	99.73	99.56
Zn	77	35	52	89	88	55	74	87	68
Cu	63	7	27	108	143	17	14	60	16
Ni	12	-4	66	5	173	43	122	7	305
Cr	9	16	240	3	499	187	504	10	1043
V	798	-3	272	348	265	224	342	383	226
Ba	8	65	17	602	44	23	22	63	36
Sc	44	0	63	26	42	50	58	45	46
Nb	0	2	0	6	4	1	0	3	1
Zr	7	76	10	87	84	25	10	91	19
Y	8	0	11	22	30	15	9	37	11
Sr	126	128	204	588	277	94	96	174	69
Rb	1	1	1	34	3	1	3	5	2
La	-2	1	1	12	4	0	0	1	0
Ce	0	8	6	23	9	3	2	12	1
Nd	-1	3	2	12	7	4	1	11	2

Appendix 3. XRF Data.

Karayaprak Melange

Sample	P001/147A	POO1/147B	P001/149	POO1/155A	POO1/155B	POO1/159A	P001/159B	POO1/159C
SiO ₂	49.36	48.90	58.54	52.28	44.10	47.21	48.14	48.82
Al ₂ O ₃	13.96	13.84	13.95	15.48	12.29	13.86	14.00	14.28
Fe ₂ O ₃	12.13	12.37	10.86	12.71	11.67	10.29	10.51	11.03
MgO	5.66	6.08	4.49	4.39	15.47	7.17	7.38	7.55
CaO	10.63	10.11	2.77	4.30	7.03	10.41	9.57	8.15
Na ₂ O	2.34	2.43	2.91	6.40	1.90	3.51	3.09	3.73
K ₂ O	1.36	1.23	0.95	0.56	0.16	0.65	1.52	1.16
TiO ₂	1.16	1.14	0.88	1.34	1.32	1.28	1.36	1.39
MnO	0.27	0.28	0.25	0.18	0.17	0.19	0.18	0.18
P ₂ O ₅	0.11	0.10	0.12	0.10	0.13	0.12	0.12	0.12
LOI	2.83	2.92	3.81	1.63	5.40	4.68	3.91	3.82
Total	99.81	99.40	99.54	99.38	99.64	99.37	99.78	100.24
Zn	82	90	129	70	100	89	92	97
Cu	35	31	114	68	97	45	43	29
Ni	72	71	5	19	704	70	81	77
Cr	146	139	17	34	963	315	304	300
V	364	319	172	552	230	315	332	310
Ba	89	100	280	255	18	42	152	126
Sc	50	44	40	44	32	45	49	53
Nb	3	3	1	1	10	3	3	3
Zr	72	71	65	64	83	80	86	85
Y	30	30	37	35	17	32	29	29
Sr	141	105	389	282	172	435	420	452
Rb	42	38	16	9	1	12	23	16
La	4	5	5	3	8	5	4	3
Ce	9	8	9	7	18	12	10	11
Nd	7	6	7	6	12	10	9	10

Appendix 3. XRF Data.

Karayaprak Melange

Sample	PO01/167A	PO01/167B	PO01/168A	PO02/E4	PO02/E6	PO02/E7	PO03/100	PO03/110
SiO ₂	48.73	49.07	56.26	47.45	43.98	55.21	58.54	53.50
Al ₂ O ₃	14.45	14.40	16.46	13.98	14.49	16.81	0.58	18.01
Fe ₂ O ₃	13.32	13.03	9.58	14.13	11.55	6.72	8.14	6.04
MgO	6.22	6.20	3.37	5.70	4.80	5.01	27.91	3.49
CaO	10.88	10.88	4.23	9.13	19.31	8.06	0.29	4.96
Na ₂ O	3.52	3.26	4.96	3.24	0.21	4.39	0.01	5.29
K ₂ O	0.18	0.26	0.09	1.41	0.05	0.62	0.00	3.43
TiO ₂	1.80	1.76	0.53	2.82	1.51	0.55	0.02	0.87
MnO	0.22	0.21	0.18	0.17	0.21	0.11	0.09	0.10
P ₂ O ₅	0.18	0.18	0.08	0.35	0.14	0.05	0.01	0.59
LOI		0.37	3.30	1.66	3.25	1.87	4.52	3.12
Total	99.50	99.62	99.03	100.05	99.49	99.40	100.10	99.40
Zn	106	102	132	141	93	105	33	77
Cu	49	56	47	95	40	160	12	19
Ni	53	55	21	110	18	95	1203	0
Cr	101	117	69	288	20	157	1652	7
V	373	370	139	312	418	299	-7	114
Ba	34	46	22	189	25	175	16	711
Sc	46	48	41	40	38	33	1	6
Nb	4	3	1	36	3	36	0	30
Zr	123	123	48	196	99	192	0	253
Y	45	46	20	34	35	25	-1	20
Sr	174	218	61	419	55	392	-2	1015
Rb	2	2	1	38	1	45	0	62
La	5	6	6	21	4	21	0	50
Ce	18	18	11	48	15	48	-1	85
Nd	15	14	7	30	13	27	0	31

Appendix 3. XRF Data.

Karadağ Formation

Sample	POO2/E28	POO2/E29	POO2/E30	POO2/E31	POO3/42	POO3/101	POO3/102	POO3/103	POO3/109
SiO ₂	57.62	54.83	47.77	58.42	70.09	50.29	57.08	55.67	54.62
Al ₂ O ₃	18.12	17.63	15.86	17.07	11.67	14.61	15.98	15.66	13.12
Fe ₂ O ₃	6.86	7.55	10.63	7.23	4.78	8.08	9.81	9.93	8.07
MgO	3.19	2.94	7.26	1.99	1.37	7.44	3.67	3.46	8.96
CaO	4.75	7.36	9.74	4.66	7.09	6.33	3.43	6.93	7.62
Na ₂ O	3.88	3.16	1.77	4.53	2.36	1.73	6.29	3.35	3.90
K ₂ O	2.45	1.61	1.23	1.08	0.03	3.51	0.09	0.09	0.06
TiO ₂	0.77	0.81	1.01	0.82	0.59	0.60	0.83	0.81	0.40
MnO	0.14	0.13	0.15	0.10	0.07	0.18	0.14	0.15	0.15
P ₂ O ₅	0.18	0.23	0.11	0.16	0.12	0.44	0.10	0.10	0.03
LOI	2.31	3.99	4.02	3.38	1.64	6.18	1.98	3.30	2.98
Total	100.28	100.25	99.55	99.44	99.81	99.40	99.40	99.45	99.91
Zn	72	76	86	58	66	64	89	72	67
Cu	11	45	108	9	19	172	10	24	29
Ni	0	9	119	0	-5	31	1	3	101
Cr	9	7	212	10	5	83	11	12	377
V	172	221	379	165	22	315	263	274	227
Ba	864	534	325	226	16	458	40	66	13
Sc	18	17	51	27	16	36	39	38	45
Nb	12	13	8	12	3	5	1	2	0
Zr	145	139	91	142	64	58	40	44	16
Y	24	20	20	24	24	18	26	27	9
Sr	508	608	355	347	178	240	74	193	41
Rb	52	38	31	35	0	32	1	1	1
La	21	19	11	15	4	22	2	1	2
Ce	40	36	26	36	12	39	7	8	2
Nd	18	16	13	16	9	19	5	7	1

Appendix 3. XRF Data.

Karadağ Formation

Sample	POO3/113	POO3/114	POO3/140	POO3/144	POO3/176	POO3/179	POO3/180	POO3/183	POO3/185
SiO ₂	50.33	49.51	55.67	45.88	45.81	52.87	59.38	50.21	57.54
Al ₂ O ₃	16.84	16.83	18.96	18.88	18.90	14.75	15.32	17.52	15.67
Fe ₂ O ₃	8.98	9.15	5.62	9.62	12.49	13.89	9.59	12.46	5.99
MgO	3.37	3.53	1.56	4.55	6.93	5.25	4.24	4.26	1.90
CaO	6.54	6.41	4.76	8.98	7.49	4.09	1.71	7.80	8.18
Na ₂ O	4.39	4.47	5.62	3.25	2.94	4.22	5.08	2.19	2.61
K ₂ O	0.63	0.46	1.99	0.83	0.08	0.23	0.31	0.49	1.24
TiO ₂	0.83	0.83	0.61	0.65	0.69	1.09	0.73	0.87	0.63
MnO	0.20	0.20	0.14	0.21	0.15	0.20	0.24	0.22	0.12
P ₂ O ₅	0.16	0.16	0.26	0.07	0.03	0.06	0.08	0.11	0.19
LOI	7.66	7.85	4.25	6.67	3.93	2.89	3.24	3.30	5.72
Total	99.93	99.40	99.44	99.58	99.44	99.54	99.92	99.43	99.78
Zn	127	124	72	104	95	201	751	96	61
Cu	229	58	46	84	132	96	16	82	21
Ni	3	2	-2	10	11	9	-5	3	4
Cr	4	4	3	24	22	11	3	5	23
V	246	242	78	350	379	459	120	365	147
Ba	273	188	632	79	20	55	53	199	504
Sc	20	20	9	35	33	43	30	44	19
Nb	4	4	8	1	0	0	0	1	11
Zr	103	103	190	20	17	16	30	41	148
Y	30	30	40	13	12	21	28	21	22
Sr	341	334	296	197	844	53	51	239	478
Rb	14	11	46	9	1	3	4	5	21
La	7	9	16	1	0	1	0	2	29
Ce	21	21	35	6	1	1	3	9	51
Nd	13	14	19	4	1	1	4	6	21

Appendix 3. XRF Data.

Kızılırmak
Ophiolite

Sample	P002/82	POO3/20	POO3/196	POO3/202	P002/236	P002/83	P002/248	POO2/249	POO3/20
SiO ₂	50.88	45.99	47.20	52.38	72.28	55.55	46.87	46.80	45.99
Al ₂ O ₃	14.53	16.73	20.83	15.96	7.24	14.08	15.54	16.35	16.73
Fe ₂ O ₃	13.32	13.71	5.89	10.42	5.17	8.45	10.09	10.53	13.71
MgO	4.71	7.42	9.21	6.18	7.31	5.48	6.35	7.79	7.42
CaO	7.89	11.57	9.51	6.35	1.81	8.48	9.49	7.31	11.57
Na ₂ O	3.84	1.34	2.37	4.51	1.43	5.15	3.71	2.93	1.34
K ₂ O	0.42	0.11	0.06	0.33	0.50	0.04	0.23	0.99	0.11
TiO ₂	2.03	0.60	0.10	0.79	0.49	0.78	1.78	1.83	0.60
MnO	0.17	0.22	0.10	0.15	0.15	0.16	0.18	0.18	0.22
P ₂ O ₅	0.21	0.03	0.01	0.07	0.08	0.05	0.24	0.26	0.03
LOI	1.64	1.92	4.41	2.28	2.95	1.72	5.05	4.97	1.92
Total	99.64	99.64	99.68	99.41	99.41	99.94	99.53	99.93	99.64
Zn	106	105	35	25	63	62	85	89	105
Cu	55	107	7	6	52	19	61	60	107
Ni	17	38	57	25	187	21	187	239	38
Cr	18	62	58	20	408	66	370	465	62
V	466	566	51	303	111	303	270	285	566
Ba	84	11	11	18	64	0	31	69	11
Sc	56	72	24	43	19	49	38	39	72
Nb	6	1	0	1	7	2	12	13	1
Zr	162	10	1	41	60	43	149	152	10
Y	50	18	0	19	14	19	34	35	18
Sr	192	116	149	154	45	51	111	125	116
Rb	6	1	1	2	18	0	5	19	1
La	8	0	-1	-1	9	2	6	5	0
Ce	25	10	0	2	23	7	20	18	10
Nd	16	2	-1	3	9	4	13	11	2

Appendix 3. XRF Data.

Kızılırmak Ophiolite

Sample	POO3/21	POO3/196	POO3/202
SiO ₂	49.59	47.20	52.38
Al ₂ O ₃	13.82	20.83	15.96
Fe ₂ O ₃	4.13	5.89	10.42
MgO	1.46	9.21	6.18
CaO	13.96	9.51	6.35
Na ₂ O	4.38	2.37	4.51
K ₂ O	0.50	0.06	0.33
TiO ₂	0.77	0.10	0.79
MnO	0.11	0.10	0.15
P ₂ O ₅	0.32	0.01	0.07
LOI	10.38	4.41	2.28
Total	99.42	99.68	99.41
Zn	78	35	25
Cu	45	7	6
Ni	33	57	25
Cr	42	58	20
V	128	51	303
Ba	2351	11	18
Sc	28	24	43
Nb	2	0	1
Zr	52	1	41
Y	57	0	19
Sr	673	149	154
Rb	7	1	2
La	21	-1	-1
Ce	29	0	2
Nd	18	-1	3

Appendix 3. XRF Data.

Kirazbaşı Melange

Sample	POO2/18	P002/21	POO2/27A	P002/34	POO2/35	P002/56	POO2/57	P002/61	P002/73
SiO ₂	44.57	45.03	47.64	31.77	52.25	47.28	50.48	43.46	48.14
Al ₂ O ₃	16.17	15.27	7.74	12.83	16.68	15.38	13.26	14.33	16.57
Fe ₂ O ₃	11.07	9.88	3.89	7.27	8.15	10.97	12.26	12.96	10.85
MgO	7.50	7.49	2.07	8.16	6.60	7.78	5.16	8.07	7.81
CaO	5.55	7.09	17.06	18.58	6.54	8.65	7.44	8.69	4.85
Na ₂ O	4.83	4.63	0.29	0.19	2.09	3.98	4.09	3.91	3.07
K ₂ O	0.10	0.01	1.58	1.46	1.37	0.52	0.11	0.16	4.56
TiO ₂	2.19	1.46	0.38	0.74	0.98	1.49	2.75	2.63	1.02
MnO	0.52	0.30	0.29	0.15	0.11	0.18	0.27	0.19	0.18
P ₂ O ₅	0.29	0.16	0.09	0.11	0.15	0.19	0.44	0.41	0.52
LOI	7.00	8.09	18.44	18.84	4.52	3.96	3.32	4.97	2.00
Total	99.78	99.41	99.46	100.10	99.43	100.38	99.57	99.78	99.57
Zn	108	92	68	81	75	94	124	100	129
Cu	83	79	54	34	44	36	88	98	154
Ni	89	233	121	66	131	50	6	77	131
Cr	362	509	198	175	286	82	6	217	7
V	353	282	88	230	179	245	299	344	371
Ba	52	13	296	187	114	92	30	66	851
Sc	77	52	0	26	22	39	31	43	31
Nb	9	4	8	1	6	15	31	32	11
Zr	181	128	83	57	148	111	255	147	106
Y	44	29	21	16	19	25	53	23	25
Sr	131	277	226	59	371	200	293	396	580
Rb	2	2	68	45	53	5	0	1	164
La	8	6	29	4	8	10	17	14	27
Ce	25	15	42	10	20	22	44	40	50
Nd	17	11	25	7	11	13	26	23	24

Appendix 3. XRF Data.

Kirazbaşı Melange

Sample	P002/77	P002/78	P002/80	P002/167	POO2/204	P002/215	POO2/239	POO2/244	P002/247
SiO ₂	48.16	49.58	50.64	48.45	52.02	48.48	64.98	39.09	47.87
Al ₂ O ₃	16.64	13.03	15.12	14.21	15.95	14.24	17.95	6.99	15.11
Fe ₂ O ₃	6.46	11.49	11.38	13.11	6.47	12.55	4.72	15.67	12.62
MgO	6.91	2.02	5.84	6.14	6.72	6.85	0.34	23.43	4.83
CaO	8.08	9.89	8.59	10.74	11.73	9.62	0.25	4.49	9.79
Na ₂ O	4.57	5.11	4.48	3.48	2.98	3.29	8.92	0.06	3.83
K ₂ O	0.34	0.15	0.40	0.17	0.44	0.13	1.22	0.07	0.76
TiO ₂	1.85	2.24	1.31	1.77	0.26	1.74	0.35	0.87	1.38
MnO	0.20	0.12	0.17	0.21	0.12	0.20	0.01	0.20	0.22
P ₂ O ₅	0.19	0.35	0.12	0.17	0.01	0.16	0.13	0.17	0.15
LOI	5.97	6.04	1.87	0.95	3.07	2.51	0.79	8.79	3.36
Total	99.36	100.01	99.93	99.39	99.77	99.76	99.66	99.82	99.92
Zn	116	116	91	67	35	107	42	104	99
Cu	274	40	65	9	9	46	11	54	66
Ni	151	73	51	54	81	61	0	1147	40
Cr	348	182	82	131	392	175	7	1189	81
V	273	306	368	278	216	293	6	109	374
Ba	25	40	136	10	21	18	97	3	69
Sc	52	32	52	51	51	46	0	6	44
Nb	12	28	3	4	1	6	165	16	4
Zr	140	170	86	66	12	142	482	65	101
Y	45	37	32	26	9	33	34	10	37
Sr	117	120	361	336	49	230	303	100	86
Rb	7	3	11	2	6	3	31	4	30
La	7	17	6	5	2	5	93	12	11
Ce	20	42	18	13	4	13	190	23	22
Nd	14	23	10	8	2	8	56	9	14

Appendix 3. XRF Data.

Kirazbaşı Melange

Sample	P002/251	P002/253	P002/258	POO2/259	P002/265	P002/267	POO2/E4	POO2/E6	POO2/E7
SiO ₂	46.54	49.36	41.06	39.17	45.97	47.66	47.45	43.98	55.21
Al ₂ O ₃	20.32	16.06	13.90	15.05	16.62	11.51	13.98	14.49	16.81
Fe ₂ O ₃	6.85	7.19	10.68	9.73	7.20	5.99	14.13	11.55	6.72
MgO	6.60	9.68	5.13	4.27	5.61	6.23	5.70	4.80	5.01
CaO	10.03	8.62	11.35	12.08	11.89	8.62	9.13	19.31	8.06
Na ₂ O	3.05	3.49	3.39	2.48	4.30	5.22	3.24	0.21	4.39
K ₂ O	0.64	0.14	0.47	1.27	0.15	0.01	1.41	0.05	0.62
TiO ₂	0.87	1.42	1.75	2.28	1.08	0.39	2.82	1.51	0.55
MnO	0.40	0.70	0.14	0.12	0.24	0.11	0.17	0.21	0.11
P ₂ O ₅	0.07	0.13	0.28	0.40	0.10	0.12	0.35	0.14	0.05
LOI	4.51	2.69	11.90	12.72	6.34	13.80	1.66	3.25	1.87
Total	99.87	99.47	100.05	99.57	99.49	99.66	100.05	99.49	99.40
Zn	57	81	95	117	68	53	141	93	105
Cu	61	91	30	34	112	16	95	40	160
Ni	85	62	128	105	241	135	110	18	95
Cr	262	177	247	93	375	427	288	20	157
V	192	294	257	342	217	238	312	418	299
Ba	59	60	44	157	23	60	189	25	175
Sc	30	58	21	31	37	32	40	38	33
Nb	3	6	31	47	1	2	36	3	36
Zr	53	95	127	169	93	38	196	99	192
Y	15	25	19	25	22	11	34	35	25
Sr	211	268	303	368	245	335	419	55	392
Rb	11	1	13	33	2	1	38	1	45
La	2	4	24	33	2	10	21	4	21
Ce	6	15	47	68	9	18	48	15	48
Nd	4	8	23	31	7	11	30	13	27

Appendix 3. XRF Data.

Kirazbaşı Melange

Sample	POO3/10	POO3/195	POO3/199	POO3/203
SiO ₂	52.59	57.70	47.78	47.20
Al ₂ O ₃	14.09	10.14	14.42	14.63
Fe ₂ O ₃	8.16	5.00	10.10	8.63
MgO	4.04	1.68	5.48	6.95
CaO	8.83	11.06	9.70	10.62
Na ₂ O	6.28	3.64	4.23	4.46
K ₂ O	0.36	0.76	1.36	0.14
TiO ₂	1.87	0.53	1.69	1.14
MnO	0.09	0.16	0.20	0.20
P ₂ O ₅	0.37	0.12	0.21	0.13
LOI	2.98	9.03	4.30	5.85
Total	99.66	99.81	99.47	99.96
Zn	106	85	106	83
Cu	81	45	90	66
Ni	103	16	144	75
Cr	189	28	219	227
V	166	107	370	259
Ba	93	64	76	40
Sc	27	20	41	41
Nb	26	11	15	8
Zr	123	108	118	75
Y	22	25	39	25
Sr	331	65	228	79
Rb	4	19	8	1
La	19	18	12	5
Ce	43	36	27	17
Nd	22	22	15	10

Appendix 3. XRF Data.

Yaylaçayı
Formation

Sample	P002/41	P002/48	P002/49	P002/67	P002/88	P002/102	P002/103	P002/104
SiO ₂	58.86	45.87	49.49	45.25	43.82	32.52	55.92	55.09
Al ₂ O ₃	8.04	17.68	16.77	15.89	13.71	12.20	16.18	16.12
Fe ₂ O ₃	5.69	12.84	5.35	11.99	7.01	8.23	7.35	8.23
MgO	5.95	8.95	1.94	5.61	2.68	4.13	2.72	2.07
CaO	9.98	8.00	6.67	10.74	16.37	21.15	9.45	8.60
Na ₂ O	2.73	0.17	4.03	4.07	2.43	1.72	2.40	2.53
K ₂ O	0.28	0.00	6.66	1.03	0.49	0.46	1.35	1.57
TiO ₂	0.13	0.78	0.62	1.00	0.68	0.48	0.61	0.63
MnO	0.13	0.13	0.14	0.23	0.36	0.24	0.20	0.22
P ₂ O ₅	0.02	0.06	0.28	0.44	0.12	0.08	0.13	0.13
LOI	7.70	5.20	7.47	3.46	11.74	18.57	3.08	4.29
Total	99.50	99.67	99.42	99.71	99.41	99.78	99.39	99.48
Zn	51	117	88	85	121	80	66	61
Cu	91	59	47	152	165	86	55	55
Ni	272	23	9	20	18	21	4	3
Cr	944	55	29	18	40	42	19	21
V	177	372	185	384	187	338	268	249
Ba	12	0	1052	893	661	140	276	284
Sc	38	44	0	28	20	18	33	39
Nb	0	0	17	9	6	0	0	3
Zr	7	24	205	101	74	25	86	82
Y	0	11	26	25	25	11	22	21
Sr	84	680	704	648	196	254	392	353
Rb	6	0	170	23	9	7	24	32
La	1	2	43	18	9	4	14	15
Ce	0	6	82	37	16	5	25	25
Nd	0	2	36	20	9	4	12	11

Appendix 3. XRF Data.

Yaylaçayı
Formation

Sample	P002/116	P002/122	POO2/126C	P002/130	P002/136	P002/150	POO2/155	P002/160	P002/176
SiO2	69.01	43.25	52.80	46.68	53.67	51.81	45.19	43.49	45.43
Al2O3	13.19	14.78	14.17	14.44	17.41	14.91	23.38	17.10	15.62
Fe2O3	3.50	7.57	8.85	9.82	8.24	12.00	2.97	12.13	12.17
MgO	1.77	4.80	7.22	7.76	3.29	6.41	8.74	3.28	6.09
CaO	3.68	13.19	9.34	10.54	7.35	7.16	15.47	10.15	9.95
Na2O	2.58	4.09	1.98	3.50	2.93	3.92	1.09	4.06	3.86
K2O	1.17	0.92	1.44	0.60	1.36	0.80	0.02	1.64	1.33
TiO2	0.38	1.40	0.68	1.43	0.61	1.39	0.07	0.85	1.03
MnO	0.07	0.16	1.99	0.17	0.13	0.27	0.05	0.10	0.23
P2O5	0.07	0.19	0.21	0.15	0.20	0.14	0.01	0.49	0.48
LOI	3.94	9.35	0.81	4.85	4.44	1.42	2.52	6.54	3.52
Total	99.37	99.69	99.49	99.94	99.62	100.23	99.51	99.83	99.71
Zn	54	79	75	83	47	99	21	86	95
Cu	45	34	3592	118	20	73	77	40	178
Ni	0	63	73	69	0	31	295	21	21
Cr	7	129	474	80	7	56	1054	9	17
V	46	218	375	314	161	393	47	367	388
Ba	344	134	481	91	233	66	0	686	1269
Sc	10	36	21	44	19	59	3	26	30
Nb	5	11	10	13	3	3	0	8	10
Zr	146	104	100	94	70	89	6	85	103
Y	31	29	21	26	20	31	0	22	28
Sr	572	404	547	423	470	304	128	553	432
Rb	13	13	31	4	23	11	0	23	38
La	12	10	16	9	14	6	0	27	21
Ce	23	24	25	20	26	15	0	50	41
Nd	12	14	11	13	13	9	0	25	23

Appendix 3. XRF Data.

Yaylaçayı Formation

Sample	P002/177	P002/178	P002/179	P002/180	P002/181	P002/182	P002/189	P002/190	P003/03
SiO ₂	44.15	43.67	43.54	43.77	43.59	43.19	53.62	76.25	38.70
Al ₂ O ₃	17.04	17.16	16.92	16.64	16.86	17.14	15.52	12.32	20.11
Fe ₂ O ₃	12.19	12.44	11.76	12.18	11.07	12.18	10.28	2.53	13.88
MgO	6.48	7.06	7.01	7.20	5.93	7.95	5.34	0.60	14.01
CaO	11.06	10.69	8.56	10.68	9.38	10.44	5.58	0.95	1.51
Na ₂ O	2.85	2.85	3.21	3.59	4.25	2.69	4.94	5.02	0.12
K ₂ O	1.24	0.89	1.74	0.42	1.37	0.68	0.24	0.74	2.39
TiO ₂	0.92	0.92	0.81	0.83	0.80	0.89	1.25	0.43	0.75
MnO	0.23	0.22	0.22	0.23	0.19	0.23	0.14	0.02	0.32
P ₂ O ₅	0.42	0.44	0.33	0.33	0.37	0.37	0.15	0.07	0.04
LOI	3.53	3.47	5.37	3.56	5.69	3.68	2.40	0.92	7.58
Total	100.10	99.81	99.47	99.43	99.50	99.44	99.46	99.85	99.42
Zn	76	82	79	89	84	75	97	50	184
Cu	81	47	102	114	86	46	26	6	115
Ni	25	24	21	38	35	29	35	-8	49
Cr	10	12	11	26	22	17	116	8	209
V	366	313	334	379	291	338	264	39	313
Ba	900	848	835	610	732	497	33	177	368
Sc	25	19	23	28	21	31	43	12	55
Nb	5	7	4	4	5	5	4	3	0
Zr	74	85	67	65	71	64	115	129	10
Y	19	22	19	19	19	18	35	25	7
Sr	485	572	602	519	349	522	204	77	9
Rb	57	43	85	11	80	23	4	12	49
La	21	23	18	17	20	16	5	10	-1
Ce	39	40	32	32	36	35	15	22	-2
Nd	21	21	17	18	18	18	10	12	0

Appendix 3. XRF Data.

Yaylaçayı
Formation

Sample	POO3/07	POO3/19	POO3/205	POO3/206	POO3/209	POO3/212	POO3/215	POO3/216	POO3/221	POO3/222
SiO ₂	47.28	54.60	44.35	60.33	47.88	58.86	42.59	43.58	47.17	48.17
Al ₂ O ₃	15.05	15.29	15.93	16.94	16.80	14.48	13.97	17.56	16.17	16.66
Fe ₂ O ₃	13.02	11.85	12.64	6.47	8.09	5.13	15.91	13.55	12.41	8.12
MgO	3.58	2.40	4.12	0.48	3.64	0.90	1.82	6.75	6.80	4.22
CaO	6.40	9.72	8.61	2.70	6.37	5.86	9.84	5.38	6.31	6.20
Na ₂ O	5.52	2.02	4.42	9.58	8.33	5.36	4.48	2.52	3.59	6.83
K ₂ O	0.03	0.02	1.03	0.39	0.09	3.57	1.29	2.44	1.07	1.89
TiO ₂	1.81	0.86	3.49	0.55	0.97	0.56	2.00	2.55	2.38	0.97
MnO	0.20	0.20	0.20	0.15	0.22	0.15	0.22	0.16	0.17	0.19
P ₂ O ₅	0.14	0.13	0.65	0.08	0.87	0.24	1.02	0.32	0.31	0.86
LOI	6.42	2.61	4.15	1.75	6.15	4.33	6.48	5.04	3.68	5.32
Total	99.45	99.70	99.59	99.41	99.41	99.43	99.60	99.85	100.05	99.43
Zn	140	99	115	67	109	29	153	150	132	98
Cu	22	60	24	5	183	18	32	82	83	175
Ni	11	27	13	-5	4	12	12	176	136	5
Cr	10	15	5	3	5	62	5	191	180	7
V	528	359	297	7	398	61	29	294	251	400
Ba	30	28	273	236	560	951	251	282	109	2331
Sc	42	42	21	0	9	15	14	30	26	10
Nb	2	1	75	187	12	12	51	24	23	12
Zr	95	43	208	680	178	136	344	168	157	176
Y	38	32	32	64	34	12	48	23	21	33
Sr	37	70	863	95	476	828	209	255	271	566
Rb	0	1	17	5	8	85	29	72	28	43
La	2	4	45	102	60	40	44	12	12	61
Ce	12	6	98	192	110	63	99	34	33	101
Nd	11	8	48	75	52	19	54	21	19	43

İkiçam Formation

Appendix 3. XRF Data.

Sample	P002/29	P002/30	P002/31	P002/32	P002/60	POO2/188	POO3/210	POO3/220
SiO ₂	55.36	53.33	61.77	54.54	51.99	44.69	45.81	53.90
Al ₂ O ₃	16.88	16.80	13.85	16.94	15.67	18.00	12.49	16.90
Fe ₂ O ₃	7.30	7.16	6.04	7.38	10.13	10.34	8.10	6.40
MgO	4.98	2.98	1.81	4.66	6.56	8.69	5.42	4.86
CaO	6.63	8.22	2.51	7.40	7.51	11.56	12.39	3.48
Na ₂ O	2.81	2.83	2.96	2.75	1.01	2.20	3.01	3.76
K ₂ O	2.23	2.13	1.24	2.15	0.26	0.58	3.27	4.03
TiO ₂	0.60	0.60	0.56	0.59	0.54	0.89	0.90	0.78
MnO	0.08	0.09	0.07	0.07	0.14	0.32	0.14	0.13
P ₂ O ₅	0.27	0.27	0.17	0.27	0.01	0.07	0.40	0.27
LOI	2.31	5.30	8.65	2.83	5.52	2.14	7.53	4.98
Total	99.45	99.70	99.62	99.57	99.33	99.47	99.45	99.49
Zn	66	66	79	69	85	77	91	101
Cu	68	73	32	64	66	78	51	69
Ni	19	22	18	21	21	150	78	49
Cr	35	41	37	37	102	1085	233	56
V	197	221	85	205	283	272	228	109
Ba	734	747	147	745	19	41	1170	1419
Sc	24	24	11	28	48	51	35	9
Nb	2	2	14	3	1	3	12	23
Zr	62	75	129	66	19	52	130	275
Y	10	11	14	10	7	17	23	30
Sr	549	804	187	647	101	302	594	594
Rb	43	52	53	45	6	12	84	123
La	12	12	27	11	3	3	36	56
Ce	20	20	51	21	4	7	62	103
Nd	9	9	19	9	1	6	28	40

Appendix 4. Electron microprobe Data.

Electron microprobe data Refahiye Complex												Total	Comment
SiO2	TiO2	Al2O3	Cr2O3	V2O3	FeO	MnO	NiO	ZnO	MgO	CaO	Na2O		
0.053	0.047	39.328	29.375	0.178	15.793	0.223	0.169	0.284	15.956	0.000	0.008	101.415	PO03188 - Spinel 1 Rim
0.000	0.000	0.000	0.000	0.000	0.000	0.000	0.000	0.000	0.000	0.000	0.000	0.000	PO03188 - Spinel 1 Rim - 37 microns in
0.000	0.000	0.000	0.000	0.000	0.000	0.000	0.000	0.000	0.000	0.000	0.000	0.000	PO03188 - Spinel 1 Rim - 37 microns in
0.066	0.008	39.010	29.793	0.184	15.842	0.240	0.170	0.265	15.882	0.016	0.016	101.493	PO03188 - Spinel 1 Rim - 37 microns in
0.164	0.016	41.710	26.750	0.178	15.246	0.243	0.184	0.266	16.699	0.004	0.020	101.480	2
0.027	0.039	38.246	30.401	0.176	16.020	0.268	0.176	0.263	15.698	0.008	0.000	101.320	PO03188 - Spinel 1 core
0.062	0.032	51.176	16.589	0.173	13.439	0.154	0.281	0.307	19.125	0.026	0.022	101.385	PO03188 - Spinel 1 rim on other side
0.022	0.028	38.344	30.457	0.185	15.955	0.259	0.177	0.244	15.806	0.005	0.012	101.494	PO03188 - Spinel 1 core 2
0.040	0.020	37.780	31.442	0.206	15.839	0.248	0.171	0.212	15.833	0.005	0.012	101.807	PO03188 - Spinel 2
0.072	0.000	0.136	145.133	0.005	0.009	0.421	0.038	0.048	0.023	0.019	0.024	145.927	Cr standard
0.027	0.000	100.368	0.014	0.001	0.000	0.001	0.014	0.018	0.021	0.010	0.007	100.481	Al standard
0.054	0.039	39.003	29.871	0.189	15.405	0.212	0.152	0.263	15.924	0.009	0.020	101.142	PO03188 Spinel 2
0.039	0.051	37.283	31.099	0.191	16.701	0.263	0.166	0.275	15.424	0.000	0.019	101.511	PO03188 Spinel 3 core
0.640	0.038	39.134	26.491	0.189	15.938	0.242	0.173	0.249	16.640	0.008	0.014	99.755	PO03188 Spinel 3 rim
0.113	0.023	40.031	28.634	0.197	15.817	0.241	0.165	0.296	15.881	0.008	0.008	101.416	PO03188 - Spinel 4 Rim
0.044	0.035	38.888	29.946	0.212	15.885	0.240	0.179	0.271	15.835	0.000	0.021	101.556	PO03188 Spinel 4
1.998	0.017	43.309	21.481	0.152	13.551	0.197	0.162	0.261	20.240	0.003	0.028	101.398	PO03188 Spinel 5 rim
1.047	0.028	37.241	28.889	0.178	15.411	0.250	0.150	0.245	16.938	0.037	0.273	100.688	PO03188 Spinel 5 core
0.064	0.022	43.838	24.352	0.184	14.771	0.243	0.197	0.273	17.128	0.016	0.018	101.107	PO03188 Spinel 6 rim
0.259	0.037	31.855	25.628	0.147	29.328	0.229	0.137	0.260	13.539	0.000	0.015	101.433	PO03188 Spinel 6 core
4.689	0.011	33.743	23.118	0.173	13.987	0.199	0.164	0.206	23.406	0.013	0.065	99.774	PO03188 Spinel 6 line
0.093	0.018	43.845	24.523	0.160	14.408	0.222	0.200	0.212	17.248	0.013	0.004	100.947	PO03188 Spinel 6 line
0.064	0.016	44.225	24.515	0.170	14.295	0.216	0.230	0.258	17.297	0.004	0.007	101.297	PO03188 Spinel 6 line
0.052	0.044	43.361	25.531	0.173	14.622	0.221	0.182	0.244	17.017	0.012	0.006	101.465	PO03188 Spinel 6 line
0.039	0.019	41.211	27.626	0.205	15.085	0.252	0.184	0.280	16.476	0.001	0.018	101.396	PO03188 Spinel 6 line
0.056	0.021	40.183	29.039	0.193	15.383	0.235	0.186	0.271	16.158	0.018	0.018	101.761	PO03188 Spinel 6 line

Appendix 4. Electron microprobe Data.

0.042	0.026	39.400	29.770	0.188	15.455	0.231	0.127	0.240	16.049	0.010	0.015	101.552	PO03188 Spinel 6 line
0.041	0.034	38.791	30.170	0.203	15.706	0.272	0.170	0.256	15.897	0.007	0.018	101.563	PO03188 Spinel 6 line
0.049	0.041	38.675	30.506	0.191	15.610	0.286	0.168	0.275	15.805	0.000	0.021	101.627	PO03188 Spinel 6 line
0.055	0.050	38.431	30.966	0.186	15.602	0.269	0.178	0.246	15.772	0.000	0.013	101.769	PO03188 Spinel 6 line
0.080	0.027	42.543	25.864	0.167	14.307	0.225	0.186	0.253	17.248	0.019	0.021	100.938	PO03188 - Spinel 7 line
0.093	0.028	42.380	26.463	0.174	14.396	0.229	0.224	0.247	17.010	0.013	0.029	101.286	PO03188 - Spinel 7 line
0.059	0.018	41.932	26.928	0.181	14.396	0.226	0.212	0.227	16.925	0.007	0.024	101.135	PO03188 - Spinel 7 line
0.064	0.033	41.485	27.269	0.188	14.640	0.227	0.193	0.236	16.765	0.012	0.016	101.127	PO03188 - Spinel 7 line
0.068	0.020	40.525	28.297	0.182	14.816	0.223	0.199	0.232	16.464	0.000	0.010	101.034	PO03188 - Spinel 7 line
0.046	0.036	40.317	28.686	0.168	14.946	0.236	0.171	0.242	16.436	0.015	0.014	101.313	PO03188 - Spinel 7 line
0.048	0.018	40.228	28.742	0.199	14.971	0.236	0.207	0.264	16.352	0.000	0.024	101.289	PO03188 - Spinel 7 line
0.049	0.038	39.879	29.275	0.198	15.014	0.242	0.175	0.219	16.337	0.000	0.008	101.433	PO03188 - Spinel 7 line
0.068	0.040	39.594	29.431	0.181	15.093	0.241	0.180	0.237	16.235	0.012	0.019	101.332	PO03188 - Spinel 7 line
0.073	0.012	39.446	29.432	0.187	15.188	0.223	0.162	0.269	16.138	0.010	0.013	101.155	PO03188 - Spinel 7 line
0.100	0.031	39.171	29.831	0.174	15.091	0.239	0.164	0.223	16.194	0.002	0.017	101.237	PO03188 - Spinel 7 line
0.457	0.037	39.158	29.691	0.190	14.544	0.246	0.182	0.193	16.286	0.380	0.015	101.379	PO03188 - Spinel 8 line
0.085	0.038	38.334	30.999	0.183	14.695	0.223	0.206	0.188	16.121	0.027	0.007	101.108	PO03188 - Spinel 8 line
0.042	0.047	37.168	32.197	0.200	14.942	0.237	0.196	0.227	15.951	0.030	0.009	101.247	PO03188 - Spinel 8 line
0.033	0.028	36.989	32.284	0.200	15.144	0.258	0.179	0.219	15.970	0.025	0.016	101.344	PO03188 - Spinel 8 line
0.067	0.045	36.850	32.518	0.190	15.247	0.252	0.174	0.220	15.960	0.019	0.012	101.556	PO03188 - Spinel 8 line
0.047	0.039	36.632	32.689	0.193	15.174	0.265	0.172	0.205	15.881	0.024	0.011	101.332	PO03188 - Spinel 8 line
0.041	0.062	36.601	33.017	0.183	15.173	0.247	0.185	0.218	15.855	0.000	0.007	101.588	PO03188 - Spinel 8 line
0.069	0.032	36.396	32.954	0.188	15.167	0.257	0.174	0.179	15.925	0.001	0.013	101.355	PO03188 - Spinel 8 line
0.195	0.069	36.233	33.015	0.177	15.163	0.243	0.186	0.181	15.939	0.018	0.016	101.434	PO03188 - Spinel 8 line
0.049	0.046	36.391	33.181	0.186	15.185	0.254	0.179	0.197	15.831	0.000	0.001	101.500	PO03188 - Spinel 8 line
0.039	0.045	36.340	33.285	0.186	15.120	0.266	0.170	0.179	15.843	0.011	0.006	101.489	PO03188 - Spinel 8 line
0.026	0.033	38.517	30.512	0.171	16.123	0.242	0.167	0.256	15.669	0.000	0.016	101.732	PO03188 - Spinel 9 core
0.048	0.048	37.219	32.091	0.179	15.571	0.285	0.149	0.207	15.667	0.001	0.002	101.468	PO03188 - Spinel 10 core
0.047	0.040	37.459	31.471	0.203	15.863	0.278	0.168	0.231	15.580	0.000	0.011	101.352	PO03188 - Spinel 11 core
0.026	0.013	39.504	29.511	0.199	15.452	0.271	0.169	0.248	15.937	0.008	0.013	101.353	PO03188 - Spinel 12 core
53.312	0.086	2.511	0.715	0.046	1.949	0.094	0.050	0.000	17.774	24.353	0.091	100.982	PO03188 - Olivine 1

Appendix 4. Electron microprobe Data.

38.138	0.007	0.982	0.689	0.019	6.098	0.181	0.336	0.035	36.473	0.100	0.011	83.069	PO03188 - serp
56.862	0.035	2.506	0.560	0.023	6.040	0.163	0.091	0.017	35.240	0.329	0.016	101.882	PO03188 - opx
41.084	0.000	0.005	0.014	0.000	9.042	0.135	0.438	0.034	50.578	0.015	0.002	101.347	PO03188 - olivine 2
0.038	0.044	37.870	30.931	0.215	15.895	0.253	0.160	0.225	15.592	0.000	0.008	101.232	PO03188 - spinel 13
3.117	0.037	0.037	0.038	0.003	86.866	0.114	0.039	0.017	1.292	0.153	0.040	91.753	PO03188 - magnetite PO03188 - spinel 14
0.076	0.041	38.395	30.498	0.193	15.768	0.266	0.201	0.303	15.784	0.005	0.023	101.552	core
0.050	0.041	40.187	27.608	0.175	15.795	0.241	0.177	0.301	16.258	0.021	0.014	100.867	PO03188 - spinel 14 rim
0.056	0.045	39.044	29.502	0.186	15.482	0.232	0.174	0.291	16.041	0.000	0.025	101.077	PO03188 - spinel 15 rim PO03188 - spinel 15
0.033	0.034	38.267	30.544	0.199	15.947	0.254	0.161	0.247	15.757	0.006	0.011	101.460	core
0.073	0.025	40.658	27.536	0.199	15.550	0.240	0.209	0.267	16.040	0.000	0.013	100.810	PO03188 - spinel 16 rim PO03188 - spinel 16
0.054	0.013	37.011	31.739	0.206	15.858	0.247	0.162	0.252	15.688	0.002	0.019	101.250	core
0.077	0.041	41.148	27.776	0.212	15.169	0.243	0.185	0.259	16.359	0.002	0.007	101.476	PO03188 - spinel 17 rim PO03188 - spinel 17
0.051	0.035	38.891	29.927	0.190	15.629	0.253	0.164	0.288	15.860	0.019	0.010	101.317	core
41.082	0.009	0.015	0.022	0.010	9.222	0.160	0.407	0.042	50.660	0.022	0.000	101.651	PO03188 - olivine 3
56.118	0.024	3.178	0.734	0.021	6.093	0.160	0.089	0.030	34.225	0.715	0.010	101.396	PO03 76 opx1
0.072	0.026	39.043	30.456	0.174	15.710	0.277	0.180	0.249	15.323	0.004	0.009	101.524	PO03 76 spinel 1
0.044	0.008	41.637	27.519	0.173	14.843	0.233	0.249	0.223	16.230	0.018	0.007	101.184	PO03 76 spinel 1 core
41.182	0.000	0.015	0.030	0.000	9.329	0.131	0.503	0.024	50.163	0.018	0.007	101.401	PO03 76 olivine 1
56.525	0.022	2.733	0.551	0.022	6.179	0.155	0.103	0.040	34.551	0.611	0.000	101.492	PO03 76 opx 2
0.032	0.040	41.377	27.286	0.159	15.038	0.227	0.199	0.268	16.323	0.022	0.004	100.976	PO03 76 spinel
0.048	0.014	39.502	29.142	0.153	16.199	0.265	0.198	0.297	15.132	0.001	0.013	100.962	PO03 76 spinel 2
1.749	0.032	40.550	26.013	0.139	14.613	0.246	0.157	0.268	17.026	0.035	0.014	100.842	PO03 76 spinel 3 rim
0.082	0.061	36.664	32.836	0.174	15.735	0.260	0.172	0.260	15.393	0.008	0.011	101.655	PO03 76 spinel 3 core
1.516	0.003	0.027	0.000	0.013	37.160	0.023	#####	0.000	1.878	0.016	0.000	82.788	PO03 76 sulphide 1
0.087	0.005	38.799	31.189	0.130	14.579	0.270	0.189	0.221	15.622	0.043	0.021	101.155	PO03 76 spinel 4
0.086	0.028	38.560	29.388	0.160	18.398	0.314	0.172	0.320	13.913	0.011	0.013	101.362	PO03 76 spinel 5 rim
0.021	0.020	42.885	26.284	0.125	14.646	0.237	0.215	0.262	16.487	0.043	0.011	101.236	PO03 76 spinel 6 line
0.038	0.013	42.422	26.607	0.140	14.615	0.238	0.204	0.272	16.462	0.021	0.013	101.044	PO03 76 spinel 6 line
0.053	0.018	41.901	27.360	0.156	14.689	0.253	0.220	0.251	16.217	0.009	0.018	101.146	PO03 76 spinel 6 line
0.040	0.018	41.813	27.697	0.146	14.947	0.244	0.219	0.289	16.207	0.017	0.012	101.648	PO03 76 spinel 6 line

Appendix 4. Electron microprobe Data.

6.369	0.021	27.457	17.121	0.093	30.435	0.261	0.147	0.220	17.081	0.036	0.023	99.263	PO03 76 spinel 6 line
0.009	0.000	0.302	32.755	0.156	1.085	0.311	0.022	0.029	16.096	0.013	0.009	50.786	PO03 76 spinel 7 rim
0.003	0.003	0.002	31.492	0.142	0.011	0.252	0.004	0.000	18.151	0.011	0.019	50.092	PO03 76 spinel 7 core
0.056	0.045	42.324	26.687	0.156	15.271	0.239	0.214	0.271	16.287	0.015	0.010	101.574	PO03 76 spinel 8
0.138	0.050	40.431	28.355	0.151	16.414	0.271	0.169	0.256	15.327	0.012	0.013	101.586	PO03 76 spinel 9 rim
0.056	0.032	41.140	28.215	0.147	14.960	0.208	0.178	0.239	16.244	0.009	0.026	101.453	PO03 76 spinel 9 core
0.105	0.027	45.281	22.635	0.158	15.568	0.225	0.230	0.321	16.456	0.017	0.007	101.030	PO03 76 spinel 10 rim
0.094	0.016	44.868	23.070	0.150	14.757	0.211	0.244	0.352	16.974	0.004	0.014	100.754	PO03 76 spinel 10 core
0.129	0.038	40.814	26.742	0.148	17.176	0.250	0.163	0.251	15.492	0.008	0.018	101.230	PO03 76 spinel 11 rim
0.059	0.039	41.437	26.398	0.156	16.953	0.238	0.181	0.251	15.765	0.010	0.006	101.492	PO03 76 spinel 11 core
0.360	0.026	44.473	23.183	0.149	14.785	0.226	0.292	0.224	17.101	0.033	0.014	100.867	PO03 76 spinel 12 rim
0.041	0.047	38.401	30.657	0.139	15.580	0.255	0.167	0.209	15.631	0.021	0.015	101.162	PO03 76 spinel 12 core
0.048	0.019	39.899	28.321	0.146	17.044	0.292	0.179	0.318	14.652	0.012	0.018	100.946	PO03 76 spinel 13 rim
0.042	0.042	39.827	28.861	0.170	15.942	0.234	0.193	0.289	15.757	0.003	0.007	101.368	PO03 76 spinel 13 core
1.259	0.016	41.517	24.047	0.136	15.450	0.230	0.226	0.245	17.951	0.007	0.007	101.091	PO03 76 spinel 14 rim
0.035	0.015	39.728	29.499	0.157	15.493	0.220	0.175	0.260	15.752	0.009	0.003	101.345	PO03 76 spinel 14 core
0.026	0.032	43.806	24.916	0.168	15.690	0.222	0.208	0.332	16.165	0.004	0.000	101.569	PO03 76 spinel 15 core
0.189	0.044	37.984	30.617	0.156	15.792	0.257	0.159	0.268	15.408	0.016	0.000	100.891	PO03 76 spinel 16 rim
0.319	0.036	38.592	30.028	0.160	15.947	0.262	0.202	0.241	15.543	0.003	0.013	101.346	PO03 76 spinel 16 core
0.386	0.005	41.871	26.518	0.141	15.603	0.254	0.164	0.275	16.281	0.014	0.008	101.520	PO03 76 spinel 17 rim
0.092	0.036	37.407	30.616	0.157	19.181	0.333	0.163	0.293	13.054	0.002	0.012	101.347	PO03 76 spinel 17 core
0.064	0.026	43.701	24.070	0.160	17.698	0.247	0.212	0.510	15.084	0.039	0.016	101.828	PO03 76 spinel 18
0.440	0.040	30.070	24.614	0.146	7.017	0.265	0.084	0.117	16.123	0.038	0.024	78.977	PO03 76 spinel 19 rim
0.001	0.046	0.000	28.895	0.158	0.014	0.230	0.007	0.001	18.169	0.006	0.009	47.536	PO03 76 spinel 19 core
0.076	0.017	43.663	25.305	0.165	14.888	0.224	0.170	0.329	16.232	0.016	0.016	101.102	PO03 76 spinel 20 rim
0.052	0.032	40.468	28.495	0.162	15.665	0.234	0.195	0.286	15.567	0.002	0.024	101.184	PO03 76 spinel 20 core
0.880	0.025	32.359	25.001	0.146	28.714	0.365	0.168	0.286	12.910	0.014	0.018	100.886	PO03 76 spinel 21 rim
0.040	0.044	39.359	29.737	0.151	15.594	0.241	0.166	0.254	15.764	0.015	0.016	101.379	PO03 76 spinel 21 core
0.053	0.034	41.586	27.749	0.136	14.948	0.247	0.207	0.263	16.207	0.001	0.009	101.439	PO03 76 spinel 22 rim
0.051	0.046	37.771	31.402	0.184	15.717	0.229	0.161	0.262	15.342	0.017	0.002	101.184	PO03 76 spinel 22 core
0.056	0.049	42.224	26.500	0.173	15.552	0.264	0.170	0.296	15.814	0.014	0.024	101.139	PO03 76 spinel 23 core
0.048	0.048	43.412	25.809	0.141	14.696	0.193	0.202	0.307	16.443	0.030	0.018	101.346	PO03 76 spinel 24 core
35.597	0.056	1.695	0.019	0.004	26.772	0.469	0.018	0.013	0.074	32.268	0.005	96.989	andradite

Appendix 4. Electron microprobe Data.

35.549	0.066	1.701	0.026	0.009	26.567	0.468	0.000	0.033	0.078	32.366	0.005	96.869	andradite2
35.492	0.051	1.708	0.023	0.004	26.854	0.467	0.001	0.064	0.063	32.436	0.012	97.176	andradite3
													andradite4 after new Fe std
35.453	0.063	1.707	0.014	0.003	27.868	0.435	0.003	0.041	0.058	32.212	0.014	97.871	std
0.063	0.086	15.553	51.159	0.213	24.080	0.455	0.077	0.246	9.995	0.015	0.015	101.956	PO03 189 Spinel 1 rim
0.170	0.115	16.109	49.878	0.210	25.517	0.499	0.071	0.289	9.277	0.000	0.022	102.157	PO03 189 Spinel 2 rim
0.062	0.125	16.247	51.506	0.207	23.048	0.426	0.068	0.268	9.939	0.000	0.018	101.914	PO03 189 Spinel 2 core
0.097	0.081	15.797	52.298	0.198	22.338	0.451	0.062	0.236	10.325	0.010	0.025	101.917	PO03 189 Spinel 3 rim
0.078	0.101	16.250	52.104	0.205	22.379	0.437	0.090	0.256	10.083	0.022	0.004	102.009	PO03 189 Spinel 3 core
0.075	0.108	15.308	51.333	0.184	23.181	0.468	0.101	0.240	10.435	0.007	0.027	101.468	PO03 189 Spinel 4 rim
0.060	0.104	16.448	52.051	0.179	22.340	0.451	0.097	0.234	10.135	0.004	0.014	102.118	PO03 189 Spinel 4 core
0.526	0.103	15.732	49.974	0.187	24.323	0.446	0.068	0.190	10.923	0.005	0.040	102.516	PO03 189 Spinel 5 rim
0.023	0.109	16.711	52.148	0.196	21.480	0.375	0.062	0.208	10.718	0.003	0.016	102.048	PO03 189 Spinel 5 core
0.045	0.103	15.679	51.681	0.187	22.075	0.429	0.072	0.220	10.547	0.000	0.041	101.077	PO03 189 Spinel 6 rim
0.047	0.129	16.484	52.240	0.211	21.197	0.413	0.077	0.195	10.951	0.023	0.018	101.985	PO03 189 Spinel 6 core
0.080	0.126	15.811	51.391	0.219	23.248	0.437	0.095	0.292	9.566	0.002	0.023	101.290	PO03 189 Spinel 7 rim
0.048	0.133	16.613	51.524	0.212	22.792	0.433	0.085	0.264	10.013	0.000	0.018	102.133	PO03 189 Spinel 7 core
0.139	0.113	11.235	50.433	0.191	29.215	0.492	0.107	0.240	8.154	0.016	0.000	100.336	PO03 189 Spinel 8 rim
0.045	0.102	8.384	51.862	0.198	31.702	0.538	0.098	0.188	7.756	0.019	0.017	100.909	PO03 189 Spinel 8 core
0.098	0.121	15.225	52.281	0.201	22.577	0.431	0.086	0.203	10.211	0.000	0.000	101.434	PO03 189 Spinel 9 rim
0.055	0.115	16.520	52.246	0.213	21.799	0.420	0.091	0.234	10.501	0.008	0.014	102.217	PO03 189 Spinel 9 core
0.065	0.106	12.262	50.639	0.208	30.158	0.600	0.097	0.308	6.135	0.013	0.010	100.602	PO03 189 Spinel 10 rim PO03 189 Spinel 10
0.050	0.127	16.920	52.143	0.203	21.343	0.439	0.063	0.228	10.643	0.014	0.021	102.194	core
0.077	0.105	14.557	50.851	0.216	26.728	0.515	0.069	0.371	7.799	0.000	0.024	101.311	PO03 189 Spinel 11 rim PO03 189 Spinel 11
0.000	0.000	0.000	0.000	0.000	0.000	0.000	0.000	0.000	0.000	0.000	0.000	0.000	core
0.071	0.111	15.229	51.382	0.209	23.736	0.437	0.088	0.277	9.442	0.027	0.038	101.047	PO03 189 Spinel 12 rim PO03 189 Spinel 12
0.051	0.095	16.167	51.133	0.206	23.131	0.454	0.076	0.262	9.847	0.018	0.027	101.467	core
0.077	0.084	15.251	51.403	0.198	23.703	0.435	0.054	0.229	9.634	0.014	0.021	101.103	PO03 189 Spinel 13 rim PO03 189 Spinel 13
0.040	0.113	16.522	51.703	0.193	21.881	0.415	0.049	0.226	10.355	0.001	0.009	101.507	core

Appendix 4. Electron microprobe Data.

0.063	0.110	15.316	52.277	0.197	23.304	0.444	0.037	0.182	9.507	0.013	0.015	101.463	PO03 189 Spinel 14 rim PO03 189 Spinel 14
0.056	0.140	16.326	52.280	0.201	22.419	0.410	0.097	0.231	9.996	0.005	0.018	102.178	core
0.207	0.320	16.502	51.781	0.192	21.912	0.422	0.079	0.203	10.371	0.024	0.030	102.045	PO03 189 Spinel 15 rim PO03 189 Spinel 15
0.073	0.124	16.685	52.143	0.200	21.138	0.425	0.066	0.168	10.985	0.006	0.013	102.027	core
0.033	0.107	15.351	52.930	0.198	21.903	0.414	0.088	0.206	10.230	0.007	0.052	101.520	PO03 189 Spinel 16 rim PO03 189 Spinel 16
0.041	0.103	16.602	52.170	0.214	21.275	0.408	0.059	0.219	10.805	0.015	0.014	101.927	core
0.294	0.127	11.003	48.505	0.207	31.672	0.512	0.113	0.249	7.714	0.024	0.021	100.442	PO03 189 Spinel 17 rim PO03 189 Spinel 17
0.049	0.135	16.611	51.076	0.218	22.863	0.454	0.104	0.195	9.988	0.000	0.019	101.712	core
0.100	0.116	15.448	51.946	0.191	22.546	0.452	0.067	0.173	10.178	0.025	0.056	101.298	PO03 189 Spinel 18 rim PO03 189 Spinel 18
0.074	0.111	16.565	52.163	0.210	21.709	0.414	0.066	0.168	10.614	0.000	0.023	102.117	core
0.054	0.118	15.805	51.186	0.189	23.342	0.436	0.072	0.211	9.840	0.002	0.001	101.255	PO03 189 Spinel 19 rim PO03 189 Spinel 19
0.030	0.115	16.766	51.612	0.197	21.837	0.419	0.086	0.180	10.618	0.000	0.015	101.876	core

SiO2	TiO2	Al2O3	Cr2O3	V2O3	FeO	MnO	NiO	ZnO	MgO	CaO	Na2O	Total	Comment
53.687	0.085	1.579	0.247	0.028	2.095	0.100	0.061	0.041	18.448	24.617	0.116	101.103	PO02 E24 spinel 1
20.080	0.302	23.776	12.698	0.084	13.028	0.190	0.198	0.103	21.253	6.905	0.021	98.636	PO02 E24 spinel 2 rim
52.812	0.136	2.307	0.402	0.012	2.314	0.095	0.089	0.000	18.191	24.217	0.125	100.699	PO02 E24 spinel 3
0.068	0.055	43.949	22.889	0.119	16.233	0.235	0.231	0.287	16.979	0.001	0.013	101.061	PO02 E24 spinel 4 rim
0.068	0.031	45.089	22.028	0.112	16.008	0.230	0.260	0.280	17.612	0.011	0.000	101.728	PO02 E24 spinel 4 core
42.638	0.008	1.124	0.010	0.000	6.382	0.105	0.040	0.022	37.753	0.045	0.012	88.137	PO02 E24 pyroxene1
2.257	0.005	0.037	0.065	0.000	90.968	0.067	0.035	0.015	0.348	0.030	0.018	93.844	PO02 E24 spinel 5
0.037	0.045	44.195	22.354	0.147	16.360	0.211	0.225	0.290	17.519	0.017	0.014	101.416	PO02 E24 spinel 6
0.653	0.077	38.651	24.955	0.141	19.313	0.277	0.197	0.278	16.779	0.012	0.036	101.369	PO02 E24 spinel 7 rim
0.034	0.054	43.567	22.531	0.149	16.876	0.199	0.273	0.297	17.004	0.005	0.006	100.993	PO02 E24 spinel 7 core
0.049	0.056	43.427	23.526	0.124	16.484	0.217	0.236	0.235	16.866	0.007	0.025	101.252	PO02 E24 spinel 8 rim
0.036	0.084	43.666	22.829	0.114	16.140	0.212	0.266	0.233	17.409	0.022	0.020	101.031	PO02 E24 spinel 8 core
0.104	0.070	44.138	22.571	0.118	15.699	0.228	0.207	0.270	17.994	0.031	0.019	101.448	PO02 E24 spinel 9 rim
0.023	0.065	43.642	23.550	0.122	16.056	0.196	0.260	0.230	17.461	0.008	0.014	101.628	PO02 E24 spinel 9 core

Appendix 4. Electron microprobe Data.

0.056	0.065	42.192	24.999	0.118	16.123	0.222	0.218	0.199	16.945	0.002	0.008	101.147	PO02 E24 spinel 10 rim
													PO02 E24 spinel 10
0.038	0.047	43.572	23.442	0.110	15.744	0.179	0.250	0.248	17.486	0.009	0.017	101.140	core
0.413	0.038	39.118	23.219	0.115	21.411	0.259	0.176	0.260	16.238	0.020	0.010	101.279	PO02 E24 spinel 11 rim
													PO02 E24 spinel 11
0.875	0.032	39.484	23.347	0.118	20.476	0.623	0.249	0.289	16.398	0.055	0.011	101.955	core
0.121	0.058	41.398	24.011	0.127	17.484	0.215	0.223	0.213	16.362	0.027	0.014	100.254	PO02 E24 spinel 12 rim
													PO02 E24 spinel 12
0.059	0.069	43.225	23.078	0.135	16.711	0.227	0.231	0.256	16.927	0.008	0.019	100.946	core
0.052	0.047	49.277	16.453	0.122	14.721	0.190	0.311	0.308	19.034	0.015	0.028	100.557	PO02 E24 spinel 13 rim
													PO02 E24 spinel 13
0.026	0.059	41.856	24.922	0.142	17.386	0.230	0.244	0.254	16.407	0.017	0.027	101.569	core
1.451	0.068	38.039	24.548	0.135	16.691	0.237	0.215	0.239	19.956	0.022	0.076	101.677	PO02 E24 spinel 14 rim
													PO02 E24 spinel 14
0.025	0.059	43.076	24.026	0.126	16.391	0.245	0.261	0.223	17.113	0.006	0.040	101.591	core
0.176	0.066	38.133	26.857	0.155	18.590	0.249	0.212	0.296	16.395	0.004	0.029	101.162	PO02 E24 spinel 15 rim
													PO02 E24 spinel 15
0.065	0.046	43.590	22.906	0.123	16.505	0.213	0.242	0.305	17.177	0.004	0.030	101.205	core
0.051	0.071	43.395	25.103	0.167	16.621	0.239	0.198	0.267	15.910	0.015	0.007	102.044	PO01 36 spinel 1 rim
0.049	0.077	41.651	26.076	0.183	16.710	0.258	0.201	0.271	15.809	0.002	0.020	101.306	PO01 36 spinel 1 core
1.230	0.056	39.826	21.281	0.129	16.457	0.243	0.180	0.229	18.713	0.025	0.041	98.412	PO01 36 spinel 2 rim
0.038	0.068	41.885	25.862	0.162	16.068	0.218	0.204	0.225	16.267	0.003	0.018	101.018	PO01 36 spinel 2 core
0.055	0.052	44.806	23.178	0.162	16.042	0.217	0.166	0.331	14.811	0.020	0.020	99.859	PO01 36 spinel 3 rim
0.040	0.049	43.447	23.847	0.158	16.993	0.226	0.192	0.337	15.898	0.010	0.017	101.216	PO01 36 spinel 3 core
0.078	0.085	37.692	28.260	0.183	18.218	0.291	0.134	0.269	15.548	0.021	0.027	100.807	PO01 36 spinel 4 rim
0.038	0.098	38.562	28.825	0.164	17.211	0.256	0.192	0.226	15.502	0.004	0.029	101.108	PO01 36 spinel 4 core
0.065	0.080	37.951	30.347	0.174	18.429	0.268	0.125	0.242	14.356	0.004	0.020	102.060	PO01 36 spinel 5 rim
0.061	0.139	36.379	30.831	0.174	18.509	0.260	0.169	0.278	14.515	0.011	0.015	101.340	PO01 36 spinel 5 core
0.039	0.087	41.704	25.183	0.165	17.860	0.257	0.186	0.294	15.074	0.009	0.016	100.874	PO01 36 spinel 6 rim
0.031	0.107	37.454	29.448	0.154	18.331	0.269	0.144	0.258	14.676	0.015	0.008	100.896	PO01 36 spinel 6 core
0.057	0.076	44.535	21.013	0.157	18.305	0.224	0.204	0.264	16.487	0.000	0.033	101.355	PO01 36 spinel 7 rim
0.038	0.109	37.943	29.859	0.175	18.020	0.269	0.178	0.235	15.004	0.000	0.009	101.839	PO01 36 spinel 7 core
1.181	0.065	38.175	27.383	0.188	17.486	0.282	0.168	0.242	16.181	0.029	0.012	101.391	PO01 36 spinel 8 rim
0.047	0.071	39.711	27.813	0.178	17.107	0.241	0.197	0.233	15.738	0.003	0.025	101.364	PO01 36 spinel 8 core

Appendix 4. Electron microprobe Data.

0.170	0.058	42.959	23.470	0.147	16.559	0.233	0.182	0.286	15.665	0.009	0.010	99.749	PO01 36 spinel 9 rim
0.054	0.051	41.530	25.771	0.175	17.017	0.264	0.183	0.247	15.562	0.004	0.013	100.871	PO01 36 spinel 9 core
0.171	0.063	39.765	27.169	0.175	16.301	0.229	0.155	0.286	16.163	0.010	0.024	100.510	PO01 36 spinel 10 rim
0.024	0.069	41.632	26.098	0.156	16.761	0.247	0.184	0.302	15.852	0.004	0.016	101.345	PO01 36 spinel 10 core
0.068	0.050	42.407	24.690	0.168	15.898	0.213	0.168	0.230	16.411	0.007	0.006	100.316	PO01 36 spinel 11 rim
0.025	0.053	42.121	25.857	0.162	15.951	0.205	0.199	0.256	16.138	0.005	0.005	100.977	PO01 36 spinel 11 core
1.089	0.089	39.125	25.284	0.151	17.505	0.264	0.158	0.236	18.503	0.002	0.015	102.422	PO01 36 spinel 12 rim
0.043	0.079	41.100	26.571	0.160	16.230	0.245	0.206	0.261	16.142	0.011	0.008	101.055	PO01 36 spinel 12 core
Kızılırmak Ophiolite													
0.228	0.047	41.112	26.677	0.188	17.221	0.251	0.210	0.303	16.247	0.004	0.012	102.499	PO02 37 spinel 1 rim
0.027	0.073	40.039	27.582	0.169	17.273	0.263	0.176	0.270	15.341	0.006	0.007	101.226	PO02 37 spinel 1 core
0.742	0.053	38.241	27.836	0.177	18.301	0.274	0.125	0.301	16.787	0.009	0.015	102.859	PO02 37 spinel 2 rim
0.041	0.046	38.946	29.106	0.162	17.748	0.247	0.173	0.306	14.946	0.000	0.009	101.731	PO02 37 spinel 2 core
0.061	0.037	40.892	26.082	0.162	16.642	0.230	0.171	0.294	15.421	0.007	0.012	100.009	PO02 37 spinel 3 rim
0.040	0.070	39.641	28.538	0.161	17.322	0.246	0.163	0.272	15.118	0.010	0.011	101.592	PO02 37 spinel 3 core
0.036	0.068	39.288	28.163	0.162	17.277	0.258	0.169	0.280	14.745	0.000	0.002	100.449	PO02 37 spinel 4 rim
0.044	0.061	39.062	28.818	0.174	17.303	0.259	0.164	0.284	15.013	0.000	0.014	101.197	PO02 37 spinel 4 core
0.047	0.040	43.048	23.229	0.135	15.625	0.218	0.192	0.314	17.175	0.006	0.015	100.045	PO02 37 spinel 5 rim
0.024	0.059	39.927	27.639	0.138	17.034	0.245	0.209	0.295	15.626	0.014	0.013	101.224	PO02 37 spinel 5 core
0.129	0.046	38.162	30.111	0.140	18.567	0.273	0.143	0.330	14.557	0.014	0.013	102.484	PO02 37 spinel 6 rim
0.059	0.042	40.959	26.431	0.153	18.031	0.272	0.157	0.370	15.076	0.000	0.008	101.558	PO02 37 spinel 6 core
0.051	0.048	39.871	27.448	0.143	17.376	0.256	0.149	0.264	15.427	0.000	0.008	101.043	PO02 37 spinel 7 rim
0.021	0.068	38.859	28.849	0.145	17.711	0.289	0.178	0.273	14.954	0.000	0.009	101.357	PO02 37 spinel 7 core
0.060	0.064	41.418	24.787	0.147	18.441	0.256	0.204	0.252	15.404	0.016	0.008	101.056	PO02 37 spinel 8 rim
0.032	0.058	39.681	27.840	0.156	17.831	0.274	0.164	0.276	15.141	0.008	0.016	101.477	PO02 37 spinel 8 core
0.019	0.062	36.344	31.142	0.170	18.886	0.304	0.173	0.273	13.940	0.020	0.009	101.341	PO02 37 spinel 9 rim
0.060	0.064	38.261	29.366	0.149	17.840	0.265	0.161	0.270	14.715	0.017	0.013	101.180	PO02 37 spinel 9 core
0.058	0.057	42.019	24.202	0.144	17.940	0.250	0.198	0.236	15.886	0.000	0.020	101.010	PO02 37 spinel 10 rim
0.033	0.095	38.416	28.894	0.172	18.015	0.255	0.174	0.251	14.809	0.021	0.002	101.137	PO02 37 spinel 10 core
0.718	0.077	34.254	30.776	0.180	20.728	0.292	0.139	0.245	14.640	0.017	0.010	102.077	PO02 37 spinel 11 rim
0.028	0.100	38.497	29.016	0.166	18.172	0.278	0.175	0.291	14.727	0.009	0.004	101.464	PO02 37 spinel 11 core
6.784	0.117	28.849	22.451	0.135	22.770	0.350	0.153	0.177	20.771	0.017	0.016	102.589	PO02 37 spinel 12 rim
0.053	0.103	36.475	31.141	0.164	18.573	0.249	0.125	0.226	14.579	0.009	0.009	101.707	PO02 37 spinel 12 core

Appendix 4. Electron microprobe Data.

Kirazbaşı Melange

0.076	0.029	15.725	51.825	0.410	22.329	0.467	0.061	0.310	9.352	0.009	0.006	100.599	PO02 71 spinel 1 rim
0.060	0.021	15.206	53.923	0.384	21.583	0.440	0.054	0.315	9.415	0.007	0.027	101.435	PO02 71 spinel 1 core
0.360	0.004	23.433	44.723	0.331	21.140	0.406	0.056	0.421	10.729	0.015	0.021	101.638	PO02 71 spinel 2 rim
0.076	0.018	20.198	47.755	0.378	21.418	0.451	0.066	0.336	9.876	0.068	0.013	100.652	PO02 71 spinel 2 core
0.048	0.027	15.452	53.870	0.348	20.652	0.449	0.059	0.246	9.732	0.021	0.013	100.916	PO02 71 spinel 3 rim
0.064	0.020	13.800	56.486	0.369	19.933	0.430	0.044	0.240	10.141	0.000	0.037	101.563	PO02 71 spinel 3 core
1.109	0.011	17.884	49.621	0.380	20.837	0.467	0.065	0.296	11.437	0.015	0.022	102.144	PO02 71 spinel 4 rim
0.076	0.017	15.088	55.038	0.369	20.680	0.465	0.047	0.255	9.656	0.021	0.015	101.726	PO02 71 spinel 4 core
57.356	0.003	0.906	0.399	0.027	5.713	0.165	0.091	0.020	35.453	1.346	0.007	101.486	PO02 71 pyroxene
0.051	0.000	16.209	54.280	0.356	19.455	0.403	0.053	0.264	10.940	0.011	0.014	102.037	PO02 71 spinel 5 rim
0.064	0.026	13.942	56.423	0.371	19.658	0.447	0.075	0.240	10.399	0.013	0.014	101.672	PO02 71 spinel 5 core
0.096	0.034	14.124	55.450	0.354	20.227	0.424	0.042	0.187	10.567	0.000	0.008	101.513	PO02 71 spinel 6 rim
0.048	0.026	13.046	56.772	0.352	20.275	0.480	0.040	0.204	10.054	0.010	0.014	101.322	PO02 71 spinel 6 core
10.152	0.012	14.813	34.587	0.267	21.458	0.333	0.162	0.256	20.848	0.032	0.029	102.948	PO02 71 spinel 7 rim
0.047	0.039	16.237	52.372	0.386	21.352	0.447	0.069	0.276	9.743	0.007	0.019	100.995	PO02 71 spinel 7 core
0.384	0.000	16.644	50.569	0.392	19.943	0.442	0.057	0.225	11.631	0.012	0.003	100.303	PO02 71 spinel 8 rim
0.109	0.032	12.841	57.864	0.340	19.518	0.427	0.049	0.176	10.397	0.028	0.008	101.790	PO02 71 spinel 8 core
0.054	0.029	14.493	54.964	0.371	20.420	0.431	0.062	0.232	9.945	0.005	0.023	101.029	PO02 71 spinel 9 rim
0.070	0.025	13.327	56.700	0.374	20.410	0.474	0.044	0.225	9.975	0.008	0.013	101.645	PO02 71 spinel 9 core
0.259	0.025	19.358	48.675	0.371	21.215	0.427	0.045	0.401	10.979	0.099	0.024	101.879	PO02 71 spinel 10 rim
0.087	0.004	18.012	50.984	0.388	21.506	0.479	0.054	0.412	9.522	0.044	0.025	101.516	PO02 71 spinel 10 core
0.075	0.011	14.698	54.615	0.370	21.628	0.474	0.038	0.264	8.976	0.003	0.023	101.176	PO02 71 spinel 11 rim
0.038	0.024	13.821	56.150	0.347	20.946	0.492	0.044	0.282	9.339	0.000	0.031	101.512	PO02 71 spinel 11 core
0.036	0.020	14.939	53.905	0.365	20.777	0.460	0.070	0.211	10.103	0.028	0.005	100.920	PO02 71 spinel 12 rim
0.081	0.049	12.431	58.242	0.337	19.411	0.442	0.065	0.203	10.545	0.018	0.015	101.839	PO02 71 spinel 12 core
14.319	0.000	17.165	25.801	0.211	18.225	0.305	0.157	0.272	25.296	0.075	0.055	101.882	PO03 5 spinel 1 rim
0.066	0.001	24.927	43.501	0.330	20.501	0.393	0.055	0.376	11.187	0.019	0.006	101.363	PO03 5 spinel 1 core
0.086	0.030	23.805	44.374	0.268	19.345	0.337	0.098	0.232	12.475	0.014	0.014	101.078	PO03 5 spinel 2 rim
0.039	0.022	20.419	49.745	0.261	18.701	0.389	0.083	0.229	11.878	0.002	0.006	101.772	PO03 5 spinel 2 core
0.145	0.020	23.226	44.551	0.282	20.411	0.383	0.079	0.255	11.806	0.009	0.013	101.182	PO03 5 spinel 3 rim
0.046	0.000	21.148	48.453	0.248	18.895	0.384	0.060	0.245	11.777	0.006	0.014	101.276	PO03 5 spinel 3 core
0.051	0.030	22.089	46.313	0.293	19.586	0.375	0.087	0.243	11.843	0.000	0.019	100.929	PO03 5 spinel 4 rim

Appendix 4. Electron microprobe Data.

0.049	0.020	20.023	48.797	0.279	18.988	0.407	0.073	0.225	11.952	0.172	0.010	100.994	PO03 5 spinel 4 core
0.324	0.023	26.726	40.653	0.305	19.230	0.345	0.079	0.391	12.258	0.033	0.019	100.388	PO03 5 spinel 5 rim
0.293	0.008	25.652	41.163	0.295	20.741	0.414	0.075	0.407	11.593	0.024	0.007	100.672	PO03 5 spinel 5 core
0.087	0.017	28.460	39.708	0.313	19.580	0.352	0.093	0.387	11.960	0.010	0.003	100.971	PO03 5 spinel 6 rim
0.056	0.010	27.339	41.078	0.318	19.563	0.364	0.083	0.392	11.730	0.031	0.018	100.983	PO03 5 spinel 6 core
0.070	0.022	26.672	41.194	0.305	19.597	0.372	0.064	0.368	11.749	0.015	0.021	100.449	PO03 5 spinel 7 rim
0.094	0.016	26.685	40.901	0.300	19.578	0.360	0.071	0.335	11.890	0.026	0.013	100.268	PO03 5 spinel 7 core
0.083	0.010	25.375	41.004	0.342	21.752	0.393	0.098	0.391	10.963	0.022	0.023	100.457	PO03 5 spinel 8 rim
0.072	0.024	25.388	40.547	0.342	22.138	0.397	0.067	0.423	11.096	0.017	0.023	100.535	PO03 5 spinel 8 core
0.097	0.022	25.397	41.896	0.324	20.637	0.416	0.082	0.365	11.279	0.005	0.041	100.562	PO03 5 spinel 9 rim
0.128	0.010	23.304	39.720	0.247	23.449	0.392	0.046	0.382	12.037	0.018	0.031	99.765	PO03 5 spinel 9 core
0.075	0.035	22.085	46.410	0.270	19.894	0.367	0.075	0.211	11.798	0.023	0.012	101.255	PO03 5 spinel 10 rim
0.058	0.020	21.201	48.420	0.271	18.706	0.375	0.056	0.232	11.907	0.018	0.007	101.272	PO03 5 spinel 10 core
0.209	0.017	27.035	40.482	0.306	20.374	0.347	0.073	0.283	12.524	0.002	0.024	101.676	PO03 5 spinel 11 rim
0.074	0.009	20.971	48.326	0.306	19.510	0.412	0.051	0.235	11.446	0.000	0.018	101.358	PO03 5 spinel 11 core
0.053	0.021	17.185	51.204	0.314	21.340	0.443	0.079	0.243	10.482	0.016	0.005	101.385	PO03 81 spinel 1 rim
0.059	0.021	15.832	54.052	0.299	19.429	0.421	0.059	0.188	11.040	0.017	0.007	101.423	PO03 81 spinel 1 core
0.758	0.026	8.428	23.383	0.131	58.677	0.243	0.447	0.115	6.671	0.000	0.007	98.886	PO03 81 spinel 2 rim
0.076	0.011	16.177	53.738	0.299	19.429	0.417	0.069	0.203	11.155	0.003	0.016	101.592	PO03 81 spinel 2 core
13.586	0.012	12.910	34.960	0.232	16.292	0.304	0.106	0.169	25.025	0.008	0.009	103.615	PO03 81 spinel 3 rim
0.045	0.019	16.959	52.214	0.339	20.489	0.414	0.061	0.233	10.610	0.004	0.011	101.398	PO03 81 spinel 3 core
0.704	0.010	17.545	39.688	0.308	30.964	0.406	0.144	0.358	9.850	0.000	0.022	99.998	PO03 81 spinel 4 rim
0.444	0.013	19.229	45.875	0.342	23.824	0.441	0.068	0.437	10.211	0.000	0.026	100.909	PO03 81 spinel 4 core
0.078	0.000	0.009	0.039	0.000	8.765	0.047	72.141	0.018	0.070	0.013	0.000	81.181	PO03 81 unknown
0.058	0.018	18.047	51.769	0.319	18.769	0.386	0.062	0.203	11.772	0.003	0.026	101.433	PO03 81 spinel 5 rim
0.053	0.021	16.057	53.584	0.300	19.483	0.387	0.071	0.209	10.958	0.006	0.015	101.144	PO03 81 spinel 5 core